Titolo

Report on the Results of Analysis of DEC Events for the ETDR (ALFRED)

Authors: G. Bandini, M. Polidori

Descrittori

Tipologia del documento: Rapporto Tecnico
Collocazione contrattuale: Contratto ENEA-EU:
Argomenti trattati: Reattori veloci
Sicurezza nucleare
Analisi di sicurezza

Sommario

This report summarizes the safety analysis results of DEC key transients (events) for the ETDR (ALFRED) plant.

Note

This report is the Deliverable DEL022 of the LEADER project of EU 7th Framework Programme (Grant agreement no. FP7-249668)

Copia n. **In carico a:**

REV.	DESCRIZIONE	DATA		REDAZIONE	CONVALIDA	APPROVAZIONE
2			NOME			
			FIRMA			
1			NOME			
			FIRMA			
0	EMISSIONE	29/04/13	NOME	G. Bandini	F. De Rosa	P. Meloni
			FIRMA			

LEADER Project - Work Package 5

Deliverable DEL022

Report on the results of analysis of DEC events for the ETDR (ALFRED)

Compiled by

G. Bandini (ENEA)
M. Polidori (ENEA)

with the contributions from:

E. Bubelis (KIT-G)
M. Schikorr (KIT-G)
A. Lázaro (JRC-IET)
K. Tuček (JRC-IET)
A. Flores y Flores (JRC-IET)
M. M. Stempniewicz (NRG)
P. Kudinov (KTH)
K. Kööp (KTH)
M. Jeltsov (KTH)
Y. Zhang (PSI)
K. Mikityuk (PSI)
G. Geffraye (CEA)
D. Kadri (CEA)
R. Lo Frano (CIRTEN)
N. Forgione (CIRTEN)
A. Pesetti (CIRTEN)
G. Barone (CIRTEN)
M. Cherubini (CIRTEN)

Executive Summary

This report is prepared to satisfy the requirements of Deliverable DEL022 of the WP5.5 in the EU 7th Framework Program's Research Project "Lead-cooled European Advanced Demonstrator Reactor (LEADER)". The main objective of Deliverable DEL022 is to report on the results of the analysis of DEC transients for the ETDR (ALFRED) reactor. ALFRED is a pool-type, Pb-cooled fast reactor of 300 MWth power. The reactor core consists of 171 fuel assemblies (57 inner core fuel assemblies and 114 outer core fuel assemblies fuelled with MOX) and 16 control/safety assemblies. The primary coolant working temperature is in the range 400–480 °C. The core power is removed by 8 steam generators (SGs), installed in an annular zone near the top of the reactor vessel, and connected with 8 secondary circuits which are fed with water at 335 °C and 188 bar. Super-heated steam at 450 °C and 180 bar pressure from the SG outlet feeds the turbine to produce a net electrical power of about 125 MWe.

The safety analysis is deterministic and the methodology is similar to that employed in the LWR safety analysis, i.e. calculate the consequences for certain postulated events that could occur in the Pb-cooled ETDR (ALFRED) reactor. The analysis presented in this report is for the design extension condition (DEC) events. The postulated DEC events are very unlikely events that foresee possible multiple failures or the failure of safety or mitigating systems, such as the reactor scram in the so-called unprotected transients. One of the major objectives of this study is to evaluate the impact of core and plant design features on the intrinsic safety behavior of the plant. Furthermore, the grace time available before critical core and vessel wall temperatures are reached, or risk of lead freezing is attained in the primary system are investigated.

For ALFRED a total of 8 transients were selected as representative of all identified DEC transients reflecting a wide range of potential transient initiators. These transients include several unprotected transients such as the ones connected with the loss of flow in the primary system and/or the loss of heat removal by the secondary system, and the overpower transient following reactivity insertion. The overcooling transients are investigated in connection with the loss of flow in the primary circuit, which are then most penalizing as related to the risk of lead freezing at the SG outlet. Furthermore, the consequences of the unlike event of the concomitant break of both SG tube walls (Steam Generator Tube Rupture - SGTR) related to: 1) potential mechanical loads on the primary system structures due to water-Pb interaction and 2) core voiding effect due to potential steam bubble transport through the core are investigated.

Different system codes adapted to deal with Pb coolant have been used for the DEC transient analysis by the partners involved in the WP5 activities of the LEADER project. These include:

- the RELAP5/MOD3.3 system code (modified by ENEA/Ansaldo/Uni-Pisa and used by ENEA, KTH and CIRTEN),
- the SIM-LFR system code (developed by KIT),
- the TRACE/FRED system code (coupled and adapted by PSI),
- the TRACE system code (adapted by JRC-IET),
- the SIMMER-III code (used by CIRTEN and JRC-IET),
- the CATHARE V2.5_2 system code (developed by CEA),
- the SPECTRA system code (developed by NRG),

The analysis of unprotected transients: UTOP, ULOF, ULOHS and ULOHS+ULOF has demonstrated the good inherent safety features of the core and plant design and the large grace time allowed for the operator to take opportune corrective action for manually shutting down the reactor and then cooling down the primary circuit towards cold safe conditions.

In case of a UTOP transient, for reactivity insertion of 250 pcm within 10 s (possibly due to: voiding of part of the active core region enveloping void introduction in case of SGTR, core compaction, fuel SA blockage, etc.), at BOC as well as at EOC core conditions, peak fuel pin cladding is not expected to fail, since there is a large margin to creep rupture limit. The more critical issue is the maximum fuel temperature that, because of the initial core nuclear power excursion (peak power up to ~ 230% the nominal value), is expected to exceed the MOX melting point in the initial phase of the transient. However, all codes agree that fuel melting is observed only in the centre of the peak fuel pin (pellets). Therefore, extended fuel rod damage can be excluded, as well as the likelihood for this transient to evolve towards a severe accident.

In case of ULOF transient, no relevant flow undershoot is expected in the initial phase of the transient and enhanced stable natural convection, around 23% of the nominal value, establishes in the primary circuit. Furthermore, the prevalent negative reactivity feedbacks reduce the core power down to about two-third of the nominal value. As a result, the ULOF transient in the ALFRED reactor can be easily accommodated, since the maximum clad temperature remains well below the creep rupture limit in the long term (maximum clad temperature stabilizes below 700 °C). Besides, very large minimum clad failure time of ~ 1.6E+5 seconds (~ 2 days), under the minimum coolant flow conditions (initial flow undershoot) at both BOC and EOC conditions, are calculated by SIM-LFR code.

In case of ULOHS transient, the maximum clad temperature is not a critical issue, since the minimum clad failure time is > 1.E6 seconds, as calculated by SIM-LFR at both BOC and EOC conditions. Because of the uniform temperature distribution establishing in the primary circuit, the main concern is on the average vessel wall temperature, which in ~ 1 hour transient time approaches 670 – 700 °C, thus questioning the long term structural integrity of the vessel under these elevated temperature conditions. The sluggish time response to this DEC transient is ascribed to the large primary loop thermal inertia and a rather large cumulative negative reactivity effect coming from the negative fuel, diagrid, pads, Pb-coolant and CRs drivelines feedback effects, resulting in a very effective decrease of the core nuclear power towards the decay level. Sufficient grace time (>> 30 minutes) is available for the operator intervention to terminate this transient by manually shutting down the reactor and cooling down the primary circuit.

The evolution of the unprotected LOOP (ULOHS+ULOF) transient is characterized first by the loss of flow with transition to natural convection in the primary circuit, such as under ULOF, and then by the loss of heat sink with core nuclear power decrease towards the decay level, such as under ULOHS. Because of the very low natural convection flow rate which stabilizes in the primary circuit and consequent significant core ΔT increase, the maximum clad temperature is about 100 - 120 °C higher than under ULOHS. On the contrary, the very low primary flow rate limits the significant vessel wall temperature increase predicted under ULOHS, and thus the long term structural integrity of the vessel is guaranteed. According to the SIM-LFR results, the minimum clad failure time is of ~ 2.1E+4 seconds at both BOC and EOC conditions.

Therefore, also under this very unlikely DEC transient, sufficient grace time (>> 30 minutes) is available for the operator intervention to terminate this transient by manually shutting down the reactor and cooling down the primary circuit.

All codes agree that the ALFRED reactor is not expected to experience any fuel pin failure during SA flow area blockages less than 75% even in case of unprotected transient. For SA flow area blockages above 75%, clad failure (creep rupture) has to expected. Clad melting point seems reached for flow area blockages above 95%, while fuel melting temperature is reached only for flow area blockages above 97.5%. The SIMMER-III results for a protected case also suggest that nearly total blockages could be well accommodated if the reactor is shutdown within 5 seconds from their detection (i.e. 10 seconds from the initiation of the accident). However, for ALFRED sudden and complete flow blockage is prevented by the SA design solution consisting in multiple inlet openings. Any other blockage caused by deposition of material will be likely gradual and can be monitored by detection of an increase of coolant outlet temperature of each SA.

The analysis of the “practically excluded” event of SCS failure with total unavailability of DHR system has highlighted a slow temperature increase of the primary system, thanks to its large thermal inertia and good coolant mixing throughout the primary pool. This transient presents no imminent safety issue to the ALFRED reactor in the first several hours. However, all primary cooling circuit temperatures, in a longer time horizon, will start increasing slowly at a rate of about 30 °C per hour and will reach ~500 °C in 3 hours. However, the operator has sufficient time for manual intervention by re-activating SCS or sub-systems of the DHR-1 system, in order to prevent overheating of the whole primary system, including the reactor vessel.

The protected loss of flow transients with simultaneous malfunction of the feedwater temperature or flow rate control system on the secondary side have no safety concern in the short term, since the perturbation on core temperatures is not significant. In all code calculations, the initial clad temperature peak produced by the loss of forced circulation in the primary circuit is below 650 °C. Furthermore, there is no risk of lead freezing at the MHX outlet, just after the DHR-1 system start-up. The major concern is on the risk of lead freezing in the medium term, since the power removal by the DHR-1 system exceeds the decay power. The Pb freezing is expected within about 2 – 4 hours, depending on the different conditions of coolant mixing calculated by the codes in the primary pool surrounding the MHX. In fact, the lack of mixing in this wide region, such as predicted by RELAP5 code, reduces significantly the effective thermal inertia of the primary system and then the elapsed time to Pb freezing. However, during this time period the operator has sufficient time to deactivate sub-systems of the DHR-1 system, in order to prevent Pb-coolant freezing at the outlet of the MHX. Future DHR design improvements are foreseen to control in a passive way the DHR-1 and DHR-2 power removal, and thus avoiding the need of operator actions in the medium and long term.

Regarding the SGTR accident, it was observed that, the steam generated by one bayonet tube rupture accident flows upward in the damaged SG and reaches the cover gas passing through the gas vents. However, as a consequence of the large amount of steam produced in the case of seven broken tubes (2.5-3.5 kg/s), traces of steam are expected to flow from the damaged SG directly and indirectly to the core. The small amount of steam enters the core downcomer mostly by the inner path, as shown by the void fraction calculated in the cells beneath the core.

However, the very low amount of vapor entering the core, the limited vapor residence time and the negative coolant expansion reactivity effect in the optimized ALFRED reactor core do not result into a positive reactivity insertion and thus represent no safety concern. Besides, in the SIMMER-III simulation, all the water injected into the Pb-coolant instantaneously fully vaporizes in contact with it at the injector tube exit region. Moreover the cover gas space, due to SIMMER-III 2D model limitation, has been modeled with separated volumes communicating only with small gas openings in the higher part, that are partially obstructed due to lead sloshing resulting in steam flowing through no realistic flow paths (e. g. downward in the pump ducts of the faulted SG). In reality, only a fraction of the injected water will be vaporized instantaneously when contacting lead and the remaining liquid water will be encapsulated in vapor bubbles and transported to the cover gas region formed by only one large volume, hence lead and steam can flow freely into the gas space. This should be kept in mind when analyzing SGTR accident simulation results.

KALLA experimental tests and Russian tests also indicated the difficulty for the vapour bubbles, generated during the lead-water interaction, to reach the core inlet section because of the drag effects produced by the liquid metal flow in the downcomer region of the reactor. A dedicated scaled facility should be foreseen to analyse in depth the SGTR phenomena further as part of the future R&D activities for LFR.

In general, the consistency of various code results for the same transient was rather good. For all DEC events the codes predicted similar transient behaviour and then similar conclusions can be drawn. Some of the observed discrepancies might be correlated to the different schematization detail of the primary and secondary circuits, or correlated to the fuel rod gap behaviour in transient conditions, due to the lack of a dedicated fuel rod gap dynamic model in some of the codes.

Finally, the analysis of the DEC transients performed for the Pb-cooled ALFRED design have demonstrated the very forgiving nature of this plant design when compared to other similar plant design, ascribable to the combination of:

- the inherently, large thermal inertia of the Pb-cooled primary system,
- the detailed focus on the optimization of all safety relevant system, in particular emphasizing appropriate design of all relevant control and safety system (as well as components), and
- optimizing the neutronic core characteristics of the ALFRED “core system” thereby assuring various reactivity feedback effects (fuel, diagrid, pads, Pb-coolant and CRs drivelines expansion reactivity) that effectively depress the reactor power under all adverse DEC transient conditions,
- as the ALFRED core is specifically designed to accommodate the ULOF transient.

This work was performed within the LEADER Project (Contract No. FP7-249668) under the auspices of the EU 7th Framework Program.

CONTENTS

1. INTRODUCTION 10

2. ANALYSED TRANSIENTS AND COMPUTER CODES USED 12

2.1 DEC transients 12
2.2 Computer codes 14

3. ETDR (ALFRED) DESIGN 15

3.1 Primary system 16
3.2 Steam generator 19
3.3 Primary pump 23
3.4 Reactor core 24

3.4.1 BOC and EOC cores: layout and main characteristics 28
3.4.2 Nuclear kinetic data and reactivity coefficients 31

3.5 Secondary circuits 33
3.6 Decay heat removal system 34

3.6.1 System actuation and operation 37
3.6.2 DHR actuation logic 39

4 BENCHMARK OF CODES 41

4.1 ULOF transient 41
4.2 UTOP transient 44
4.3 ULOHS transient 48
4.4 Conclusions from code benchmark 51

5 DEC TRANSIENT RESULTS 52

5.1 TR-4: Unprotected reactivity insertion (UTOP) 52

5.1.1 TR-4 transient: SIM-LFR results (KIT-G) 52
5.1.2 TR-4 transient: TRACE/FRED results (PSI) 55
5.1.3 TR-4 transient: TRACE results (JRC-IET) 56
5.1.4 TR-4 transient: RELAP5 results (ENEA) 58
5.1.5 TR-4 transient: CATHARE results (ENEA/CEA) 59
5.1.6 TR-4 transient: SPECTRA results (NRG) 60

5.2 T-DEC1: Unprotected loss of flow (ULOF) 63

5.2.1 T-DEC1 transient: SIM-LFR results (KIT-G) 63
5.2.2 T-DEC1 transient: TRACE/FRED results (PSI) 66
5.2.3 T-DEC1 transient: TRACE results (JRC-IET) 68
5.2.4 T-DEC1 transient: RELAP5 results (ENEA) 70
5.2.5 T-DEC1 transient: CATHARE results (ENEA/CEA) 72
5.2.6 T-DEC1 transient: SPECTRA results (NRG) 73
5.2.7 T-DEC1 transient: RELAP5 results (KTH) 76
5.2.8 T-DEC1 transient: RELAP5 results (CIRTEN) 77

5.3 T-DEC3: Unprotected loss of heat sink (ULOHS) 79

5.3.1 T-DEC3 transient: SIM-LFR results (KIT-G) 79

5.3.2 T-DEC3 transient: TRACE/FRED results (PSI) 83
5.3.3 T-DEC3 transient: RELAP5 results (ENEA) 84
5.3.4 T-DEC3 transient: CATHARE results (ENEA/CEA) 85
5.3.5 T-DEC3 transient: SPECTRA results (NRG) 86

5.4 T-DEC4: Unprotected loss of offsite power (ULOHS+ULOF) 89

5.4.1 T-DEC4 transient: SIM-LFR results (KIT-G) 89
5.4.2 T-DEC4 transient: RELAP5 results (ENEA) 92
5.4.3 T-DEC4 transient: CATHARE results (ENEA/CEA) 93
5.4.4 T-DEC4 transient: SPECTRA results (NRG) 94
5.4.5 T-DEC4 transient: RELAP5 results (KTH) 96

5.5 T-DEC5: Unprotected partial blockage in the hottest fuel assembly 97

5.5.1 T-DEC5 transient: SIM-LFR results (KIT-G) 98
5.5.2 T-DEC5 transient: RELAP5 results (ENEA) 103
5.5.3 T-DEC5 transient: SPECTRA results (NRG) 103
5.5.4 T-DEC5 transient: SIMMER results (JRC-IET) 105

5.6 T-DEC6: Failure of secondary cooling circuits 109

5.6.1 T-DEC6 transient: SIM-LFR results (KIT-G) 109
5.6.2 T-DEC6 transient: RELAP5 results (ENEA) 113
5.6.3 T-DEC6 transient: SPECTRA results (NRG) 115

5.7 TO-3: Reduction of FW temperature with all primary pumps trip 118

5.7.1 TO-3 transient: SIM-LFR results (KIT-G) 118
5.7.2 TO-3 transient: RELAP5 results (ENEA) 122
5.7.3 TO-3 transient: SPECTRA results (NRG) 124

5.8 TO-6: Increase of FW flowrate with all primary pumps trip 126

5.8.1 TO-6 transient: SIM-LFR results (KIT-G) 127
5.8.2 TO-6 transient: RELAP5 results (ENEA) 130
5.8.3 TO-6 transient: SPECTRA results (NRG) 132

5.9 Steam generator tube rupture (SGTR) event (CIRTEN) 135

5.10 CFD simulation of bubble transport in SGTR/SGTL event (KTH) 141

6. CONCLUSIONS 146

REFERENCES 149

APPENDIX A. Description of computer codes used 150

A.1 SIM-LFR code used by KIT-G 151
A.2 TRACE/FRED code used by PSI 153
A.3 TRACE code used by JRC-IET 154
A.4 RELAP5/MO3.3 code used by ENEA, KTH and CIRTEN 156
A.5 CATHARE V2.5_2 code used by ENEA / CEA 158
A.6 SPECTRA code used by NRG 159
A.7 SIMMER-III code used by CIRTEN 161
A.8 SIMMER-III code used by JRC-IET 164

APPENDIX B. KIT-G contribution to Deliverable DEL022 165

APPENDIX C. PSI contribution to Deliverable DEL022 201

APPENDIX D. JRC-IET contribution to Deliverable DEL022 ……. 217
APPENDIX E. NRG contribution to Deliverable DEL022 ……..……..…....239
APPENDIX F. KTH contribution to Deliverable DEL022 ……..……..……..291
APPENDIX G. CIRTEN contribution to Deliverable DEL022 ……..…….304

1. INTRODUCTION

This report is prepared to satisfy the requirements of Deliverable DEL022 of the WP5.5 in the EU 7th Framework Program's Research Project "Lead-cooled European Advanced Demonstrator Reactor (LEADER)". The main objective of Deliverable DEL022 is to report on the results of the analysis of DEC transients for the ETDR (ALFRED) reactor.

ALFRED is a pool-type, Pb-cooled fast reactor of 300 MWth power. The reactor core consists of 171 fuel assemblies (57 inner core fuel assemblies and 114 outer core fuel assemblies fuelled with MOX) and 16 control/safety assemblies. The primary coolant working temperature is in the range 400–480 °C. The core power is removed by 8 steam generators (SGs), installed in an annular zone near the top of the reactor vessel, and connected with 8 secondary circuits which are fed with water at 335 °C and 188 bar. Super-heated steam at 450 °C and 180 bar pressure from the SG outlet feeds the turbine to produce a net electrical power of about 125 MWe.

The Decay Heat Removal system (DHR) of ALFRED is constituted of two independent and redundant systems: 1) DHR-1: 4 Isolation Condenser systems (ICs) connected to 4 Steam Generators (SGs); 2) DHR-2: 4 Isolation Condenser systems (ICs) connected to the remaining 4 Steam Generators (SGs).

The safety analysis is deterministic and the methodology is similar to that employed in the LWR safety analysis, i.e. calculate the consequences for certain postulated events that could occur in the Pb-cooled ETDR (ALFRED) reactor. The analysis presented in this report is for the design extension condition (DEC) events. The postulated DEC events are very unlikely events that foresee possible multiple failures or the failure of safety or mitigating systems, such as the reactor scram in the so-called unprotected transients. One of the major objectives of this study is to evaluate the impact of core and plant design features on the intrinsic safety behavior of the plant. Furthermore, the grace time available before critical core and vessel wall temperatures are reached, or risk of lead freezing is attained in the primary system are investigated.

For ALFRED a total of 8 transients were selected as representative of all identified DEC transients reflecting a wide range of potential transient initiators. These transients include several unprotected transients such as the ones connected with the loss of flow in the primary system and/or the loss of heat removal by the secondary system, and the overpower transient following reactivity insertion. The overcooling transients are investigated in connection with the loss of flow in the primary circuit, which are then most penalizing as related to the risk of lead freezing at the SG outlet. Furthermore, the consequences of the unlike event of the concomitant break of both SG tube walls (Steam Generator Tube Rupture - SGTR) related to: 1) potential mechanical loads on the primary system structures due to water-Pb interaction and 2) core voiding effect due to eventual steam bubble transport through the core are investigated.

Different system codes adapted to deal with Pb coolant have been used for the DEC transient analysis by the partners involved in the WP5 activities of the LEADER project. These include (see Appendix A):

- the RELAP5/MOD3.3 system code (modified by ENEA/Ansaldo/Uni-Pisa and used by ENEA, KTH and CIRTEN),

- the SIM-LFR system code (developed by KIT),
- the TRACE/FRED system code (coupled and adapted by PSI),
- the TRACE system code (adapted by JRC-IET),
- the SIMMER-III code (used by CIRTEN and JRC-IET),
- the CATHARE V2.5_2 system code (developed by CEA),
- the SPECTRA system code (developed by NRG),

This report is organized as follows:

Section 2 first provide a table of the DEC (unprotected and protected) transients that were selected for the safety analysis described in this report. Section 3 provides a short overview of the ALFRED design and main parameters that play an important role during postulated DEC transients (detailed information is provided in DEL015 along with the results of steady-state operation at full power). Section 4 presents the results of the code benchmark on several representative unprotected transients (UTOP, ULOF and ULOHS), performed with the aim to verify the consistency of code results. Section 5 present the results of the analyses for each DEC transient as obtained by the various partners employing their codes. As indicated in section 5, not all the transients have been analyzed by all the partners, but at least three partners have analyzed the same transient, thus providing the possibility to compare and better judge the consistency of code results. The conclusions obtained during this study are described in Section 6.

This report responds to the Deliverable D022 and is a joint report to which all Task 5.5 partners have contributed. Thus, the report consists of a compilation of information, made available by different colleagues from various organizations, extracted from the following reports, which are also being published in their full length as appendixes to the LEADER Deliverable DEL022. Direct use of the appropriate parts of these reports has been made for the main part of the Deliverable DEL022.

2. ANALYSED TRANSIENTS AND COMPUTER CODES USED

The representative accident initiators for both Design Basis Conditions (DBC) and Design Extension Conditions (DEC) have been defined in Deliverable DEL011-2012. On the basis of the design solution adopted for the ETDR (ALFRED), a simplified line-of-defense strategy was applied for identification of accident initiators. Furthermore, the identified event initiators were categorized and the most representative for each category were selected for safety analysis to be carried out in tasks 5.4 and 5.5 of the LEADER project.

2.1 DEC transients

The list of DEC transients analyzed by various research organizations using different system codes is reported in Table 2-1. These events of very low frequency are characterized either by the failure of reactor scram (so-called unprotected accidents) involving:

- TR-4: Unprotected reactivity insertion transient (UTOP),
- T-DEC1: Unprotected loss of flow transient (ULOF),
- T-DEC3: Unprotected loss of heat sink transient (ULOHS),
- T-DEC4 (LOOP): Unprotected loss of offsite power transient (ULOF+ULOHS),
- T-DEC5: Unprotected partial SA blockage,

or by the simultaneous occurrence of multiple failures in some protected transients:

- T-DEC6: Loss of all secondary circuits with total unavailability of DHR system,
- TO-3: Loss of all primary pumps with reduction of feedwater temperature,
- TO-6: Loss of all primary pumps with increase of feedwater flowrate by 20%.

The unprotected transients (TR-4, T-DEC1, T-DEC3, T-DEC4 and T-DEC5) are mainly investigated to obtain insights on the intrinsic safety behavior of ALFRED and thus verifying the adequacy of the solutions adopted for the core and the plant design.

The analysis of the extremely unlikely T-DEC6 event characterized by the failure of all secondary circuits with total unavailability of any DHR system, leading to a progressive increase of the primary temperatures, is investigate to determine the grace time left to the operator before reaching limiting temperatures for the core and the vessel structures.

The protected transients TO-3 and TO-6 are mainly investigated to assess an important aspect for LFR systems related to the risk of lead freezing in the primary cooling circuit. This specifically concerns situations after reactor shutdown and activation of the DHR system, since, in the medium term, heat removed by the DHR system (which is almost constant in time) is expected to exceed the decreasing decay heat. In this case the lead freezing might become an issue and then the grace time left to the operator to undertake appropriate corrective actions must be evaluated.

In addition to the transient list in Table 2-1, the steam generator tube rupture (SGTR) event has been analyzed within DEC, despite of the very low frequency expected for this event through the adoption of double-wall steam generator tubes, along with the possibility to detect single tube wall break by the continuous monitoring the gas pressure inside the gap. The SGTR transient has been analyzed by CIRTEN using the SIMMER-III code postulating the concomitant break of both walls.

Table 2-1: DEC transients analyzed for the Pb-cooled ETDR (ALFRED)

Transients to be analyzed for Pb-cooled ALFRED Design (LEADER project)												
Case Number	Transient	Description	Burnup State									
Transients analyzed for Pb-cooled **ALFRED** Design			BOC (***)	EOC	ENEA	KIT-G	NRG	JRC-IET	KTH	PSI	ENEA / CEA	CIRTEN
					RELAP5	SIM-LFR	SPECTRA	SIMMER / TRACE	RELAP5 / CFD	TRACE/ FRED	CATHARE	RELAP5 / SIMMER (*)
DEC Transients												
TR-4	**Reactivity insertion (enveloping SGTR, flow blockage, core compaction)**	Reactivity insertion (voiding of part of active region enveloping voids introduction due SGTR, core compaction, fuel blockage) = 250 pcm Reactor at hot full power (HFP)	X	X	X	X	X	X	X (**)	X	X	
TO-3	**Reduction of FW temperature + all pumps stop**	Loss of one preheater (feedwater temperature reduction from 335oC down to 300oC) All primary pumps are stopped Reactor is tripped	X	X	X	X	X					
TO-6	**Increase of FW flowrate+ all pumps stop**	20 % increase in feedwater flowrate All primary pumps are stopped Reactor is tripped	X	X	X	X	X					
T-DEC1	**Complete loss of forced flow + Reactor trip fails (total ULOF)**	All primary pumps are stopped Feedwater system available Reactor trip fails	X	X	X	X	X	X	X	X	X	X
T-DEC3	**Loss of SCS+ Reactor trip fails (ULOHS)**	All primary pumps are operating DHR system is operating Reactor trip fails	X	X	X	X	X			X	X	
T-DEC4	**Loss of off-site power (LOOP) + Reactor trip fails (ULOHS + ULOF)**	All primary pumps are stopped SCS is lost DHR system is operating Reactor trip fails	X	X	X	X	X		X		X	
T-DEC5	**Partial blockage in the hottest fuel assembly**	Reactor trip fails The maximum acceptable flow reduction factor has to be determined	X	X	X	X	X	X		X		
T-DEC6	**SCS failure**	All primary pumps are operating DHR system totally fails Reactor is tripped	X	X	X	X	X					
Note (*)	**SIMMER-III code has been used by CIRTEN for the analysis of SGTR transient (DEC event not included in this list)**											
Note (**)	**KTH plans to look at core voiding due to leak from steam generator by CDF analysis** (simulation of bubble transport to the core in Lagrangian framework by turbulent coolant voiding taking into account uncertainties in: bubble size distribution, different correlations for bubble drag in lead, locations of possible leakage from SG, leak rate, etc.)											
Note (***)	**Only KIT-G with SIM-LFR code for all DEC transients and JRC-IET for T-DEC5 transient**											

In general, all DEC transients have been analyzed starting with the reactor in steady-state conditions at full power (300 MWth) from the end of cycle (EOC) condition, which seems more conservative with respect to the beginning of cycle (BOC) condition, from the safety point of view. Only KIT with SIM-LFR code has investigated all DEC transients starting from both BOC and EOC conditions. Their analyses confirm that the general situation at BOC condition does not differ significantly from EOC condition, and thus similar conclusions apply in both cases.

2.2 Computer codes

For the DEC transient analysis different computers codes are used by various organizations. In general, already validated computer codes developed for safety analysis of nuclear power reactor using different coolants have been modified by introducing a consistent set of physical and thermodynamic properties and empirical correlations for Pb in the modules devoted to evaluating heat and mass transport phenomena.

The validation phase of these codes for LFR reactor applications is in progress on the basis of the available experimental database.

The issues associated with each of the different system codes used are discussed in more detail in Appendix A.

3. ETDR (ALFRED) DESIGN

The ETDR (ALFRED) configuration is illustrated in Fig. 3-1 [1].

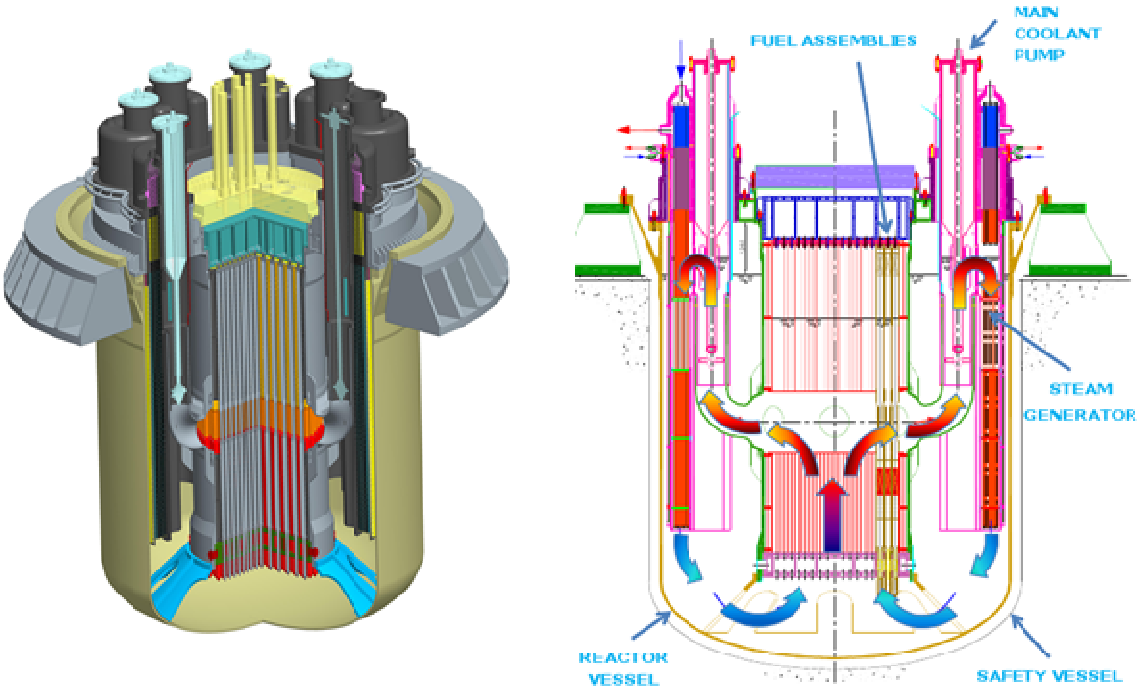


Fig. 3-1: ALFRED configuration (3D view on the left and 2D vertical section on the right)

Main features of the ALFRED design are:

- Pool type configuration characterized by a reactor vessel and the cavity liner safety vessel,
- Hexagonal wrapped fuel assemblies extended to cover gas to simplify fuel handling (FAs weighted down by tungsten ballast for refueling and kept in position by upper grid springs during operation),
- Mechanical pumps located in the hot collector,
- Double-walled straight SG tubes with continuous monitoring of tube leakages.

The thermal cycle is completely consistent with the ELFR thermal cycle: primary lead temperature being between 400-480°C, secondary side pressure 180 bars, once through SGs with water/steam temperature range from 335 to 450°C in superheated conditions, the overall efficiency has been evaluated higher than 42%. ALFRED will also allow for testing the connection to the electrical grid, with a generated power of about 125 MWe.

Safety of ALFRED is extensively based on the use of the defense in depth criteria, enhanced by the use of passive safety systems (actively actuated through locally stored energy source, always available, and fully passively operated). Safety features of the LFR system have been designed since the beginning of the activities to face challenging conditions and events, thanks to the very forgiving and benign characteristics of the coolant. As an example, there is no need of off-site or emergency AC electrical power supply to manage the design basis accident

conditions; the only action needed is the addition of water to maintain the level in the decay heat removal (DHR) pools which are already sized to guarantee at least three days of unassisted fully passive operation and can be easily re-filled in the following days.

The reference design configuration for the plant safety analysis, presented in details in Ref. [2], is summarized in the following sub-sections. Besides, in the DEL015-2013 devoted to DBC transient analysis, the results of the steady-state calculations for ALFRED at nominal power with different codes are also reported, along with a code benchmark.

3.1 Primary system

Fig. 3.1-1 and Fig. 3.1-2 present the general layout of the primary system. The main ETDR (ALFRED) parameters are listed in Table 3.1-1 [11].

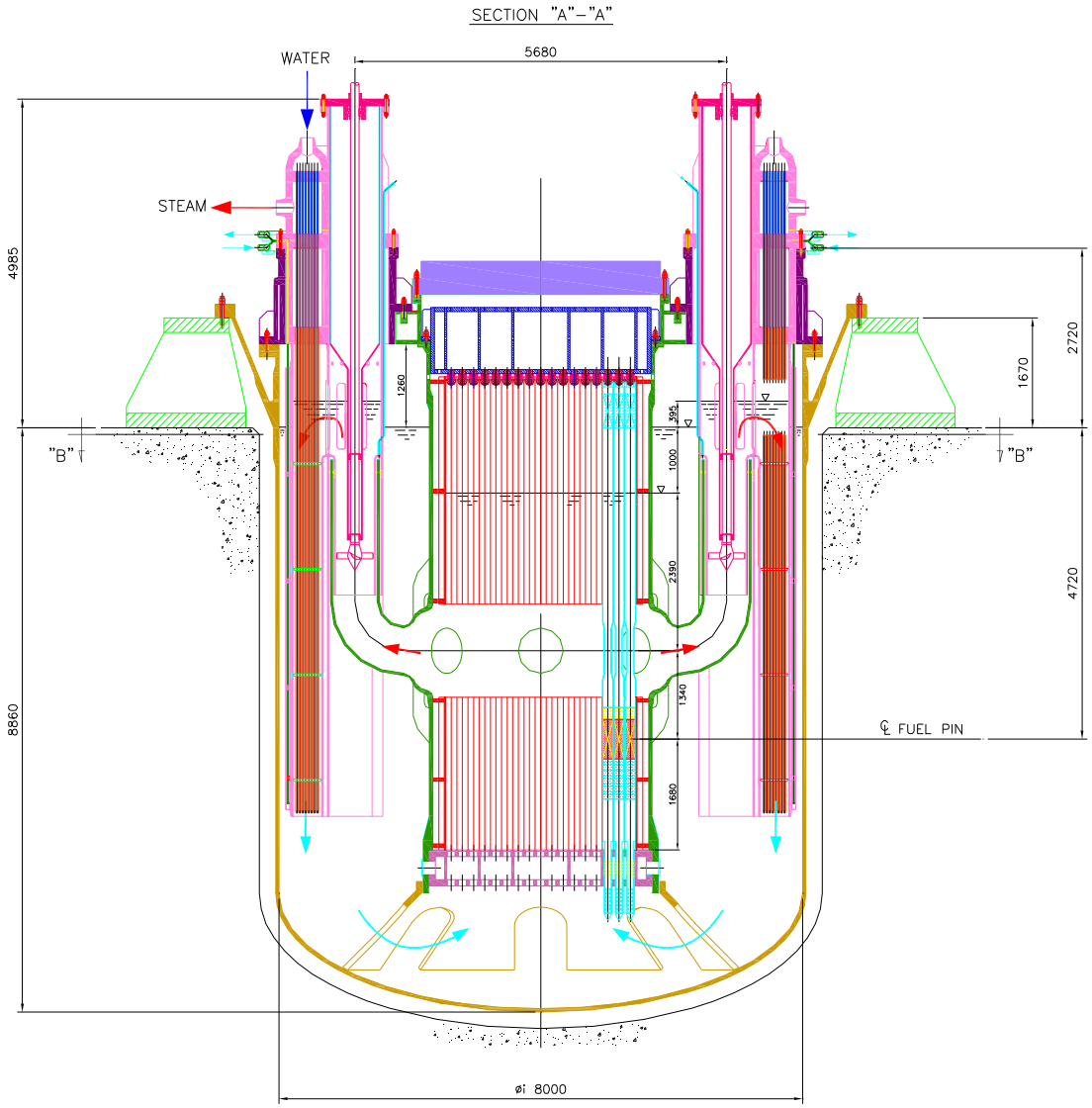


Fig. 3.1-1: Reactor block configuration – vertical view [4]

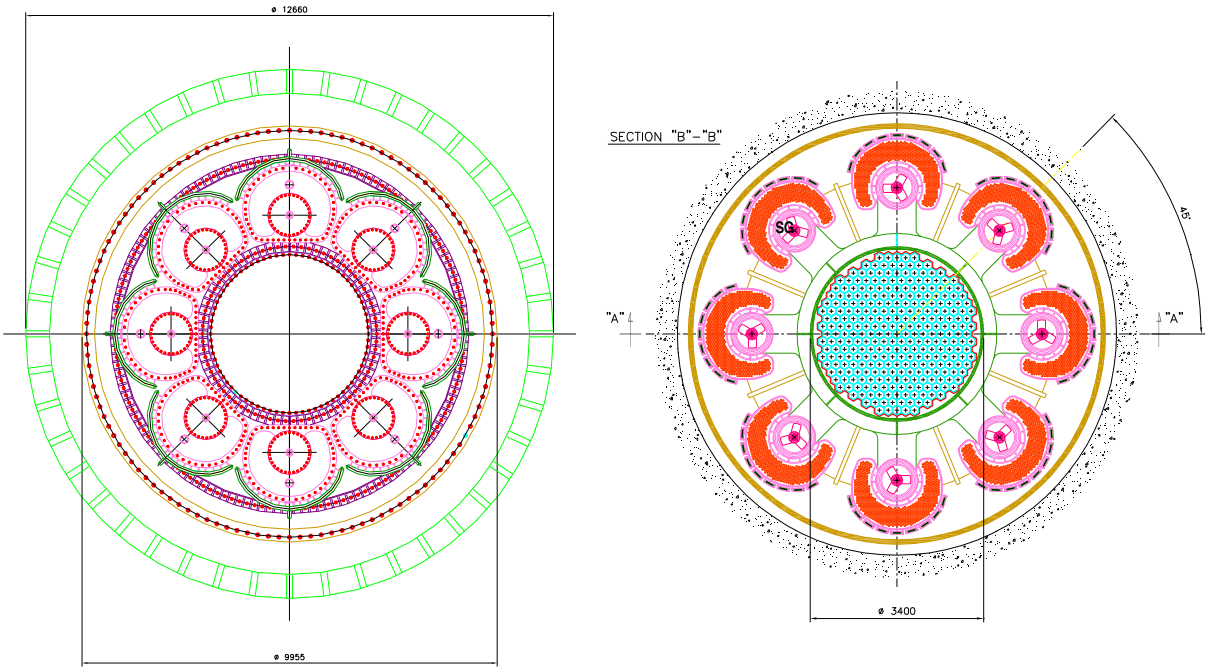


Fig. 3.1-2: Reactor block configuration – top view [4]

Table 3.1-1: ETDR (ALFRED) main parameters [11]

ALFRED Main Parameters	
Power	300 MWth
Thermal efficiency	> 40%
Primary system	Pool, compact
Primary circulation	8 mechanical pumps
Primary pressure loss	1.5 bar
Primary thermal cycle	400 – 480 °C
Fuel	MOX
Fuel cladding	15-15/Ti + coating
Fuel clad max temperature	550 °C
Main & safety vessel	Austenitic SS
Steam generators	8 - integrated
Secondary cycle	180 bar, 335 – 450 °C
Internals	Removable
Seismic design	2D isolators

Reactor inner vessel

ALFRED inner vessel (Fig. 3.1-3) is made of 3 sub-assemblies as schematized in Fig. 3.1-4:

- The cylindrical vessel [6],
- The core lower grid [7],
- The core upper grid [8].

The inner vessel (see Fig. 3.1-3) is a double wall shell: the outer thick wall has a structural function, while the inner thin wall follows the core section profile. Lead flow is guided from the FAs outlet towards the primary pump (PP) inlet pipes by a toroidal half-ring The inner vessel is fixed to the cover by bolts and is radially restrained at the bottom.

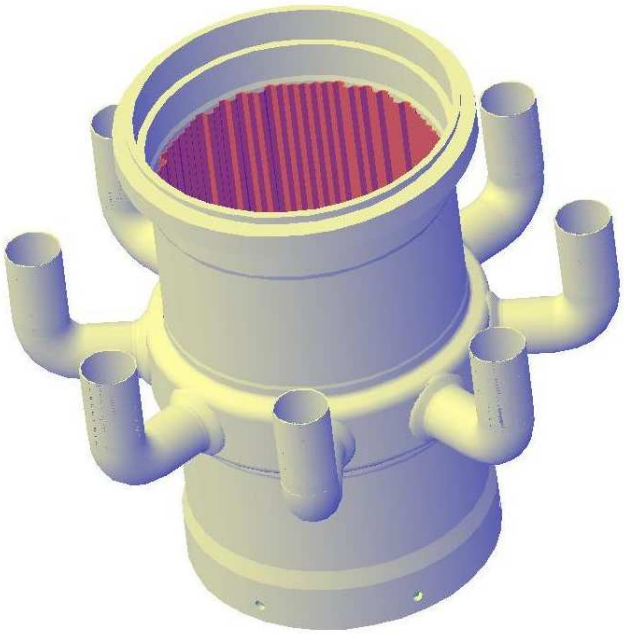


Fig. 3.1-3: 3D view of the cylindrical inner vessel [3]

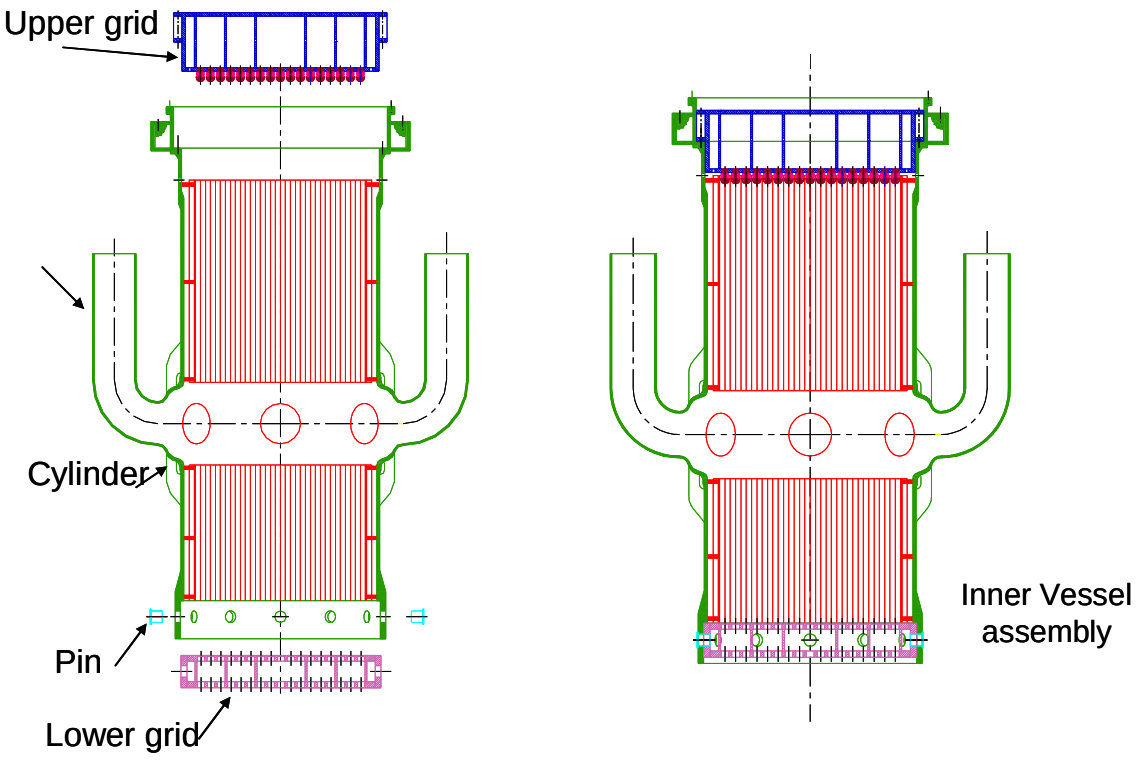


Fig. 3.1-4: ALFRED inner vessel assembly schematics [3]

Core lower grid has a box structure with two horizontal perforated plates connected by vertical plates. Plates holes are the housing of FAs foots. The plates distance must be sufficient to assure the verticality of FAs. Core upper grid has a box structure similar to the core lower grid but more stiff. It has the function to push down the FAs during the reactor operation. A series of preloaded disk springs presses each FA on its lower housing.

Reactor outer vessel

The reactor outer vessel [9] is a cylindrical vessel with a torospherical bottom head. It is anchored to the reactor pit from the top. Reactor outer vessel is closed by a roof that supports the core and all the primary components. Its upper part is divided in two branches by a "Y" junction: the conical skirt that supports the whole weight and the cylindrical that supports the Reactor Cover. A cone frustum welded to the bottom head has the function of bottom radial restraint of the Inner Vessel.

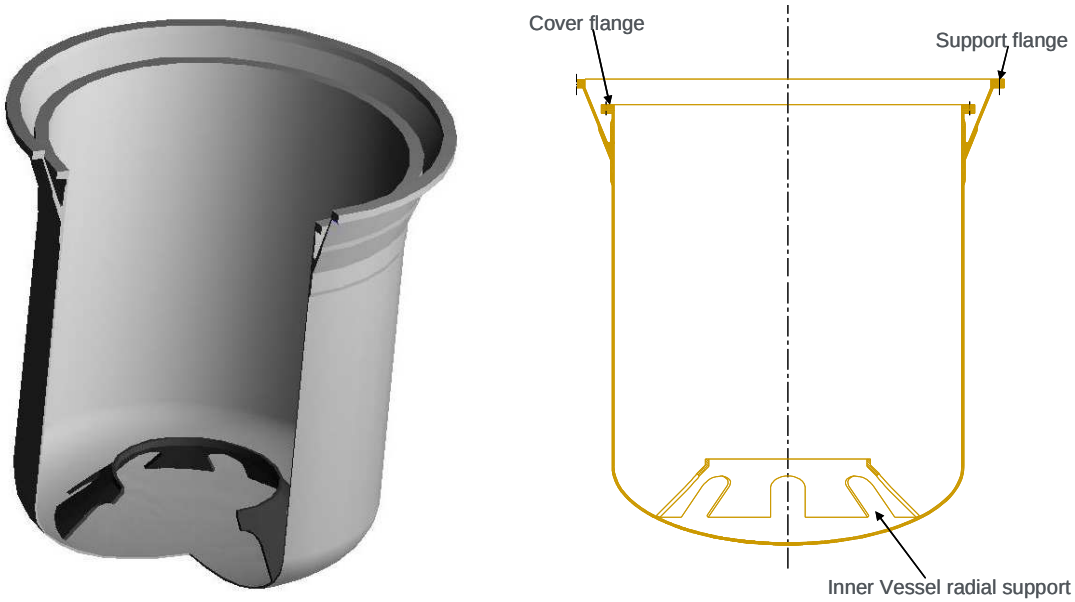


Fig. 3.1-5: ALFRED reactor outer vessel schematics [9]

3.2 Steam generator

Steam Generators (SG) [10] (called also MHX in this transient analysis) are distributed around the Inner Vessel. It is a bayonet tubes Steam Generator made by 4 tubes bayonets with an intermediate medium between lead and water/steam. This solution mitigates the SGTR effects: the intermediate medium allows an instantaneous identifying of a tube rupture event. An independent cooling loop made by a series of U-tubes avoids the heating of Reactor Vessel removing the heat dispersions from the hot zone. The main SG operation parameters are listed in Table 3.2-1.

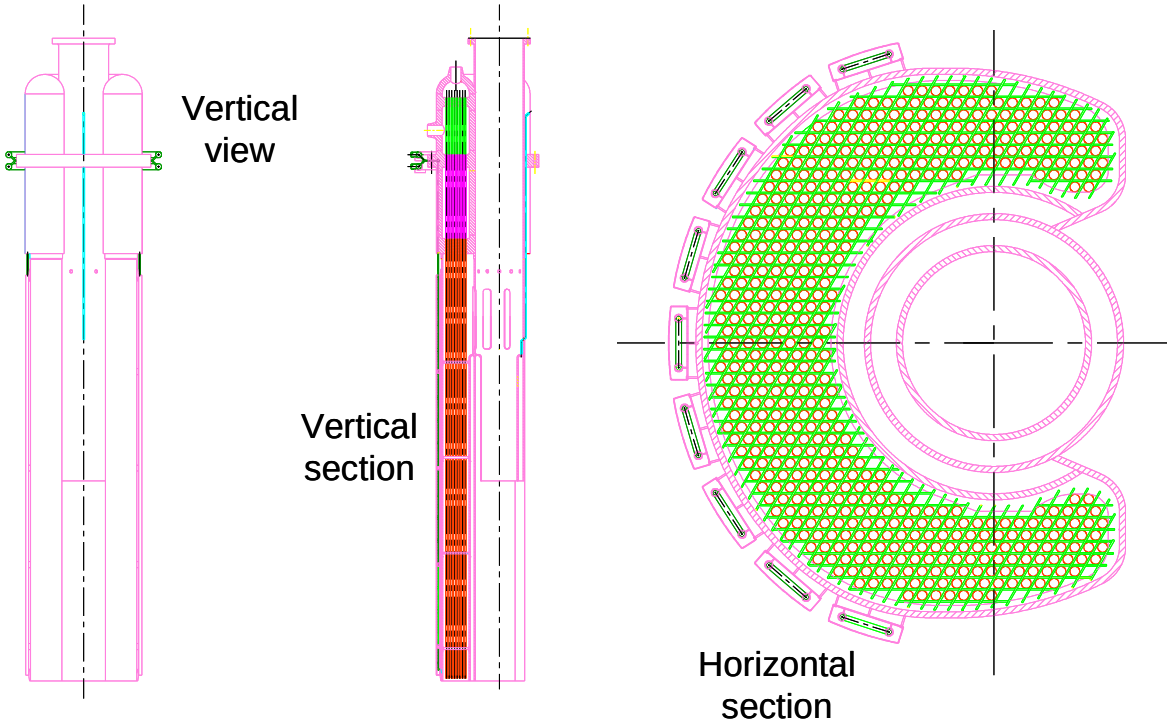


Fig. 3.2-1: ALFRED steam generator schematics [10]

Table 3.2-1: Main SG operation parameters [12]

Main SG Parameters	
Nominal reactor core power	300 MWth
Number of steam generators	8
Number of primary pumps	8
Power removed by 1 SG	37.5 MWth
Lead (Primary system)	
SG outlet T (Core inlet T)	400 °C
SG inlet T (Core outlet T)	480 °C
Mass flow rate (1 SG)	3247.5 kg/s
Water/Steam (Secondary system)	
Pressure	180 bar
Water inlet T	335 °C
Steam outlet T	450 °C
Mass flow rate	24.1 kg/s

The height difference between the core mid-plane and SG mid-plane is about 1.87 m (see Fig. 3.2-2). The main SG design data are given in Table 3.2-2, while the main SG tube geometric data and design are schematized in Fig. 3.2-3 [12].

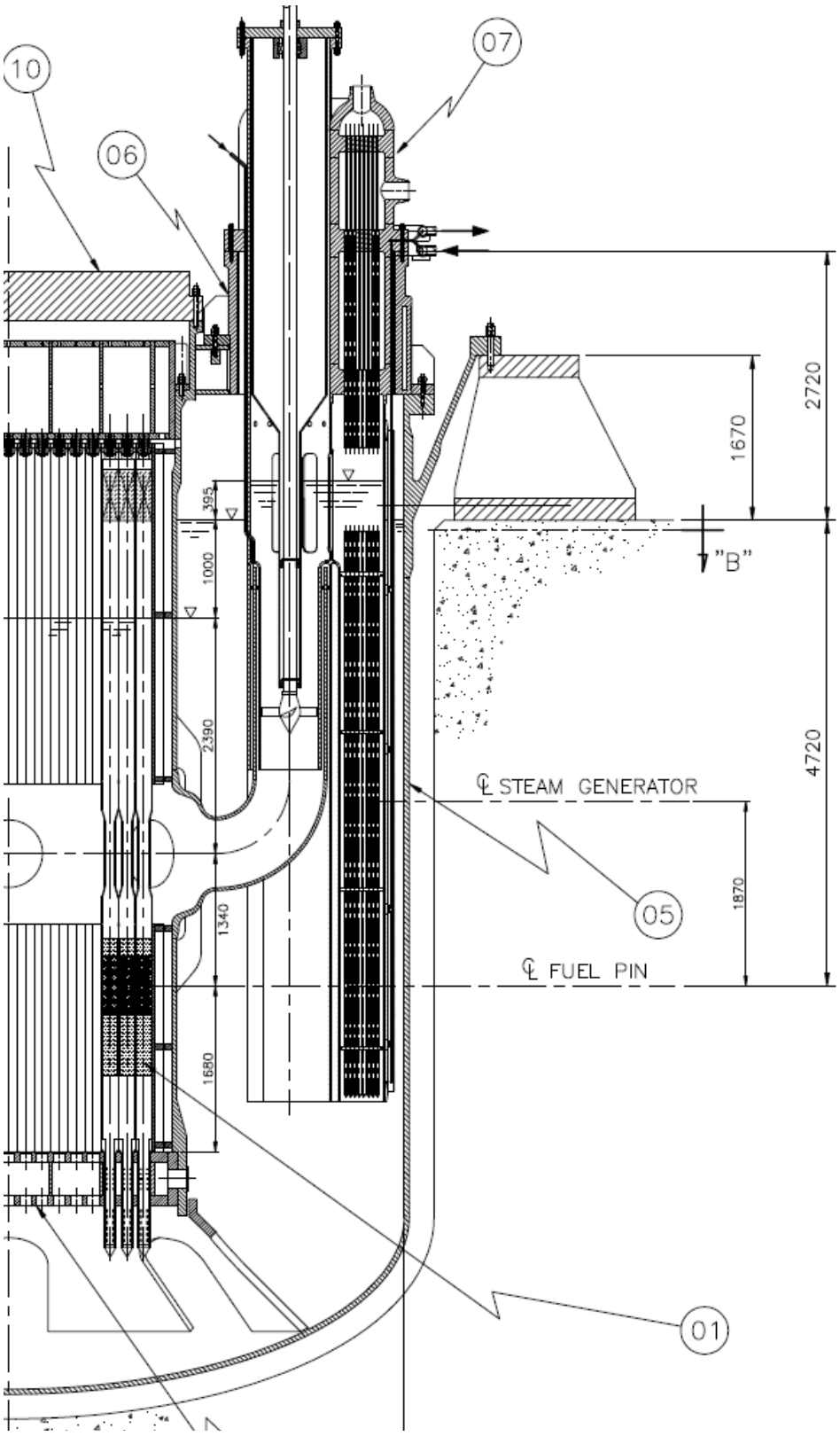
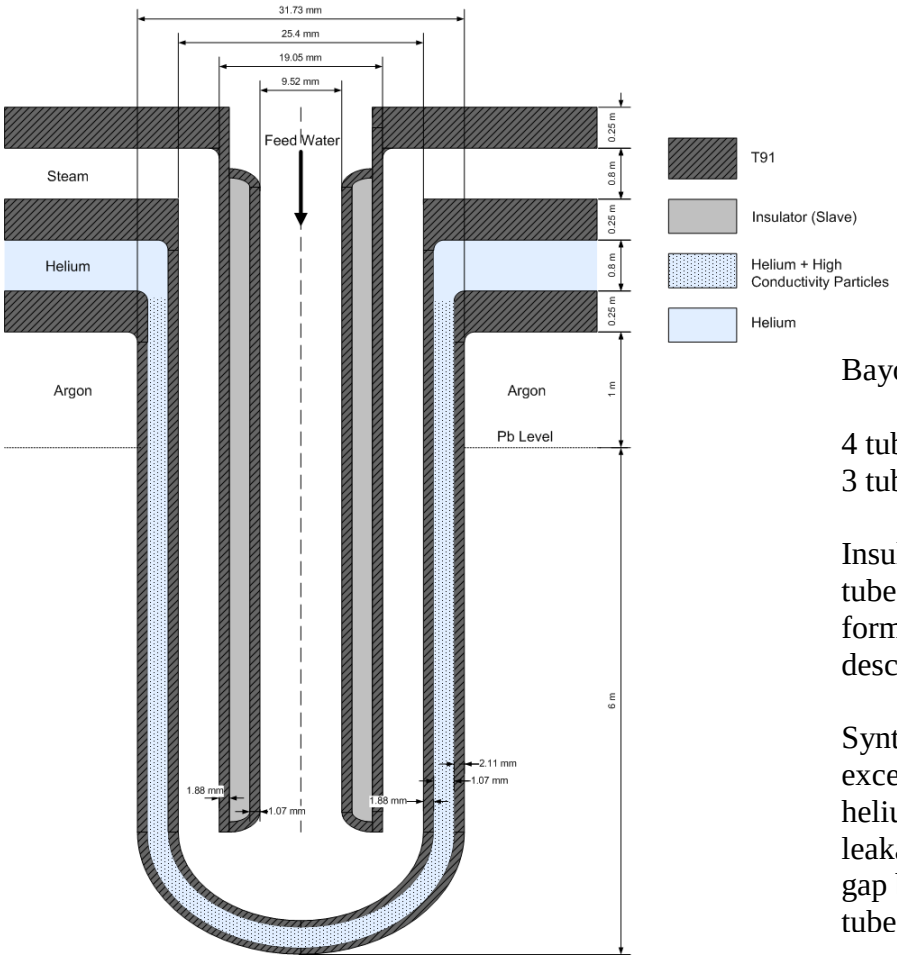


Fig. 3.2-2: Height difference between the core mid-plane and SG mid-plane

Table 3.2-2: Main SG design data [12]

Steam Generator Geometry	Bayonet tube
Number of coaxial tubes	4
Slave tube O.D	9.52 mm
Slave tube thickness	1.07 mm
Inner tube O.D	19.05 mm
Inner tube thickness	1.88 mm
Outer tube O.D	25.4 mm
Outer tube thickness	1.88 mm
Outermost tube (Gap) O.D	31.73 mm
Outermost tube thickness	2.11 mm
Length of exchange	6 m
Argon Plenum Height	1 m
Helium Plenum Height	0.8 m
Steam Plenum Height	0.8 m



Bayonet tube specifics [12]:

4 tubes
3 tube sheets

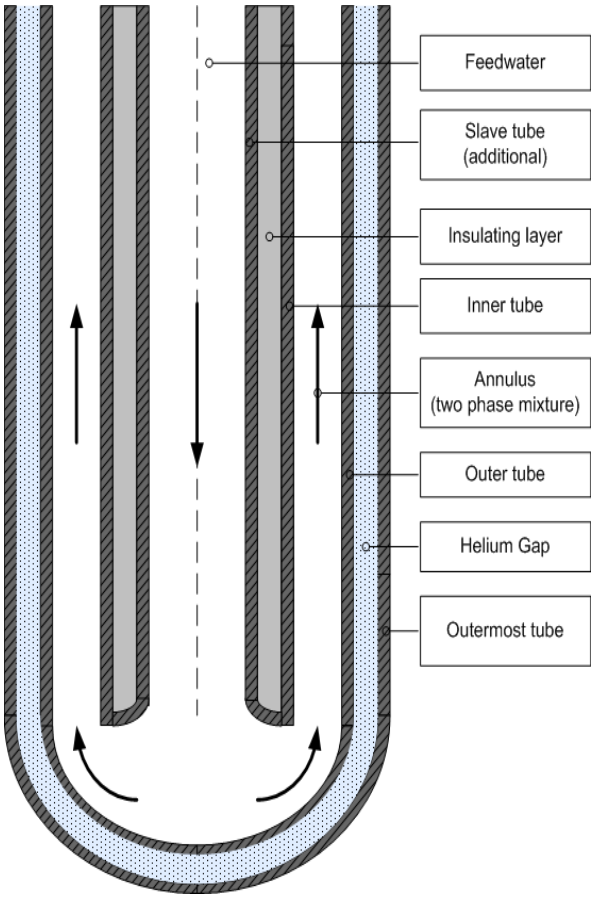
Insulation between the inner tubes used to avoid steam formation during the water descent down the inner tube.

Synthetic diamonds (for excellent heat transfer) and helium (for continuous water leakage monitoring) filling the gap between the two outer tubes.

Fig. 3.2-3: Main SG bayonet tube geometric data and design [11]

Steam Generator Bayonet Tube Concept

- Bayonet vertical tube with external safety tube and internal insulating layer
- The internal insulating layer (delimited by the Slave tube) has been introduced to ensure the production of superheated dry steam. Without an insulating system the high ΔT (≈115°C) between the rising steam and the descending feedwater promotes steam condensation in the upper part of the steam generator.
  Sensitivity on materials and extension of this layer has been performed and the results will be discussed later.
- The gap between the outermost and the outer bayonet tube is filled with pressurized helium and high thermal conductivities particles to enhance the heat exchange capability.
  In case of an external tube break this arrangement guarantees that primary lead does not interact with the secondary water. Moreover a tube break can be easily detected monitoring the Helium gap pressure.



3.3 Primary pump

The Primary Pump (PP) is located in the hot side of a SG. It is surrounded by the SG tube bundle and its housing is the SG casing. The Pump is fixed to the top of SG casing by a bolted joint. This allows an easy removal of the component.

The Primary Pump studies are in progress. Based on analyses performed during previous LFR projects (EUROTRANS, ELSY) an axial pump has been adopted.

The PP impeller material is an issue. The stainless steel (SS) cannot be used because the high speed achieved at the top of the impeller blades induces a very fast material corrosion. Maxthal ceramic material has been proposed. Test campaigns must be performed still to select the proper PP impeller material.

The primary pump outline, the SG and PP schematics, as well as the Inner Vessel, PP and SG coupling schematic are illustrated in Fig. 3.3-1 [3].

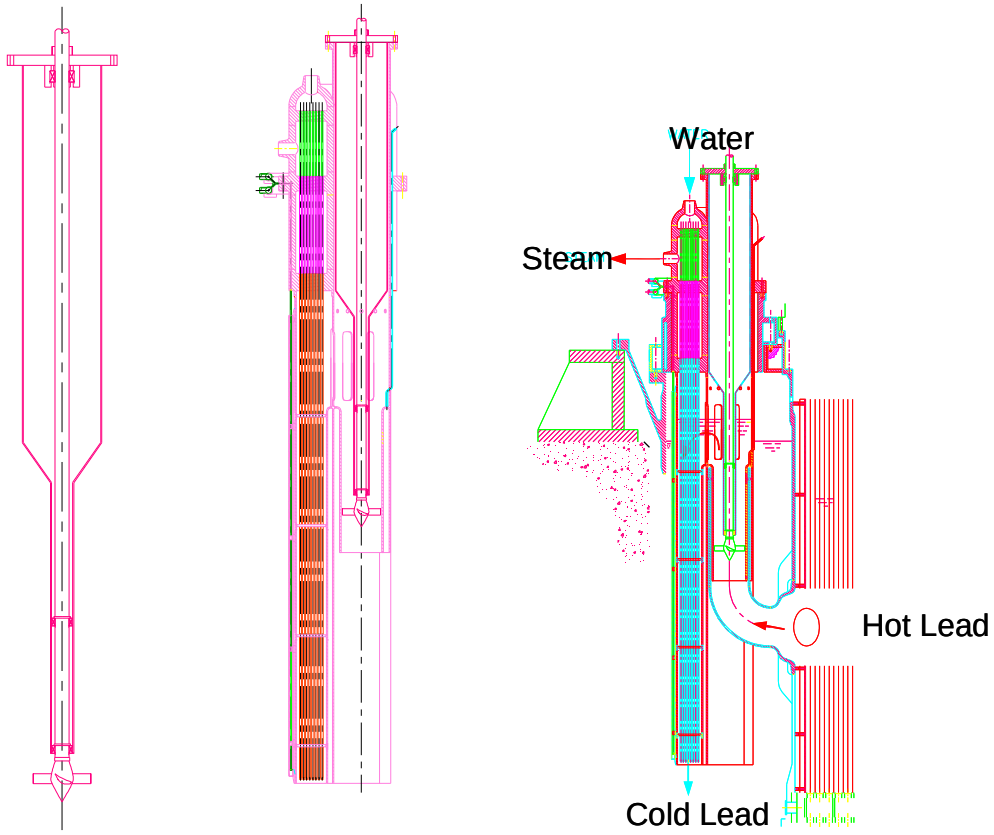


Fig. 3.3-1: a) Primary pump outline; b) SG and PP coupling schematics;
c) Inner Vessel, Primary Pump and Steam Generator coupling schematics [3]

3.5 Reactor core

In the framework of the LEADER project [13], the ALFRED core is devoted to the demonstration of a fast reactor cooled by lead.

The considered fuel is MOX (conventional MOX): the Pu vector is estimation from the reprocessing of PWR spent UO_2 fuel burnt up to 45 GWd t^{-1}; with a 4.5% initial enrichment in ^{235}U and 15 years of cooling period. The assumed ratio of $^{241}Am/Pu$ is 1.3%. The specifications for the assumed isotopic composition and densities for the MOX fuel, the Pb coolant, the structural materials and the B_4C can be found in [14].

The core parameters are reported in Table 3.4-1 and Table 3.4-2 below.

Table 3.4-1: ALFRED core parameters

Parameter	Unit	Value
Pellet radius	mm	4.5
Gap thickness	mm	0.15
Clad thickness	mm	0.6
Pin diameter	mm	10.5
Wrapper thickness	mm	4.0
Distance between 2 wrappers	mm	5.0
Lattice pitch (hexagonal)	mm	13.86
Pins per FA	-	127
Inner vessel radius	cm	165
Inner / Outer FAs number	-	57 / 114
Inner / Outer enrichment (Pu+^{241}Am) / (Pu+^{241}Am+U)	atom%	21.7% / 27.8%
Mass inventory of actinides: BOC - U / Pu / Minor Actinides EOC - U / Pu / Minor Actinides	tons	 5.27 / 1.78 / 0.038 5.19 / 1.74 / 0.043
Fuel residence time	month	60
Number of batches	-	5
Cycle length	month	12
Δk_{eff} swing	pcm	≈ -2600
BoC/EoC k_{eff} (with CR extracted)	-	1.025 / 0.999
Assumed grace time for cladding failure (in ULOF conditions)	minutes	30

Table 3.4-2: Fuel pin geometric parameters [5, 15]

Description	Length
Bottom plug [mm]	50
Gas plenum [mm]	550
Bottom insulator ZrO_2-Y_2O_3 [mm]	10
Active length [mm]	600
Upper insulator ZrO_2-Y_2O_3 [mm]	10
Spring [mm]	120
Upper plug [mm]	50

Fig. 3.4-1 presents the proposed ALFRED core configuration made of 171 Fuel Assemblies, 12 Control Rods and 4 Safety Rods, surrounded by 108 Dummy Elements (ZrO_2-Y_2O_3) shielding the Inner Vessel.

The Fuel Assembly and Fuel Pin drawing are reported in Ref. [5]. Fig. 3.4-2 to Fig. 3.4-4 present the fuel sub-assembly design, while Fig. 3.4-5 presents the fuel pin design for this ALFRED core configuration.

The preliminary (until final design calculations will become available) foreseen core pressure drop is ~1.0 bar, that is approximately two-third of the total primary circuit pressure drop (~1.5 bar).

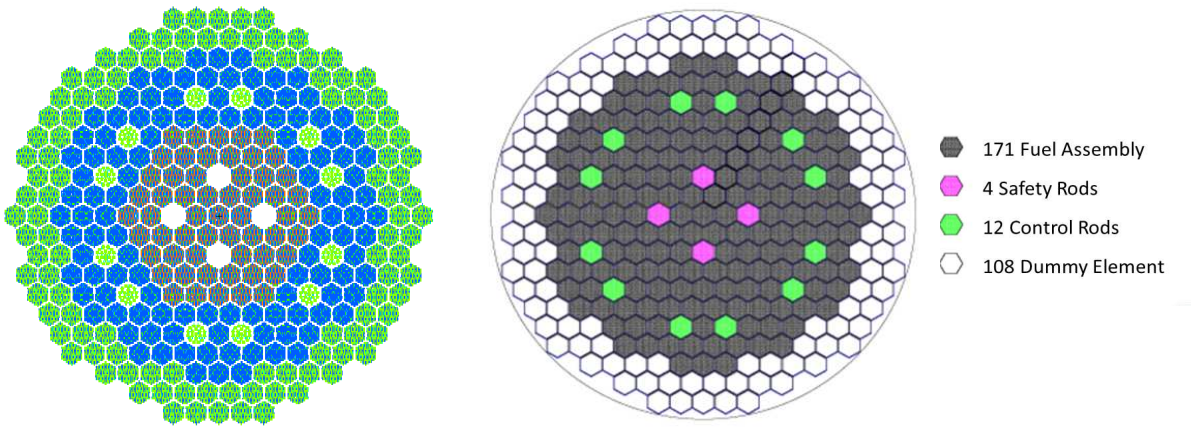


Fig. 3.4-1: ALFRED core configuration.
Inner zone (57 violet FA) and outer zone (114 blue FA) [15].

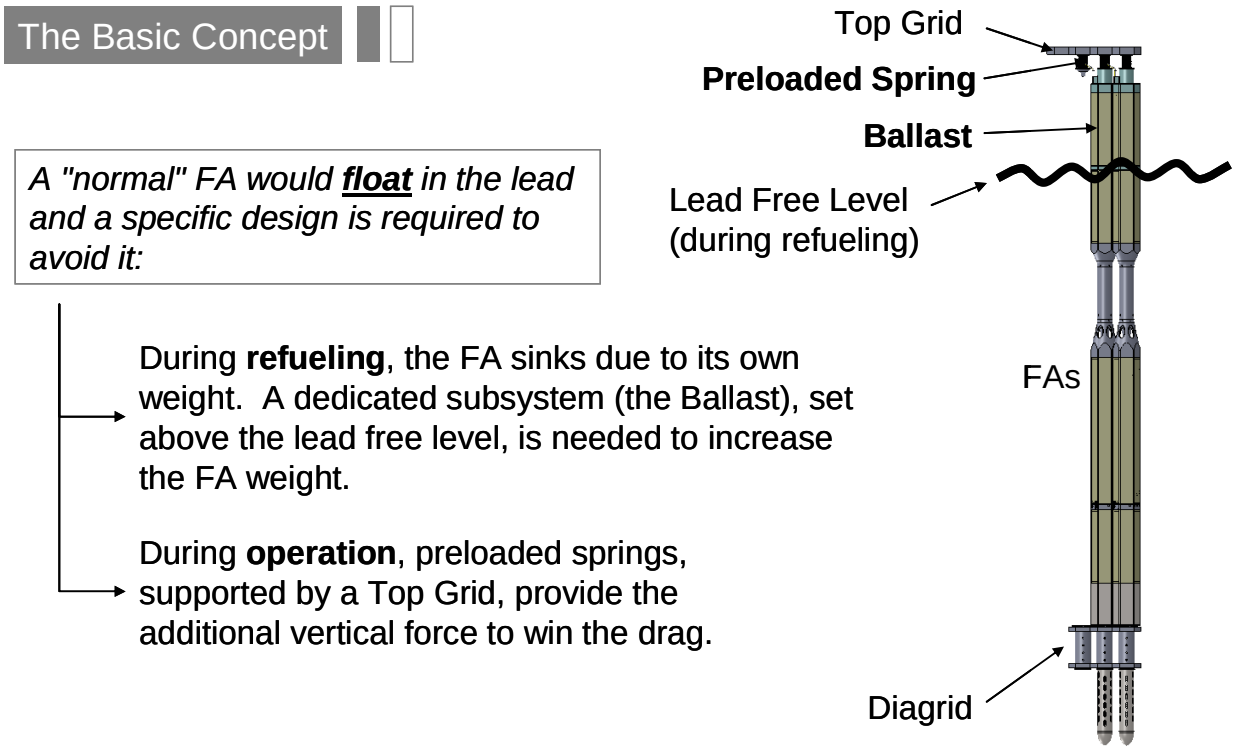


Fig. 3.4-2: ALFRED fuel sub-assembly (FA) basic concept [16]

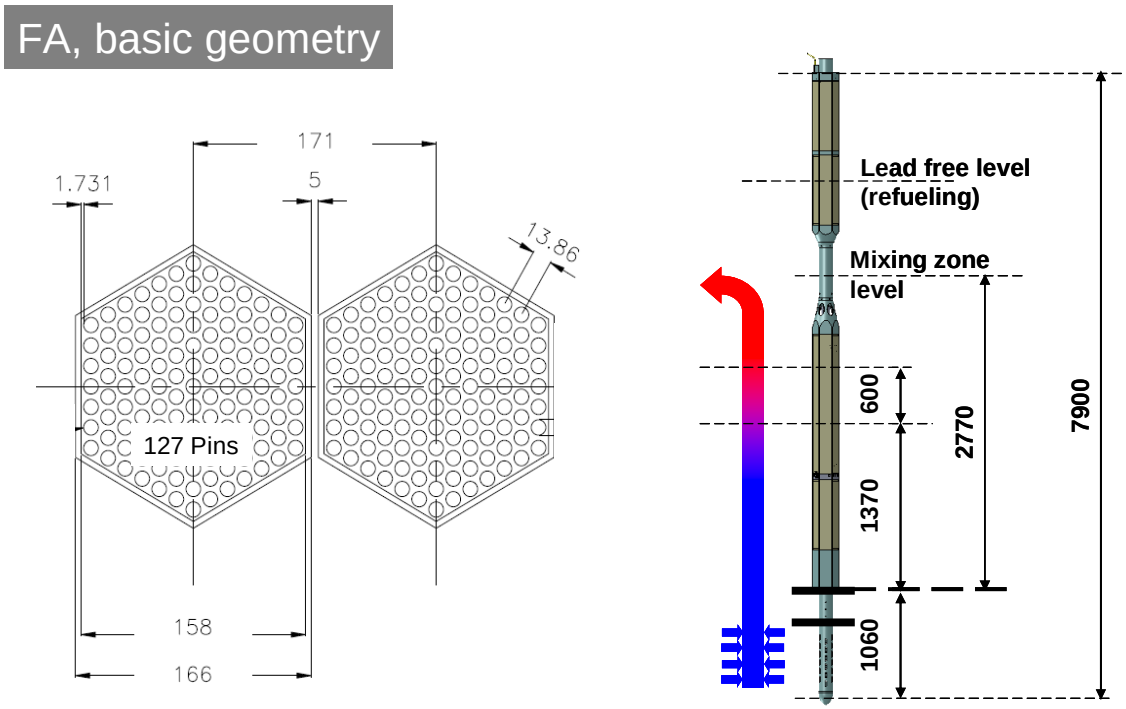


Fig. 3.4-3: Fuel sub-assembly (FA) design for ALFRED core configuration [5, 16]

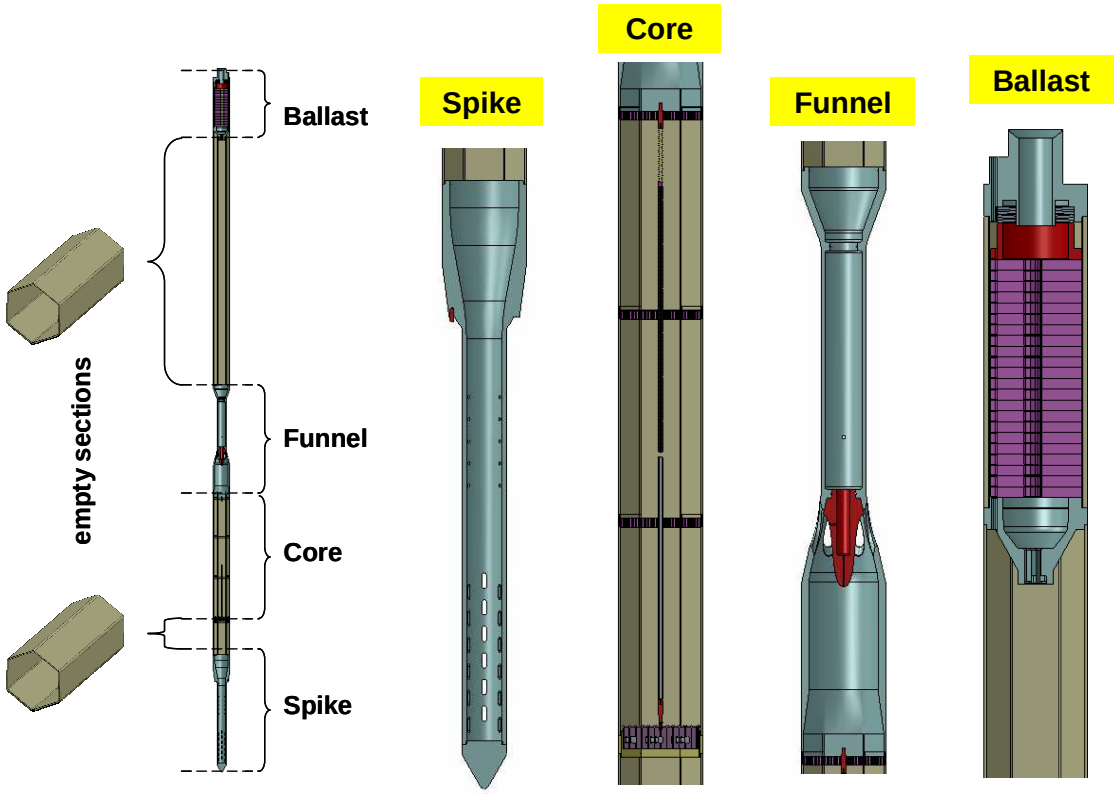


Figure 3.4-4: ALFRED fuel sub-assembly design - schematic mechanical drawings [5, 16]

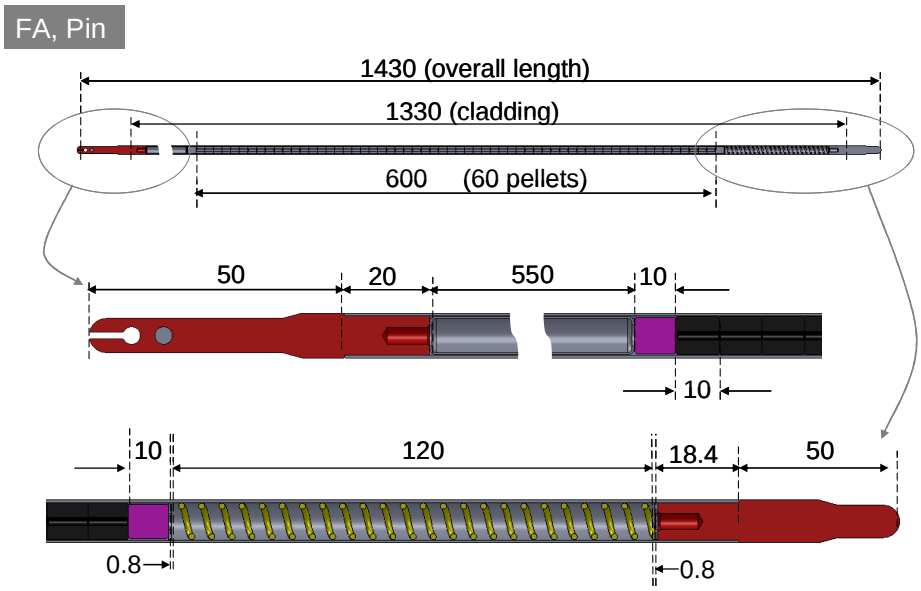


Fig. 3.4-5: ALFRED FA pin - schematic mechanical drawings [5, 16]

3.4.1 BOC and EOC core: layouts and main characteristics

The core power distribution has been calculated by both MCNPX and ERANOS [15]. Only the results obtained by MCNPX are reported here.

The power generation in the Fuel Assemblies is shown in Fig. 3.4.1-1 (1/4 of the core), calculated at BOC (CR inserted of 17 cm in the active zone) and at EOC (CR withdrawn).

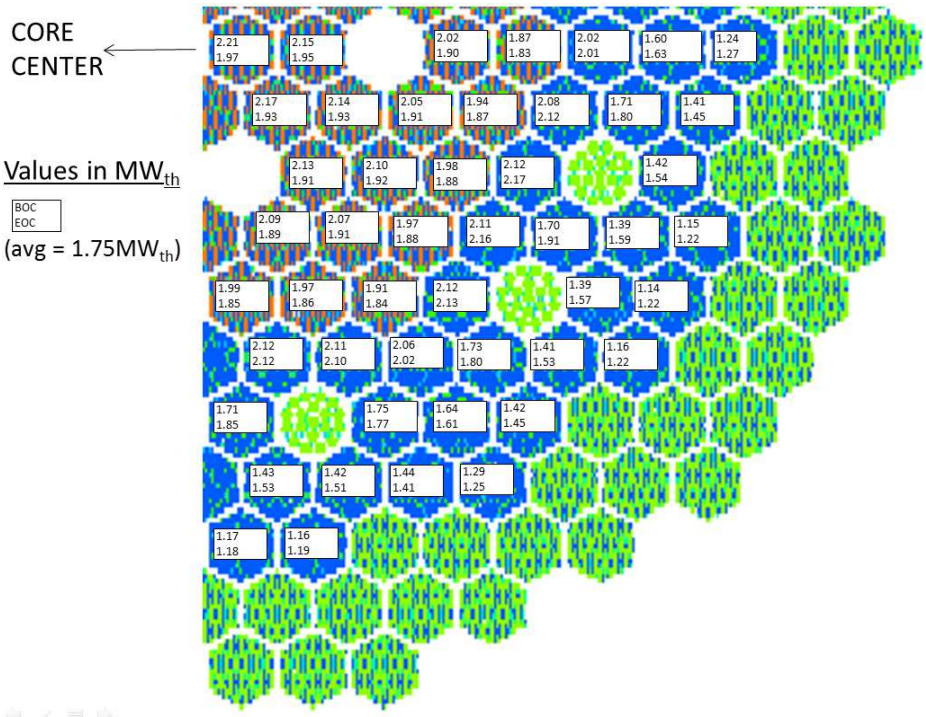


Fig. 3.4.1-1: Power generation at BOC and at EOC

The maximum value is at the center at BOC (2.21 MW_{th}) and in the outer zone at EOC (2.17 MW_{th}), but the hottest pin is not in these FAs, but in the outer zone, as depicted in Fig. 3.4.1-2. Here also the axial form factors, as calculated in some FAs, are shown.

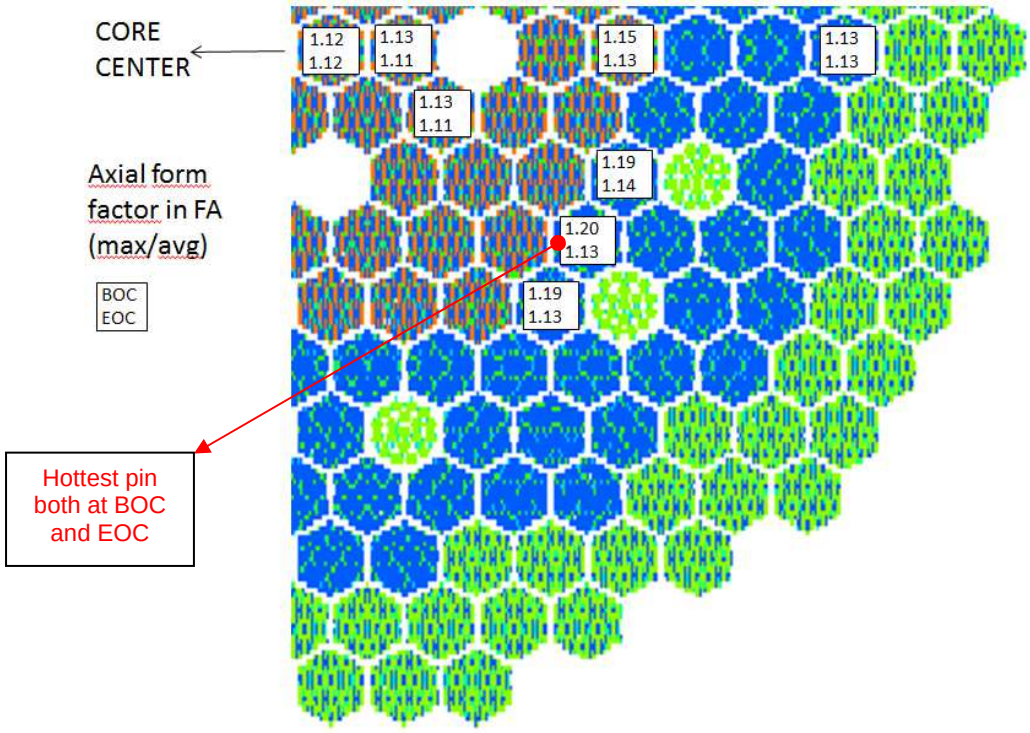


Fig. 3.4.1-2: Axial form factors in some FAs at BOC and at EOC

The power is deposited not only in the fuel, but also in the other materials, due to the gamma and neutron emission in the fission process. The power distribution at BOL (CR inserted of 17 cm; SR extracted), according to the materials and to the different zones is shown in Table 3.4.1-1 and Table 3.4.1-2.

Table 3.4.1-1: Power distribution according to different materials

Material	**%**	**MW_{th}**
MOX fuel	93.06%	279.17
Ti 15-15	0.48%	1.44
Pb	4.89%	14.66
T91	0.85%	2.55
ZrO_2-Y_2O_3	0.32%	0.96
B_4C	0.40%	1.21
Total	***100.00%***	***300***

Table 3.4.1-2: Power distribution according to different zones

Zone	**%**	**MW_{th}**
MOX fuel	93.06%	279.17
FA - outside MOX	4.91%	14.74
Dummies	0.95%	2.84
Control Rods	0.57%	1.71
Safety Rods	0.17%	0.50
Pb between dummies and vessel	0.09%	0.26
exterior	0.26%	0.79
Total	***100.00%***	***300***

A maximum linear power value of 350 W/cm can be assumed, as deduced from Table 3.4.1-3.

Table 3.4.1-3: Maximum power deposition in the hottest pin

	BOC	EOC
Power deposition on the FA (MW_{th})	2.11	2.16
Axial form factor of the FA	1.20	1.13
Pinwise form factor of the power deposition within the FA (max pin/avg pin)	1.089	
% deposition in the fuel	93.1%	
Correction for more realistic batch approximation description in MCNPX	~+4%	~+4%
Estimated max linear power (W/cm)	~350	~340

The average linear power and the axial form factors for the whole core are shown in Table 3.4.1-4.

Table 3.4.1-4: Average power deposition and axial form factors in the whole core

	Average FA
MW_{th}	1.75
% deposition in the fuel	93.1%
Estimated average linear power in the pellets (W/cm)	214
Average axial form factor of the FAs	1.16 (BOC) 1.13 (EOC)

The average neutron flux in the fuel pellets is $1.54 \cdot 10^{15}$ cm^{-2} s^{-1}.

The linear power axial distribution of the average pin in the average FA and of the hottest pin are shown in Fig. 3.4.1-3.

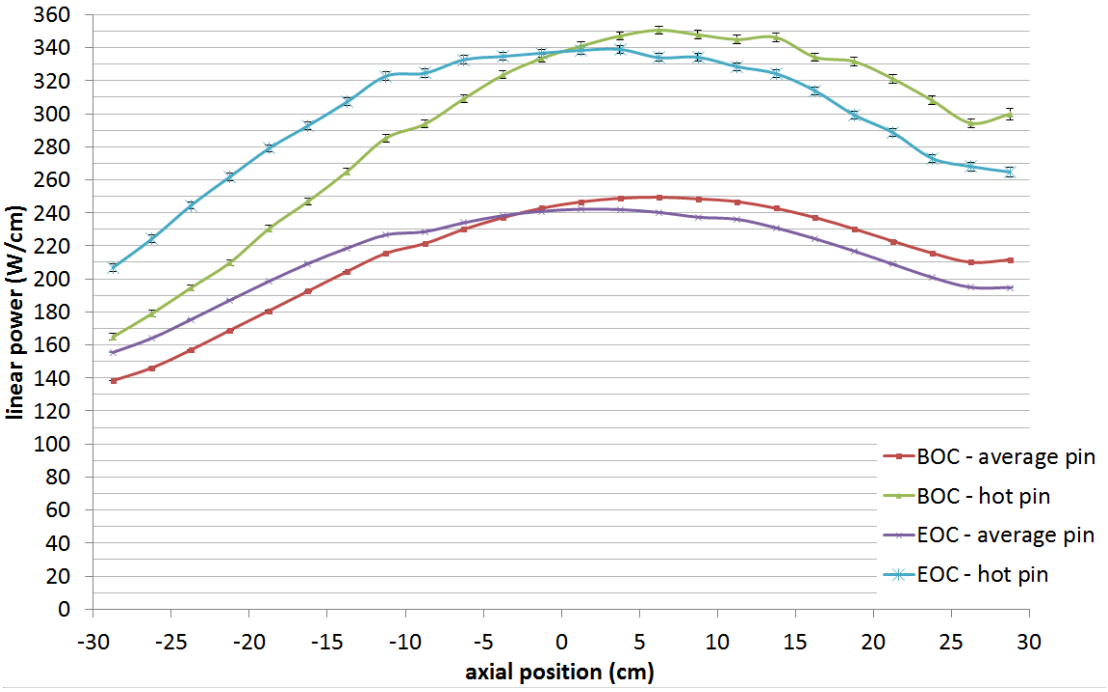


Fig. 3.4.1-3: Linear power axial distribution

3.4.2 Nuclear kinetic data and reactivity coefficients

The kinetic characteristics of the reactor core, i.e. the effective delayed neutron fraction and the effective prompt neutron lifetime, determine the response of the core to reactivity changes due to changing plant conditions or to operator adjustments made during normal operation, as well as in abnormal transients and accidents.

The effective delayed neutron fraction at the End Of Cycle (EOC) conditions was determined to be 335 pcm [15].

Corresponding to the 8 groups of the JEFF3.1 library, the description of the effective neutron fraction and precursor life time is given in Table 3.4.2-1 at EOC.

Table 3.4.2-1: Description of the kinetic constants on the 8 groups of the JEFF3.1 library [15]

Group	1	2	3	4	5	6	7	8
β (pcm)	5,9	57,9	21,8	50,5	106,5	38,5	37,4	16,1
λ (s^{-1})	0,0125	0,0283	0,0425	0,1330	0,2925	0,6665	1,6348	3,5546
Global precursor disintegration constant: λ = 0,0867 s^{-1} Life time on the whole reactor : 6,296.10^{-07} s								

The reactivity changes with the insertion of the 12 CRs is shown in Fig. 3.4.2-1 [15]. The reactivity introduced for full CRs insertion (64 cm) at BOL, such as during automatic reactor scram, is of -8476 pcm.

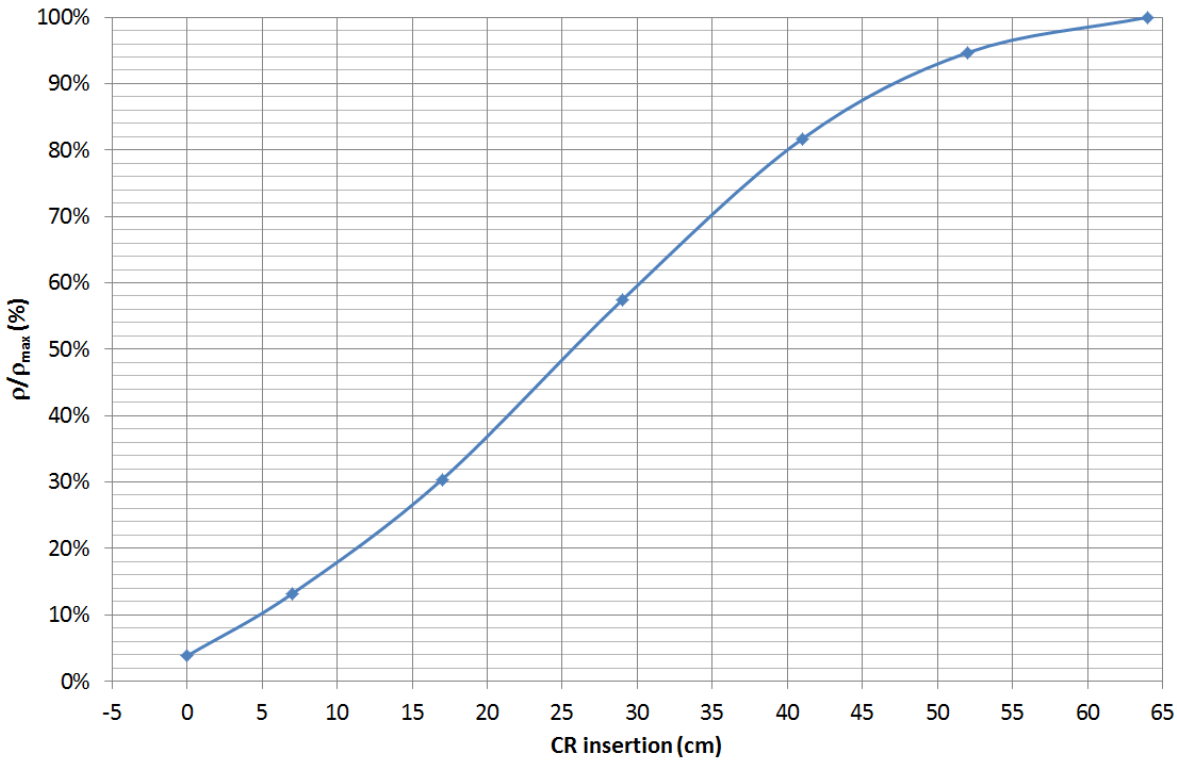


Fig. 3.4.2-1: Reactivity worth of the 12 CR at different insertion lengths (core mid-plane at 30 cm; full extraction corresponds to -4 cm).

Some performances of the ALFRED core are reported in Table 3.4.2-2, as calculated by CEA with ERANOS in [16].

Table 3.4.2-2: ALFRED core characteristics and performances

Average burn-up	73,3 GWd.t^{-1}
Max. burn-up	103 GWd.t^{-1}
Max. DPA NRT (Fe)	85
Effective delayed neutron fraction at EOC	335 pcm*
Lead void effect at EOC (fuel zones)	2 $
Doppler effect at EOC	-1,7 $
**** : pcm = % Δk/k***	

The positive lead void effect is calculated by voiding only the fissile media. The Doppler constant has been evaluated between the nominal fuel temperature (~1500 K) and an hottest one, near the melting point (~2500 K).

The evaluation of the reactivity feedbacks during the fifth equilibrium cycle is presented in Table 3.4.2-3. It is important to notice that all these coefficients are calculated at a fixed temperature. Thus, it would not be discerning to apply these ones to the calculation of transients on the core in a very different situation: beginning of fusion of the core for example.

Table 3.4.2-3: Reactivity feedbacks

	Driving temperature	BOC	EOC
Effective delayed neutron fraction (pcm)	-	336	335
Control and Safety rods differential expansion (pcm/K) – prompt response	Coolant Temp at core outlet	-0,455	-0,218
Control and Safety rods differential expansion (pcm/K) – delayed response	Cold-to-hot leg by-pass Temp*	-0,897	-0,429
Lead expansion coefficient (pcm/K)**	Average coolant Temp in core	-0,271	-0,268
Axial clad expansion (pcm/K)	Average coolant Temp in core	0,037	0,039
Axial wrapper tube expansion (pcm/K)	Clad Temp	0,022	0,023
Radial clad expansion (pcm/K)	Average coolant Temp in core	0,008	0,011
Radial wrapper tube expansion (pcm/K)	Clad Temp	0,002	0,003
Diagrid expansion ($T_{outlet} > T_c$) ***	Coolant Temp at core inlet	-0,147	-0,152
Diagrid expansion ($T_{outlet} < T_c$) ***		-0,519	-0,430
Pad expansion ($T_{outlet} > T_c$) ***	Coolant Temp at core outlet	-0,415	-0,430
Pad expansion ($T_{outlet} < T_c$) ***		0	0
Axial fuel expansion: free (pcm/K)	Fuel Temp	-0,148	-0,155
Axial fuel expansion: linked (pcm/K)	Clad Temp	-0,232	-0,242
Doppler constant (pcm)	Fuel Temp	-555	-566
Iron part of the Doppler constant (pcm)	Clad Temp	-74	-66
Fissile part of the Doppler constant (pcm)	Fuel Temp	-481	-500

****: the region here referred to is the one within the Inner Vessel, above the mixing chamber at core outlet, fed by a by-pass flow entering from the cold flow outside the Inner Vessel***

*****: calculated on the whole height of the fissile sub-assemblies (the other feedbacks are calculated only in the fissile zone)***

******: the critical temperature for pads to enter in contact is $T_c = 480 + 0.6552 * (T_{inlet} – 400)$ [°C].***

Concerning the control rods differential expansion effect, for the calculation it is assumed:

- At BOC: CR inserted by 16 cm into the active region; SR extracted.
- At EOC: CR extracted (4 cm below the active region); SR extracted.

3.5 Secondary circuits

The layout of the ALFRED secondary circuits with Main Steam and Feed Water lines in the proximity of the reactor vessel in schematized in Fig. 3.5-1. The secondary system is constituted by 8 independent circuits connected to the 8 SGs. Both Feed Water and Main Steam lines are provided with isolation valves, which guarantee a very fast isolation of the circuits. Each Main Steam line is provided with 4 relief valves to avoid over-pressurization of the secondary circuits during transients.

Each secondary circuit is linked to one DHR sub-system with connections on both Feed Water and Main Steam pipes.

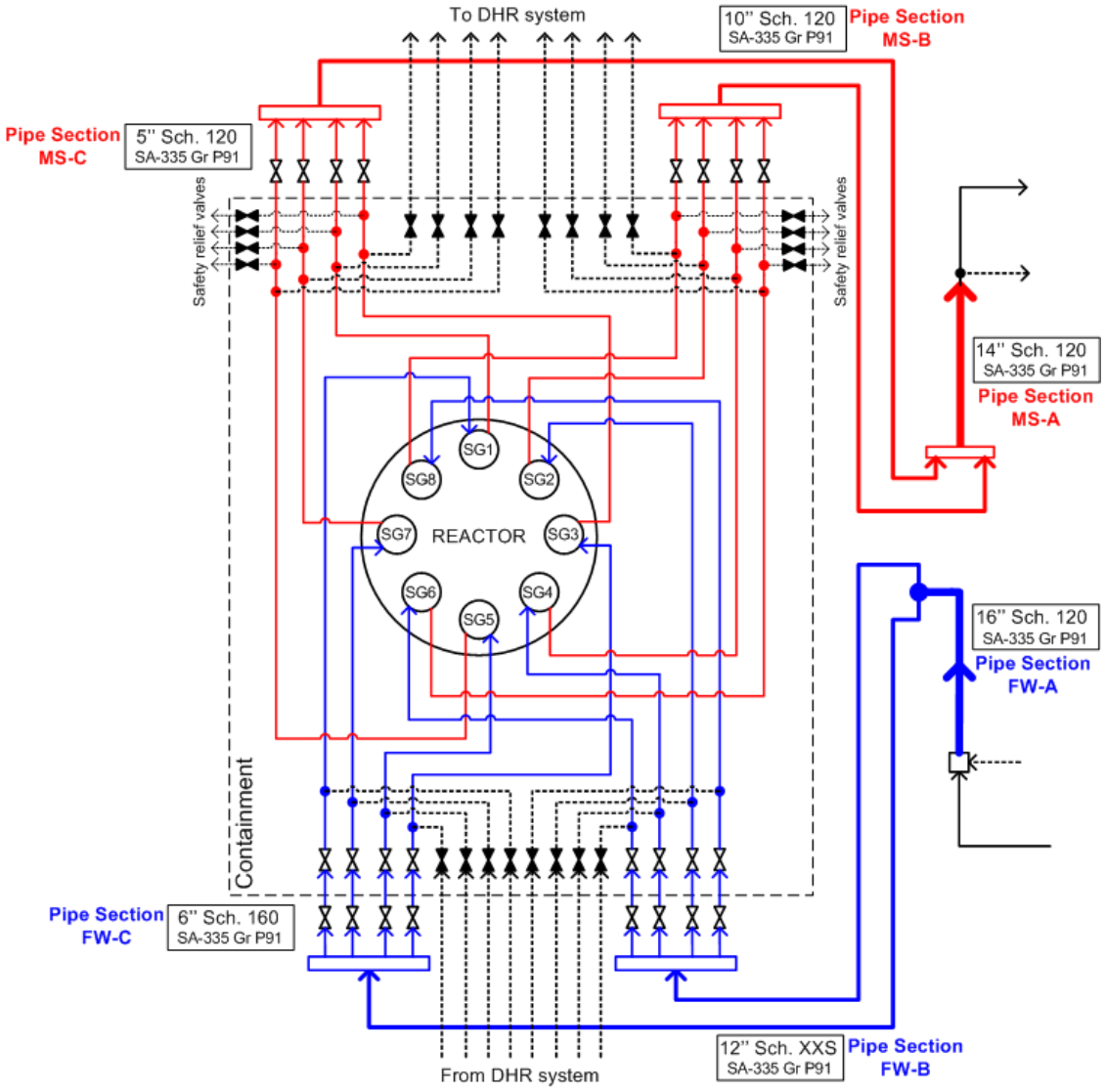


Fig. 3.5-1: Layout with Main Steam and Feed Water pipes in the proximity of the reactor

3.6 Decay heat removal system

The general safety requirement is to have two independent, diverse, high reliable and redundant safety-related Decay Heat Removal systems (DHR-1 and DHR-2). In ALFRED a different approach has been used replacing the diversity with a higher redundancy: eight independent systems with three systems sufficient to fulfill the DHR safety function. In case of unavailability of the secondary cooling system, the DHR system is called upon to evacuate the decay heat.

DHR system main features:

- High Redundancy is obtained by means of three out of four loops (of each system) sufficient to fulfill the DHR safety function even if a single failure occurs.

- To ensure that the decay heat is removed from the primary coolant and rejected to the ultimate heat sink to prevent the primary system structures and core fuel from reaching high temperatures at which their integrity might be compromised.
- To ensure that the decay heat is removed from the primary coolant and rejected to the ultimate heat sink preventing any excessive cooling of the primary coolant leading to fluid solidification with an adequate time grace period.
- To maintain an adequate flow of primary coolant through the core in order to ensure that the decay heat is transferred from the fuel to the primary coolant.

As DHR system, isolation condenser system is foreseen for the ETDR (ALFRED). This DHR system uses the 8 SGs connected to 8 isolation condensers. In this way, fully redundant DHR system has been proposed for the decay heat removal purposes for the ALFRED reactor system. The knowledge of the SG status is fundamental for the possibility to conceive it as an integral part of a safety reactor DHR system. That's why the selection of a SG bundle as composed by bayonet tubes provided with additional external tube with pressurized Helium gap continuously monitored, allows to check the integrity of each SG in operation.

The DHRs systems are the safety-grade decay heat removal system. Each DHR system (DHR-1 and DHR-2) consists of four independent isolation condenser subsystems, for a total of eight isolation condensers. The DHR1 system is composed by four isolation condensers connected to four different steam generators; only three out of four machines are necessary to fulfill the required function of removing the decay heat power from the core. The DHR-2 system is composed by four isolation condensers connected to four different steam generators; only three out of four machines are necessary to fulfill the required function of removing the decay heat power from the core.

Each isolation condenser subsystem is comprehensive of (see Fig. 3.6-1):

- One heat exchanger (isolation condenser), constituted by a vertical tube bundle with an upper and lower header.
- One water pool, where the isolation condenser is immersed; the amount of water contained in the pool is sufficient to guarantee 3 operation days.
- One condensate isolation valve (to meet the single failure criteria this function shall be performed at least by two parallel valves).

As stated above, each isolation condenser is connected to a steam generator:

- The main steam line of a steam generator is connected to the upper header of the isolation condenser.
- The lower header of the isolation condenser is connected to the main feed water line of a steam generator. This connection includes a condensate isolation valve which isolate the isolation condenser from the secondary system (i.e. the isolation valve is full closed during normal operation).

In the following a short description of one DHR system is reported. It should be evidenced since now that the operation of the isolation condensers foresees the actuation of the steam generator safety valves: these, as well as the other components, are described in the following.

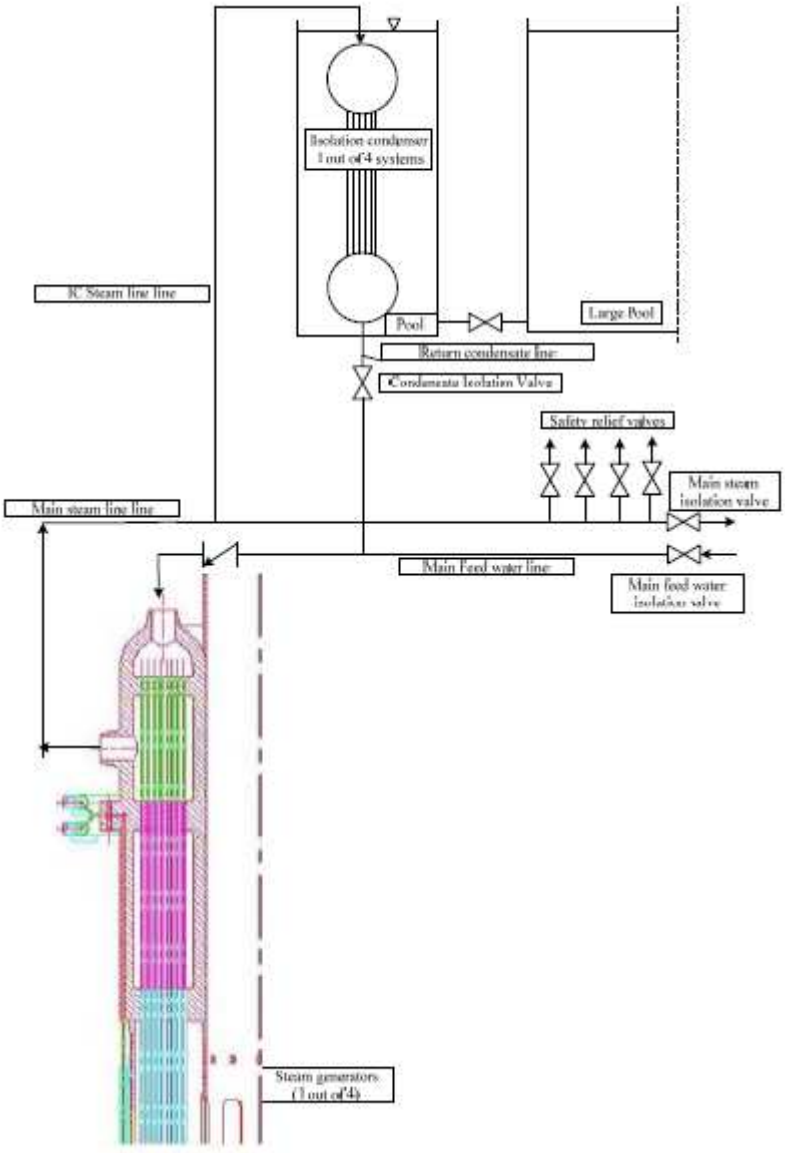


Fig. 3.6-1: DHR system schematics

Condensate Isolation Valve

The condensate isolation valve is located on the condensate return line from isolation condenser to the feed water line. The condensate isolation valve begins to open 0.5 seconds after the reactor trip signal; the valve stroke time is assumed to be 20 seconds. The valve is assumed to operate as orifice, in order to prevent and to limit flow instabilities at low decay heat power levels: the valve flow area has been assumed to be about 1/10 of the connected pipe area.

Safety Relief Valves

The safety relief valves are considered since the operation of the isolation condensers foresees the actuation of the steam generator safety valves. Each main steam line is equipped with 4

safety relief valves, whose purpose is to maintain the pressure of the secondary system below 195 bar(a). The safety relief valves discharge to the atmosphere. Each steam generator is equipped with four safety valves located upstream the main steam isolation valves, in the 4'' steam line connecting the steam generator to the main steam header.

Isolation Condenser

In this preliminary design the isolation condenser consists of one module composed by a vertical tube bundle with an upper and a lower spherical header [29]. The main sizes of each of the four condensers are listed here below.

- **Upper and lower spherical header**

-	External Diameter	560 mm
-	Thickness:	60 mm
-	Material:	Inconel 600

- **Tube bundle**

-	Number of tubes:	16
-	Average active tube length:	2000 mm
-	Tube external diameter:	38.1 mm
-	Tube thickness:	3.0 mm
-	Triangular tube arrangement:	
-	P/D	1.36
-	material:	Inconel 600

- **Condenser connection piping**

-	Steam inlet	Ø 114.3 x 11.13 (4" sch 120)
-	Water condensate outlet	Ø 114.3 x 11.13 (4" sch 120)

Pools

The DHR system design includes the pools which constitute the final heat sink of the system. In the present design four independent water pools are conceived each one dedicated to one isolation condenser. It is foreseen that interconnecting piping, provided with isolation valves, should allow connecting the different pools. The total amount of the stored water for each DHR system should be at least of 520 m^3 (4 * 173.3 m^3) in order to comply with the requirement of 3 days of operation.

3.6.1 System actuation and operation

The DHR is called to operate in case of decay heat removal necessity and failure of the secondary system decay heat removal function (i.e. unavailability of the by-pass to the condenser). The DHR full operation is achievable only by actuating (i.e. opening) the condensate isolation valve; the DHR actuation logic is described in Section 3.6.2, however the following signals are necessary both in case of DHR-1 actuation or DHR-2 actuation:

- Reactor Trip signal following the initiating event.
- Main Steam Isolation Valve and Main Feed Water Isolation Valve closure signal following the Reactor Trip signal.

The isolation of the main feedwater and main steam line causes a pressure increase due to the core decay heat power which heats up the primary coolant as well as the secondary coolant through the steam generators. The safety relief valves of the main steam lines actuate to limit at 195 bars(a) the secondary system pressure rise caused by the main supply lines isolation.

As the isolation condenser subsystem is called to operate, the condensate isolation valve starts opening (0.5 seconds delay and 20 seconds valve stroke are assumed) and the sub-cooled water stored into the isolation condenser tube bundle drains into the steam generator, due to the hydrostatic head existing between the reactor and the isolation condenser. The isolation condenser tubes and headers become empty and their internal cold surface starts to condensate the steam coming from the steam generator and hence to transfer heat to the cold pool water. The steam condensation causes a pressure reduction which calls other steam from the steam generator. The water injected into the secondary system from the isolation condenser during the draining phase, vaporizes into the steam generator tube bundle contributing to the secondary system pressure rise: the safety relief valves continue to operate to reject to the atmosphere the excess of steam and to guarantee a secondary side pressure of 195 bar. In parallel, the isolation condenser reaches its steady state condition (i.e. the condensate isolation valve is fully open, the draining phase is terminated and a constant steam flow rate is condensed into the IC tubes) and starts to remove the thermal power from the primary coolant: this decreases and finally stops the secondary side pressure rise and leads to close the safety relief valves on the main steam line once the secondary pressure falls below the valves blowdown pressure[1].

Thermal stresses on the structures (piping, steam generator plates, etc.) due to the cold sub-cooled water flowing from the isolation condenser during the draining phase are mitigated by water preheating:

- Heat exchange in the steam generator bayonet tube between the cold water descending through the inner pipe and the hot steam ascending through the annular riser.
- Mixing with the hot feedwater still present in the main feedwater line and in the steam generator inlet plenum.

Each condenser is located and immersed in an independent water pool at atmospheric pressure. Pool water can heat up to about 100°C. The steam produced vents from the steam space above each condenser segment where it is released to the atmosphere through large-diameter discharge vents. A moisture separator is installed at the entrance of the discharge vent lines to preclude excessive moisture carryover.

[1] The valve blowdown pressure is the pressure at which the relief valve can be considered fully closed. This pressure is lower than the relief valve set point pressure, which is the pressure causing the valve opening. The blowdown pressure has been assumed equal to 194 bar(a) for the analysis.

3.6.2 DHR actuation logic

The DHR systems actuation logic should fulfill the following requirements:

- Each DHR system is called to operate when the reactor trip signal, the main feedwater line and the main steam line isolation signal take place.
- First DHR-1 system is called to operate; the DHR-2 system is called to operate only in case of DHR-1 failure.
- In case of DHR-1 system failure and DHR-2 actuation, the overall power removal capacity provided by the operating isolation condensers of DHR-1 system and DHR-2 system should avoid reaching the primary coolant solidification temperature for at least one hour, which is the minimum time period credited the operator to limit the DHR power removal capacity.

In case of necessity, the DHR-1 is the first system called to operate. When the following signals become true, all the four DHR-1 isolation condenser subsystems start working:

- Reactor trip signal.
- Main feedwater and main steam lines isolation signal.

The same signals put the DHR-2 system in stand-by condition, ready to operate in case of DHR-1 system failure.

The DHR-1 system failure occurs when one or more isolation condenser subsystems fail re-circulating condensate water to the steam generators:

- Isolation condenser failure: the condensate isolation valve does not open or isolation condenser piping break.
- The initiating event is the main feedwater line break upstream the main isolation valve or the main steam line break downstream the main isolation valve.

The DHR-1 system failure can be detected monitoring specific parameters that can indicate if each isolation condenser subsystem is effectively operating or not. A first preliminary example of parameters to monitor is the following:

- Isolation condenser lower header temperature: when the condensate isolation valve is closed, the isolation condenser is filled with sub-cooled water in thermal equilibrium with the cold water of the pool in which the isolation condenser is immersed. Differently, when the isolation condenser works, the temperature of the fluid contained into the isolation condenser lower header is higher and it corresponds to the fluid saturation temperature at the operating pressure (i.e. 180 ÷ 195 bar(a)).
- Isolation condenser water level: when the condensate isolation valve is closed, the isolation condenser is filled with sub-cooled water in thermal equilibrium with the cold water of the pool in which the isolation condenser is immersed. When the condensate isolation valve actuates, the water stored into the isolation condenser headers and tube bundle drains into the steam generators, due to the hydrostatic head existing between the reactor and the isolation condenser: the machine becomes almost empty.

- Isolation condenser pressure: when the condensate isolation valve is closed, the isolation condenser is at the secondary system normal operating pressure (i.e. about 180 bar(a)). A pressure decrease to low values respect the expected one during normal operation indicates a line break on the secondary side. It should be reminded that each steam generator system is provided with a dedicated main feedwater line and a main steam line which are physically separated inside the reactor containment (i.e. downstream the main feedwater isolation valve and upstream the main steam isolation valve, which are closed in case of DHR actuation signal).

The monitoring of the first two parameters can indicate the effective or not isolation condenser subsystem actuation, while the third one shows if the initiating event can affect the isolation condenser operation, as in case of secondary side line break.

The DHR-1 system failure is detected as soon as one out of four isolation condenser sub-systems fail to actuate or to correctly operate. In this case the DHR-2 system, which is in stand-by condition as a consequence of the DHR-1 actuation signals, activates; however not all the four DHR-2 isolation condenser subsystems should start operating simultaneously, in order to avoid a too high DHR heat power removal capacity (DHR-2 four isolation condenser sub-systems plus the still operating DHR-1 isolation condenser sub-systems) causing an excessively fast primary coolant temperature decrease, which could lead to violate the requirement of sufficient grace time period before to reach the lead solidification temperature (i.e. one hour).

The DHR-2 isolation condenser subsystem should activate one per time, as defined in a dedicated sequence of activation; the DHR-2 system activates when all the following signals become true:

- Reactor trip signal.
- Main feed water and main steam lines isolation signal.
- One or more DHR1 isolation condenser subsystems failure.

The number of DHR-2 isolation condenser subsystems called to operate is function of the number of DHR-1 isolation condenser subsystems that have failed. The activation sequence of the DHR-2 isolation condenser subsystems should also foresee the DHR-2 single failure: the isolation condenser subsystem next in the sequence list should start in case the DHR-2 isolation condenser subsystem called to operate fails to activate or to operate.

The parameters to monitor, to understand if the DHR-2 isolation condenser subsystem called to operate has failed or not, are the same as for DHR-1 system (i.e. isolation condenser water temperature, level and pressure).

A detailed description and the functional analysis of the ETDR (ALFRED) DHR system are provided in Refs, [11] and [17].

4. BENCHMARK OF CODES

The results of some representative unprotected transients: ULOF, UTOP and ULOHS have been compared in order to verify the consistency of different code results.

4.1 ULOF transient

This transient is initiated by the loss of power supply to all primary pumps. The reactor scram is supposed to fail and then the core power is driven by reactivity feedbacks. The secondary circuits are supposed to remain in normal operation with no control of the feedwater flow rate.

The natural circulation which stabilizes in the primary circuit after primary pumps coastdown is shown in Fig. 4.1-1. All codes predict similar natural convection flow rate in the range 20-25% of nominal value. Similarly, all codes predict a significant reduction of core power which stabilizes around 200 MW (two-third of the nominal value).

The core coolant inlet temperature reduces, as shown in Fig. 4.1-2, due to sudden temperature decrease at MHX outlet, while the coolant temperature at core outlet suddenly increases at the beginning of the transient because of the disbalance between core flow rate and power. All codes predict similar coolant temperature peak and then reduction and stabilization of temperature in the range of 600 – 650 °C.

The maximum clad and fuel temperatures evolution is shown in Fig. 4.1-3. There are some discrepancies in the initial temperature peak predicted by the codes. The largest peak is calculated by CIRTEN with RELAP5. Most of the codes predict maximum clad temperature stabilization around 650 °C. The maximum fuel temperature in steady-state conditions varies in the range 1980 – 2080 °C. Even a larger spread of maximum fuel temperature is predicted during the ULOF transient which is related to the difference in the obtained core power and likely also due to differences in fuel rod gap dynamic behavior modelling.

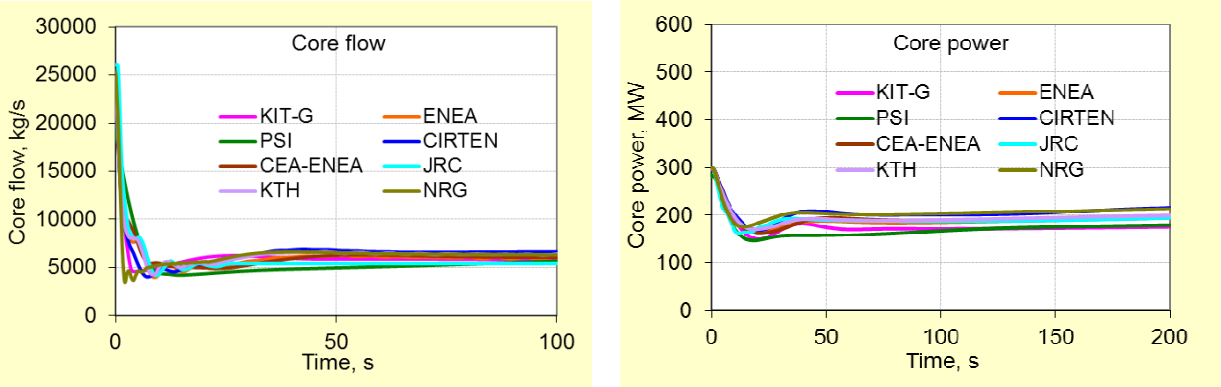


Fig. 4.1-1: Core mass flow rate (left) and core power (right) evolution

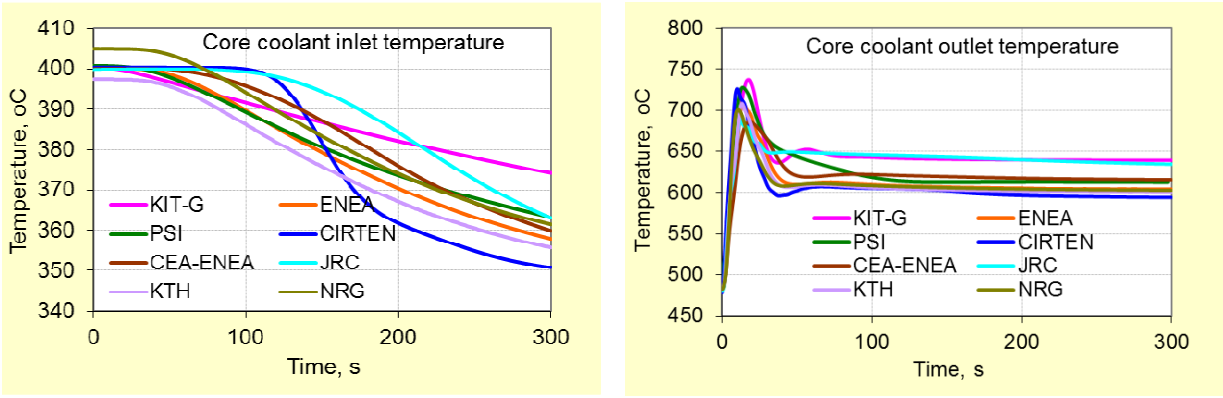


Fig. 4.1-2: Core coolant inlet (left) and outlet (right) temperature evolution

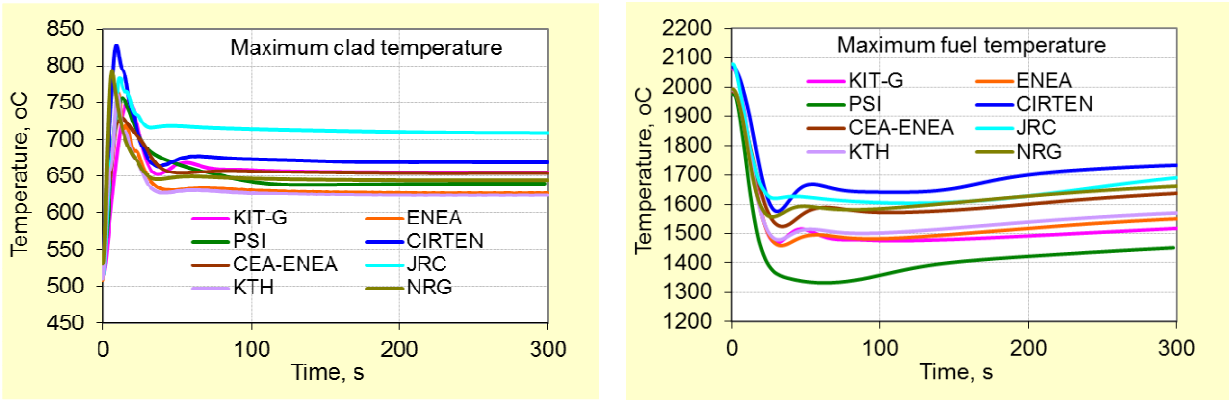


Fig. 4.1-3: Maximum clad (left) and fuel (right) temperature evolution

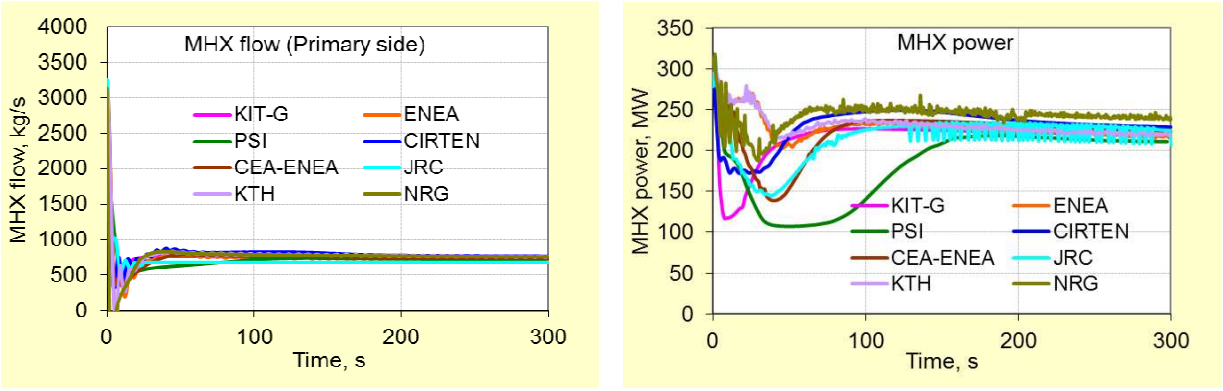


Fig. 4.1-4: MHX lead mass flow rate (left) and MHX power (right) evolution

The power removed by the MHX reduces first according to the reduced primary flow rate as shown in Fig. 4.1-4 and then increases according to the temperature increase at MHX inlet (see Fig. 4.1-5). The temperature at MHX outlet reduces significantly down to 340 – 350 °C. There are some significant deviations in the prediction of MHX lead inlet temperature by JRC-IET with TRACE, which are not clearly understood.

The total reactivity evolution is compared in Fig. 4.1-6 along with different feedback effects. At the same time as the total reactivity exhibits a similar behavior, there are significant differences in some of the feedback components. Major differences are observed when

comparing axial expansion and Doppler effects as related to different obtained fuel temperatures and dynamic gap behavior. Further important deviations are observed in radial expansion feedback by JRC-IET with TRACE and in control rod drive expansion feedback by CIRTEN with RELAP5.

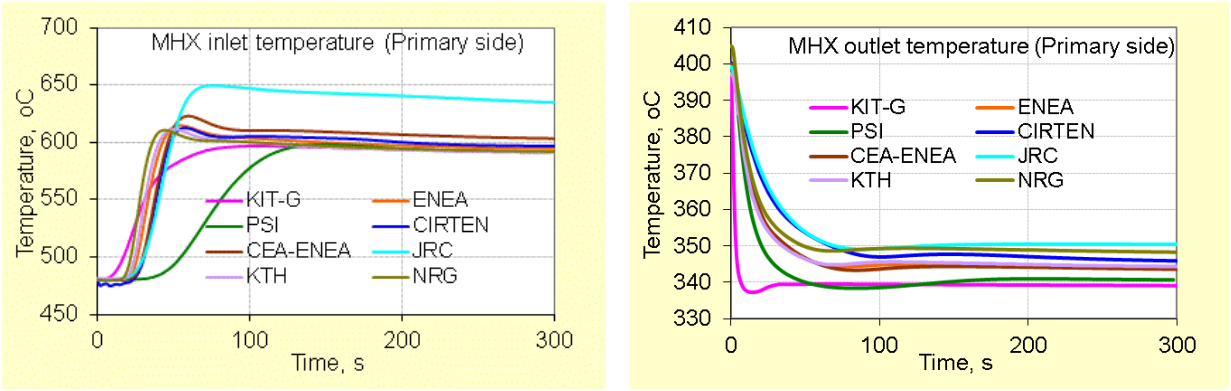
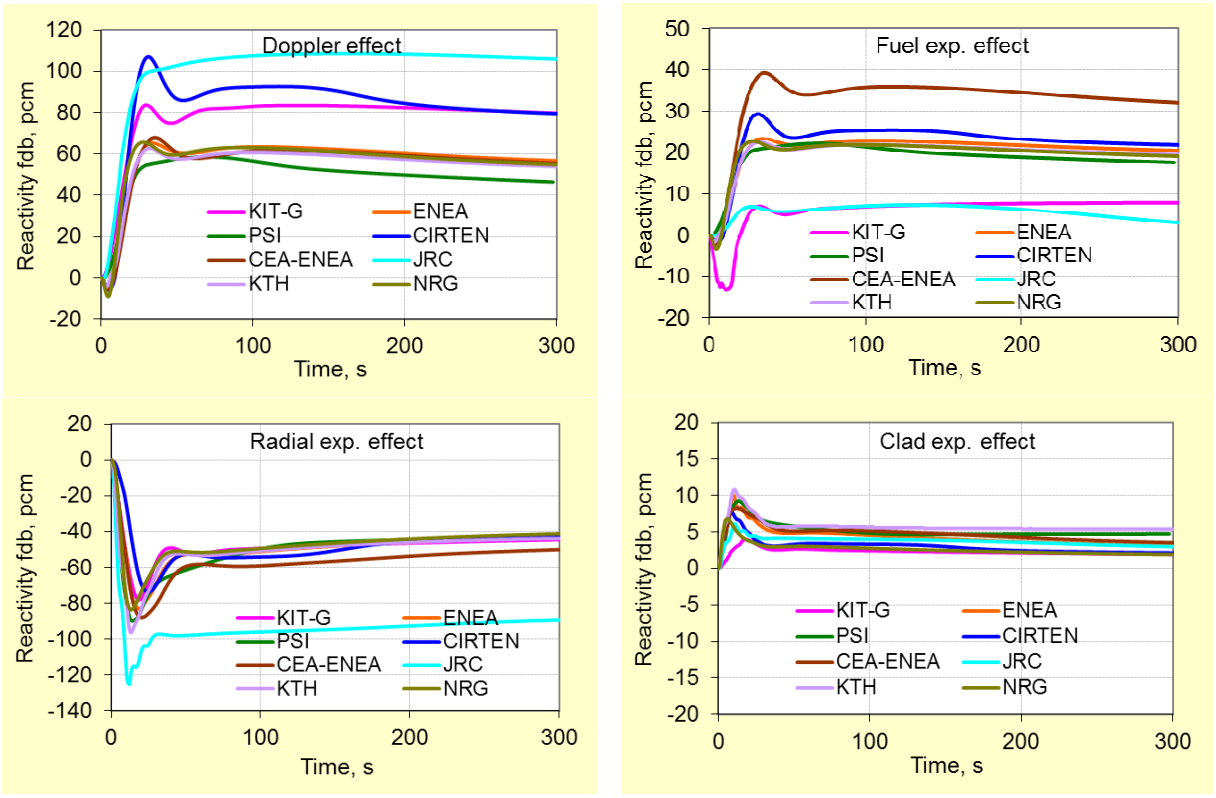


Fig. 4.1-5: MHX lead inlet (left) and outlet (right) temperature evolution



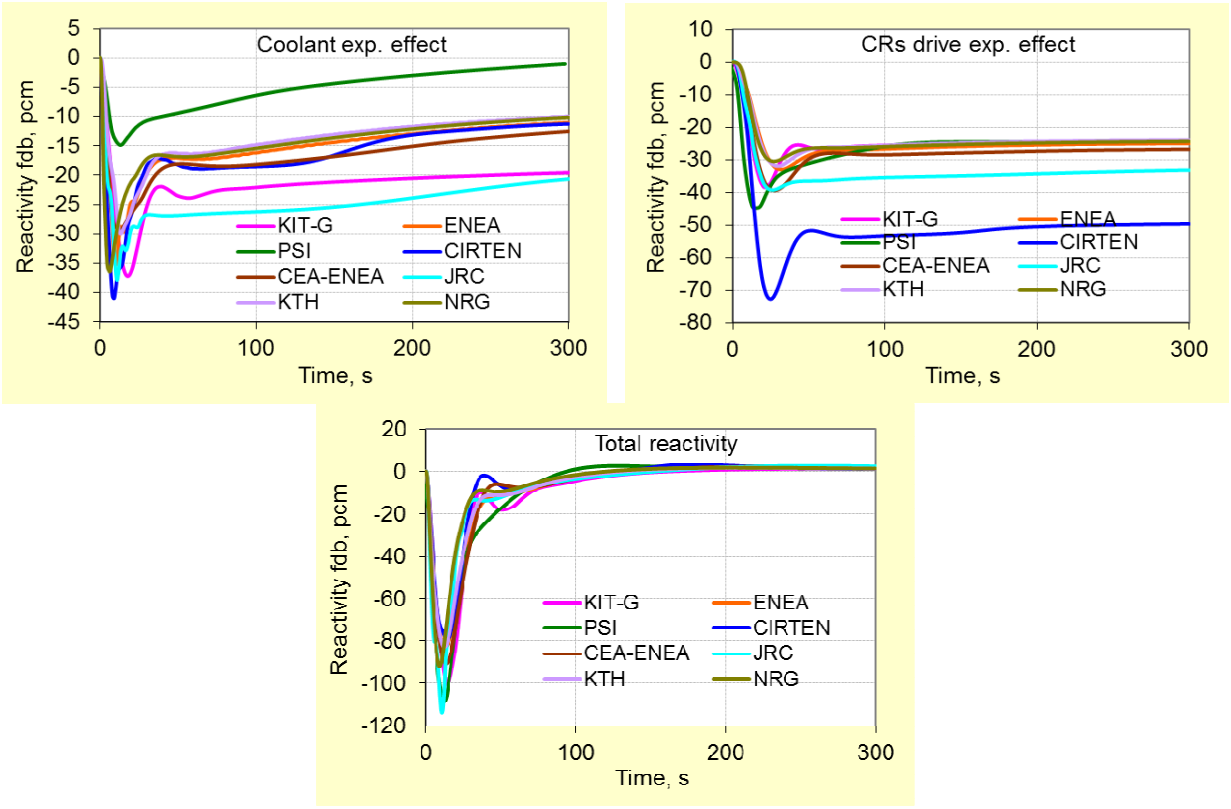


Fig. 4.1-6: Total reactivity and feedbacks

Apart from separate parameter deviations in code results, similar general behavior is predicted by the codes under ULOF transient conditions.

4.2 UTOP transient

This transient is initiated by a reactivity insertion of 250 pcm in 10 s without reactor scram. The secondary circuits are supposed to remain in normal operation with no control of the feedwater flow rate.

The primary system remains in forced circulation as evidenced in Fig. 4.2-1. The reactivity insertion results in a power excursion which is limited by negative reactivity feedbacks. All codes predicts similar power excursion (Fig. 4.2-1) up to around 700 MW and then a power decrease and stabilization around 480 MW. Only TRACE by JRC-IET predicts a larger power decrease at t = 200 s down to ~ 430 MW.

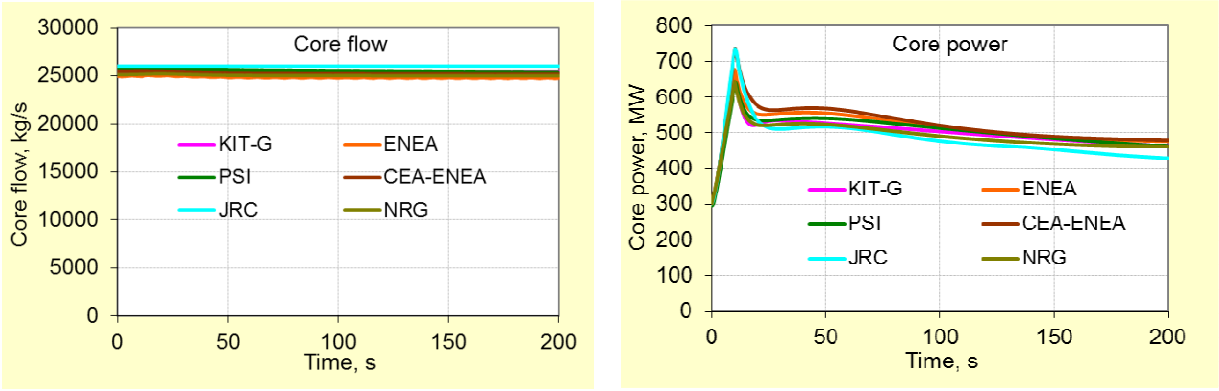


Fig. 4.2-1: Core mass flow rate (left) and core power (right) evolution

All codes predict a sudden increase of temperature at core outlet at the beginning of the transient and then a progressive increase of temperature according to temperature increase at core inlet (Fig. 4.2-2). The code temperature differences are rather consistent with the deviations in nuclear power evolution. Similarly, there are some deviations in the prediction of maximum clad temperature as evidenced in Fig. 4.2-3. Some larger deviations are observed in the calculation of maximum fuel temperature in the hottest FA, also because of the different fuel rod gap dynamic model used by the codes. However, all codes confirm that only local fuel melting is expected in the centre of the pellets of the hottest FAs of the core.

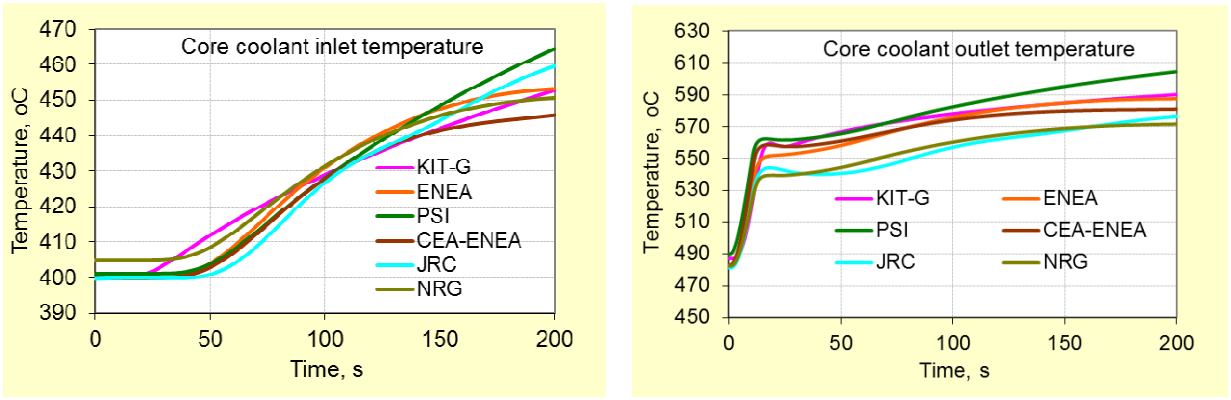


Fig. 4.2-2: Core coolant inlet (left) and outlet (right) temperature evolution

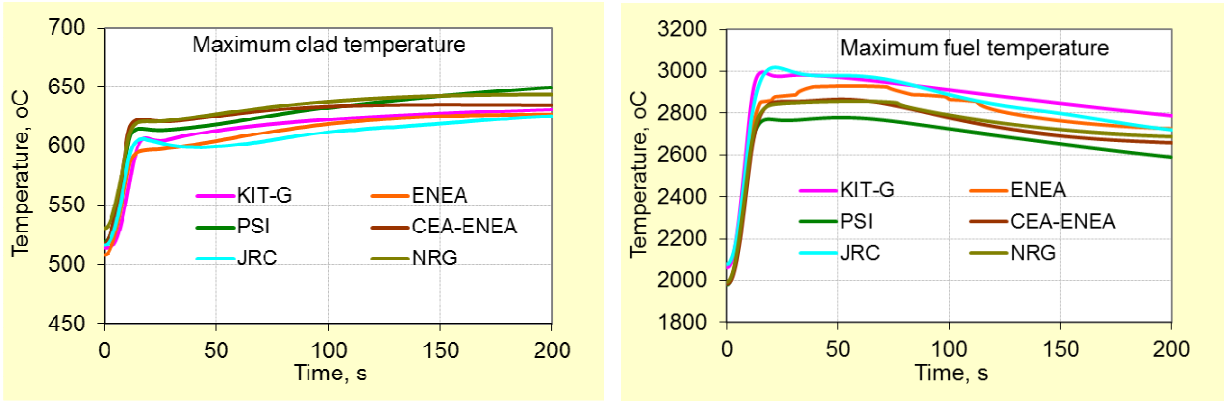


Fig. 4.2-3: Maximum clad (left) and fuel (right) temperature evolution

All codes predict similar increase of power removal by the secondary side (Fig. 4.2-4) according to the average coolant temperature increase on primary side, and corresponding evolution of temperature increase at the inlet and outlet of MHX (Fig. 4.2-5).

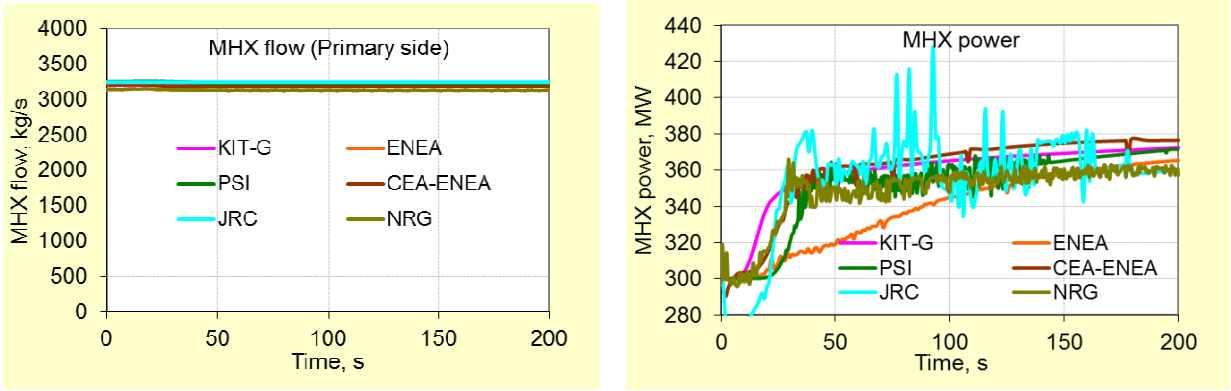


Fig. 4.2-4: MHX lead mass flow rate (left) and MHX power (right) evolution

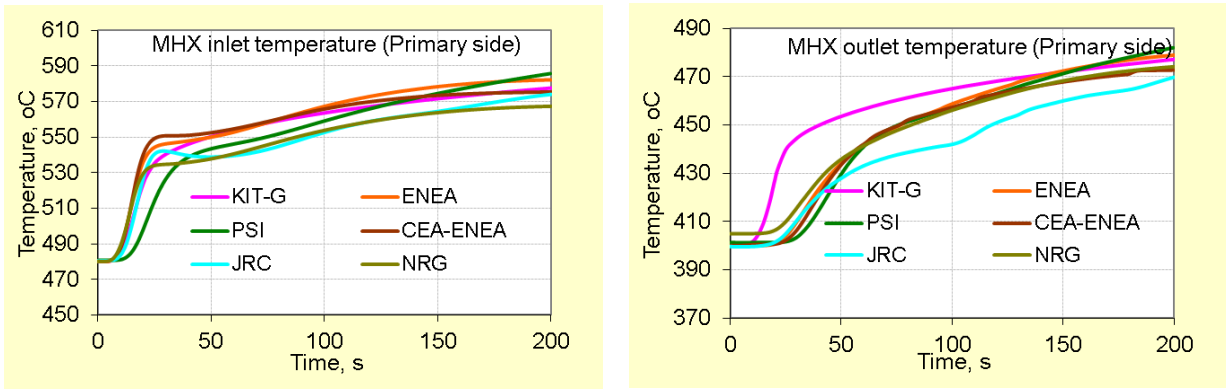


Fig. 4.2-5: MHX lead inlet (left) and outlet (right) temperature evolution

All codes predict similar increase of total reactivity at the beginning of the transient (Fig. 4.2-6) and their compensation by negative feedbacks. The inserted reactivity is mainly counterbalanced by prompt Doppler effect. The deviations observed in fuel expansion effect seem mainly caused by different fuel rod gap dynamic modelling. The deviations in other feedback effects are rather small.

As a general conclusions, all codes agree on rather low clad temperature increase in the core which is below clad failure safety limits and only local fuel melting in the central part of the fuel pellets in the hottest FA is being predicted.

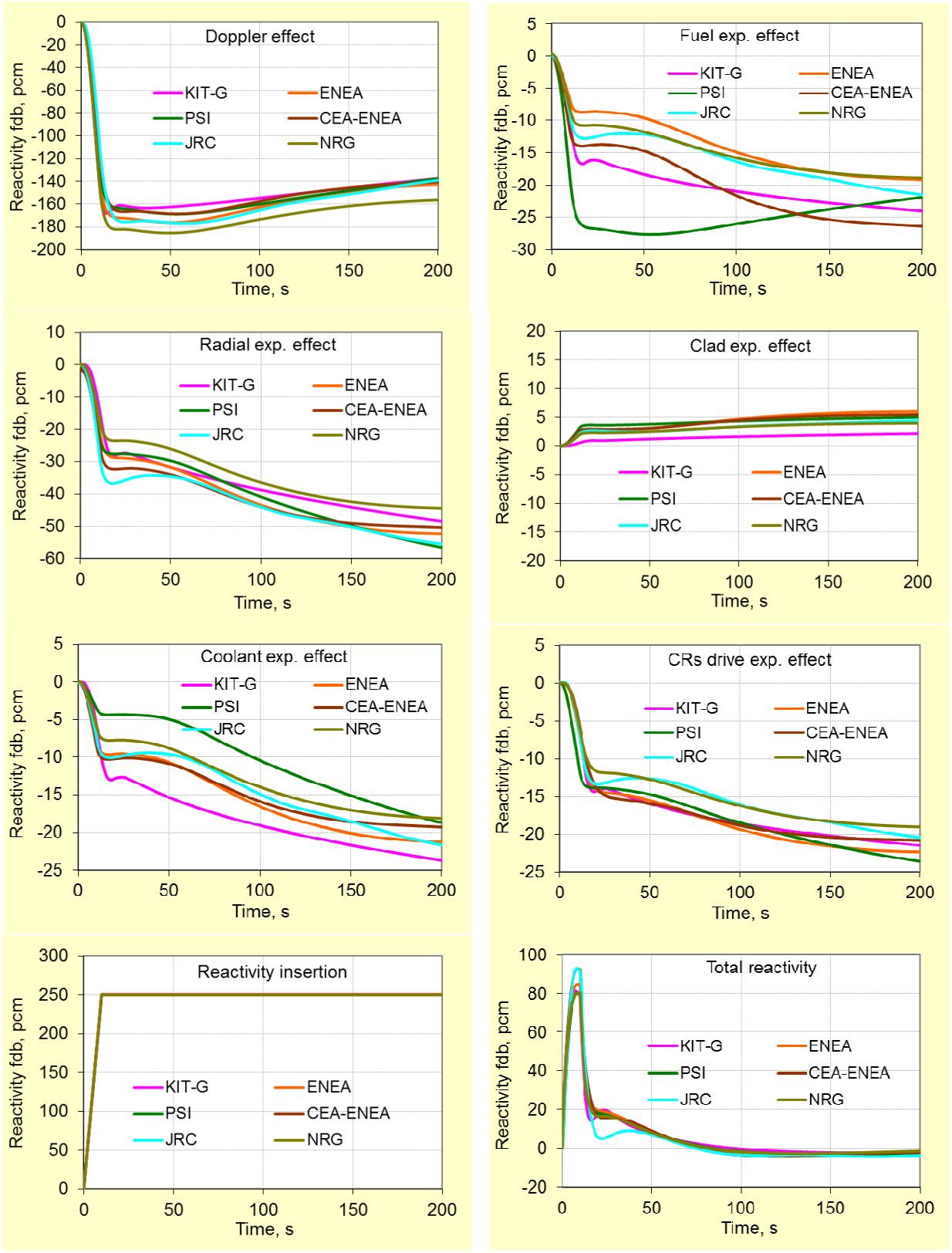


Fig. 4.2-6: Total reactivity and feedbacks

4.3 ULOHS transient

This transient is initiated by the simultaneous loss of feedwater to all MHX, which leads to turbine trip and isolation of secondary circuits and startup of DHR-1 system. The reactor scram is supposed to fail and as a conservative assumption only 3 out of 4 DHR-1 sub-systems are supposed to be in service.

The primary system remains in forced circulation as evidenced in Fig. 4.3-1. All codes predict progressive core power reduction towards the decay level during one hour transient due to negative feedbacks introduced following primary coolant and core temperature increase.

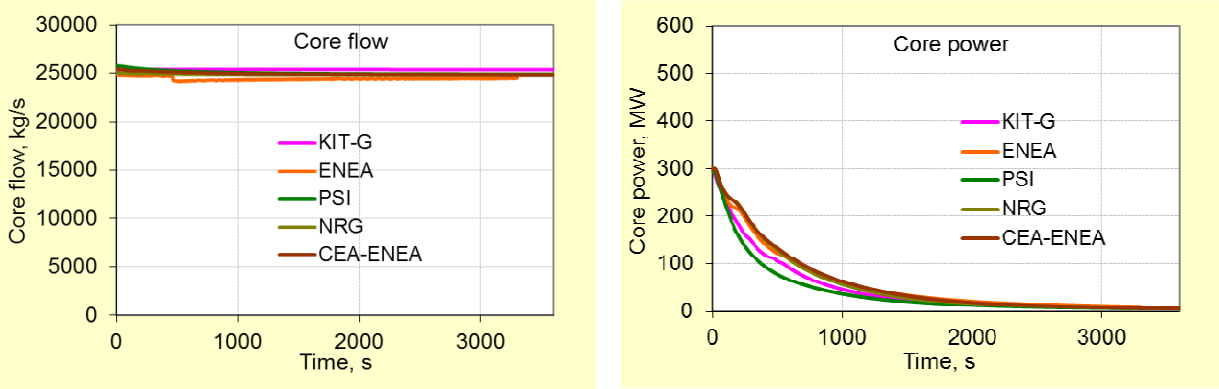


Fig. 4.3-1: Core mass flow rate (left) and core power (right) evolution

Due to reduced core power with constant primary flowrate, the temperature difference between core inlet and outlet significantly reduces, while the maximum core coolant temperature tends to stabilize around 700 °C (Fig. 4.3-2). According to uniform primary temperature increase, all codes predict similar maximum clad temperature with strong decrease of maximum fuel temperature as shown in Fig. 4.3-3.

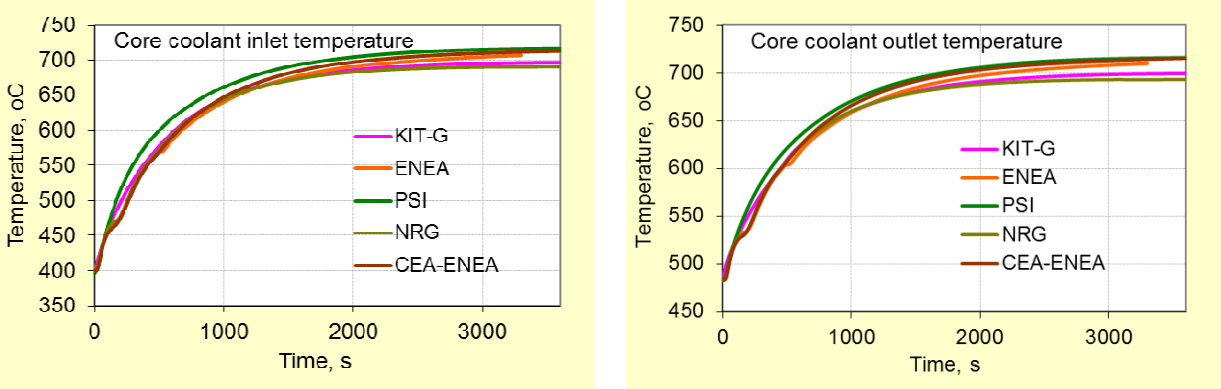


Fig. 4.3-2: Core coolant inlet (left) and outlet (right) temperature evolution

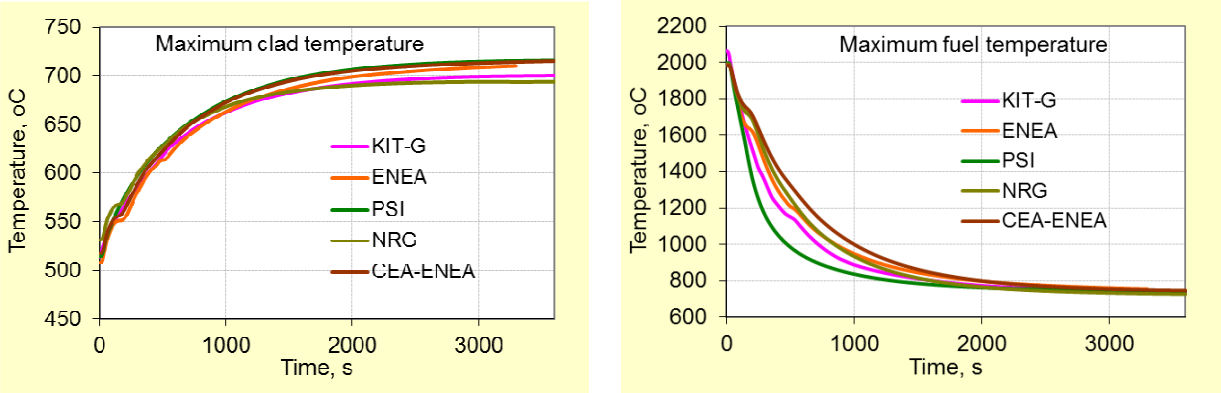


Fig. 4.3-3: Maximum clad (left) and fuel (right) temperature evolution

A critical safety issue for this transient is the relevant increase in vessel wall temperature that approaches 700 °C during one hour transient (Fig. 4.3-4). The largest vessel wall temperature values are predicted by ENEA and CEA with RELAP5 and CATHARE codes likely because radiative heat losses from the external vessel wall surface are not taken into account. After the initial transient phase, the MHX power is removed through the IC by boiling on the secondary side and steam condensation on the primary side. The semi-stationary state values are about 5 MW by 3 DHR-1 sub-systems. NRG with SPECTRA code predicts somewhat larger power removal by DHR-1. It should be noted that higher IC power was also observed by ENEA/CEA with CATHARE, but the IC power was tuned to obtain design values by adjusting the tube exchange area in the model. SPECTRA results (as well as ENEA RELAP5) are the best-estimate code results. The difference in IC power may come from condensation correlations (at high pressures) or boiling correlations in the codes and should be investigated in the future.

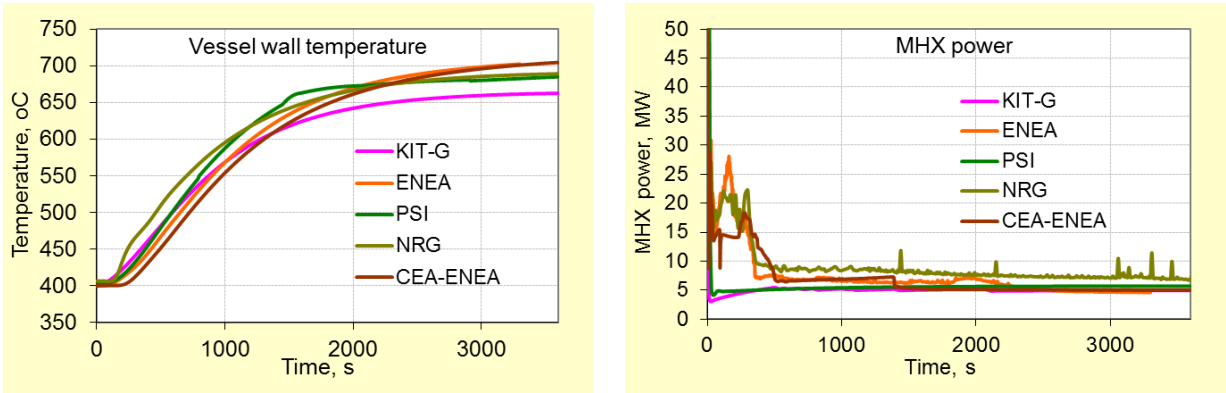


Fig. 4.3-4: Evolution of maximum vessel wall temperature (left) and power removed by secondary side (right)

The total reactivity evolution shown in Fig. 4.3-5 shows that all codes predict negative reactivity during the whole transient associated to negative feedback effects related to radial core expansion, coolant expansion and control rod drive expansion which are only partially counterbalanced by positive Doppler, fuel expansion and clad expansion effects. The relative deviations among the code values are rather small. Once again, the largest differences are exhibited in fuel expansion effect likely due to different gap dynamic behavior. Wrapper expansion effect is included along with the clad expansion effect in the ENEA and CEA

calculations with RELAP5 and CATHARE and thus this may contribute to enhance the deviation with other code results when predicting clad expansion feedback.

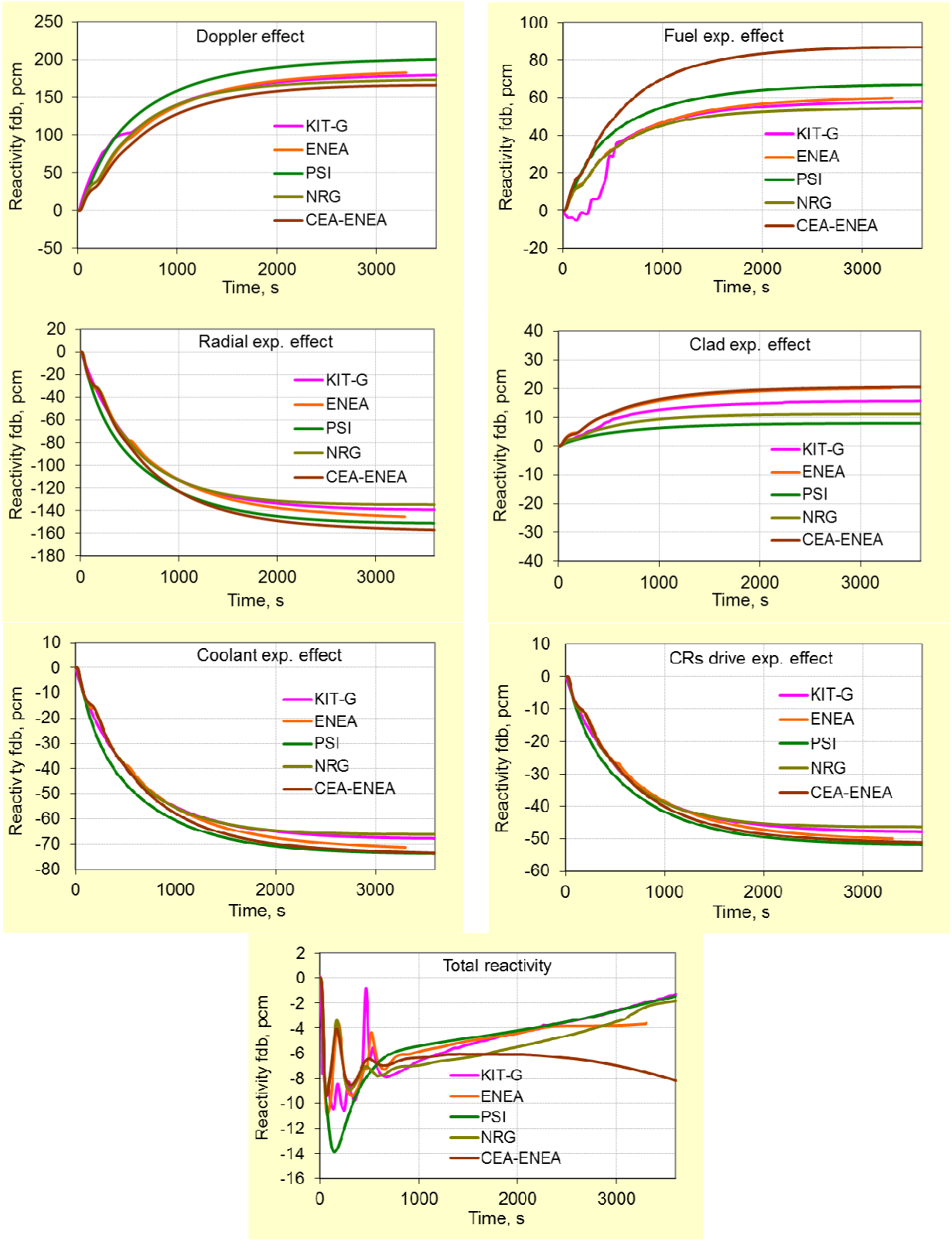


Fig. 4.3-5: Total reactivity and feedbacks

4.4 Conclusions from the code benchmark

The results of the code benchmark on representative unprotected transients: UTOP, ULOF and ULOHS have highlighted a general consistency of different code results. Similar conclusions can be drawn from the analysis of different DEC transients analyzed using different codes. Some certain parameter deviations have been encountered that are likely due to different modeling detail of primary and secondary circuits. Furthermore, the largest deviations on reactivity feedbacks seem to be related to the lack of consistent fuel rod gap dynamic behavior modeling under transient conditions.

5. DEC TRANSIENT RESULTS

In the Deliverable DEL011-2012, the more representative DEC events have been selected for the safety analysis to be carried out within the Task 5.5 of the LEADER project. The list of analyzed transients has been already presented in Table 2-1 of Section 2.

In the following subsections the main results of the DEC transient analysis performed by various organizations using different codes (see Section 2) are presented.

5.1 TR-4: Unprotected reactivity insertion (UTOP)

This transient is initiated by an unexpected positive reactivity insertion of 250 pcm in 10 s following possible perturbations in the primary system induced by steam generator tube rupture (SGTR), FA flow blockage or core compaction.

The transient is unprotected and then the reactor scram is assumed to fail, while forced circulation is maintained in the secondary circuits with no control of the feedwater flow rate, which remains constant at its nominal value.

This transient has been analyzed by several partners using different codes: KIT-G with SIM-LFR at BOC and EOC conditions, PSI with TRACE/FRED, JRC-IET with TRACE, ENEA with RELAP5, ENEA/CEA with CATHARE and NRG with SPECTRA at EOC conditions. The main results of these analyses are presented in the following subsections.

A CFD simulation approach has been developed by KTH for evaluating the core voiding which could arise from steam bubble transport through the core in case of SGTR/SGTL event. This CFD simulation approach is presented in section 5.10 of this report and with more details in Appendix F.

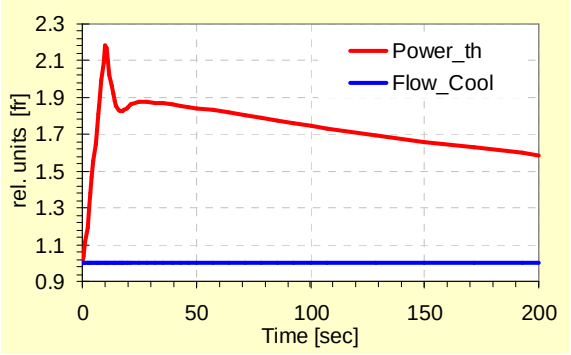
5.1.1 TR-4 transient: SIM-LFR results (KIT-G)

ALFRED overpower transient at HFP (Hot Full Power) and BOC, as well as EOC core conditions is reported in this section, namely:

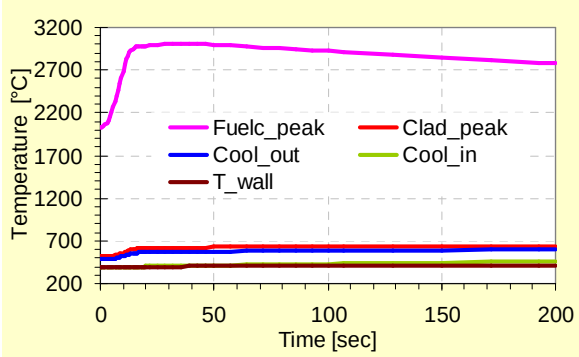
- 250 pcm reactivity insertion within 10 sec time interval at HFP conditions. This amount of reactivity might be inserted into the core due to: voiding of part of active core region enveloping voids introduction in case of SGTR, core compaction, fuel SA blockage, etc.

As can be observed in Fig. 5.1.1-1c, an insertion of 250 pcm in 10 sec time interval at BOC conditions, leads to a power jump of ~ 2.17 nominal (see Fig. 5.1.1-1a). The maximum fuel and clad temperatures under BOC conditions increase from 2028 °C and 516 °C to 3011 °C and 641 °C respectively (see Fig. 5.1.1-1b) resulting in short-term local fuel melting (fuel center) of the peak fuel pins.

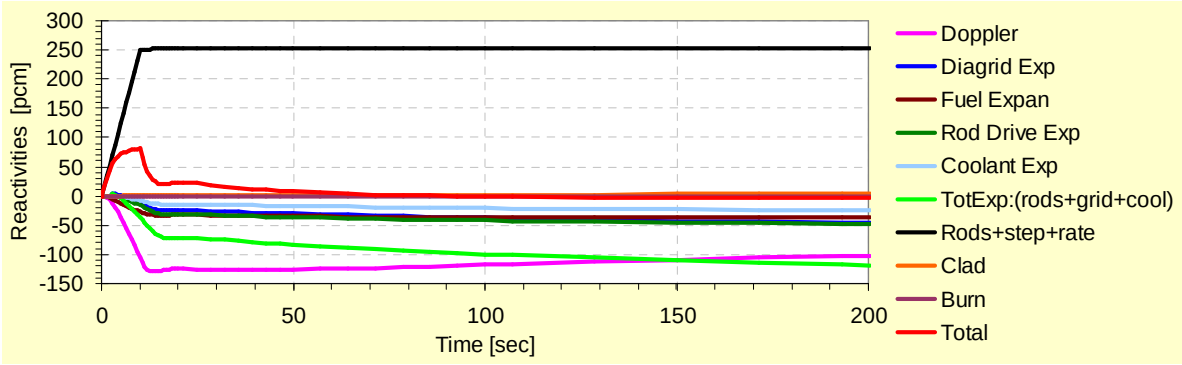
The corresponding clad failure time remains above 1E+8 sec (see Fig. 5.1.1-1d) as peak clad temperatures remain relatively low (< 700 °C).



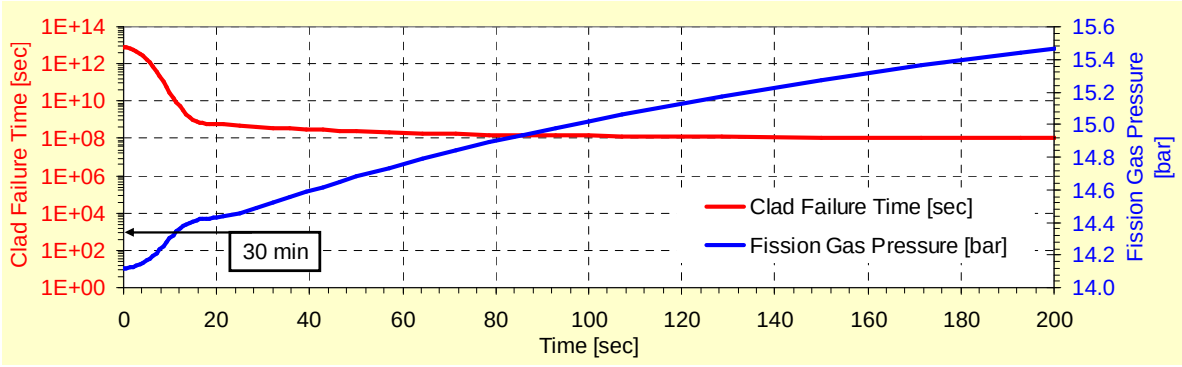
a) Relative core thermal power and flow rate



b) Peak fuel-, clad-, coolant- and vessel wall temperatures



c) Reactivity effects

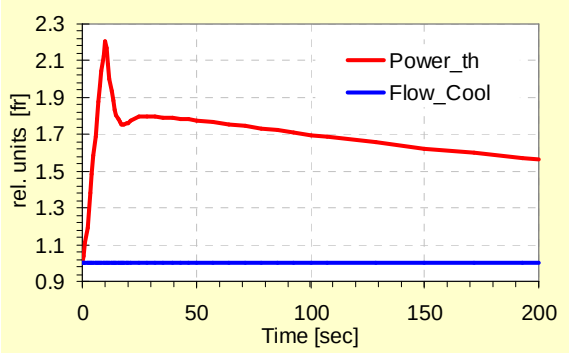


d) Peak pin fission gas pin pressure and clad failure time

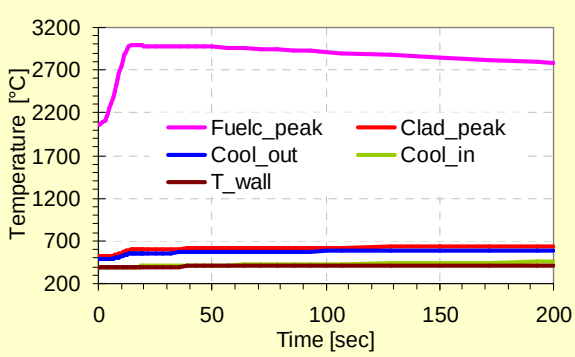
Fig. 5.1.1-1: Results for TR-4: (UTOP: 250 pcm in 10 sec) transient at HFP - BOC conditions at an average burnup of 730 EFPD as calculated by SIM-LFR (KIT)

As can be observed in Fig. 5.1.1-2c, an insertion of 250 pcm in 10 sec time interval at EOC conditions, leads to a power jump of ~ 2.2 nominal (see Fig. 5.1.1-2a). The maximum fuel and clad temperatures under EOC conditions increase from 2064°C and 514°C to 2996 °C and 631 °C respectively (see Fig. 5.1.1-2b) resulting in short-term local fuel melting (fuel center) of the peak fuel pins..

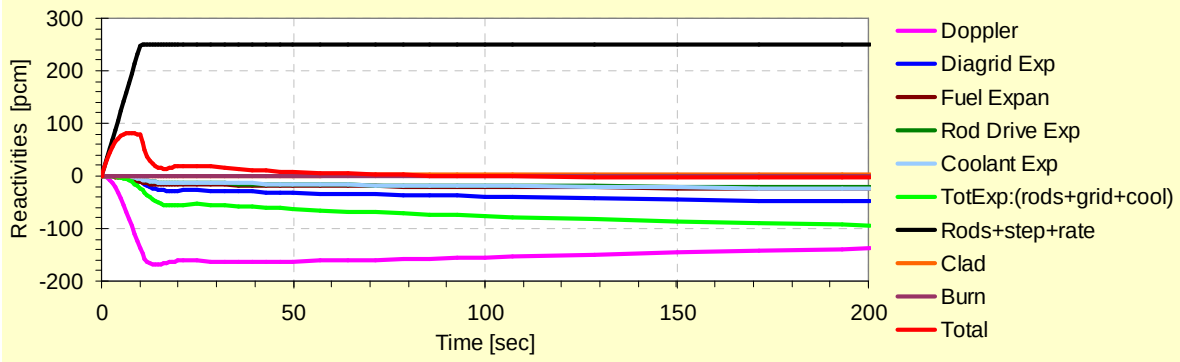
The corresponding clad failure time remains above 1E+8 sec (see Fig. 5.1.1-2d) as peak clad temperatures remain relatively low (< 700 °C).



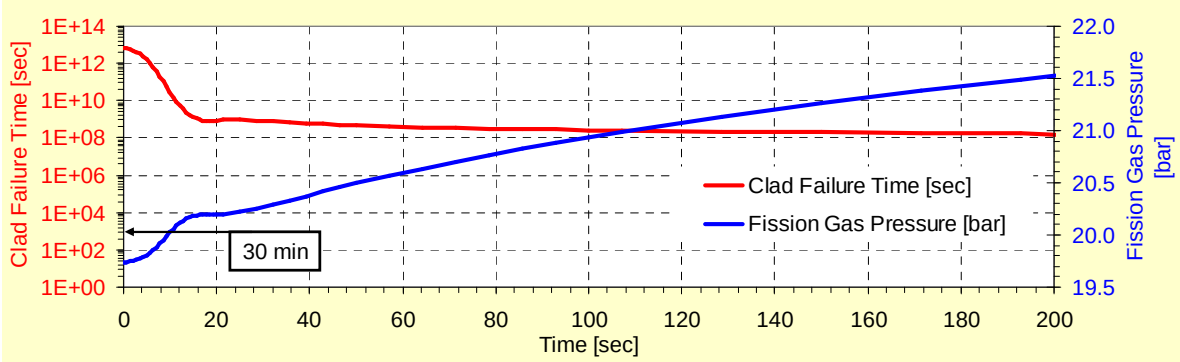
a) Relative core thermal power and flow rate



b) Peak fuel-, clad-, coolant- and vessel wall temperatures



c) Reactivity effects



d) Peak pin fission gas pin pressure and clad failure time

Fig. 5.1.1-2: Results for TR-4: (UTOP: 250 pcm in 10 sec) transient at HFP - EOC conditions at an average burnup of 1095 EFPD as calculated by SIM-LFR (KIT)

As related to the above study, one can observe that:

- For reactivity insertion of 250 pcm in 10 sec time interval (due to: voiding of part of active core region enveloping voids introduction in case of SGTR, core compaction, fuel SA blockage, etc.) at BOC, as well as EOC conditions, ALFRED reactor peak fuel pin cladding survives this transient, but local fuel melting is observed in the center of the peak fuel pins (pellets).

5.1.2 TR-4 transient: TRACE/FRED results (PSI)

The Unprotected Transient over Power (UTOP) was defined to be initiated by a linearly introduction of 250 pcm positive reactivity within 10 seconds. During the whole accident, the scram protection system fails to work. Meanwhile, the primary circulation pump, MHX and secondary circuit will work normally.

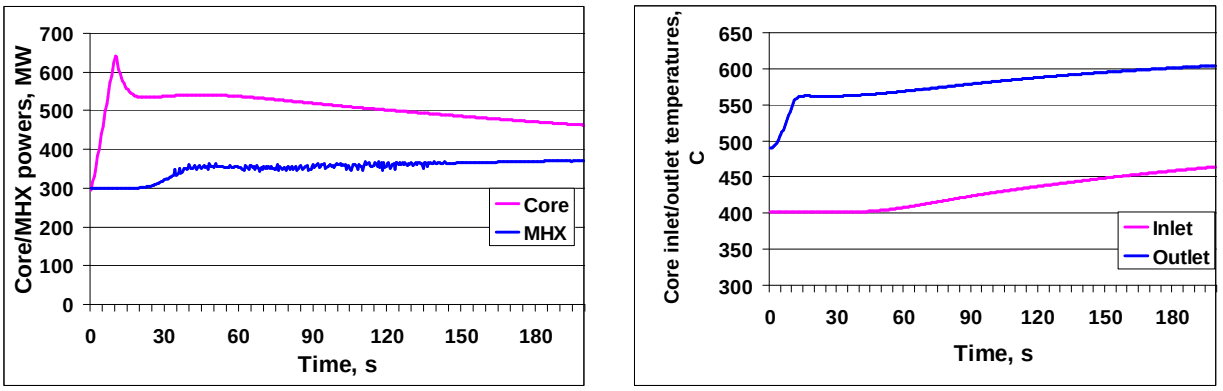


Fig. 5.1.2-1: Evolutions of core/SG powers (left) and core inlet/outlet temperature (right) with time

When 250 pcm positive reactivity starts to be introduced, core power begins increasing as shown in Fig. 5.1.2-1. After around 15 seconds, core power reaches its peak level, being equal to 642 MW (214% of the initial level). The fuel temperature increase due to power increase leads to negative reactivity feedback incurred by the Doppler effect as shown in Fig. 5.1.2-3. This significant negative reactivity feedback, together with negative reactivity feedbacks incurred by fuel axial expansion and pad/diagrid expansion, will be higher than the introduced positive reactivity feedback. This stabilizes core power at around 154% of its initial level after 200 seconds.

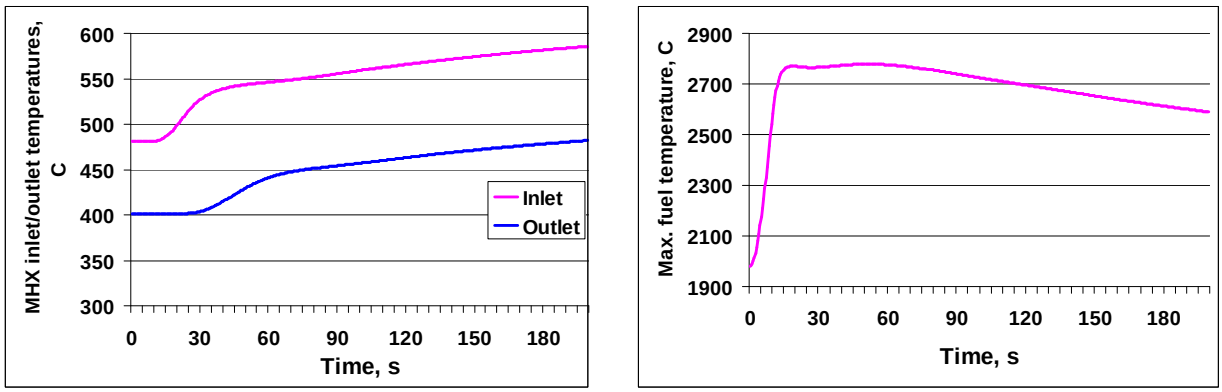


Fig. 5.1.2-2: Evolutions of SG inlet/outlet temperatures (left) and the maximum fuel temperature (right) with time

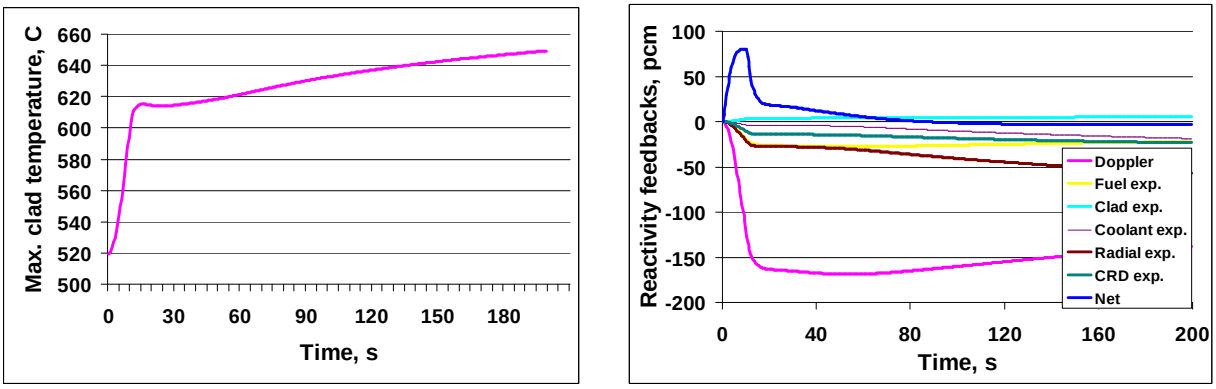


Fig. 5.1.2-3 Evolutions of the maximum clad temperature (left) and reactivity feedbacks (right) with time

Around 12 seconds into the UTOP transient, the power of SG also increases and eventually stabilizes at around 370 MW, which is equal to 123% of its initial level. As shown in Fig. 5.1.2-1, 5.1.2-2 and 5.1.2-3, the coolant temperatures at core inlet/outlet, SG inlet/outlet, and maximum clad temperature will continuously increase after 200 seconds into the transient, since heat removing capability provided by MHX is obviously lower than that of the reactor core. However, thanks to negative reactivity feedbacks, the net reactivity become slightly negative around 100 seconds into the transient, which leads to the slow reduction of the maximum fuel temperature as shown in Fig. 5.1.2-2. Furthermore, it can be noticed that the maximum fuel temperature in the hottest pin that can be achieved during UTOP is around 2770 ^{o}C, which is close to the working limit of MOX fuel (melting point).

5.1.3 TR-4 transient: TRACE results (JRC-IET)

The UTOP transient is initiated by the reactivity insertion of 250 pcm during 10 seconds. This leads to net positive reactivity in the initiation phases of the transient, resulting in an increase of the core power and correspondingly also coolant and structure temperatures. As it can be seen in Fig. 5.1.3-1, the reactivity insertion initiates a power excursion up to a value of 730 MWth (243% Pnom). As this transient is unprotected, the system evolves to a new equilibrium state at higher power (~400 MW).

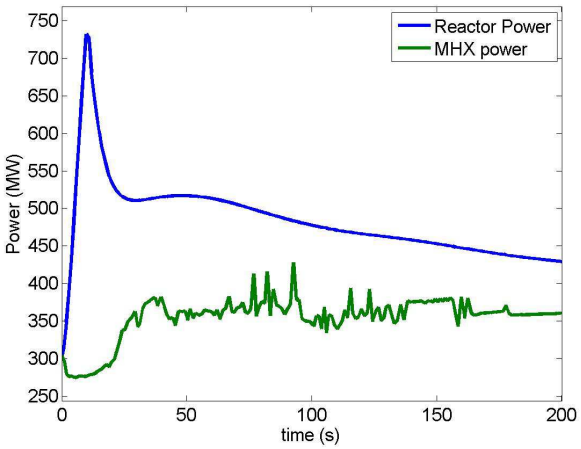


Fig. 5.1.3-1: Core and MHX power trace – UTOP

Fig. 5.1.3-2 shows that the increase in the temperature of the primary lead is limited as the heat transfer to the secondary side in the MHX also increases in a constant rate all along the transient.

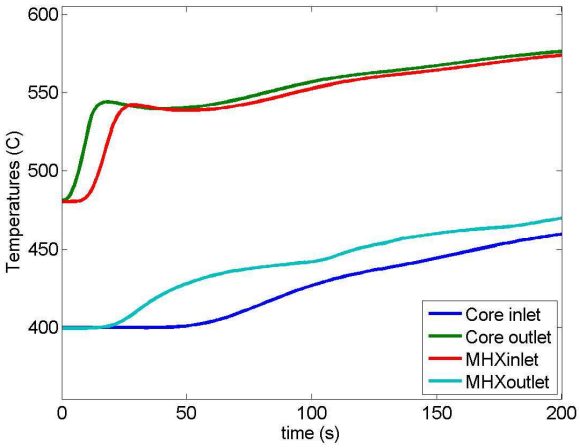


Fig. 5.1.3-2: Coolant temperatures – UTOP

A maximum fuel temperature (Fig. 5.1.3-3) of about 3000 °C is predicted in the hot fuel assembly, which is already above the melting temperature of the mixed-oxide fuel. Consequently, fuel melting in the centre of the fuel pellet is to be expected. The maximum cladding temperature is of 625 °C.

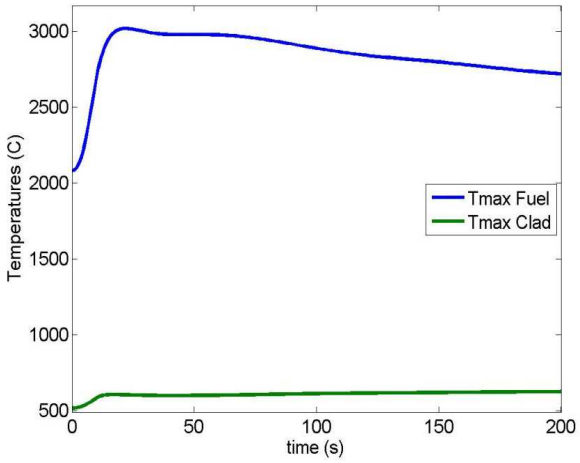


Fig. 5.1.3-3: Fuel & cladding temperatures – UTOP

The reactivity feedback components following the transient evolution are shown in Fig. 5.1.3-4. The initial positive reactivity due to the reactivity insertion of 250 pcm in 10 seconds is thereafter counterbalanced mainly by negative reactivity feedbacks due to the Doppler effect and fuel expansion, together with the radial core expansion and the control rod driveline expansion, the contribution of the latter being however relatively small.

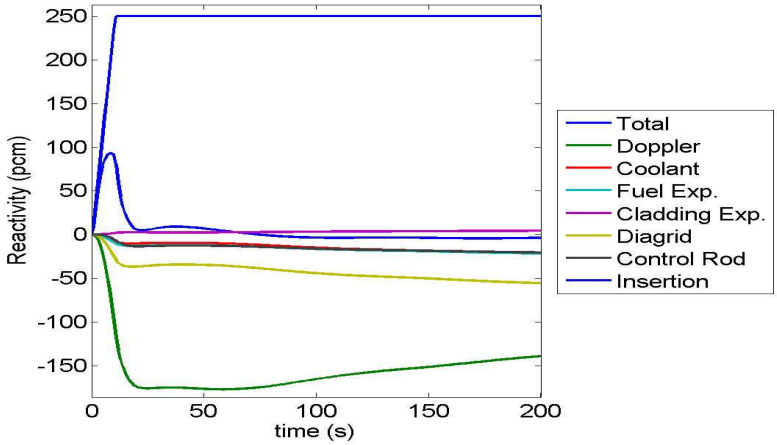


Fig. 5.1.3-4: Reactivity feedback evolution - UTOP

5.1.4 TR-4 transient: RELAP5 results (ENEA)

This transient is initiated by a reactivity insertion of 250 pcm in 10 s without reactor scram. The primary and secondary circuits remain in operation in forced circulation. No feedwater control is performed on the secondary side. The main results of the TR-4 transient analysis are illustrated in Fig. 5.1.4-1.

The reactivity insertion of 250 pcm is mainly counterbalanced by prompt and negative Doppler effect as shown in Fig. 5.1.4-1a. The fuel expansion feedback is rather limited, since the fuel-clad linked effect has been considered in this analysis, because of the large fuel temperature increase, which leads to almost complete closure of the fuel rod gap. The total core reactivity reaches a maximum of 85 pcm after 10 s and then reduces. The core power shows a maximum of 680 MW at t = 10 s and then progressively reduces (Fig. 5.1.4-1b), while the power removed by the secondary side increases due to lead temperature increase at MHX inlet.

The core temperatures evolution is shown in Fig. 5.1.4-1c. The maximum clad temperature suddenly rises up to ~600 °C in 10 s and then progressively increases up to 627 °C in 200 s, following temperature increase at core inlet. The more critical issue in this transient is the fuel maximum temperature that approximates 2930 °C after 50 s and then progressively reduces down to 2725 °C at 200 s (Fig. 5.1.4-1d). However, this is the hottest point located in the centre of the fuel pellet of the hottest FA around the middle core plane. For this reason, only local fuel melting is expected in the hottest FAs, and thus extended fuel melting can be excluded.

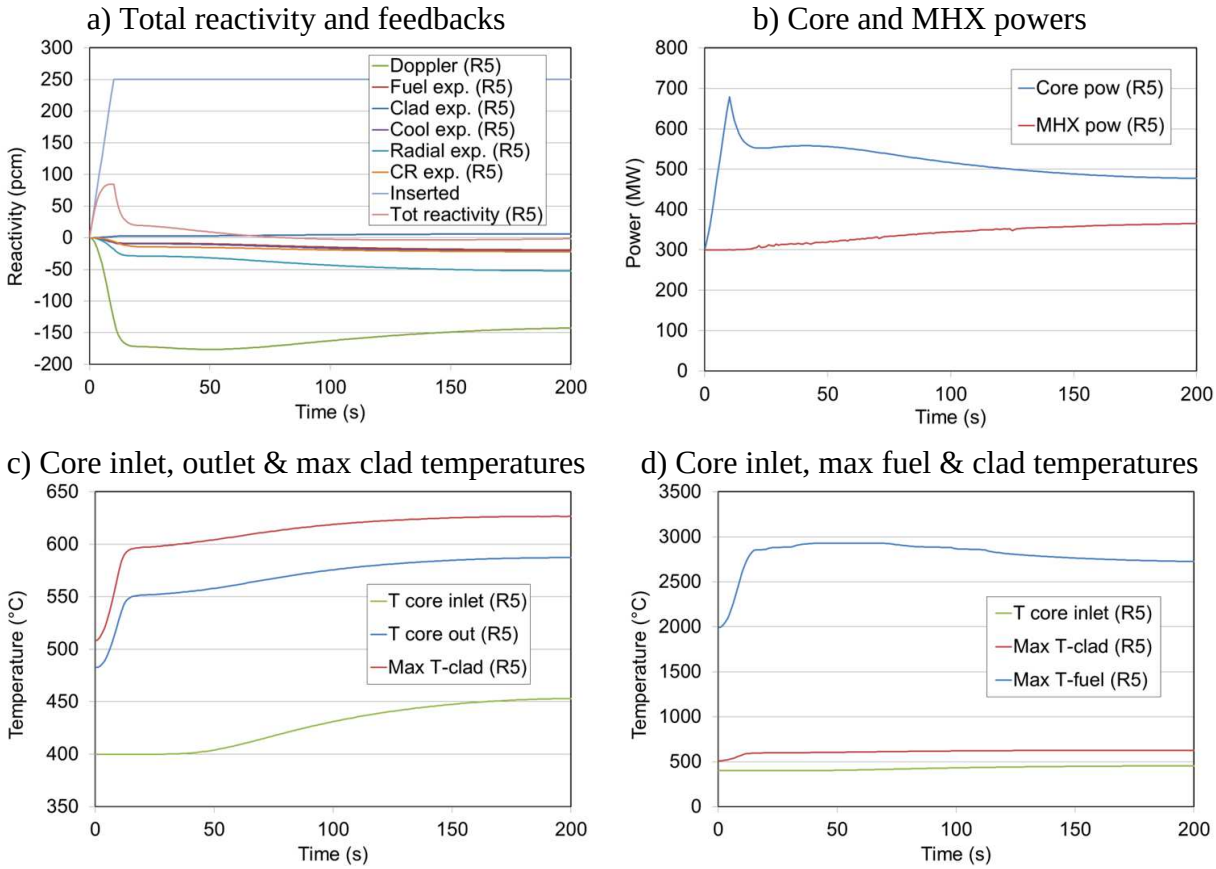


Fig. 5.1.4-1: Main RELAP5 results of the TR-4 transient

5.1.5 TR-4 transient: CATHARE results (ENEA/CEA)

This transient is initiated by a reactivity insertion of 250 pcm in 10 s without reactor scram. The primary and secondary circuits remain in operation in forced circulation. No feedwater control is performed on the secondary side. The main results of the TR-4 transient analysis are illustrated in Fig. 5.1.5-1.

The reactivity insertion of 250 pcm is mainly counterbalanced by prompt and negative Doppler effect as shown in Fig. 5.1.5-1a. The fuel expansion feedback is rather limited, since the fuel-clad linked effect has been considered in this analysis, because of the large fuel temperature increase, which leads to almost complete closure of the fuel rod gap. The total core reactivity reaches a maximum of 93 pcm after 10 s and then reduces. The core power shows a maximum of 735 MW at t = 10 s and then progressively reduces (Fig. 5.1.5-1b), while the power removed by the secondary side increases due to lead temperature increase at MHX inlet.

The core temperatures evolution is shown in Fig. 5.1.5-1c. The maximum clad temperature suddenly rises up to ~620 °C in 10 s and then progressively increases up to 635 °C in 200 s, following temperature increase at core inlet. The more critical issue in this transient is the fuel maximum temperature that approximates 2870 °C after 50 s and then progressively reduces down to 2660 °C at 200 s (Fig. 5.1.5-1d). However, this is the hottest point located in the centre

of the fuel pellet of the hottest FA around the middle core plane. For this reason, only local fuel melting is expected in the hottest FAs, and thus extended fuel melting can be excluded.

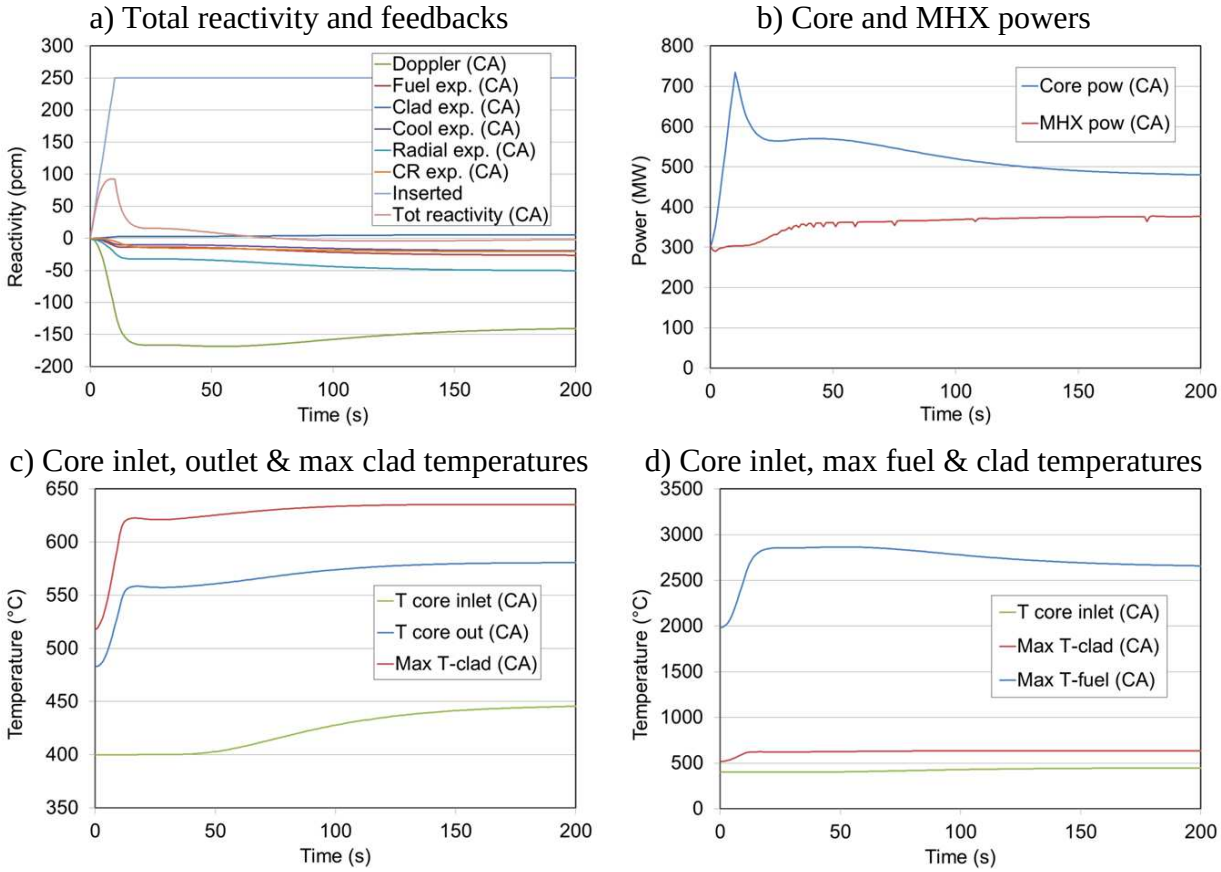


Fig. 5.1.5-1: Main CATHARE results of the TR-4 transient

5.1.6 TR-4 transient: SPECTRA results (NRG)

The Unprotected Transient Over-Power (UTOP) scenario is as follows:

- Reactivity of 250 pcm (0.7463 $) is inserted in 10 seconds.
- Reactor trip (scram signal) is disabled.
- Fuel-clad linked effect - fuel expansion according to linked effect with clad temperature.

In this transients all loops are symmetrical. The model with all loops combined into one is used. The NRG SPECTRA results are shown in Fig. 5.1.6-2 through Fig. 5.1.6-5.

Core power is shown in Fig. 5.1.6-2. The core power reaches 645 MW and decreases to about 460 MW.

Fuel temperatures are shown in Fig. 5.1.6-3. The maximum fuel temperature reaches 2856 °C at 57 s. The maximum fuel temperature exceeds for a short period the melting temperature (MOX melting point ~2670 °C). Only local fuel melting is expected (~ 1 mm) – Fig. 5.1.6-1.

Coolant and cladding temperatures are shown in Fig. 5.1.6-4. The maximum cladding temperature remains below 650 °C the core outlet temperature slowly increases following the temperature increase at core inlet.

The total reactivity as well as the reactivity feedbacks are shown in Fig. 5.1.6-5. The inserted reactivity is counterbalanced mainly by negative Doppler effect induced by fuel temperature increase. Total reactivity reaches a maximum of about 80 pcm at 10 s and then reduces due to negative feedbacks.

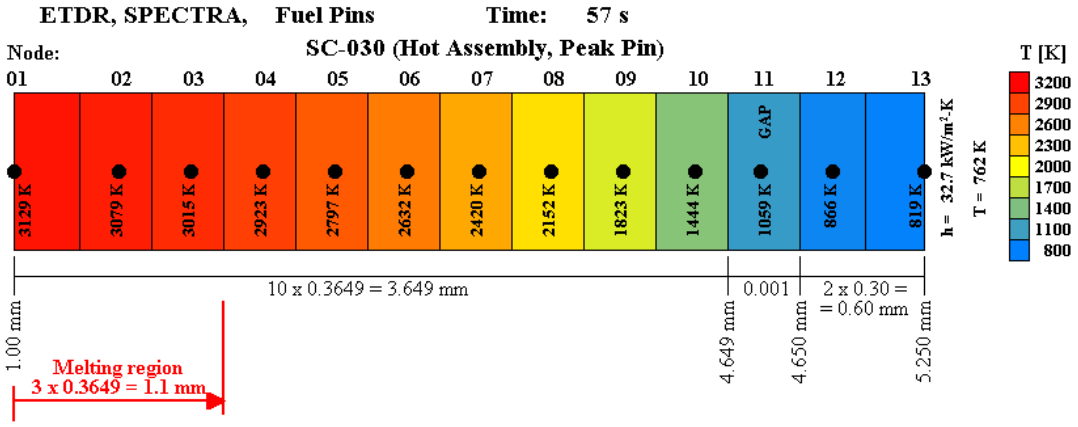


Fig. 5.1.6-1: Maximum fuel temperatures, SPECTRA

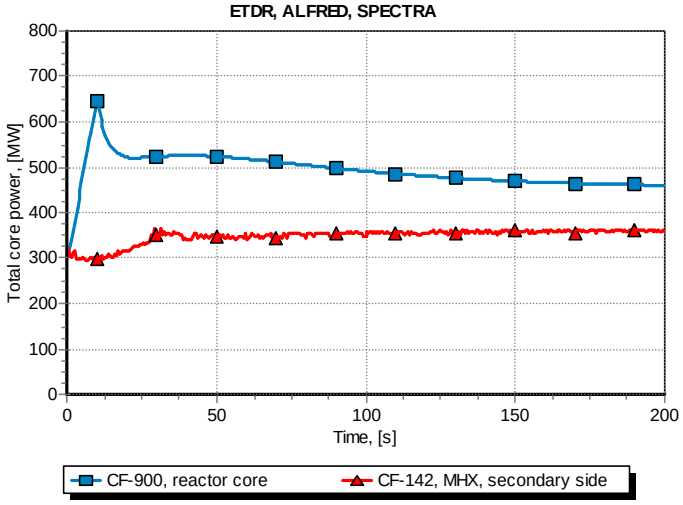


Fig. 5.1.6-2: Core and MHX powers

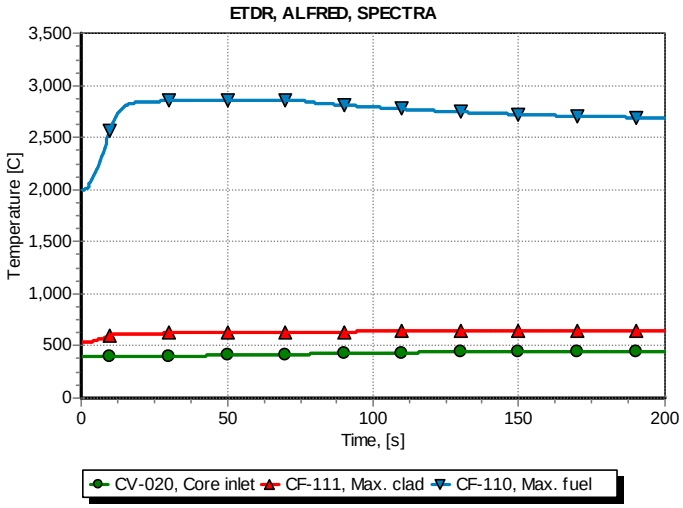


Fig. 5.1.6-3: Core inlet, max clad and fuel temperatures

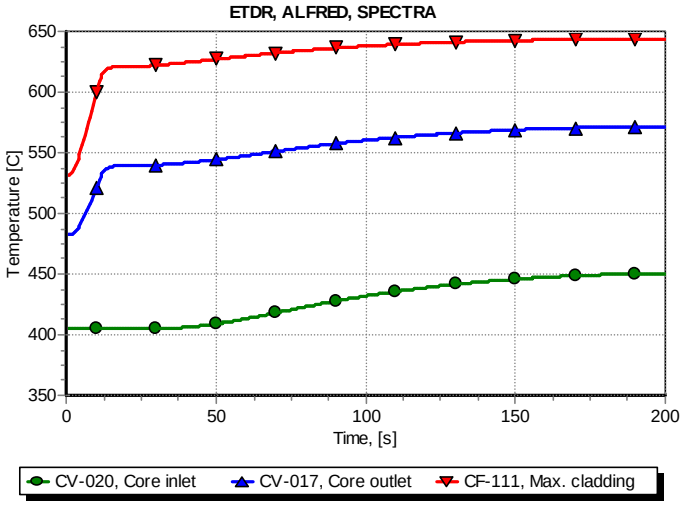


Fig. 5.1.6-4: Coolant and max clad temperatures

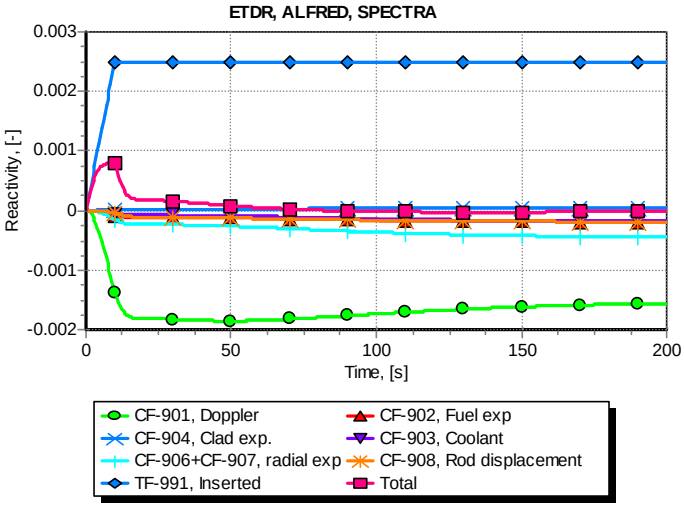


Fig. 5.1.6-5: Total reactivity and feedbacks

5.2 T-DEC1: Unprotected loss of flow (ULOF)

The unprotected loss of flow transient (ULOF) foresees the loss of power supply to all primary pumps and then their simultaneous coastdown. The reactor scram is assumed to fail and then the core power evolution is driven by reactivity feedbacks. In the present analyses the secondary circuits are supposed to remain in operation in nominal condition with no control of the feedwater flow rate.

This transient has been analyzed by several partners using different codes: KIT-G with SIM-LFR at BOC and EOC conditions, PSI with TRACE/FRED, JRC-IET with TRACE, ENEA with RELAP5, ENEA/CEA with CATHARE, NRG with SPECTRA, KTH with RELAP5 and CIRTEN with RELAP5 at EOC conditions. The main results of these analyses are presented in the following subsections.

5.2.1 T-DEC1 transient: SIM-LFR results (KIT-G)

For these calculations all primary pumps are assumed to fail simultaneously and the secondary heat transport system is assumed fully functional (forced convection mode). The reactor shut-down systems are also assumed to fail. The coast-down characteristics of the primary pumps (or primary system mass flow rate) subsequent to pump failure was presumed to correspond to the flow rate characteristics as calculated by SIM-LFR implying a flow undershoot down to ~19% nominal flow ~ 6 sec after the transient initiation, and a recovery to the natural convection asymptotic flow fraction of ~ 24 % ~ 60 sec after the flow undershoot minimum.

Two cases were analyzed to investigate the clad and fuel temperature response of the peak pin and the likelihood of peak pin clad rupture during the flow undershoot, namely at BOC and EOC core state conditions.

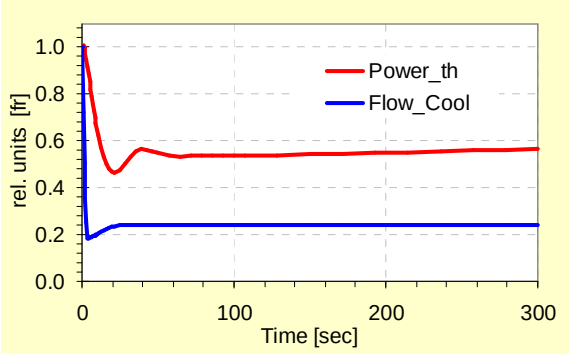
Under BOC conditions, the fuel temperature of the peak pin are the highest at the beginning of the transient (~2030 ^{o}C), but later, due to reactor power decrease caused by the negative reactivity feedback effects, the fuel temperature decreases. Clad temperature of the peak pin, due to the coolant flow undershoot increases from 516 ^{o}C up to 738 ^{o}C (Fig. 5.2.1-1b) at transient time t = 17.8 sec during the ULOF transient. At the same time point minimum clad failure time of the peak pin decreases to 4.7E+5 sec (Fig. 5.2.1-1d), but later, when the coolant flowrate increases to ~ 24% of nominal, increases to ~ 3.7E+8 sec. During this transient, due to reactor power suppression by the negative reactivity feedback effects (Fig. 5.2.1-1c), the reactor power level decreases down to ~56% for BOC conditions (see Fig. 5.2.1-1a).

Under EOC conditions, the fuel temperature of the peak pin are the highest at the beginning of the transient (~2064 ^{o}C), but later, due to reactor power decrease caused by the negative reactivity feedback effects, fuel temperature decreases. Clad temperature of the peak pin, due to the coolant flow undershoot increases from 514 ^{o}C up to 751 ^{o}C (Fig. 5.2.1-2b) at transient time t = 17.8 sec during the ULOF transient. At the same time point minimum clad failure time of the peak pin decreases to 1.6E+5 sec (Fig. 5.2.1-2d), but later, when the coolant flowrate increases to ~ 24% of the nominal, increases to ~ 7.8E+7 sec. During this transient, due to reactor power suppression by the negative reactivity feedback effects (Fig. 5.2.1-2c), the reactor power level decreases down to ~ 60% for EOC core conditions (see Fig. 5.2.1-2a).

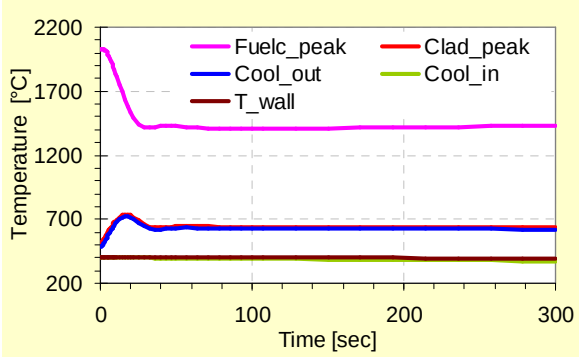
The coast-down characteristics of the primary system mass flow rate are governed by the coast-down, inertial characteristics of the pump, and are thus independent of the burn-up state of the core. The asymptotic natural convection flow rate is ~ 24%, as is determined by the heights differential between the mid-planes of core and the heat exchanger, as well as the pressure drop characteristics of the entire primary cooling system. As both of these parameters do not change during the burn-up of the plant, core temperatures during the ULOF transient are thus primarily determined by the flow undershoot that must be expected during flow coast-down before the asymptotic natural convection flow rate is attained. It must be stated, that the SIM-LFR calculated flow undershoot is an estimation based on RELAP5 calculations of the same transient performed by ENEA. The actual flow characteristic of the ALFRED primary cooling system during pump-coast down can only be determined to a higher degree of confidence in case of experimental measurements of the actual primary system layout. CFD-type calculations should be able to narrow down the current uncertainty in the estimation of the flow undershoot for the ALFRED.

Of particular importance are the calculated fuel and cladding temperatures during the ULOF transient since the ALFRED primary system was specifically designed with the intention of being able to accommodate the ULOF transient without significant pin failures. Thus, it is important to estimate the minimum clad failure time for the peak pin during the ULOF transient. That’s why this important investigation was performed during the ALFRED safety analysis. The analysis showed, that at transient time t ~ 17.8 sec minimum clad failure time of the peak pin decreases to ~1.6E+5 sec at the minimum, thus clad failure (rupture) should not be expected during ULOF transient.

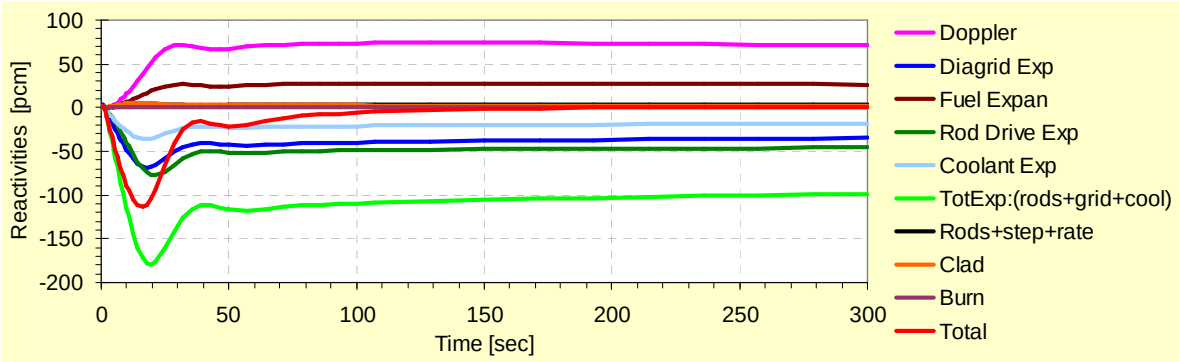
This clearly demonstrates, that the clad of the peak pins of the ALFRED has a very large margin to clad failure (rupture), that is primarily due to the relatively high Pb natural convection core mass flow rate of ~ 24% nominal and the relatively low fission gas pin pressure at EOC of ~ 20 bar during ULOF conditions.



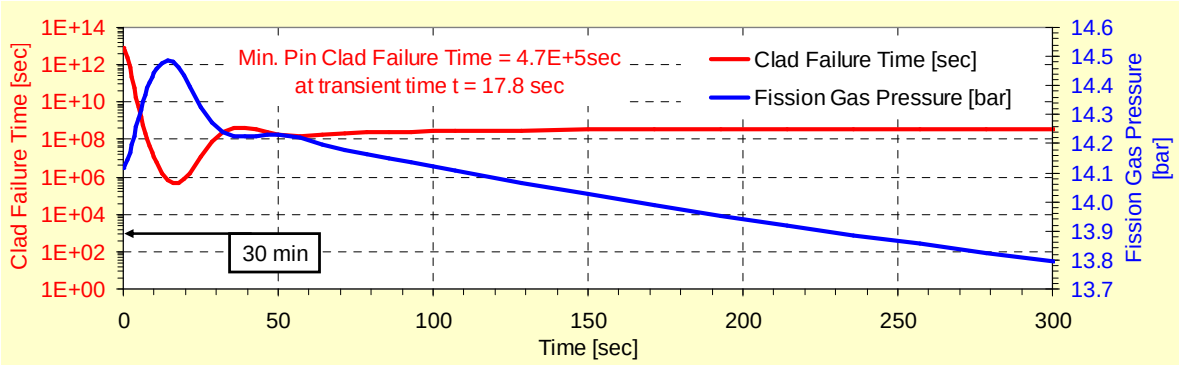
a) Relative core thermal power and flow rate



b) Peak fuel-, clad-, coolant- and vessel wall temperatures

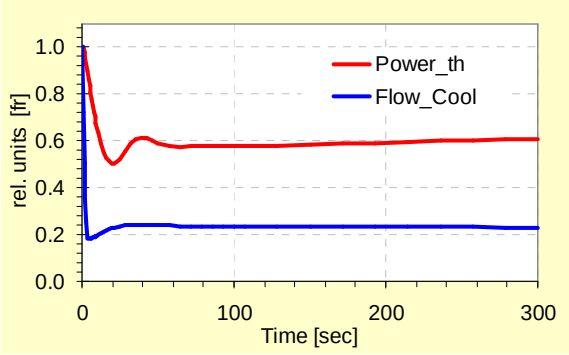


c) Reactivity effects

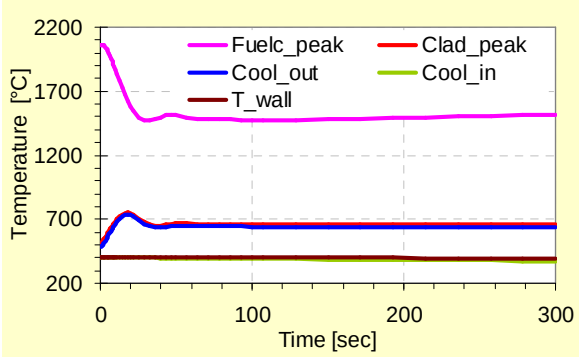


d) Peak pin fission gas pin pressure and clad failure time

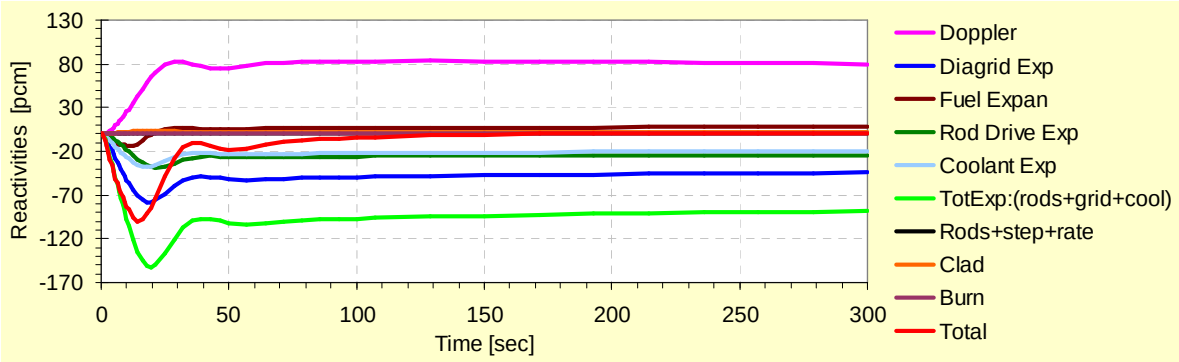
Fig. 5.2.1-1: Results for T-DEC1: (ULOF) transient at BOC conditions at an average burnup of 730 EFPD as calculated by SIM-LFR (KIT)



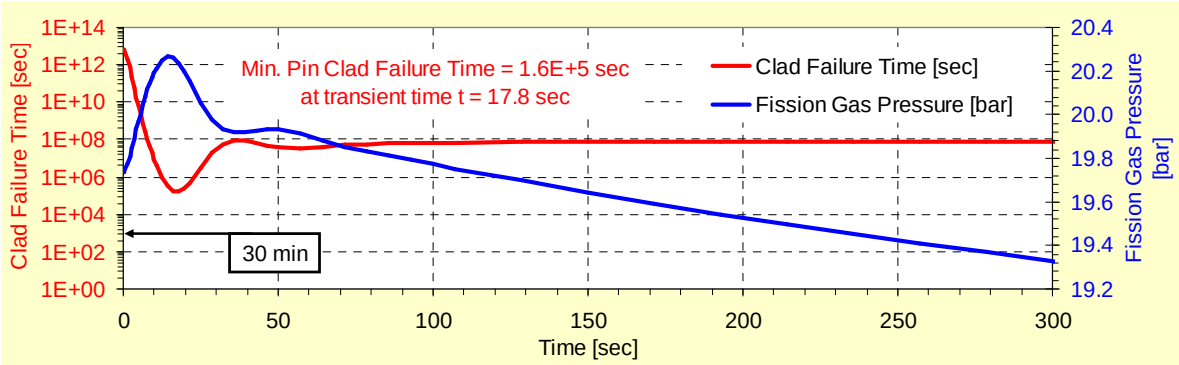
a) Relative Core Thermal Power and Flow rate



b) Peak fuel-, clad-, coolant- and vessel wall temperatures



c) Reactivity effects



d) Peak Pin Fission Gas Pin Pressure and Clad Failure Time

Fig. 5.2.1-2: Results for T-DEC1: (ULOF) transient at EOC conditions at an average burnup of 1095 EFPD as calculated by SIM-LFR (KIT)

Finally, under BOC and EOC conditions, the ULOF transient in the ALFRED can be accommodated, implying minimum clad failure time of ~1.6E+5 sec under the minimum coolant flow conditions (flow undershoot conditions). Taking this fact into account one can state that the ULOF transient is not a critical transient for the ALFRED plant.

5.2.2 T-DEC1 transient: TRACE/FRED results (PSI)

The Unprotected Loss of Flow (ULOF) accident was initiated by the drop of primary pump head with the halving time of 0.56 second. During the whole ULOF transient, the scram

protection system fails to work, but the MHX and secondary circuits of the plant work normally.

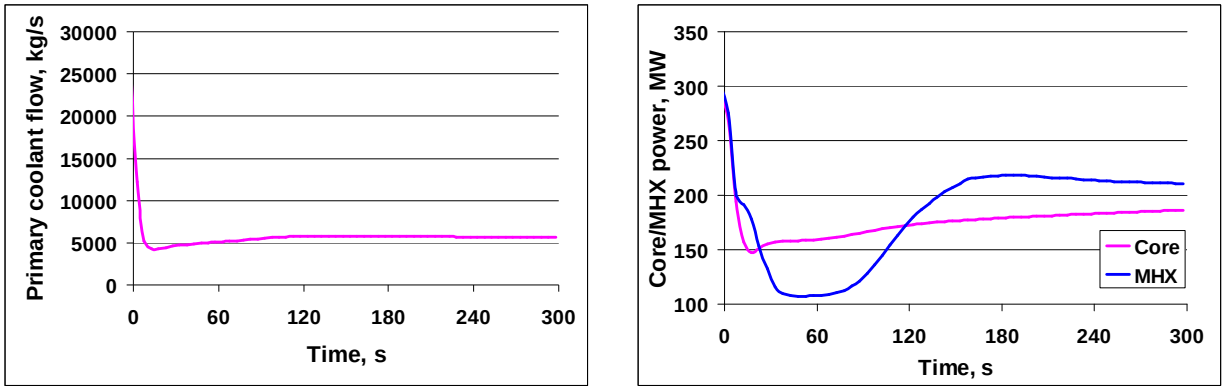


Fig. 5.2.2-1: Evolutions of primary coolant flowrate (left) and core/MHX power (right) with time

As the primary coolant flowrate starts to decrease (Fig. 5.2.2-1), the core power first has a small increase up to around 305 MW because of positive reactivity feedback coolant temperature will increase due to less flow rate provided. Then, after the coolant temperature increase moves to the diagrid and pad, a big negative reactivity feedback incurred by the radial expansion of diagrid and pad will be generated as shown in Fig. 5.2.2-3. This negative feedback, together with other negative reactivity responses incurred by fuel axial expansion and the Doppler effect, may take over the positive reactivity feedback caused by coolant density decrease, which leads to the reduction of core power, as well as coolant temperatures and temperatures of fuel and clad.

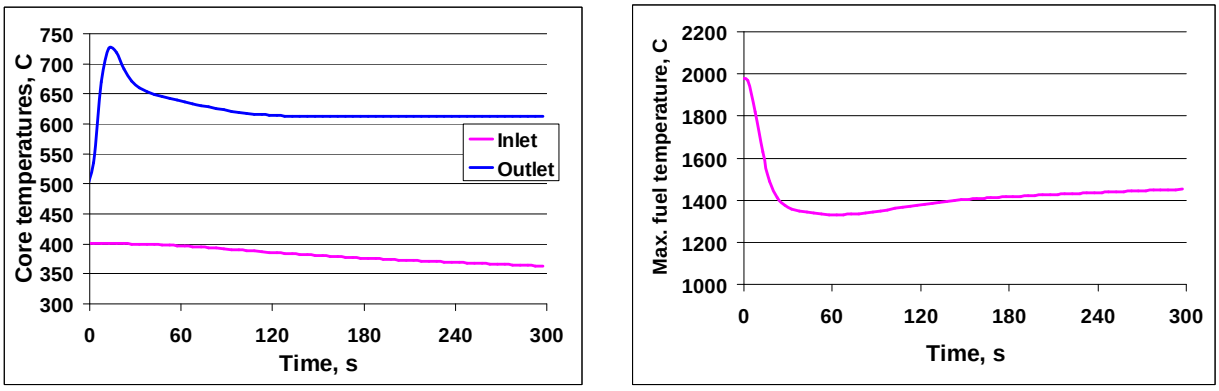


Fig. 5.2.2-2: Evolutions of core inlet/outlet temperature (left) and the maximum fuel temperature (right) with time

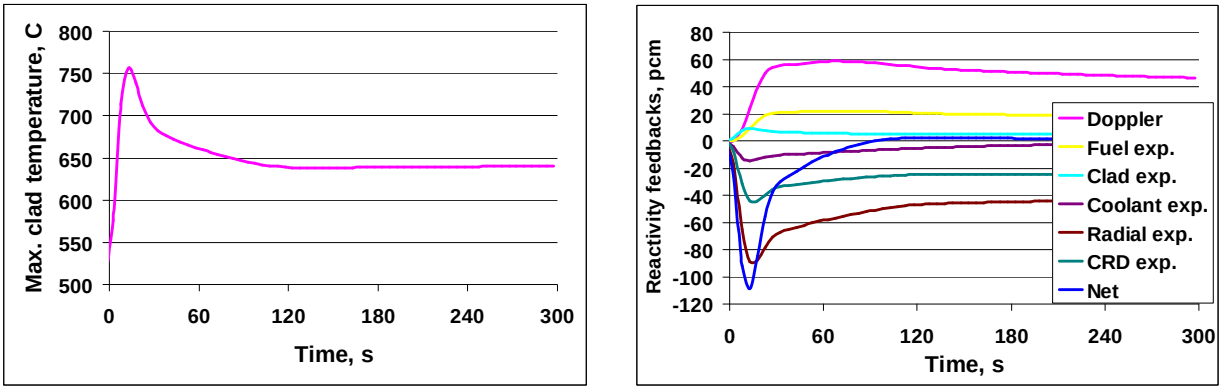


Fig. 5.2.2-3 Evolutions of the maximum clad temperature (left) and reactivity feedback (right) with time

The maximum temperatures of fuel and clad will decrease slowly because of the higher MHX power comparing to the core power after around 120 seconds. The highest temperatures that can be achieved by fuel and clad of the peak fuel pin during ULOF are 1977 ^{o}C and 756 ^{o}C respectively (Fig. 5.2.2-2), which are certainly lower than their own working limits.

5.2.3 T-DEC1 transient: TRACE results (JRC-IET)

The ULOF transient is initiated by the coast-down of all primary pumps. Consequently, the system gradually evolves in a continuous decrease of primary coolant mass flow rate until the natural convection process takes over. The natural circulation core mass flow rate is of 5420 kg/s (21% of the nominal value). Fig. 5.2.3-1 shows this core mass flow rate evolution. The secondary circuits remain in operation in forced circulation.

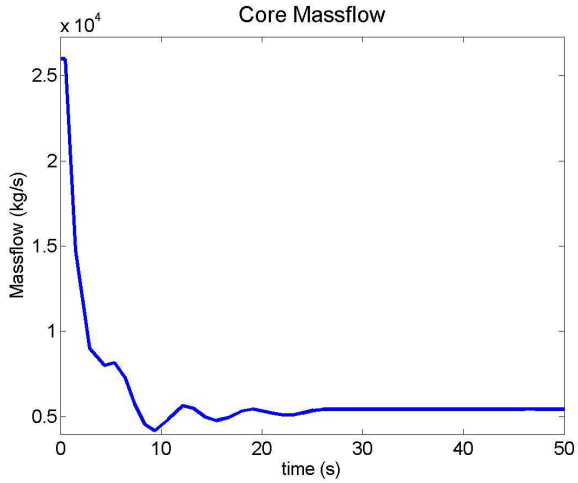


Fig. 5.2.3-1: Core mass flow rate - ULOF

As it can be seen in Fig. 5.2.3-2 the transient is characterized by an abrupt increase of the primary coolant temperatures as a consequence of the reduced coolant mass flow through the core.

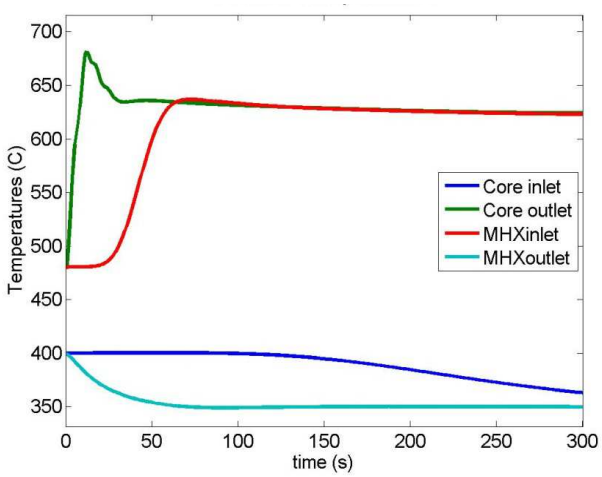


Fig. 5.2.3-2: Coolant temperatures in the core inlet and outlet (hot fuel assembly) and in the MHX inlet and outlet - ULOF

The maximum fuel and cladding temperature is shown in Fig. 5.2.3-3. Even though the reduced coolant mass flow results in an abrupt increase in the cladding temperature (Tmax 782°C), the safety margins can be maintained during the transient and no deterministic clad ruptures are to be expected. Equally, safety margins can be kept with respect to fuel melting or coolant boiling.

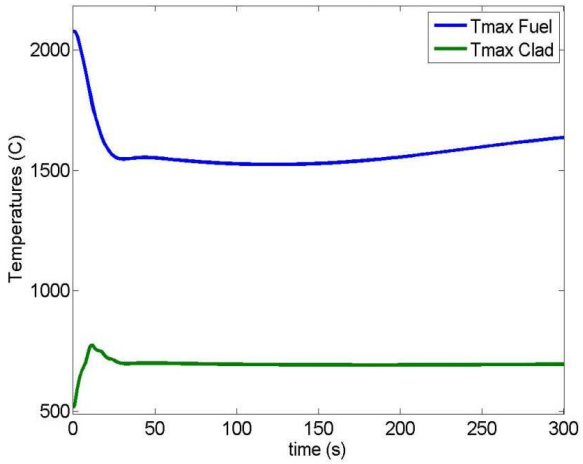


Fig. 5.2.3-3: Fuel and cladding temperatures for the hot fuel assembly - ULOF

This increase in temperatures of coolant and structures implies the insertion of reactivity feedbacks (Fig. 5.2.3-4), out of which dominating is the negative feedback due to the diagrid (radial) expansion. The control rod (due to the driveline expansion) and the coolant expansion effects also introduce negative reactivity, which leads to further decrease of the net reactivity. In the longer term, however, as a consequence of decreased fuel temperatures, the positive reactivity insertion is observed due to the Doppler and fuel expansion reactivity feedbacks.

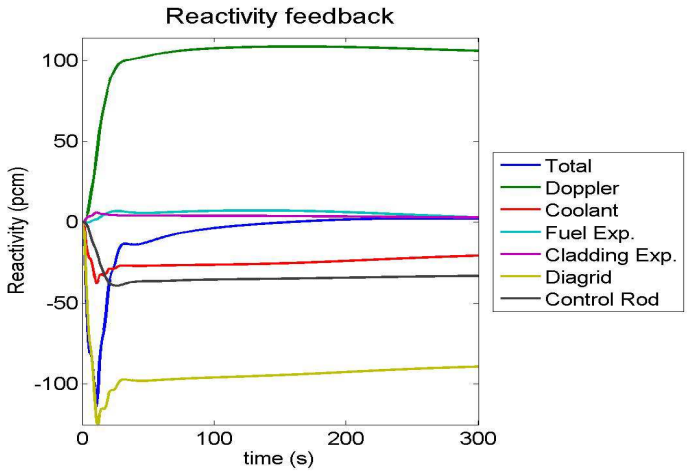


Fig. 5.2.3-4: Reactivity feedback evolution - ULOF

Fig. 5.2.3-5 shows the core power evolution during the transient. As a consequence of the reactivity evolution, the core is subcritical during the first seconds into the transient with a remarkable decrease in power, after which the core power slowly attains a new equilibrium state at about 180 MWth (60% Pnom).

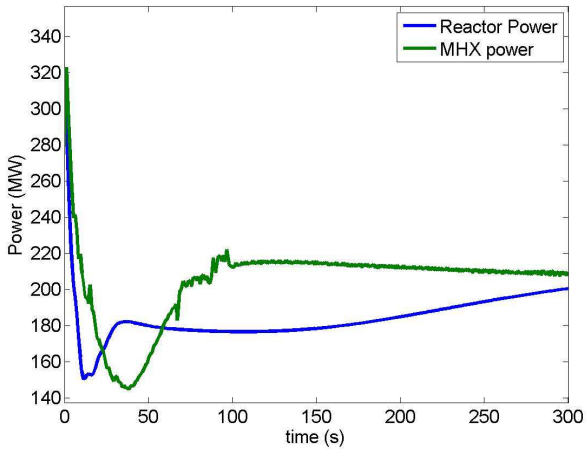


Fig. 5.2.3-5: Core and MHX power evolution - ULOF

Thus, the analyses show that the ALFRED design is robust with respect to a ULOF transient providing sufficient grace times for corrective actions to be taken to terminate the transient.

5.2.4 T-DEC1 transient: RELAP5 results (ENEA)

This transient is initiated by the loss of all primary pumps at t = 0 s without reactor scram. The secondary circuits remain operational in forced circulation providing a nominal feedwater flowrate at the SG inlet and a constant steam pressure at the SG outlet. The main results of the T-DEC1 transient analysis are illustrated in Fig. 5.2.4-1.

The simultaneous coastdown of all primary pumps leads to the transition from forced to natural circulation in the primary circuit. The choice by design of low pressure loss through the core and the whole primary circuit (1.0 bar and 1.5 bar in normal operation, respectively), connected

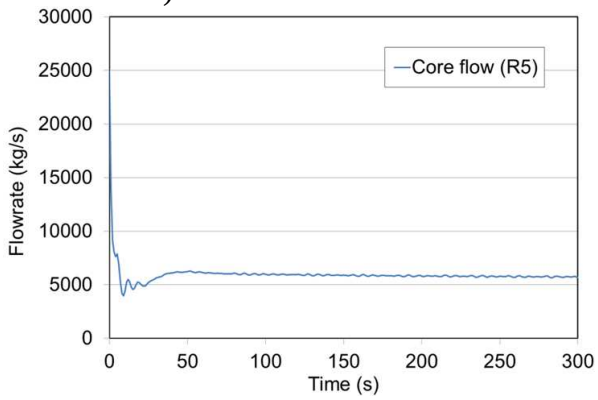
with the differential height between the mid-planes of the core and SGs, favours the establishment of natural convection in the primary circuit, and thus limits the core temperatures rise during the ULOF transient.

As calculated by the RELAP5 code, after a small initial core flowrate undershoot related to the equalization of the lead free levels inside the reactor vessel, the natural circulation flowrate through the core stabilizes at ~5800 kg/s (~23% of nominal value) as it is shown in Fig. 5.2.4-1a. The resulting core temperature rise and corresponding negative reactivity feedback effects (due to the expansion of FA spacer pads, coolant and control rod drivelines, see Fig. 5.2.4-1e) leads to a progressive reduction in the core power, which stabilizes at ~200 MW after t = 300 s (Fig. 5.2.4-1b) and later on tends to come into equilibrium with the power removed by the secondary circuits.

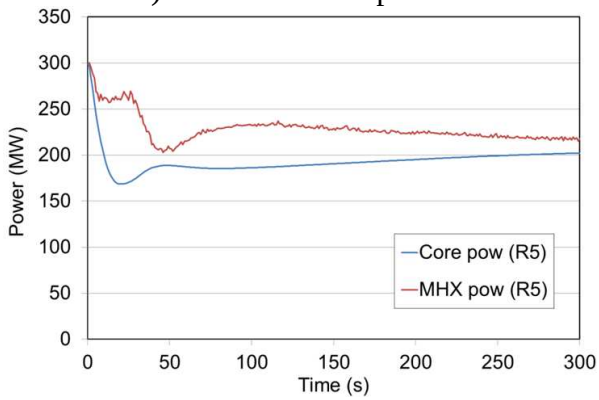
Because of the initial core flow rate undershoot, the clad temperature of the hottest pin increases from 508 °C up to 764 °C at t = 10 s, and then decreases down until stabilizing below 650 °C (Fig. 5.2.4-1c). Due to the very low amplitude of the initial clad temperature peak, clad failures are not expected during the ULOF transient. The peak fuel temperature reduces during the transient, according to the core power decrease, from the initial value of ~2000 °C down to ~1550 °C (Fig. 5.2.4-1d).

Of particular importance are the rather low calculated fuel and cladding temperatures during the ULOF transient, since the ALFRED primary system was specifically designed with the intention of being able to accommodate the ULOF transient without significant pin failures.

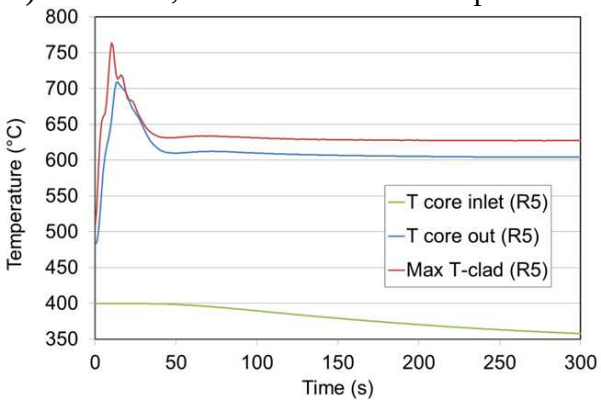
a) Active core flow rate



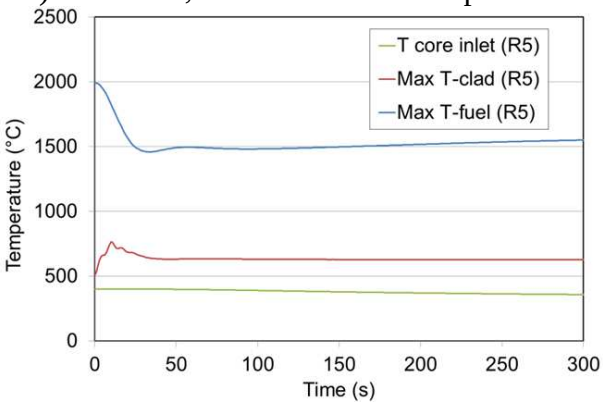
b) Core and MHX powers



c) Core inlet, outlet & max clad temperatures



d) Core inlet, max fuel & clad temperatures



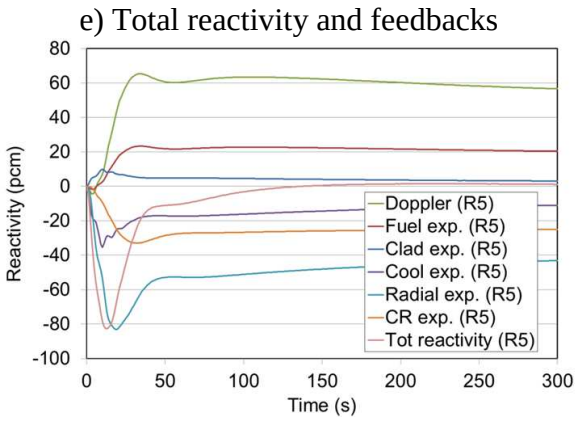


Fig. 5.2.4-1: Main RELAP5 results of the T-DEC1 transient

5.2.5 T-DEC1 transient: CATHARE results (ENEA/CEA)

This transient is initiated by the loss of all primary pumps at t = 0 s without reactor scram. The secondary circuits remain operational in forced circulation providing a nominal feedwater flowrate at the SG inlet and a constant steam pressure at the SG outlet. The main results of the T-DEC1 transient analysis are illustrated in Fig. 5.2.5-1.

The simultaneous coastdown of all primary pumps leads to the transition from forced to natural circulation in the primary circuit. The choice by design of low pressure loss through the core and the whole primary circuit (1.0 bar and 1.5 bar in normal operation, respectively), connected with the differential height between the mid-planes of the core and SGs, favours the establishment of natural convection in the primary circuit, and thus limits the core temperatures rise during the ULOF transient.

As calculated by the RELAP5 code, after a small initial core flowrate undershoot related to the equalization of the lead free levels inside the reactor vessel, the natural circulation flowrate through the core stabilizes at ~5800 kg/s (~23% of nominal value) as it is shown in Fig. 5.2.5-1a. The resulting core temperature rise and corresponding negative reactivity feedback effects (due to the expansion of FA spacer pads, coolant and control rod drivelines, see Fig. 5.2.5-1e) leads to a progressive reduction in the core power, which stabilizes at ~205 MW after t = 300 s (Fig. 5.2.5-1b) and later tends to come into equilibrium with the power removed by the secondary circuits.

Because of the initial core flow rate undershoot, the clad temperature of the hottest pin increases from 508 °C up to 728 °C at t = 10 s, and then decreases down until stabilizing at 654 °C (Fig. 5.2.5-1c). Due to the very low amplitude of the initial clad temperature peak, clad failures are not expected during the ULOF transient. The peak fuel temperature reduces during the transient, according to the core power decrease, from the initial value of ~2000 °C down to ~1640 °C (Fig. 5.2.5-1d).

Of particular importance are the rather low calculated fuel and cladding temperatures during the ULOF transient, since the ALFRED primary system was specifically designed with the intention of being able to accommodate the ULOF transient without significant pin failures.

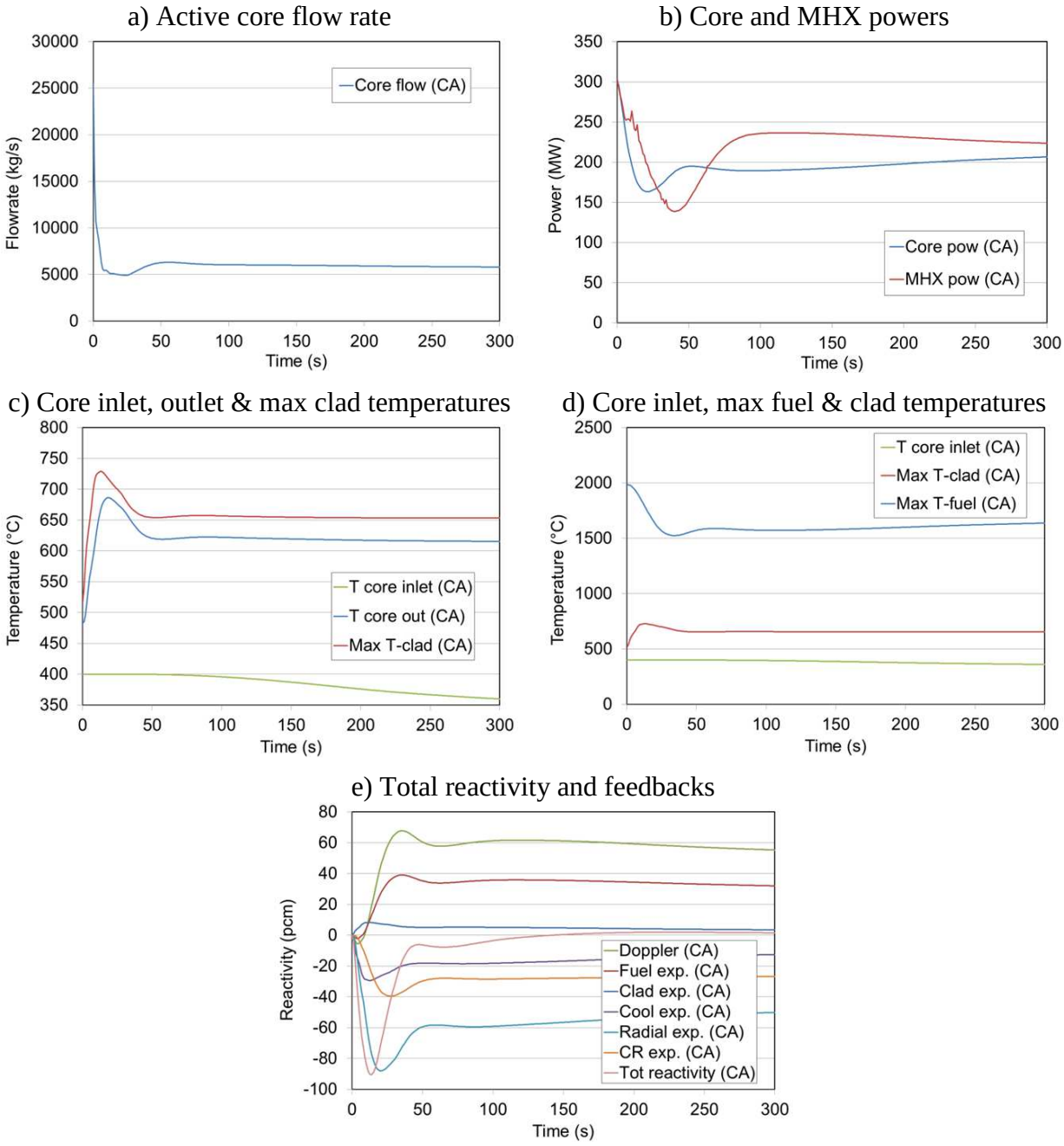


Fig. 5.2.5-1: Main CATHARE results of the T-DEC1 transient

5.2.6 T-DEC1 transient: SPECTRA results (NRG)

The Unprotected Loss of Flow (ULOF) scenario is as follows:

- Coastdown of all primary pumps. Pump speed halving time 0.56 s.
- The secondary circuits remain in operation in forced circulation
- Reactor trip (scram signal) is disabled.

In this transients all loops are symmetrical. The model with all loops combined into one is used. The NRG SPECTRA results are shown in Fig. 5.2.6-1 through Fig. 5.2.6-5.

The core inlet flow is shown in Fig. 5.2.6-1. After an initial small core flow rate undershot natural circulation stabilizes in the primary circuit a little above 5000 kg/s.

The core and MHX powers are shown in Fig. 5.2.6-2. The core power initially reduces due to negative reactivity feedbacks and then stabilizes at about 210 MW, in equilibrium with the MHX power. The MHX power initially decreases due to reduced primary flow and then increases with the lead temperature increase at the MHX inlet.

The fuel, cladding, and core inlet temperatures are shown in Fig. 5.2.6-3. The peak and average fuel temperatures reduce according to the decrease of core power level. The maximum fuel temperature stabilizes at about 1660 ˚C.

The coolant and cladding temperatures are shown in Fig. 5.2.6-4. Initially the maximum core outlet temperature increases. The maximum value is 794 °C. The maximum core outlet temperature stabilizes at about 600 °C. The core inlet temperature slowly decreases, at 300 s it is about 360 °C.

The total reactivity as well as the reactivity feedbacks are shown in Fig. 5.2.6-5. The positive reactivity come from Doppler effect and fuel expansion and is counterbalanced by negative coolant density effect, radial expansion and control rod displacement feedbacks. Total reactivity decreases and reaches a minimum of about –92 pcm at about 10 s and then approaches zero.

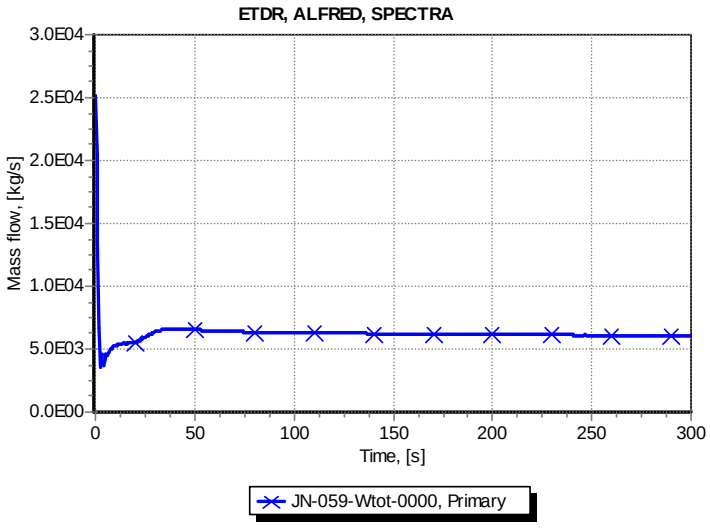


Fig. 5.2.6-1: Primary mass flow rate

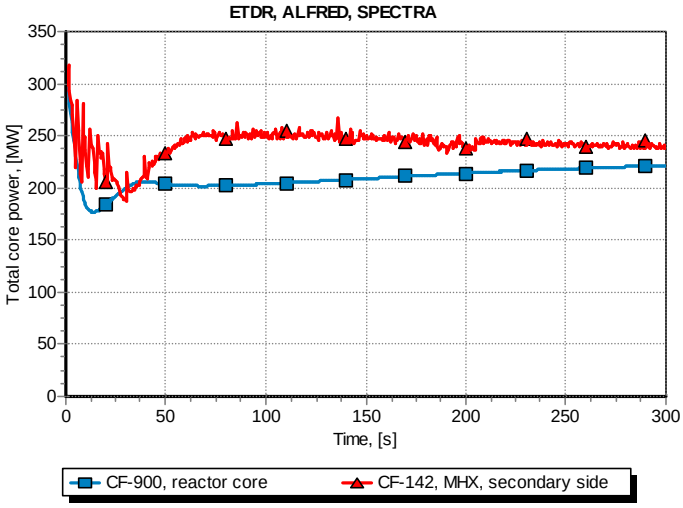


Fig. 5.2.6-2: Core and MHX powers

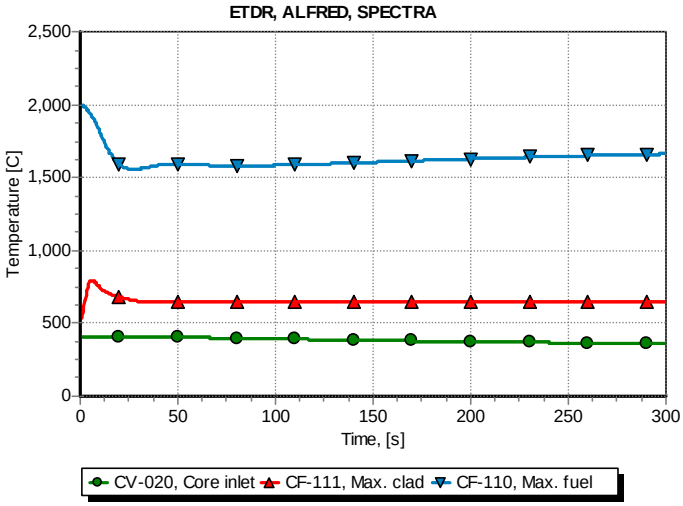


Fig. 5.2.6-3: Fuel, cladding, and core inlet temperatures

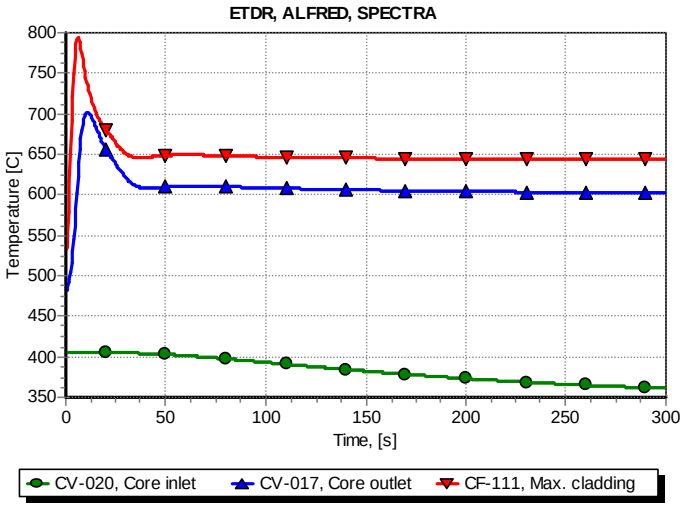


Fig. 5.2.6-4: Coolant and cladding temperatures

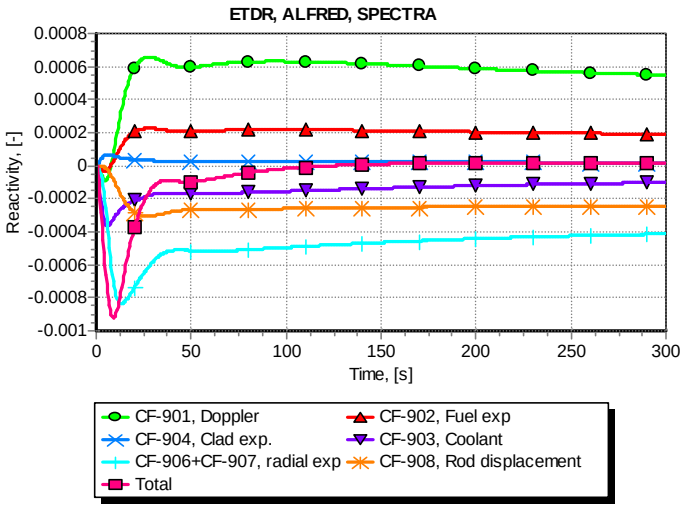
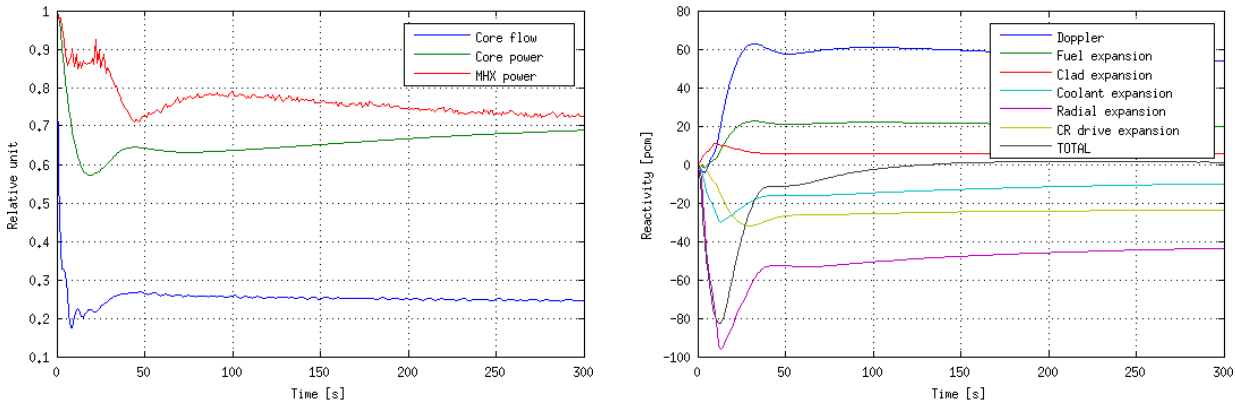


Fig. 5.2.6-5: Total reactivity and feedbacks

5.2.7 T-DEC1 transient: RELAP5 results (KTH)

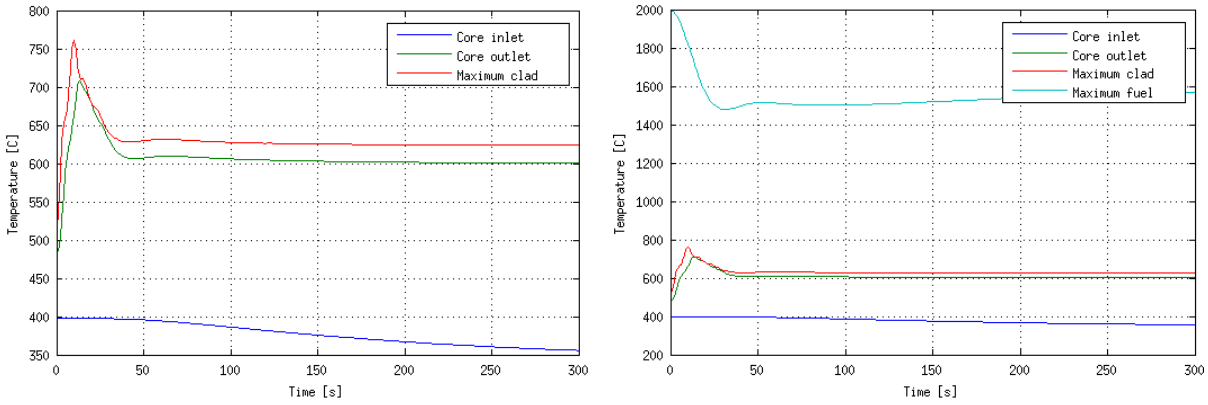
In case of unprotected loss of flow transient, all pumps are tripped at time 0 after a 1000 seconds steady state calculation. Scram signal is deactivated throughout the transient and secondary cooling system is kept operational.



a) b)

Fig. 5.2.7-1: a) Core flow, power and MHX power in relative units -
b) Reactivity components and total feedback for ULOF

The power of the reactor decreases from its initial value of 300 MW down to around 57% in the first 20 seconds as the pumps coast down. This is largely due to the negative reactivity feedback from the radial expansion.



a) b)

Fig. 5.2.7-2: a) Core inlet, outlet and maximum clad temperatures
b) Same with added maximum fuel temperature for ULOF

Core outlet temperature rises steadily from its initial value of 484 °C to about 700 °C and then stabilizes around 600 °C as natural circulation in the system is achieved at around 24% of the nominal mass flow. After about 50 seconds, the inlet temperature of the core starts decreasing. This is the effect of overcooling, as MHX power is still higher than that of the core. The power of the core increases because of the inlet temperature change. In the initial phase of the transient, the maximum fuel temperature decreases rapidly to about 1500 °C and then increases steadily with power.

Based on the simulation results, no cladding or vessel failure is expected in case of ULOF transient.

5.2.8 T-DEC1 transient: RELAP5 results (CIRTEN)

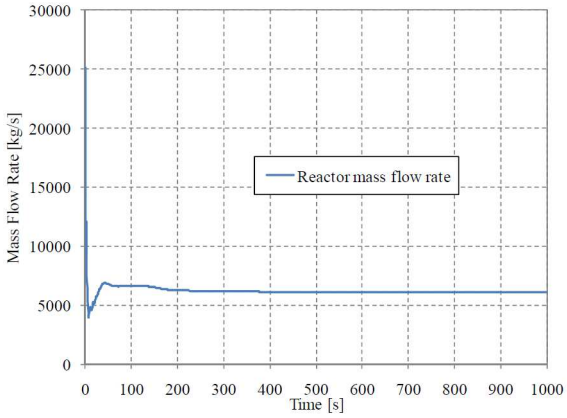
The transient starts with the simultaneous coastdown of all primary pumps. This causes a fast drop of the reactor mass flow rate (see Fig. 5.2.8-1a) down to about 4000 kg/s. Once the natural circulation conditions are established, the reactor mass flow rate stabilizes around a value of 6100 kg/s.

The core power, driven by neutron feedbacks only, experiences a drop down to about 170 MW, further it stabilizes at a level close to 225 MW, as shown in Fig. 5.2.8-1b. The same figure reports also the total power exchanged by all SGs (cooling power). The first drop is caused by the immediate and drastic primary mass flow rate reduction, a slow oscillatory trend of the parameter is predicted till 400 s in the transient. Oscillations are caused by the transition between forced circulation and natural circulation establishing in the reactor. Moreover, an extra cooling is computed by the code, since that cooling power is greater than that generated in the core in the time interval 50–350 s (this is reflected in the lead temperature distribution). Further on the core power is completely transferred by the SG reaching a new steady state condition.

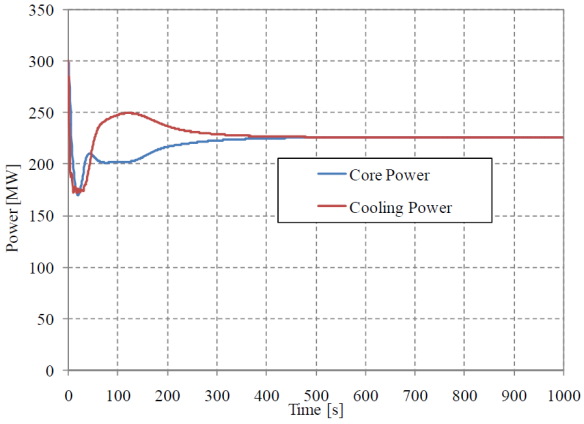
Fig. 5.2.8-1c and Fig. 5.2.8-1d show all the considered contributions to the reactivity. Among the others major feedbacks can be recognized: Doppler effect which inserts a positive contribution up to about 110 pcm; pad and control rod expansion which on contrary contributes

for a negative value whose minimum is about -75 pcm. The total core reactivity rapidly decreases down to -80 pcm in the first 10 s, then Doppler feedback starts to give its contribution (because of decreasing in fuel temperature due to lower power level) and the total reactivity consequently increases. At the end of the simulation (i.e. 1000 s) the total reactivity is equal to 0.0 pcm establishing new reactor conditions.

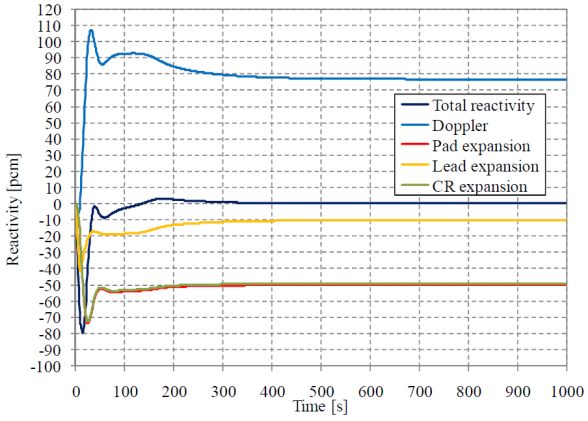
a) Reactor mass flow rate



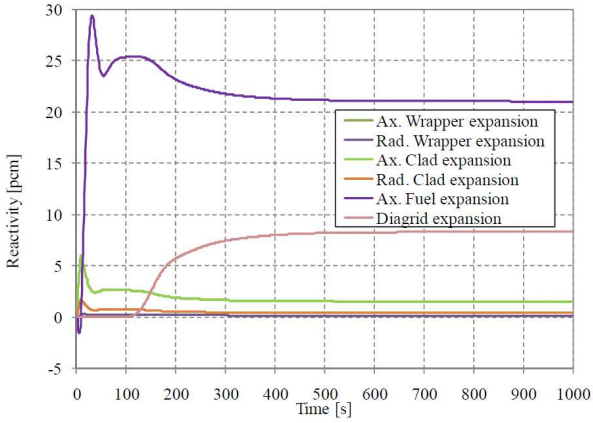
b) Core and total cooling power



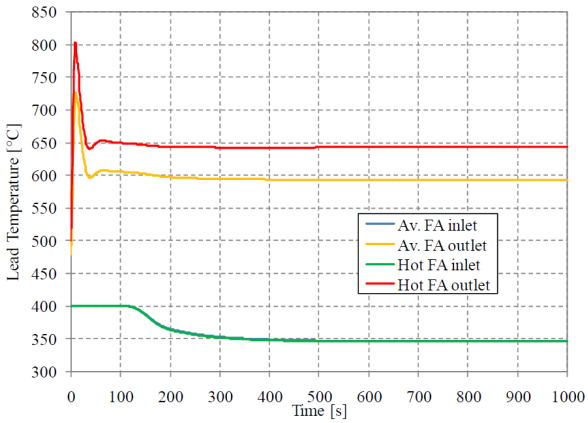
c) Neutron reactivity feedbacks (large)



d) Neutron reactivity feedbacks (small)



e) Lead inlet and outlet temperature



f) Maximum clad temperature

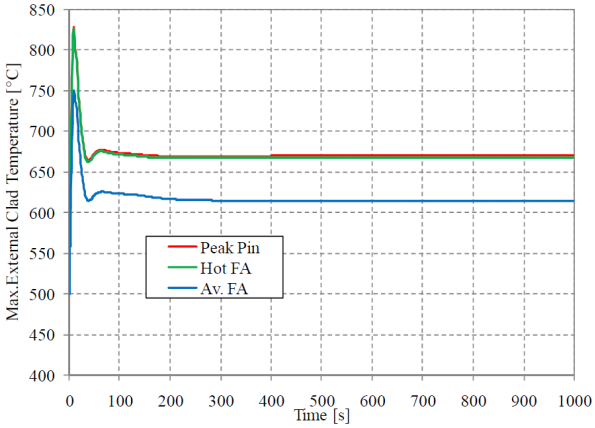


Fig. 5.2.8-1: Main RELAP5 results of the T-DEC1 transient

Primary fluid temperature behaviour is shown in Fig. 5.2.8-1e. A steep increase of core exit temperature is due to the fast mass flow rate decrease. In the meantime core inlet temperature

stays close to its nominal value (400 °C), still fed by the lead nominally cooled by the SGs. Going on in the transient, inlet temperature decreases (because of extra cooling by SGs as discussed above) and a much larger (than in nominal conditions) core ΔT is established (350 °C and 597 °C inlet and outlet temperature respectively in the FA with average power). It should be noted that the margin from solidification threshold is sensibly reduced. Clad temperature basically follows the same trend of the lead (see Fig. 5.2.8-1f). A maximum value of 828 °C is reached in the hot pin at 9 s. Afterwards, the maximum clad temperature stabilizes just below 650 °C.

As described above, core power decreases due to the initial negative reactivity balance. As a consequence fuel temperature decreases too. At the end of the simulation a lower (than steady state conditions) temperature is reached. A decrease of about 260 °C in respect to the nominal steady state condition is computed for the FA with average power, maximum power and for the hot pin.

5.3 T-DEC3: Unprotected loss of heat sink (ULOHS)

The unprotected loss of heat sink (ULOHS) transient foresees the loss of feedwater to all MHXs. The reactor scram is assumed to fail and then the core power is driven by the reactivity feedbacks. Forced circulation is maintained in the primary system, while the secondary circuits are isolated and the DHR-1 system is activated for decay heat removal.

This transient has been analyzed by several partners using different codes: KIT-G with SIM-LFR at BOC and EOC conditions, PSI with TRACE/FRED, ENEA with RELAP5, ENEA/CEA with CATHARE and NRG with SPECTRA at EOC conditions. The main results of these analyses are presented in the following subsections.

5.3.1 T-DEC3 transient: SIM-LFR results (KIT-G)

For these calculations the primary heat transport path through the MHXs was assumed to fail at time t = 0 sec. Additionally, despite of the various signals for reactor shutdown, it was assumed that all reactor shut-down systems are inoperable. The reactor is not being shut-down by a reactor shutdown system, so the LOHS transient is simulated as an unprotected transient. In order to get even more conservative analysis results, we postulated a simultaneous failure of one DHR-1 subsystem (IC). It means that from that time point onwards, only three DHR-1 subsystems (ICs) are responsible for removing heat from the primary cooling circuit. DHR-2 system is not activated (logic failure). The primary pumps are assumed operational thereby assuring an even heat distribution throughout the primary cooling system providing a nominal coolant flow rate.

Two cases were analyzed to investigate the clad and fuel temperature response of the peak pin and the likelihood of peak pin clad rupture during this LOHS transient, namely at BOC and EOC conditions.

Under BOC conditions, the power level in the core is seen in Fig. 5.3.1-1 to reduce down to ~ 3% at 3600 sec (1 hour) into the transient due to negative temperature reactivity feedback effects (fuel, diagrid, pads, lead and CRs drivelines expansion reactivity effects).

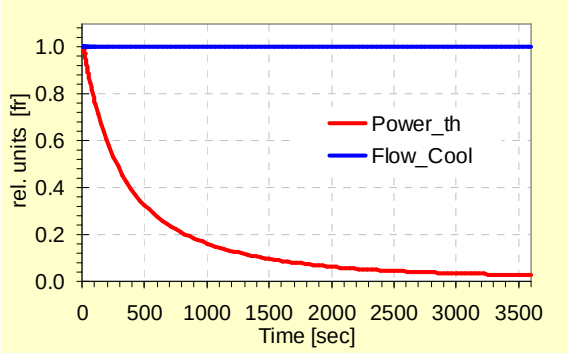
As a result of the unprotected loss of heat sink, all core and vessel temperatures will heat up fairly uniformly at a rate of ~3.2 °C/min based on the masses of coolant (~3570 tons), and structural materials inside the primary cooling circuit.

At the end of the simulation (at t = 3600 sec (1 hour) into the transient), the average vessel wall temperature approaches ~ 670 °C, thus questioning the long term structural integrity of the vessel under these elevated temperature conditions. At t = 3600 sec into the transient peak pin clad temperatures will reach ~ 710 ^{o}C, but due to rather low fission gas pressure of ~20 bar, the clad of the peak power pin will stay intact, having the clad failure time of ~3.6E+6 sec. All these temperatures will still continue to increase if the operator will not interact to terminate this transient. Even in 1 hour transient time the power generated in the core is still higher than the heat removal capacity of three DHR-1 subsystems.

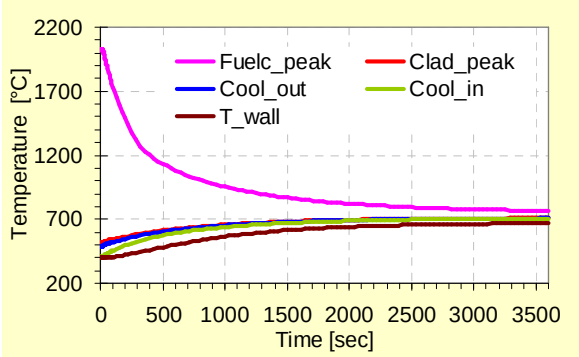
Under EOC conditions, the power level in the core is seen in Fig. 5.3.1-2 to reduce down to ~ 2.5% at 3600 sec (1 hour) into the transient due to negative temperature reactivity feedback effects (fuel, diagrid, pads, lead and CRs drivelines expansion reactivity effects).

As a result of the unprotected loss of heat sink, all core and vessel temperatures will heat up fairly uniformly at a rate of ~3.1 °C/min based on the masses of coolant (~3570 tons), and structural materials inside the primary cooling circuit.

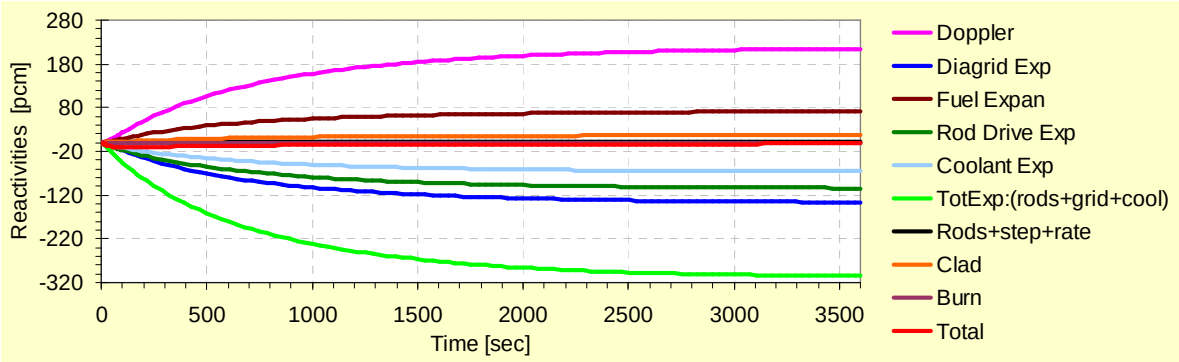
At the end of the simulation (at t = 3600 sec (1 hour) into the transient), the average vessel wall temperature approaches 662 °C, thus questioning the long term structural integrity of the vessel under these elevated temperature conditions. At t = 3600 sec into the transient peak pin clad temperatures will reach ~ 700 ^{o}C, but due to rather low fission gas pressure of ~ 28 bar, the clad of the peak power pin will stay intact, showing clad failure time of ~ 4.9E+6 sec. All these temperatures will still continue to increase if the operator will not interact to terminate this transient. Even in 1 hour transient time the power generated in the core is still higher than the heat removal capacity of three DHR-1 subsystems.



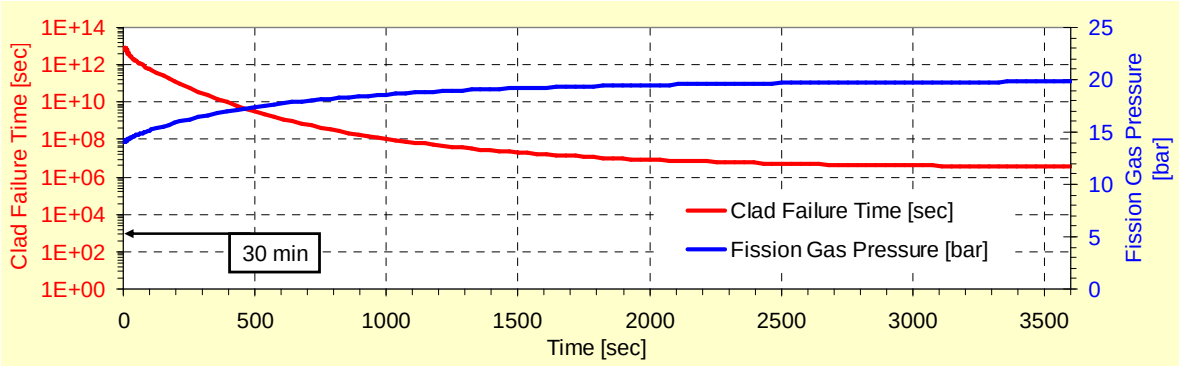
a) Relative core thermal power and flow rate



b) Peak fuel-, clad-, coolant- and vessel wall temperatures

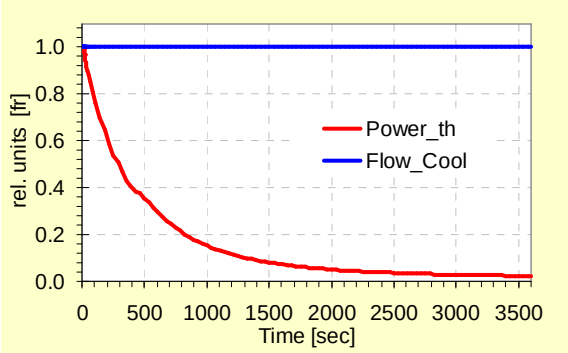


c) Reactivity effects

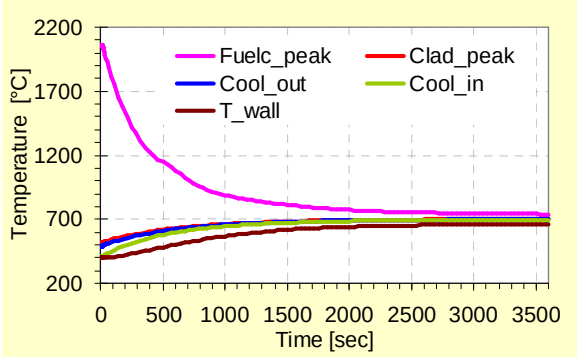


d) Peak pin fission gas pin pressure and clad failure time

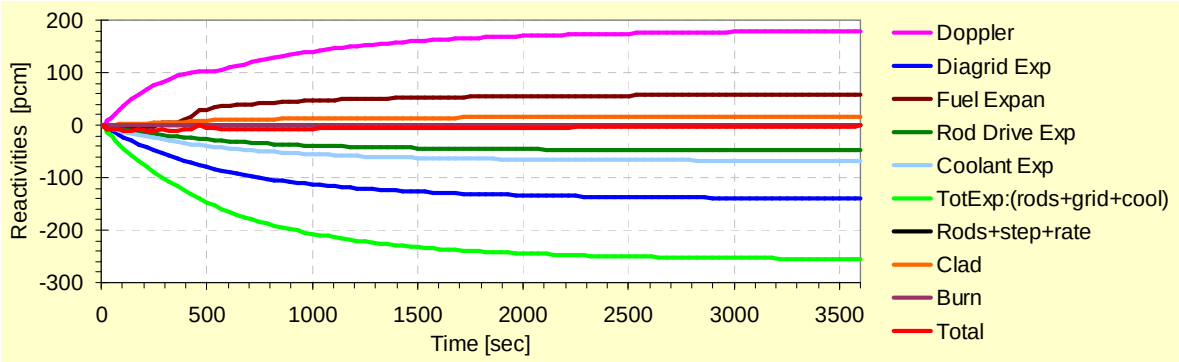
Fig. 5.3.1-1: Results for T-DEC3: (ULOHS) transient at HFP - BOC conditions at an average burnup of 730 EFPD as calculated by SIM-LFR (KIT)



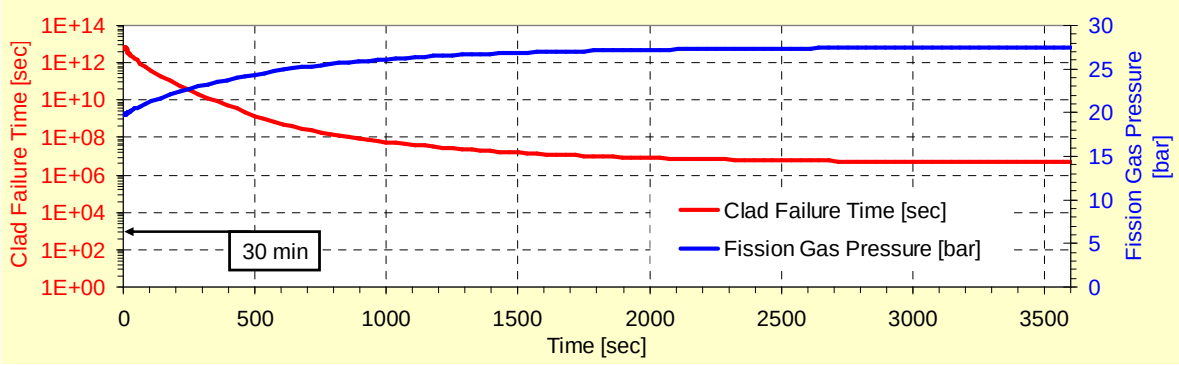
a) Relative core thermal power and flow rate



b) Peak fuel-, clad-, coolant- and vessel wall temperatures



c) Reactivity effects



d) Peak pin fission gas pin pressure and clad failure time

Fig. 5.3.1-2: Results for T-DEC3: (ULOHS) transient at HFP - EOC conditions at an average burnup of 1095 EFPD as calculated by SIM-LFR (KIT)

The timely response to this DEC transient is ascribed to a rather large cumulative negative reactivity feedback effect coming from the negative fuel, diagrid, pads, lead and CRs drivelines expansion reactivity effects. Sufficient grace time (>> 30 min) is available for the manual operator intervention to terminate this transient by manually shutting down the reactor and cooling down the primary cooling circuit.

5.3.2 T-DEC3 transient: TRACE/FRED results (PSI)

The Unprotected Loss of Heat Sink (ULOHS) transient initiates from a total loss of feedwater flow into the secondary side of MHX, leaving one DHR working to remove heat from core. One DHR is able to provide a maximum 7 MW heat removal capability.

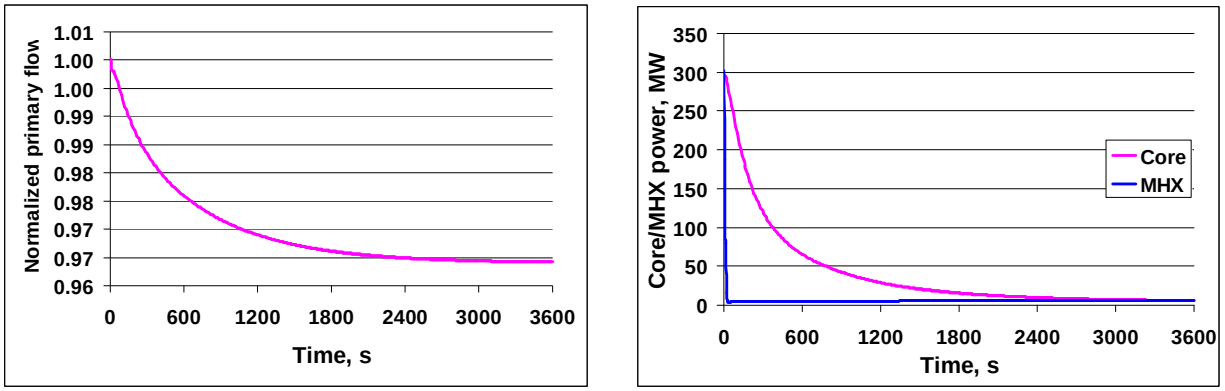


Fig. 5.3.2-1: Primary coolant flow (left) and core/MHX power (right) evolutions with time

When MHX power was suddenly removed (Fig. 5.3.2-1), both core inlet and outlet temperatures start to increase significantly as shown in Fig. 5.3.2-2, leading to negative reactivity feedback incurred by radial expansions of pad and diagrid as can be noticed from Fig. 5.3.2-3. This negative feedback is higher than the positive one mainly caused by the coolant density decrease. This leads to core power reduction and fuel temperature decrease.

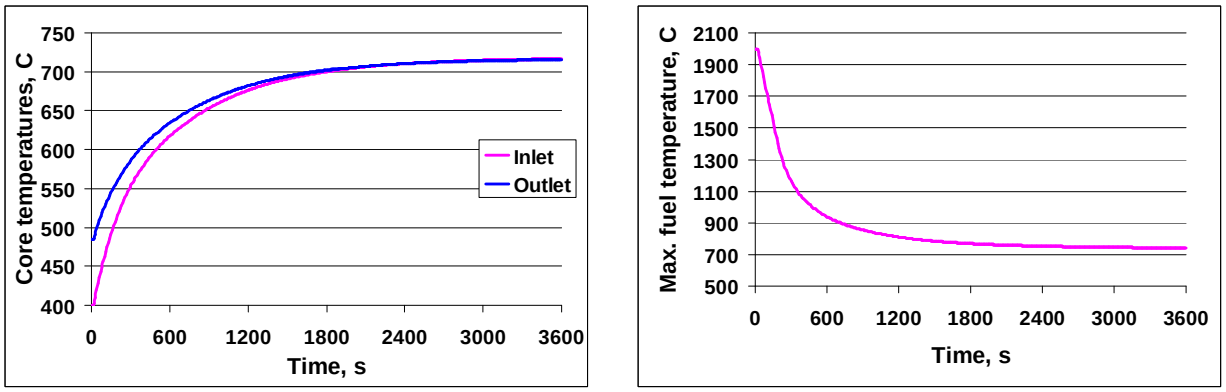


Fig. 5.3.2-2: Evolutions of core inlet/outlet coolant temperatures (left) and the maximum fuel temperature (right) with time

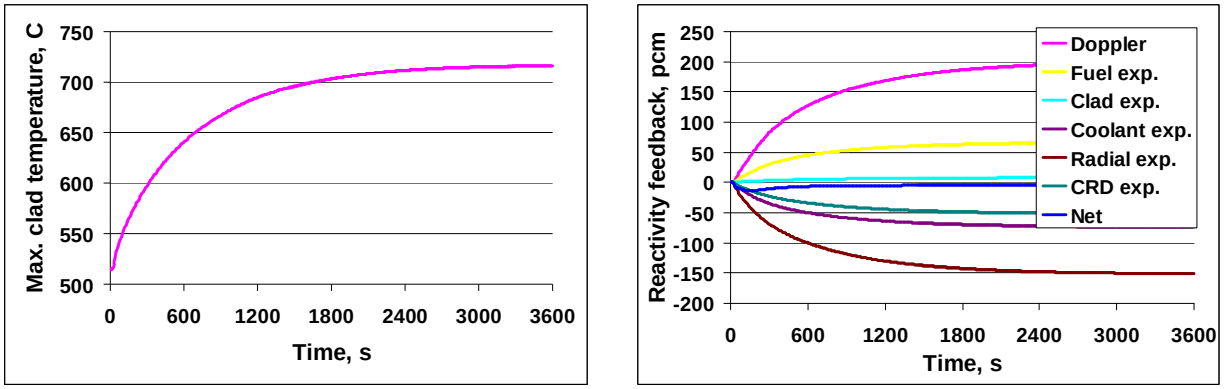


Fig. 5.3.2-3: Evolutions of the maximum cad temperature (left) and reactivity feedback (right) with time

After 3000 seconds, the whole primary system becomes stabilized. The asymptotic fuel and clad temperatures at the hottest spot are 742 ^{o}C and 716 ^{o}C respectively, which are well below their own working limits.

5.3.3 T-DEC3 transient: RELAP5 results (ENEA)

This transient is initiated by the loss of feedwater to all MHXs without reactor scram. The secondary circuits are promptly isolated by the MSIV closure and the DHR-1 system is started for core decay heat removal. As a conservative assumption, only 3 out of 4 IC loops of DHR-1 system are supposed in service. The main results of the T-DEC3 transient analysis are illustrated in Fig. 5.3.3-1.

The sudden reduction in heat removal by the secondary side leads to progressive increase of temperatures of the primary system with consequent negative reactivity feedbacks which tend to reduce the core neutronic power. The core power decreases towards the decay level in about 1 hour transient (see Fig. 5.3.3-1a), while the heat removed by the secondary side, through the 3 IC loops of the DHR-1 system stabilizes around 5 MW.

With the reducing core power, the temperatures in the primary system tend to stabilize around 700 °C (see Fig. 5.3.3-1b). Since the primary pumps remain in operation at nominal speed, the ΔT through the core becomes negligible and almost uniform temperature distribution is calculated in the primary circuit due to good coolant mixing in the cold pool surrounding the MHX. The maximum clad temperature is limited to 705 °C and no clad failure is expected in the medium and long term. The more critical issue is the vessel wall temperature which approximates 700 °C after about one hour transient, so that vessel integrity cannot be guaranteed in the long term. However, enough grace time (> 30 min) is left to the operator for corrective actions. Furthermore, as a conservative assumption, no radiative heat losses are taken into account from the external vessel wall.

The positive reactivity introduced by Doppler and fuel expansion effects, following large fuel temperature decrease (Fig. 5.3.3-1c), is counterbalanced by negative radial core (diagrid and pad effects), coolant and control rod expansion feedbacks (Fig. 5.3.3-1d).

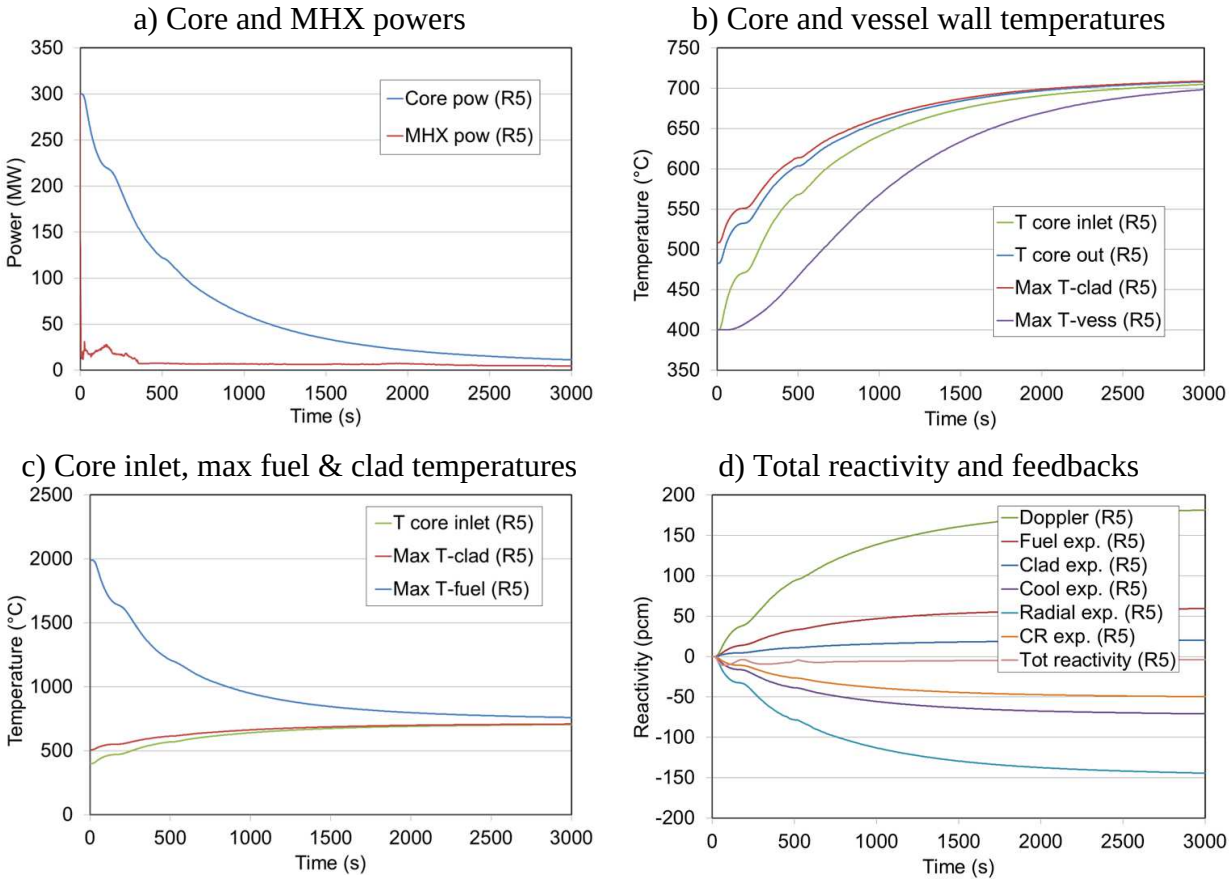


Fig. 5.3.3-1: Main RELAP5 results of the T-DEC3 transient

5.3.4 T-DEC3 transient: CATHARE results (ENEA/CEA)

This transient is initiated by the loss of feedwater to all MHX without reactor scram. The secondary circuits are promptly isolated by the MSIV closure and the DHR-1 system is started for core decay heat removal. As a conservative assumption, only 3 out of 4 IC loops of DHR-1 system are supposed in service. The main results of the T-DEC3 transient analysis are illustrated in Fig. 5.3.4-1.

The sudden reduction in heat removal by the secondary side leads to progressive increase of temperatures of the primary system with consequent negative reactivity feedbacks which tend to reduce the core neutronic power. The core power decreases towards the decay level in about one hour transient (see Fig. 5.3.4-1a), while the heat removed by the secondary side, through the 3 IC loops of the DHR-1 system stabilizes around 5 MW.

With the reducing core power, the temperatures in the primary system tend to stabilize around 700 °C (see Fig. 5.3.4-1b). Since the primary pumps remain in operation at nominal speed, the ΔT through the core becomes negligible and almost uniform temperature distribution is calculated in the primary circuit due to good coolant mixing in the cold pool surrounding the MHX. The maximum clad temperature is limited to 710 °C and no clad failure is expected in the medium and long term. The more critical issue is the vessel wall temperature which approximates 700 °C after about one hour transient, so that vessel integrity cannot be

guaranteed in the long term. However, enough grace time (> 30 min) is left to the operator for corrective actions. Furthermore, as a conservative assumption, no radiative heat losses are taken into account from the external vessel wall.

The positive reactivity introduced by Doppler and fuel expansion effects, following large fuel temperature decrease (Fig. 5.3.4-1c), is counterbalanced by negative radial core (diagrid and pad effects), coolant and control rod expansion feedbacks (Fig. 5.3.4-1d).

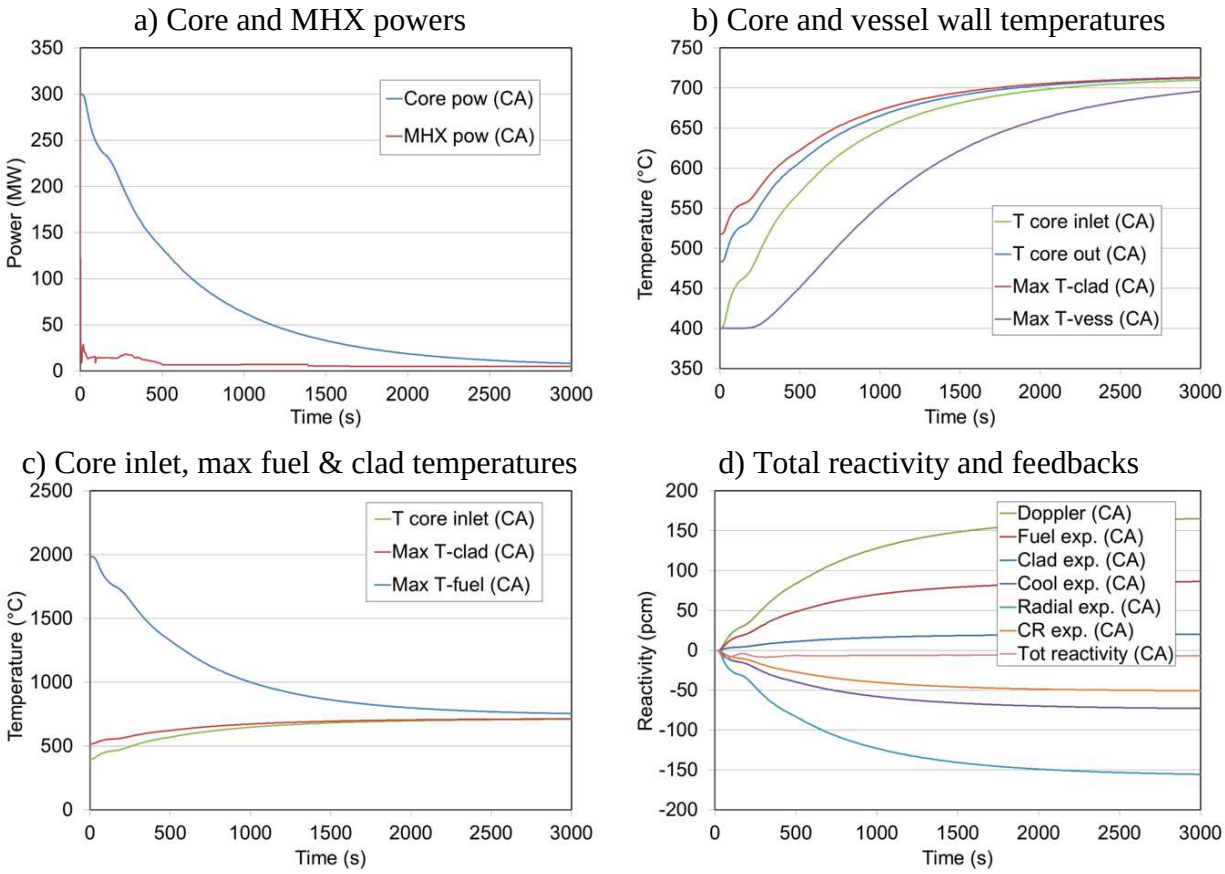


Fig. 5.3.4-1: Main CATHARE results of the T-DEC3 transient

5.3.5 T-DEC3 transient: SPECTRA results (NRG)

The Unprotected Loss of Heat Sink (ULOHS) scenario is as follows:

- Loss of feedwater on all MHX-s. Mass flow halving time 1.0 s.
- MSIV closes at 0.0 s. IC valve opens at 1.0 s. Valve opening/closing time 1.0 s.
- Startup of DHR-1 (three out of four DHR-1 loops available).
- Reactor trip (scram signal) is disabled.

In this transient there are three loops with IC operating and five loops with IC closed. In the model two loops are used. The first loop represents three real loops with IC-s, combined into one. The second loop represents five real loops without IC-s. The NRG SPECTRA results are shown in Fig. 5.3.5-1 through Fig. 5.3.5-4

The core and MHX powers are shown in Fig. 5.3.5-1. The core power decreases gradually. At t = 3000 s the total power is 8.58 MW, consisting of 3.38 MW fission power and 5.20 MW decay power.

The coolant, cladding and vessel temperatures are shown in Fig. 5.3.5-2. The temperatures rise to about 700˚C. No fuel rod cladding rupture nor vessel failure is expected in the medium term. Enough grace time is left to the operator to take the opportune corrective actions and bring the plant in safe conditions in the medium and long term.

The coolant, cladding and fuel temperatures are shown in Fig. 5.3.5-3. The maximum fuel temperatures continuously decrease. At the end of calculations it is equal to 732 °C. The maximum cladding temperatures slowly increases. At the end of calculations it is equal to 694 °C. The core inlet temperature slowly increases. At the end of calculations it is equal to 691 °C.

The total reactivity as well as the reactivity feedbacks are shown in Fig. 5.3.5-4. The main positive feedback is from Doppler effect and fuel expansion. The main negative feedbacks are from radial expansions (diagrid, pads), coolant density, and control rod displacement. The total reactivity is constantly slightly below zero, resulting in gradual power decrease.

At the end of calculations the three operating IC-s remove about 6.98 MW (3×2.33 MW) power.

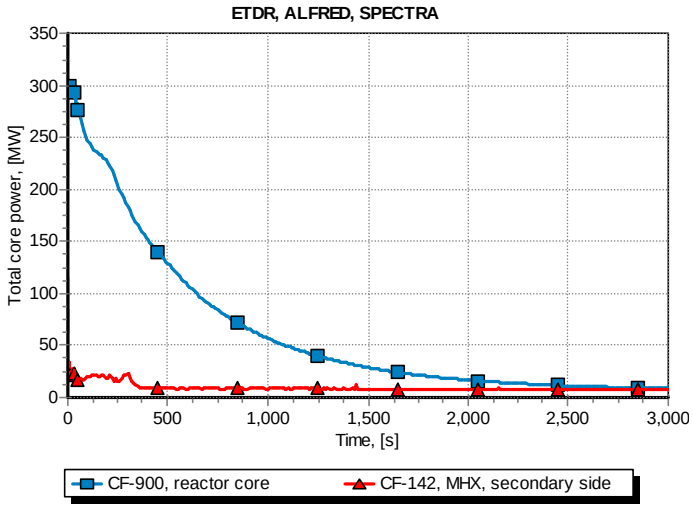


Fig. 5.3.5-1: Core power and MHX powers

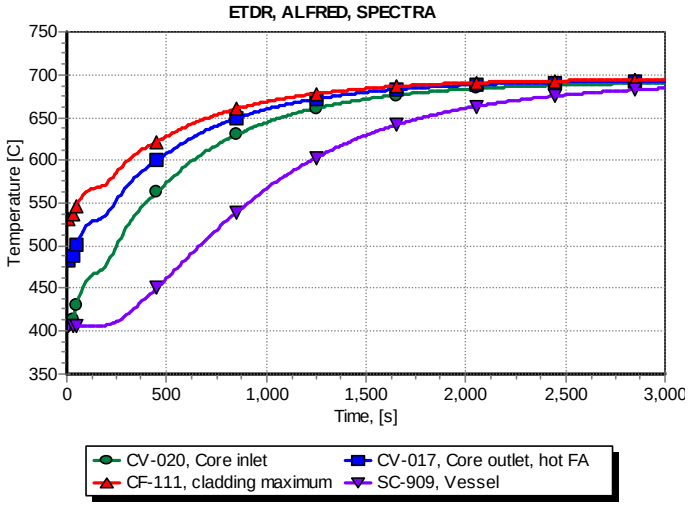


Fig. 5.3.5-2: Coolant, cladding, and vessel wall temperatures

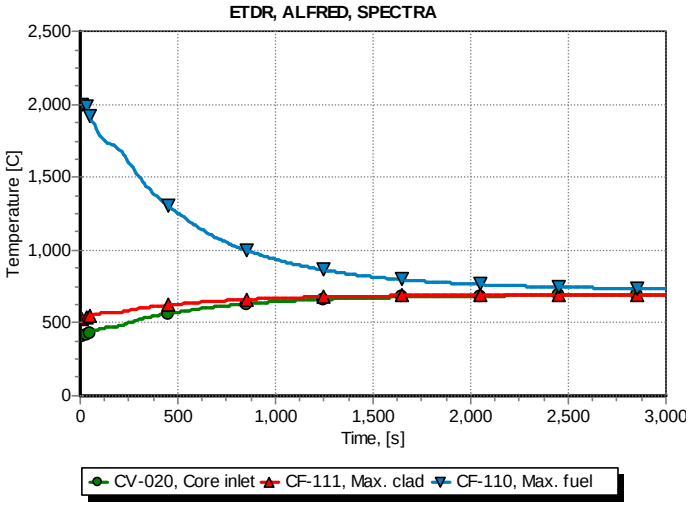


Fig. 5.3.5-3: Coolant, cladding and fuel temperatures

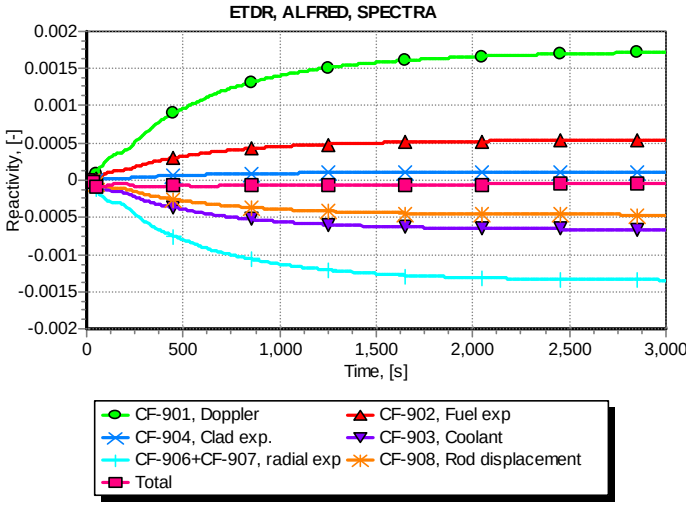


Fig. 5.3.5-4: Total reactivity and feedbacks

5.4 T-DEC4: Unprotected loss of offsite power (ULOHS+ULOF)

The loss of offsite power (LOOP) in analyzed as unprotected transient, that is without reactor scram, assuming the simultaneous loss of all primary pumps and feedwater to all MHXs. The secondary circuits are isolated and the DHR-1 system is started for decay heat removal. For conservative analysis only 3 out of 4 subsystems of DHR-1 are supposed available.

This transient has been analyzed by several partners using different codes: KIT-G with SIM-LFR at BOC and EOC conditions, ENEA with RELAP5, ENEA/CEA with CATHARE and NRG with SPECTRA at EOC conditions. The main results of these analyses are presented in the following subsections.

5.4.1 T-DEC4 transient: SIM-LFR results (KIT-G)

For these calculations loss-of-offsite power (LOOP), which means that the primary pumps and the primary heat transport path through the MHXs are assumed to fail simultaneously, takes place at time t = 0 sec. Additionally, despite of the various signals for reactor shutdown, it was assumed that all reactor shut-down systems fail, so that the LOOP (LOF & LOHS) transient is simulated as an unprotected transient. In order to achieve even more conservative analysis results, we postulated a simultaneous failure of one DHR-1 subsystem (IC). It means that from that time point onwards, only three DHR-1 subsystems (ICs) are responsible for removing heat from the primary cooling circuit. DHR-2 system is not activated (logic failure). Stopping of the primary pumps at the beginning of the transient means that primary coolant circulation in the primary cooling circuit is only by natural convection, thus it does not provide a well-mixed, uniform temperature distribution throughout the primary system, as is the case when the primary pumps are operating normally.

Two cases were analyzed to investigate the clad and fuel temperature response of the peak pin and the likelihood of peak pin clad rupture during this unprotected LOOP (LOF & LOHS) transient, namely at BOC and EOC conditions.

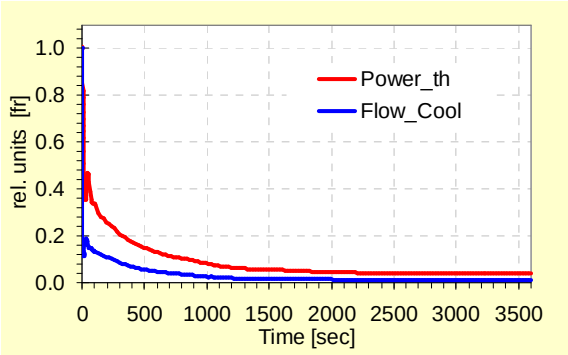
Under BOC conditions, the power level in the core is seen in Fig. 5.4.1-1 decreases to ~3.8% at 3600 sec (1 hour) into the transient due to negative temperature reactivity feedback effects (fuel, diagrid, pads, lead and CRs drivelines expansion reactivity effects).

As a result of the unprotected loss-of-offsite power (LOOP), all core and vessel temperatures will heat up fairly uniformly at a rate of ~ 2.2 °C/min (due to faster reduction of the reactor power level in comparison with the ULOHS case above) based on the masses of coolant (~3570 tons) and structural materials inside the primary cooling circuit.

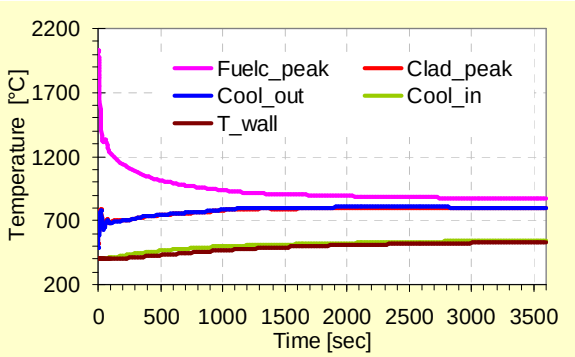
At the end of the simulation (at t = 3600 sec (1 hour) into the transient), the average vessel wall temperature approaches ~ 535 °C, thus the long term structural integrity of the vessel is still guaranteed. At t = 3600 sec into the transient peak pin clad temperatures will reach ~ 795 ^{o}C, but due to rather low fission gas pressure of ~ 17 bar, the clad of the peak power pin will stay intact, having the clad failure time of ~ 2.1E+4 sec. All the core temperatures seem to be increasing further only very slightly after 1 hour of the transient time. Even in 1 hour transient time the power generated in the core is still higher than the heat removal capacity of three DHR-1 subsystems.

Under EOC conditions, the power level in the core is seen in Fig. 5.4.1-2 to reduce down to ~ 2.9% at 3600 sec (1 hour) into the transient due to negative temperature reactivity feedback effects (fuel, diagrid, pads, lead and CRs drivelines expansion reactivity effects).

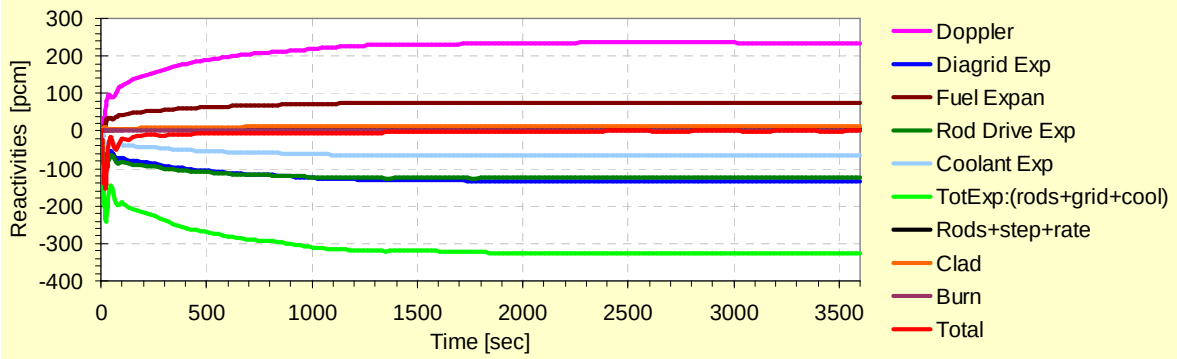
As a result of the unprotected loss-of-offsite power (LOOP), all core and vessel temperatures will heat up fairly uniformly at a rate of ~ 2.5 °C/min (due to faster reduction of the reactor power level in comparison with the ULOHS case above) based on the masses of coolant (~3570 tons) and structural materials inside the primary cooling circuit.



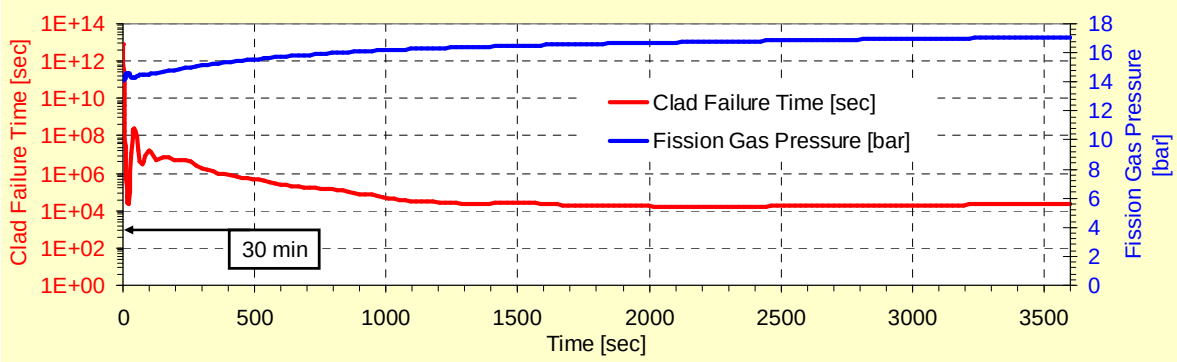
a) Relative core thermal power and flow rate



b) Peak fuel-, clad-, coolant- and vessel wall temperatures



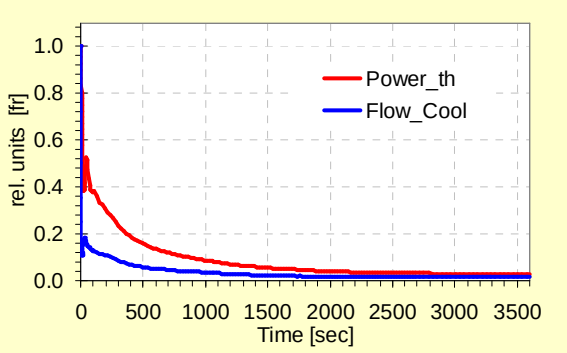
c) Reactivity effects



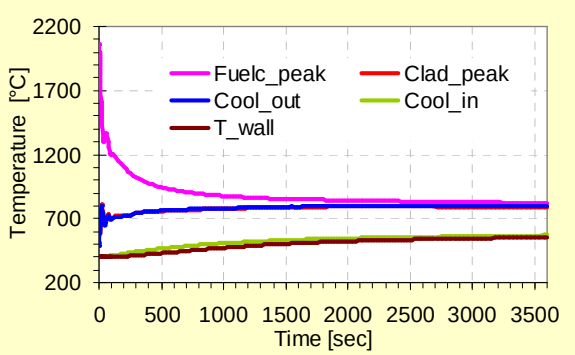
d) Peak pin fission gas pin pressure and clad failure time

Fig. 5.4.1-1: Results for T-DEC4: (ULOOP) transient at HFP - BOC conditions at an average burnup of 730 EFPD as calculated by SIM-LFR (KIT)

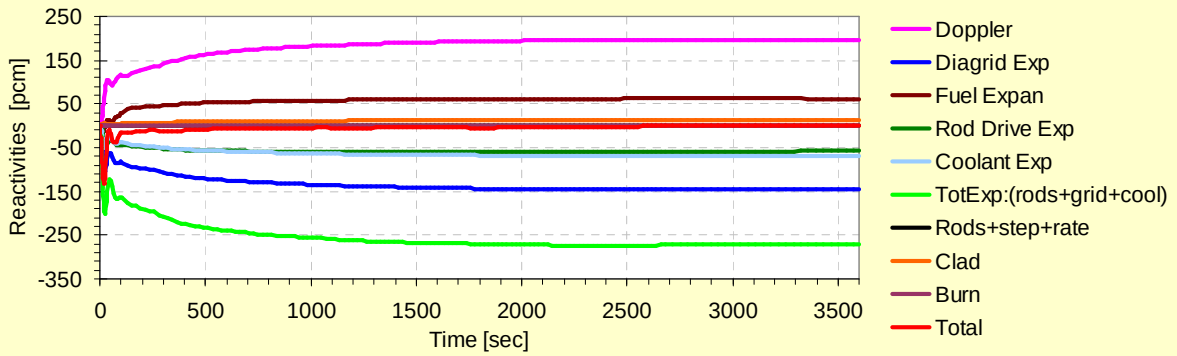
At the end of the simulation (at t = 3600 sec (1 hour) into the transient), the average vessel wall temperature approaches ~ 555 °C, thus the long term structural integrity of the vessel is still guaranteed. At t = 3600 sec into the transient peak pin clad temperatures will reach ~790 ^{o}C, but due to rather low fission gas pressure of ~ 24.5 bar, the clad of the peak power pin will stay intact, having the clad failure time of ~ 2.2E+4 sec. All the core temperatures seem to be increasing further only very slightly after 1 hour of the transient time. Even in 1 hour transient time the power generated in the core is still higher than the heat removal capacity of three DHR-1 subsystems.



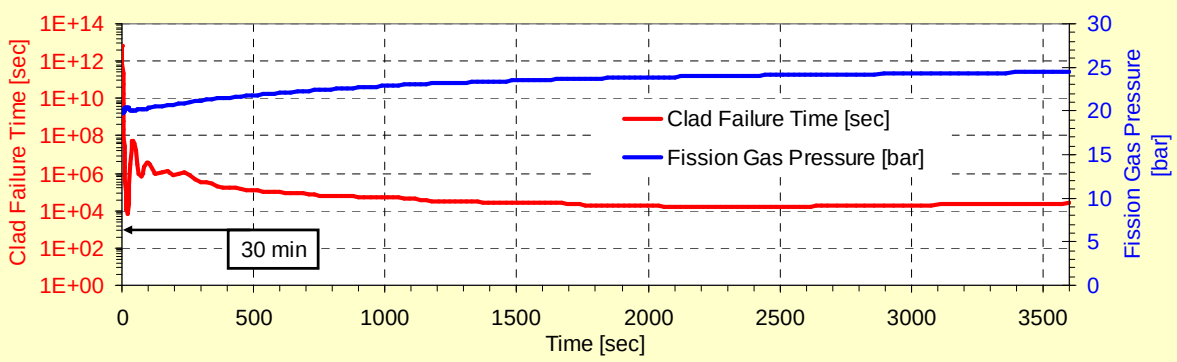
a) Relative core thermal power and flow rate



b) Peak fuel-, clad-, coolant- and vessel wall temperatures



c) Reactivity effects



d) Peak pin fission gas pin pressure and clad failure time

Fig. 5.4.1-2: Results for T-DEC4: (ULOOP) transient at HFP - EOC conditions at an average burnup of 1095 EFPD as calculated by SIM-LFR (KIT)

The timely response to this DEC transient is ascribed to a rather large cumulative negative

reactivity feedback effect coming from the negative fuel, diagrid, pads, lead and CRs drivelines expansion reactivity effects. Sufficient grace time (>> 30 min) is available for the manual operator intervention to terminate this transient by manually shutting down the reactor and cooling down the primary cooling circuit.

5.4.2 T-DEC4 transient: RELAP5 results (ENEA)

This transient is initiated by the loss of offsite power supply without reactor scram. The simultaneous loss of all primary pumps and feedwater to all MHXs in the secondary circuits is taken into account. The secondary circuits are promptly isolated by the MSIV closure and the DHR-1 system is started for core decay heat removal. As a conservative assumption, only 3 out of 4 IC loops of DHR-1 system are supposed in service. The main results of the T-DEC4 transient analysis are illustrated in Fig. 5.4.2-1.

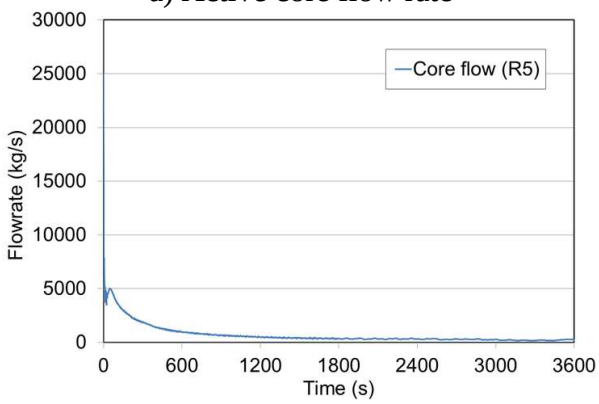
The initial phase of this transient is mainly characterized by the loss of primary pumps and consequent transition from forced to natural circulation in the primary circuit (Fig. 5.4.2-1a). After a sudden decrease down to about 160 MW, the core power progressively reduces according with the primary temperature increase and induced negative reactivity feedbacks. The core power approximates the decay level in about 1 hour, while the DHR-1 removed power (3 IC loops) stabilizes around 5 MW (Fig. 5.4.2-1b).

After the initial temperature peak induced by the loss of forced primary flow, the maximum clad temperature increases again and then stabilizes around 825 °C as shown in Fig. 5.4.2-1c. A large ΔT through the core is calculated, because of the low natural circulation flow rate that is exhibited in the primary circuit (around 1% of nominal value as shown in Fig. 5.4.2-1a).

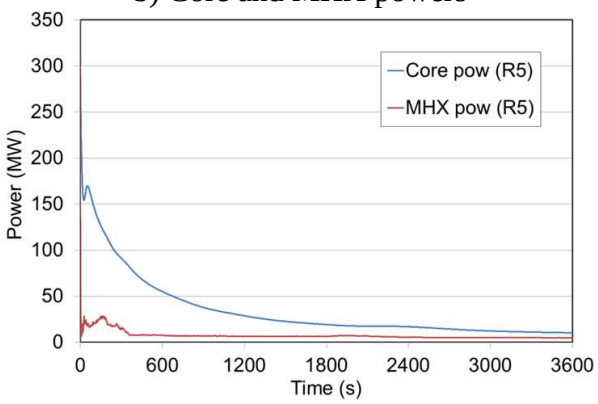
Because of the rather high maximum clad temperature, clad integrity cannot be guaranteed in the long term. On the contrary, the vessel wall temperature increase is rather limited (below 500 °C after 1 hour as shown in Fig. 5.4.2-1c), therefore, the vessel integrity is guaranteed in the long term.

The positive reactivity introduced by Doppler and fuel expansion effects, following large fuel temperature decrease, is counterbalanced by negative radial core (diagrid and pad effects), coolant and control rod expansion feedbacks (Fig. 5.4.2-1d).

a) Active core flow rate



b) Core and MHX powers



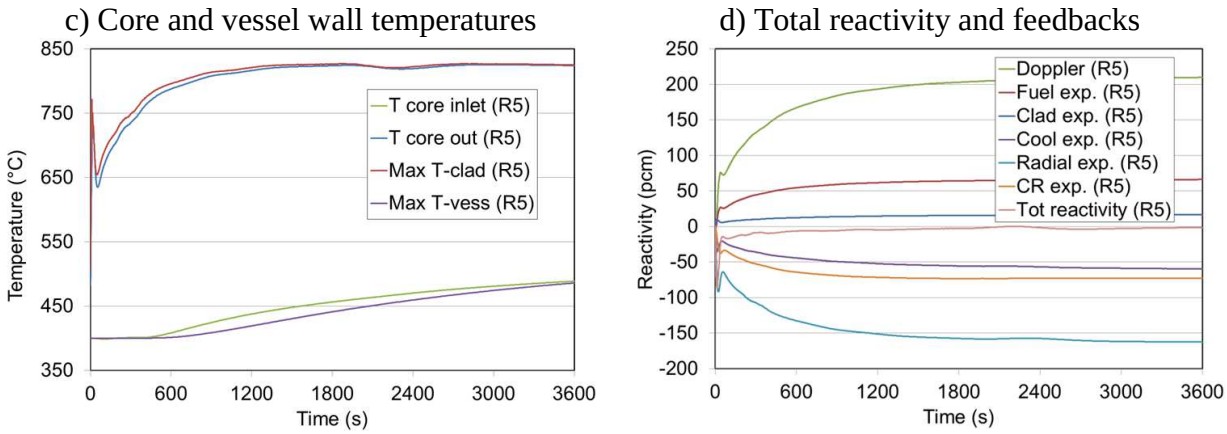


Fig. 5.4.2-1: Main RELAP5 results of the T-DEC4 transient

5.4.3 T-DEC4 transient: CATHARE results (ENEA/CEA)

This transient is initiated by the loss of offsite power supply without reactor scram. The simultaneous loss of all primary pumps and feedwater to all MHXs in the secondary circuits is taken into account. The secondary circuits are promptly isolated by the MSIV closure and the DHR-1 system is started for core decay heat removal. As a conservative assumption, only 3 out of 4 IC loops of DHR-1 system are supposed in service. The main results of the T-DEC4 transient analysis are illustrated in Fig. 5.4.3-1.

The initial phase of this transient is mainly characterized by the loss of primary pumps and consequent transition from forced to natural circulation in the primary circuit (Fig. 5.4.3-1a). After a sudden decrease down to about 170 MW, the core power progressively reduces according with the primary temperature increase and induced negative reactivity feedbacks. The core power approximates the decay level in about 1 hour, while the DHR-1 removed power (3 IC loops) stabilizes around 5 MW (Fig. 5.4.3-1b).

After the initial temperature peak induced by the loss of forced primary flow, the maximum clad temperature increases again and then stabilizes around 825 °C as shown in Fig. 5.4.3-1c. A large ΔT through the core is calculated, because of the low natural circulation flow rate that is exhibited in the primary circuit (around 1% of nominal value as shown in Fig. 5.4.3-1a).

Because of the rather high maximum clad temperature, clad integrity cannot be guaranteed in the long term. On the contrary, the vessel wall temperature increase is rather limited (~510 °C after 1 hour as shown in Fig. 5.4.3-1c), so that the vessel integrity is guaranteed in the long term.

The positive reactivity introduced by Doppler and fuel expansion effects, following large fuel temperature decrease, is counterbalanced by negative radial core (diagrid and pad effects), coolant and control rod expansion feedbacks (Fig. 5.4.3-1d).

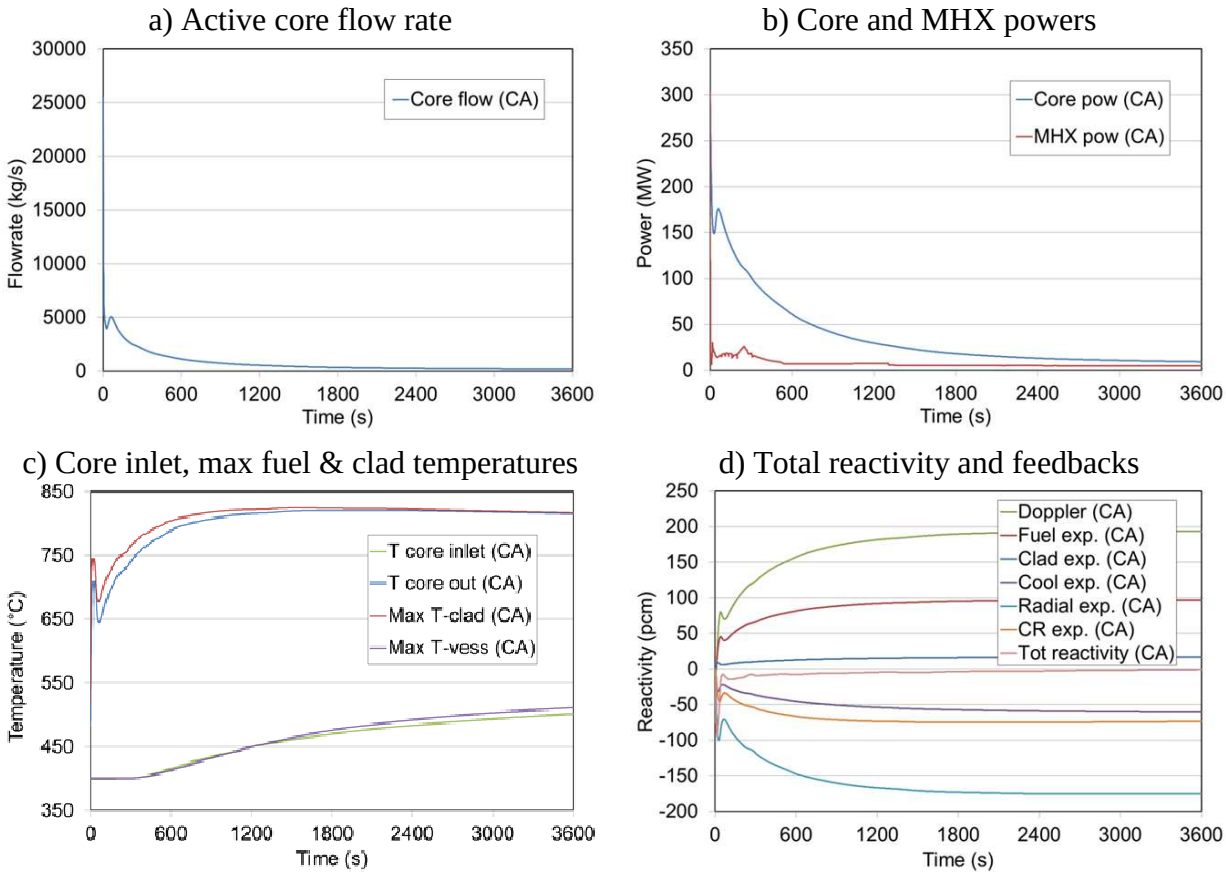


Fig. 5.4.3-1: Main CATHARE results of the T-DEC4 transient

5.4.4 T-DEC4 transient: SPECTRA results (NRG)

The Loss of offsite power (ULOHS+ULOF) scenario is as follows:

- Loss of all primary pumps. Pump speed halving time 0.56 s.
- Loss of feedwater on all MHX-s. Mass flow halving time 1.0 s.
- MSIV closes at 0.0 s. IC valve opens at 1.0 s. Valve opening/closing time 1.0 s.
- Startup of DHR-1 (three out of four DHR-1 loops available).
- Reactor trip (scram signal) is disabled.

In this transient there are three loops with IC operating and five loops with IC closed. In the model two loops are used. The first loop represents three real loops with IC-s, combined into one. The second loop represents five real loops without IC-s. The NRG SPECTRA results are shown in Fig. 5.4.4-1 through Fig. 5.4.4-4.

The core inlet flow is shown in Fig. 5.4.4-1. Natural circulation in primary circuit reduces down to very low value (around 1%).

Core power and MHX power are shown in Fig. 5.4.4-2. The core power decreases gradually. At t = 3600 s the total power is 10.79 MW, consisting of 5.98 MW fission power and 4.81 MW decay power. The MHX power decreases due to feedwater trip.
Coolant, cladding, and vessel temperatures are shown in Fig. 5.4.4-3. The maximum cladding temperatures rises to about 808 ˚C at about 1300 s and slowly decreases to about 800 ˚C at the end of the run. No fuel rod cladding rupture nor vessel failure is expected in the medium term. Enough grace time is left to the operator to take the opportune corrective actions and bring the plant in safe conditions in the medium and long term.

The total reactivity as well as the reactivity feedbacks are shown in Fig. 5.4.4-4. The main positive feedback is from Doppler effect and fuel expansion. The main negative feedbacks are from radial expansions (diagrid, pads), control rod displacement, and coolant density. The total reactivity is constantly slightly below zero, resulting in gradual power decrease.

The three operating IC-s remove about 6.24 MW (3×2.08 MW) power. The corresponding three steam generators remove similar power 6.32 MW (3×2.11 MW) from the primary system. There is practically no power removal through the remaining five steam generators. The total power is 0.08 MW (5×0.02 MW).

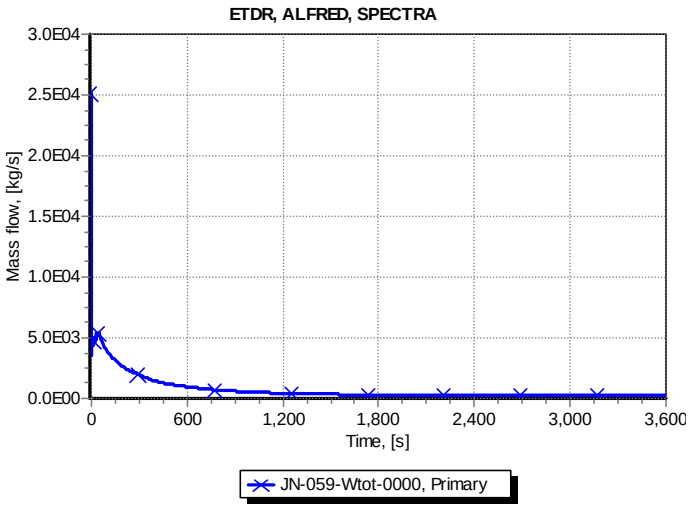


Fig. 5.4.4-1: Core inlet flow rate

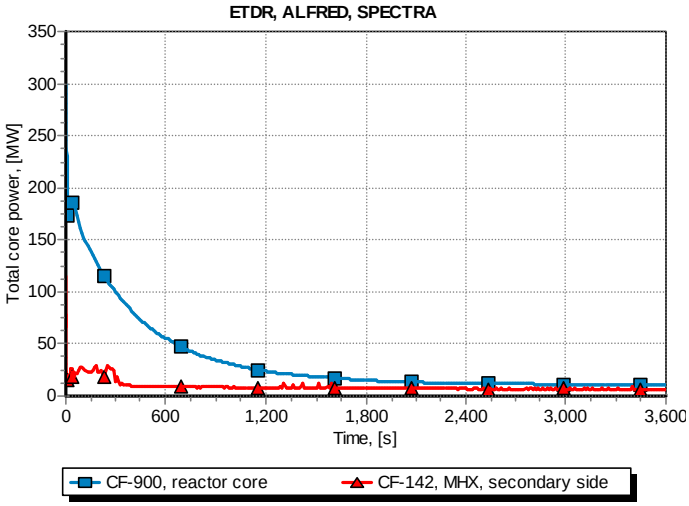


Fig. 5.4.4-2: Core power and MHX powers

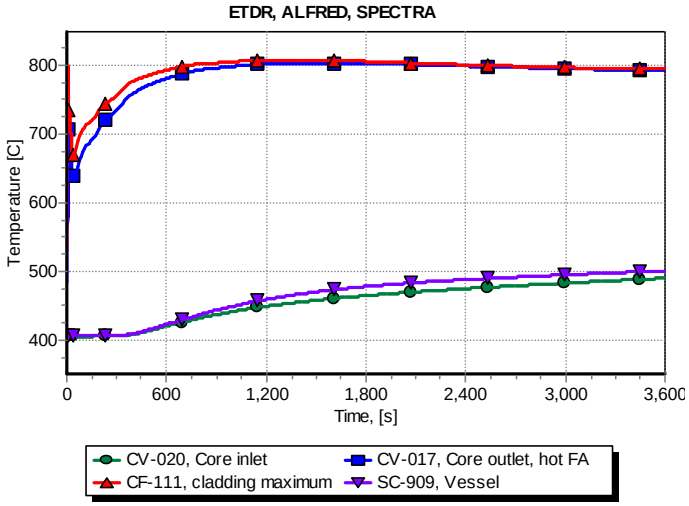


Fig. 5.4.4-3: Coolant, cladding and vessel wall temperatures

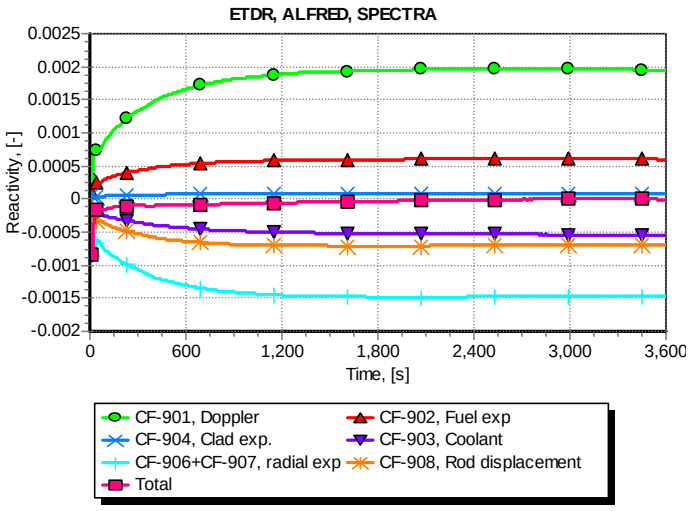


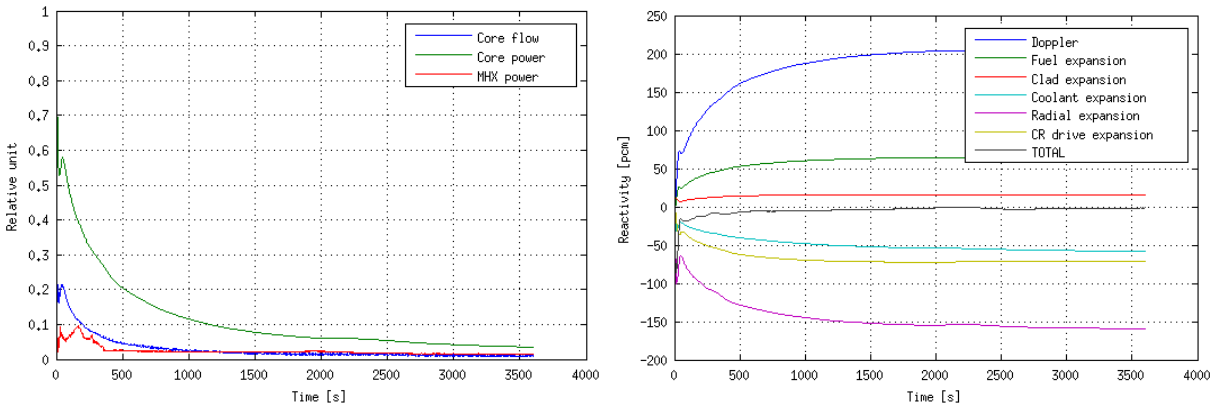
Fig. 5.4.4-4: Total reactivity and feedbacks

5.4.5 T-DEC4 transient: RELAP5 results (KTH)

In case of unprotected loss of flow and secondary cooling system transient, all pumps are tripped at time 0 after a 1000 seconds steady state calculation, at 1 second the main steam isolation valves are closed and at 2 seconds DHR-1 (with 3 out of 4 IC loops) is initiated. Scram signal is deactivated throughout the transient.

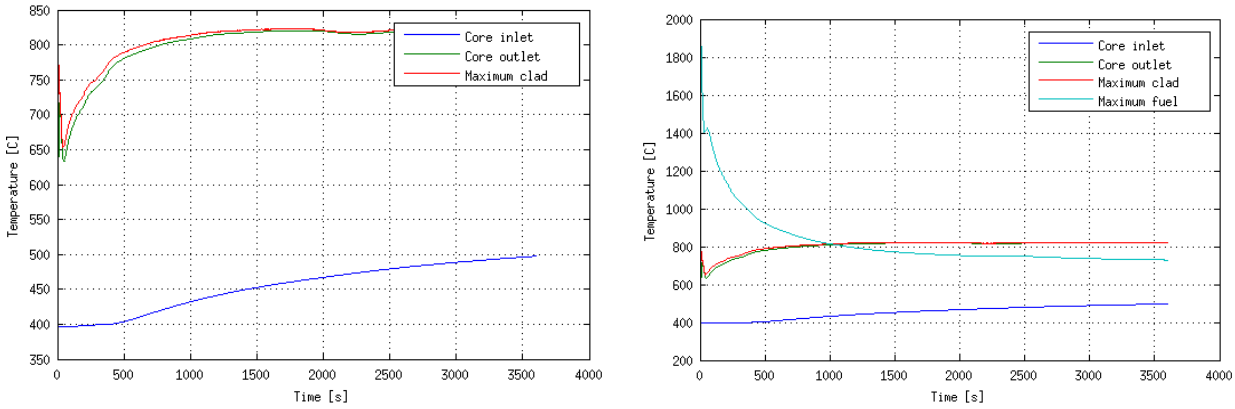
The initial sharp decrease of the power in the first 100 seconds reduces the power from 300 MW to nearly half of that value. The power decrease continues as temperatures of the lead and cladding continue to rise. At around 20 minutes into the transient, the power of the core has decreased to 30 MW and continues to decrease due to inlet temperature rise.

The inlet temperature of the core starts steadily increasing, as the MHX is not powerful enough to remove the heat from the coolant. The inlet temperature increases 100 degrees in around 50 minutes. Dominant reactivity feedbacks are negative radial expansion and positive Doppler.



a) b)

Fig. 5.4.5-1: a) Core flow, power and MHX power in relative units
b) Reactivity components and total feedback for ULOF+ULOHS



a) b)

Fig. 5.4.5-2: a) Core inlet, outlet and maximum clad temperatures
b) Same with added maximum fuel temperature for ULOF+ULOHS

In case of ULOF+ULOHS transient, vessel temperature continues to rise with coolant temperature and might pose an issue in the long term.

5.5 T-DEC5: Unprotected partial blockage in the hottest fuel assembly

Parametric studies on partial blockage in the hottest SA has been investigated in the unprotected case without reactor scram, in order to evaluate the maximum reduction of cross flow area or flow rate through the SA that might be sustained without leading to significant fuel rod damage. In general, conservative assumptions have been taken with respect to heat transfer through the inter-wrapper gap with the surrounding SAs.

This transient has been analyzed by: KIT-G with SIM-LFR at BOC and EOC, JRC-IET with SIMMER at BOC, ENEA with RELAP5 and NRG with SPECTRA at EOC. The main results of these analyses are presented in the following subsections.

5.5.1 T-DEC5 transient: SIM-LFR results (KIT-G)

Two different calculations were performed (for both cases nominal power at HFP, no reactor trip and no radial heat transfer are assumed):

Case 1: The flow area through the hottest SA is blocked 97.5%. Thus a flow area of 2.5% remains open for the flow of coolant. Of interest here will be time to clad failure after blockage initiation.

Case 2: The maximum clad temperatures of the peak pin as a function of blockage area are determined.

Note: SIM-LFR assumption - in both cases it is assumed that coolant flow in the blocked SA is linearly proportional to the SA blocked flow area. Since

flow rate [kg/s] = density[kg/ m^3] *Flow_Area[m^2]*velocity[m/sec]

the flow rate may in reality not change exactly in proportion to the reduced flow area during the transient as the channel velocity may also change due to changing pressure conditions of the blocked sub-assembly (SA).

Case 1: 97.5% SA blockage area

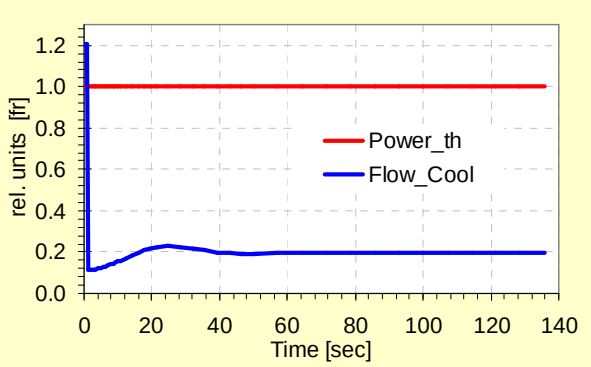
Sub-assembly blockage (97.5%) is assumed to be initiated instantly at 1 sec transient time.

The sub-assembly outlet temperature is assumed to be monitored but corresponding signal is assumed to fail in this transient.

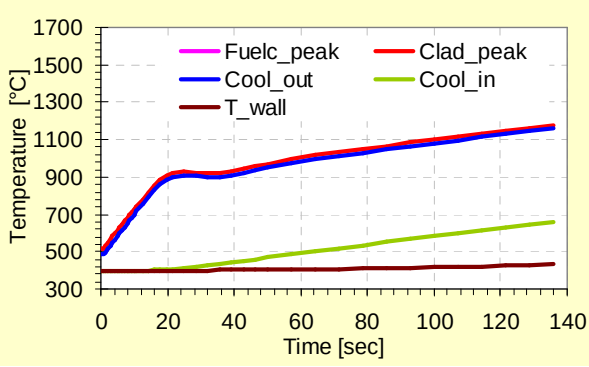
Several different cases are run at BOC and EOC conditions, varying the blockage area ranging from 20% to 97.5% (20, 40, 60, 65, 70, 75, 80, 90, 95 and 97.5%).

For the 97.5% SA blockage transient at BOC, the peak pin will fail ~57 sec into the transient due to clad rupture (transient initiation at 1 sec transient time) as the cladding temperature will reach 996 °C (see Fig. 5.5.1-1b), with a peak pin fission gas pressure of ~16.6 bar (see Fig. 5.5.1-2).

As a result of the SA blockage, the flow rate will initially decrease to ~ 12% nominal, gradually recovering to about 20% flow rate at ~50 sec into the transient due to changing SA pressure conditions. The power remains at 100% nominal throughout the transient (see Fig. 5.5.1-1a).

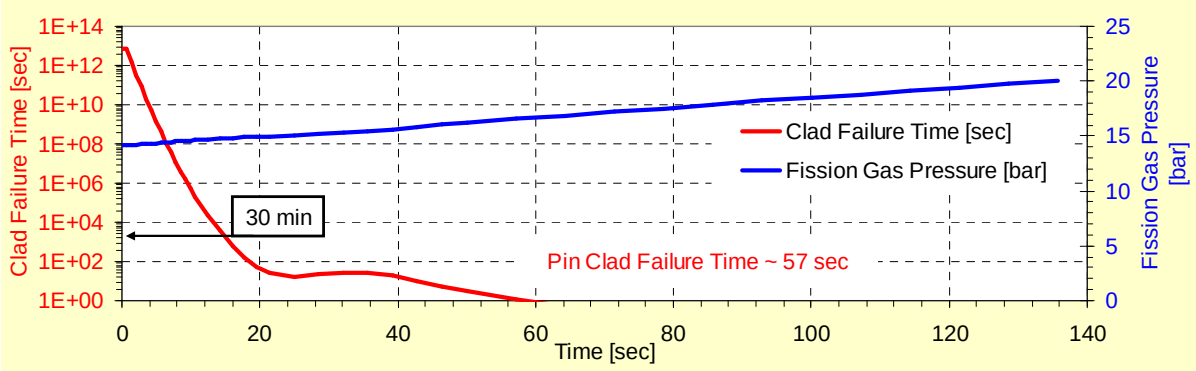


a) Relative core thermal power and hot SA flow rate



b) Peak fuel-, clad-, coolant- and vessel wall temperatures

Fig. 5.5.1-1: Results for T-DEC5: SA Blockage transient (flow area of hottest SA 97.5% blocked; w/o radial heat transfer, BOC conditions) as calculated by SIM-LFR (KIT)

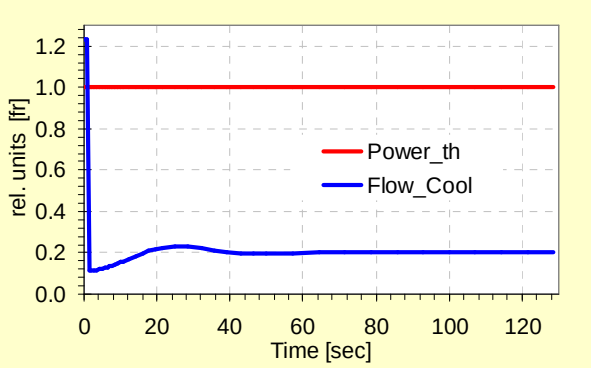


Peak pin plenum pressure and clad failure time

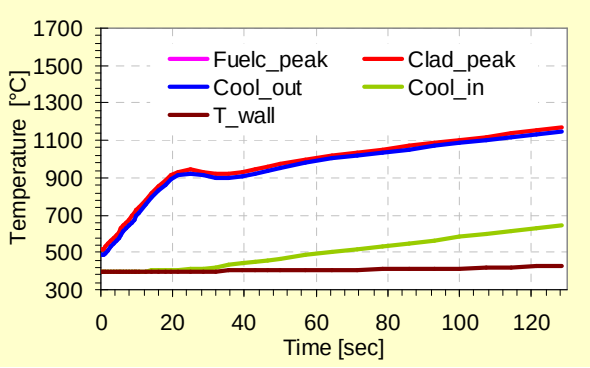
Fig. 5.5.1-2: Results for T-DEC5: SA Blockage transient (flow area of hottest SA 97.5% blocked; w/o radial heat transfer, BOC conditions) as calculated by SIM-LFR (KIT)

For the 97.5% SA blockage transient at EOC, the peak pin will fail ~56 sec into the transient (transient initiation at 1 sec transient time) as the cladding temperature will reach 1000 °C (see Fig. 5.5.1-3b), with a peak pin fission gas pressure of ~23 bar (see Fig. 5.5.1-4).

As a result of the SA blockage, the flow rate will initially decrease to ~ 12% nominal, gradually recovering to about 20% flow rate at ~50 sec into the transient due to changing SA pressure conditions. The power remains at 100% nominal throughout the transient (see Fig. 5.5.1-3a).

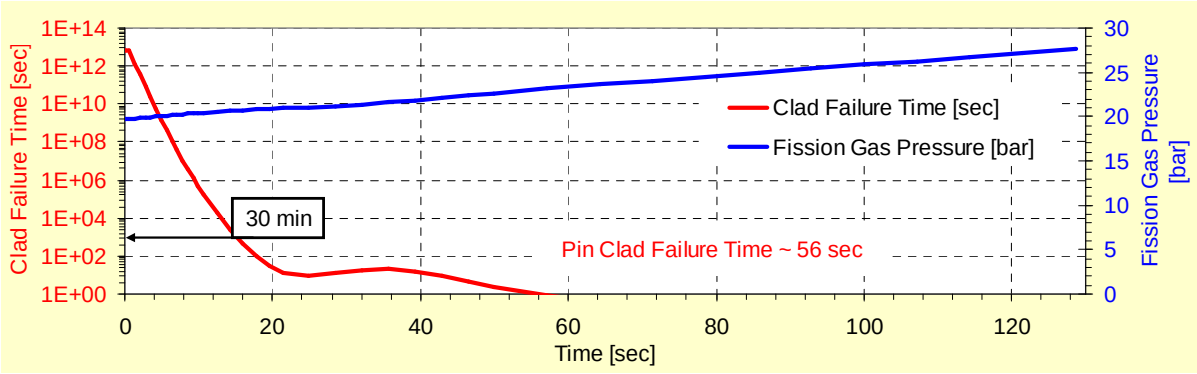


a) Relative core thermal power and hot SA flow rate



b) Peak fuel-, clad-, coolant- and vessel wall temperatures

Fig. 5.5.1-3: Results for T-DEC5: SA Blockage transient (flow area of hottest SA 97.5% blocked; w/o radial heat transfer, EOC conditions) as calculated by SIM-LFR (KIT)



Peak pin plenum pressure and clad failure time

Fig. 5.5.1-4: Results for T-DEC5: SA Blockage transient (flow area of hottest SA 97.5% blocked; w/o radial heat transfer, EOC conditions) as calculated by SIM-LFR (KIT)

Case 2: Different SA blockage areas

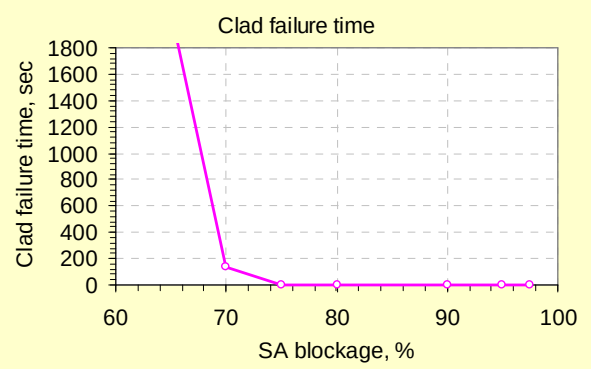
Table 5.5.1-1 and Fig. 5.5.1-5 display the corresponding clad failure times and clad melting times as a function of blockage area (from 20% to 97.5%) for BOC conditions, while Table 5.5.1-2 and Fig. 5.5.1-6 display the corresponding clad failure times and clad melting times as a function of blockage area (from 20% to 97.5%) for EOC conditions. The following can be observed:

- The ALFRED will not experience any fuel pin failure for blockage areas less than 75% for both BOC and EOC conditions, even under unprotected conditions;
- For blockages above 75%, clad failures must be expected (see 5.5.1-5a and Fig. 5.5.1-6a) for both BOC and EOC conditions;
- Fuel melting is not an issue for ALFRED. Fuel melting temperatures are not reached even in 97.5% SA blockage case (see Fig. 5.5.1-5b and Fig. 5.5.1-6b) for both BOC and EOC conditions.

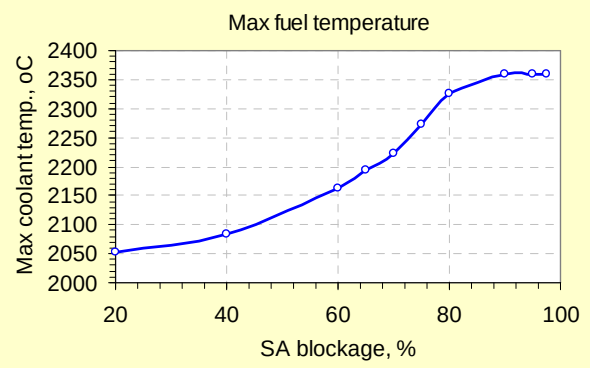
Table 5.5.1-1: ALFRED clad failure time and max SA channel temperatures as a function of SA blockage area for BOC under unprotected blockage transients (T-DEC5) conditions.

Blockage	Clad failure time*	Max. cool. SA outlet temp.	Max clad temp (peak pin)	Max fuel temp (peak pin)
%	sec	°C	°C	°C
20	4.00E+10	542	573	2052
40	2.20E+08	608	638	2083
60	4.20E+04	742	771	2162
65	2057	799	826	2194
70	136	873	898	2222
75	0	974	997	2272
80	0	1091	1110	2326
90	0	1158	1176	2359
95	0	1158	1176	2359
97.5	0	1158	1176	2359

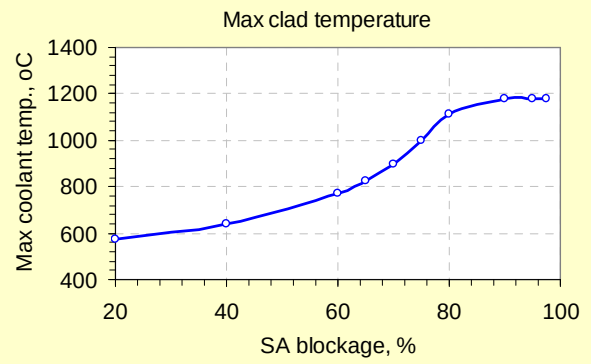
* - max fission gas pressure ~18 bar



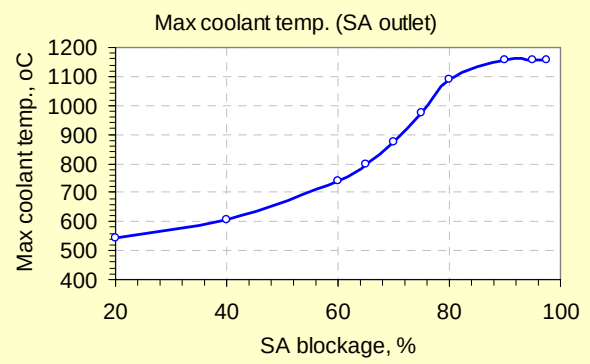
a) Clad failure time [s] as a function of SA channel blockage area



b) Max fuel temperature [°C] as a function of SA channel blockage area



c) Max clad temperature [°C] as a function of SA channel blockage area



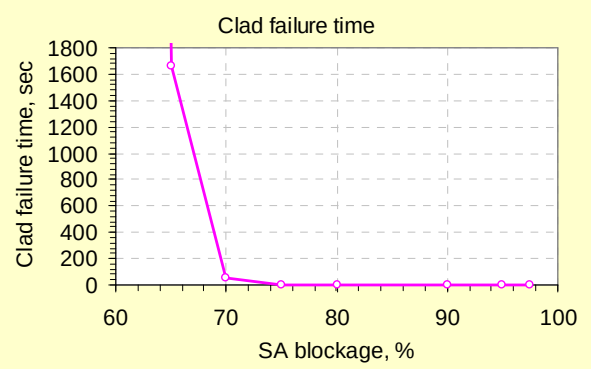
d) Max coolant temperature [°C] as a function of SA channel blockage area

Fig. 5.5.1-5: Results for T-DEC5: SA Blockage transient. Clad failure time and max SA channel temperatures as function of SA blockage area for BOC conditions as calculated by SIM-LFR (KIT)

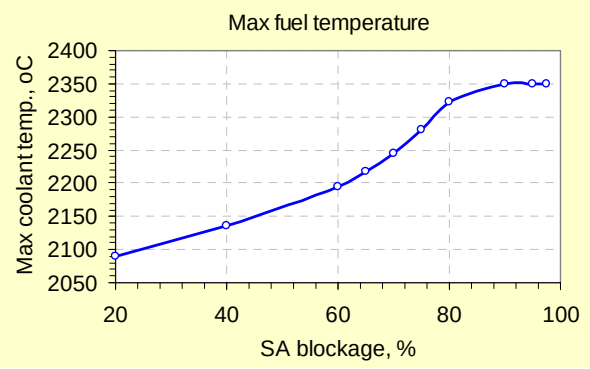
Table 5.5.1-2: ALFRED clad failure time and max SA channel temperatures as a function of SA blockage area for EOC under unprotected blockage transients (T-DEC5) conditions.

Blockage	Clad failure time*	Max. cool. SA outlet temp.	Max clad temp (peak pin)	Max fuel temp (peak pin)
%	sec	°C	°C	°C
20	2.70E+10	545	574	2089
40	1.50E+08	612	641	2136
60	3.00E+04	745	772	2194
65	1661	801	827	2218
70	53	874	898	2245
75	0	974	996	2280
80	0	1084	1103	2322
90	0	1148	1165	2349
95	0	1148	1165	2350
97.5	0	1148	1165	2350

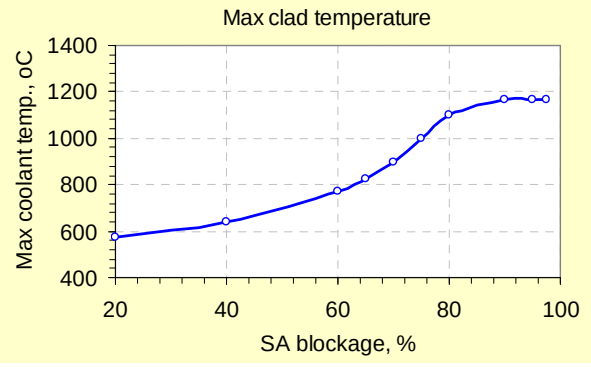
* - max fission gas pressure ~25 bar



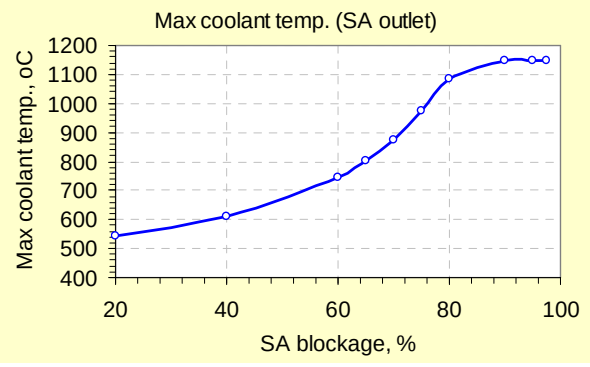
a) Clad failure time [s] as a function of SA channel blockage area



b) Max fuel temperature [°C] as a function of SA channel blockage area



c) Max clad temperature [°C] as a function of SA channel blockage area



d) Max coolant temperature [°C] as a function of SA channel blockage area

Fig. 5.5.1-6: Results for T-DEC5: SA Blockage transient. Clad failure time and max SA channel temperatures as function of SA blockage area for EOC conditions as calculated by SIM-LFR (KIT)

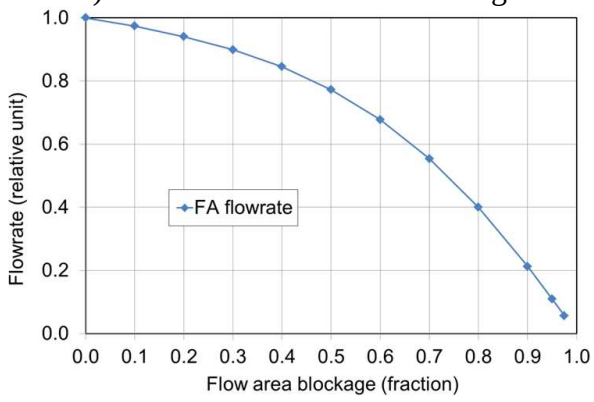
5.5.2 T-DEC5 transient: RELAP5 results (ENEA)

The progressive reduction of FA inlet flow area in the hottest FA has been assumed in the RELAP5 calculations up to a maximum of 97.5% of blocked inlet flow area. The local pressure loss at the FA inlet has been evaluated to about 22% of the entire FA pressure loss that is equal to 1 bar. For a conservative analysis the heat exchange with surrounding FAs through the inter-wrapper gap is neglected. The main results of the RELAP5 analysis are illustrated in Fig. 5.5.2-1.

As a result of the reducing inlet flow area, the mass flow rate in the hottest FA decreases as shown in Fig. 5.5.2-1a. A 75% blockage at the FA inlet leads to about 50% mass flow rate reduction inside the FA. The corresponding maximum FA temperature increase for the coolant, the clad and the fuel is represented in Fig. 5.5.2-1b. The maximum clad temperature reaches the temperature limit of 700 °C after an inlet area blockage of about 85%. Clad melting (Tmelt ~1500 °C) is not expected for blockages below 95%. The fuel melting temperature (Tmelt ~2670 °C) in the center of the peak power fuel pellets is exceeded only if the area blockage is close to 97.5%.

The partial FA blockage has been simulated under unprotected conditions, that is without reactor scram. However, temperature measurements are provided by thermocouples positioned at the outlet of each FA, in order to detect an eventual flow area blockage in a FA. From the above results it appears that a 50% blockage at the FA inlet would lead to a temperature increase at the FA outlet sufficient to overcome the reactor scram threshold set-point value (ΔT through the FA greater than 1.2 nominal value), thus limiting and terminating the FA temperature increase well within the safety limits.

a) Flowrate vs. flow area blockage



b) Max temperatures vs. flow area blockage

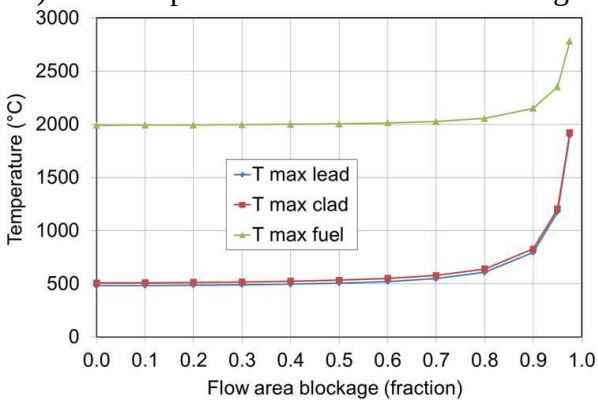


Fig. 5.5.2-1: Main RELAP5 results of the T-DEC5 transient

5.5.3 T-DEC5 transient: SPECTRA results (NRG)

The T-DEC5 scenario is as follows:

- Partial blockage of the hottest fuel assembly, inlet junction (JN-001) assumed to be blocked.

- Blockage is defined by a decrease of flow area, with constant loss factor, overall core ΔP = ~1.0 bar.
- Blockage fractions: 10, 20, 30, 40, 50, 60, 70, 80, 90, 95, 97% (subcooled boiling leading to code termination was observed for 97.5%, therefore 97% is the highest blockage reported here).
- Reactor trip (scram signal) is disabled. No heat exchange with surrounding assemblies.

In this transients all loops are symmetrical. The model with all loops combined into one is used. The NRG SPECTRA results are shown in Fig. 5.5.3-1 and Fig. 5.5.3-2. Each case is a separate run, performed for 100 s since start of blockage. During this time stable parameters are obtained.

Relative flow versus blockage fraction is shown in Fig. 5.5.3-1. Reduction of flow rate to 50% corresponds to 75% of area reduction.

Maximum fuel, cladding, and coolant temperatures versus blockage fraction are shown in Fig. 5.5.3-2. The maximum cladding temperature of 700˚C is exceeded at about 85% blockage. No cladding melting is expected for blockage ≤95% (T91 clad melts at ~1450˚C). No fuel melting is expected for blockage ≤90% (MOX fuel melts at ~2670˚C). Coolant T ~580 °C at 50% blockage can be detected by TC-s at assembly outlet. Note that scram signal at ΔT > 1.2×nominal (502 ˚C) (blockage ≥ 50%) is disabled here.

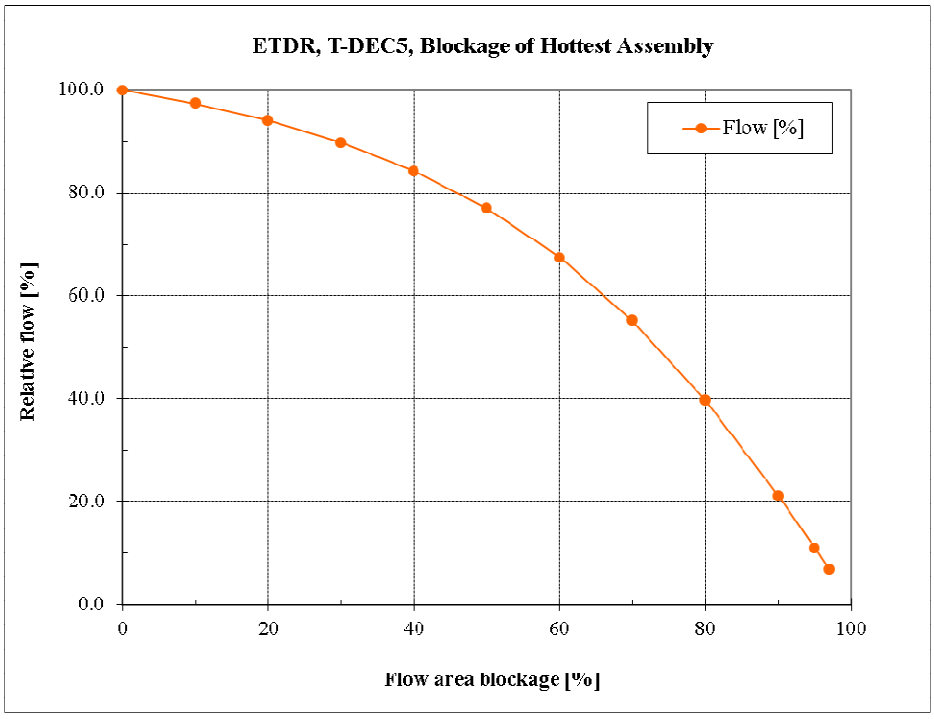


Fig. 5.5.3-1: Relative coolant flow rate vs. flow area blockage

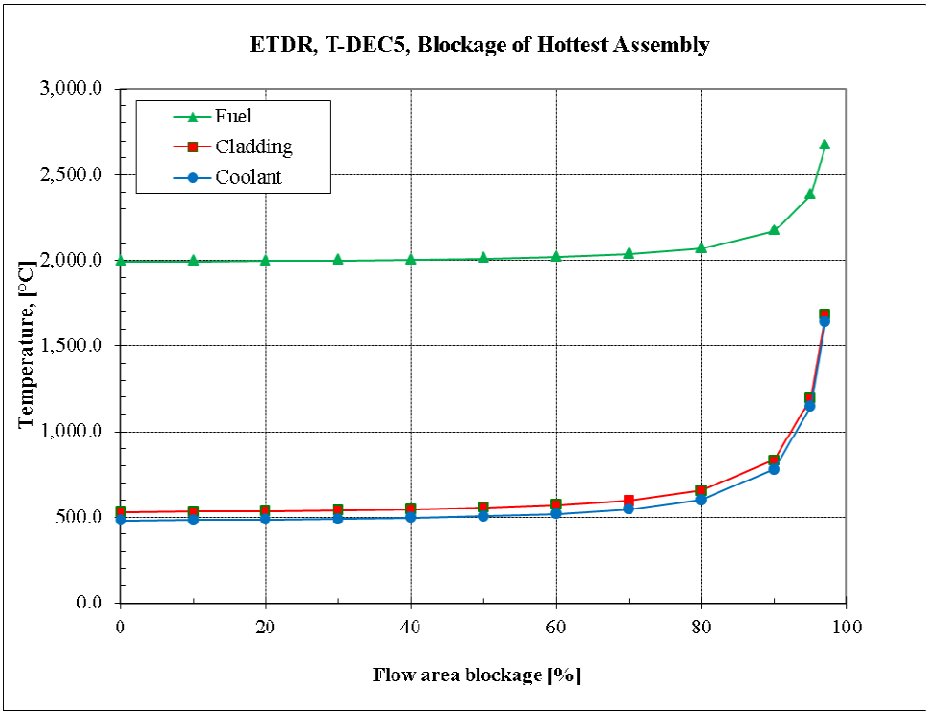


Fig. 5.5.3-2: Fuel, cladding and coolant temperatures vs. flow area blockage

5.5.4 T-DEC5 transient: SIMMER results (JRC-IET)

A SIMMER-III 2D geometrical model, representing the central blocked sub-assembly as well as the surrounding ring of six sub-assemblies, has been set-up for the purpose of these analyses (see Fig. 5.5.4-1) The details of the modelling and the simulation approach are presented in Appendix D.

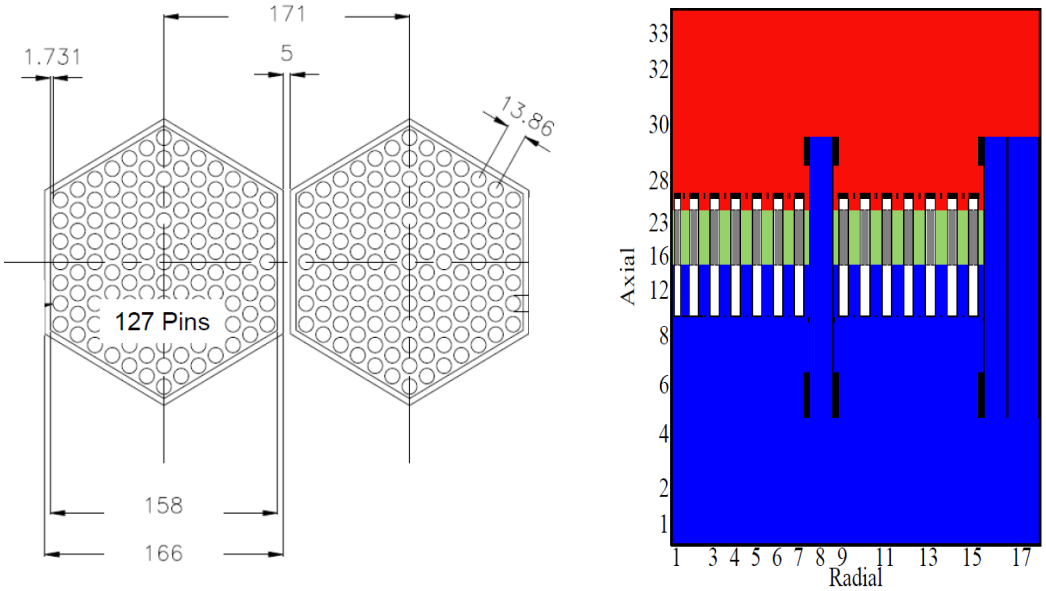


Fig. 5.5.4-1: Cross-section of the ALFRED fuel sub-assembly (left) and R-Z representation of the calculation mesh for the analyses of partial sub-assembly blockages in SIMMER-III (right)

Steady state

The steady state corresponding to peak power conditions was established with the coolant temperature gradient being 87 K and the corresponding pressure drop between the SA inlet and outlet predicted at 0.73 bar. The steady state conditions are typically established rather fast – within several seconds after the initiation of the simulation.

Coolant blockages (Unprotected cases)

A parametric study of unprotected coolant blockages was performed assuming blockages ranging from 65% to 75% of the coolant flow cross-section. The blockages were introduced at the location of the pin grid in all internal sub-channels (axial cell no. 10). In the simulations, no radial coolant cross-flow has been assumed. The results of the analyses are summarised in Table 5.5.4-1. The results of the SIMMER-III analyses are somewhat different from RELAP5 and SPECTRA results of previous sections 5.5.2 and 5.5.3, depending on the different location of the flow area blockage. In fact, same percentage of flow area blockage at the FA inlet in RELAP5 and SPECTRA calculations leads to much larger flow rate reduction with respect to flow area blockage at the lower pin grid location considered in the SIMMER-III analysis.

Table 5.5.4-1 - Results of analyses of the unprotected sub-assembly blockages

Coolant flow area blockage [%]	Maximum predicted temperature [K(°C)]		Outlet coolant temperature [°C]	%ΔT*
	Cladding	Coolant		
65	804(531)	777(504)	493	7
70	817(544)	789(516)	497	11.5
75	833(560)	807(534)	505	20.7

*Taken into account the nominal inlet and outlet coolant temperatures of 400°C and 487°C, respectively

As for the 65% coolant flow area blockage (cf. Fig. 5.5.4-2), the maximum predicted coolant temperature is 504 °C, while 531 °C for the cladding. The SA coolant outlet temperature is 493 °C, which corresponds to only a small increase with respect to the corresponding nominal value (487 °C) and as such might not be detectable and would not be prevented by a reactor scram signal. However, also no systematic fuel pin damage is to be expected.

As for the 70% coolant flow cross-section blockage (cf. Fig. 5.5.4-3), the maximum predicted coolant temperature is 516 °C, while 544 °C for the cladding. Hence, no systematic fuel pin damage is again to be expected. In this case, the predicted increase in SA outlet temperature is only 10 °C and again this initiator might not be prevented by a reactor scram signal.

As a consequence of a blockage of 75% of the coolant flow area (cf. Fig. 5.5.4-4) the maximum coolant temperature of 534 °C is predicted, while 560 °C for the pin cladding. The estimated increase in the SA coolant outlet temperature is greater than 18 °C representing more than 20% increase in the coolant temperature gradient compared to its nominal value (87 °C), which is expected to trigger a reactor scram signal subsequently resulting in the shut-down of the reactor. However, since cladding temperatures are still well below the threshold for fast creep

(~830 °C), no systematic damage is expected to the fuel pin cladding even if the blockages are not protected in the short time frame after the initiation of the accident (< 30 min).

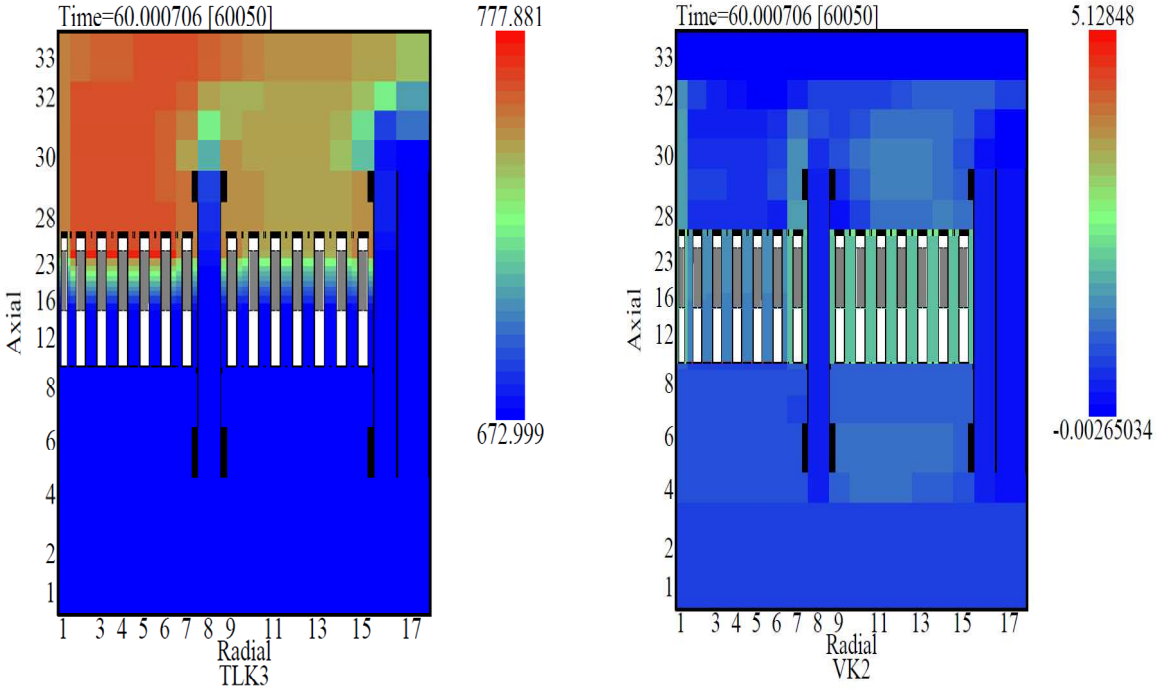


Fig. 5.5.4-2: Coolant temperature (left) and axial velocity distribution (right) corresponding to 65% coolant flow area blockage of all internal sub-channels

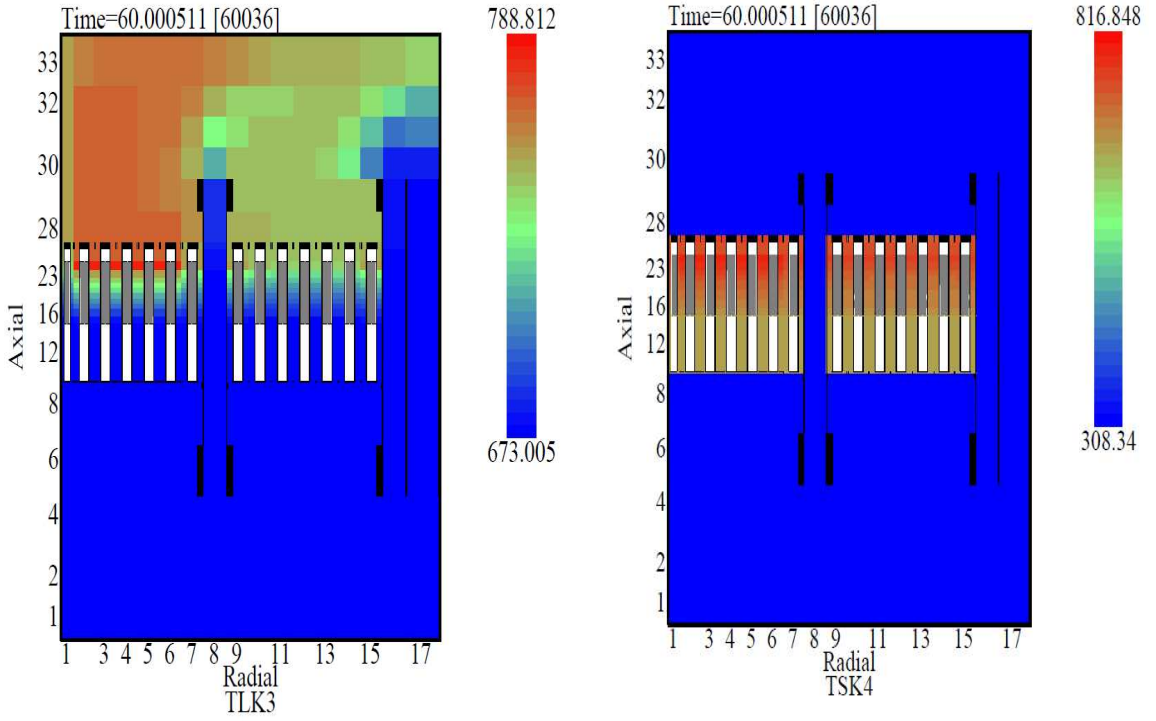


Fig. 5.5.4-3: Coolant temperature (left) and cladding temperature (right) distributions corresponding to 70% coolant flow area blockage of all internal sub-channels

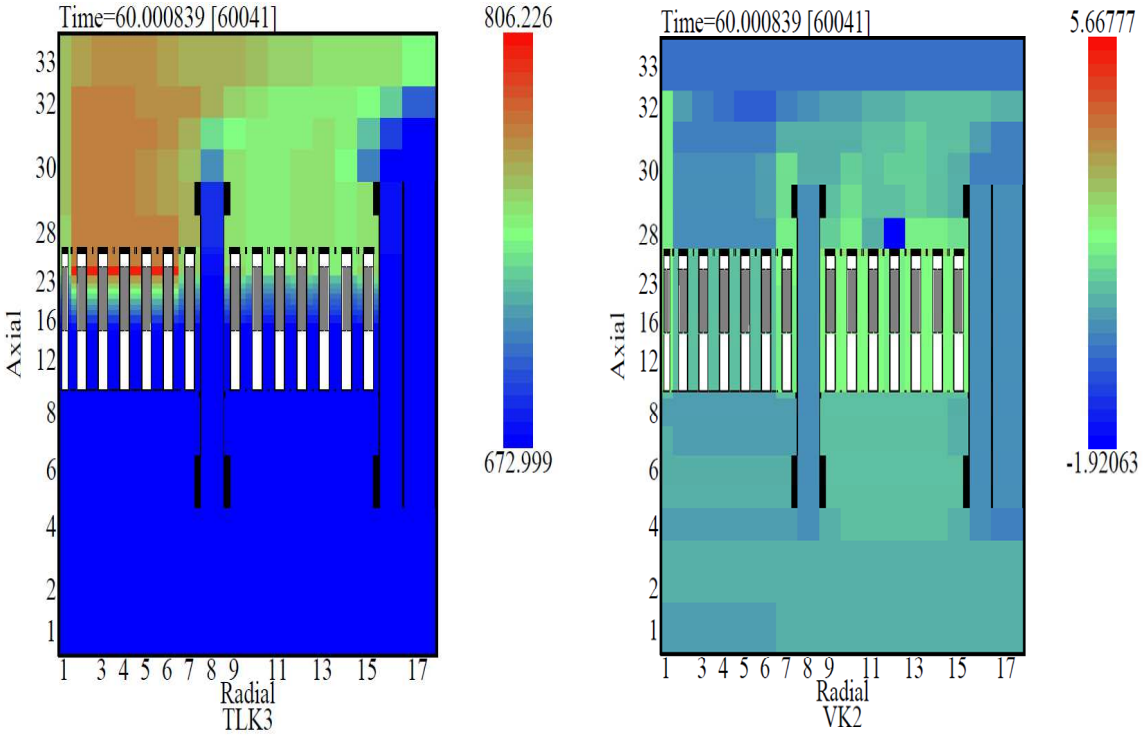


Fig. 5.5.4-4: Coolant temperature (left) and axial velocity distribution (right) corresponding to 75% coolant flow area blockage of all internal sub-channels

Coolant blockages (Protected case)

The situation of nearly total blockages protected by the reactor scram signal was also considered in the analyses as a Design Extension Condition. The SA blockage was expected to be detected 5 seconds into the transient, well within the interval when SA coolant temperature gradient is expected to exceed 120% of its nominal value [DEL015-2013]. Subsequently, the delay of the reactor scram is parametrically assumed to occur 1, 2, 3, 5, and 10 seconds from the detection of the SA blockage. The corresponding reactor scrams therefore occur at 6, 7, 8, 10, and 15 seconds into the transient. Similarly to the analyses of the unprotected blockages, radial cross-flow has not been modelled in these cases. Decay heat was taken into account corresponding to the BOC conditions.

The first results indicate that thanks to the high thermal inertia of lead, even if the shut-down is delayed by up to 5 seconds following the detection of the blockage, clad temperatures remain below the threshold for which clad ruptures initiated by fast creep would occur (~830 °C). On the other hand, our analyses also suggest that 10 seconds delay in reactor scram would likely result in systematic fuel pin clad failures possibly leading to severe core damage. In this case, preliminary indications are that residual coolant flow between 7-10% of the nominal value would be sufficient to remove the resulting decay heat such that a systematic clad damage can be effectively prevented. These qualitative conclusions are also supported by an analytical assessment of the heat balance in the modelled geometry.

It is important to note that in LFRs, in contrast to the phenomenology of SFRs, the clad ruptures and melting will occur well before a coherent coolant boiling is to be expected (T_{boil} = 1749°C at atmospheric pressure).

5.6 T-DEC6: Failure of secondary cooling circuits

The sudden depressurization of all secondary circuits is postulated in the T-DEC6 event. Even if T-DEC6 is classified as a “practically-excluded” event in the DEL011-2012 of the LEADER project, the associated transient is analyzed to give indications on the grace time left to the operator for corrective actions. Also both DHR systems are postulated to be unavailable.

This transient has been analyzed by: KIT-G with SIM-LFR at BOC and EOC conditions, ENEA with RELAP5 and NRG with SPECTRA at EOC conditions. The main results of these analyses are presented in the following subsections.

5.6.1 T-DEC6 transient: SIM-LFR results (KIT-G)

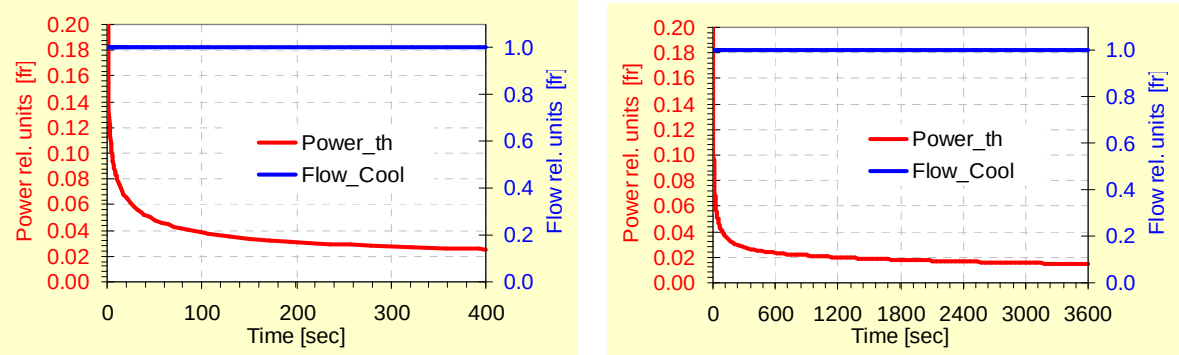
For these calculations SCS failure was postulated - the primary heat transport path through the MHXs was assumed to fail at time t = 0 sec. One second later two signals for reactor shutdown are generated: 1) MHX outlet temperature on the primary (lead) side becomes more than 430 ^{o}C, and 2) Turbine trip signal on the failure of SCS (turbine stop valve closure). Based on these two reactor scram signals (even if the first one is being neglected), the reactor is being shut-down by a reactor shutdown system - the SCS failure (LOHS) transient is simulated as a protected transient. In order to achieve even more conservative analysis results, a simultaneous failure of both DHRS (DHR-1 and DHR-2 subsystems) is being postulated. This implies that from that time point onwards, the power generated in the reactor core remains within the primary cooling circuit. Following the reactor scram, all relevant core temperatures first will decrease, but later will start increasing due the primary cooling system heat-up by the decay heat (the only heat sink available is the radiation heat loss of the primary system). The primary pumps are assumed operational thereby assuring an even heat distribution throughout the primary cooling system providing a nominal primary coolant flow rate.

Two cases were analyzed to investigate the clad and fuel temperature response of the peak pin during this SCS failure (PLOHS) transient, namely at BOC and EOC conditions.

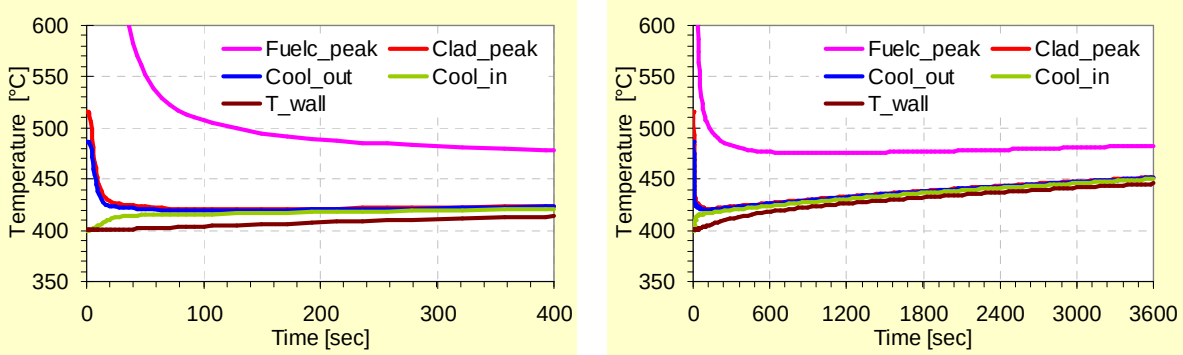
Under BOC (Fig. 5.6.1-1), as well as EOC (Fig. 5.6.1-2) conditions, the power level in the core is observed to rapidly decrease to the decay heat level, following the reactor scram. All core temperatures, as a result of the decreasing reactor power, decrease during the initial phase of the transient. Later, due to the SCS and DHRS failures (no decay heat is being transferred through the MHX to the secondary cooling circuit), fuel, clad, coolant and vessel temperatures start increasing. In 1 hour transient time, fuel temperature will reach ~ 480 ^{o}C, clad and coolant temperatures will reach ~ 450 ^{o}C and reactor vessel temperature will reach ~445 ^{o}C. Based on the lead temperature gradients around the primary cooling circuit, one can estimate that clad and coolant temperatures will reach ~ 500 ^{o}C in 3 hours from the start of the transient. During this time period the operator has sufficient time for manual intervention by activating SCS or subsystems of DHR-1 system in order to prevent overheating of the whole primary system.

The very slow increase in the primary cooling circuit temperatures is due to the very large thermal inertia of the primary cooling system, continuously decreasing decay heat, as well as some radiation heat losses from the primary cooling circuit.

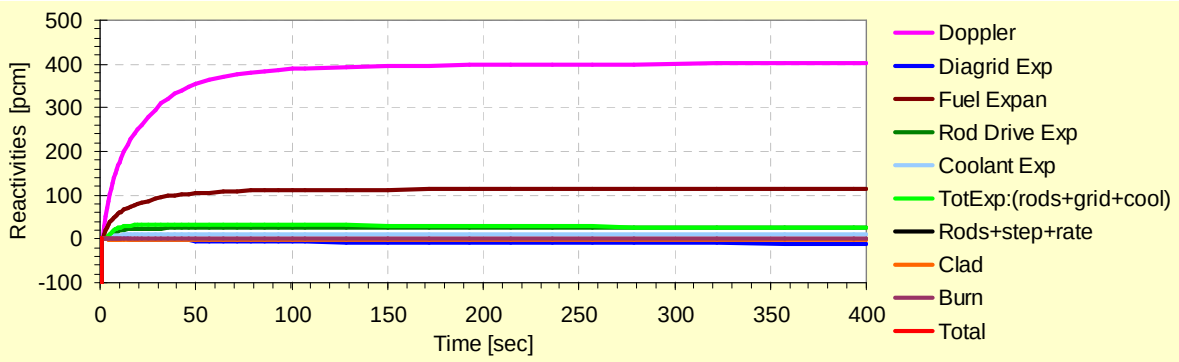
A conclusion can be made here, that a protected SCS failure transient, even assuming the complete failure of the DHRS (DHR-1 and DHR-2 subsystems), presents no imminent safety issue to the ALFRED reactor in the first several hours, following the event. However, all primary cooling circuit temperatures, in a longer time period, will start increasing slowly and will reach ~500 ^{o}C in 3 hours, but the operator has sufficient time for manual intervention by re-activating SCS or sub-systems of DHR-1 system in order to prevent overheating of the whole primary system, including the reactor vessel.

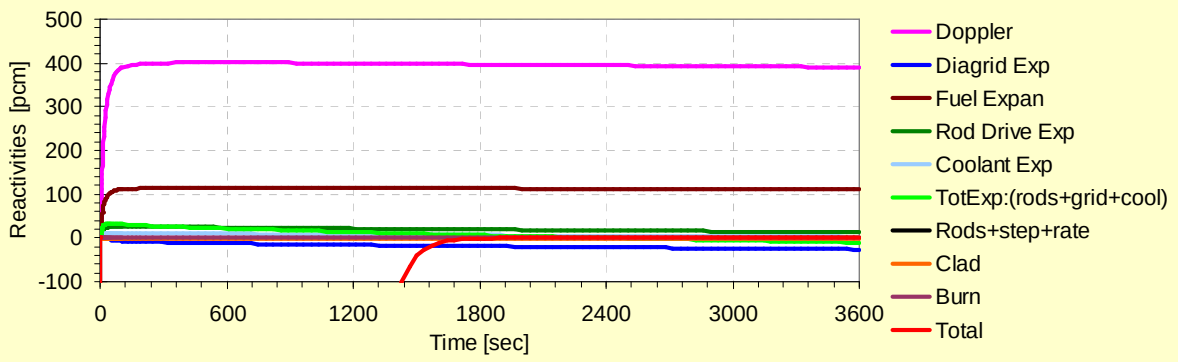


a) Relative core thermal power and flow rate

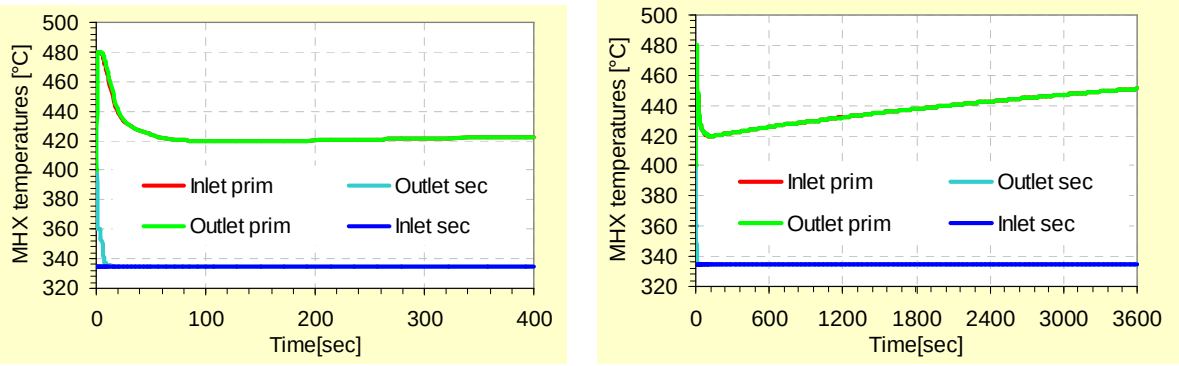


b) Peak fuel-, clad-, coolant- and vessel wall temperatures

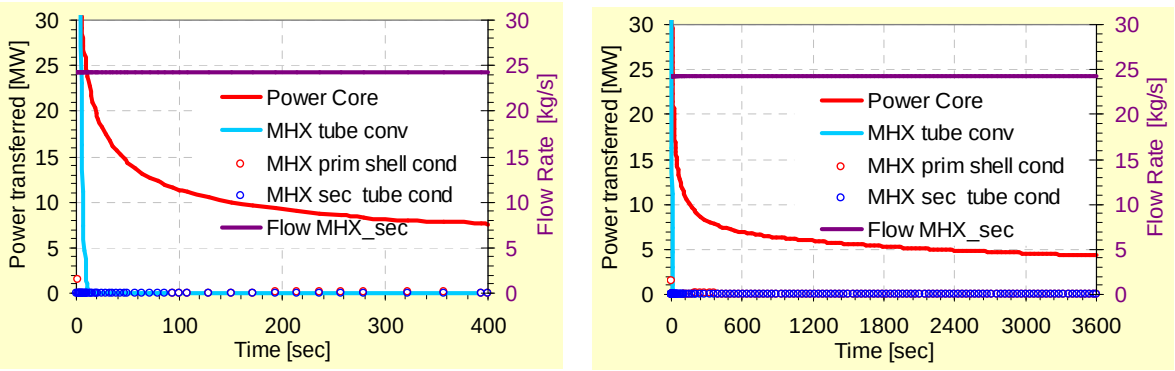




c) Reactivity effects

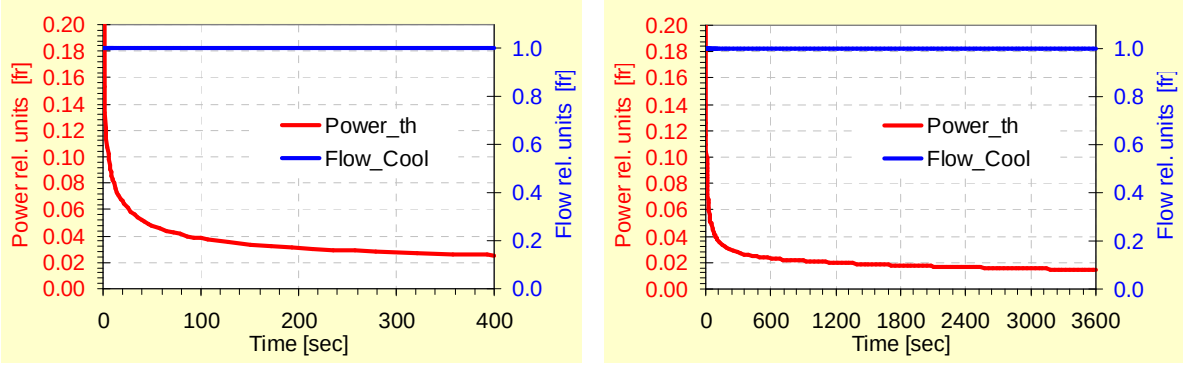


d) MHX temperatures

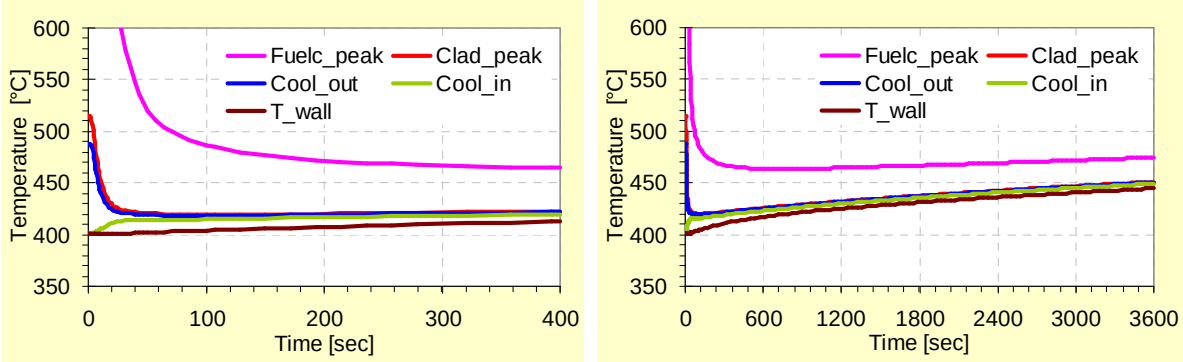


e) Core and MHX powers, plus MHX sec. side water flow rate

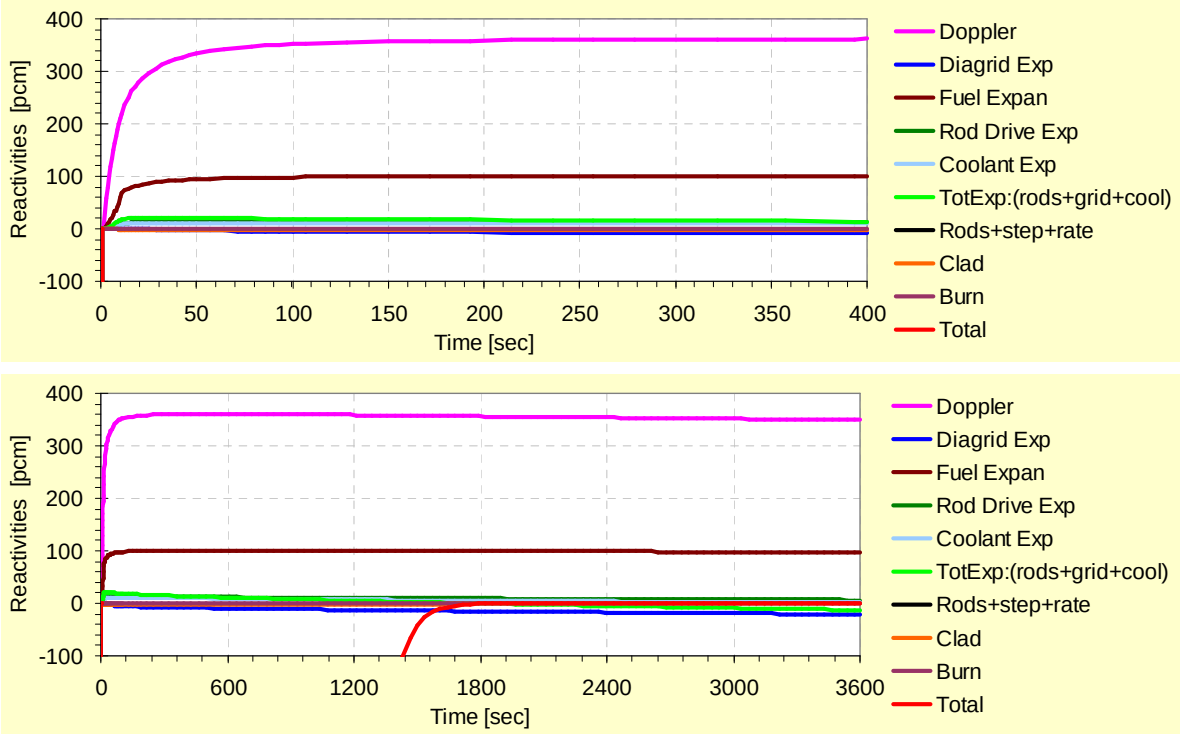
Fig. 5.6.1-1: Results for T-DEC6: SCS failure (PLOHS) transient at HFP - BOC conditions at peak burnup of 730 EFPD as calculated by SIM-LFR (KIT)



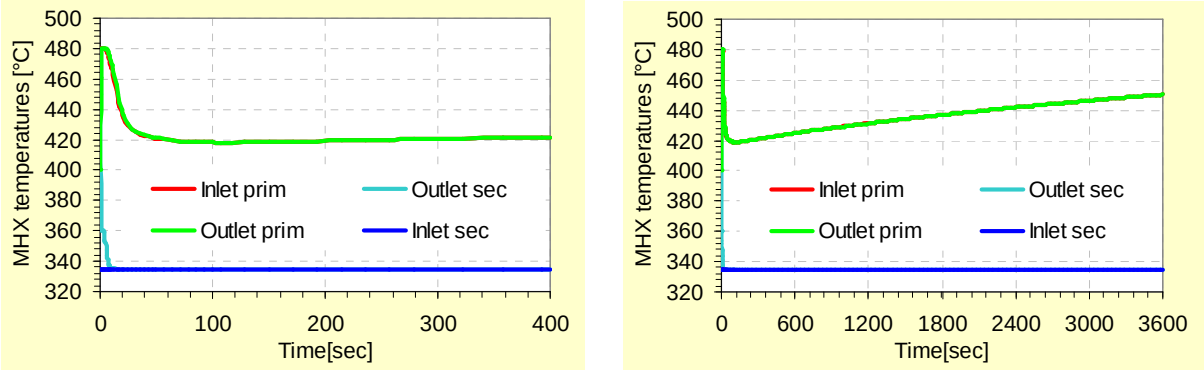
a) Relative core thermal power and flow rate



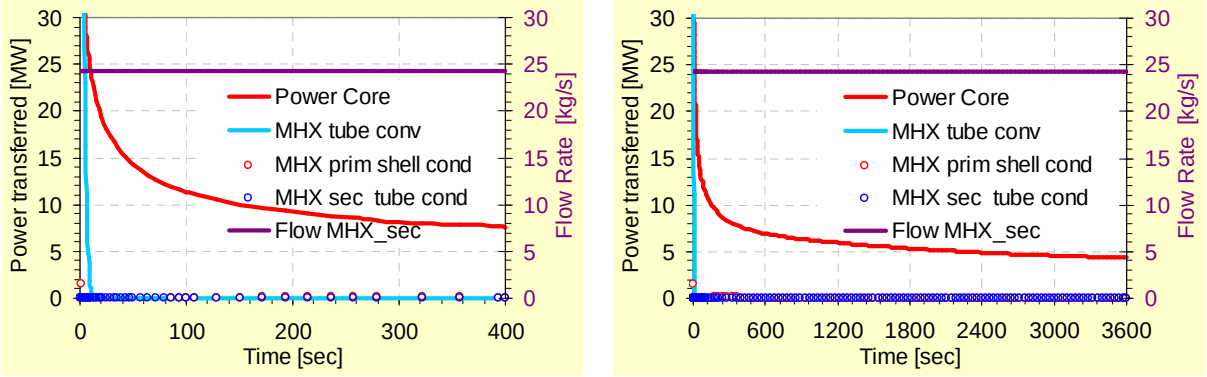
b) Peak fuel-, clad-, coolant- and vessel wall temperatures



c) Reactivity effects



d) MHX temperatures



e) Core and MHX Powers, plus MHX sec. side water flow rate

Fig. 5.6.1-2: Results for T-DEC6: SCS failure (PLOHS) transient at HFP - EOC conditions at peak burnup of 1095 EFPD as calculated by SIM-LFR (KIT)

5.6.2 T-DEC6 transient: RELAP5 results (ENEA)

This transient is initiated by the sudden depressurization of all secondary circuits. The reactor scram is actuated at t = 2 s on low secondary pressure signal. Also the DHR systems are postulated to be unavailable. The primary circuit remains in forced circulation. The main results of the T-DEC6 transient analysis are illustrated in Fig. 5.6.2-1 and Fig. 5.6.2-2 for the short term and the long term, respectively.

The secondary circuit pressure evolution is shown in Fig. 5.6.2-1a. The secondary pressure fall down to 130 bar in 2 s, when saturated conditions are reached, and then more slowly down to ambient pressure in about 40 s. The core power reduces down to decay level after reactor scram at t = 2 s, while the sudden water evaporation inside the MHX in the initial phase of the transient results in enhanced power removal by the secondary side (see Fig. 5.6.2-1b). The MHX power removal reaches a maximum of 843 MW at t = 2 s and then reduces down to zero after about 40 s, according to the full depressurization of the secondary circuits.

The enhanced power removal by the MHX produces a significant reduction in the lead temperature at the MHX outlet, in the initial phase, as shown in Fig. 5.6.2-1c. The minimum lead temperature reached at t = 15 s is of 353 °C, that is still far enough from the lead solidification point (327 °C). Therefore, no risk of lead freezing is expected in the primary circuit.

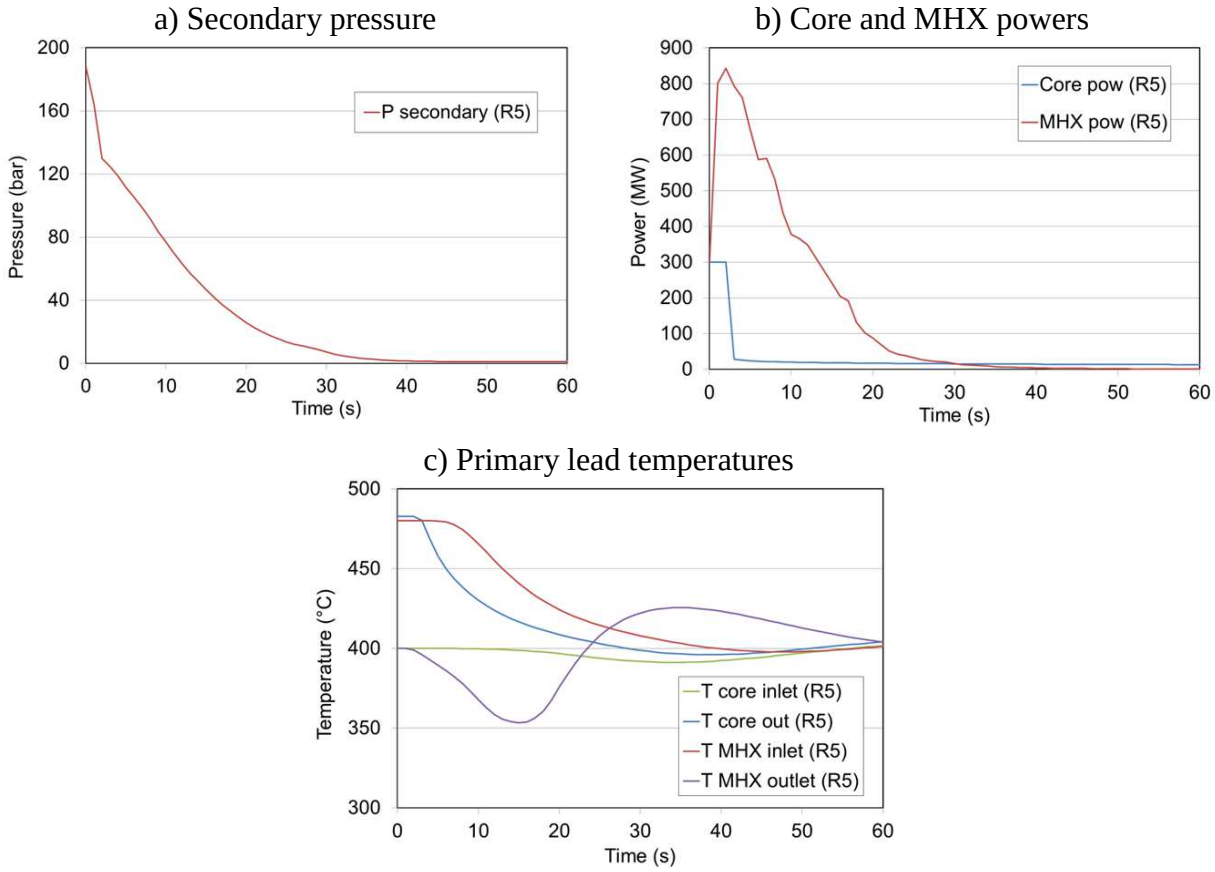


Fig. 5.6.2-1: Main RELAP5 results of the T-DEC6 transient *(short term)*

In the long term, the temperatures in the primary circuit rise slowly according to the decay power level (Fig. 5.6.2-2) and the large thermal inertia of the primary system (lead + structures). A rather uniform temperature distribution is reached in the primary circuit due to forced circulation and good mixing in the lead pool surrounding the MHXs. After about two hours, the primary temperatures are still rather low (below 470 °C). Therefore, there is large grace time for operator actions. Possible recovery actions consist in the isolation of some secondary circuits and activation of corresponding IC loops of DHR system for decay heat removal and primary temperature control.

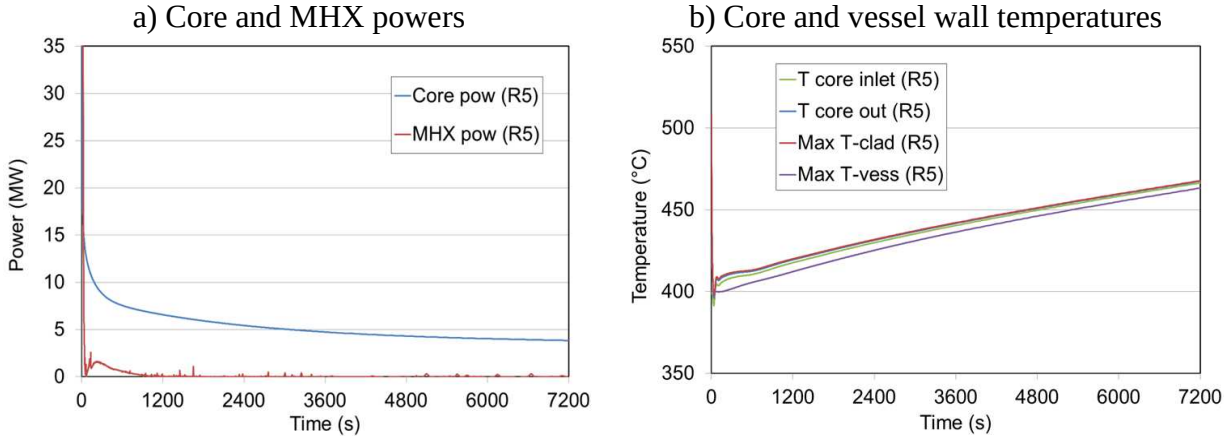


Fig. 5.6.2-2: Main RELAP5 results of the T-DEC6 transient *(long term)*

5.6.3 T-DEC6 transient: SPECTRA results (NRG)

The T-DEC6 scenario is as follows:

- Depressurization of all secondary circuits at 0.0 s, MSDV-s open in 1.0 s, MSIV-s close in 1.0 s.
- Isolation Condensers not available.
- FW stops at t = 10.0 s. Pump speed halving time assumed 1.0 s.
- Reactor trip (scram) at t = 2 s on low secondary pressure.

In this transient all loops are symmetrical. The model with all loops combined into one is used. The NRG SPECTRA results are shown in Fig. 5.6.3-1 through Fig. 5.6.3-7.

Secondary pressures are shown in Fig. 5.6.3-1. The secondary pressure decreases to atmospheric in about 40 s. Core power and MHX power are shown in Fig. 5.6.3-2. Due to reactor scram at 2.0 s, the core power decreases and follows the decay power. The MHX power shortly increases to 802 MW and then decreases to about zero. Note that the height of the initial peak is very short and is strongly governed by the valve closing/opening time. In the current analyses 1.0 s was assumed for MSIV/MSDV opening/closing. If this time was 5 seconds, the peak power would be about 675 MW.

The coolant temperatures are shown in Fig. 5.6.3-3. Lead temperatures in the core decrease to about 400 °C in about 60 s. Similar lead temperatures (~400 °C) are observed at the inlet and outlet of the MHX.
The fuel and cladding temperatures are shown in Fig. 5.6.3-4 and Fig. 5.6.3-5. The maximum fuel temperature decreases after the reactor scram (at 2.0 s). The maximum cladding temperature decreases after the reactor scram.

Long term power of core and MHX is shown in Fig. 5.6.3-6. The core power follows the decay power; at 2 hours the power is 3.5 MW. The MHX power is approximately zero after about half a hour.

The long term coolant temperatures are shown in Fig. 5.6.3-7. Because the decay heat is not removed by MHX, the temperatures rise slowly. After 2 hours the lead temperature at the core outlet is still below the initial temperature. This gives large grace time for the operator to take corrective actions (activate Isolation Condensers). The slow primary temperature increase is due to large thermal inertia of the primary system and effective mixing in the cold pool surrounding the MHX-s. In steady state (a) the pool surrounding the MHX-s is at ~400 °C. Two hours into T-DEC6 (b), the pool surrounding the MHX-s is at ~ 450 °C; similar temperature is observed in the core.

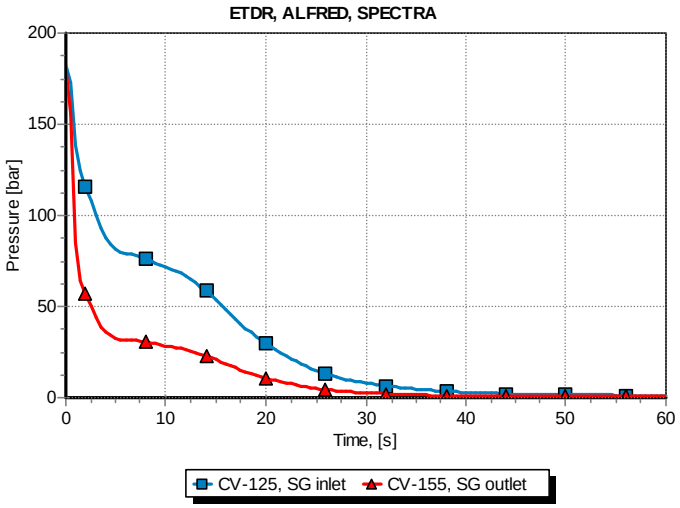


Fig. 5.6.3-1: Secondary pressure

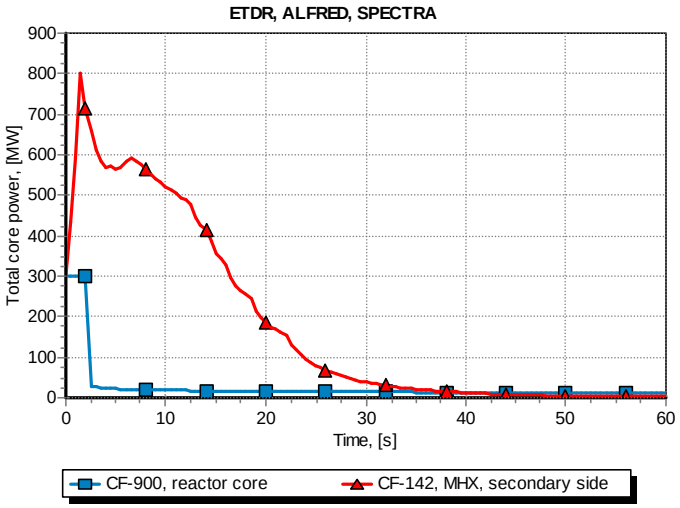


Fig. 5.6.3-2: Core power and MHX powers

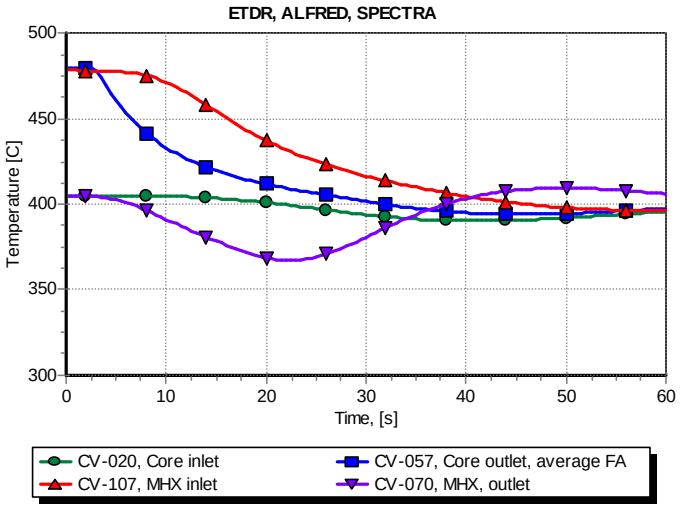


Fig. 5.6.3-3: Primary coolant temperatures – short term

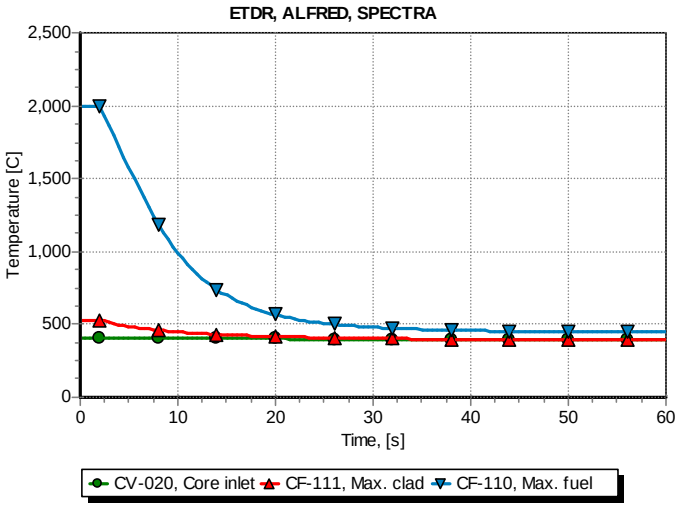


Fig. 5.6.3-4: Core inlet, cladding and fuel temperatures – short term

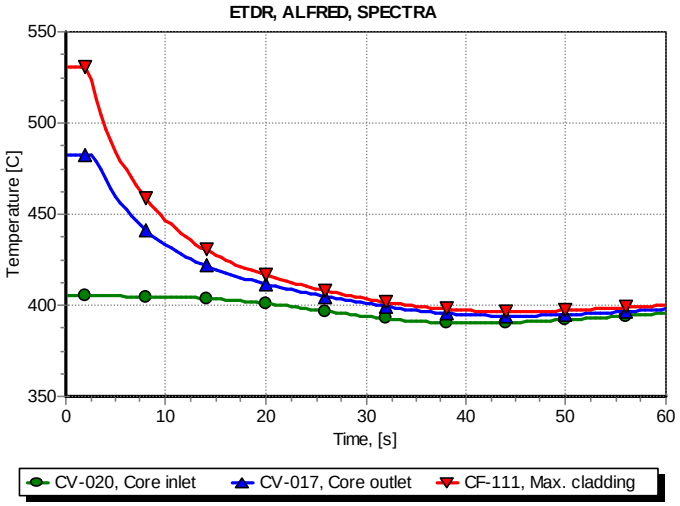


Fig. 5.6.3-5: Core inlet, outlet and cladding temperatures – short term

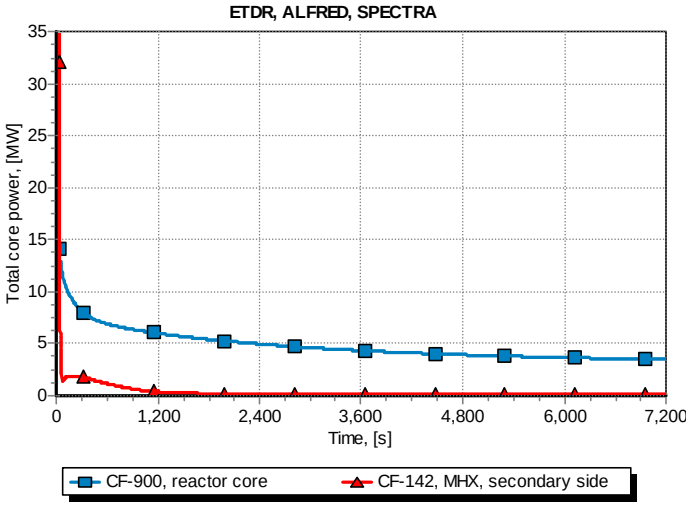


Fig. 5.6.3-6: Core power and MHX powers - long term

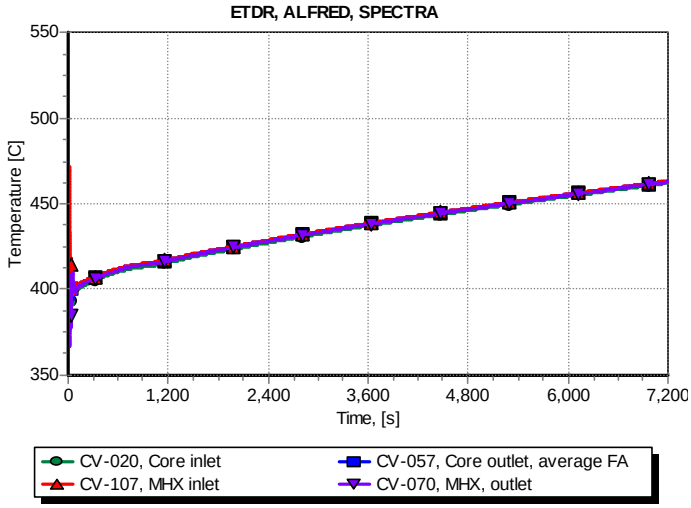


Fig. 5.6.3-7: Primary coolant temperatures - long term

5.7 TO-3: Reduction of FW temperature with all primary pumps trip

The simultaneous loss of primary pumps and feedwater temperature reduction on the secondary side is taken into account in this transient. The feedwater temperature is assumed to reduce from 335 °C down to 300 °C in 1 s, because of the partial loss of pre-heating function. The reactor scram is considered on low primary pump speed signal. Following reactor scram, the secondary circuits are isolated and the DHR-1 system is started for decay heat removal. All four sub-systems of the DHR-1 system are supposed available to be conservative against the risk of lead freezing in the primary circuit in the long term.

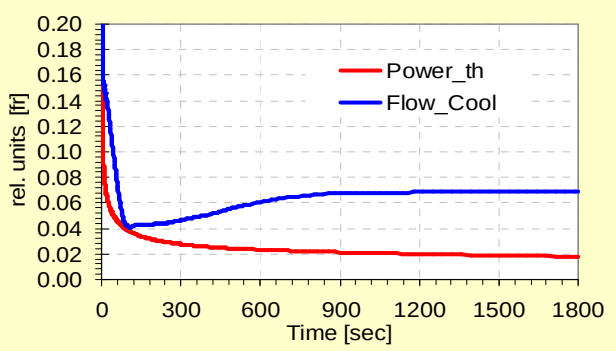
This transient has been analyzed by: KIT-G with SIM-LFR at BOC and EOC conditions, ENEA with RELAP5 and NRG with SPECTRA at EOC conditions. The main results of these analyses are presented in the following subsections.

5.7.1 TO-3 transient: SIM-LFR results (KIT-G)

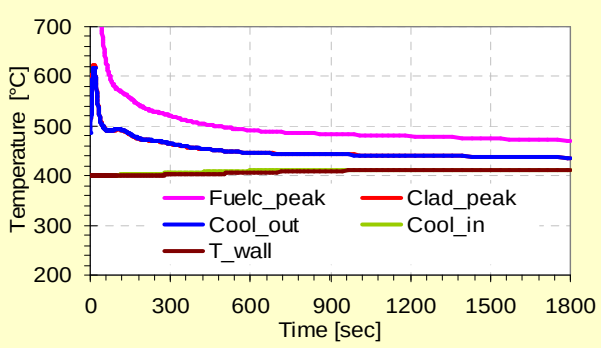
For this simulation it was assumed that: 1) at t = 0 sec, all primary pumps stop and feedwater temperature drops down (in ~ 1 sec) to 300 ^{o}C; 2) at t = 1 sec, two reactor scram signals are generated based on primary pumps under-speed (< 90 %) and feedwater temperature decreasing below 327 ^{o}C; 3) based on one of the two reactor scram signals (one of the signals is being neglected) the reactor is being shutdown at t = 2 sec into the transient; 4) main steam lines and main feedwater lines are being closed in ~2 sec time period, while condensate isolation valves of four ICs of the DHR-1 system fully opens in ~ 20 sec, thus then removing maximal 7 MW of heat from the primary cooling circuit; 5) water temperature leaving the ICs and directed to the MHXs is also 300 ^{o}C (same as that of feedwater).

Two cases were analyzed to investigate the clad and fuel temperature response of the peak pin and the likelihood of Pb-coolant freezing at the outlet of the MHX (primary side) during this PLOF with FW temperature decreasing down to 300 ^{o}C, namely at BOC and EOC core state conditions.

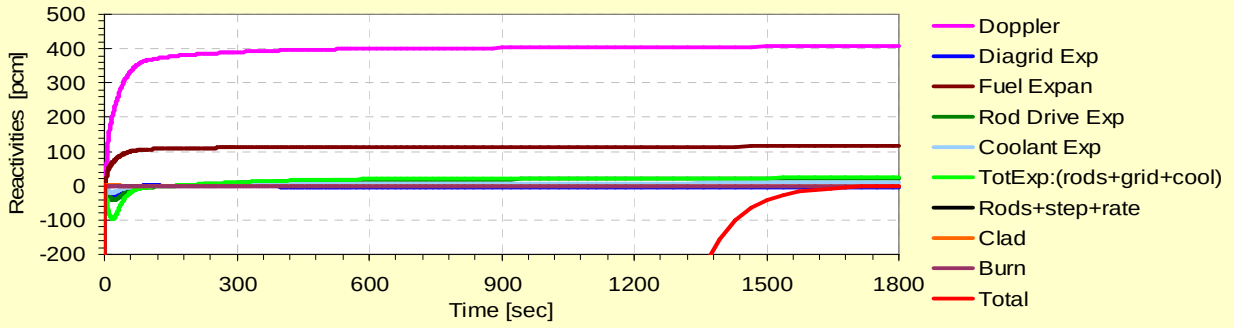
Under BOC conditions, following reactor scram, reactor power rapidly decreases approaching the decay heat level (see Fig. 5.7.1-1a). Due to the primary pumps stopping, the Pb-coolant mass flowrate through the core (see Fig. 5.7.1-1a) decreases to ~ 4% of nominal flow, later recovering to ~7% at ~ 15 min into the transient. Related to the water temperature decrease on the secondary side of the MHX to 300 ^{o}C, Pb-coolant temperature at the outlet of the MHX decreases to ~360 ^{o}C in ~ 4 sec (see Fig. 5.7.1-1d), but later, after the FW lines valves closure, increases to ~490 ^{o}C at its maximum, later decreasing again to ~405 ^{o}C in 0.5 hour transient time (Fig. 5.7.1-1d). As the feedwater temperature decreases by 35 ^{o}C, power transferred to the secondary cooling circuit through the MHX also shortly increases, but later due to the reactor scram starts decreasing (see Fig. 5.7.1-1e). In the first ~15 sec of the transient, clad and coolant (at core outlet) temperatures, due to core flowrate decrease (when primary pumps stop), increase up to ~ 620 ^{o}C. Fuel temperatures during this time period, due to the reactor scram, decreases to ~ 910 ^{o}C (see Fig. 5.7.1-1b). Pb temperature at the inlet of the core and vessel temperature changes only by ~ 10 ^{o}C during the simulated time period of 0.5 hour. From the calculation results one can observe, that in case feedwater temperature decreases suddenly down to 300 ^{o}C (note: $T_{melting}^{Pb} \sim 327\,^{\circ}C$) at the inlet of the secondary side of the MHX, in the time period of 0.5 hour the lead temperature at the outlet of the MHX on its primary side reaches ~405 ^{o}C, which is still far from the lead freezing temperature. Based on the lead temperature gradients around the MHX, one can estimate, that lead at the outlet from the MHX will start freezing only ~3.9 hours into the transient, when the lead temperature will reach ~327 ^{o}C at that location of the primary cooling circuit. So this transient presents a potential safety issue as related to possible Pb-freezing for the ALFRED reactor only ~3.9 hours into the transient. During this time period the operator has more than sufficient time for manual intervention by deactivating sub-systems of DHR-1 system in order to prevent lead freezing at the outlet of the MHX. Reactivities behavior during this transient is shown in Fig. 5.7.1-c.



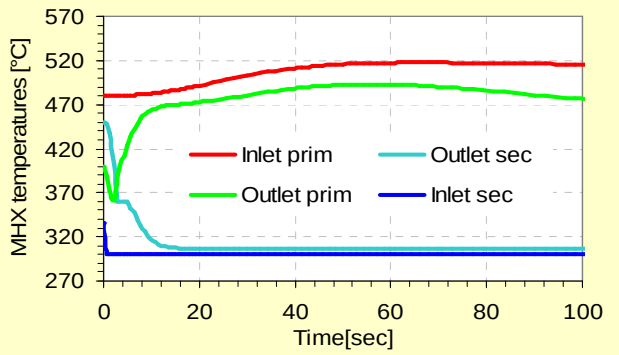
a) Relative core thermal power and Pb flowrate

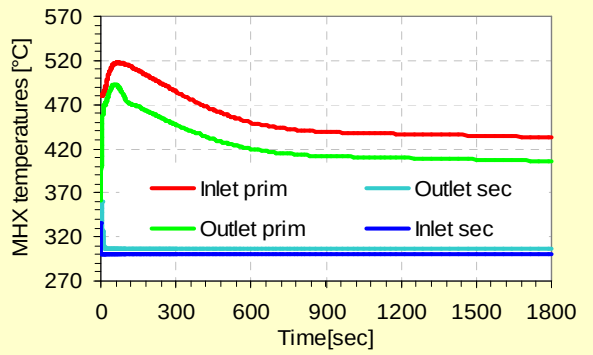


b) Peak fuel-, clad-, coolant- and vessel wall temperatures

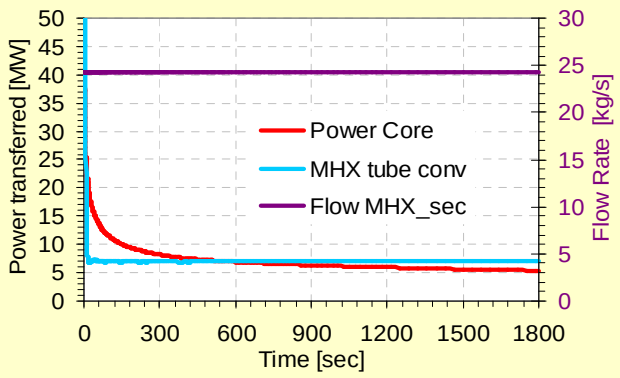


c) Reactivity feedbacks





d) MHX temperatures

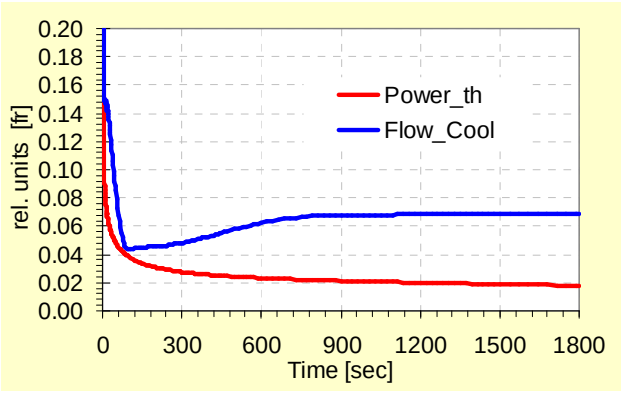


e) Core and MHX powers, plus MHX sec. side water flow rate

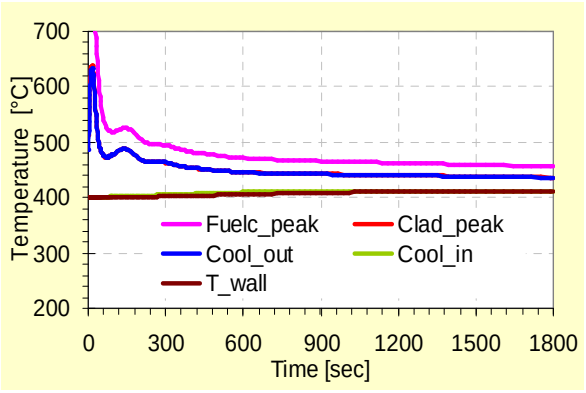
Fig. 5.7.1-1: Results for TO-3 (overcooling following reactor trip) transient: HFP BOC conditions at an average burnup of 730 EFPD as calculated by SIM-LFR (KIT)

Under EOC conditions, following the reactor scram, reactor power quickly decreases approaching the decay heat level (see Fig. 5.7.1-2a). Due to the primary pumps stopping, Pb-coolant mass flowrate through the core (see Fig. 5.7.1-2a) decreases to ~ 4% of nominal flow, later recovering to ~7% at ~ 15 min into the transient. Related to the water temperature decrease on the secondary side of the MHX down to 300 ^{o}C, lead temperature at the outlet of the MHX drops down to ~360 ^{o}C in ~ 4 sec (see Fig. 5.7.1-2d), but later, after the FW lines valves closure, increases to ~490 ^{o}C at its maximum, later decreasing again to ~405 ^{o}C in 0.5 hour transient time (Fig. 5.7.1-2d). As the feedwater temperature decreases by 35 ^{o}C, power transferred to the secondary cooling circuit through the MHX also shortly increases, but later due to the reactor scram starts decreasing (see Fig. 5.7.1-2e). In the first ~15 sec of the transient, clad and coolant (at core outlet) temperatures, due to core flowrate decrease (when primary pumps stop), increase up to ~ 630 ^{o}C. Fuel temperatures during this time period, due to the reactor scram, decreases down to ~ 870 ^{o}C (see Fig. 5.7.1-2b). Pb temperature at the inlet of the core and vessel temperature changes only by ~ 10 ^{o}C during the simulated time period of 0.5 hour. From the calculation results one can observe, that in case feedwater temperature decreases suddenly down to 300 ^{o}C (note: $T_{melting}^{Pb} \sim 327\,°C$) at the inlet of the secondary side of the MHX, in the time period of 0.5 hour the lead temperature at the outlet of the MHX on its primary side reaches ~405 ^{o}C, which is still far from the lead freezing temperature. Based on the lead temperature gradients around the MHX, one can estimate, that lead at the outlet from the MHX will start freezing only ~3.8 hours into the transient, when the lead temperature will

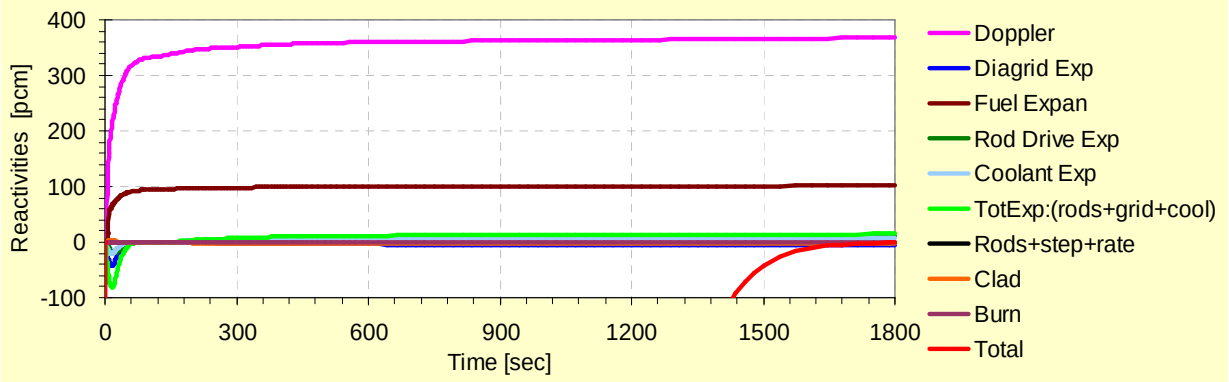
reach ~327 °C at that location of the primary cooling circuit. So this transient presents a potential safety issue as related to possible Pb-freezing for the ALFRED reactor only ~3.8 hours into the transient. During this time period operator has more than sufficient time for manual intervention by deactivating sub-systems of DHR-1 system in order to prevent lead freezing at the outlet of the MHX. Reactivities behavior during this transient is shown in Fig. 5.7.1-2c.



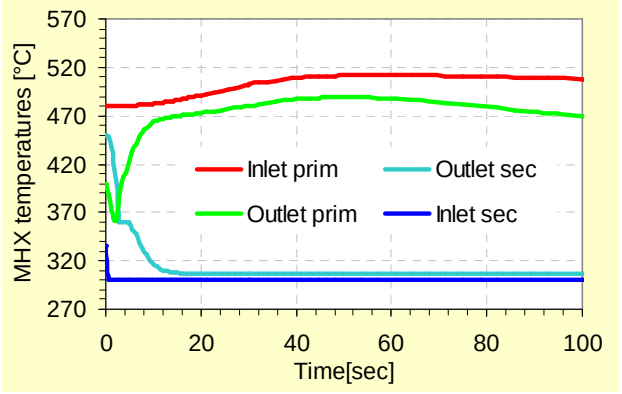
a) Relative core thermal power and Pb flowrate

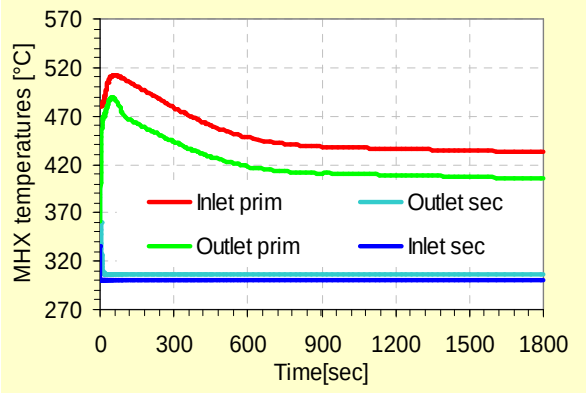


b) Peak fuel-, clad-, coolant- and vessel wall temperatures

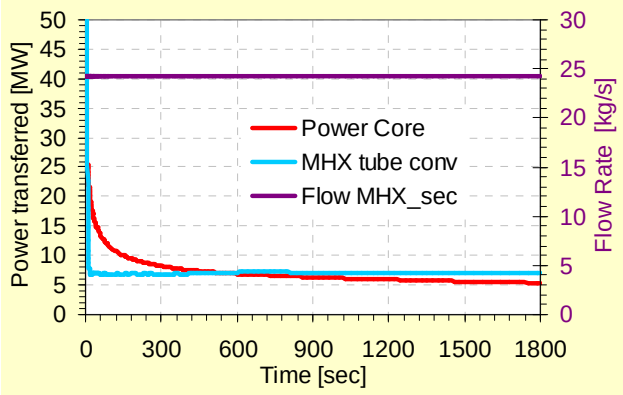


c) Reactivity feedbacks





d) MHX temperatures



e) Core and MHX powers, plus MHX sec. side water flow rate

Fig. 5.7.1-2: Results for TO-3 (overcooling following reactor trip) transient: HFP EOC conditions at an average burnup of 1095 EFPD as calculated by SIM-LFR (KIT)

Normally Pb-overcooling anywhere in the primary cooling loop below 335°C should be prevented under all plant transient conditions in order to prevent freezing of the Pb coolant thereby endangering an assured flow pattern throughout the primary system, in particular the core region. The feedwater temperature on the secondary side of the MHX must never be allowed to go below 335°C in order to assure that the primary system is always maintained at temperatures above 335°C. This requires an assured preheater system of the secondary side of the MHX.

5.7.2 TO-3 transient: RELAP5 results (ENEA)

This transient is initiated by the simultaneous loss of primary pumps and feedwater temperature reduction on the secondary side. The feedwater temperature is assumed to reduce down to 300 °C in 1 s, because of the partial loss of pre-heating function. The reactor scram is considered at t = 2 s on low primary pump speed signal. Following reactor scram, the secondary circuits are isolated and the DHR-1 system is started for decay heat removal. All 4 IC loops of the DHR-1 system are supposed available to be conservative against the risk of lead freezing in the primary circuit in the long term. The main results of the TO-3 transient are illustrated in Fig. 5.7.2-1 and Fig. 5.7.2-2 for the short term and the long term, respectively.

Following the coastdown of primary pumps at t = 0 s, natural circulation stabilizes in the primary circuit as shown in Fig. 5.7.2-1a. Because of the 2 s delay in reactor scram, the temperature at the core outlet increases and the clad temperature reaches a maximum of 613 °C at t = 3 s as shown in Fig. 5.7.2-1b.

In the long term, the natural circulation flow rate in the primary circuit reduces down to about 1-2% of nominal value (Fig. 5.7.2-2a), while the core power is at the decay level (Fig. 5.7.2-2b). The MHX power in excess to IC power in the initial phase of the transient is removed by steam release through the relief valves, following water vaporization inside the MHX and over pressurization of the secondary circuits. The power removed by the secondary side exceeds the decay power over the whole transient and thus there is no primary temperature increase after the initial peak. The total IC power (4 loops) is around 7 MW and exceeds the decay power after about 1100 s.

The minimum lead temperature is exhibited at MHX outlet as shown in Fig. 5.7.2-2c. In the short term, the lead temperature reaches a minimum of 350 °C at t = 180 s far enough from lead freezing point (327 °C). In the long term, the lead freezing point at the MHX outlet is approached after about two hours, thus leaving enough grace time for operator action and control of DHR-1 power removal. Automatic control of IC power removal is the one of the objectives of further DHR design development, in order to avoid the risk of lead freezing, indefinitely with time, without the need of operator actions.

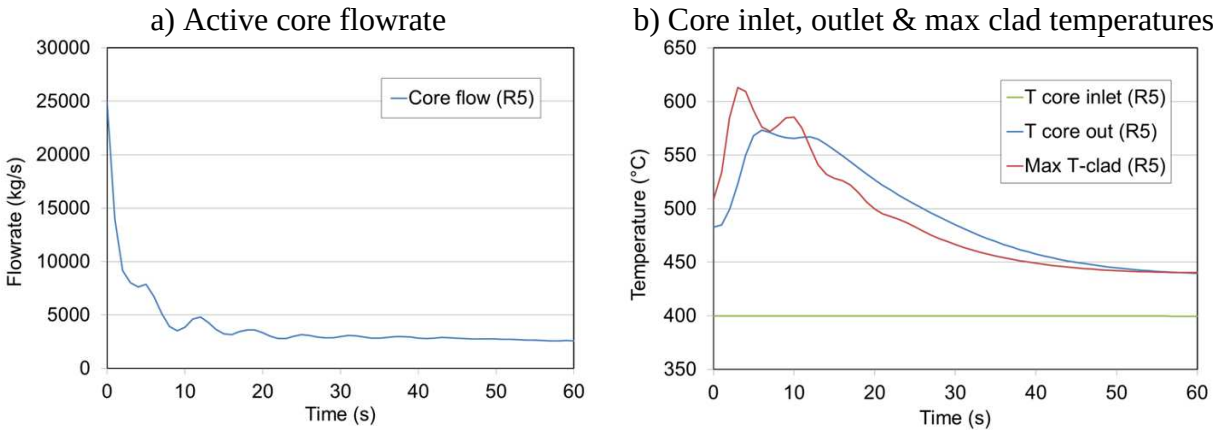


Fig. 5.7.2-1: Main RELAP5 results of the TO-3 Transient *(short term)*

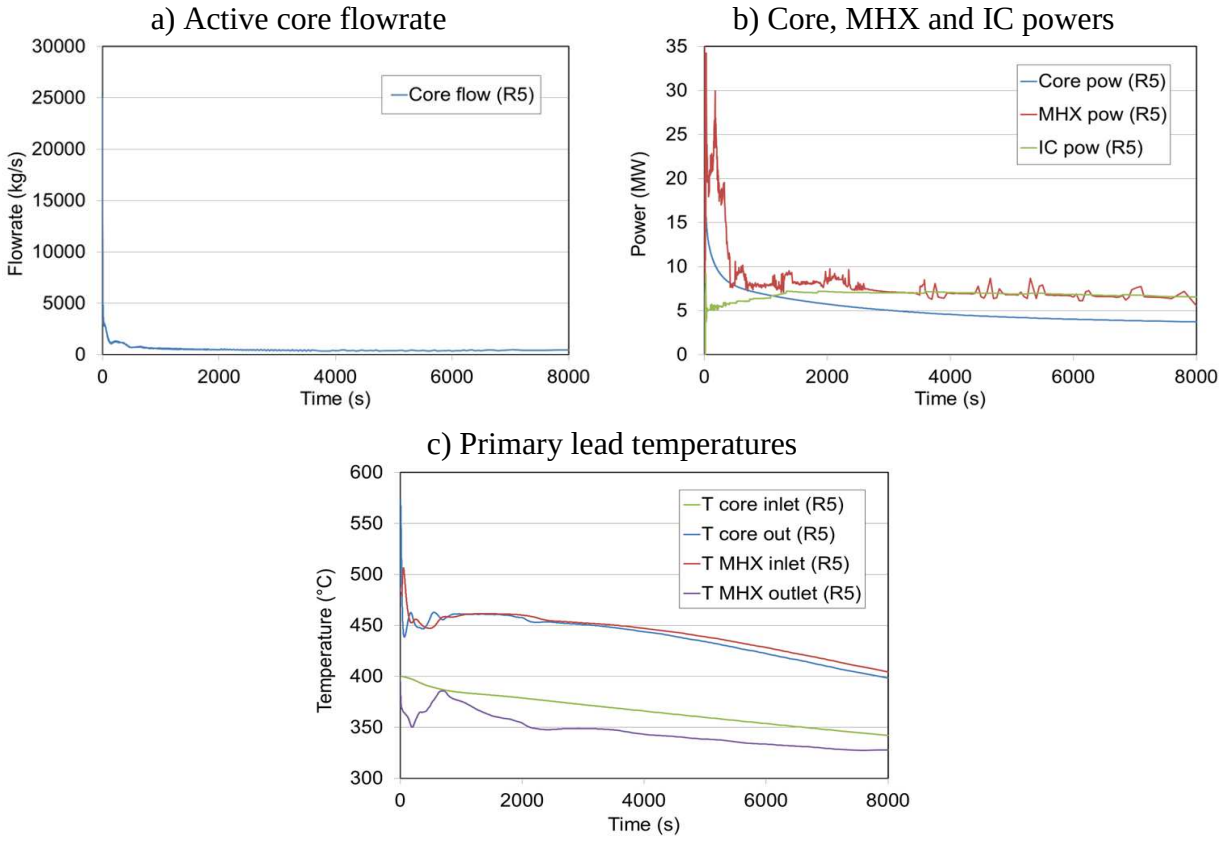


Fig. 5.7.2-2: Main RELAP5 results of the TO-3 Transient *(long term)*

It is worthwhile to mention here that the time to lead freezing at the MHX outlet is limited by the absence of coolant mixing in the lead pool surrounding the MHX. This means that the cold lead at the MHX outlet flows directly to core inlet, while temperature stratification develops in the lead pool, thus significantly reducing the effective thermal inertia of the primary system.

5.7.3 TO-3 transient: SPECTRA results (NRG)

The scenario is as follows:

- Loss of one preheater, FW temperature drops from 335 ºC to 300 ºC in 1.0 s.
- All primary pumps coastdown at t = 0.0 s, pump speed halving time 0.56 s.
- FW trip at 2.0 s. FW flow halving time 1.0 s.
- MSIV closes at 2.0 s. Closing time 1.0 s.
- Reactor trip (scram signal) on low primary pump speed signal.
- Startup of DHR-1, four IC-s available.

In this transient there are four loops with IC operating and four loops with IC closed. In the model two loops are used. The first loop represents four real loops with IC-s, combined into one. The second loop represents four real loops without IC-s. The NRG SPECTRA results are shown in Fig. 5.7.3-1 through Fig. 5.7.3-5.

Core inlet flow is shown in Fig. 5.7.3-1 and Fig. 5.7.3-2. The primary mass flow decreases quickly. Natural circulation is established at about 4000 kg/s. In the long term the natural circulation flow decreases to about 800 kg/s – about 3% of the nominal flow.

Core power and MHX power are shown in Fig. 5.7.3-3. The core power decreases to decay power after scram. The MHX power is close to the IC power, about 7 MW and exceeds the decay power.

Primary coolant temperatures are shown in Fig. 5.7.3-4. The liquid lead temperatures continuously decrease, because the power removed by the 4 IC units exceeds the decay power. The lead freezing temperature (327.4 ˚C) is reached at MHX outlet after about 2 hours.

Coolant and cladding temperatures are shown in Fig. 5.7.3-5. The maximum cladding temperature reaches about 650 °C at about 5 s and then decreases. The core outlet temperature reaches about 580 °C at about 10 s and then decreases. The core inlet temperature is stable at approximately initial values.

The four operating IC-s remove about 5.35 MW (4×1.34 MW) power. The corresponding four steam generators remove similar power 5.16 MW (4×1.29 MW) from the primary system. There is practically no power removal through the remaining four steam generators. The total power is 0.07 MW (4×0.02 MW).

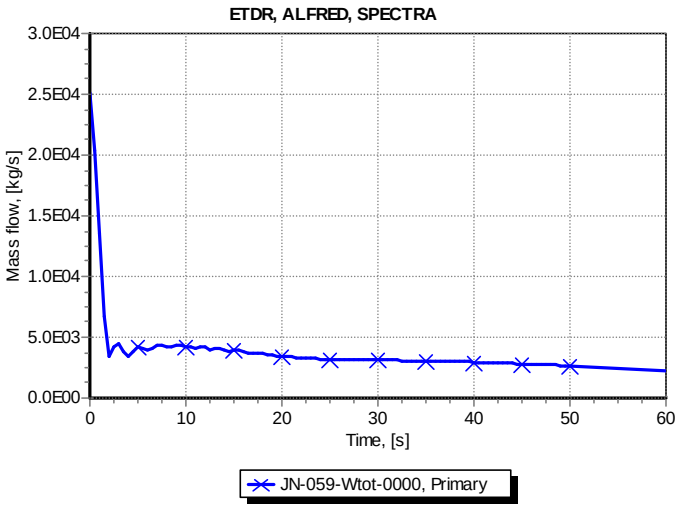


Fig. 5.7.3-1: Core inlet flow rate - short term

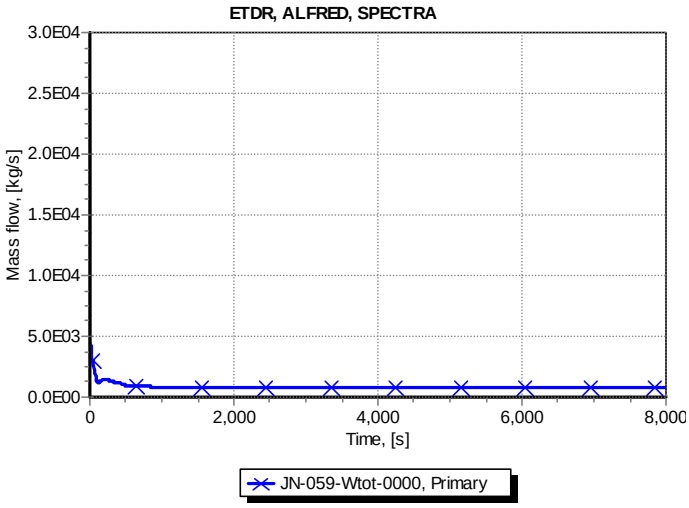


Fig. 5.7.3-2: Core inlet flow rate - long term

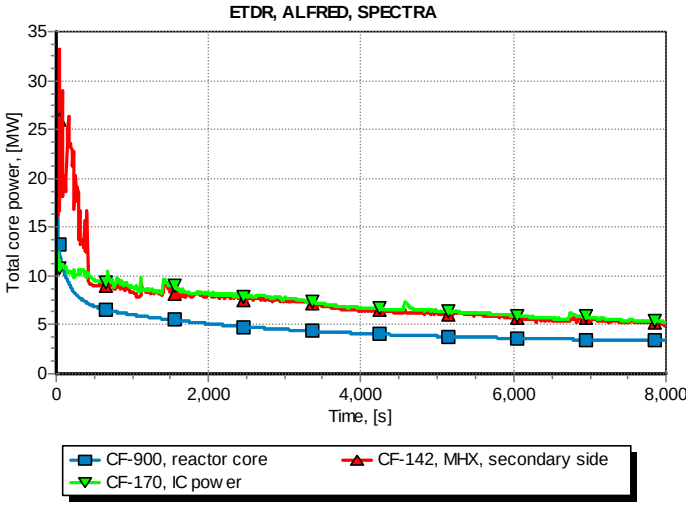


Fig. 5.7.3-3: Core, MHX and IC powers

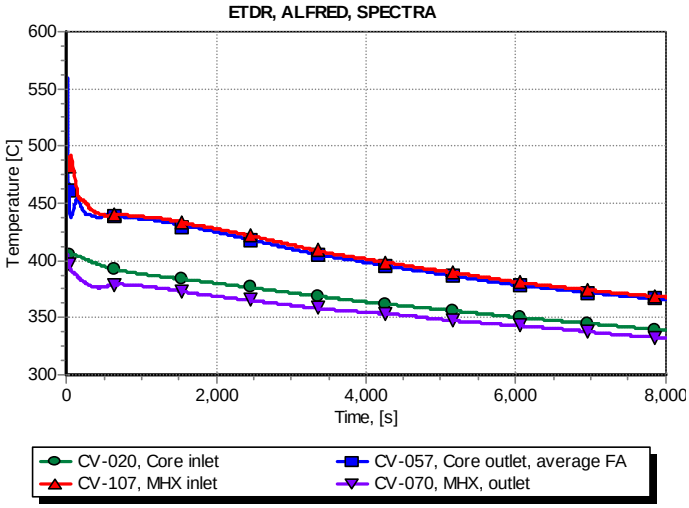


Fig. 5.7.3-4: Primary coolant temperatures

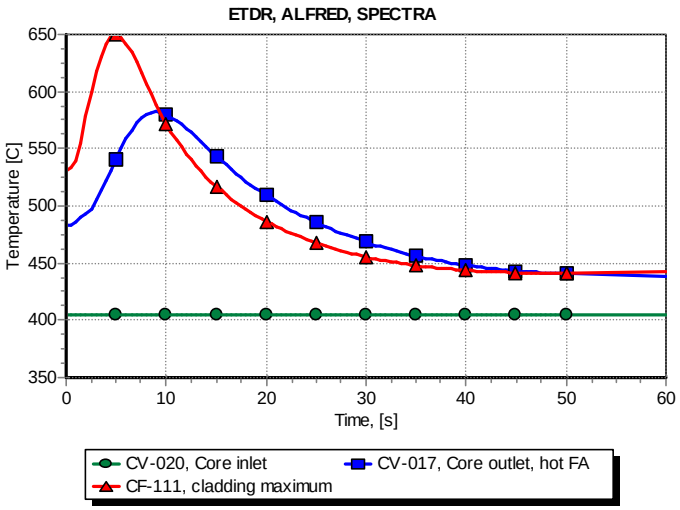


Fig. 5.7.3-5: Coolant and cladding temperatures

5.8 TO-6: Increase of FW flowrate with all primary pumps trip

The simultaneous loss of primary pumps and feedwater temperature increase on the secondary side is taken into account in this transient. The feedwater temperature is assumed to increase by 20% due to control system malfunction. The reactor scram is considered on low primary pump speed signal. Following reactor scram, the secondary circuits are isolated and the DHR-1 system is started for decay heat removal. All four sub-systems of the DHR-1 system are supposed available to be conservative against the risk of lead freezing in the primary circuit in the long term.

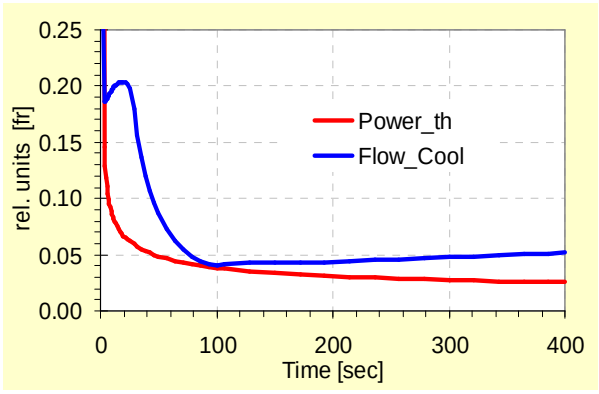
This transient has been analyzed by: KIT-G with SIM-LFR at BOC and EOC conditions, ENEA with RELAP5 and NRG with SPECTRA at EOC conditions. The main results of these analyses are presented in the following subsections.

5.8.1 TO-6 transient: SIM-LFR results (KIT-G)

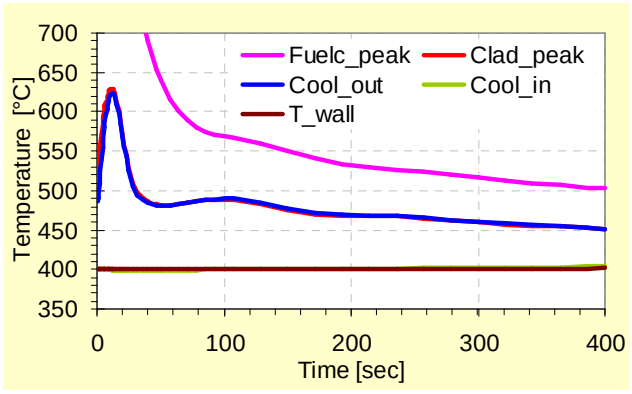
For this simulation it was assumed that: 1) at t = 0 sec, all primary pumps stop and feedwater flowrate increases by 20%; 2) at t = 1 sec, reactor scram signal is generated based on primary pumps under-speed (< 90 %), but is being neglected; 3) at t = 3 sec, two reactor scram signals are generated based on average core temperature difference, as well as on peak SA temperature difference being > 1.2 times their nominal values; 4) based on these reactor scram signals, reactor is being shutdown at t = 4 sec into the transient; 5) main steam lines and main feedwater lines are being closed in ~2 sec time period, while condensate isolation valves of four ICs of the DHR-1 system fully opens in ~ 20 sec, thus then removing maximal 7 MW of heat from the primary cooling circuit.

Two cases were analyzed to investigate the clad and fuel temperature response of the peak pin and the likelihood of Pb-coolant freezing at the outlet of the MHX (primary side) during this PLOF with FW flowrate increase by 20 %, namely at BOC and EOC core state conditions.

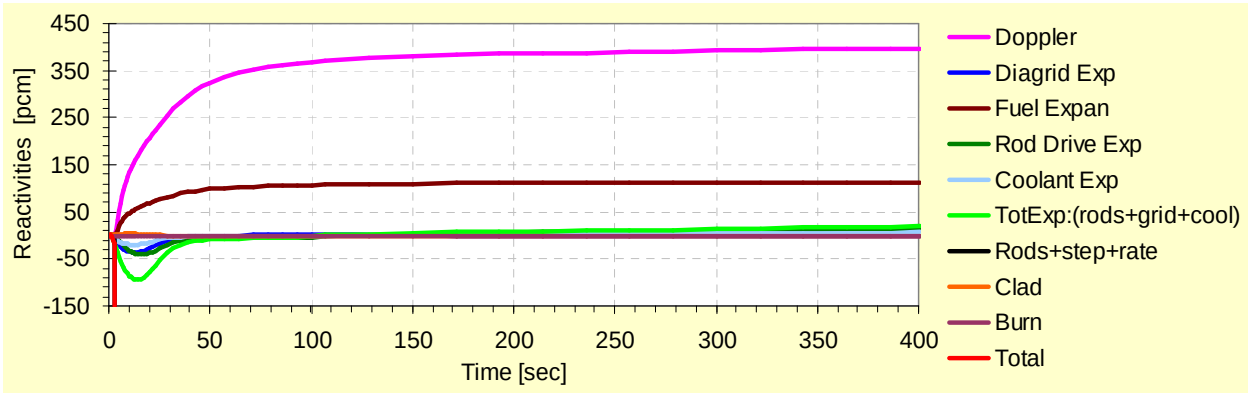
Under BOC conditions, following the reactor scram, reactor power quickly decreases to the decay heat level (see Fig. 5.8.1-1a). Due to the primary pumps stopping, lead-coolant mass flowrate through the core (see Fig. 5.8.1-1a) first decreases to ~ 19% of nominal flow, then recovers up to ~ 20%, but later due to the switch-over to DHR-1 sub-system the core flowrate decreases again to ~ 5% of nominal flow. Related to the feedwater flowrate increase on the secondary side of the MHX by 20%, lead temperature at the outlet of the MHX decreases to 335 ^{o}C (only 8 ^{o}C to the Pb-freezing point of 327°C), but later due to the switch-over to DHR-1 sub-system (lead flowrate decreases down to ~5 % of the nominal flow on the primary side of the MHX and heat transfer to the secondary side of the MHX suddenly decreases down to ~7 MW) it increases sharply up to ~ 500 ^{o}C, being close to the lead inlet temperature at the inlet of the MHX (see Fig. 5.8.1-1d). As the feedwater flowrate increases by 20%, power transferred to the secondary cooling circuit through the MHX also increases (see Fig. 5.8.1-1e) sharply, but later due to the switch-over to DHR-1 sub-system it decreases down to ~ 7 MW. Clad and coolant (at core outlet) temperatures, first (due to core flowrate decrease, when primary pumps stop) increase up to ~ 620 ^{o}C, but later, due to the reactor scram and reactor power decrease to the decay heat level, decreases to ~ 450 ^{o}C. Fuel temperatures during this transient decreases down to ~ 500 ^{o}C at t = 400 sec transient time (see Fig. 5.8.1-b) due to reactor scram. A large Pb mass (~ 3570 tons) in the primary loop and lower plenum provides a large heat inertia. Due to this, Pb temperature at the inlet of the core and vessel temperature hardly changes during the simulated time period of 400 sec. As long as the feedwater temperature remains at 335 ^{o}C (note: $T_{melting}^{Pb} \sim 327\,^{\circ}C$), there is a marginal danger of lead freezing anywhere in the primary cooling circuit. So this transient presents some marginal safety issue as related to Pb-freezing for the ALFRED reactor. Reactivities behavior during this transient is shown in Fig. 5.8.1-1c).



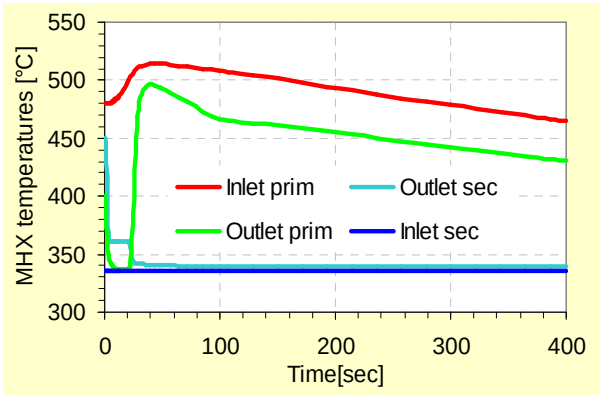
a) Relative core thermal power and Pb flow rate



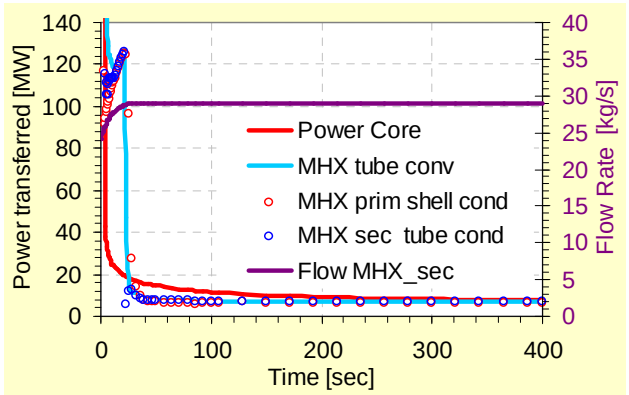
b) Peak fuel-, clad-, coolant- and vessel wall Temperatures



c) Reactivity feedbacks



d) MHX temperatures

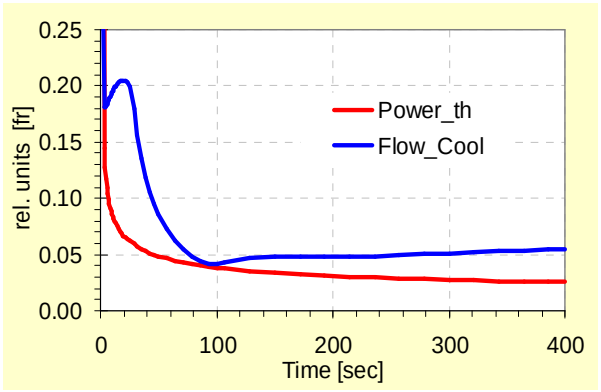


e) Core and MHX powers, plus MHX sec. side water flow rate

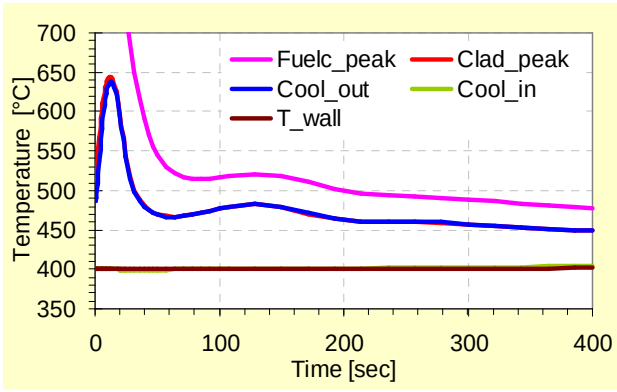
Fig. 5.8.1-1: Results for TO-6 (overcooling following reactor trip) transient: HFP BOC conditions at an average burnup of 730 EFPD as calculated by SIM-LFR (KIT)

Under EOC conditions, following the reactor scram, reactor power quickly decreases to the decay heat level (see Fig. 5.8.1-2a). Due to the primary pumps stopping, lead-coolant flowrate through the core (see Fig. 5.8.1-2a) first decreases to ~ 18% of nominal flow, then recovers up to ~ 20%, but later due to the switch-over to DHR-1 sub-system the core flowrate decreases to ~ 5-6% of the nominal flow. Related to the feedwater flowrate increase on the secondary side

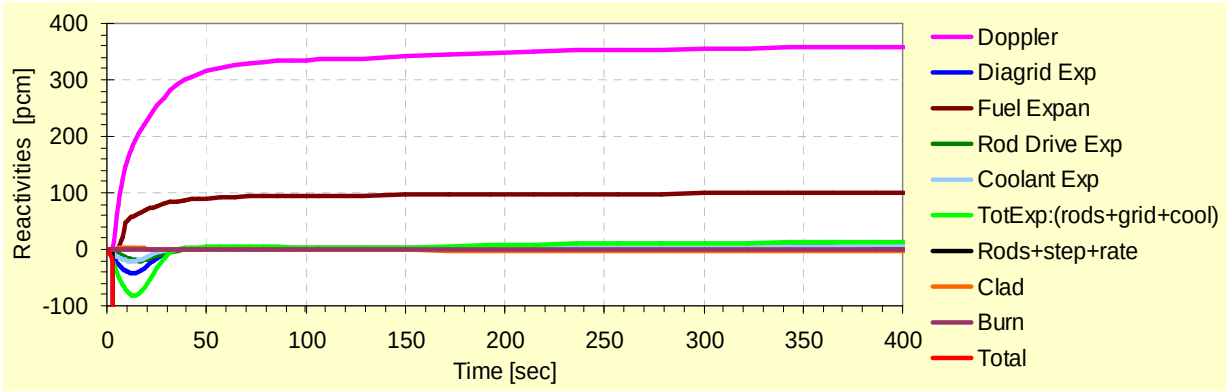
of the MHX by 20%, lead temperature at the outlet of the MHX drops down to 335 ^{o}C, but later due to the switch-over to DHR-1 sub-system (lead flowrate decrease to ~ 5-6% of the nominal flow) it increases sharply up to ~ 495 ^{o}C, being close to the lead inlet temperature at the inlet of the MHX (see Fig. 5.8.1-2d). As the feedwater flowrate increases by 20%, power transferred to the secondary cooling circuit through the MHX also increases (see Fig. 5.8.1-2e) rapidly, but later due to the switch-over to DHR-1 sub-system it decreases down to ~ 7 MW. Clad and coolant (at core outlet) temperatures, first (due to core flowrate decrease, when primary pumps stop) increase up to ~ 640 ^{o}C, but later, due to the reactor scram and reactor power decrease to the decay heat level, decreases to ~ 450 ^{o}C. Fuel temperatures during this transient, due to the reactor scram, decrease to ~ 480 ^{o}C at t = 400 sec transient time (see Fig. 5.8.1-2b). A large Pb mass (~ 3570 tons) in the primary loop and lower plenum provides a large heat inertia. Due to this, Pb temperature at the inlet of the core and vessel temperature hardly changes during the simulated time period of 400 sec. As long as the feedwater temperature remains at 335 ^{o}C (note: $T_{melting}^{Pb} \sim 327\,^{\circ}C$), there is a marginal danger of lead freezing anywhere in the primary cooling circuit. So this transient presents some marginal safety issue as related to Pb-freezing for the ALFRED reactor. Reactivities behavior during this transient is shown in Fig. 5.8.1-2c).



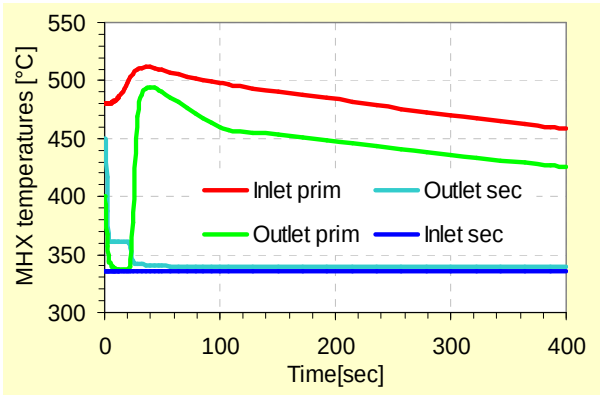
a) Relative core thermal power and Pb flow rate



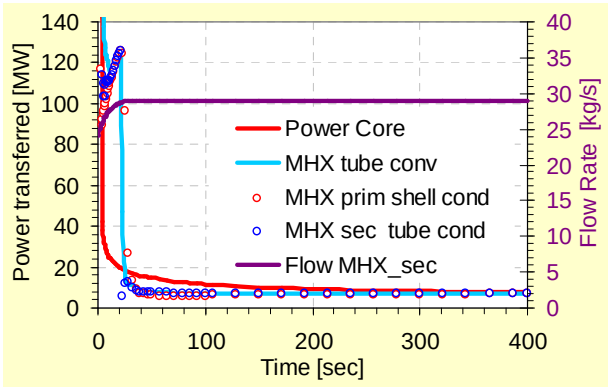
b) Peak fuel-, clad-, coolant- and vessel wall temperatures



c) Reactivity feedbacks



d) MHX temperatures



e) Core and MHX powers, plus MHX sec. side water flow rate

Fig. 5.8.1-2: Results for TO-6 (overcooling following reactor trip) transient: HFP EOC conditions at an average burnup of 1095 EFPD as calculated by SIM-LFR (KIT)

In the longer term for BOC as well as EOC conditions, lead temperature at the outlet from the MHX will continue to decrease further, slowly approaching lead freezing temperature (note: $T_{melting}^{Pb} \sim 327\,°C$), as the heat removed by DHR-1 system becomes larger than the decay heat generated in the reactor core. Usually this process occurs during a time stretching over several hours [DEL010-2012], providing the operator sufficient time to deactivate sub-systems of the DHR-1 system, in order to prevent Pb-coolant freezing at the outlet of the MHX.

As a conclusion, this transient has the potential to lead to a safety issue as related to possible Pb-freezing for the ALFRED reactor. Reactor safety is ensured by the reactor protection system, shutting down the reactor, as well as by the tightly controlled heat removal by the DHRS (also by an operator in the medium and long term), removing only controlled amounts of decay heat from the reactor primary cooling circuit to assure prevention of freezing of the Pb-coolant at any location of the primary cooling circuit.

5.8.2 TO-6 transient: RELAP5 results (ENEA)

This transient is initiated by the simultaneous loss of primary pumps and feedwater temperature flow rate increase on the secondary side. The feedwater flow rate is assumed to increase by 20%. The reactor scram is considered at t = 2 s on low primary pump speed signal. Following reactor scram, the secondary circuits are isolated and the DHR-1 system is started for decay heat removal. All four IC loops of the DHR-1 system are supposed available to be conservative against the risk of lead freezing in the primary circuit in the long term. The main results of the TO-6 transient are illustrated in Fig. 5.8.2-1 and Fig. 5.8.2-2 for the short term and the long term, respectively.

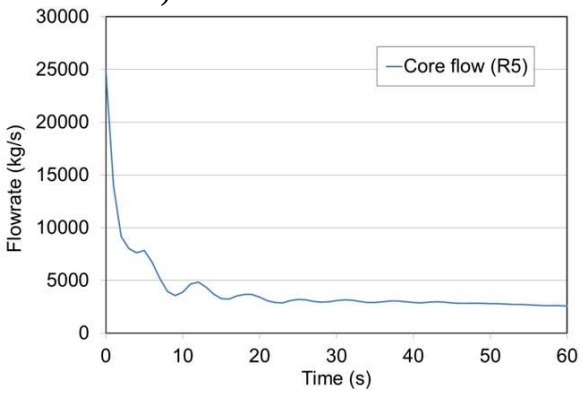
Following the coastdown of primary pumps at t = 0 s, natural circulation stabilizes in the primary circuit as shown in Fig. 5.8.2-1a. Because of the 2 s delay in reactor scram, the temperature at the core outlet increases and the clad temperature reaches a maximum of 613 °C at t = 3 s as shown in Fig. 5.8.2-1b.

In the long term, the natural circulation flow rate in the primary circuit reduces down to about 1-2% of nominal value (Fig. 5.8.2-2a), while the core power is at the decay level (Fig. 5.8.2-2b). The MHX power in excess to IC power in the initial phase of the transient is removed by steam release through the relief valves, following water vaporization inside the MHX and over pressurization of the secondary circuits. The power removed by the secondary side exceeds the decay power over the whole transient and thus there is no primary temperature increase after the initial peak. The total IC power (4 loops) is around 7 MW and exceeds the decay power after about 1100 s.

The minimum lead temperature is exhibited at MHX outlet as shown in Fig. 5.8.2-2c. In the short term, the lead temperature reaches a minimum of 350 °C at t = 180 s far enough from the lead freezing point (327 °C). In the long term, the lead freezing point at the MHX outlet is approached after about 2 hours, thus leaving enough grace time for operator action and control of DHR-1 system power removal. Automatic control of IC power removal is the one of the objectives of further DHR design development, in order to avoid the risk of lead freezing, indefinitely with time, without the need of operator actions.

It is worthwhile to mention here that the time to lead freezing at the MHX outlet is limited by the absence of coolant mixing in the lead pool surrounding the MHX. This means that the cold lead at the MHX outlet flows directly to core inlet, while temperature stratification develops in the lead pool, thus significantly reducing the effective thermal inertia of the primary system.

a) Active core flowrate



b) Core inlet, outlet & max clad temperatures

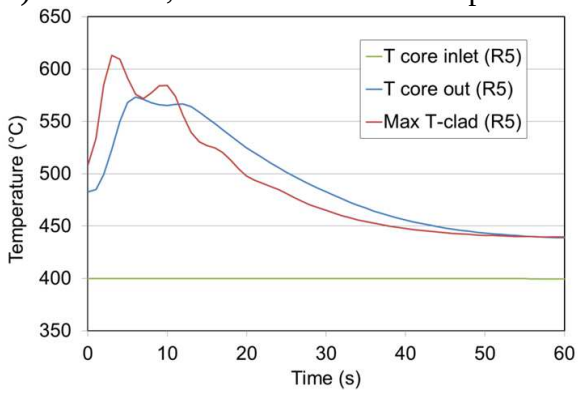
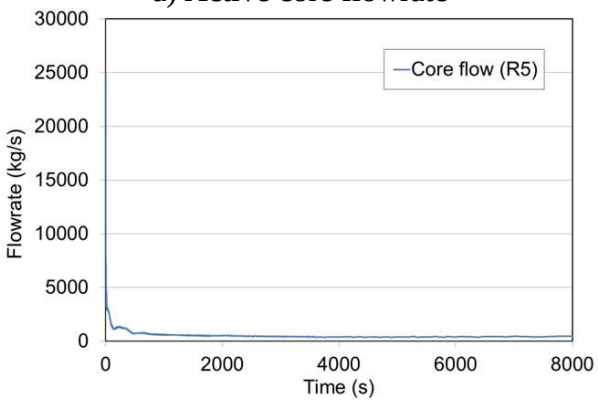
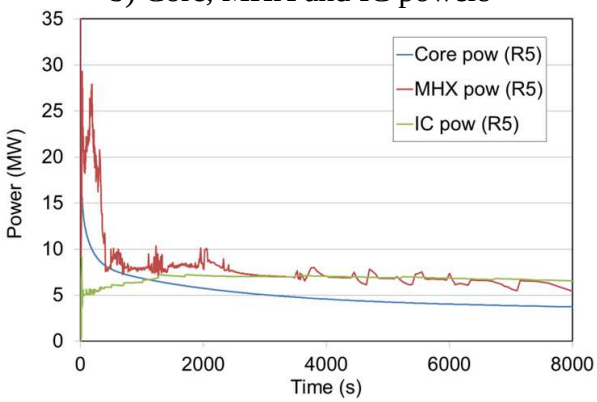


Fig. 5.8.2-1: Main RELAP5 results of the TO-6 Transient *(short term)*

a) Active core flowrate



b) Core, MHX and IC powers



c) Primary lead temperatures

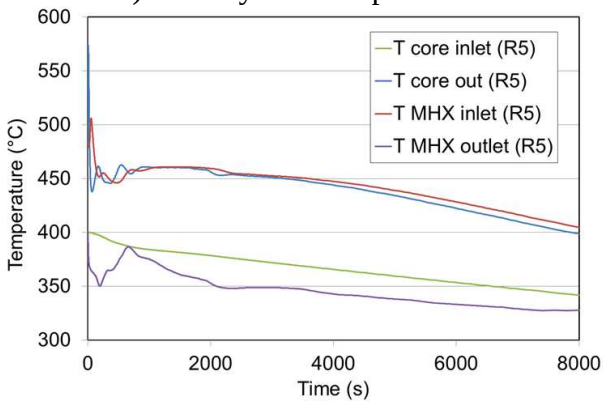


Fig. 5.8.2-2: Main RELAP5 results of the TO-6 Transient *(long term)*

5.8.3 TO-6 transient: SPECTRA results (NRG)

The scenario is as follows:

- FW flow increases by 20% in 1.0 s.
- All primary pumps coastdown at t = 0.0 s, pump speed halving time 0.56 s.
- FW trip at 2.0 s. FW flow halving time 1.0 s.
- MSIV closes at 2.0 s. Closing time 1.0 s.
- Reactor trip (scram signal) on low primary pump speed signal.
- Startup of DHR-1, four IC-s available.

In this transient there are four loops with IC operating and four loops with IC closed. In the model two loops are used. The first loop represents four real loops with IC-s, combined into one. The second loop represents four real loops without IC-s. The NRG SPECTRA results are shown in Fig. 5.8.3-1 through Fig. 5.8.3-5.

Core inlet flow rate is shown in Fig. 5.8.3-1 and Fig. 5.8.3-2. The primary mass flow decreases quickly. Natural circulation is established at about 4000 kg/s. In the long term the natural circulation flow decreases to about 800 kg/s – about 3% of the nominal flow.

Core, MHX, and IC power is shown in Fig. 5.8.3-3. The core power decreases to decay power after scram. The MHX power is close to the IC power, about 7 MW and exceeds the decay power.

Coolant temperatures are shown in Fig. 5.8.3-4. Lead temperatures continuously decrease, because the power removed by the 4 IC units exceeds the decay power. The lead freezing temperature (327.4˚C) is reached at MHX outlet after about 2 hours.

Coolant and cladding temperatures are shown in Fig. 5.8.3-5. The maximum cladding temperature reaches about 650 °C at about 5 s and then decreases. The core outlet temperature reaches about 580 °C at about 10 s and then decreases. The core inlet temperature is stable at approximately initial values.

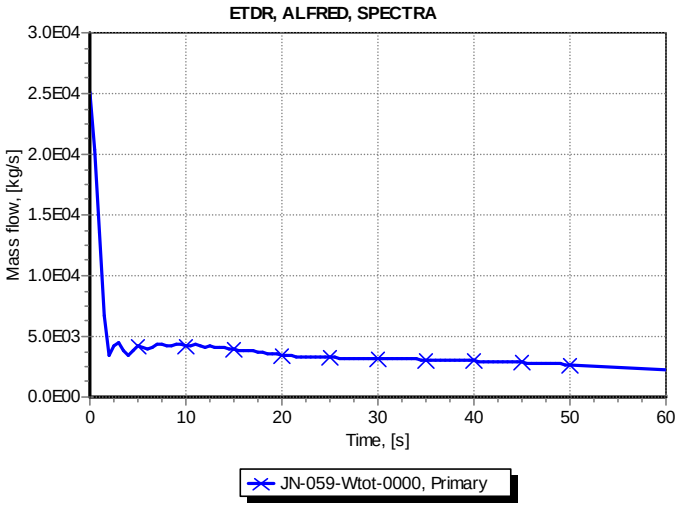


Fig. 5.8.3-1: Core inlet flow rate - short term

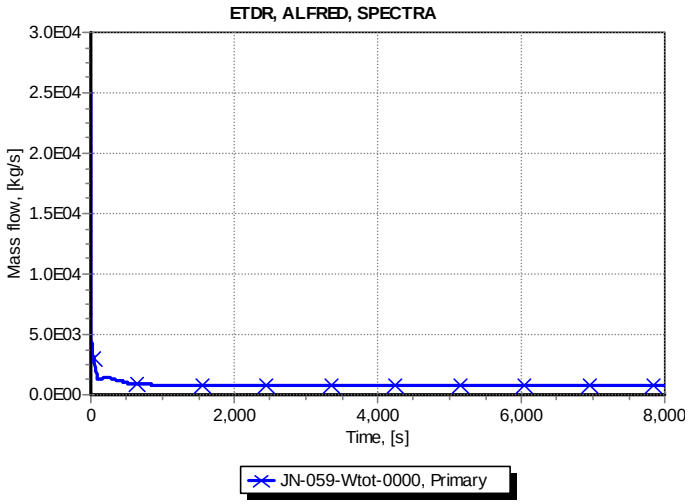


Fig. 5.8.3-2: Core inlet flow rate - long term

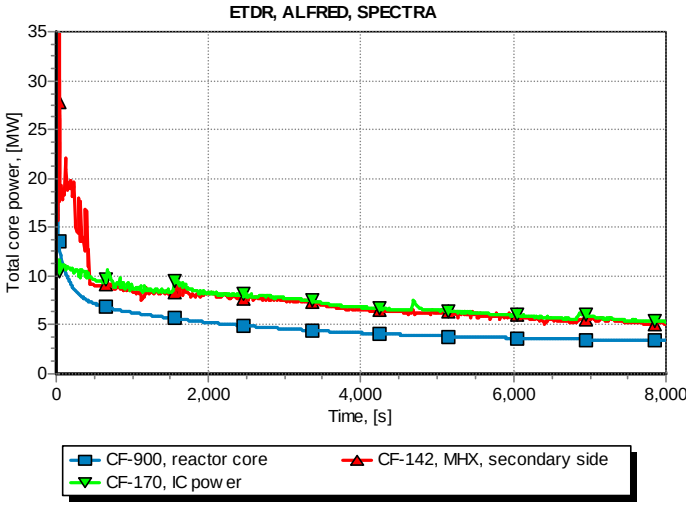


Fig. 5.8.3-3: Core, MHX, and IC power

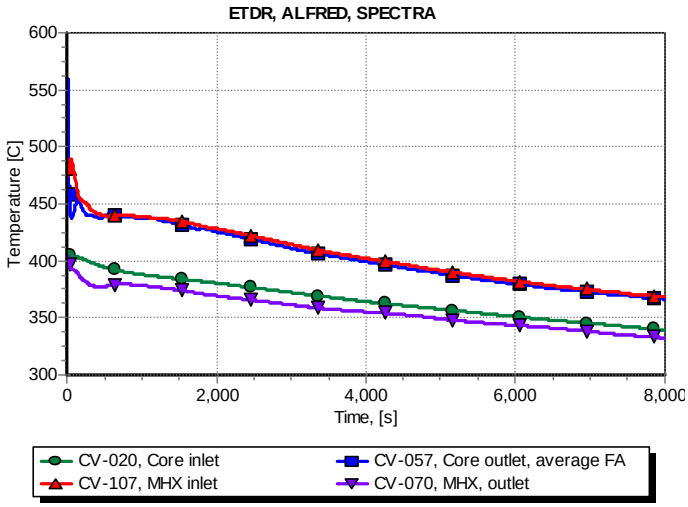


Fig. 5.8.3-4: Primary temperatures

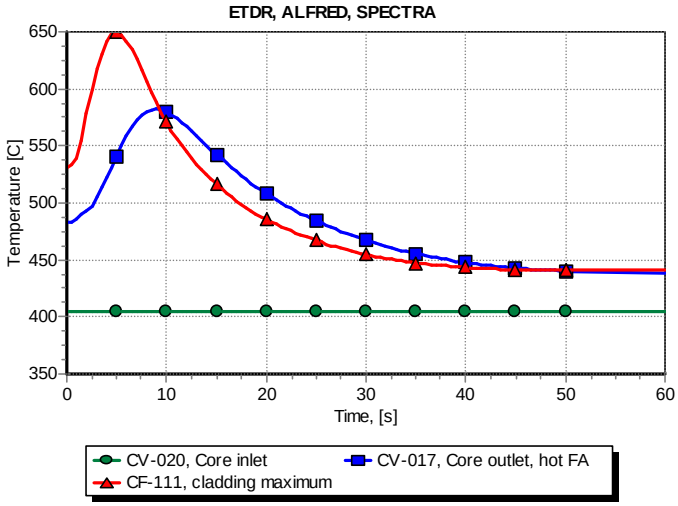


Fig. 5.8.3-5: Coolant and cladding temperatures

The four operating IC-s remove about 5.31 MW (4×1.33 MW) power. The corresponding four steam generators remove similar power 5.04 MW (4×1.26 MW) from the primary system. There is practically no power removal through the remaining four steam generators. The total power is 0.07 MW (4×0.02 MW).

5.9 Steam generator tube rupture (SGTR) event (CIRTEN)

The SGTR accident scenario (guillotine rupture of one or more double-wall SG tubes), that could endanger the integrity of the reactor internals was numerically analyzed considering the two cases of one and seven broken bayonet tubes. In this latter (extremely conservative) case, it was assumed that the broken tube damages the surrounding six tubes (Fig. 5.9-1), although such an event is considered as a very improbable event.

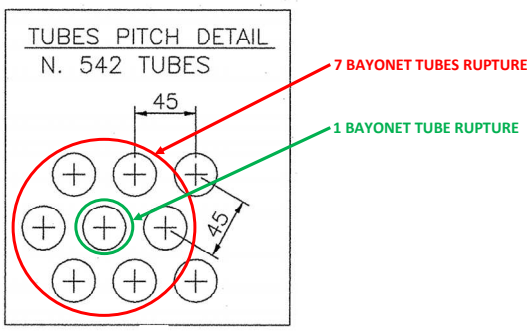


Fig. 5.9-1: Tubes pitch detail

The SGTR induced effects were evaluated by adopting SIMMER-III code and implementing an axisymmetric (R-Z) quite simplified model of the ALFRED reactor (Fig. 5.9-2).

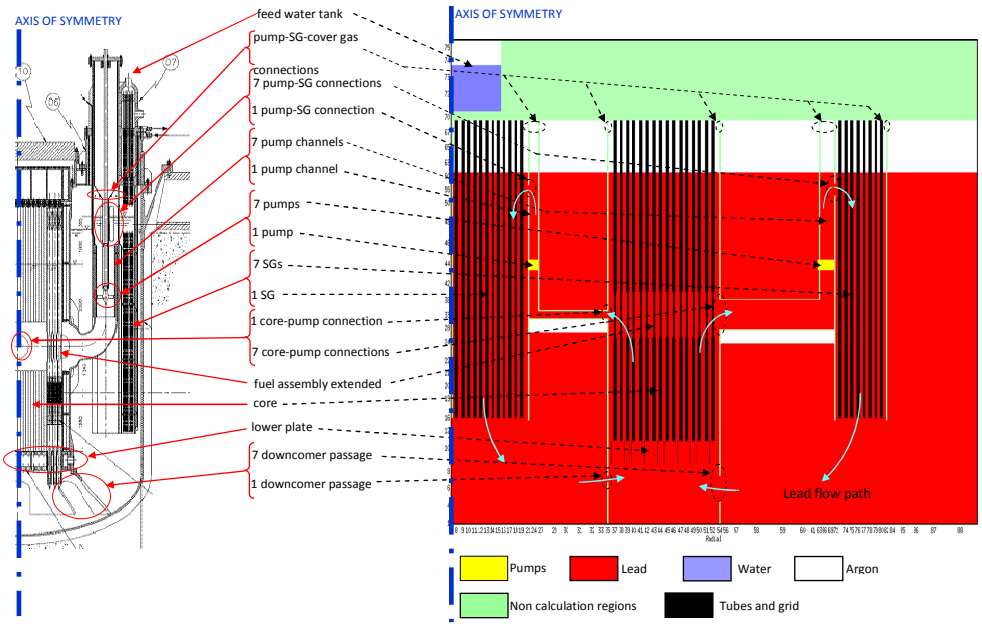


Fig. 5.9-2: ALFRED reactor geometrical model

The model geometrical domain consists of 88 radial and 75 axial cells: the lead is represented in red, the water in blue, the argon (cover gas) in white; non calculation regions (structural parts) in light green, pins and grids in black and pumps in yellow. The cyan arrows indicate the lead flow path. The SG, where the SGTR is assumed to occur, is positioned near the symmetry axis, while the other seven SGs are merged together (the same is done for the pumps as well)

and are located in the outer region. The reactor core is positioned between 1SG-1PP and 7PPs-7SGs. Moreover, Fig. 5.9-3 shows the details of the modeled water injector tube, with its main radial dimensions, for the both analyzed SGTR accident scenarios.

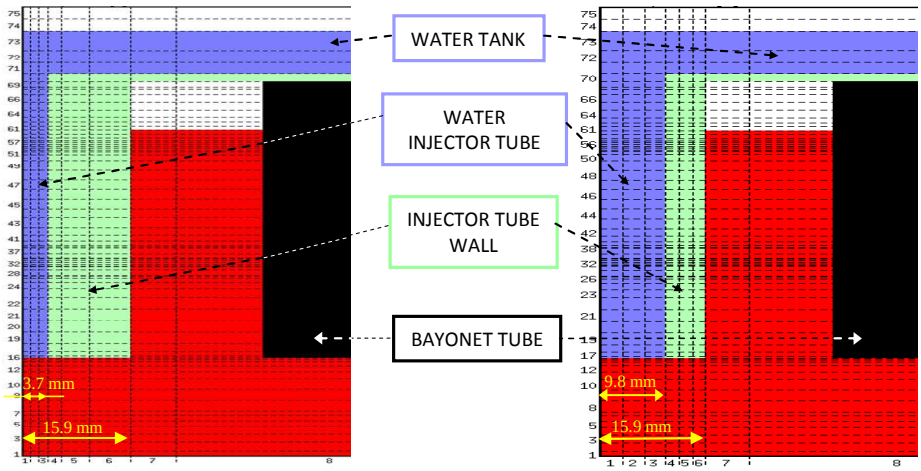


Fig. 5.9-3: Water injector tube detail for one (left) and seven (right) tubes rupture tests

Obtained results for one single bayonet tube rupture

In the performed simulations, the water was injected into the lead (Fig. 5.9-4) at t = 100 s after the start of the calculation: this time interval (100 s) represents the transient period to reach the ALFRED operative stationary conditions.

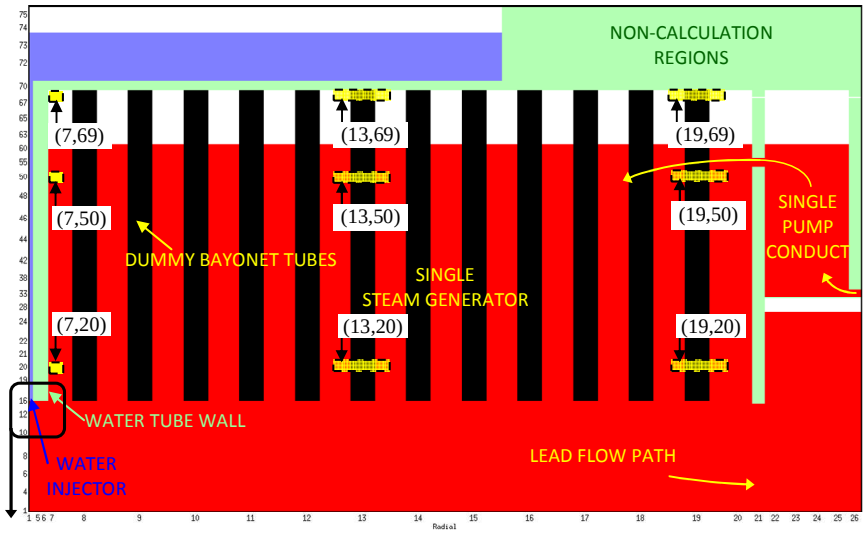


Fig. 5.9-4: Detailed view of the injector tube, single SG and single pump conduct

The white regions represent the cells filled by argon gas. Fig. 5.9-4 shows also the nine cells ((7,20), (13,20), (19,20), (7,50), (13,50), (19,50), (7,69), (13,69) and (19,69)), chosen as reference cells to represent the pressure behavior in the single SG, as well as six cells in the 13th, 14th and 15th vertical rows, positioned beneath the injector tube.

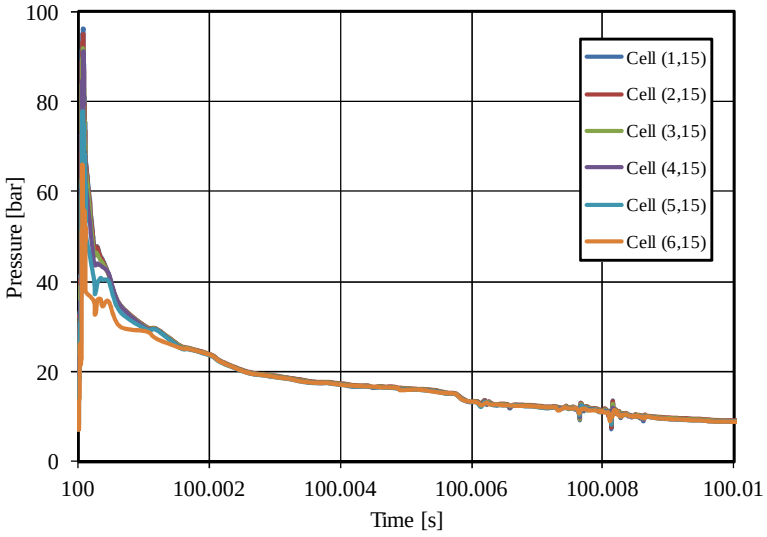


Fig. 5.9-5: Pressure peaks at the beginning of water injection

The obtained results in terms of pressure (transient analysis ranges from 100 to almost 126 s) indicate that the pressure increases near the broken tube in the first tenths of a second after the water injection (Fig. 5.9-5); the presence of the rupture disks and the safety valves on the vessel cover, not considered in the SIMMER model, would allow to limit the cover gas pressurization. The peak pressure value (peaks in Fig. 5.9-5) is about 96 bar; this value was located in the cell (1,15), nearest and central position in respect to the injector tube. In the other cells, the maximum pressure value decreases. The calculated peaks occur almost at the same instant (10^{-4}s from the water injection); after that the pressure decreases rapidly to its initial value. After 2 ms and till the end of the tube rupture transient the six pressure profiles show almost the same pressure value. After 0.01 s starting from the water injection, the computed pressures reach the stationary value of almost 7 bar, observed before the water injection.

In the simulation, the water injected into the liquid metal instantaneously fully vaporizes in contact with it at the injector tube exit region; the steam generated flows down reaching the ninth axial cell, then moves radially and goes up into the cover gas region. In reality, all the injected water would not vaporize instantly when contacting lead (only part of it will do so), but will be encapsulated in water vapor bubbles and transported to the cover gas region instead. This fact should be kept in mind when analyzing the simulation results.

The Fig. 5.9-6 represents the water mass flow rate injected into the lead (the water flow through the upper surface of the cells beneath the injection orifice (1-3,15)): during the first 26 s the injected water mass resulted almost in 0.4-0.5 kg/s.

It is worth noting that both the distributed and the singular pressure drops have been considered. The former represents the friction effect inside the tube while the latter (ΔP = 10 bar) the schematization of a device (like a Venturi nozzle to be put on the feed water line), foreseen to limit the mass flow rate exiting from the bayonet tube in case of tube rupture. The total mass of water injected during the whole transient resulted in almost 11 kg.

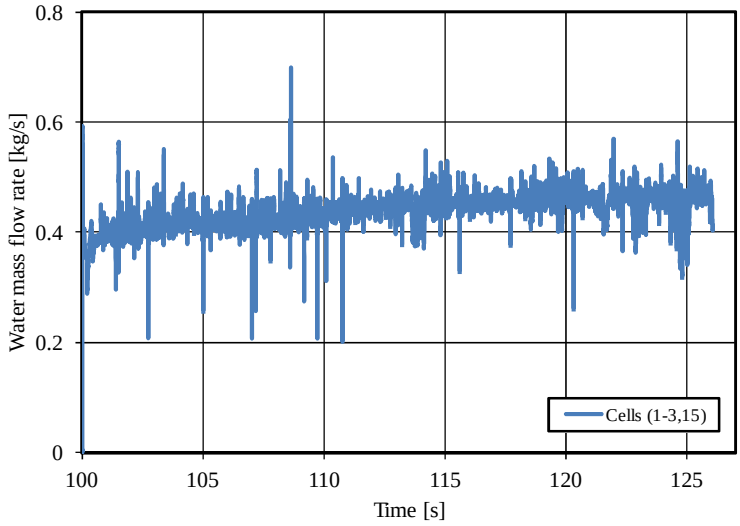


Fig. 5.9-6: Behavior of the injected water mass flow rate

The shown results highlighted also the fact that the steam does not enter into the reactor core.

Obtained results for seven bayonet tubes rupture

The analysis of a bayonet tube rupture involving/propagating to the six surrounding tubes ("domino effect") has been performed to evaluate the consequence of SGTR in a very conservative case. The set up SIMMER model is almost the same of that one used to analyze a single bayonet tube rupture; the only difference being the diameter of the water injector tube, assumed equal to 19.6 mm in order to represent a flow section area seven times greater than that of a single bayonet tube.

Fig. 5.9-7 shows the pressure behaviour obtained in the first six radial cells (1-6) and in the row 15 beneath the water injection orifice: only the first 0.3 s are represented in order to highlight the peak values (greater than those shown in Fig. 5.9-5) that did arise at the beginning of the water injection and its interaction with the lead.

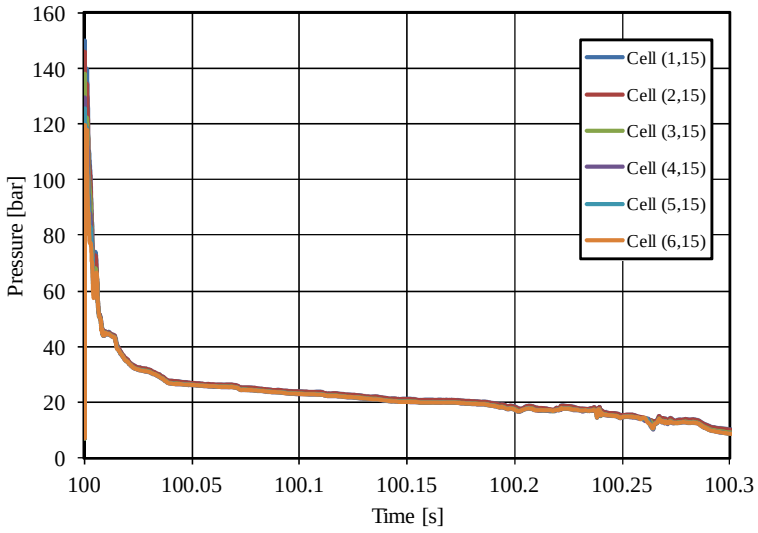


Fig. 5.9-7: Pressure time trends in the cells (1-6,15)

In addition, Fig. 5.9-8 shows the void fraction calculated in the cells below the core. To better analyze the steam that enters into the core by "J" path, 50 s of transient have been simulated. The obtained results confirmed that an "appreciable quantity" of vapor enters only in the left part of the core (peripheral region close to the SG where the accident takes place). In the center (cell (45,10)) and in the radially opposed side of the core (cell (52,10)) the void fraction is lower than 10^{-3}.

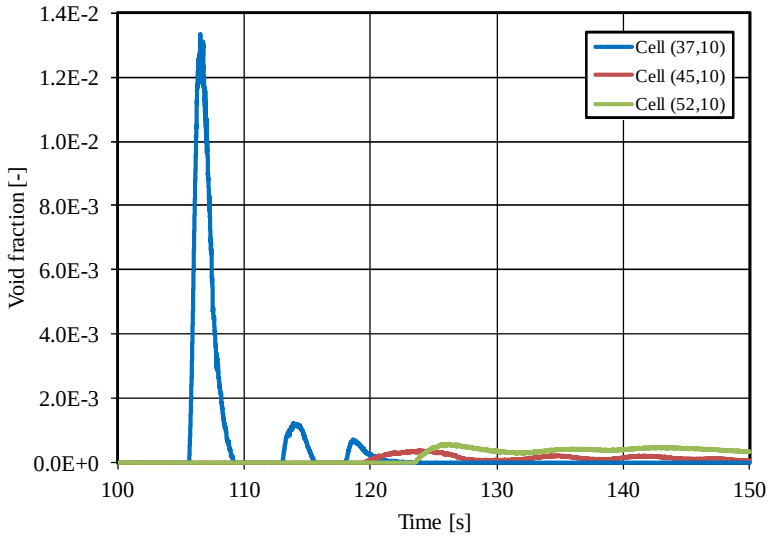


Fig. 5.9-8: Void fraction time trends in the cells (37,10), (45,10) and (52,10)

As shown in Fig. 5.9-8, the vapor (blue trend) enters the core by "B" path only during three time intervals (three blue peaks in the first 20 s of the water injection), each one of almost 2 s duration, the first of which reaches a void fraction value almost ten times greater than those reached in the subsequent intervals. The vapor void fraction in the center and right hand cells is computed by the SIMMER-III code only after almost 20 s from the water injection instant; this time partially is required by the vapor to flow from the lower region of the 1SG to the core downcomer passing through the "J" path.

Conclusions

The analysis of two SGTR accidents in the ALFRED reactor has been performed by means of the SIMMER-III code, in order to assess the consequences arisen from the water-lead interaction. In fact, the formation of vapor coupled to the pressure waves propagation could represent a risk for the internals integrity, such as damages of the neighboring SG tubes.

The ALFRED reactor has been modelled using the axisymmetric SIMMER-III code model, conserving the component axial dimensions and the lead flow cross-section areas. The broken bayonet tube was simulated by a cylindrical water injector tube, set coaxially to the model. All the other ALFRED components are modelled by outer annuli.

Two simulations have been performed, the former considering the rupture of only one bayonet tube and the latter assuming that also the six surrounding tubes are damaged (seven tubes are broken). The two models set up for the simulation differ only in the water injector tube diameter.

The highest pressure values were computed in the cell (1,15) at the first transient instants, beneath the water injector tube. Its value was almost 100 and 150 bar for one and seven broken tubes cases, respectively.

In the SIMMER-III simulation, the water injected into the liquid metal instantaneously fully vaporizes in contact with it at the injector tube exit region. In reality, all the injected water would not vaporize instantly when contacting lead (only part of it will do so), but will be encapsulated in vapor bubbles and transported to the cover gas region instead. Moreover the cover gas space, due to SIMMER-III 2D model limitation, has been modeled with separated volumes communicating only with small gas openings in the higher part, that are partially obstructed due to lead sloshing resulting in steam flowing through no realistic flow paths (e. g. downward in the pump ducts of the faulted SG). This fact should be kept in mind when analyzing the simulation results.

After 0.3 s starting from the water injection, the pressure peak disappears and the pressure reaches its initial stationary value; afterwards it increases again due to the cover gas pressurization. Not so far from the injector the pressure peaks disappear, as observed in both performed simulations, preventing any risk (from a structural point of view) for the SG and the core.

The steam generated by one bayonet tube rupture accident flows upward in the 1SG and reaches the cover gas passing through the gas vents. Instead, as consequence of the large amount of steam produced in the case of seven broken tubes, traces of steam flow from the 1SG directly and indirectly to the core. The steam enters the core downcomer mostly by the inner path, as shown by the void fraction calculated in the cells beneath the core. The very low amount of vapor entering the core, the limited vapor residence time and the negative coolant expansion reactivity effect in the optimized ALFRED reactor core do not result into a hazard of positive reactivity insertion, even if they are to be carefully taken into account for the neutronic feedback consequences.

For a more detailed description of the performed SGTR accident analysis for ALFRED done by CIRTEN using SIMMER-III code, refer to Appendix G of this report.

5.10 CFD simulation of bubble transport in SGTR/SGTL event (KTH)

Close proximity of steam generator to the core increases the risks associated with Steam Generator Tube Rupture/Leakage (SGTR/SGTL) such as voiding of the core and resulting reactivity insertion and/or local damage (burnout) of fuel rod cladding. Analysis of consequences of SGTL provided in the following suggests that small bubbles of steam can be dragged by the turbulent coolant flow into the core region. Trajectories of the bubbles are determined by location of the leak, bubbles size and turbulent flow field of lead coolant. The influence of epistemic uncertainty in drag coefficient on prediction of the fraction of bubbles that can reach the core and accumulate in the primary coolant system is discussed in detail in Appendix F.

The main objective of the present study for ALFRED is to quantify the likelihood that a steam bubble is transported in the primary coolant system to the core in case of SG tube leakage. The ALFRED pool-type 300MWth LFR is used as a reference design (see Section 3).

General approach

A commercial CFD code Star-CCM+ version 8.02.008 [18] is used for modelling of coolant flow field and bubble transport. We are considering the steady state liquid lead flow in the primary system of the ALFRED design at nominal full power operation conditions.

The consequences of SGT leakage are studied by injecting bubbles with different diameters into the steam generator region. Bubbles are modelled as Lagrangian particles. Bubble transport to the core region is contingent upon the balance between the gravity and hydrodynamic drag forces. To account for the effects of fluctuating turbulent velocity field on the trajectories of the bubbles, a turbulent dispersion model, which employs so-called random-walk technique, is employed. A fraction of the bubbles that can reach the core region is calculated by counting the number of bubbles at the core inlet and relating this number to the total number of bubbles released. Similar approach is used to determine the fraction of bubbles that can accumulate in the primary coolant system. We vary the size of the bubbles and location of bubble injection inside the SG to identify the most dangerous bubble size and positions of the leak. The influence of epistemic uncertainty in the correlations for bubble drag in liquid lead is addressed by comparing the probabilities of bubble transport to the core obtained with different correlations.

Bubble drag coefficient

Drag force is a result of skin and form friction of a body. The most common method to mathematically model the drag force is:

$$F_D = \frac{1}{2}\rho v^2 C_D A \qquad (1)$$

The balance between drag and buoyancy forces defines the terminal rise velocity of a bubble in lead. Essentially, bubble will be dragged down by coolant flow if the terminal rise velocity of a bubble is smaller than local downward velocity of the coolant. Therefore the drag coefficient is one of the most important factors determining the bubble transport in the primary system.

Verification of drag coefficient correlation for steam bubble in liquid lead is performed. For that purpose, terminal rise velocity of a steam bubble in steady liquid lead column is calculated using different drag correlations. The predicted velocity is then compared with available analytical and experimental data about the terminal rise velocity of a bubble in heavy liquid metals.

Modeling bubble motion in lead

Motion of a bubble in liquid and its terminal rise velocity have been studied extensively in the past. Bubble dynamics is affected by many factors (i.e. temperature, viscosity, pressure, purity). Therefore, prediction of terminal rise velocity is not a trivial task, especially taking into account a nonlinear nature of drag coefficient versus bubble size curve (nonlinearity rises with bubble size).

In this work, Lagrangian model for bubble transport in a continuum flow field of liquid lead is used [19]. Steam inside the bubble was assumed to be incompressible and bubble size was not a function of hydrostatic pressure. Density and viscosity of the bubble gas was assumed equal to water vapour density at 100 °C under atmospheric pressure. Bubbles with diameter ranging from 0.2 mm to 10 mm are studied. This range of bubble sizes was observed in experiments performed air injection into water with different sizes and geometries of the orifice [20] and also in experiments with water injection into lead [21].

Four different drag coefficient correlations were tested and the results of relevant applications are discussed in detail in Appendix F.

Bubble transport in the primary system

In this section we address the possibility of transport of a bubble from the steam generator to the core region in the ALFRED design at nominal operation conditions. First, we resolve the averaged steady state flow at full power operation in a realistic configuration of the primary system. Then we study behavior of individual bubbles in the flow field with Lagrangian approach, taking into account dispersion of the bubbles by turbulent vortices. The probability that a bubble of certain size can reach the core region and then stay in the primary coolant system is assessed for the bubbles released at different locations in the SG.

ALFRED nominal operational conditions

Simulation domain represents $1/8^{th}$ of the whole reactor pool, comprising of a SG, a pump and a slice of the core region with corresponding sections of the hot/cold plenum and downcomer.

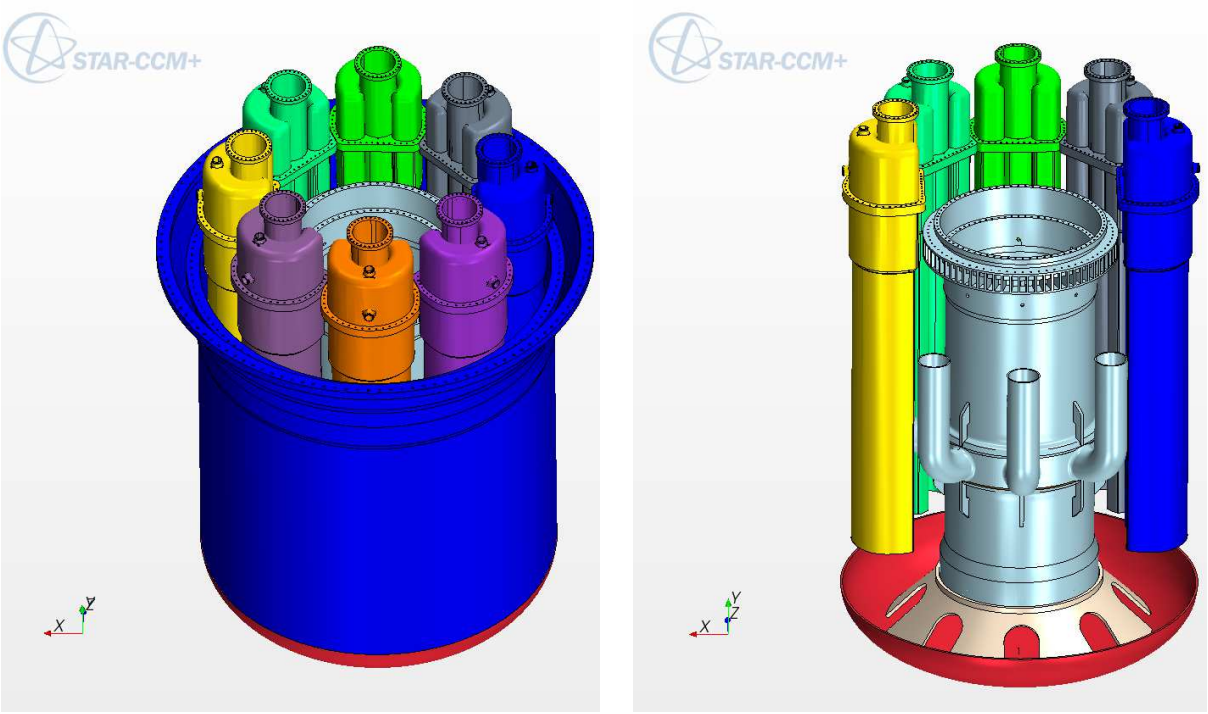


Fig. 5.10-1: ALFRED 3D CAD model. Left image shows all components, right image shows internals

CFD simulations will be set up to first achieve nominal operational conditions given by [2]. The simulations are in the phase of preparing the geometry according to ALFRED 3D CAD model in Fig. 5.10-1, and therefore no results are provided at this moment. Results could be made available in a future revision of deliverable DEL022-2013.

Approach to estimate the fraction of bubbles reaching the core

The following three-step method is used in assessment of void accumulation rate in the core (and in the primary system). Bubbles are injected at three different height levels within the SG region simulating different leakage locations. Then the bubbles have three possibilities to escape the system (see Fig. 5.10-2) depending on their size, leak location and coolant flow characteristics:

1. Bubble escapes after injection immediately to the cold free surface above the downcomer and the SG.
2. Bubble is dragged down to the core for the first time and then escapes from the loop to the hot free surface above the core.
3. Bubble stays in the primary coolant flow, travels through the hot leg and pump and reaches the SG again. Then it emerges to the cold free surface.

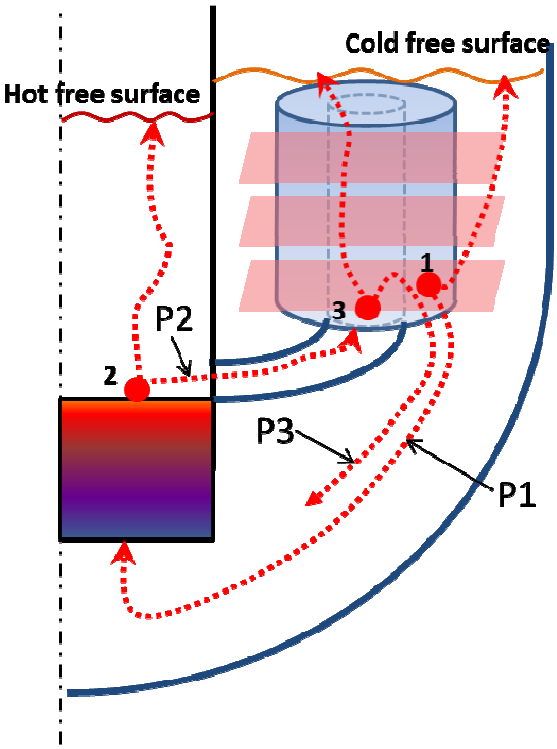


Fig. 5.10-2: Illustration of different locations of bubble injection (1-3) and respective probabilities that injected bubble can stay in the loop (P1-P3)

All the bubbles which do not escape from the coolant will be carried by the coolant flow through the primary loop again to the core. In order to assess the consequences of the SGTL and different scenarios of void behaviour in the primary system we need to calculate the probabilities that a bubble will escape from the coolant given the abovementioned three possibilities.

P1 is the probability that a bubble can reach the core after entering the primary coolant flow through the SG tube leak. We calculate this probability by injecting bubbles at one of the three injection levels in the SG and counting the number of the bubbles that reach the core inlet boundary. P2 is the probability that a bubble can reach SG after passing through the core. To estimate the P2, we inject bubbles at the exit of the core and count those that escape to the hot free surface. One minus obtained fraction of the bubbles that escape from the coolant is equal to P2. Finally, P3 is the probability that a bubble stays in the primary loop after passing through the core and the pump. To calculate the P3 we inject bubbles at the exit of the pump and count those that reach the core inlet.

If leak rate and bubble size distribution in case of SGTL are known, one can estimate the total rate of void accumulation in the coolant in the form of the bubbles that are circulating in the primary system:

$$Q_{primary}(t) = Q_{leak}(t) \sum_{i=1,N} f_{d_i} P_{1_{d_i}} P_{2_{d_i}} P_{3_{d_i}} \qquad (2)$$

where Q_{leak} is volumetric leak rate [litres/day], $f_{d_i}, P_{1_{d_i}}, P_{2_{d_i}}, P_{3_{d_i}}$ are volume fraction and respective probabilities for a bubble with size d_i, and N is the number of bubbles sizes considered in the bubble size distribution.

It is also interesting to estimate the void accumulation rate in the core (assuming that all bubbles that reach the core will stick in the core, e.g. below spacers):

$$Q_{core}(t) = Q_{leak}(t) \sum_{i=1,N} f_{d_i} P_{1_{d_i}} \qquad (3)$$

To estimate the realistic rate of void accumulation in the core one needs to consider the probability that bubble will pass or stuck in the core given detailed geometry of the core internals. This task is beyond the scope of the present work.

Future considerations

The future work foresees finishing the CAD model that is, preparing the surface for CFD meshing. Then surface and volume mesh will be created. Simulation of nominal operational flow conditions are then performed on several meshes to evaluate the mesh sensitivity and use the fastest (read: coarser) mesh.

After the solution for nominal operational conditions is resolved, Lagrangian framework is utilized to simulate bubble transport in the primary system. Then the above described methodology to estimate the void accumulation rates in the primary system and in the core are calculated.

6. CONCLUSIONS

The representative DEC accidental transients for the ALFRED reactor have been simulated by various organizations using different computer codes with the main objective to investigate the inherent safety features of the plant and the suitability of the design solution adopted for ALFRED.

The analysis of unprotected transients: UTOP, ULOF, ULOHS and ULOHS+ULOF has demonstrated the good inherent safety features of the core and plant design and the large grace time allowed for the operator to take opportune corrective action for manually shutting down and cooling down the primary circuit towards cold safe conditions.

In case of a UTOP transient, for reactivity insertion of 250 pcm within 10 s (possibly due to: voiding of part of the active core region enveloping void introduction in case of SGTR, core compaction, fuel SA blockage, etc.), at BOC as well as at EOC core conditions, peak fuel pin cladding is not expected to fail, since there is a large margin to creep rupture limit. The more critical issue is the maximum fuel temperature that, because of the initial core nuclear power excursion (peak power up to ~ 230% the nominal value), is expected to exceed the MOX melting point in the initial phase of the transient. However, all codes agree that fuel melting is observed only in the centre of the peak fuel pin (pellets). Therefore, extended fuel rod damage can be excluded, as well as the likelihood for this transient to evolve towards a severe accident.

In case of ULOF transient, no relevant flow undershoot is expected in the initial phase of the transient and enhanced stable natural convection, around 23% of the nominal value, establishes in the primary circuit. Furthermore, the prevalent negative reactivity feedbacks reduce the core power down to about two-third of the nominal value. As a result, the ULOF transient in the ALFRED reactor can be easily accommodated, since the maximum clad temperature remains well below the creep rupture limit in the long term (maximum clad temperature stabilizes below 700 °C). Besides, very large minimum clad failure time of ~ 1.6E+5 seconds (~ 2 days), under the minimum coolant flow conditions (initial flow undershoot) at both BOC and EOC conditions, are calculated by SIM-LFR code.

In case of ULOHS transient, the maximum clad temperature is not a critical issue, since the minimum clad failure time is > 1.E6 seconds, as calculated by SIM-LFR at both BOC and EOC conditions. Because of the uniform temperature distribution establishing in the primary circuit, the main concern is on the average vessel wall temperature, which in ~ 1 hour transient time approaches 670 – 700 °C, thus questioning the long term structural integrity of the vessel under these elevated temperature conditions. The sluggish time response to this DEC transient is ascribed to the large primary loop thermal inertia and a rather large cumulative negative reactivity effect coming from the negative fuel, diagrid, pads, Pb-coolant and CRs drivelines feedback effects, resulting in a very effective decrease of the core nuclear power towards the decay level. Sufficient grace time (>> 30 minutes) is available for the operator intervention to terminate this transient by manually shutting down the reactor and cooling down the primary circuit.

The evolution of the unprotected LOOP (ULOHS+ULOF) transient is characterized first by the loss of flow with transition to natural convection in the primary circuit, such as under ULOF, and then by the loss of heat sink with core nuclear power decrease towards the decay level,

such as under ULOHS. Because of the very low natural convection flow rate which stabilizes in the primary circuit and consequent significant core ΔT increase, the maximum clad temperature is about 100 - 120 °C higher than under ULOHS. On the contrary, the very low primary flow rate limits the significant vessel wall temperature increase predicted under ULOHS, and thus the long term structural integrity of the vessel is guaranteed. According to the SIM-LFR results, the minimum clad failure time is of ~ 2.1E+4 seconds at both BOC and EOC conditions. Therefore, also under this very unlikely DEC transient, sufficient grace time (>> 30 minutes) is available for the operator intervention to terminate this transient by manually shutting down the reactor and cooling down the primary circuit.

All codes agree that the ALFRED reactor is not expected to experience any fuel pin failure during SA flow area blockages less than 75% even in case of unprotected transient. For SA flow area blockages above 75%, clad failure (creep rupture) has to expected. Clad melting point seems reached for flow area blockages above 95%, while fuel melting temperature is reached only for flow area blockages above 97.5%. The SIMMER-III results for a protected case also suggest that nearly total blockages could be well accommodated if the reactor is shutdown within 5 seconds from their detection (i.e. 10 seconds from the initiation of the accident). However, for ALFRED sudden and complete flow blockage is prevented by the SA design solution consisting in multiple inlet openings. Any other blockage caused by deposition of material will be likely gradual and can be monitored by detection of an increase of coolant outlet temperature of each SA.

The analysis of the “practically excluded” event of SCS failure with total unavailability of DHR system has highlighted a slow temperature increase of the primary system, thanks to its large thermal inertia and good coolant mixing throughout the primary pool. This transient presents no imminent safety issue to the ALFRED reactor in the first several hours. However, all primary cooling circuit temperatures, in a longer time horizon, will start increasing slowly at a rate of about 30 °C per hour and will reach ~500 °C in 3 hours. However, the operator has sufficient time for manual intervention by re-activating SCS or sub-systems of the DHR-1 system, in order to prevent overheating of the whole primary system, including the reactor vessel.

The protected loss of flow transients with simultaneous malfunction of the feedwater temperature or flow rate control system on the secondary side have no safety concern in the short term, since the perturbation on core temperatures is not significant. In all code calculations, the initial clad temperature peak produced by the loss of forced circulation in the primary circuit is below 650 °C. Furthermore, there is no risk of lead freezing at the MHX outlet, just after the DHR-1 system start-up. The major concern is on the risk of lead freezing in the medium term, since the power removal by the DHR-1 system exceeds the decay power. The Pb freezing is expected within about 2 – 4 hours, depending on the different conditions of coolant mixing calculated by the codes in the primary pool surrounding the MHX. In fact, the lack of mixing in this wide region, such as predicted by RELAP5 code, reduces significantly the effective thermal inertia of the primary system and then the elapsed time to Pb freezing. However, during this time period the operator has sufficient time to deactivate sub-systems of the DHR-1 system, in order to prevent Pb-coolant freezing at the outlet of the MHX. Future DHR design improvements are foreseen to control in a passive way the DHR-1 and DHR-2 power removal, and thus avoiding the need of operator actions in the medium and long term.

Regarding the SGTR accident, it was observed that, the steam generated by one bayonet tube rupture accident flows upward in the damaged SG and reaches the cover gas passing through the gas vents. However, as a consequence of the large amount of steam produced in the case of seven broken tubes (2.5-3.5 kg/s), traces of steam are expected to flow from the damaged SG directly and indirectly to the core. The small amount of steam enters the core downcomer mostly by the inner path, as shown by the void fraction calculated in the cells beneath the core. However, the very low amount of vapor entering the core, the limited vapor residence time and the negative coolant expansion reactivity effect in the optimized ALFRED reactor core do not result into a positive reactivity insertion and thus represent no safety concern. Besides, in the SIMMER-III simulation, all the water injected into the Pb-coolant instantaneously fully vaporizes in contact with it at the injector tube exit region. Moreover the cover gas space, due to SIMMER-III 2D model limitation, has been modeled with separated volumes communicating only with small gas openings in the higher part, that are partially obstructed due to lead sloshing resulting in steam flowing through no realistic flow paths (e. g. downward in the pump ducts of the faulted SG). In reality, only a fraction of the injected water will be vaporized instantaneously when contacting lead and the remaining liquid water will be encapsulated in vapor bubbles and transported to the cover gas region formed by only one large volume, hence lead and steam can flow freely into the gas space. This should be kept in mind when analyzing SGTR accident simulation results.

KALLA experimental tests [22] and Russian tests [23] also indicated the difficulty for the vapour bubbles, generated during the lead-water interaction, to reach the core inlet section because of the drag effects produced by the liquid metal flow in the downcomer region of the reactor. A dedicated scaled facility should be foreseen to analyse in depth the SGTR phenomena further as part of the future R&D activities for LFR.

In general, the consistency of various code results for the same transient was rather good. For all DEC events the codes predicted similar transient behaviour and then similar conclusions can be drawn. Some of the observed discrepancies might be correlated to the different schematization detail of the primary and secondary circuits, or correlated to the fuel rod gap behaviour in transient conditions, due to the lack of a dedicated fuel rod gap dynamic model in some of the codes.

Finally, the analysis of the DEC transients performed for the Pb-cooled ALFRED design have demonstrated the very forgiving nature of this plant design when compared to other similar plant design, ascribable to the combination of:

- the inherently, large thermal inertia of the Pb-cooled primary system,
- the detailed focus on the optimization of all safety relevant system, in particular emphasizing appropriate design of all relevant control and safety system (as well as components), and
- optimizing the neutronic core characteristics of the ALFRED “core system” thereby assuring various reactivity feedback effects (fuel, diagrid, pads, Pb-coolant and CRs drivelines expansion reactivity) that effectively depress the reactor power under all adverse DEC transient conditions,
- as the ALFRED core is specifically designed to accommodate the ULOF transient.

REFERENCES

1. A. Alemberti et al., “The Lead fast reactor - Demonstrator (ALFRED) and ELFR design”, International Conference on Fast Reactors and Related Fuel Cycles: Safe Technologies and Sustainable Scenarios (FR13), Paris, France (2013).
2. E. Bubelis, K. Mikityuk, “Plant data for the safety analysis of the ETDR (ALFRED)”, FP7 LEADER Project technical report TEC058-2012, PSI report, May 2012.
3. G. Ramò, M. Reale, “LEADER Task 3.3: ALFRED Reactor Block”, LEADER WP3 meeting presentation, Bologna, October 25th, 2011.
4. Drawing LEADER33DMMX013 Rev. 0 – ALFRED Project – Reactor Block General Assembly.
5. Drawing LEADER33DMMX014 Rev. 0 – ALFRED Project – Fuel Assembly Outline.
6. Drawing LEADER33DMMX015 Rev. 0 – ALFRED Project – Inner Vessel Outline.
7. Drawing LEADER33DMMX016 Rev. 0 – ALFRED Project – Core Lower Grid Outline.
8. Drawing LEADER33DMMX017 Rev. 0 – ALFRED Project – Core Upper Grid Outline.
9. Drawing LEADER33DMMX018 Rev. 0 – ALFRED Project – Reactor Vessel Outline.
10. Drawing LEADER33DMMX020 001 / 002 Rev. 0 – ALFRED Project – Steam Generator outline.
11. M. Gregorini, “Conceptual design of the DHR system of the ETDR (ALFRED)”, FP7 LEADER project deliverable DEL010-2012, Ansaldo Nucleare report, April 2012.
12. M. Palmero, F. Fionelli, “ALFRED steam generator design”, LEADER WP3 meeting presentation, Genova, May 11th, 2011.
13. Lead-cooled European Advanced DEmonstration Reactor (LEADER) – Annex I Description of work (3 May 2010), Rev. 0.
14. G. Ramò, M. Reale “LEADER Task 3.1, Reference Plant Configuration of ALFRED”, LEADER WP3 meeting presentation, Genova, May 11th, 2011.
15. C. Petrovich et al., P. Sciora, “Definition of the ETDR core and neutronic characterization”, FP7 LEADER project deliverable DEL007-2012, ENEA/CEA report, March 2012.
16. F. Manni, D. Vitale Di Maio “WP2.4: ALFRED core. Fuel assembly”, LEADER WP3 meeting presentation, Bologna, October 25th, 2011.
17. Drawing LEADER35DMBX036 Rev. 0, ALFRED Project Isolation Condenser Outline.
18. CD-adapco, Star-CCM+ User Guide version 8.02.
19. M. Jeltsov and P. Kudinov, “Simulation of steam bubble transport in primary system of pool type lead cooled fast reactors,” 14th International Topical Meeting on Nuclear Reactor Thermalhydraulics (NURETH-14), Toronto, Ontario, Canada, September 25-29, 2011.
20. E. Krepper, D. Lucas, and H.-M. Prasser, “On the modelling of bubbly flow in vertical pipes”, Nucl. Eng. Des., Vol. 235, 2005, 597-611.
21. A. V. Beznosov, S. S. Pinaev, D. V. Davydov, A. A. Molodtsov, T. A. Bokova, P. N. Martynov and V. I. Rachkov, “Experimental studies of the characteristics of contact heat exchange between lead coolant and the working body”, *Atomic Energy*, Vol. 98, Issue 3, 2005.
22. L. Marocco, A. Friedrich, T. Wetzel, “Final Report on the SGTR-experiments at KIT”, 2009-2010.
23. A. V. Beznosov, et al., “Experimental Studies of the Characteristics of Contact Heat Exchange Between Lead Coolant and the Working Body”, Atomic Energy, Vol. 98, No. 3, 2005.

APPENDIX A

Description of Computer Codes Used

A.1 SIM-LFR code used by KIT-G

SIM-LFR [1] is a PC-based; multi node point kinetic model that describes the nuclear and thermal-hydraulic characteristics of both critical and sub-critical reactor cores. Two separate neutronic core models are run simultaneously, namely a single node PK model that acts as driver for a multi-node (16-axial nodes) thermo-hydraulic model, and a multi-node neutronic model (16 axial neutronically coupled nodes) which allows the axial power profile to change during the transient according to nodal temperature and nodal reactivity variations. In the single node PK neutronic model, the axial power profile is assumed to remain unchanged during the transient.

Under “normal”, simple transient conditions that are not dependent on a transient axial power profile, both neutronic models (single node and 16-axial nodes) should yield identical results in core averaged parameters, thereby serving as a constant calculational cross-check.

The neutron kinetics of each nuclear model is described by 6-delayed neutron precursor groups on the nodal level, and a complete set of nodal dependent reactivity feedback coefficients such as Doppler, coolant, fuel expansion, diagrid expansion, void, control rod, Xenon (for thermal reactors), etc. The nodal time characteristics of the decay heat after shutdown is described by 6 decay heat groups.

The 16-axial node, full-scope thermal-hydraulic model assumes an initial axial and radial power distribution (provided as input to the kinetics models and supplied by the detailed neutronic analysis performed during the design phase of the core), and then calculates the radial heat transfer through a typical fuel pin consisting of the detailed description of the heat transfer mechanisms between cladding and coolant, the heat transfer through the clad material, the heat transfer in the gap between clad and fuel, and the fuel matrix itself assuming appropriate material property data and applicable coolant type dependent heat transfer correlations (correlation for Nusselt numbers, friction factors, etc.). This heat transfer analysis is performed for the peak pin and the average pin of the core where the radial core power distribution is assumed to be representable by radial power form factors.

The primary loop is nodalized into several appropriate hydraulic nodes with corresponding volumes, internal masses and surface areas (lower vessel plenum, the 16 axial core nodes, upper vessel plenum, the piping to and from the HX, (HX and DHRS itself are modeled by appropriate internal nodalization)) to account for all relevant thermal-hydraulic effects including radiation (from vessel wall) to the ambient and all relevant pressure loss calculations inside the core region (i.e. due to grid or wire-wrap spacers) and the primary system (heat exchangers, pumps, loops, etc.).

Particular attention is placed on the correct formulation of all relevant heat transfer mechanisms between cladding surface and coolant (such as for example roughened surface areas) in the core region and in the HX and DHRS systems, in particular accounting for the physical phenomena encountered in various flow regimes (i.e turbulent and laminar flow under forced flow and natural convection conditions) for heavy metals (Na, or Pb, or LBE), water or gas coolants (He, Air or CO_2).

The codes system SIM-LFR has been used to perform the transient analysis of both the LBE-cooled and He-cooled PDS-XADS ADS designs during the PDS-XADS project and the EFIT-Pb, EFIT-He and XT-ADS designs during the EUROTRANS project, critical and sub-critical FASTEF reactor designs during the CDT project, as well as the AMSTER molten salt reactor extensively against actual LWR plant data (plant transient data) for both PWRs and BWRs, Superphenix (SPX1) plant data, and by code to code comparisons of results obtained using various releases of RELAP5, SAS4A, TRAC, TRACE, SIMMER and other large transient code systems.

References:

1. W. M. SCHIKORR, Assessment of the kinetic and dynamic transient behavior of subcritical systems (ADS) in comparison to critical reactor systems, Nuclear Engineering and Design 210, 95-123, 2001.

A.2 TRACE/FRED code used by PSI

FRED code

The transient thermal-mechanics code FRED was originally developed to model the transient behavior of LWR fuel rods. The FRED code is used to calculate the transient changes of temperature, heat flux, stress, strain and thus failure probability for structural elements in fuel rods. The FRED code was implemented into the FAST code system. The data library in the FRED code includes thermo-mechanical properties of different cladding materials (zircaloy alloy, Zr-1%Nb, several types of stainless steel), fuels (UO_2, MOX and so on) and gases (He, Ar, Xe, Kr, H_2 and N_2) and coolants (D_2O, H_2O, He, liquid Na, and LBE) [1].

TRACE code

The advanced system code TRACE (TRAC/RELAP Advanced Computational Engine) was developed by the United States Nuclear Regulatory Commission (US NRC), in order to perform simulations of real and postulated transients in pressurized and boiling water reactors. The code can also model a wide variety of thermal-hydraulic experiments in reduced-scale facilities [2]. Being a part of the FAST code system, the TRACE code is being extended and used at PSI for the thermal-hydraulic assessment of Generation IV fast reactor systems. In particular, the modifications include adding equations of state for new coolants and the corresponding heat transfer and friction models [3]. In the present work, TRACE was used for the steady-state and transient analysis of the ALFRED system.

References:

1. K. Mikityuk and A. Shestopalov. ”FRED fuel behaviour code: Main models and analysis of Halden IFA-503.2 tests”. Nuclear Engineering and Design 241 (2011), 2455–2461. DOI:10.1016/j.nucengdes.2011.04.033.

2. Division of Safety Analysis, Office of Nuclear Regulatory Research, U. S. Nuclear Regulatory Commission, "TRACE V5.435 Theory Manual", DC 20555-0001.

3. Konstantin Mikityuk, Sandro Pelloni, Paul Coddington, Evaldas Bubelis, Rakesh Chawla, "FAST: An advanced code system for fast reactor transient analysis", Annals of Nuclear Energy 32 (2005), 1613–1631.

A.3 TRACE code used by JRC-IET

Concerning its applicability to heavy liquid metal modeling, the TRACE code is capable of performing analyses only using lead-bismuth eutectic (LBE) as a coolant in liquid state. Therefore, to perform detailed and more accurate assessments applicable to ALFRED LFR, equations of state for lead have been implemented into the TRACE source. These data are based on experiments and their evaluations carried out by ENEA-ANSALDO [1].

An exhaustive comparison of the main thermal properties was performed between the lead-bismuth correlations embedded in the TRACE source, the ones extracted from the abovementioned data, and the ones proposed in the OECD/NEA Handbook for lead and lead-bismuth eutectic [2]. Some physical quantities (as saturation temperatures and pressures) appeared to be nearly identical, so they were left unmodified. Others, for which remarkable differences had been observed, were substituted, namely: the internal energy and its derivative over temperature (Fig. A.3-1), the specific heat as a function of temperature (Fig. A.3-1), the density (Fig. A.3-2) and its derivative over temperature as a function of temperature. As there is no experimental data available for the thermal conductivity, a comparison was made between the correlations available in literature. Finally, the original correlation embedded in TRACE code was substituted by the Takamichi [1] to be consistent with other partners of the LEADER project. Fig. A.3-2 shows the comparison between the different correlations together with the relative difference between them.

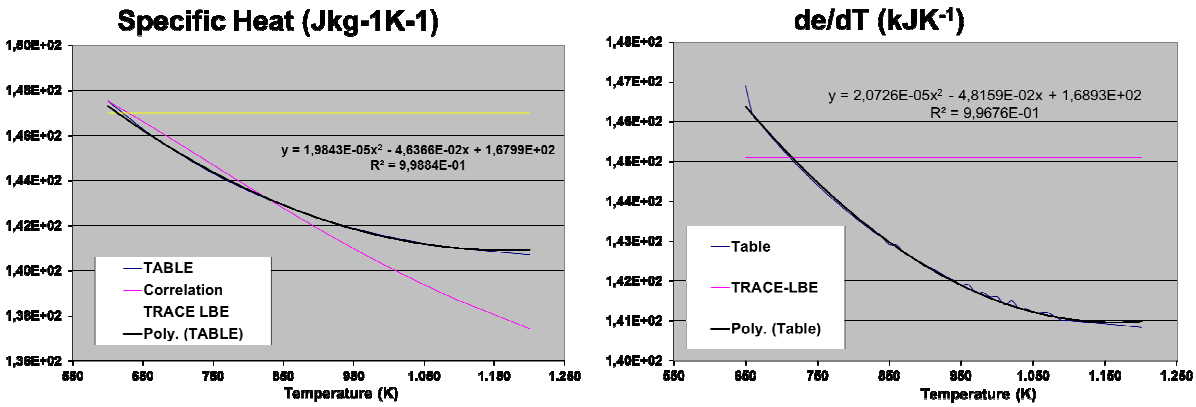


Fig. A.3-1: Left – Internal energy with displayed experimental data (blue) , the corresponding correlation (black) and in TRACE-LBE embedded correlation (magenta). Right – Specific Heat, with displayed experimental data (blue), the corresponding correlation (black), correlation given in the NEA Handbook (magenta), and in TRACE-LBE embedded correlation (yellow)

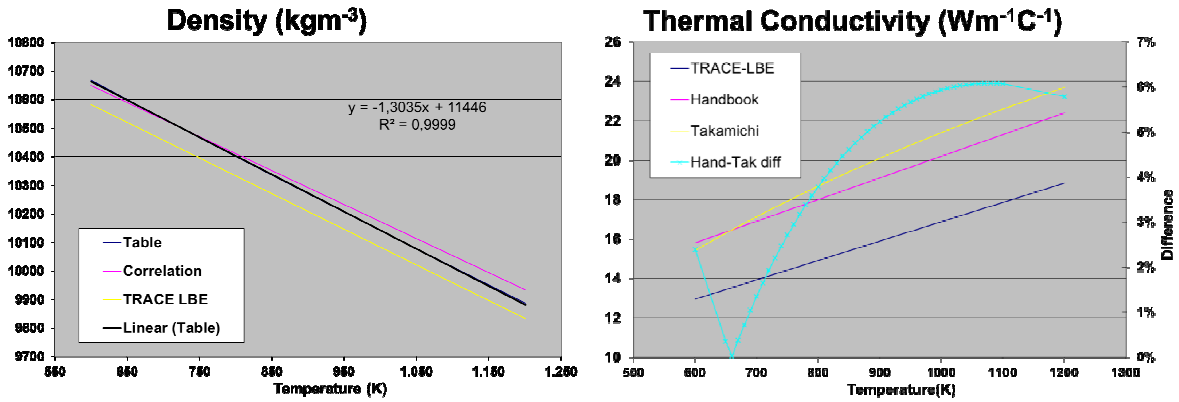


Fig. A.3-2: Left – Density - displayed are the experimental data (blue) and the corresponding correlation (black), correlation given in the NEA handbook (magenta) and in TRACE-LBE embedded correlation (yellow). Right – Thermal conductivity – displayed are in TRACE-LBE embedded correlation (blue), correlation given in the NEA handbook (magenta), the Takamichi correlation (yellow) and the relative difference between the two latter correlations

References:

1. Private Communication, ENEA –ANSALDO (Mr. L. Mansani) (2012).

2. Handbook on Lead-bismuth Eutectic Alloy and Lead Properties, Materials Compatibility, Thermal-hydraulics and Technologies, Edition 2007, Chapters 2 and 3, NEA No. 6195, OECD (2007).

A.4 RELAP5/MOD3.3 code used by ENEA and KTH

The DBC transient analysis of the lead-cooled ALFRED reactor has been carried out by using the RELAP5/MOD3.2.2 code developed by INEL for the USNRC and modified by ENEA/Ansaldo to include properties of lead alloys used as coolant in LFR reactors.

The standard RELAP5 code [1] is widely used and qualified for thermal-hydraulic transient analysis of LWRs reactors. Lead thermo-physical property data and heat transfer correlations for heavy liquid metal in different geometries have been taken from the literature and available studies and introduced in the modified code [2].

The modified RELAP5 code has been validated against experimental data from tests conducted on the LBE-cooled CHEOPE, NACIE and CIRCE facilities at ENEA/Brasimone centre [3, 4, 5]. More recently, the code has been validated by the post-test analysis of accidental transients (ULOF and ULOHS) simulated on the large scale CIRCE facility within the EUROTRANS EU project [6]. A new experimental program conducted on CIRCE within the current THINS EU project has recently provided further valuable data for code validation and verification.

The modified RELAP5 code has been extensively used by ENEA for the transient analysis of the lead-cooled ADS EFIT [7, 8] and for the thermal-hydraulic and transient analysis of the lead-cooled ELSY critical reactor [9, 10], in the frame of EUROTRANS and ELSY EU projects. The results of these analyses have been successfully compared with other codes.

References:

1. C.D. Fletcher, R.R. Scuhltz, RELAP5/MOD3 Code manual, NUREG/CR–5535, INEL–95/174, Idaho National Engineering Laboratory, June 1995.

2. P. Meloni, et al., “Implementation and Preliminary Verification of the RELAP5/PARCS Code for Pb-Bi Cooled Subcritical System”, International Conference on Accelerator Applications AccApp01, Nuclear American Society, Reno, USA, 2001.

3. P. Agostini, et al., “Natural Circulation of Lead-Bismuth in a One-Dimensional Loop: Experiments and Code Predictions”, 10th International Conference on Nuclear Engineering (ICONE-10), Arlington, Virginia, USA, April 14-18, 2002.

4. P. Meloni, A.D. Wagner, F: Castiglia, M. Casamirra, P. Agostini, G. Bertacci, “Investigation of RELAP Capability to Simulate the LBE Cooling System Thermal-Hydraulic”, 8th Information Exchange Meeting on Actinide and Fission Product Partitioning & Transmutation, Las Vegas, Nevada, USA, November 9-11, 2004.

5. M. Casamirra, F. Castiglia, M. Giardina, P. Meloni, “RELAP5 Modification for CHEOPE Simulations”, International Conference Nuclear Energy for New Europe, Bled, Slovenia, September 5-8, 2005.

6. G. Bandini, et al., “Analysis of Integral Circulation and Decay Heat Removal Experiments in the Lead-Bismuth CIRCE Facility with RELAP5 codes”, 14th International Topical

Meeting on Reactor Thermal-hydraulics (NURETH-14), Toronto, Ontario, Canada, September 25-30, 2011.

7. G. Bandini et al., “Decay Heat Removal and Transient Analysis in Accidental Conditions in the EFIT Reactor”, International Conference on Nuclear Energy for New Europe 2007, Portoroz, Slovenia, September 10-13, 2007.

8. G. Bandini et al., “Analysis of Protected Accidental Transients in the EFIT Reactor with the RELAP5 Thermal-Hydraulic Code”, 16th International Conference on Nuclear Engineering (ICONE-16), Orlando, Florida, USA, May 11-15, 2008.

9. M. Polidori, G. Bandini, P. Meloni, “Reactivity Insertion Accident Simulation of ELSY Lead Fast Reactor with RELAP5 Code”, 8th International Topical Meeting on Nuclear Thermal-Hydraulics, Operation and Safety (NUTHOS-8), Shanghai, China, October 10-14, 2010.

10. G. Bandini, P. Meloni, M. Polidori, “Thermal-Hydraulics Analyses of ELSY Lead Fast Reactor with Open Square Core Option”, Nuclear Engineering and Design, doi: 10.1016/j.nucengdes. 2010.04.034 (2010).

A.5 CATHARE V2.5_2 used by ENEA / CEA

The DBC transient analysis of the lead-cooled ALFRED reactor has been carried out by using the CATHARE system code. This code is the result of a joint effort of CEA, EDF, Framatome ANP and IRSN.

The CATHARE system code [1] is commonly used for thermal-hydraulic transient analysis and best-estimate safety analysis of light water reactors. The CATHARE V2.5_2/mod5.1 can be also applied for safety analysis of gas-cooled and sodium-cooled fast reactors.

The lead-bismuth eutectic (LBE) and lead thermo-physical properties have been recently implemented in the CATHARE code, in the frame of a bilateral collaboration between ENEA and CEA, for the safety analysis of lead-cooled fast reactors. The validation of the code for lead-cooled systems is still in its initial phase. Some validation works have been performed or are in progress at ENEA on the basis of:

- The experiments conducted in the Korean LBE-cooled HELIOS loop in the frame of the OECD LACANES benchmark, including a comparison with RELAP5 code;
- The experiments carried out in the LBE-cooled NACIE facility of ENEA/Brasimone;
- The experiments carried out on the LBE-cooled TALL loop of KTH/Stockholm within the on-going activities of the THINS European project.

The capabilities introduced in CATHARE for sodium-cooled fast reactors, regarding reactivity feedbacks calculation and fuel rod gap dynamic behaviour modelling, have been used for the lead-cooled ALFRED applications.

The whole core, primary system and secondary system discretization of the ALFRED reactor used in the CATHARE simulation has been harmonized with the one used in the RELAP5 simulation performed by ENEA, in order to better compare the code results. The systematic comparison of CATHARE results with the results of the more validated RELAP5 code, regarding both DBC and DEC transient analysis, has confirmed the good applicability of CATHARE for ALFRED transient simulations.

References:

1. G. Geffraye et al., “CATHARE 2 V2.5_2: a Single Version for Various Applications”, Proc. 13th International Topical Meeting on Nuclear Reactor Thermal-Hydraulics (NURETH-13), Kanazawa, Japan, Sept. 27-Oct. 2, 2009.

A.6 SPECTRA code used by NRG

The SPECTRA [1] is a thermal-hydraulic system code for transient analyses in Light Water Reactors, High Temperature Reactors and Liquid Metal Fast Reactors. The SPECTRA model of ETDR consists of the following elements:

- Reactor primary system
- MHX loops
- DHR decay heat removal loops

Properties of Liquid Lead

Liquid lead properties were tabulated based on approximation formulae for the following properties of liquid lead 2.

- Saturation pressure, [Pa] (2, section 2.8.1):

$$p_{sat}(T) = 6.5715\times10^{9}\cdot\exp\left(-\frac{22{,}247.0}{T}\right)$$

Here T is temperature, [K].

- Enthalpy of saturated liquid, [J/kg] (2, section 3.2):

$$h_{liq}(T) = h_0(T_{melt}) + \Delta h(T - T_{melt})$$

Here h_0 is the enthalpy at the melting point, T_{melt}, (=600.6 K 2) and Δh is the enthalpy change from the melting temperature to the temperature T. These values of h_0 and T_{melt}, expressed in [J/mol] and Δh isotherms are given by:

$$\begin{aligned} h_0(T_{melt}) = &-5.13300\times10^{-4}\cdot T_{melt}^2 + \\ &+3.03623\times10^{1}\cdot T_{melt} - \\ &-4.67191\times10^{3} \end{aligned}$$

$$\begin{aligned} \Delta h(T - T_{melt}) = &\ 3.3756\times10^{+1}\cdot(T - T_{melt}) - \\ &-3.1310\times10^{-3}\cdot(T - T_{melt})^2 + \\ &+5.7614\times10^{-7}\cdot(T - T_{melt})^3 \end{aligned}$$

Finally the value of enthalpy should be expressed in [J/kg]. Therefore the value given by the above formulae is multiplied by 1000 and divided by the molar weight of lead, equal to 207.2 kg/kmol.

- Density of saturated liquid, [kg/m^3] (2, section 2.10.1):

$$\rho_{liq}(T) = 1.1367\times10^{4} - 1.1944\cdot T$$

- Specific heat of saturated liquid, [J/kg-K] (2, section 2.13.1):

$$\begin{aligned} c_p(T) = {} & 175.1 - 4.961\times10^{-2}\cdot T + \\ & + 1.985\times10^{-5}\cdot T^2 - \\ & - 2.099\times10^{-9}\cdot T^3 - \\ & - 1.524\times10^{6}\cdot T^{-2} \end{aligned}$$

- Thermal conductivity, [W/m-K] (2, section 2.17.1):

$$k_{liq}(T) = 9.2 + 0.011\cdot T$$

- Viscosity of saturated liquid, [kg/m/s] (2, section 2.15.1):

$$\eta_{liq}(T) = 4.55\times10^{-4}\cdot\exp\left(\frac{1069}{T}\right)$$

- Surface tension, [N/m] (2, section 2.9.1):

$$\sigma(T) = 0.519 - 1.13\times10^{-4}\cdot T$$

- Speed of sound, [m/s] (2, section 2.12.1):

$$c(T) = 1951.75 - 0.3423\cdot T + 7.635\times10^{-5}\times T$$

References:

1. M.M. Stempniewicz, “SPECTRA Sophisticated Plant Evaluation Code for Thermal-Hydraulic Response Assessment, Version 3.60, August 2009, Volume 1 – Program Description, Volume 2 – User’s Guide, Volume 3 – Subroutine Description, Volume 4 - Verification and Validation”, NRG report K5024/10.101640, Arnhem, April 24, 2009.

2. “Handbook on Lead-bismuth Eutectic Alloy and Lead Properties, Materials Compatibility, Thermal-hydraulics and Technologies”, OECD/NEA Nuclear Science Committee. ISBN 978-92-64-99002-9, 2007.

A.7 SIMMER-III code used by CIRTEN

SIMMER-III is a two-dimensional, three-velocity field, multi-phase, multi-component, Eulerian, fluid-dynamics code coupled with a space dependent neutron kinetics model [1, 2, 3].

The entire code consists of three elements: the fluid-dynamics model, the structure (fuel pin) model, and the neutronics model. The fluid-dynamics portion, which interests this work, constitutes about two thirds of the code and interfaced with the structure model through heat and mass transfer at structure surfaces (see Fig. A.7-1).

A two-dimensional *R*-Z cylindrical coordinate system is utilized to define the SIMMER-III geometrical structure, although optionally an *X*-*Z* or one-dimensional system can also be used for various fluid-dynamic calculations.

The structure of the SIMMER-III code is shown in Fig. A.7-2. In each fluid-dynamics mesh cell, the structure-field volume fraction is composed of fuel pin and can wall component, which are stationary and provide walls containing fluid flow. The remaining volume is occupied by fluid having three velocity fields. When the cell vapour volume fraction falls below a certain non-zero value (for example 10^{-4}, with the default value in SIMMER-III being 10^{-2}) the mesh cell is regarded as single phase. This treatment is necessary for the numerical reason.

Finally, to increase the computational efficiency, an optimized hierarchy of a three-level time-step control is implemented in the code.

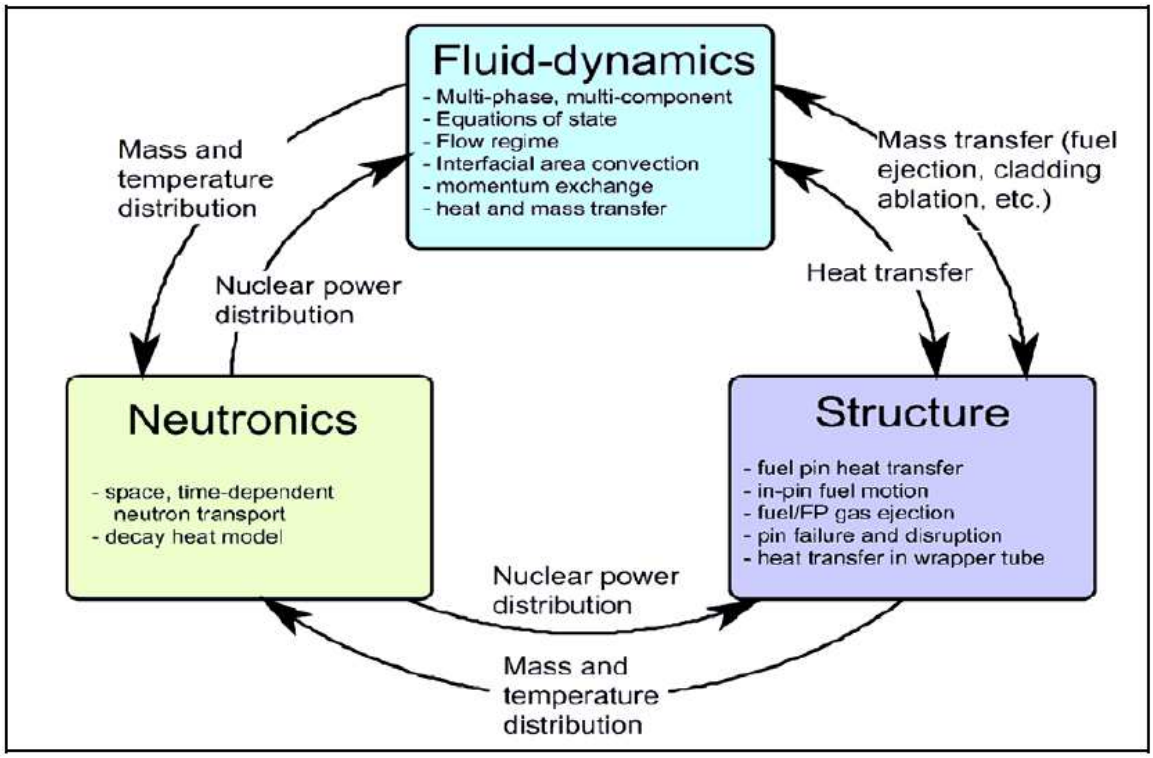


Fig. A.7-1: SIMMER-III code structure

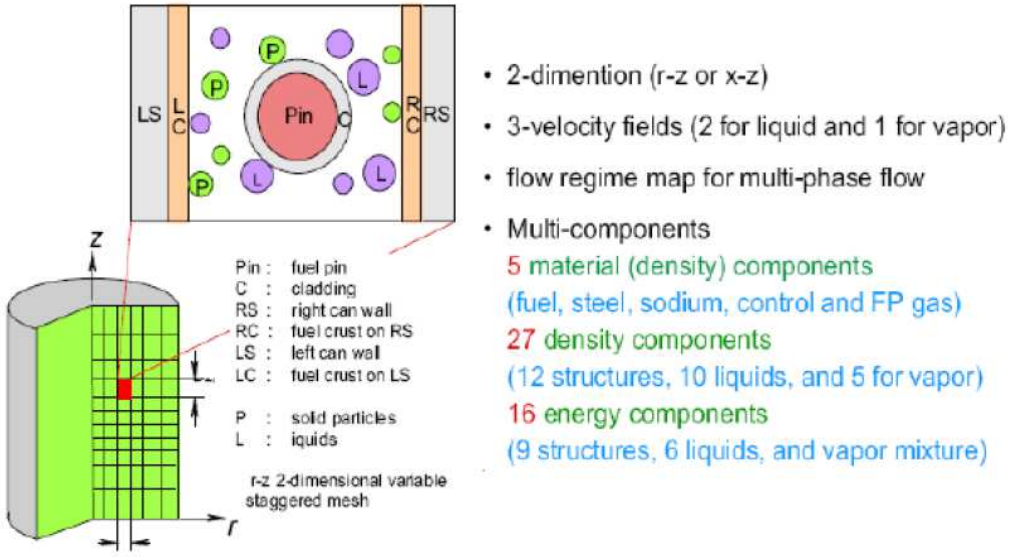


Fig. A.7-2: Geometrical, fluid-dynamics, multiphase and multicomponent models

Disparate simulations for the analysis of the interaction between liquid metal and water have been previously carried out on the base of experimental data attained on the LIFUS 5 facility. It aims to provide the validation of SIMMER-III code for thermo-hydraulic studies on liquid metals [4, 5]. In this work, the code has been used to accomplish the transient analysis of the SGTR accident.

Several simulations have been performed by the code and collected in two main series, which indicate a different approach to the problem and a different geometrical approximation level of the SG. In each series, simulations will be classified in several groups according to the size of the injector section, the total concentrated pressure drop values along the injector tube, the presence or not, of outer shell porosity of the SG, the presence of tubes near to the injector and of internal structures (grid) in the upper side of the component.

References:

1. AA.VV. “SIMMER-III Structure model: model and method description”, Research Document, O-arai Engineering Center, Japan Nuclear Cycle Development Institute, JNC TN 9400 2004-043.

2. Morita K., et al., “SIMMER-III applications to fuel-coolant interactions”, Nucl.Eng.Des. 189 (1999) 337-357.

3. Tobita Y., et al., “Evaluation in a CDA Energetics in the Prototype LMFBR with Latest Knowledge and Tools”, Proc.7th Int. Conf. Nuclear Engineering, (ICONE 7), Tokio, Japan, 12-23 April 1999.

4. N. Forgione, D. Pellini, F. Oriolo, W. Ambrosini, “Summary of previous applications and critical review on models and applications”, Milestone N° 4.2.11 for the THINS FP7-EU Project, 14th June 2012.

5. N. Montagnani, “Progettazione ed analisi di prove sperimentali di interazione tra metallo liquido ed acqua mediante il codice SIMMER”, Master’s thesis, Università di Pisa, December 2010.

A.8 SIMMER-III code used by JRC-IET

Computational analyses of partial SA flow blockage by JRC-IET were performed with the SIMMER-III (S_n Implicit Multi-field Multi-component Eulerian Recriticality) code, version 3.F [1].

The SIMMER-III code is a 2D multi-velocity field, multi-phase, multi-component, Eulerian fluid-dynamics code system capable of the integrated thermal-hydraulic, mechanics and structural modelling of fuel pins, wrappers and general structures with coupled space-time and energy-dependent neutron kinetics model. The core/pin structure model calculates the configuration and the time-dependent disintegration of fuel pins and sub-assembly wrappers. The neutronic part solves the time-dependent multi-group neutron transport equation with the improved quasi-static method. The flux shape calculations are based on TWODANT.

The current strength and uniqueness of SIMMER is its capability to analyse transient and expansion phases of severe accidents in fast reactors. In its present version, the code has also been successfully used as a system code to study design basis accidents and its capabilities are further being extended to encompass analysis of initiation phases of severe accidents as well.

In our present analyses, neutronic reactivity feedbacks (e.g., due to coolant voiding or Doppler) and the corresponding power change were not considered since the reactivity change corresponding to a single sub-assembly blockage is relatively small. Also, the applied “sub-channel” flow model is not conventional in SIMMER, but for our purposes it is deemed to be suitable for the modelling of sub-assembly blockages.

References:

1. Kondo, S. et al., “SIMMER-III: An Advanced Computer Program for LMFBR Severe Accident Analysis”, ANP’92, Tokyo, Japan, 1992.

APPENDIX B

KIT-G Contribution to LEADER Deliverable DEL022:

Summary of Transient Simulation Results for ALFRED with the SIM-LFR Code

E. Bubelis, M. Schikorr (KIT-G)

1.1.1 List of DEC transients simulated by KIT

The following DEC transients were simulated for ALFRED reactor using the SIM-LFR code:

DEC transients analyzed for Pb-cooled ALFRED Design (LEADER project)					
Case Number	Transient	Description	Burnup State		
Transients analyzed for Lb-cooled **ALFRED** Design			BOC	EOC	KIT
					SIM-LFR
DEC Transients					
TR-4	**Reactivity insertion (enveloping SGTR, flow blockage, core compaction)**	Reactivity insertion (voiding of part of active region enveloping voids introduction due SGTR, core compaction, flow blockage) = 250 pcm Reactor at hot full power (HFP)	X	X	**X**
TO-3	**Reduction of FW temperature + all pumps stop**	Loss of one preheater (feedwater temperature reduction from 335oC down to 300oC) All primary pumps are stopped Reactor is tripped	X	X	**X**
TO-6	**Increase of FW flowrate+ all pumps stop**	20 % increase in feedwater flowrate All primary pumps are stopped Reactor is tripped	X	X	**X**
T-DEC1	**Complete loss of forced flow + Reactor trip fails (total ULOF)**	All primary pumps are stopped Feedwater system available Reactor trip fails	X	X	**X**
T-DEC3	**Loss of SCS+ Reactor trip fails (ULOHS)**	All primary pumps are operating DHR system is operating Reactor trip fails	X	X	**X**
T-DEC4	**Loss of off-site power (LOOP) + Reactor trip fails (ULOHS + ULOF)**	All primary pumps are stopped SCS is lost DHR system is operating Reactor trip fails	X	X	**X**
T-DEC5	**Partial blockage in the hottest fuel assembly**	Reactor trip fails The maximum acceptable flow reduction factor has to be determined	X	X	**X**
T-DEC6	**SCS failure**	All primary pumps are operating DHR system totally fails Reactor is tripped	X	X	**X**

In the above table, the “EOC” core state is represented by a fuel pin average burnup equivalent to 1095 EFPD, whereas the “BOC” core state is represented by a fuel pin average burnup equivalent to 730 EFPD as specified in LEADER project deliverable DEL007-2012, pg.11-12 and Table 10.

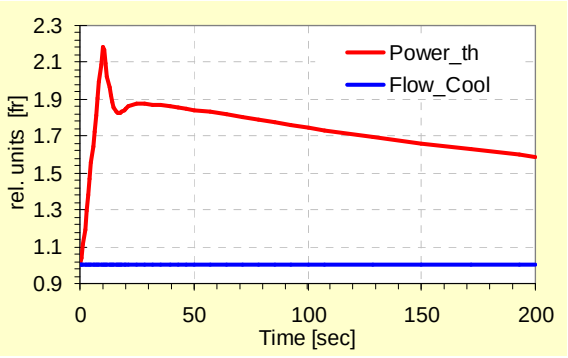
1.1.1.1 TR-4: Unprotected Overpower Transient at HFP (UTOP): SIM-LFR (KIT)

ALFRED overpower transient at HFP (Hot Full Power) and BOC, as well as EOC core conditions is reported in this section, namely:

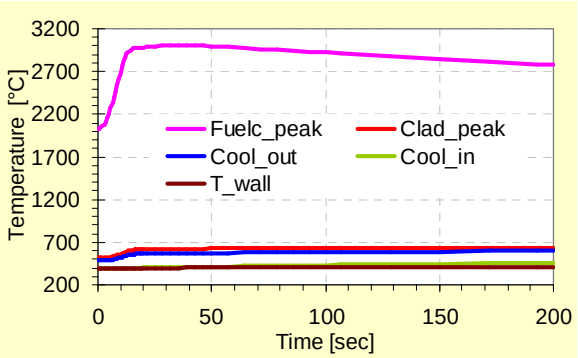
- 250 pcm reactivity insertion within 10 sec time interval at HFP conditions. This amount of reactivity might be inserted into the core due to: voiding of part of active core region enveloping voids introduction in case of SGTR, core compaction, fuel SA blockage, etc.

As can be observed in **Fig. 1.1.1.1-1-c**, an insertion of 250 pcm in 10 sec time interval at BOC conditions, leads to a power jump of ~ 2.17 nominal (see **Fig. 1.1.1.1-1-a)**. The maximum fuel and clad temperatures under BOC conditions increase from 2028°C and 516°C to 3011 °C and 641 °C respectively (see **Fig. 1.1.1.1-1-b)** resulting in short-term local fuel melting (fuel center) of the peak fuel pins.

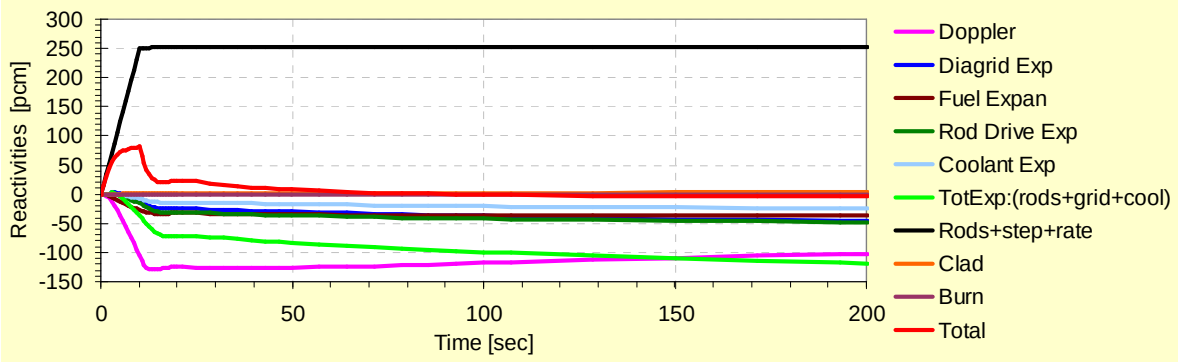
The corresponding clad failure time remains above 1E+8 sec (see **Fig. 1.1.1.1-1-d)** as peak clad temperatures remain relatively low (< 700°C)**.**



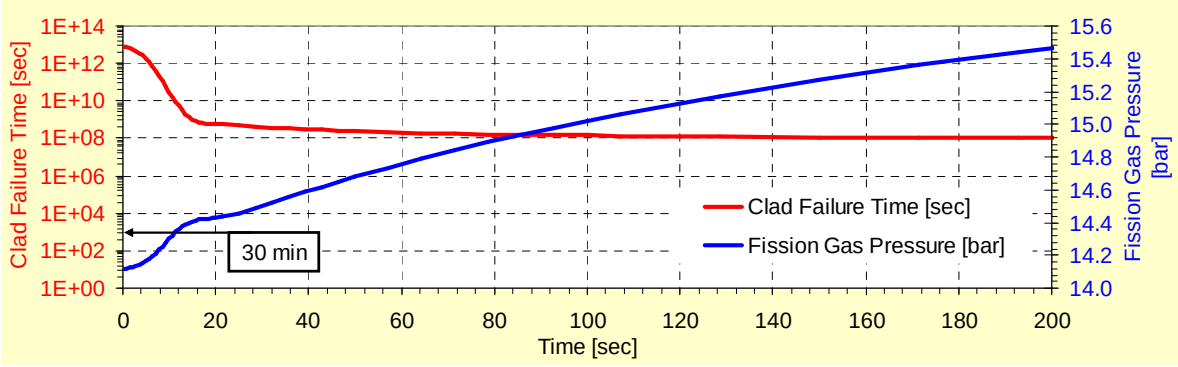
a) Relative Core Thermal Power and Flow rate



b) Peak Fuel-, Clad-, Coolant- and Vessel Wall Temperatures



c) Reactivity effects

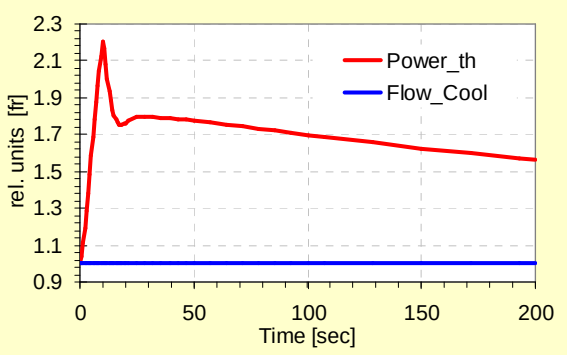


d) Peak Pin Fission Gas Pin Pressure and Clad Failure Time

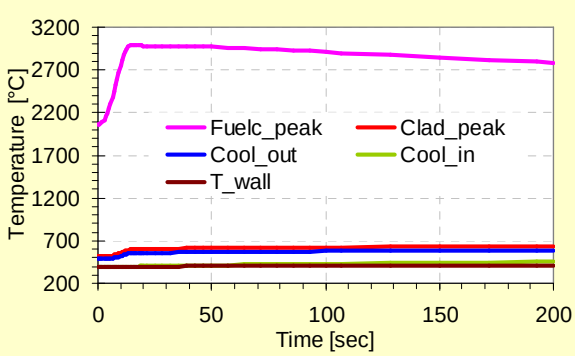
Fig. 1.1.1.1-1 Results for TR-4: (UTOP: 250 pcm in 10 sec) transient at HFP - **BOC** conditions at an average burnup of 730 EFPD as calculated by SIM-LFR (KIT)

As can be observed in **Fig. 1.1.1.1-2-c**, an insertion of 250 pcm in 10 sec time interval at EOC conditions, leads to a power jump of ~ 2.2 nominal (see **Fig. 1.1.1.1-2-a)**. The maximum fuel and clad temperatures under EOC conditions increase from 2064°C and 514°C to 2996 °C and 631 °C respectively (see **Fig. 1.1.1.1-2-b)** resulting in short-term local fuel melting (fuel center) of the peak fuel pins..

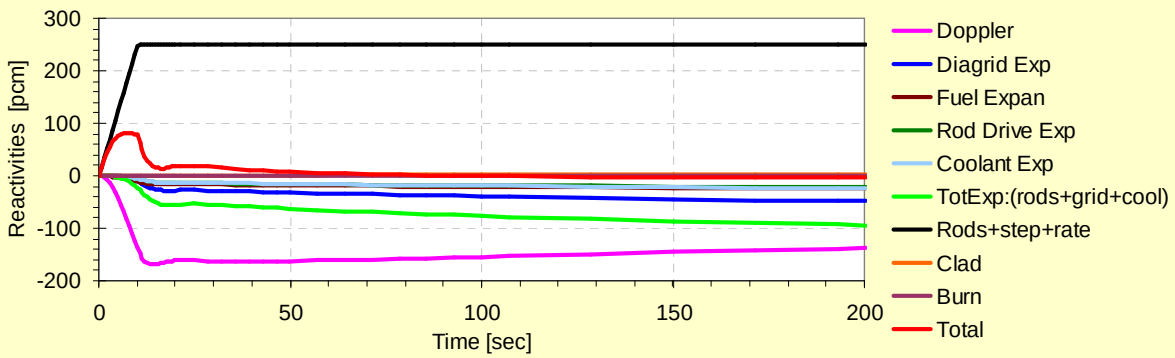
The corresponding clad failure time remains above 1E+8 sec (see **Fig. 1.1.1.1-2-d)** as peak clad temperatures remain relatively low (< 700°C)**.**



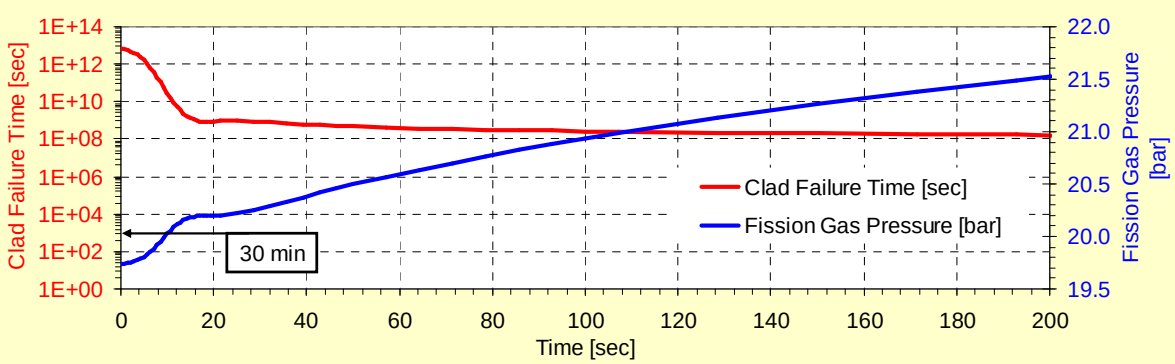
a) Relative Core Thermal Power and Flow rate



b) Peak Fuel-, Clad-, and Coolant- and Vessel Wall Temperatures



c) Reactivity effects



d) Peak Pin Fission Gas Pin Pressure and Clad Failure Time

Fig. 1.1.1.1-2 Results for TR-4: (UTOP: 250 pcm in 10 sec) transient at HFP - **EOC** conditions at an average burnup of 1095 EFPD as calculated by SIM-LFR (KIT)

As related to the above study, one can observe that:

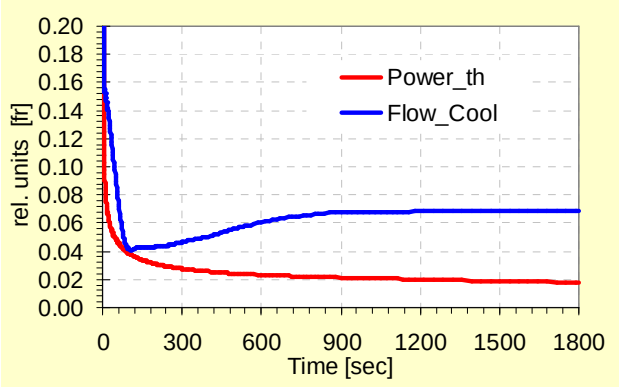
- For reactivity insertion of 250 pcm in 10 sec time interval (due to: voiding of part of active core region enveloping voids introduction in case of SGTR, core compaction, fuel SA blockage, etc.) at BOC, as well as EOC conditions, ALFRED reactor peak fuel pin cladding survives this transient, but local fuel melting is observed in the center of the peak fuel pins (pellets).

1.1.1.2 TO-3: Protected Loss-Of-Flow Transient (PLOF) With FW Temperature Reduction at HFP: SIM-LFR (KIT)

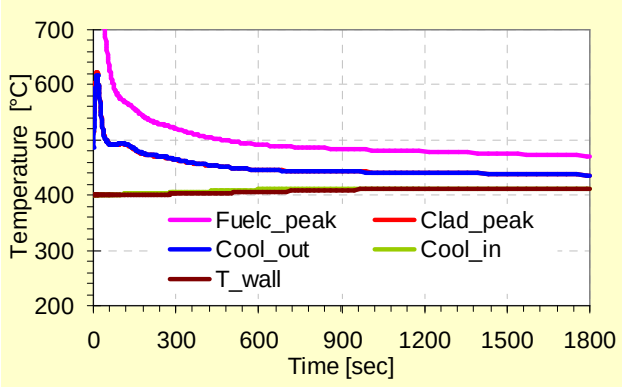
For this simulation it was assumed that: 1) at t = 0 sec, all primary pumps stop and feedwater temperature drops down (in ~ 1 sec) to 300 ^{o}C; 2) at t = 1 sec, two reactor scram signals are generated based on primary pumps under-speed (< 90 %) and feedwater temperature decreasing below 327 ^{o}C; 3) based on one of the two reactor scram signals (one of the signals is being neglected) the reactor is being shutdown at t = 2 sec into the transient; 4) main steam lines and main feedwater lines are being closed in ~2 sec time period, while condensate isolation valves of four ICs of the DHR-1 system fully opens in ~ 20 sec, thus then removing maximal 7 MW of heat from the primary cooling circuit; 5) water temperature leaving the ICs and directed to the MHXs is also 300 ^{o}C (same as that of feedwater).

Two cases were analyzed to investigate the clad and fuel temperature response of the peak pin and the likelihood of Pb-coolant freezing at the outlet of the MHX (primary side) during this PLOF with FW temperature decreasing down to 300 ^{o}C, namely at BOC and EOC core state conditions.

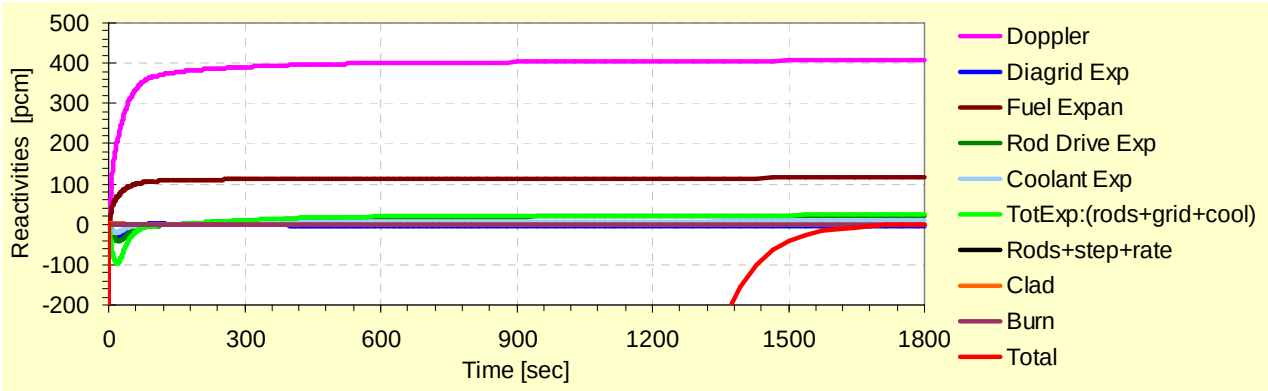
Under BOC conditions, following reactor scram, reactor power rapidly decreases approaching the decay heat level (see **Fig. 1.1.1.2-1-a**). Due to the primary pumps stopping, the Pb-coolant mass flowrate through the core (see **Fig. 1.1.1.2-1-a**) decreases to ~ 4 % of nominal flow, later recovering to ~7 % at ~ 15 min into the transient. Related to the water temperature decrease on the secondary side of the MHX to 300 ^{o}C, Pb-coolant temperature at the outlet of the MHX decreases to ~360 ^{o}C in ~ 4 sec (see **Fig. 1.1.1.2-1-d**), but later, after the FW lines valves closure, increases to ~490 ^{o}C at its maximum, later decreasing again to ~405 ^{o}C in 0.5 hour transient time **Fig. 1.1.1.2-1-d**). As the feedwater temperature decreases by 35 ^{o}C, power transferred to the secondary cooling circuit through the MHX also shortly increases, but later due to the reactor scram starts decreasing (see **Fig. 1.1.1.2-1-e**). In the first ~15 sec of the transient, clad and coolant (at core outlet) temperatures, due to core flowrate decrease (when primary pumps stop), increase up to ~ 620 ^{o}C. Fuel temperatures during this time period, due to the reactor scram, decreases to ~ 910 ^{o}C (see **Fig. 1.1.1.2-1-b**). Pb temperature at the inlet of the core and vessel temperature changes only by ~ 10 ^{o}C during the simulated time period of 0.5 hour. From the calculation results one can observe, that in case feedwater temperature decreases suddenly down to 300 ^{o}C (note: $T_{melting}^{Pb}$~327 °C) at the inlet of the secondary side of the MHX, in the time period of 0.5 hour the lead temperature at the outlet of the MHX on its primary side reaches ~405 ^{o}C, which is still far from the lead freezing temperature. Based on the lead temperature gradients around the MHX, one can estimate, that lead at the outlet from the MHX will start freezing only ~3.9 hours into the transient, when the lead temperature will reach ~327 ^{o}C at that location of the primary cooling circuit. So this transient presents a potential safety issue as related to possible Pb-freezing for the ALFRED reactor only ~3.9 hours into the transient. During this time period the operator has more than sufficient time for manual intervention by deactivating sub-systems of DHR-1 system in order to prevent lead freezing at the outlet of the MHX. Reactivities behavior during this transient is shown in **Fig. 1.1.1.2-1-c**).



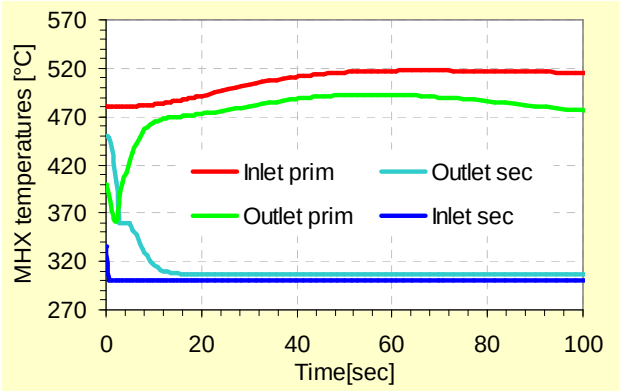
a) Relative Core Thermal Power and Pb Flowrate

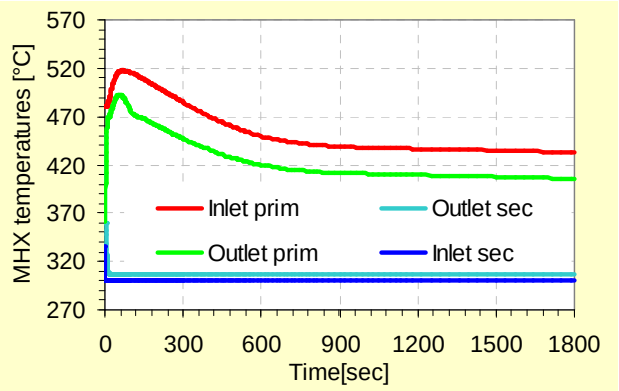


b) Peak Fuel-, Clad-, Coolant- and Vessel Wall Temperatures

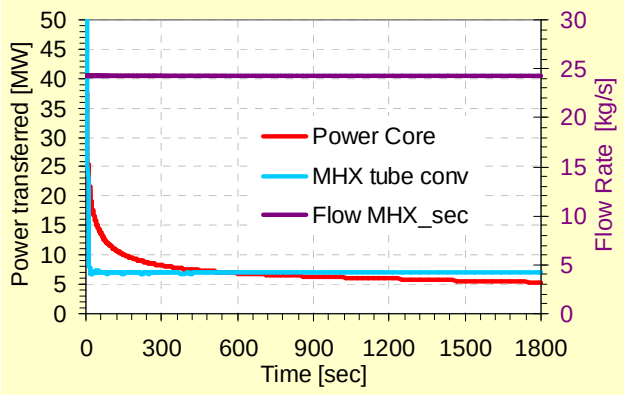


c) Reactivity feedbacks





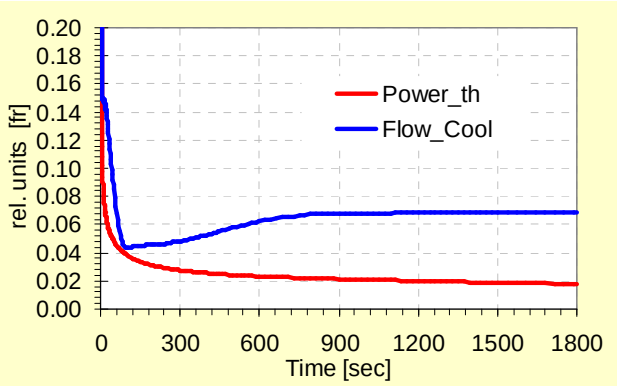
d) MHX temperatures



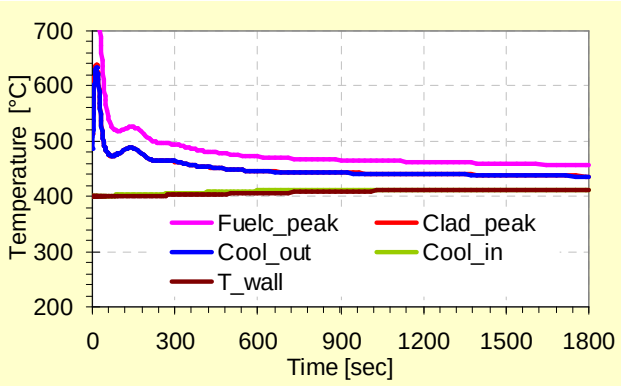
e) Core and MHX Powers, plus MHX sec. side water flow rate

Fig. 1.1.1.2-1 Results for TO-3 (overcooling following reactor trip) transient: HFP **BOC** conditions at an average burnup of 730 EFPD as calculated by SIM-LFR (KIT)

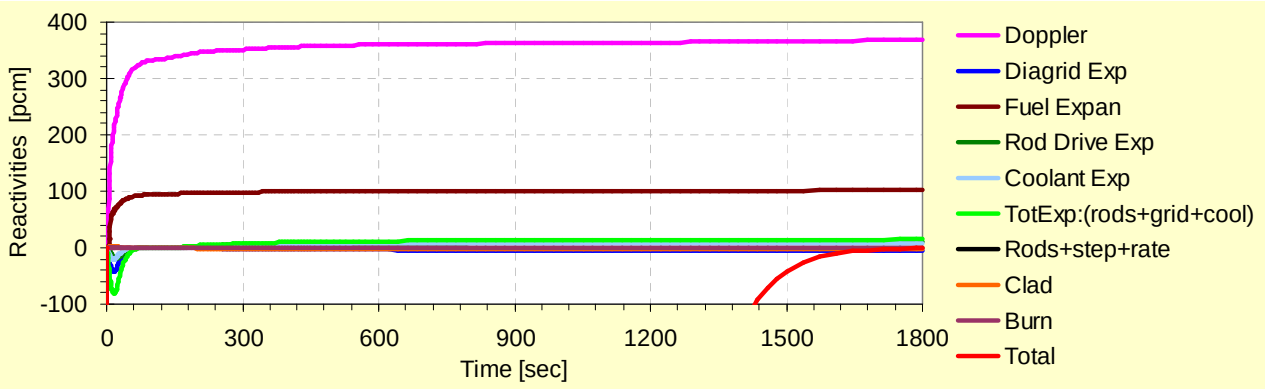
Under EOC conditions, following the reactor scram, reactor power quickly decreases approaching the decay heat level (see **Fig. 1.1.1.2-2-a**). Due to the primary pumps stopping, Pb-coolant mass flowrate through the core (see **Fig. 1.1.1.2-2-a**) decreases to ~ 4 % of nominal flow, later recovering to ~7 % at ~ 15 min into the transient. Related to the water temperature decrease on the secondary side of the MHX down to 300 ^{o}C, lead temperature at the outlet of the MHX drops down to ~360 ^{o}C in ~ 4 sec (see **Fig. 1.1.1.2-2-d**), but later, after the FW lines valves closure, increases to ~490 ^{o}C at its maximum, later decreasing again to ~405 ^{o}C in 0.5 hour transient time (**Fig. 1.1.1.2-2-d**). As the feedwater temperature decreases by 35 ^{o}C, power transferred to the secondary cooling circuit through the MHX also shortly increases, but later due to the reactor scram starts decreasing (see **Fig. 1.1.1.2-2-e**). In the first ~15 sec of the transient, clad and coolant (at core outlet) temperatures, due to core flowrate decrease (when primary pumps stop), increase up to ~ 630 ^{o}C. Fuel temperatures during this time period, due to the reactor scram, decreases down to ~ 870 ^{o}C (see **Fig. 1.1.1.2-2-b**). Pb temperature at the inlet of the core and vessel temperature changes only by ~ 10 ^{o}C during the simulated time period of 0.5 hour. From the calculation results one can observe, that in case feedwater temperature decreases suddenly down to 300 ^{o}C (note: $T_{melting}^{Pb}$~327$\,^{\circ}C$) at the inlet of the secondary side of the MHX, in the time period of 0.5 hour the lead temperature at the outlet of the MHX on its primary side reaches ~405 ^{o}C, which is still far from the lead freezing temperature. Based on the lead temperature gradients around the MHX, one can estimate, that lead at the outlet from the MHX will start freezing only ~3.8 hours into the transient, when the lead temperature will reach ~327 ^{o}C at that location of the primary cooling circuit. So this transient presents a potential safety issue as related to possible Pb-freezing for the ALFRED reactor only ~3.8 hours into the transient. During this time period operator has more than sufficient time for manual intervention by deactivating sub-systems of DHR-1 system in order to prevent lead freezing at the outlet of the MHX. Reactivities behavior during this transient is shown in **Fig. 1.1.1.2-2-c**).



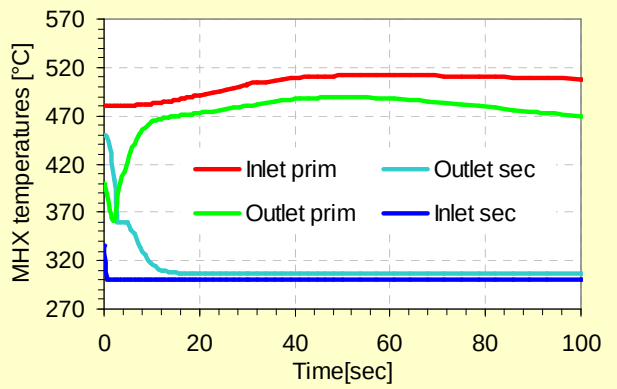
a) Relative Core Thermal Power and Pb Flowrate

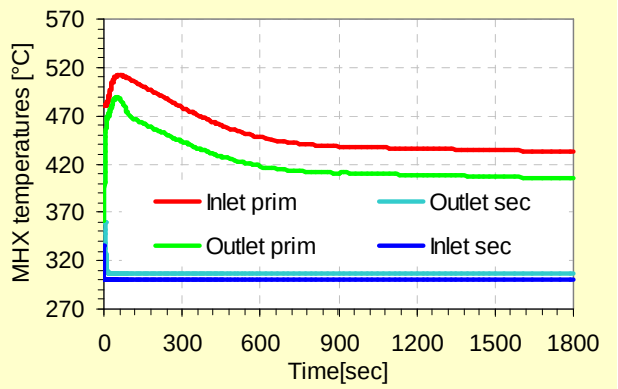


b) Peak Fuel-, Clad-, Coolant- and Vessel Wall Temperatures

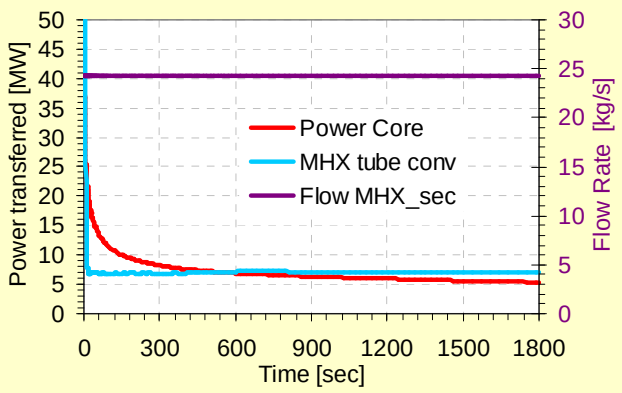


c) Reactivity feedbacks





d) MHX temperatures



e) Core and MHX Powers, plus MHX sec. side water flow rate

Fig. 1.1.1.2-2 Results for TO-3 (overcooling following reactor trip) transient: HFP **EOC** conditions at an average burnup of 1095 EFPD as calculated by SIM-LFR (KIT)

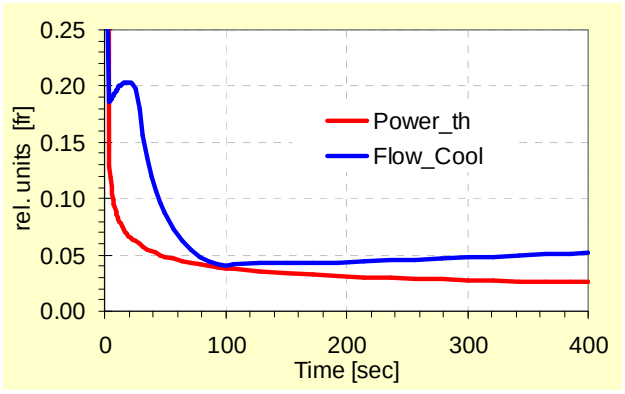
Normally Pb-overcooling anywhere in the primary cooling loop below 335°C should be prevented under all plant transient conditions in order to prevent freezing of the Pb coolant thereby endangering an assured flow pattern throughout the primary system, in particular the core region. The feedwater temperature on the secondary side of the MHX must never be allowed to go below 335°C in order to assure that the primary system is always maintained at temperatures above 335°C. This requires an assured preheater system of the secondary side of the MHX.

1.1.1.3 TO-6: Protected Loss-Of-Flow Transient (PLOF) With FW Flowrate Increase at HFP: SIM-LFR (KIT)

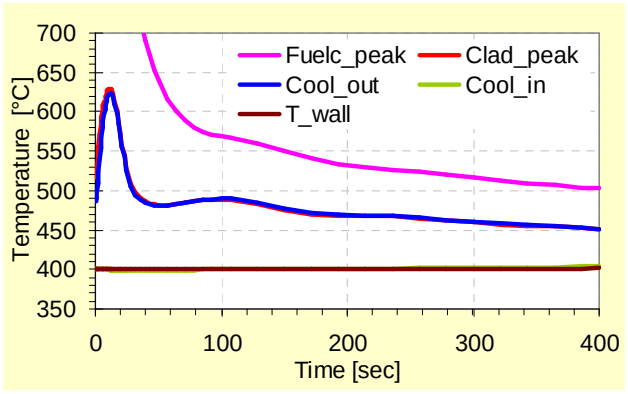
For this simulation it was assumed that: 1) at t = 0 sec, all primary pumps stop and feedwater flowrate increases by 20 %; 2) at t = 1 sec, reactor scram signal is generated based on primary pumps under-speed (< 90 %), but is being neglected; 3) at t = 3 sec, two reactor scram signals are generated based on average core temperature difference, as well as on peak SA temperature difference being > 1.2 times their nominal values; 4) based on these reactor scram signals, reactor is being shutdown at t = 4 sec into the transient; 5) main steam lines and main feedwater lines are being closed in ~2 sec time period, while condensate isolation valves of four ICs of the DHR-1 system fully opens in ~ 20 sec, thus then removing maximal 7 MW of heat from the primary cooling circuit.

Two cases were analyzed to investigate the clad and fuel temperature response of the peak pin and the likelihood of Pb-coolant freezing at the outlet of the MHX (primary side) during this PLOF with FW flowrate increase by 20 %, namely at BOC and EOC core state conditions.

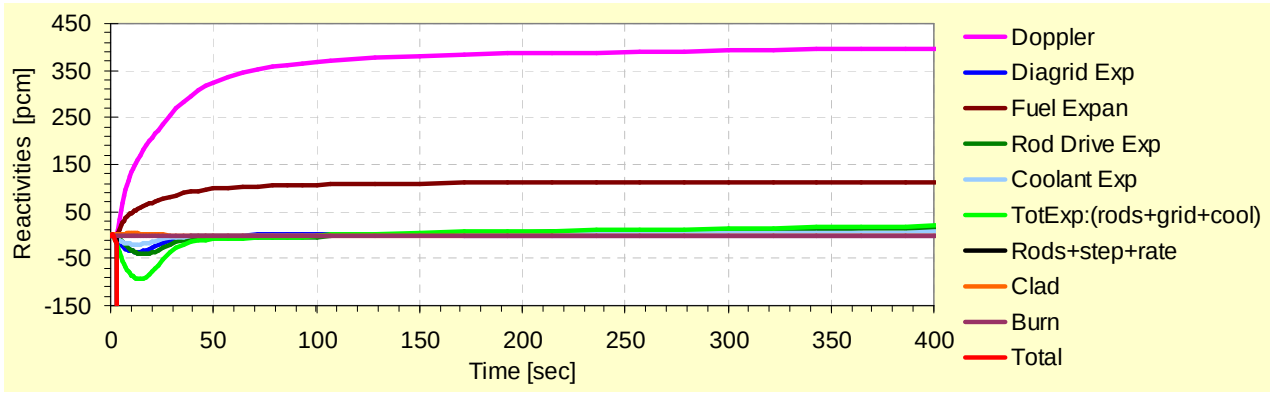
Under BOC conditions, following the reactor scram, reactor power quickly decreases to the decay heat level (see **Fig. 1.1.1.3-1-a**). Due to the primary pumps stopping, lead-coolant mass flowrate through the core (see **Fig. 1.1.1.3-1-a**) first decreases to ~ 19 % of nominal flow, then recovers up to ~ 20 %, but later due to the switch-over to DHR-1 sub-system the core flowrate decreases again to ~ 5 % of nominal flow. Related to the feedwater flowrate increase on the secondary side of the MHX by 20 %, lead temperature at the outlet of the MHX decreases to 335 ^{o}C (only 8 ^{o}C to the Pb-freezing point of 327°C), but later due to the switch-over to DHR-1 sub-system (lead flowrate decreases down to ~5 % of the nominal flow on the primary side of the MHX and heat transfer to the secondary side of the MHX suddenly decreases down to ~7 MW) it increases sharply up to ~ 500 ^{o}C, being close to the lead inlet temperature at the inlet of the MHX (see **Fig. 1.1.1.3-1-d**). As the feedwater flowrate increases by 20 %, power transferred to the secondary cooling circuit through the MHX also increases (see **Fig. 1.1.1.3-1-e**) sharply, but later due to the switch-over to DHR-1 sub-system it decreases down to ~ 7 MW. Clad and coolant (at core outlet) temperatures, first (due to core flowrate decrease, when primary pumps stop) increase up to ~ 620 ^{o}C, but later, due to the reactor scram and reactor power decrease to the decay heat level, decreases to ~ 450 ^{o}C. Fuel temperatures during this transient decreases down to ~ 500 ^{o}C at t = 400 sec transient time (see **Fig. 1.1.1.3-1-b**) due to reactor scram. A large Pb mass (~ 3570 tons) in the primary loop and lower plenum provides a large heat inertia. Due to this, Pb temperature at the inlet of the core and vessel temperature hardly changes during the simulated time period of 400 sec. As long as the feedwater temperature remains at 335 ^{o}C (note: $T_{melting}^{Pb} \sim 327\,^{\circ}C$), there is a marginal danger of lead freezing anywhere in the primary cooling circuit. So this transient presents some marginal safety issue as related to Pb-freezing for the ALFRED reactor. Reactivities behavior during this transient is shown in **Fig. 1.1.1.3-1-c**).



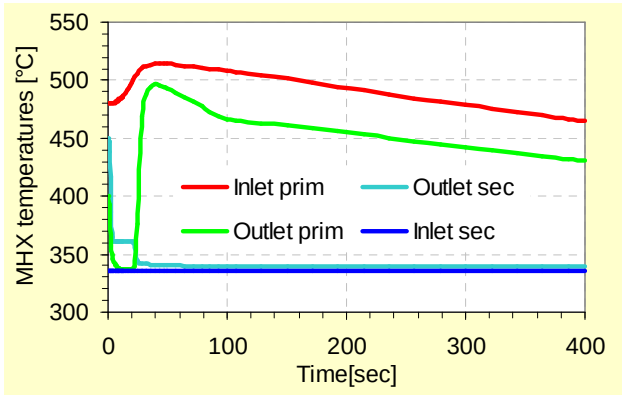
a) Relative Core Thermal Power and Pb Flowrate



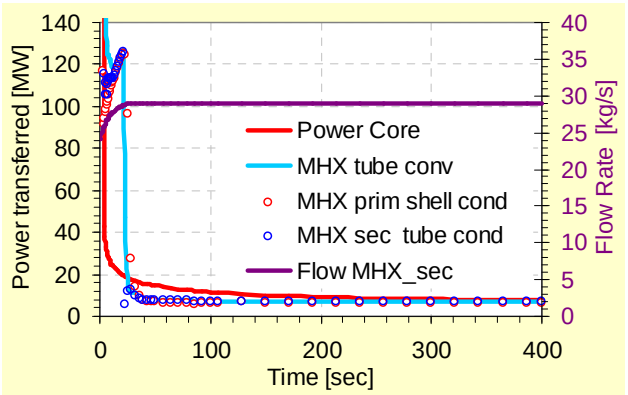
b) Peak Fuel-, Clad-, Coolant- and Vessel Wall Temperatures



c) Reactivity feedbacks



d) MHX temperatures

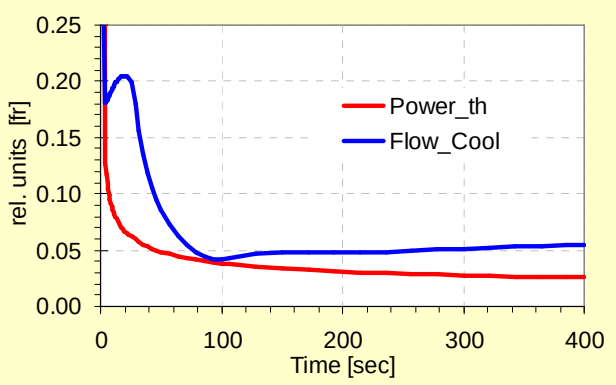


e) Core and MHX Powers, plus MHX sec. side water flow rate

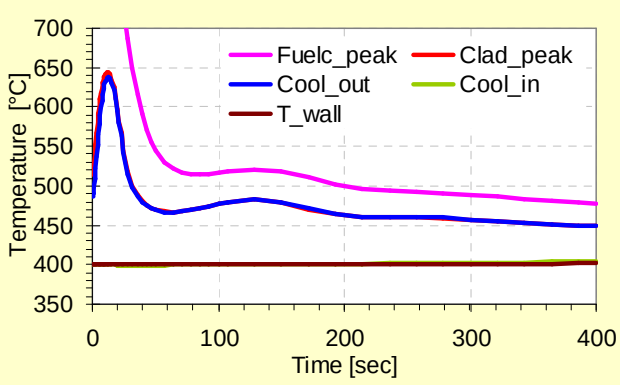
Fig. 1.1.1.3-1 Results for TO-6 (overcooling following reactor trip) transient: HFP **BOC** conditions at an average burnup of 730 EFPD as calculated by SIM-LFR (KIT)

Under EOC conditions, following the reactor scram, reactor power quickly decreases to the decay heat level (see **Fig. 1.1.1.3-2-a**). Due to the primary pumps stopping, lead-coolant flowrate through the core (see **Fig. 1.1.1.3-2-a**) first decreases to ~ 18 % of nominal flow, then recovers up to ~ 20 %, but later due to the switch-over to DHR-1 sub-system the core flowrate decreases to ~ 5-6 % of the nominal flow. Related to the feedwater flowrate increase on the

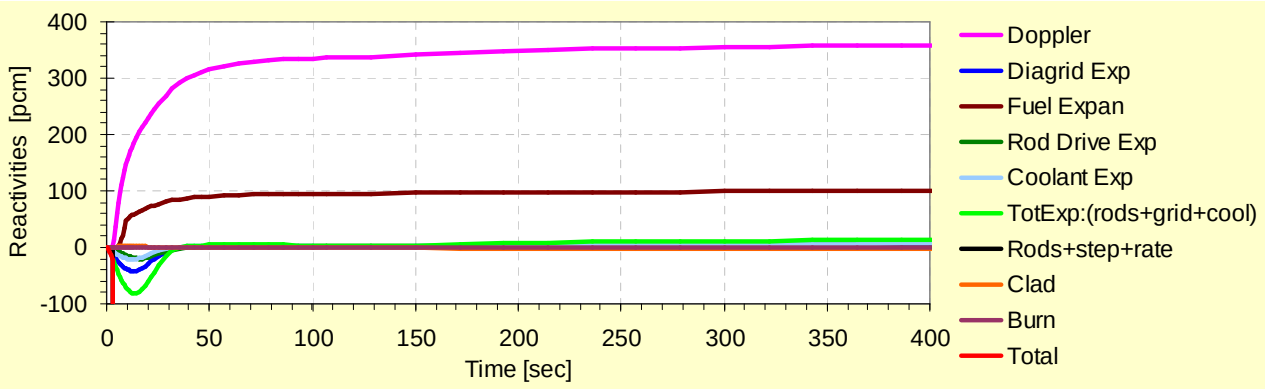
secondary side of the MHX by 20 %, lead temperature at the outlet of the MHX drops down to 335 °C, but later due to the switch-over to DHR-1 sub-system (lead flowrate decrease to ~ 5-6 % of the nominal flow) it increases sharply up to ~ 495 °C, being close to the lead inlet temperature at the inlet of the MHX (see **Fig. 1.1.1.3-2-d**). As the feedwater flowrate increases by 20 %, power transferred to the secondary cooling circuit through the MHX also increases (see **Fig. 1.1.1.3-2-e**) rapidly, but later due to the switch-over to DHR-1 sub-system it decreases down to ~ 7 MW. Clad and coolant (at core outlet) temperatures, first (due to core flowrate decrease, when primary pumps stop) increase up to ~ 640 °C, but later, due to the reactor scram and reactor power decrease to the decay heat level, decreases to ~ 450 °C. Fuel temperatures during this transient, due to the reactor scram, decrease to ~ 480 °C at t = 400 sec transient time (see **Fig. 1.1.1.3-2-b**). A large Pb mass (~ 3570 tons) in the primary loop and lower plenum provides a large heat inertia. Due to this, Pb temperature at the inlet of the core and vessel temperature hardly changes during the simulated time period of 400 sec. As long as the feedwater temperature remains at 335 °C (note: $T_{melting}^{Pb} \sim 327\,°C$), there is a marginal danger of lead freezing anywhere in the primary cooling circuit. So this transient presents some marginal safety issue as related to Pb-freezing for the ALFRED reactor. Reactivities behavior during this transient is shown in **Fig. 1.1.1.3-2-c**).



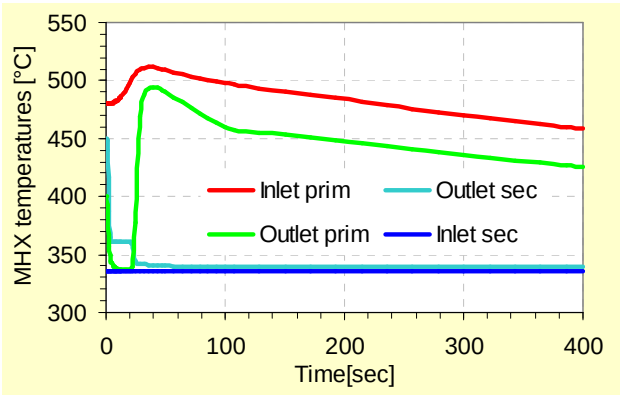
a) Relative Core Thermal Power and Pb Flowrate



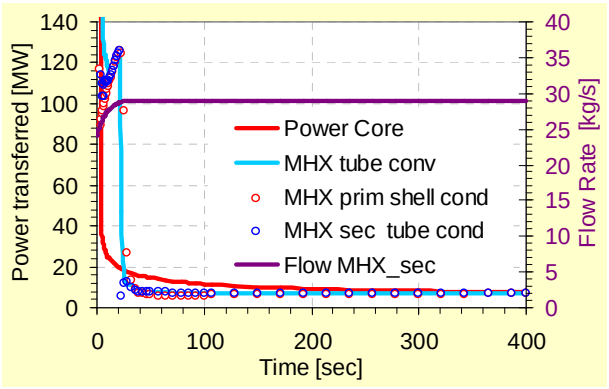
b) Peak Fuel-, Clad-, Coolant- and Vessel Wall Temperatures



c) Reactivity feedbacks



d) MHX temperatures



e) Core and MHX Powers, plus MHX sec. side water flow rate

Fig. 1.1.1.3-2 Results for TO-6 (overcooling following reactor trip) transient: HFP **EOC** conditions at an average burnup of 1095 EFPD as calculated by SIM-LFR (KIT)

In the longer term for BOC as well as EOC conditions, lead temperature at the outlet from the MHX will continue to decrease further, slowly approaching lead freezing temperature (note: $T_{melting}^{Pb} \sim 327\,°C$), as the heat removed by DHR-1 system becomes larger than the decay heat generated in the reactor core. Usually this process occurs during a time stretching over several hours [DEL010-2012], providing the operator sufficient time to deactivate sub-systems of the DHR-1 system, in order to prevent Pb-coolant freezing at the outlet of the MHX.

As a conclusion, this transient has the potential to lead to a safety issue as related to possible Pb-freezing for the ALFRED reactor. Reactor safety is ensured by the reactor protection system, shutting down the reactor, as well as by the tightly controlled heat removal by the DHRS (also by an operator in the medium and long term), removing only controlled amounts of decay heat from the reactor primary cooling circuit to assure prevention of freezing of the Pb-coolant at any location of the primary cooling circuit.

1.1.1.4 T-DEC1: Unprotected Loss of Flow (ULOF): SIM-LFR (KIT)

For these calculations all primary pumps are assumed to fail simultaneously and the secondary heat transport system is assumed fully functional (forced convection mode). The reactor shut-down systems are also assumed to fail. The coast-down characteristics of the primary pumps (or primary system mass flow rate) subsequent to pump failure was presumed to correspond to the flow rate characteristics as calculated by SIM-LFR implying a flow undershoot down to ~19% nominal flow ~ 6 sec after the transient initiation, and a recovery to the natural convection asymptotic flow fraction of ~ 24 % ~ 60 sec after the flow undershoot minimum.

Two cases were analyzed to investigate the clad and fuel temperature response of the peak pin and the likelihood of peak pin clad rupture during the flow undershoot, namely at BOC and EOC core state conditions.

Under BOC conditions, the fuel temperature of the peak pin are the highest at the beginning of the transient (~2030 ^{o}C), but later, due to reactor power decrease caused by the negative reactivity feedback effects, the fuel temperature decreases. Clad temperature of the peak pin, due to the coolant flow undershoot increases from 516 ^{o}C up to 738 ^{o}C (**Fig. 1.1.1.4-1-b**) at transient time t = 17.8 sec during the ULOF transient. At the same time point minimum clad failure time of the peak pin decreases to 4.7E+5 sec (**Fig. 1.1.1.4-1-d**), but later, when the coolant flowrate increases to ~ 24 % of nominal, increases to ~ 3.7E+8 sec. During this transient, due to reactor power suppression by the negative reactivity feedback effects (**Fig. 1.1.1.4-1-c**), the reactor power level decreases down to ~56% for BOC conditions (see **Fig. 1.1.1.4-1-a**).

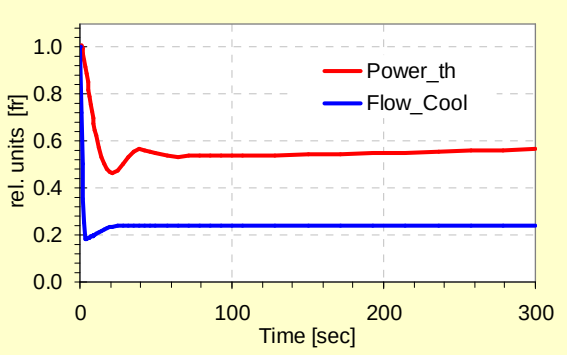
Under EOC conditions, the fuel temperature of the peak pin are the highest at the beginning of the transient (~2064 ^{o}C), but later, due to reactor power decrease caused by the negative reactivity feedback effects, fuel temperature decreases. Clad temperature of the peak pin, due to the coolant flow undershoot increases from 514 ^{o}C up to 751 ^{o}C (**Fig. 1.1.1.4-2-b**) at transient time t = 17.8 sec during the ULOF transient. At the same time point minimum clad failure time of the peak pin decreases to 1.6E+5 sec (**Fig. 1.1.1.4-2-d**), but later, when the coolant flowrate increases to ~ 24 % of the nominal, increases to ~ 7.8E+7 sec. During this transient, due to reactor power suppression by the negative reactivity feedback effects (**Fig. 1.1.1.4-2-c**), the reactor power level decreases down to ~60% for EOC core conditions (see **Fig. 1.1.1.4-2-a**).

The coast-down characteristics of the primary system mass flow rate are governed by the coast-down, inertial characteristics of the pump, and are thus independent of the burn-up state of the core. The asymptotic natural convection flow rate is ~ 24 %, as is determined by the heights differential between the mid-planes of core and the heat exchanger, as well as the pressure drop characteristics of the entire primary cooling system. As both of these parameters do not change during the burn-up of the plant, core temperatures during the ULOF transient are thus primarily determined by the flow undershoot that must be expected during flow coast-down before the asymptotic natural convection flow rate is attained. It must be stated, that the SIM-LFR calculated flow undershoot is an estimation based on RELAP5 calculations of the same transient performed by ENEA. The actual flow characteristic of the ALFRED primary cooling system during pump-coast down can only be determined to a higher degree of confidence in

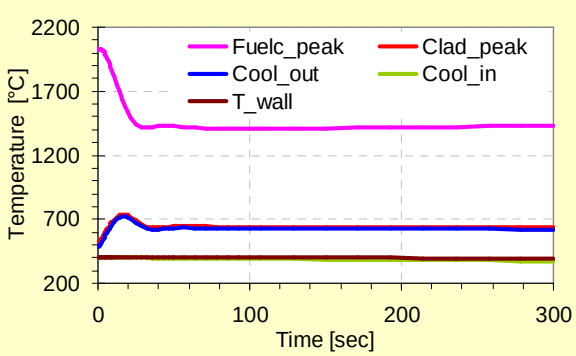
case of experimental measurements of the actual primary system layout. CFD-type calculations should be able to narrow down the current uncertainty in the estimation of the flow undershoot for the ALFRED.

Of particular importance are the calculated fuel and cladding temperatures during the ULOF transient since the ALFRED primary system was specifically designed with the intention of being able to accommodate the ULOF transient without significant pin failures. Thus, it is important to estimate the minimum clad failure time for the peak pin during the ULOF transient. That's why this important investigation was performed during the ALFRED safety analysis. The analysis showed, that at transient time t ~ 17.8 sec minimum clad failure time of the peak pin decreases to ~1.6E+5 sec at the minimum, thus clad failure (rupture) should not be expected during ULOF transient.

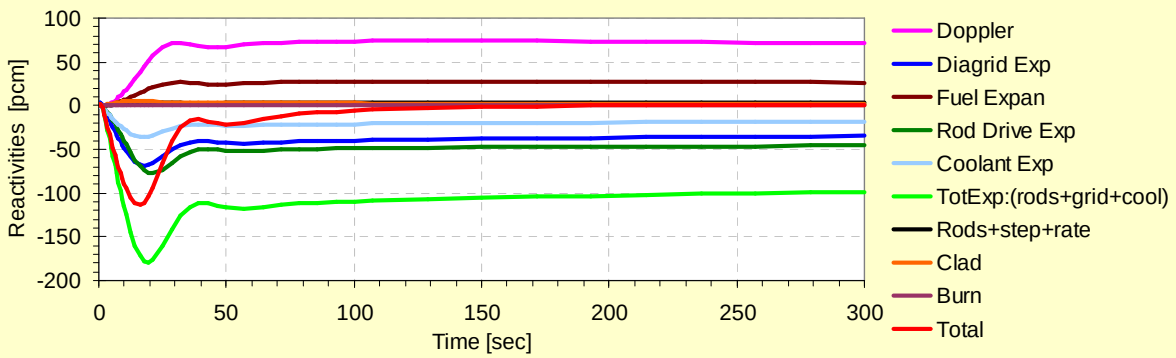
This clearly demonstrates, that the clad of the peak pins of the ALFRED has a very large margin to clad failure (rupture), that is primarily due to the relatively high Pb natural convection core mass flow rate of ~ 24 % nominal and the relatively low fission gas pin pressure at EOC of ~ 20 bar during ULOF conditions.



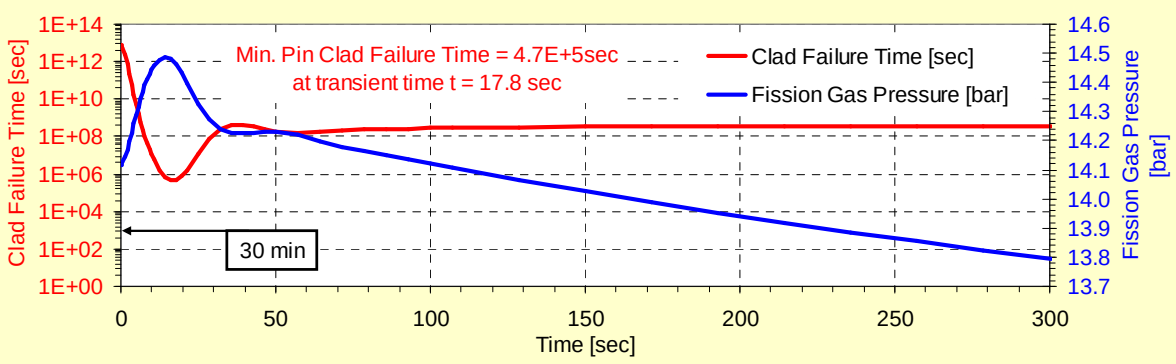
a) Relative Core Thermal Power and Flow rate



b) Peak Fuel-, Clad-, Coolant- and Vessel Wall Temperatures

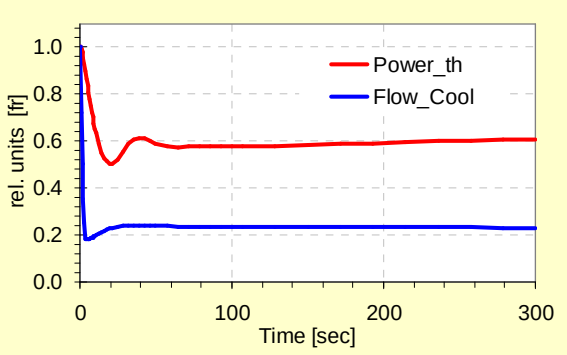


c) Reactivity effects

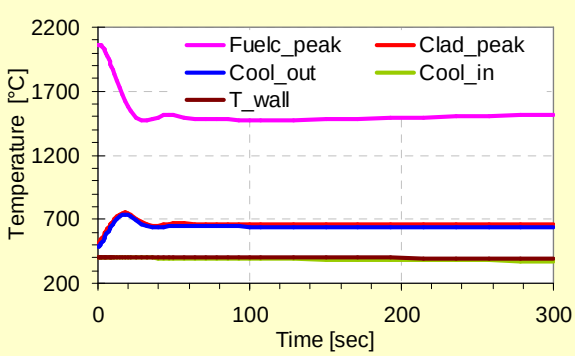


d) Peak Pin Fission Gas Pin Pressure and Clad Failure Time

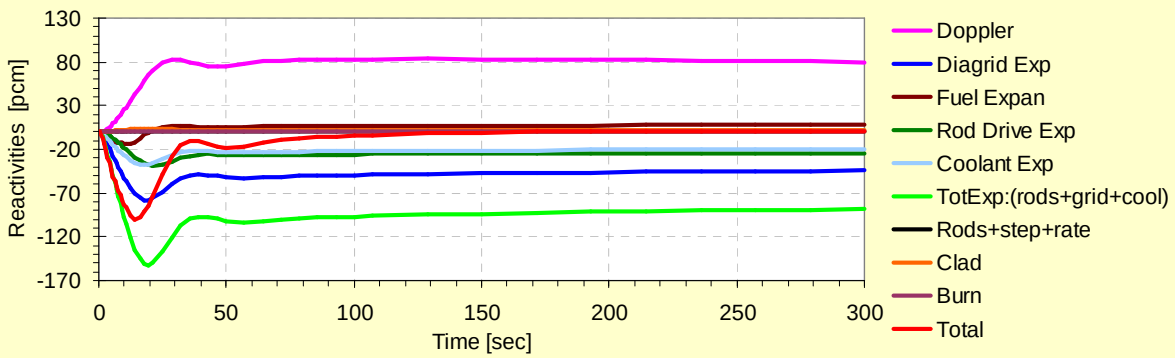
Fig. 1.1.1.4-1 Results for T-DEC1: (ULOF) transient at **BOC** conditions at an average burnup of 730 EFPD as calculated by SIM-LFR (KIT)



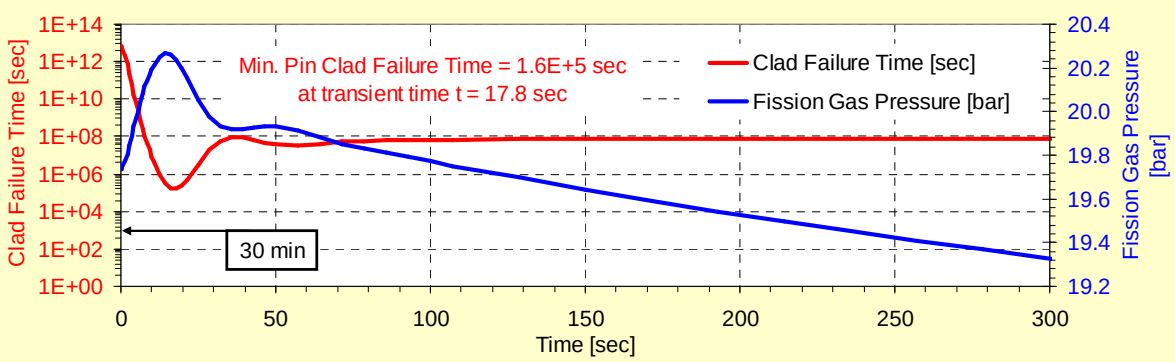
a) Relative Core Thermal Power and Flow rate



b) Peak Fuel-, Clad-, Coolant- and Vessel Wall Temperatures



c) Reactivity effects



d) Peak Pin Fission Gas Pin Pressure and Clad Failure Time

Fig. 1.1.1.4-2 Results for T-DEC1: (ULOF) transient at **EOC** conditions at an average burnup of 1095 EFPD as calculated by SIM-LFR (KIT)

Finally, under BOC and EOC conditions, the ULOF transient in the ALFRED can be accommodated, implying minimum clad failure time of ~1.6E+5 sec under the minimum coolant flow conditions (flow undershoot conditions). Taking this fact into account one can state that the ULOF transient is not a critical transient for the ALFRED plant.

1.1.1.5 T-DEC3: Loss of SCS - Unprotected Loss of Heat Sink (ULOHS): SIM-LFR (KIT)

For these calculations the primary heat transport path through the MHXs was assumed to fail at time t = 0 sec. Additionally, despite of the various signals for reactor shutdown, it was assumed that all reactor shut-down systems are inoperable. The reactor is not being shut-down by a reactor shutdown system, so the LOHS transient is simulated as an unprotected transient. In order to get even more conservative analysis results, we postulated a simultaneous failure of one DHR-1 subsystem (IC). It means that from that time point onwards, only three DHR-1 subsystems (ICs) are responsible for removing heat from the primary cooling circuit. DHR-2 system is not activated (logic failure). The primary pumps are assumed operational thereby assuring an even heat distribution throughout the primary cooling system providing a nominal coolant flow rate.

Two cases were analyzed to investigate the clad and fuel temperature response of the peak pin and the likelihood of peak pin clad rupture during this LOHS transient, namely at BOC and EOC conditions.

Under BOC conditions, the power level in the core is seen in **Fig. 1.1.1.5-1** to reduce down to ~ 3 % at 3600 sec (1 hour) into the transient due to negative temperature reactivity feedback effects (fuel, diagrid, pads, lead and CRs drivelines expansion reactivity effects).

As a result of the unprotected loss of heat sink, all core and vessel temperatures will heat up fairly uniformly at a rate of ~3.2 °C/min based on the masses of coolant (~3570 tons), and structural materials inside the primary cooling circuit.

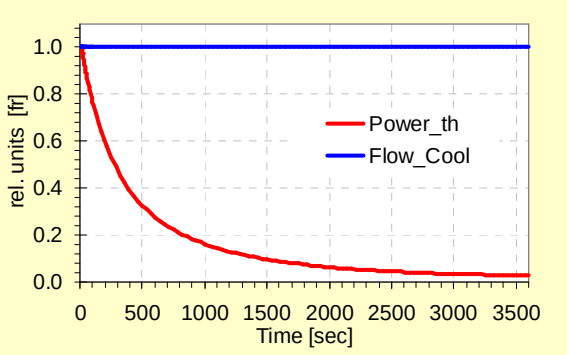
At the end of the simulation (at t = 3600 sec (1 hour) into the transient), the average vessel wall temperature approaches ~ 670 °C, thus questioning the long term structural integrity of the vessel under these elevated temperature conditions. At t = 3600 sec into the transient peak pin clad temperatures will reach ~ 710 ^{o}C, but due to rather low fission gas pressure of ~20 bar, the clad of the peak power pin will stay intact, having the clad failure time of ~3.6E+6 sec. All these temperatures will still continue to increase if the operator will not interact to terminate this transient. Even in 1 hour transient time the power generated in the core is still higher than the heat removal capacity of three DHR-1 subsystems.

Under EOC conditions, the power level in the core is seen in **Fig. 1.1.1.5-2** to reduce down to ~ 2.5 % at 3600 sec (1 hour) into the transient due to negative temperature reactivity feedback effects (fuel, diagrid, pads, lead and CRs drivelines expansion reactivity effects).

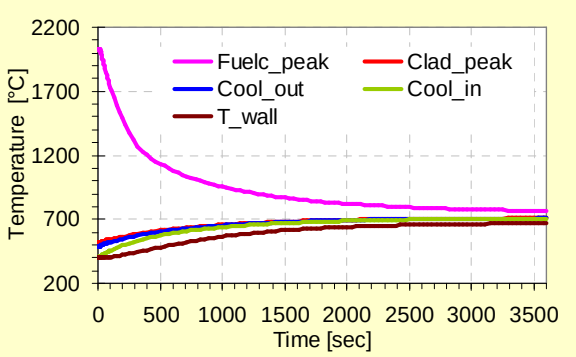
As a result of the unprotected loss of heat sink, all core and vessel temperatures will heat up fairly uniformly at a rate of ~3.1 °C/min based on the masses of coolant (~3570 tons), and structural materials inside the primary cooling circuit.

At the end of the simulation (at t = 3600 sec (1 hour) into the transient), the average vessel wall temperature approaches 662 °C, thus questioning the long term structural integrity of the vessel under these elevated temperature conditions. At t = 3600 sec into the transient peak pin clad temperatures will reach ~ 700 ^{o}C, but due to rather low fission gas pressure of ~ 28 bar, the clad of the peak power pin will stay intact, showing clad failure time of ~ 4.9E+6 sec. All these

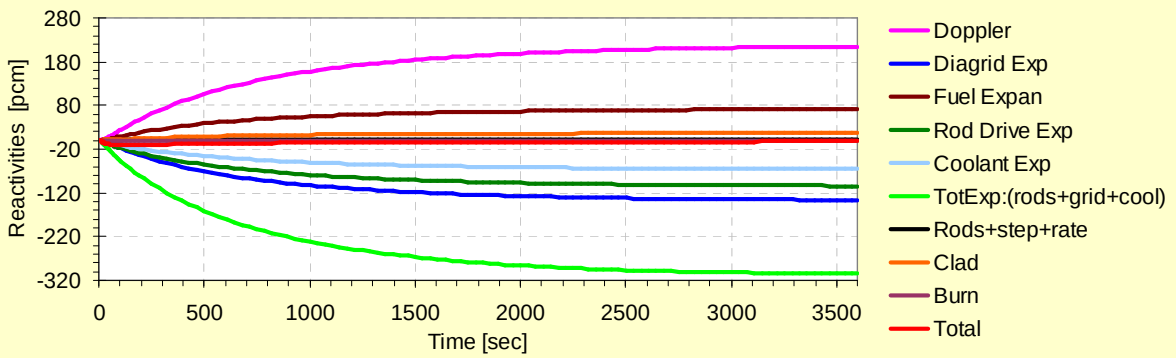
temperatures will still continue to increase if the operator will not interact to terminate this transient. Even in 1 hour transient time the power generated in the core is still higher than the heat removal capacity of three DHR-1 subsystems.



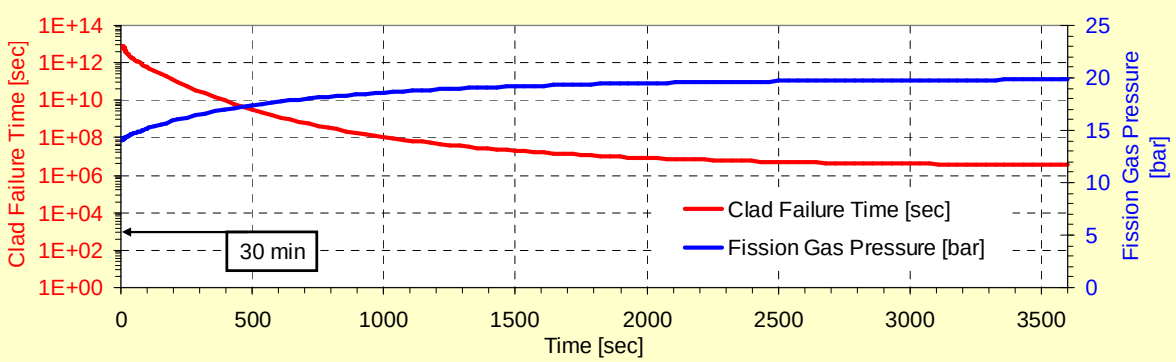
a) Relative Core Thermal Power and Flow rate



b) Peak Fuel-, Clad-, Coolant- and Vessel Wall Temperatures

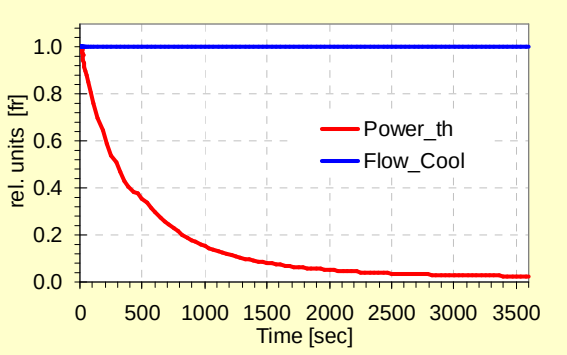


c) Reactivity effects

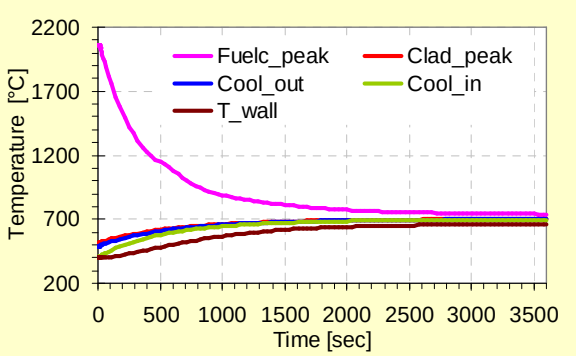


d) Peak Pin Fission Gas Pin Pressure and Clad Failure Time

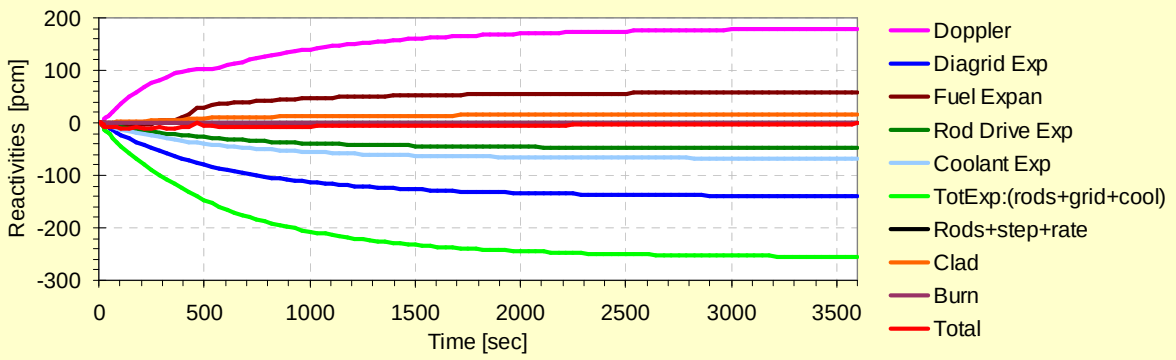
Fig. 1.1.1.5-1 Results for T-DEC3: (ULOHS) transient at HFP - **BOC** conditions at an average burnup of 730 EFPD as calculated by SIM-LFR (KIT)



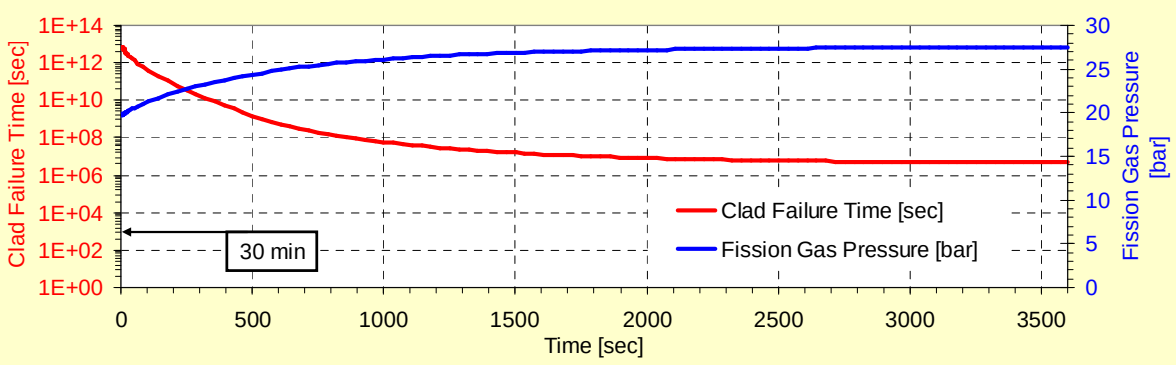
a) Relative Core Thermal Power and Flow rate



b) Peak Fuel-, Clad-, Coolant- and Vessel Wall Temperatures



c) Reactivity effects



d) Peak Pin Fission Gas Pin Pressure and Clad Failure Time

Fig. 1.1.1.5-2 Results for T-DEC3: (ULOHS) transient at HFP - **EOC** conditions at an average burnup of 1095 EFPD as calculated by SIM-LFR (KIT)

The timely response to this DEC transient is ascribed to a rather large cumulative negative reactivity feedback effect coming from the negative fuel, diagrid, pads, lead and CRs drivelines expansion reactivity effects. Sufficient grace time (>> 30 min) is available for the manual operator intervention to terminate this transient by manually shutting down the reactor and cooling down the primary cooling circuit.

1.1.1.6 T-DEC4: Loss of Off-site Power (LOOP) - Unprotected Loss of Flow and Loss of Heat Sink (ULOF & ULOHS): SIM-LFR (KIT)

For these calculations loss-of-offsite power (LOOP), which means that the primary pumps and the primary heat transport path through the MHXs are assumed to fail simultaneously, takes place at time t = 0 sec. Additionally, despite of the various signals for reactor shutdown, it was assumed that all reactor shut-down systems fail, so that the LOOP (LOF & LOHS) transient is simulated as an unprotected transient. In order to achieve even more conservative analysis results, we postulated a simultaneous failure of one DHR-1 subsystem (IC). It means that from that time point onwards, only three DHR-1 subsystems (ICs) are responsible for removing heat from the primary cooling circuit. DHR-2 system is not activated (logic failure). Stopping of the primary pumps at the beginning of the transient means that primary coolant circulation in the primary cooling circuit is only by natural convection, thus it does not provide a well mixed, uniform temperature distribution throughout the primary system, as is the case when the primary pumps are operating normally.

Two cases were analyzed to investigate the clad and fuel temperature response of the peak pin and the likelihood of peak pin clad rupture during this LOOP (LOF & LOHS) transient, namely at BOC and EOC conditions.

Under BOC conditions, the power level in the core is seen in **Fig. 1.1.1.6-1** decreases to ~3.8 % at 3600 sec (1 hour) into the transient due to negative temperature reactivity feedback effects (fuel, diagrid, pads, lead and CRs drivelines expansion reactivity effects).

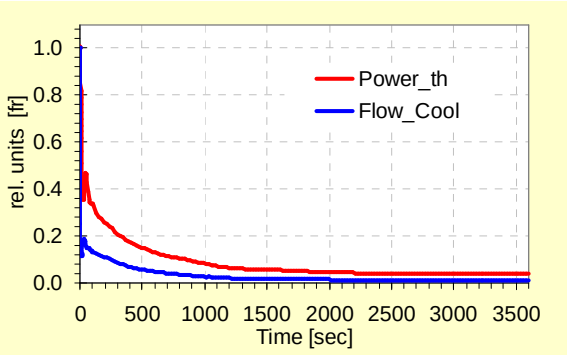
As a result of the unprotected loss-of-offsite power (LOOP), all core and vessel temperatures will heat up fairly uniformly at a rate of ~ 2.2 °C/min (due to faster reduction of the reactor power level in comparison with the ULOHS case above) based on the masses of coolant (~3570 tons) and structural materials inside the primary cooling circuit.

At the end of the simulation (at t = 3600 sec (1 hour) into the transient), the average vessel wall temperature approaches ~ 535 °C, thus the long term structural integrity of the vessel is still guaranteed. At t = 3600 sec into the transient peak pin clad temperatures will reach ~ 795 ^{o}C, but due to rather low fission gas pressure of ~ 17 bar, the clad of the peak power pin will stay intact, having the clad failure time of ~ 2.1E+4 sec. All the core temperatures seem to be increasing further only very slightly after 1 hour of the transient time. Even in 1 hour transient time the power generated in the core is still higher than the heat removal capacity of three DHR-1 subsystems.

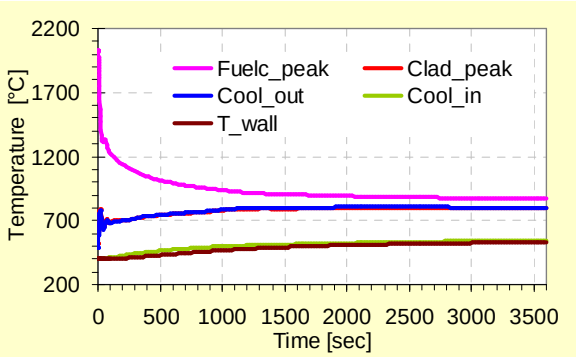
Under EOC conditions, the power level in the core is seen in **Fig. 1.1.1.6-2** to reduce down to ~ 2.9 % at 3600 sec (1 hour) into the transient due to negative temperature reactivity feedback effects (fuel, diagrid, pads, lead and CRs drivelines expansion reactivity effects).

As a result of the unprotected loss-of-offsite power (LOOP), all core and vessel temperatures will heat up fairly uniformly at a rate of ~ 2.5 °C/min (due to faster reduction of the reactor power level in comparison with the ULOHS case above) based on the masses of coolant (~3570 tons) and structural materials inside the primary cooling circuit.

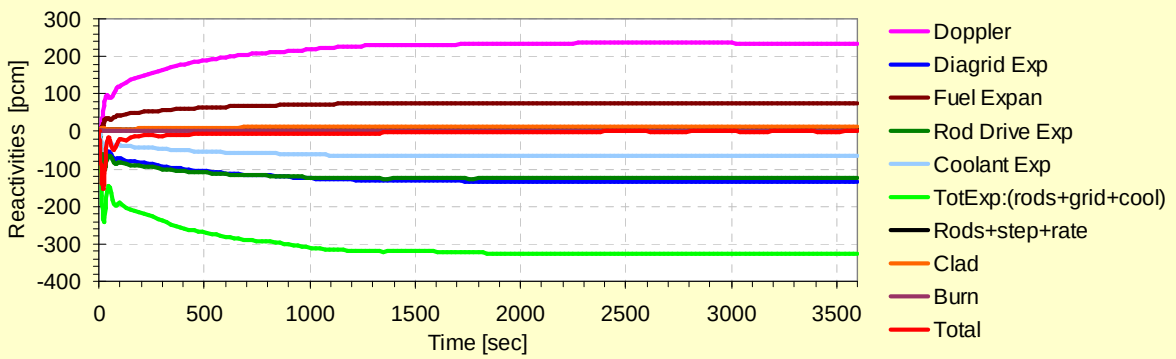
At the end of the simulation (at t = 3600 sec (1 hour) into the transient), the average vessel wall temperature approaches ~ 555 °C, thus the long term structural integrity of the vessel is still guaranteed. At t = 3600 sec into the transient peak pin clad temperatures will reach ~790 ^{o}C, but due to rather low fission gas pressure of ~ 24.5 bar, the clad of the peak power pin will stay intact, having the clad failure time of ~ 2.2E+4 sec. All the core temperatures seem to be increasing further only very slightly after 1 hour of the transient time. Even in 1 hour transient time the power generated in the core is still higher than the heat removal capacity of three DHR-1 subsystems.



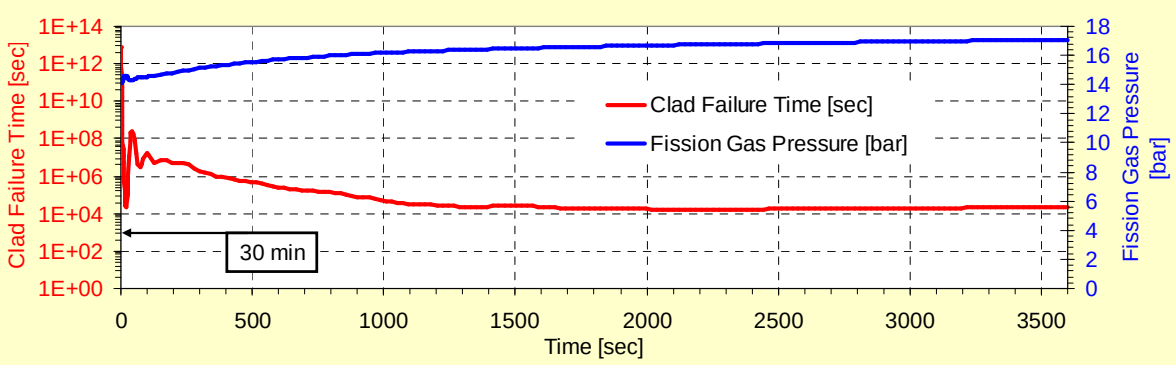
a) Relative Core Thermal Power and Flow rate



b) Peak Fuel-, Clad-, Coolant- and Vessel Wall Temperatures

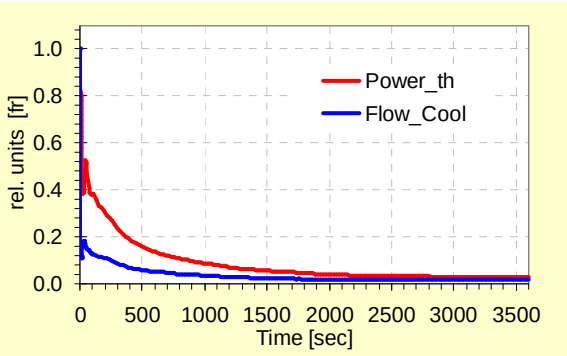


c) Reactivity effects

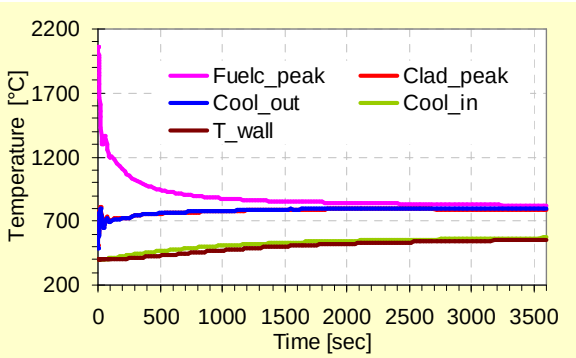


d) Peak Pin Fission Gas Pin Pressure and Clad Failure Time

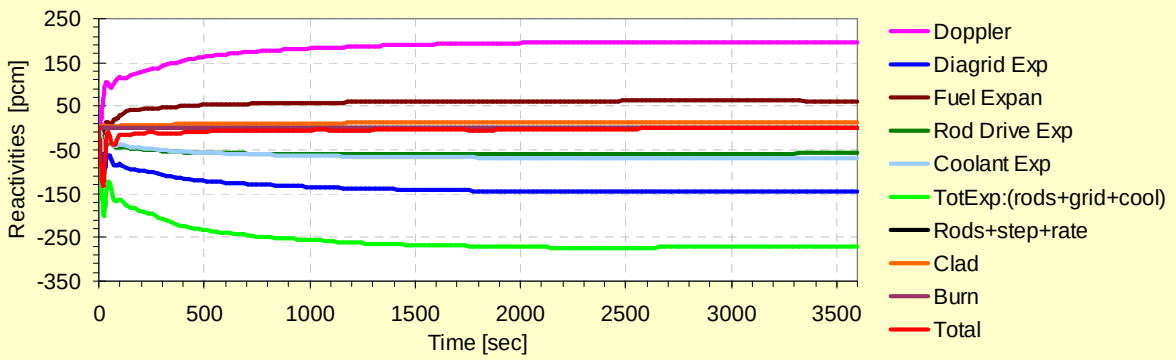
Fig. 1.1.1.6-1 Results for T-DEC4: (ULOOP) transient at HFP - **BOC** conditions at an average burnup of 730 EFPD as calculated by SIM-LFR (KIT)



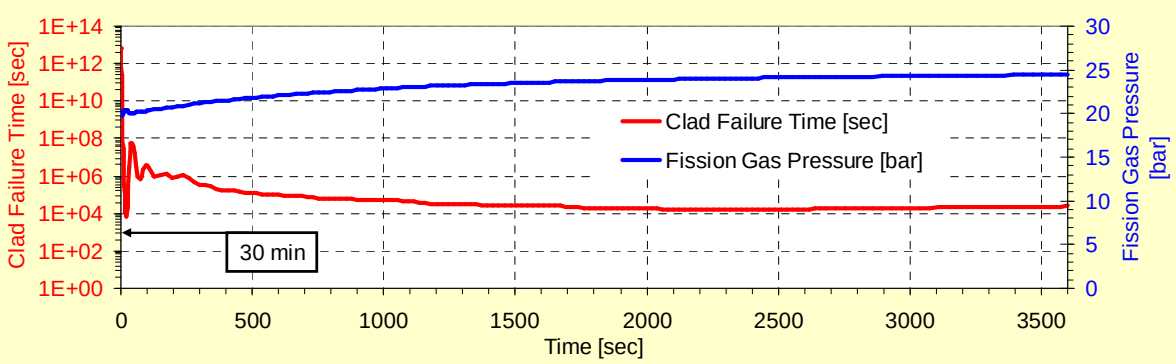
a) Relative Core Thermal Power and Flow rate



b) Peak Fuel-, Clad-, Coolant- and Vessel Wall Temperatures



c) Reactivity effects



d) Peak Pin Fission Gas Pin Pressure and Clad Failure Time

Fig. 1.1.1.6-2 Results for T-DEC4: (ULOOP) transient at HFP - **EOC** conditions at an average burnup of 1095 EFPD as calculated by SIM-LFR (KIT)

The timely response to this DEC transient is ascribed to a rather large cumulative negative reactivity feedback effect coming from the negative fuel, diagrid, pads, lead and CRs drivelines expansion reactivity effects. Sufficient grace time (>> 30 min) is available for the manual operator intervention to terminate this transient by manually shutting down the reactor and cooling down the primary cooling circuit.

1.1.1.7 T-DEC5: Unprotected Blockage of SA w/o radial Heat Transfer (UBA): SIM-LFR (KIT)

Two different calculations were performed (for both cases nominal power at HFP, no reactor trip and no radial heat transfer are assumed):

Case 1: The flow area through the hottest SA is blocked 97.5%. Thus a flow area of 2.5% remains open for the flow of coolant. Of interest here will be time to clad failure after blockage initiation.

Case 2: The maximum clad temperatures of the peak pin as a function of blockage area are determined.

Note: SIM-LFR assumption - in both cases it is assumed that coolant flow in the blocked SA is linearly proportional to the SA blocked flow area. Since

$$\text{flow rate [kg/s]} = \text{density[kg/ m}^3\text{]} * \text{Flow_Area[m}^2\text{]} * \text{velocity[m/sec]}$$

the flow rate may in reality not change exactly in proportion to the reduced flow area during the transient as the channel velocity may also change due to changing pressure conditions of the blocked sub-assembly (SA).

Case 1: 97.5% SA blockage area

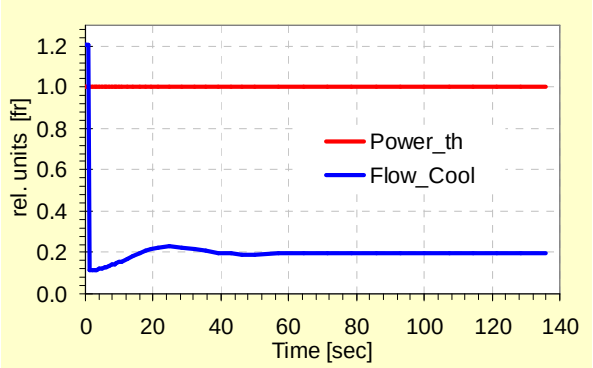
Sub-assembly blockage (97.5%) is assumed to be initiated instantly at 1 sec transient time.

The sub-assembly outlet temperature is assumed to be monitored but corresponding signal is assumed to fail in this transient.

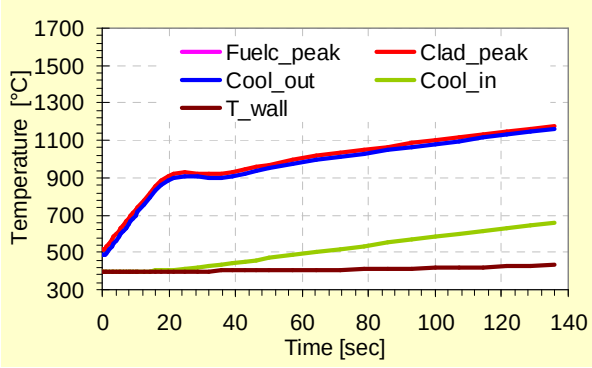
Several different cases are run at BOC and EOC conditions, varying the blockage area ranging from 20% to 97.5% (20, 40, 60, 65, 70, 75, 80, 90, 95 and 97.5%).

For the 97.5% SA blockage transient at BOC, the peak pin will fail ~57 sec into the transient due to clad rupture (transient initiation at 1 sec transient time) as the cladding temperature will reach 996 °C (see **Fig. 1.1.1.7-1-b**), with a peak pin fission gas pressure of ~16.6 bar (see **Fig. 1.1.1.7-2**).

As a result of the SA blockage, the flow rate will initially decrease to ~ 12% nominal, gradually recovering to about 20% flow rate at ~50 sec into the transient due to changing SA pressure conditions. The power remains at 100% nominal throughout the transient (see **Fig. 1.1.1.7-1-a**).

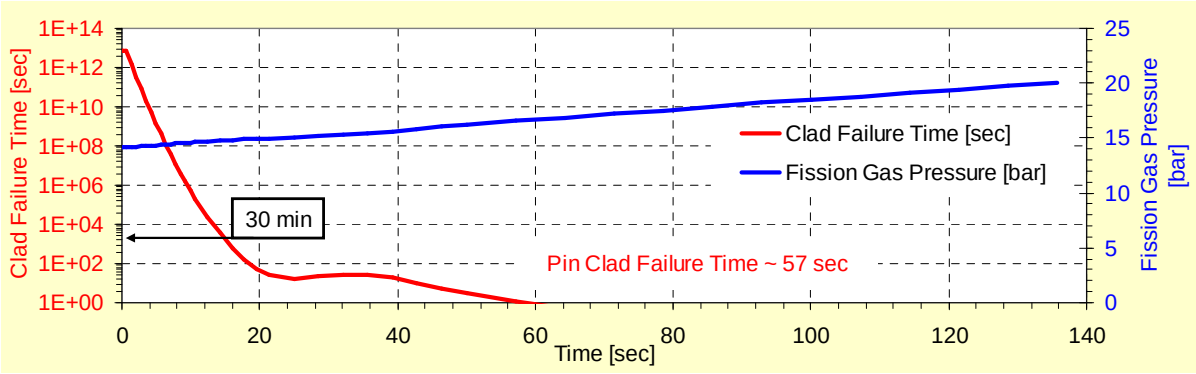


a) Relative Core Thermal Power and Hot SA Flow rate



b) Peak Fuel-, Clad-, Coolant- and Vessel Wall Temperatures

Fig. 1.1.1.7-1 Results for T-DEC5: SA Blockage transient (flow area of hottest SA 97.5% blocked; w/o radial heat transfer, **BOC** conditions) as calculated by SIM-LFR (KIT)

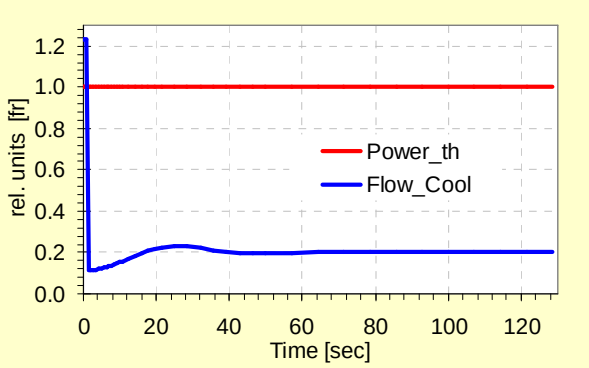


Peak pin plenum pressure and clad failure time

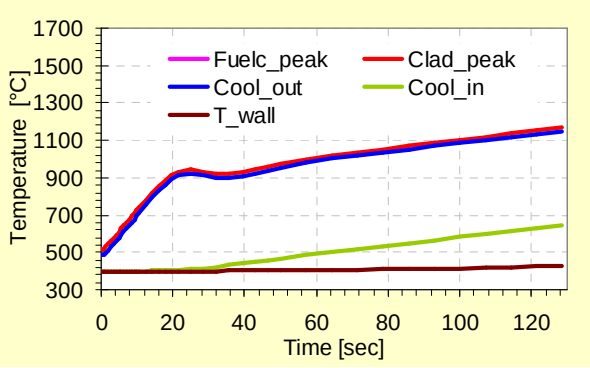
Fig. 1.1.1.7-2 Results for T-DEC5: SA Blockage transient (flow area of hottest SA 97.5% blocked; w/o radial heat transfer, **BOC** conditions) as calculated by SIM-LFR (KIT)

For the 97.5% SA blockage transient at EOC, the peak pin will fail ~56 sec into the transient (transient initiation at 1 sec transient time) as the cladding temperature will reach 1000 °C (see **1.1.1.7-3-b**), with a peak pin fission gas pressure of ~23 bar (see **Fig. 1.1.1.7-4**).

As a result of the SA blockage, the flow rate will initially decrease to ~ 12 % nominal, gradually recovering to about 20% flow rate at ~50 sec into the transient due to changing SA pressure conditions. The power remains at 100% nominal throughout the transient (see **1.1.1.7-3-a**).

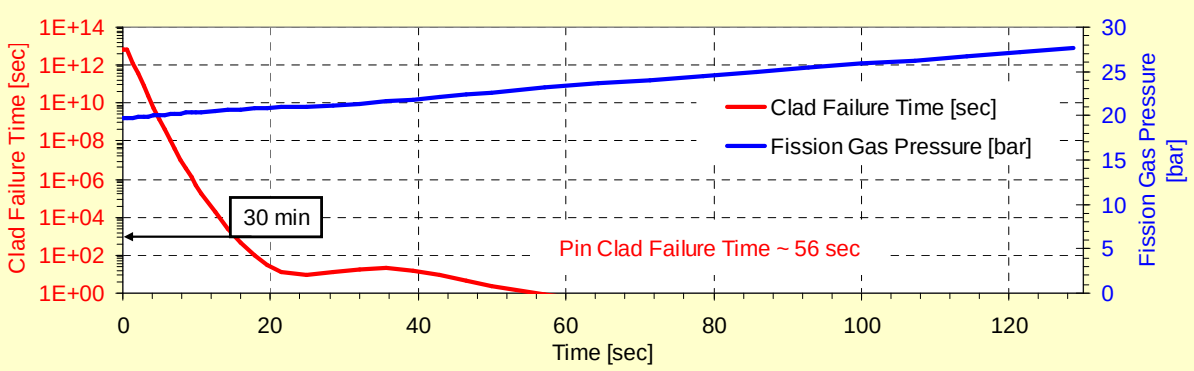


a) Relative Core Thermal Power and Hot SA Flow rate



b) Peak Fuel-, Clad-, Coolant- and Vessel Wall Temperatures

Fig. 1.1.1.7-3 Results for T-DEC5: SA Blockage transient (flow area of hottest SA 97.5% blocked; w/o radial heat transfer, **EOC** conditions) as calculated by SIM-LFR (KIT)



Peak pin plenum pressure and clad failure time

Fig. 1.1.1.7-4 Results for T-DEC5: SA Blockage transient (flow area of hottest SA 97.5% blocked; w/o radial heat transfer, **EOC** conditions) as calculated by SIM-LFR (KIT)

Case 2: Different SA blockage areas

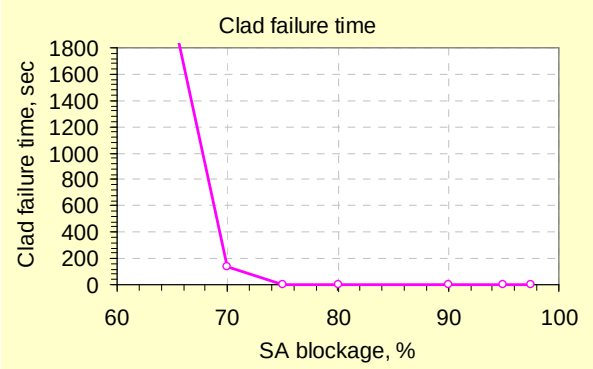
Table 1.1.1.7-1 and **Fig. 1.1.1.7-5** display the corresponding clad failure times and clad melting times as a function of blockage area (from 20% to 97.5%) for BOC conditions, while **Table 1.1.1.7-2** and **Fig. 1.1.1.7-6** display the corresponding clad failure times and clad melting times as a function of blockage area (from 20% to 97.5%) for EOC conditions. The following can be observed:

- The ALFRED will not experience any fuel pin failure for blockage areas less than 75% for both BOC and EOC conditions, even under unprotected conditions;
- For blockages above 75%, clad failures must be expected (see **Fig. 1.1.1.7-5a** and **Fig. 1.1.1.7-6a)** for both BOC and EOC conditions;
- Fuel melting is not an issue for ALFRED. Fuel melting temperatures are not reached even in 97.5% SA blockage case (see **Fig. 1.1.1.7-5b** and **1.1.1.7-6b)** for both BOC and EOC conditions.

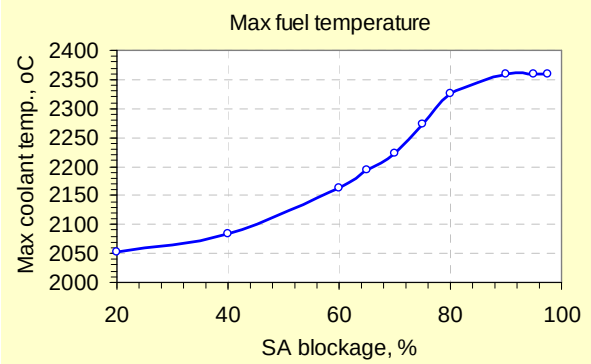
Table 1.1.1.7-1 ALFRED clad failure time and max SA channel temperatures as a function of SA blockage area for **BOC** under unprotected blockage transients (T-DEC5) conditions.

Blockage	Clad failure time*	Max. cool. SA outlet temp.	Max clad temp (peak pin)	Max fuel temp (peak pin)
%	sec	^{o}C	^{o}C	^{o}C
20	4.00E+10	542	573	2052
40	2.20E+08	608	638	2083
60	4.20E+04	742	771	2162
65	2057	799	826	2194
70	136	873	898	2222
75	0	974	997	2272
80	0	1091	1110	2326
90	0	1158	1176	2359
95	0	1158	1176	2359
97.5	0	1158	1176	2359

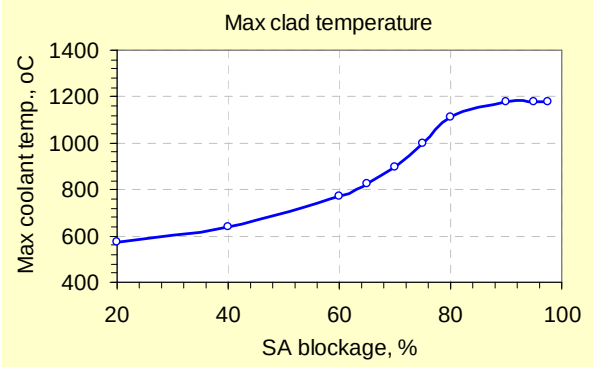
* - max fission gas pressure ~18 bar



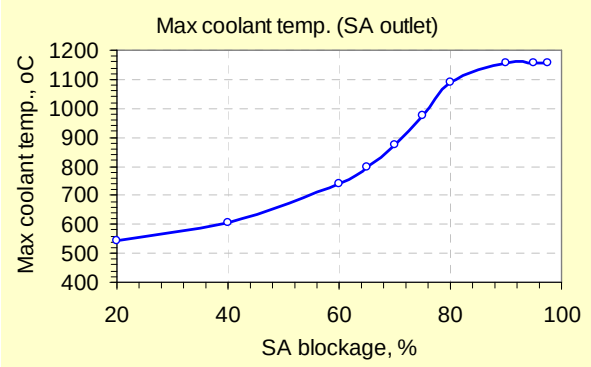
a) Clad failure time [sec] as a function of SA channel blockage area



b) Max fuel temperature [^{o}C] as a function of SA channel blockage area



c) Max clad temperature [^{o}C] as a function of SA channel blockage area



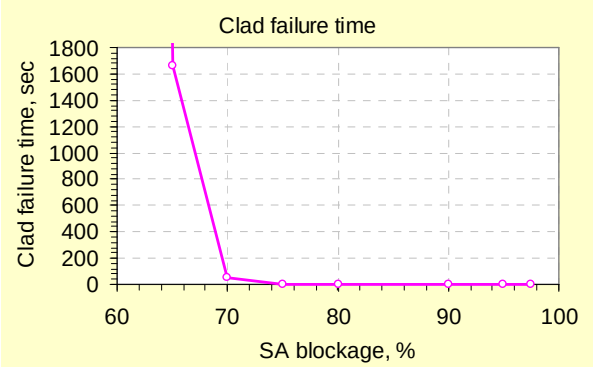
d) Max coolant temperature [^{o}C] as a function of SA channel blockage area

Fig. 1.1.1.7-5 Results for T-DEC5: SA Blockage transient. Clad failure time and max SA channel temperatures as function of SA blockage area for **BOC** conditions as calculated by SIM-LFR (KIT)

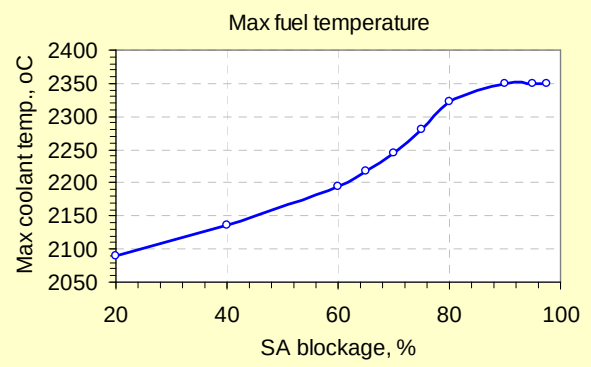
Table 1.1.1.7-2 ALFRED clad failure time and max SA channel temperatures as a function of SA blockage area for **EOC** under unprotected blockage transients (T-DEC5) conditions.

Blockage	Clad failure time*	Max. cool. SA outlet temp.	Max clad temp (peak pin)	Max fuel temp (peak pin)
%	sec	^{o}C	^{o}C	^{o}C
20	2.70E+10	545	574	2089
40	1.50E+08	612	641	2136
60	3.00E+04	745	772	2194
65	1661	801	827	2218
70	53	874	898	2245
75	0	974	996	2280
80	0	1084	1103	2322
90	0	1148	1165	2349
95	0	1148	1165	2350
97.5	0	1148	1165	2350

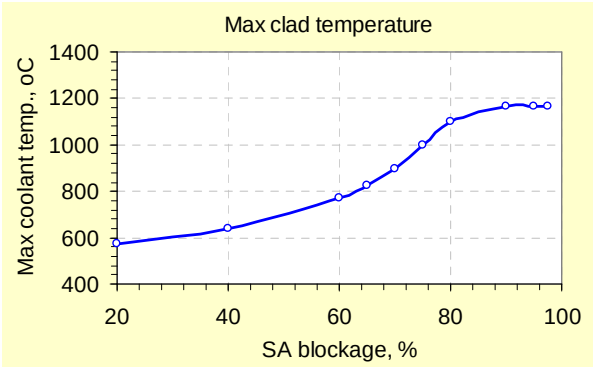
* - max fission gas pressure ~25 bar



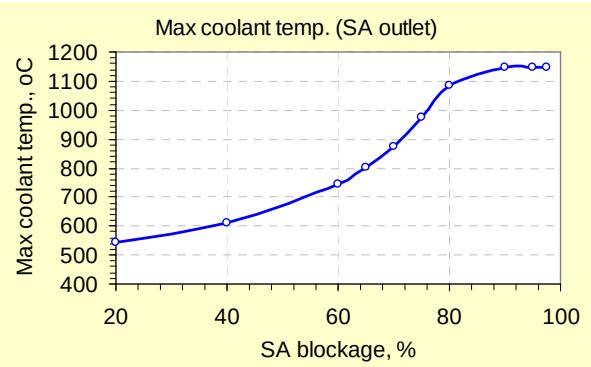
a) Clad failure time [sec] as a function of SA channel blockage area



b) Max fuel temperature [^{o}C] as a function of SA channel blockage area



c) Max clad temperature [^{o}C] as a function of SA channel blockage area



d) Max coolant temperature [^{o}C] as a function of SA channel blockage area

Fig. 1.1.1.7-6 Results for T-DEC5: SA Blockage transient. Clad failure time and max SA channel temperatures as function of SA blockage area for **EOC** conditions as calculated by SIM-LFR (KIT)

1.1.1.8 T-DEC6: SCS failure - Protected Loss of Heat Sink (PLOHS): SIM-LFR (KIT)

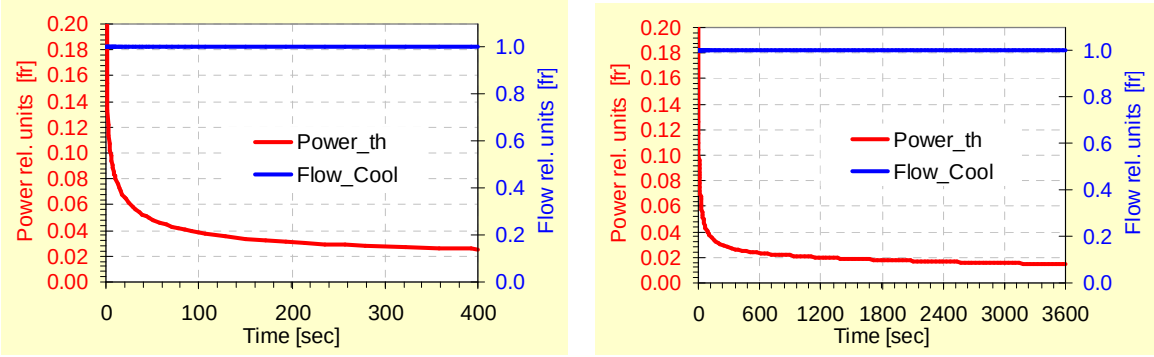
For these calculations SCS failure was postulated - the primary heat transport path through the MHXs was assumed to fail at time t = 0 sec. One second later two signals for reactor shutdown are generated: 1) MHX outlet temperature on the primary (lead) side becomes more than 430^{o}C, and 2) Turbine trip signal on the failure of SCS (turbine stop valve closure). Based on these two reactor scram signals (even if the first one is being neglected), the reactor is being shut-down by a reactor shutdown system - the SCS failure (LOHS) transient is simulated as a protected transient. In order to achieve even more conservative analysis results, a simultaneous failure of both DHRS (DHR-1 and DHR-2 subsystems) is being postulated. This implies that from that time point onwards, the power generated in the reactor core remains within the primary cooling circuit. Following the reactor scram, all relevant core temperatures first will decrease, but later will start increasing due the primary cooling system heat-up by the decay heat (the only heat sink available is the radiation heat loss of the primary system). The primary pumps are assumed operational thereby assuring an even heat distribution throughout the primary cooling system providing a nominal primary coolant flow rate.

Two cases were analyzed to investigate the clad and fuel temperature response of the peak pin during this SCS failure (PLOHS) transient, namely at BOC and EOC conditions.

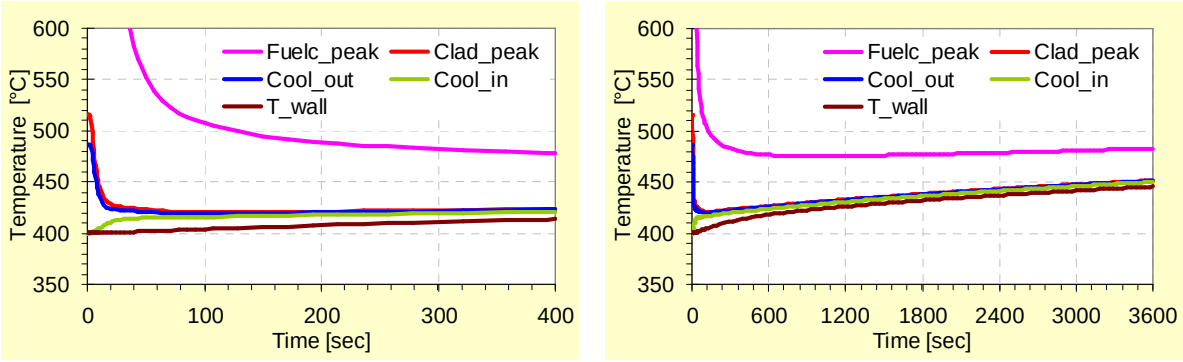
Under BOC (**Fig. 1.1.1.8-1**), as well as EOC (**Fig. 1.1.1.8-2**) conditions, the power level in the core is observed to rapidly decrease to the decay heat level, following the reactor scram. All core temperatures, as a result of the decreasing reactor power, decrease during the initial phase of the transient. Later, due to the SCS and DHRS failures (no decay heat is being transferred through the MHX to the secondary cooling circuit), fuel, clad, coolant and vessel temperatures start increasing. In 1 hour transient time, fuel temperature will reach ~ 480 ^{o}C, clad and coolant temperatures will reach ~ 450 ^{o}C and reactor vessel temperature will reach ~445 ^{o}C. Based on the lead temperature gradients around the primary cooling circuit, one can estimate that clad and coolant temperatures will reach ~ 500 ^{o}C in 3 hours from the start of the transient. During this time period the operator has sufficient time for manual intervention by activating SCS or sub-systems of DHR-1 system in order to prevent overheating of the whole primary system.

The very slow increase in the primary cooling circuit temperatures is due to the very large thermal inertia of the primary cooling system, continuously decreasing decay heat, as well as some radiation heat losses from the primary cooling circuit.

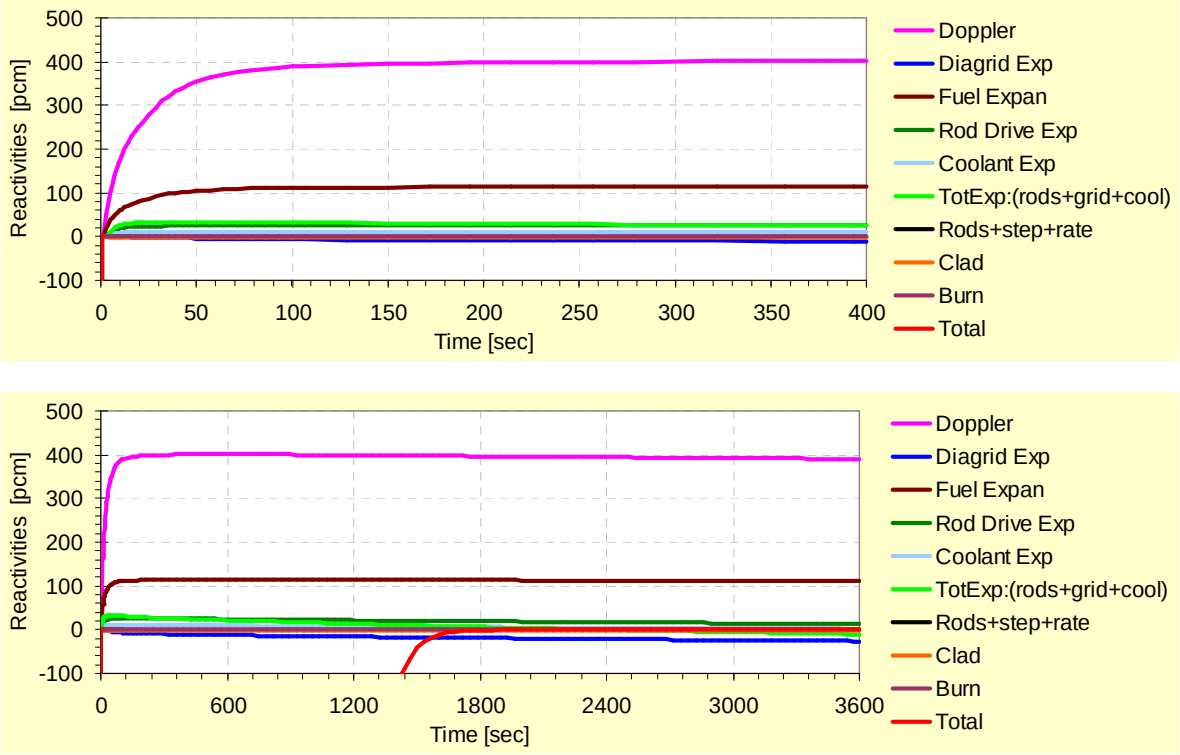
A conclusion can be made here, that a protected SCS failure transient, even assuming the complete failure of the DHRS (DHR-1 and DHR-2 subsystems), presents no imminent safety issue to the ALFRED reactor in the first several hours, following the event. However, all primary cooling circuit temperatures, in a longer time period, will start increasing slowly and will reach ~500 ^{o}C in 3 hours, but the operator has sufficient time for manual intervention by re-activating SCS or sub-systems of DHR-1 system in order to prevent overheating of the whole primary system, including the reactor vessel.



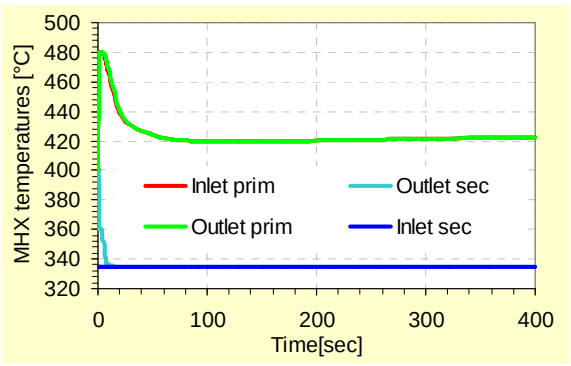
a) Relative Core Thermal Power and Flow rate

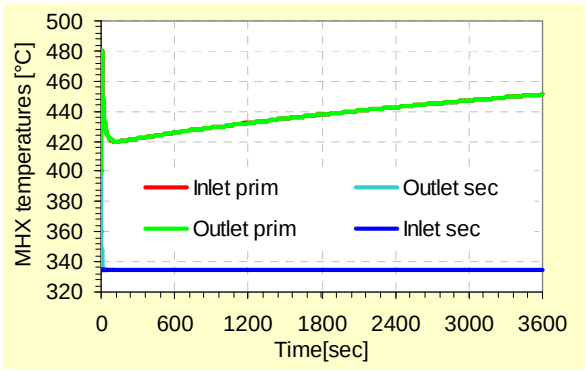


b) Peak Fuel-, Clad-, Coolant- and Vessel Wall Temperatures

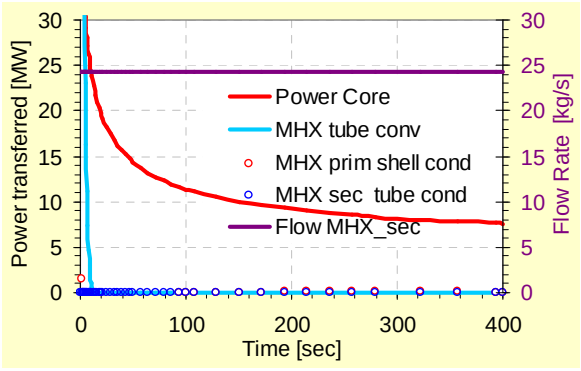


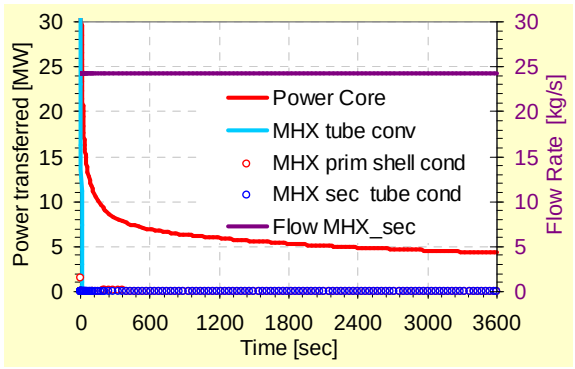
c) Reactivity effects





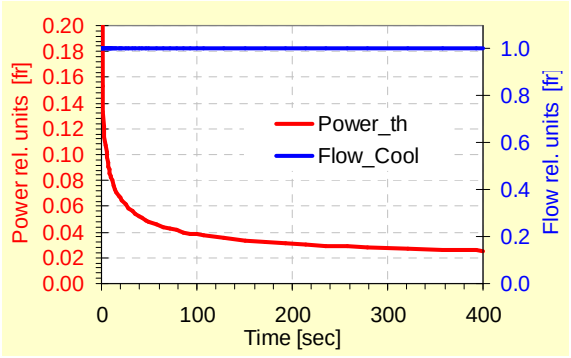
d) MHX temperatures

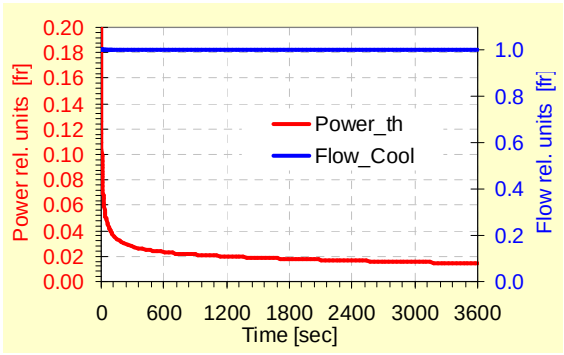




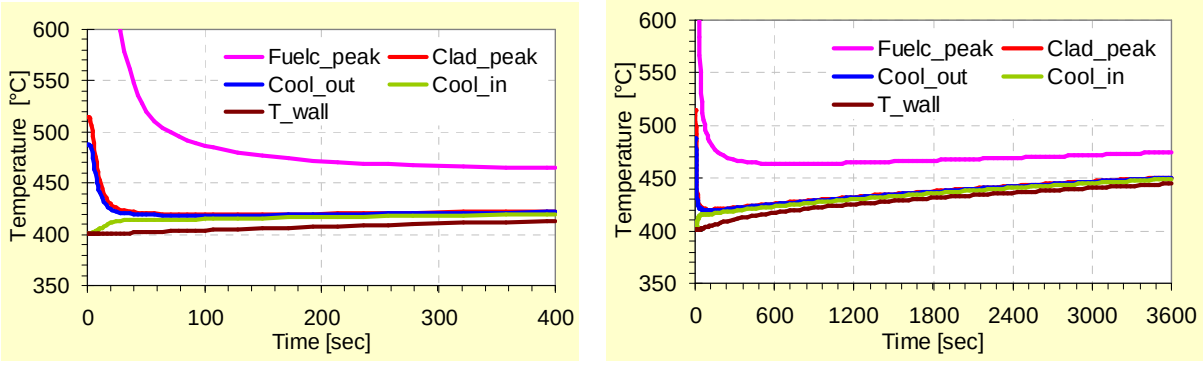
e) Core and MHX Powers, plus MHX sec. side water flow rate

Fig. 1.1.1.8-1 Results for T-DEC6: SCS failure (PLOHS) transient at HFP - **BOC** conditions at peak burnup of 730 EFPD as calculated by SIM-LFR (KIT)

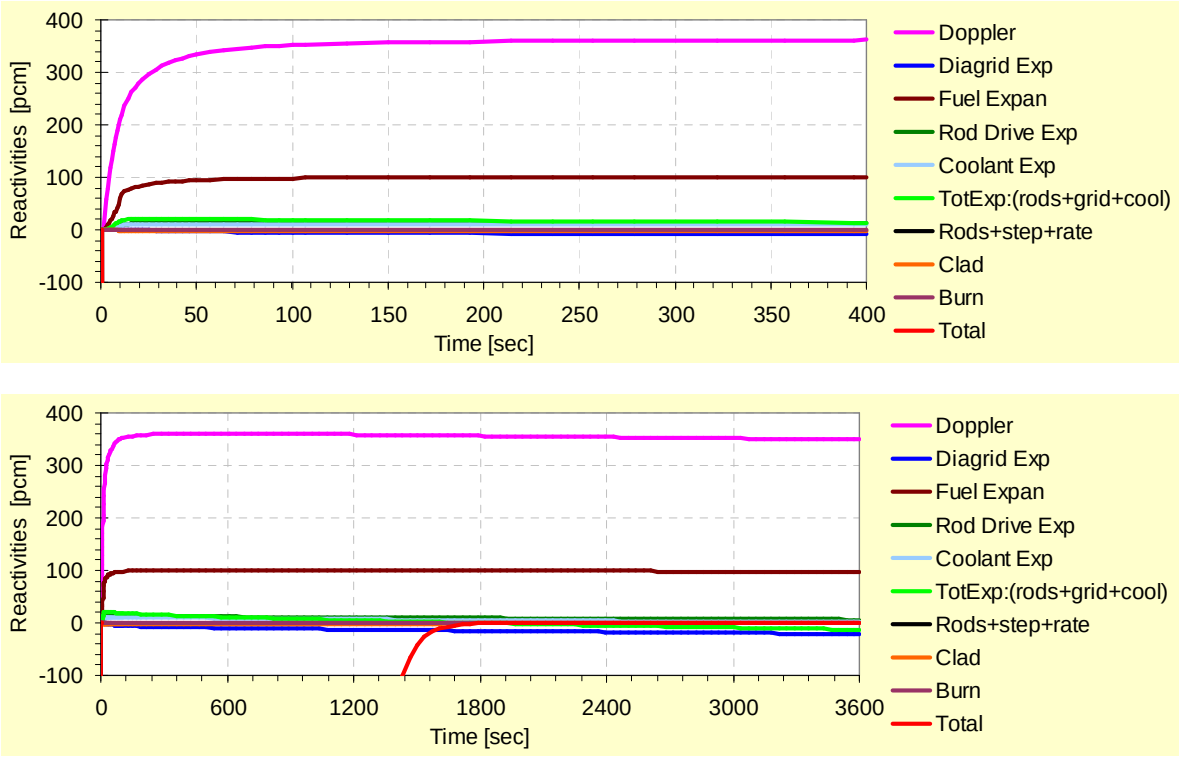




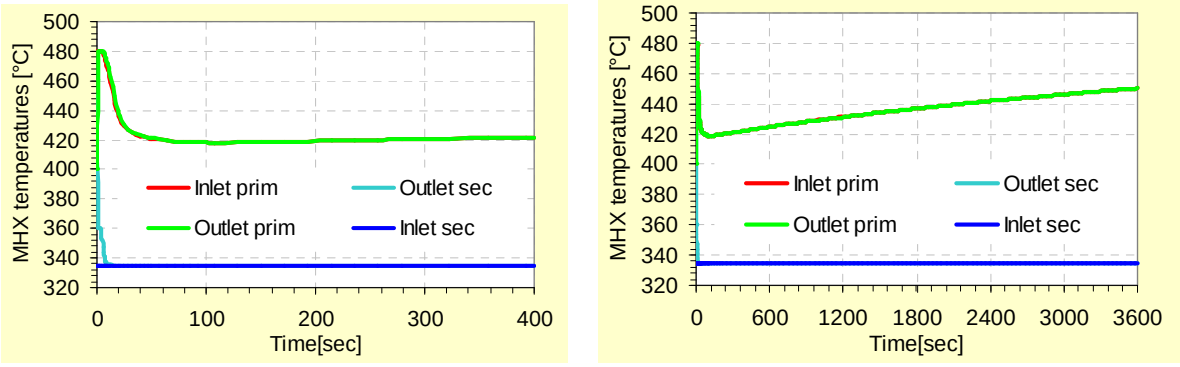
a) Relative Core Thermal Power and Flow rate



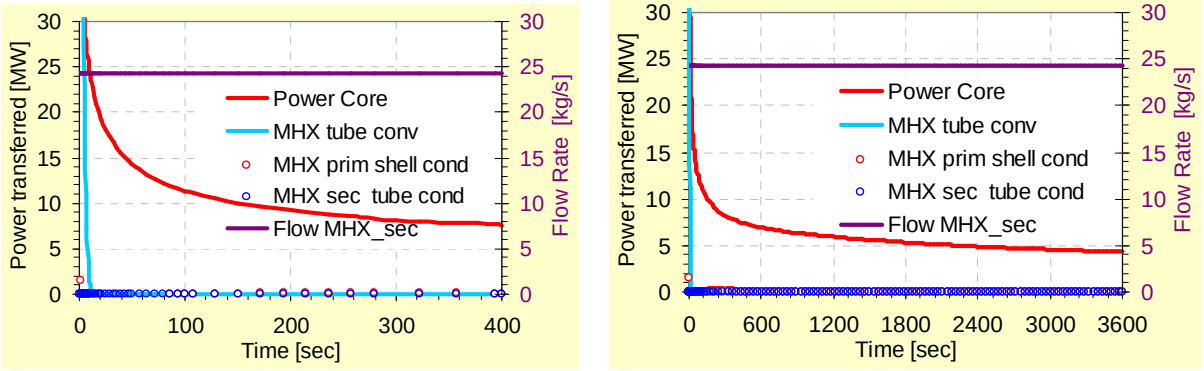
b) Peak Fuel-, Clad-, Coolant- and Vessel Wall Temperatures



c) Reactivity effects



d) MHX temperatures



e) Core and MHX Powers, plus MHX sec. side water flow rate

Fig. 1.1.1.8-2 Results for T-DEC6: SCS failure (PLOHS) transient at HFP - **EOC** conditions at peak burnup of 1095 EFPD as calculated by SIM-LFR (KIT)

1.1.1.9 Conclusions

The protected SCS failure transient, even assuming the complete failure of the DHRS (DHR-1 and DHR-2 subsystems), presents no imminent safety issue to the ALFRED reactor in the first several hours into the transient. However, all primary cooling circuit temperatures, in a longer time horizon, will start increasing slowly and will reach ~500 ^{o}C in 3 hours, but the operator has sufficient time for manual intervention by re-activating SCS or sub-systems of DHR-1 system in order to prevent overheating of the whole primary system, including the reactor vessel.

The protected LOF transient with FW flow-rate increase by 20 % presents a safety issue as related to possible Pb-freezing for the ALFRED reactor. Reactor safety is ensured by the reactor protection system, shutting down the reactor, as well as by the tightly controlled heat removal by the DHRS (also by an operator in the medium and long term), removing only controlled amounts of decay heat from the reactor primary cooling circuit to assure prevention of freezing of the Pb-coolant at any location of the primary cooling circuit.

Protected LOF with corresponding FW temperature decrease to 300 ^{o}C will lead to a safety issue as Pb-freezing will have to be expected ~3.8 hours into the transient. During this time period the operator has sufficient time to deactivate sub-systems of the DHR-1 system, in order to prevent Pb-coolant freezing at the outlet of the MHX.

Normally, Pb-overcooling anywhere in the primary cooling loop below 335°C should be prevented under all plant transient conditions in order to assure prevention of freezing of the Pb-coolant thereby endangering an assured flow pattern throughout the primary system, in particular the core region. The feedwater temperature on the secondary side of the MHX must never be allowed to go below 335°C in order to assure that the primary system is always maintained at temperatures above 335°C. This requires an assured preheater system of the secondary side of the MHX for all times under all conceivable, adverse transient conditions.

For reactivity insertion of 250 pcm within 10 sec (possibly due to: voiding of part of the active core region enveloping voids introduction in case of SGTR, core compaction, fuel SA blockage, etc.) at BOC, as well as EOC core conditions, ALFRED reactor peak fuel pin cladding is not expected to fail (rupture), but local fuel melting is observed in the center of the peak fuel pins (pellets).

Under BOC and EOC conditions, the ULOF transient in the ALFRED can be accommodated, as very large minimum clad failure times of ~1.6E+5 sec under the minimum coolant flow conditions (flow undershoot conditions) are calculated by SIM-LFR. The ULOF transient is thus not a “critical” transient for the ALFRED plant.

As related to the ULOHS transient, the main concern is the average vessel wall temperature which in ~ 1 hour transient time approaches ~670 °C, thus questioning the long term structural integrity of the vessel under these elevated temperature conditions. The sluggish time response to this DEC transient is ascribed to the large primary loop thermal inertia and a rather large cumulative negative reactivity feedback effect coming from the negative fuel, diagrid, pads,

Pb-coolant and CRs drivelines expansion reactivity feedback effects resulting in a very effective decrease of the reactor power. Sufficient grace time (>> 30 min) is available for the manual operator intervention to terminate this transient by manually shutting down the reactor and cooling down the primary cooling circuit.

The ULOOP (ULOF+ULOHS) transient revealed no additional relevant safety issues as observed during the ULOHS transient (as described above). A large influence in coping with this DEC transient is associated with the negative fuel, diagrid, pads, Pb-coolant and CRs drivelines expansion reactivity feedback effects, effectively reducing reactor power to a “safe” power level (~ 3-4 % of the nominal power) in a timely manner.

The ALFRED reactor is not expected to experience any fuel pin failure during SA flow blockages less than 75% blockage area, even under unprotected conditions. However, for SA flow blockages above 75%, clad failure (creep rupture) has to be expected. Fuel melting is not an issue for the ALFRED reactor; as fuel melting temperatures are not reached even in the 97.5% SA flow blockage case.

The analysis of DEC transients performed for the Pb-cooled ALFRED design demonstrated the very forgiving nature of this plant design when compared to other similar plant designs, ascribable to the combination of:

1. the inherently, large thermal inertia of the Pb-cooled primary system,

2. the detailed focus on the optimization of all safety relevant systems, in particular emphasizing appropriate designs of all relevant control and safety systems (as well as components), and

3. optimizing the neutronic core characteristics of the ALFRED “core system” thereby assuring various reactivity feedback effects (fuel, diagrid, pads, Pb-coolant and CRs drivelines expansion reactivity) that effectively depress the reactor power under all adverse DEC transient conditions,

4. as the ALFRED core is specifically designed to accommodate the ULOF transient.

APPENDIX C

PSI Contribution to LEADER Deliverable DEL022:

Summary of Transient Simulation Results for ALFRED (DBC and DEC) with the TRACE/FRED Code

Summary of transient simulation results for ALFRED

Youpeng Zhang; Mikityuk Konstantin

Paul Scherrer Institut

1. TRACE/FRED model construction

1.1.1 Introduction of the FRED code

The transient thermal-mechanics code FRED was originally developed to model the transient behavior of LWR fuel rods. The FRED code is used to calculate the transient changes of temperature, heat flux, stress, strain and thus failure probability for structural elements in fuel rods. The FRED code was implemented into the FAST code system. The data library in the FRED code includes thermo-mechanical properties of different cladding materials (zircalloy alloy, Zr-1%Nb, several types of stainless steel), fuels (UO_2, MOX and so on) and gases (He, Ar, Xe, Kr, H_2 and N_2) and coolants (D_2O, H_2O, He, liquid Na, and LBE) [1].

1.1.2 FRED model creation

Based on different linear power rating and burnup levels, fuel pins in ALFRED core can be categorized into three different types: the hottest fuel pin, the average fuel pin in the peak assembly and the average fuel pins. Hence, three different types of fuel pins were modeled into the FRED code correspondingly.

Since all these three types of pins were considered to have the same geometrical and compositional details, differences that will be considered for the FRED model are only burnup levels and axial power profile as shown in Fig. 1.1.1. The burnup level of the hottest fuel pin, average pins in hot assembly and average fuel pins at BOC are 38.9, 35.7 and 29.6 MWd/kgHM respectively. At EOC state, these values are 59.7, 54.8 and 44.4 MWd/kgHM

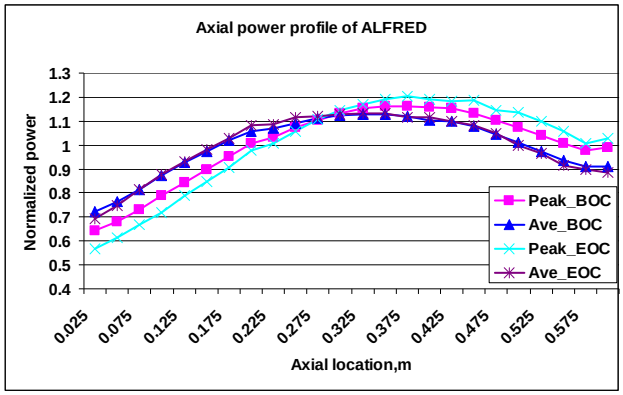


Fig. 1.1.1 TRACE model for ELFR primary and secondary circuits

Other parameters used for the FRED model creation of all three types of fuel pins are listed in Table 1.1.1.

Table 1.1.1 Design specifications of fuel pins [2]

Fuel TD, kg/m^3	10430	Pu content, %	30.0
Inner hole radius, mm	1.00	Pellet outer radius, mm	4.50
Fuel surface roughness, mm	0.002	Stoichiometric deviation	0.03
Initial gap size, mm	0.15	Initial pressure in gas plenum, bar	1.4
Gas plenum volume, mm^3	39.10	Cladding material	15-15Ti
Cladding material density, kg/m^3	8074	Cladding inner surface roughness, mm	0.003
Fission gas release fraction	0.90	Fuel swelling rate, % per MWd/kgHM	1.1
Clad swelling rate, % per MWd/kgHM	0.40		

1.2.1 Introduction of the TRACE code

The advanced system code TRACE (TRAC/RELAP Advanced Computational Engine) was developed by the United States Nuclear Regulatory Commission (US NRC), in order to perform simulations of real and postulated transients in pressurized and boiling water reactors. The code can also model a wide variety of thermal-hydraulic experiments in reduced-scale facilities [3]. Being a part of the FAST code system, the TRACE code is being extended and used at PSI for the thermal-hydraulic assessment of Generation IV fast reactor systems. In particular, the modifications include adding equations of state for new coolants and the corresponding heat transfer and friction models [4]. In the present work, TRACE was used for the steady-state and transient analysis of the ALFRED system.

1.2.2 TRACE model creation

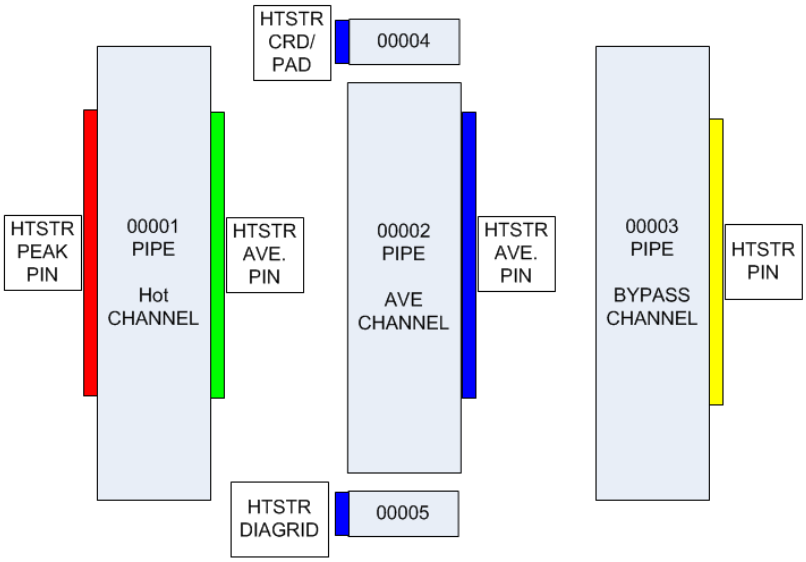


Fig. 1.2.1 TRACE model for the active zone of ALFRED

Heat structures, representing peak and average pins in both the hottest assembly and average assemblies, were attached on hot and average coolant channels as shown in Fig. 1.2.1. The full model for core primary, secondary and DHR systems are shown in Fig. 1.2.2.

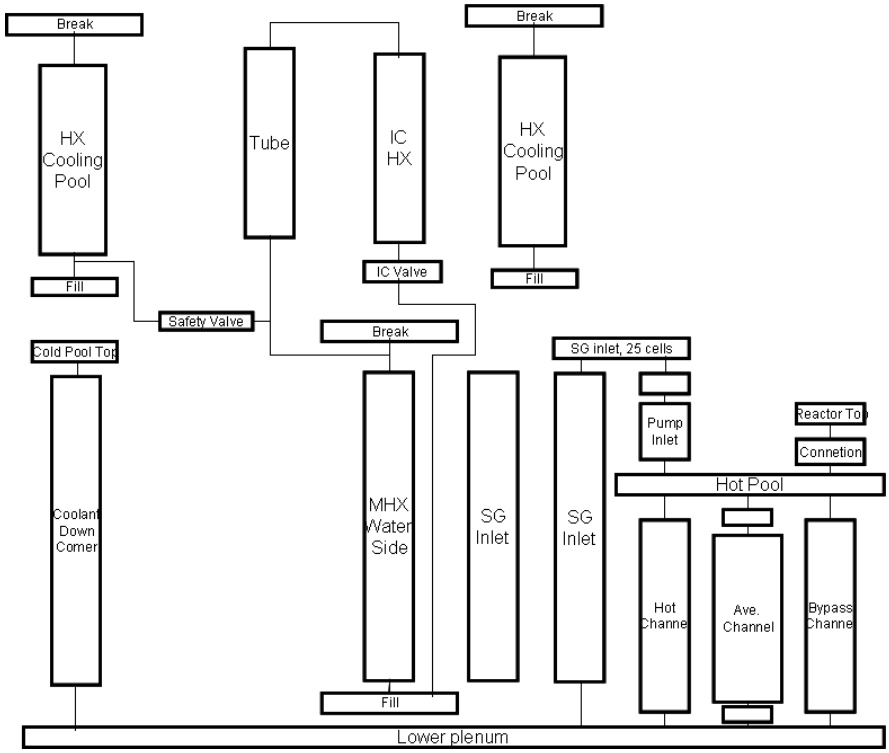


Fig. 1.2.2 TRACE model for the whole system of ALFRED

The point-kinetic model was applied to calculate power evolution with time during accidental situations.

The ANS-79 decay heat constants were used for decay heat production calculation and delayed neutron parameters were listed in Table 1.2.1. The prompt neutron lifetime is 0.0867 second.

Table 1.2.1 Delayed neutron specifications

Time group number	β-effective	λ, 1/s
1	57.9000E-05	0.0283
2	21.8000E-05	0.0425
3	50.5000E-05	0.1330
4	106.500E-05	0.2925
5	38.5000E-05	0.6665
6	37.4000E-05	1.6348

2. Transient scenarios and simulation results for transients at EOC

2.1 UTOP

The Unprotected Transient over Power (UTOP) was defined to be initiated by a linearly introduction of 250 pcm positive reactivity within 10 seconds. During the whole accident, the SCRAM protection system fails to work. Meanwhile, the primary circulation pump, MHX and secondary circuit will work normally.

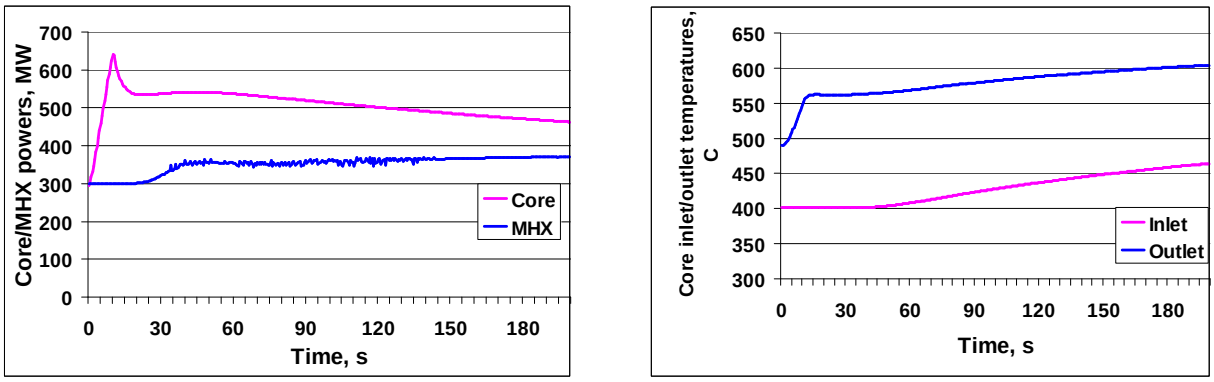


Fig. 2.1.1 Evolutions of core/SG powers (left) and core inlet/outlet temperature (right) with time

When 250 pcm positive reactivity starts to be introduced, core power begins increasing as shown in Fig. 2.1.1. After around 15 seconds, core power reaches its peak level, being equal to 642 MW (214% of the initial level). The fuel temperature increase due to power increase leads to negative reactivity feedback incurred by the Doppler Effect

as shown in Fig. 2.1.3. This significant negative reactivity feedback, together with negative reactivity feedbacks incurred by fuel axial expansion and pad/diagrid expansion, will be higher than the introduced positive reactivity feedback. This stabilizes core power at around 154% of its initial level after 200 seconds.

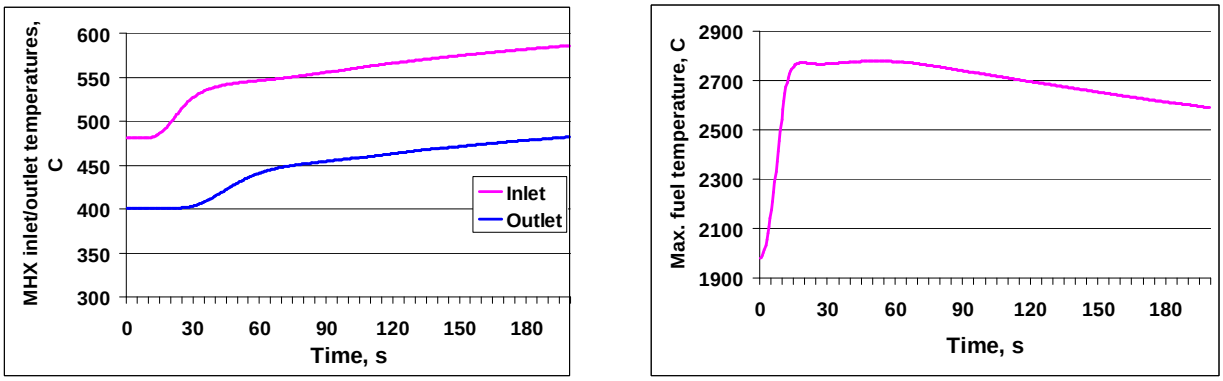


Fig. 2.1.2 Evolutions of SG inlet/outlet temperatures (left) and the maximum fuel temperature (right) with time

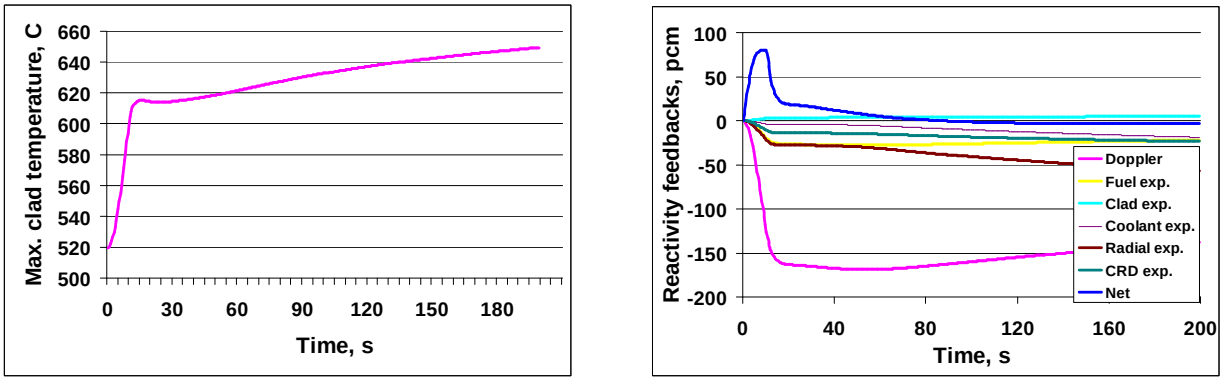


Fig. 2.1.3 Evolutions of the maximum clad temperature (left) and reactivity feedbacks (right) with time

Around 12 seconds into the UTOP transient, the power of SG also increases and eventually stabilizes at around 370 MW, which is equal to 123% of its initial level. As shown in Fig 2.1.1, 2.1.2 and 2.1.3, the coolant temperatures at core inlet/outlet, SG inlet/outlet, and maximum clad temperature will continuously increase after 200 seconds into the transient, since heat removing capability provided by MHX is obviously lower than that of the reactor core. However, thanks to negative reactivity feedbacks, the net reactivity become slightly negative around 100 seconds into the transient, which leads to the slow reduction of the maximum fuel temperature as shown in Fig. 2.1.2. And it can be noticed that the maximum fuel temperature in the hottest pin that can be achieved during UTOP is around 2770 ^{o}C, which is still much lower than the working limit of MOX fuel.

2.2 ULOF

The Unprotected Loss of Flow (ULOF) accident was initiated by the drop of primary pump head with the halving time of 0.56 second. During the whole ULOF transient, the SCRAM protection system fails to work, but the MHX and secondary circuit of core work normally.

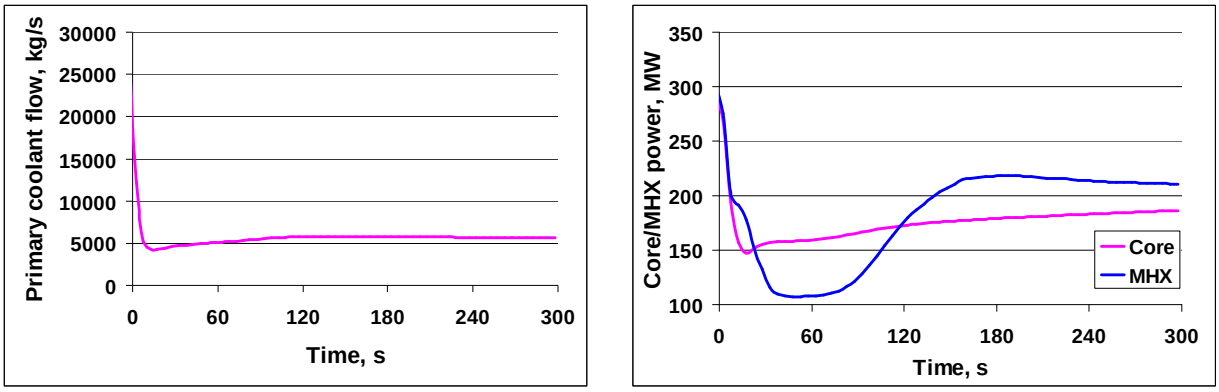


Fig. 2.2.1 Evolutions of primary coolant flowrate (left) and core/SG power (right) with time

As the primary coolant flowrate starts to decrease, the core power first has a small increase up to around 305 MW because of positive reactivity feedback coolant temperature will increase due to less flowrate provided. Then, after the coolant temperature increase moves to the diagrid and pad, a big negative reactivity feedback incurred by the radial expansion of diagrid and pad will be generated as shown in Fig. 2.2.3. This negative feedback, together with other negative reactivity responses incurred by fuel axial expansion and the Doppler Effect, may take over the positive reactivity feedback caused by coolant density decrease, which leads to the reduction of core power, as well as coolant temperatures and temperatures of fuel and clad.

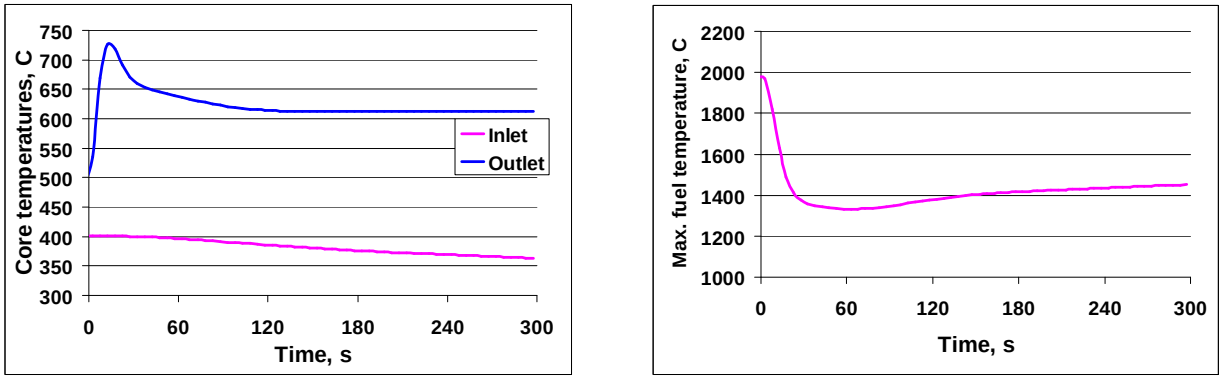


Fig. 2.2.2 Evolutions of core inlet/outlet temperature (left) and the maximum fuel temperature (right) with time

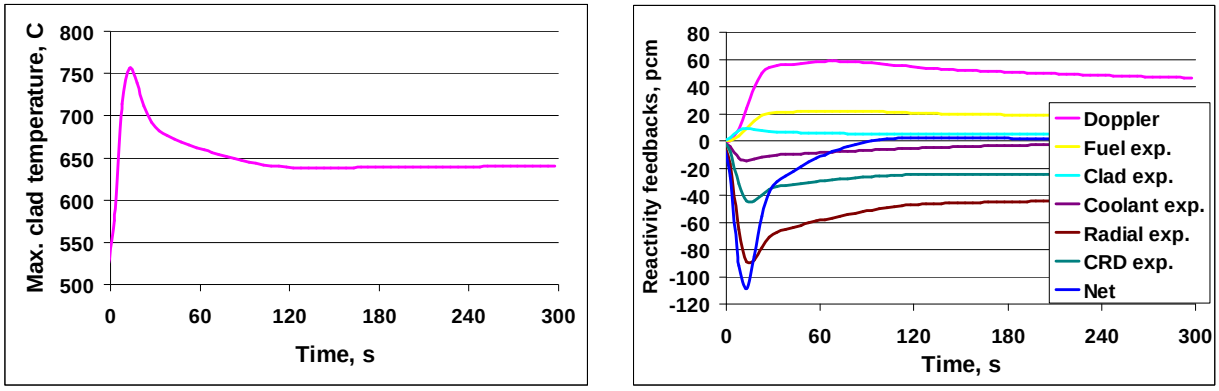


Fig. 2.2.3 Evolutions of the maximum clad temperature (left) and reactivity feedback (right) with time

The maximum temperatures of fuel and clad will decrease slowly because of the higher SG power comparing to the core power after around 120 seconds. The highest temperatures that can be achieved by fuel and clad of the peak fuel pin during ULOF are 1977 ^{o}C and 756 ^{o}C respectively, which are certainly lower than their own working limits.

2.3 ULOHS

The Unprotected Loss of Heat Sink (ULOHS) transient initiates from a total loss of feedwater flow into the secondary side of SG, leaving one DHR working to remove heat from core. One DHR is able to provide a maximum 7 MW heat removal capability.

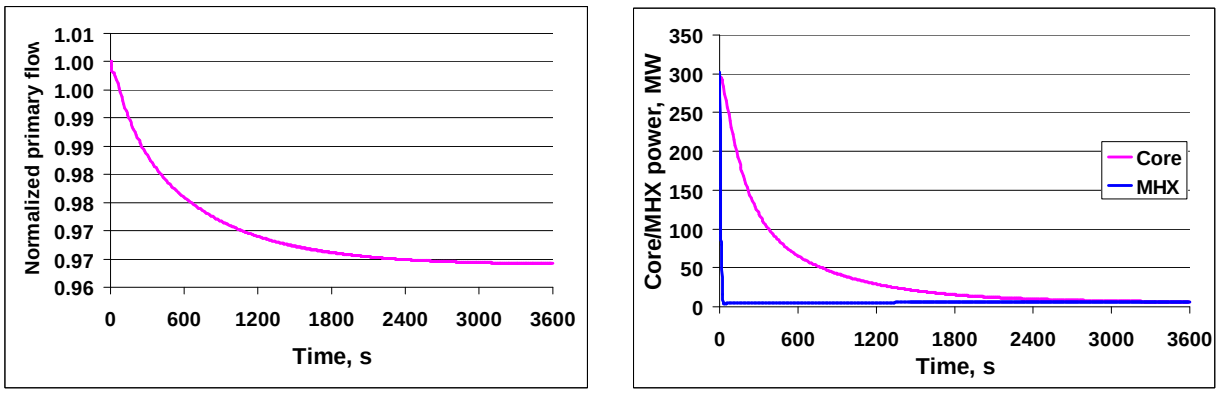
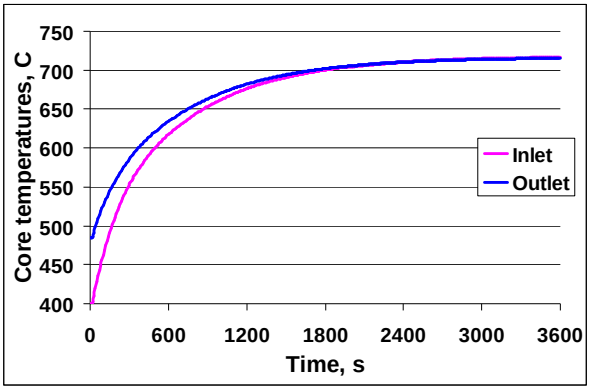


Fig. 2.3.1 Primary coolant flow (left) and core/SG power (right) evolutions with time

When SG power was suddenly removed, both core inlet and outlet temperatures start to increase significantly as shown in Fig. 2.3.2, leading to negative reactivity feedback incurred by radial expansions of pad and diagrid as can be noticed from Fig. 2.3.3. This negative feedback is higher than the positive one mainly caused by the coolant density decrease. This leads to core power reduction and fuel temperature decrease.



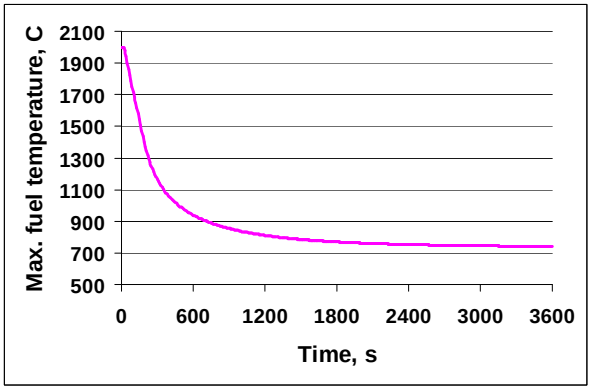
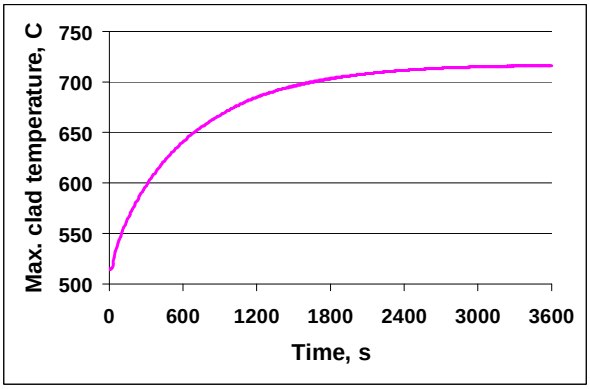


Fig. 2.3.2 Evolutions of core inlet/outlet coolant temperatures (left) and the maximum fuel temperature (right) with time



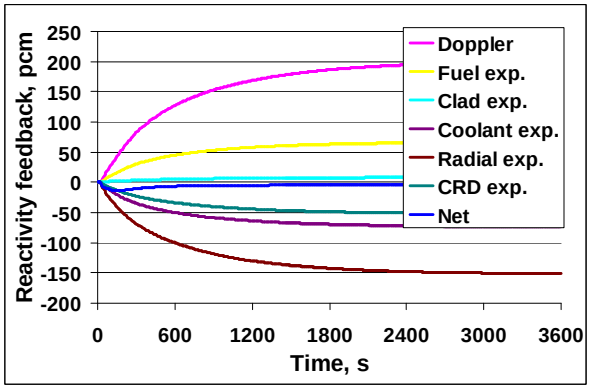


Fig. 2.3.3 Evolutions of the maximum cad temperature (left) and reactivity feedback (right) with time

After 3000 seconds, the whole primary system becomes stabilized. The asymptotic fuel and clad temperatures at the hottest spot are 742 ^{o}C and 716 ^{o}C respectively, which are well below their own working limits.

2.4 PLOOP (TD-3)

The Protected Loss of Off-site Power transient was initiated by the loss of secondary feedwater. When reactor scram criteria were met, trip signal will be generated and core will be shut down after 1.0 seconds delay as a protection action. At the same time, steam turbines and primary pumps were also tripped. Simulation results for short-term and long-term time scales will be discussed.

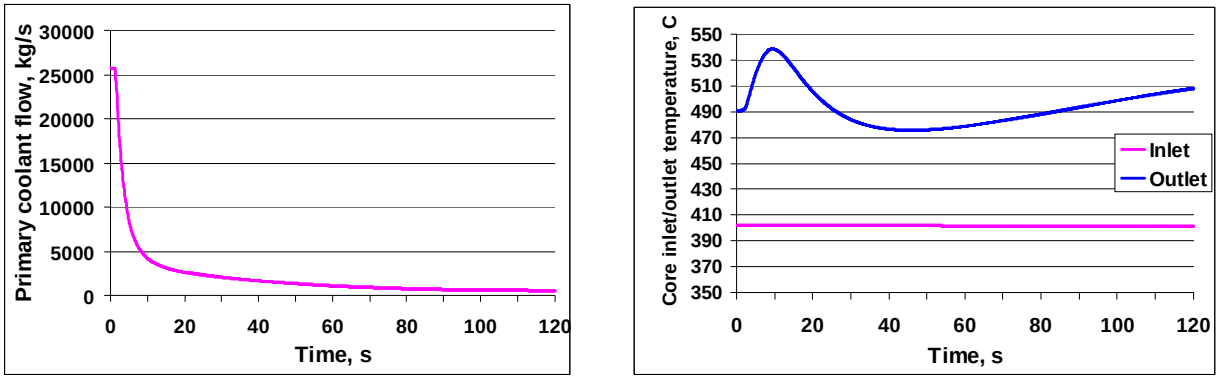


Fig. 2.4.1 Evolutions of primary coolant flow (left) and the maximum clad temperature (right) in short-term time scale

When the feedwater and primary pump head start to be removed, a significant increase of coolant temperature at core outlet would be expected as shown in Fig. 2.4.1. At the same time, 1$ negative reactivity was introduced to shut down the reactor, leading to coolant temperature drop, as well as decreasing of clad and fuel temperatures. Later, since the core decay power decreases slower than the primary coolant flow from 20 seconds into the transient as shown in Fig. 2.4.2, the primary coolant will be heated up again.

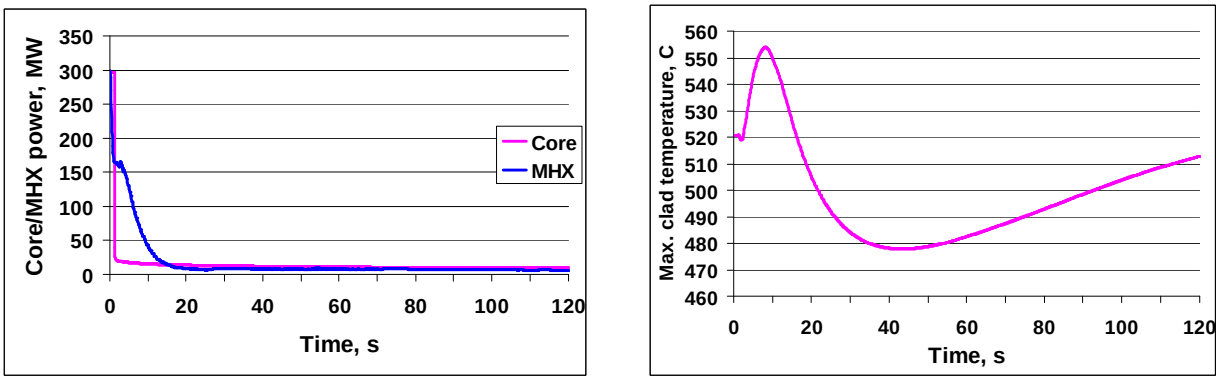


Fig. 2.4.2 Evolutions of core/MHX power (left) and the maximum clad temperature (right) in short-term time scale

With the drop of fuel and clad temperatures, significant positive reactivity response mainly incurred by the Doppler Effect and fuel axial shrinkage were generated as shown in Fig. 2.4.4. However, these positive reactivity responses are still much smaller than the negative reactivity that was introduced for reactor SCRAM. Hence, core power will keep decaying with time, leading to further reduction of fuel, clad and coolant temperatures, as shown in Fig. 2.4.3 and 2.4.4.

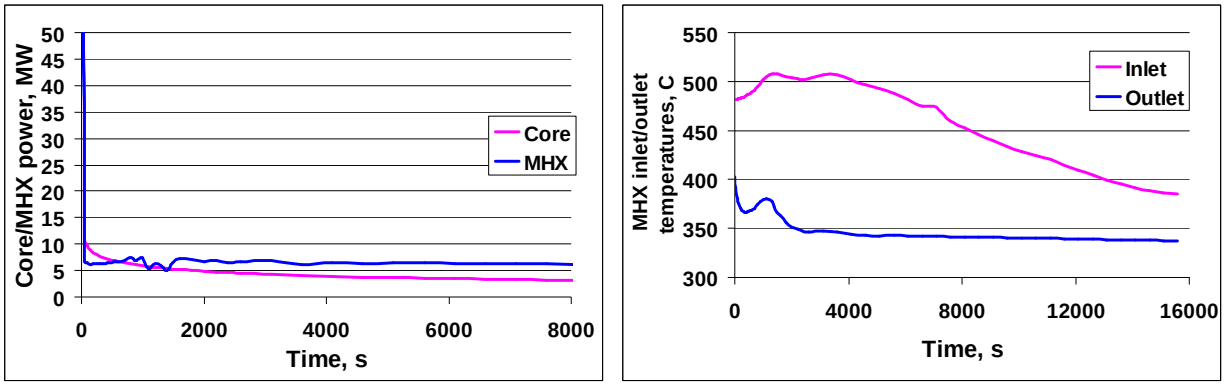


Fig. 2.4.3 Evolutions of core/MHX powers (left) and MHX inlet/outlet temperatures in long-term time scale

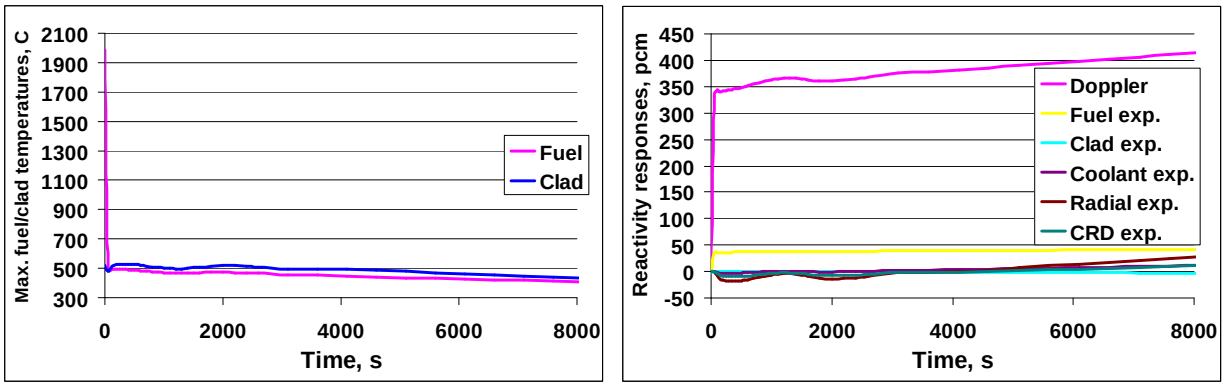


Fig. 2.4.4 Evolutions of maximum fuel/clad temperatures (left) and reactivity responses in long-term time scale

With the reductions of core power and MHX power, temperature difference between core inlet and outlet, as well as temperature difference between MHX outlet and inlet, will decrease as shown in Fig. 2.4.3. Coolant temperature at MHX outlet, being considered to be the lowest one in the primary system, will approach the freezing point of liquid Pb after 16000 seconds into the transient.

The maximum fuel and clad temperatures that could be achieved during the PLOOP transient is 1984 ^{o}C and 554 ^{o}C respectively, which are certainly lower than their corresponding working limits.

2.5 OVC

The Over Cooling (OVC) transient was initiated by the reduction of feedwater temperature from 335 °C to 300 °C within 1.0 second. When feedwater temperature

was lower than 327 °C, the SCRAM signal was triggered to shutdown the reactor with 1.0 second delay. Later, main steam lines and main feedwater lines in SG system was closed in 2.0 seconds. At the same time, condensate isolation valves will be fully opened, leading to DHR system functioning, which is able to provide 7.0 MW heat removal capability. The opening process of condensate isolation valves will take 20.0 seconds.

During the whole transient, safety valves will maintain the pressure in isolation condensers under 195 bar and temperature of liquid water leaving isolation condensers will be kept at 300 °C.

Simulation results of the OVC transient were discussed for both short-term and long-term time scales.

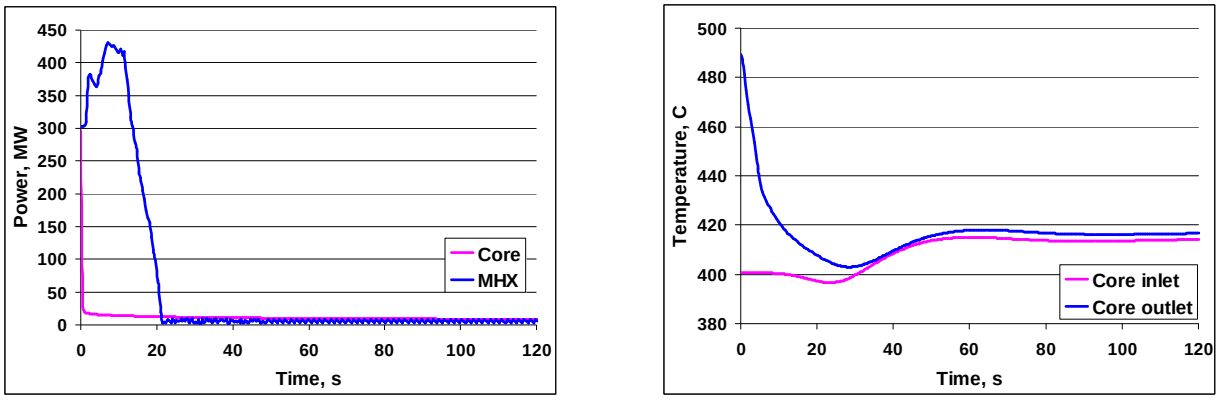


Fig. 2.5.1 Evolutions of core/SG powers (left) and core inlet/outlet coolant temperature (right) in short-term time scale

When condensate isolation valves start to open, liquid water stored in isolation condensers will flow into steam lines and evaporate instantly, leading to a significant increase of MHX power up to 140% of its rated level. Thereafter, MHX power will continuously decrease with core power, but is still sufficient to reduce the temperature difference between core outlet and core inlet, until only negligible temperature difference between core inlet and outlet was left as shown in Fig. 2.5.1.

As a design basis, the rated power of one DHR system is 7 MW, which will be higher than core power after 900 seconds decay. Hence, primary coolant temperature may decreases slowly as shown in Fig. 2.5.2. After around 14000 seconds, the lowest

coolant temperature in the primary circuit (at the MHX outlet) will be lower than the freezing point of liquid lead (~ 327 °C).

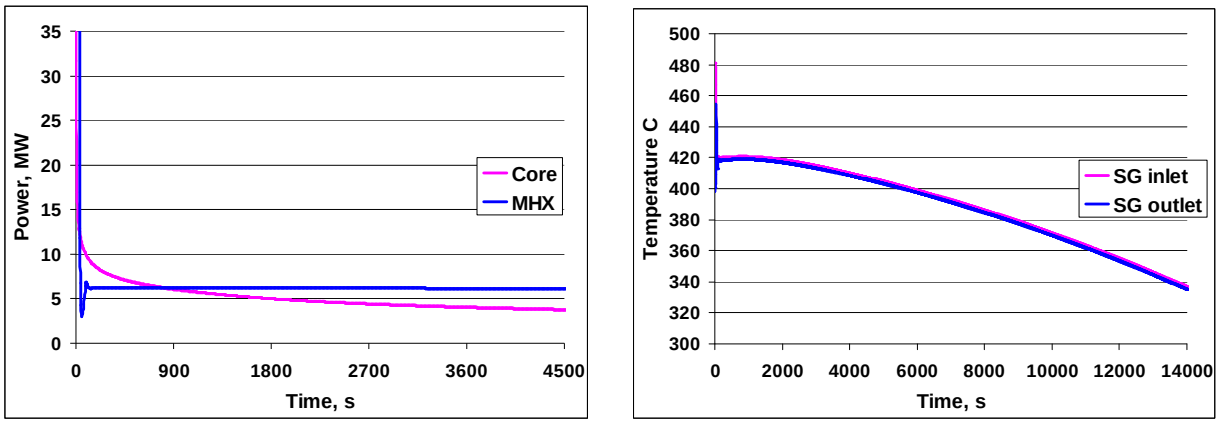


Fig. 2.5.2 Evolutions of core/SG powers (left) and core inlet/outlet coolant temperature (right) in long-term time scale

2.6 SLB

The Steam Line Break (SLB) transient was initiated by a depressurization of steam pipes in SG. In this report, we studied the case with the depressurization of all 8 SG units. During the depressurization of SG, feedwater flowrate and temperature will also change. When the steam pressure in the secondary system is lower than 160 bar, reactor trip signal will be generated and core will be shut down by inserting -1.0 $ reactivity. The secondary system will be switched to DHR mode as described for the OVC transient.

Simulation results of the SLB transient were shown in short-term and long-term time scales.

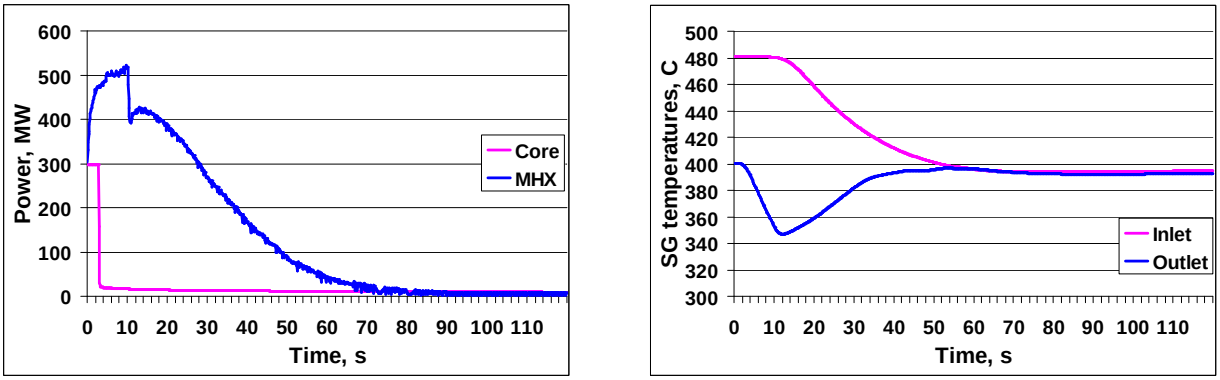


Fig. 2.6.1 Evolutions of core/SG powers (left) and SG inlet/outlet coolant temperature (right) in short-term time scale

Similar to what happened during OVC transient, the SG power will significantly increase at the beginning of the SLB transient mainly due to water evaporation in SG pipes, which leads to a jump of secondary flowrate and therefore heat removing in SG as shown in Fig. 2.6.1. Together with core SCRAM, this jump of heat removing capability leads to the reduction of coolant temperatures at core inlet and outlet. However, switching MHX to DHR mode leads to the reduction of secondary coolant mass flowrate, and thus the heat removing capability of MHX as shown in Fig. 2.6.1.

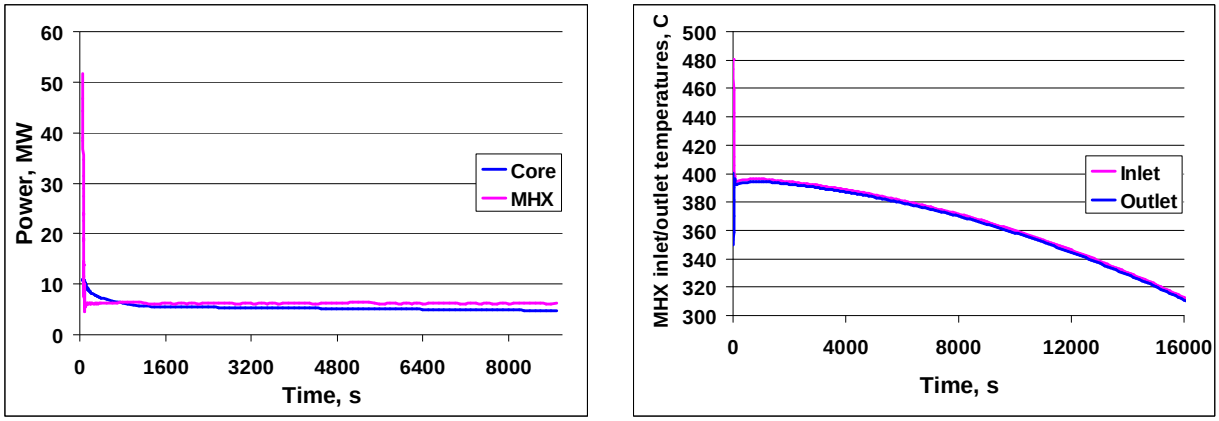


Fig. 2.6.2 Evolutions of core/SG powers (left) and SG inlet/outlet coolant temperature (right) in long-term time scale

As can be noticed from Fig. 2.6.2, the MHX power will oscillate at a level of around 7 MW after around 700 seconds into transient. Meanwhile, core decay power will keep decreasing. This causes a slow decrease of the primary coolant temperature as shown in Fig. 2.6.2. After around 14500 seconds, the lowest coolant temperature in the primary system will be lower than the freezing point of liquid Pb.

2.7 Withdrawal of the most reactive control rod (TR-2)

The TR-2 transient was initiated by an unpredicted withdrawal of the most valuable control rod, leading to a maximum 250 pcm positive reactivity insertion with the ramp rate of 0.15 pcm/s. After 606 seconds into the transient, coolant temperature at the MHX outlet becomes higher than 430 °C, which generates the SCRAM signal as a protection action. Reactor core is then shut down after 1.0 second delay.

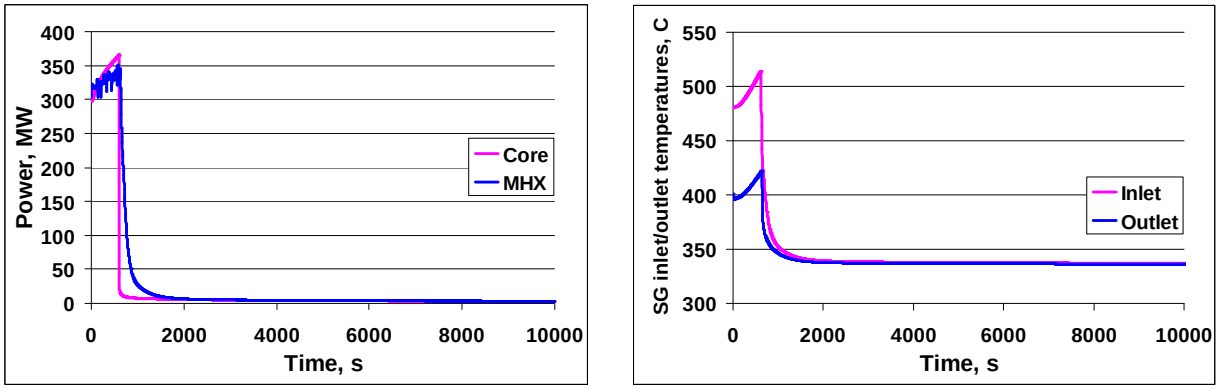


Fig. 2.7.1 Evolutions of core/MHX powers (left)
and SG inlet/outlet coolant temperature (right)

As can be noticed from Fig. 2.7.1, both core and MHX power will first increase until core SCRAM signal was generated. After core was tripped, core power will drop down to decay power level instantly, which leads to a fast drop of fuel, structure and coolant temperatures. The significant drop of fuel temperature leads to a big positive reactivity feedback caused by the Doppler Effect as shown in Fig. 2.7.2. After around 13000 seconds into the transient, coolant temperature will still be higher than 330 °C.

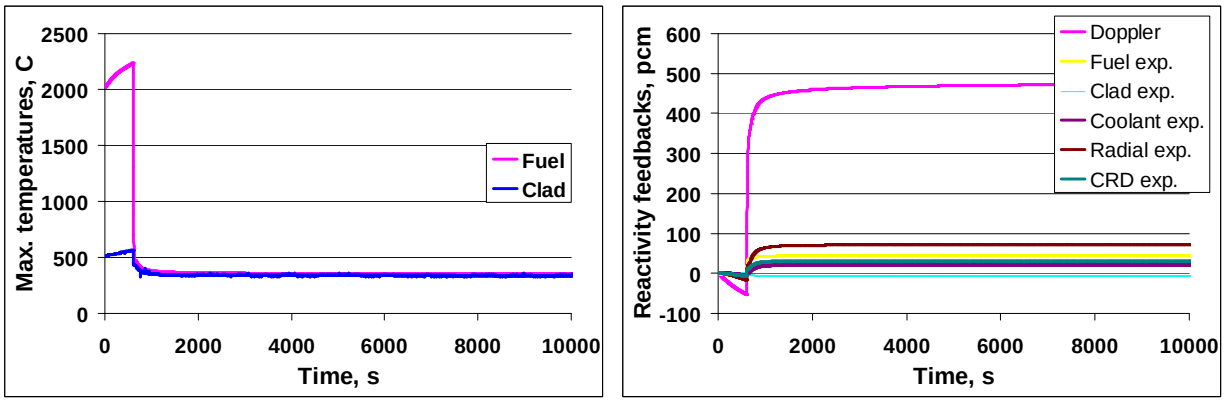


Fig. 2.7.2 Evolutions of Max. fuel/clad temperatures (left)
and reactivity feedbacks (right)

During the whole transient, working limits of fuel, cladding material and coolant will not be met.

2.8 FA loading error (TR-3)

The fuel assembly loading error accident, when reactor is at hot zero power state, was considered to cause 100 pcm positive reactivity introduction. In the TRACE simulation model, the hot zero power state was modeled by reducing the core power to 5.0 MW, which is considered to be the decay power level, and then let the core stabilize by 5000 seconds. Simulation for the fuel loading error transient will start from this status.

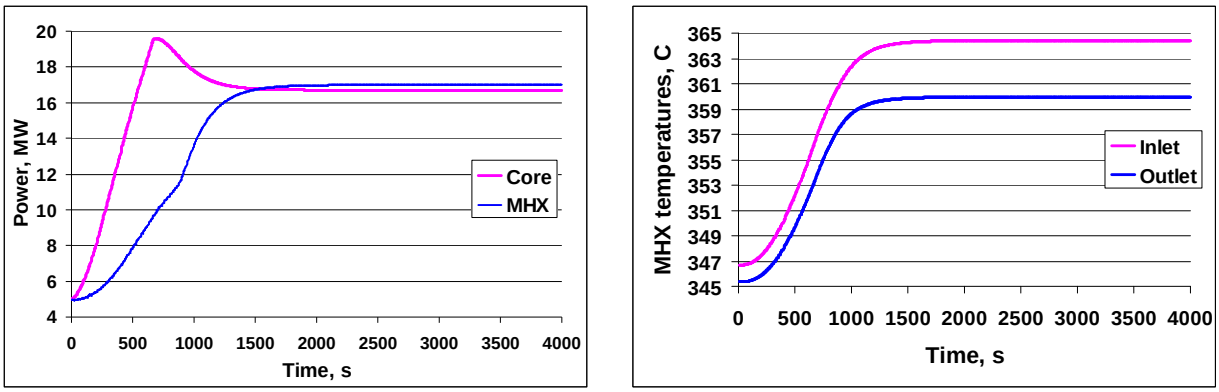


Fig. 2.8.1 Evolutions of core/MHX powers (left)
and SG inlet/outlet coolant temperature (right)

When the positive reactivity was introduced, core power started to increase, leading to the increase of coolant temperatures as can be noticed from Fig. 2.8.1. After approximate 700 seconds into the transient, negative reactivity feedbacks may take over the introduced positive reactivity, which stabilized core power at 17 MW. Since SG power increased slower than core power, coolant temperature at SG outlet (core inlet) may also increase. With the increase of MHX power, temperature difference between SG inlet and outlet will also increase.

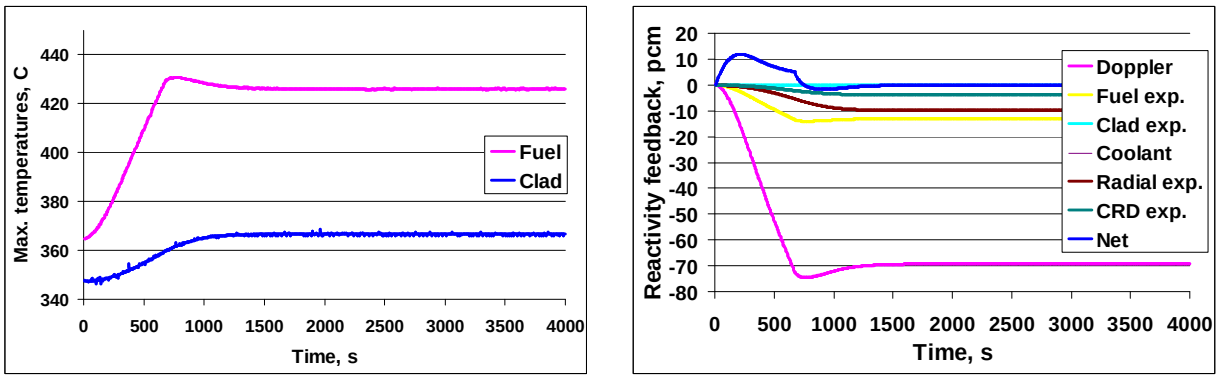


Fig. 2.8.2 Evolutions of Max. fuel/clad temperatures (left)
and reactivity feedbacks (right)

During the whole transient, reactor SCRAM will not be triggered, since the trip criteria were not met. The maximum temperatures of fuel, clad and coolant are far below their respective working limits.

3. Conclusion

For all postulated transients, the maximum fuel temperature that can be achieved is at least 200 °C lower than the solidus temperature of MOX fuel with 30% Pu content [5]. The maximum cladding temperature is more than 300 °C lower than its creep rupture limit. Liquid Pb boiling will therefore not be an issue.

However, during DBC transients with protection actions, coolant temperature will continuously decrease with core power decay. Hence, coolant freezing may happen. During the OVC transient, the shortest time (~14000 seconds) is needed for liquid Pb coolant in the primary system to reach its freezing point.

References:

1. Petr Petkevich, Doctoral Thesis "Development and Application of an Advanced Fuel Model for the Safety Analysis of the Generation IV Gas-cooled Fast Reactor", 2008.

2. Lead-cooled European Advanced Demonstrator Reactor, Plant Data for the Safety Analysis of the ETDR (ALFRED), Grant agreement no. FP7-249668.

3. Division of Safety Analysis, Office of Nuclear Regulatory Research, U. S. Nuclear Regulatory Commission, "TRACE V5.435 Theory Manual", DC 20555-0001.

4. Konstantin Mikityuk, Sandro Pelloni, Paul Coddington, Evaldas Bubelis, Rakesh Chawla, "FAST: An advanced code system for fast reactor transient analysis", Annals of Nuclear Energy 32 (2005) 1613–1631.

5. Edwards, J. et al., 1990. Fast Reactor Data Manual. Fast Reactor European Collaboration Report.

APPENDIX D

JRC-IET Contribution to LEADER Deliverable DEL022:

a) Preliminary analyses of sub-assembly blockages with the SIMMER-III code, and b) Development of a thermal-hydraulic model for DEC transient analysis of the ALFRED design using the system code TRACE

(Pag. 229)

Preliminary analyses of sub-assembly blockages with the SIMMER-III code

Contribution to Deliverable DEL022 of the LEADER FP7 collaborative project

Kamil Tuček and Alain Flores y Flores
European Commission, Joint Research Centre, Institute for Energy and Transport,
Westerduinweg 3, NL-1755 LE Petten, the Netherlands

1 Introduction

The FERMI-1 experience [1] as well as experimental evidence gathered, in particular in MOL7C and SCARABEE program experiments [2,3], suggest that sub-assembly (SA) blockages might be a viable precursor to severe core damage.

Key questions are therefore to evaluate:

- grace period to fuel damage following the blockage of a sub-assembly and the corresponding viability for the detection of the blockage;
- potential for the failure propagation from the blocked SA to the neighbouring SAs, which could be a precursor to a large severe core damage;
- related phenomena, particularly what concerns the behaviour and transport of fuel chunks in the heavy liquid metal coolant (which are of similar density) and could pose a specific challenge to the integrity of confinement barriers (in particular in the steam generator).

Specifically, for **Phénix SFR**, Total Instantaneous Blockages (TIBs) were considered as a beyond design basis event. It has been concluded that in the case of a TIB, the temperature measurement at the SA outlet is not effective to quickly shut-down the reactor and to prevent fuel melting in the blocked SA. This was predicted to occur in a few seconds from the initiation of the transient [4].

The reactor was expected to undergo an emergency shut-down by other signals (e.g., by the detection of fission products or delayed neutrons from ruptured fuel pins or reactivity/power changes) and as such the damage propagation and fuel melting was predicted to be limited to the six sub-assemblies neighbouring the blocked one.

It was also shown that the configuration of molten materials remains sub-critical and coolable.

For **ALFRED LFR**, the instantaneous blockage of the fuel sub-assembly is to be prevented by the design through the adoption of multiple openings at the inlet to the sub-assembly (Fig. 1).



Fig. 1. Schematic drawing of the ALFRED fuel sub-assembly spike.

However, solid particles could be formed in the coolant in the presence of oxygen, hydrogen or other impurities, which could result in circuit fouling and slagging leading to a possible reduction of the coolant flow cross section as a consequence (specifically at the location of the pin grid), potentially causing coolant flow blockages.

In particular for lead- and LBE-cooled reactors, the coolant blockage could be caused by an excessive amount of lead oxides (e.g., PbO) and other impurities in lead.

In fact, an accident occurred in the USSR LBE-cooled submarine reactor during reactor operation in 1968. In this case, impurities (mainly oxides) were accumulated in the circuit resulting in an abrupt deterioration of heat removal in the core, causing a partial core meltdown [5].

Consequently, the unprotected partial blockages in the hottest fuel sub-assembly are considered as a Design Extension Condition (TDEC-5). Moreover, as a Design Extension Condition, protected blockages of nearly entire internal coolant flow cross-section of the hottest fuel sub-assembly were investigated as well. The goal of our studies was to determine consequences of both of these blockage conditions as well as the acceptable degree of the coolant flow blockage that can be accommodated by the ALFRED design. In the protected case, the acceptable delay of the reactor scram from the detection of the SA blockage was also investigated.

2 Method

2.1 Model

A 2D geometrical model, representing the central blocked sub-assembly as well as the surrounding ring of six sub-assemblies, has been set-up for the purpose of our analyses. The geometrical parameters of the ALFRED sub-assembly and fuel pin are recounted in Tables 1 & 2 and Fig. 2 [6].

Table 1. Sub-assembly geometry parameters for the ALFRED core [6].

Parameter	Value
Sub-assembly	
Number of pins per sub-assembly (SA)	127
SA outer flat-to-flat [m]	1.660E-01
SA unit cell (with inter-wrapper space) [m]	1.710E-01
SA inner flat-to-flat [m]	1.580E-01
SA outer flat-to-flat [m]	1.660E-01
Gap between SA's [m]	5.000E-03
Wrapper thickness [m]	4.000E-03
Fuel pin	
Fuel pin diameter [m]	1.050E-02
Fuel pin pitch [m]	1.386E-02
Pin pitch over diameter	1.320
Clad	
Clad thickness [m]	6.000E-04
Clad inner diameter [m]	9.300E-03
Clad outer diameter [m]	1.050E-02
Pellet	
Pellet-gap [m]	1.500E-04
Pellet diameter [m]	9.000E-03
Pellet hole diameter [m]	2.000E-03

Table 2. Fuel pin geometry parameters for the ALFRED core [6].

Parameter	Value [m]
Upper core plenum height	1.200E-01
Upper axial insulator	1.000E-02
Active core height	6.000E-01
Lower axial insulator	1.000E-02
Lower core plenum height	5.500E-01

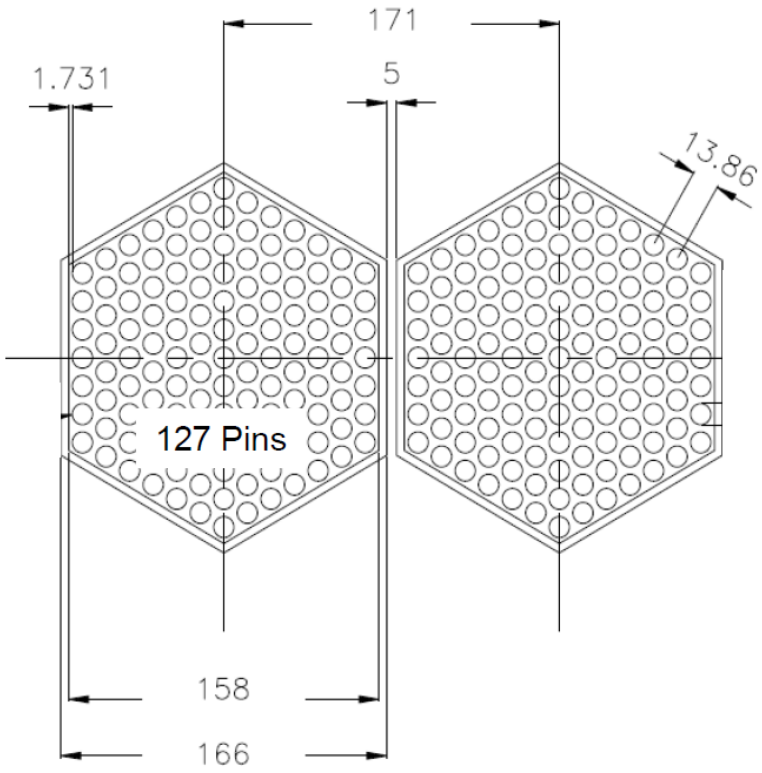


Fig. 2. Cross-section of the ALFRED fuel sub-assembly [6].

In the axial direction, the model (cf. Fig. 3) represents the fuel sub-assembly geometry with the corresponding inlet and outlet coolant pools. The following regions are explicitly modelled: lower part pool (cells 1-4, total length 1.4 m), SA input section (cells 5-6, length 0.51 m), lower coolant plenum (cells 7-8, length 0.55 m), pin grid plate (cell 9, length 5 cm), pin bottom plug (cell 10, length 2 cm), lower gas plenum (cells 11-13, length 0.55 m), lower axial insulator (cell 14, length 10 cm), core (cells 15-24, length 0.6 m), upper axial insulator (cell 25, length 1 cm), upper gas plenum (cell 26, length 12 cm), pin top plug (cell 27, length 6.84 cm), upper coolant plenum (cell 28, length 0.3 m), SA head (cell 29, length 0.32 m), and upper part pool (cells 30-33, length 1.4 m).

In the radial direction, the model consists of seven internal rings representing the central fuel sub-assembly, where the blockage is introduced (cells 1-7), an inter-wrapper gap (cell 8), additional seven outer rings representing the six neighbouring fuel sub-assemblies (cells 9-15), an additional inter-wrapper gap (cell 16), and the external channel (cell 17). The six neighbouring SAs are treated in a simplified manner and represented by seven equidistant-meshed rings along the apothem of the fuel sub-assembly.

The assumed power deposition corresponds to the peak power conditions at the Beginning-of-Cycle (BOC) with an axial power profile as depicted in Fig. 4.

The equivalent total thermal power in our model of seven sub-assemblies is 10.044 MW with the core inlet temperature being 673 K (400°C).

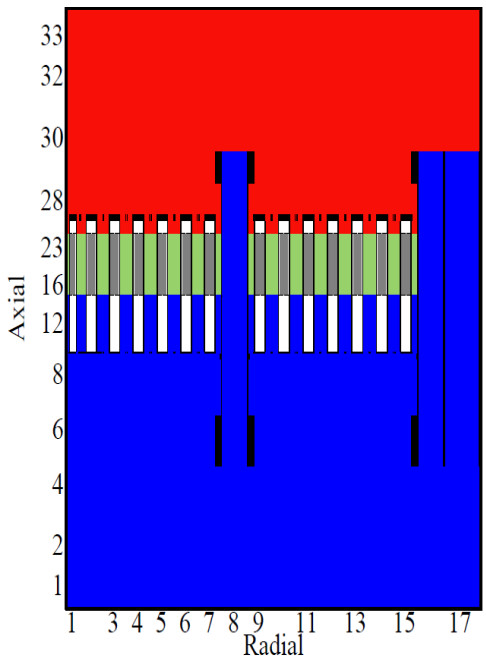


Fig. 3. R-z representation of the calculation mesh for the analyses of partial sub-assembly blockages in SIMMER-III.

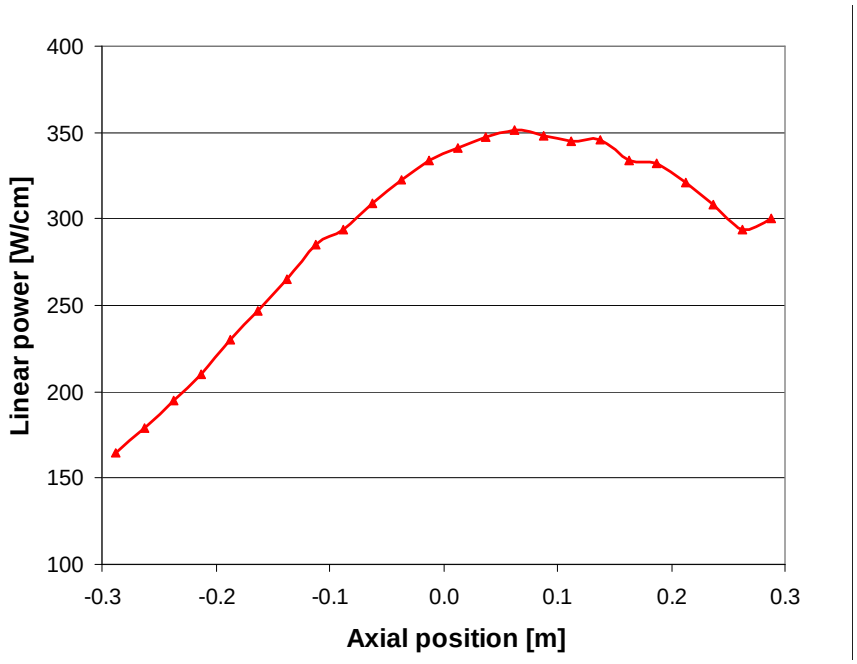


Fig. 4. Axial representation of the peak pin linear power at the Beginning-of-Cycle conditions.

2.2 Computational tool

Computational analyses were performed with the SIMMER-III (S_n Implicit Multi-field Multi-component Eulerian Recriticality) code, version 3.F [7].

The SIMMER-III code is a 2D multi-velocity field, multi-phase, multi-component, Eulerian fluid-dynamics code system capable of the integrated thermal-hydraulic, mechanics and structural modelling of fuel pins, wrappers and general structures with coupled space-time and energy-dependent neutron kinetics model. The core/pin structure model calculates the configuration and the time-dependent disintegration of fuel pins and sub-assembly wrappers. The neutronic part solves the time-dependent multi-group neutron transport equation with the improved quasi-static method. The flux shape calculations are based on TWODANT.

The current strength and uniqueness of SIMMER is its capability to analyse transient and expansion phases of severe accidents in fast reactors. In its present version, the code has also been successfully used as a system code to study design basis accidents and its capabilities are further being extended to encompass analysis of initiation phases of severe accidents as well.

In our present analyses, neutronic reactivity feedbacks (e.g., due to coolant voiding or Doppler) and the corresponding power change were not considered since the reactivity change corresponding to a single sub-assembly blockage is relatively small. Also, the applied "sub-channel" flow model is not conventional in SIMMER, but for our purposes it is deemed to be suitable for the modelling of sub-assembly blockages.

3 Results

3.1 Steady state

The steady state corresponding to peak power conditions was established with the coolant temperature gradient being 87 K and the corresponding pressure drop between the SA inlet and outlet predicted at 0.73 bar. The steady state conditions are typically established rather fast – within several seconds after the initiation of the simulation.

3.2 Coolant blockages

3.2.1 Unprotected cases

A parametric study of unprotected coolant blockages was performed assuming blockages ranging from 65% to 75% of the coolant flow cross-section. The blockages were introduced at the location of the pin grid in all internal sub-channels (axial cell no. 10). In our simulations, no radial coolant cross-flow has been assumed. The results of our analyses are summarised in Table 3.

Table 3. Results of analyses of the unprotected sub-assembly blockages.

Coolant flow area blockage [%]	Maximum predicted temperature [K(°C)]		Outlet coolant temperature [°C]	%ΔT*
	Cladding	Coolant		
65	804(531)	777(504)	493	7
70	817(544)	789(516)	497	11.5
75	833(560)	807(534)	505	20.7

*Taken into account the nominal inlet and outlet coolant temperatures of 400°C and 487°C, respectively.

As for the 65% coolant flow area blockage (cf. Fig. 5), the maximum predicted coolant temperature is 777 K (~504°C), while 804 K (~531°C) for the cladding. The SA coolant outlet temperature is 493°C, which corresponds to only a small increase with respect to the corresponding nominal value (487°C) and as such might not be detectable and would not be prevented by a reactor scram signal. However, also no systematic fuel pin damage is to be expected.

As for the 70% coolant flow cross-section blockage (cf. Fig. 6), the maximum predicted coolant temperature is 789 K (~516°C), while 817 K (~544°C) for the cladding. Hence, no systematic fuel pin damage is again to be expected. In this case, the predicted increase in SA outlet temperature is only 10 K and again this initiator might not be prevented by a reactor scram signal.

As a consequence of a blockage of 75% of the coolant flow area (cf. Fig. 7) the maximum coolant temperature of 807 K (~534°C) is predicted, while 833 K (~560°C) for the pin cladding. The estimated increase in the SA coolant outlet temperature is greater than 18 K representing more than 20% increase in the coolant temperature gradient compared to its nominal value (87 K), which is expected to trigger a reactor scram signal subsequently resulting in the shut-down of the reactor. However, since cladding temperatures are still well below the threshold for fast creep (~830°C [8]), no systematic damage is expected to the fuel pin cladding even if the blockages are not protected in the short time frame after the initiation of the accident (< 30 min).

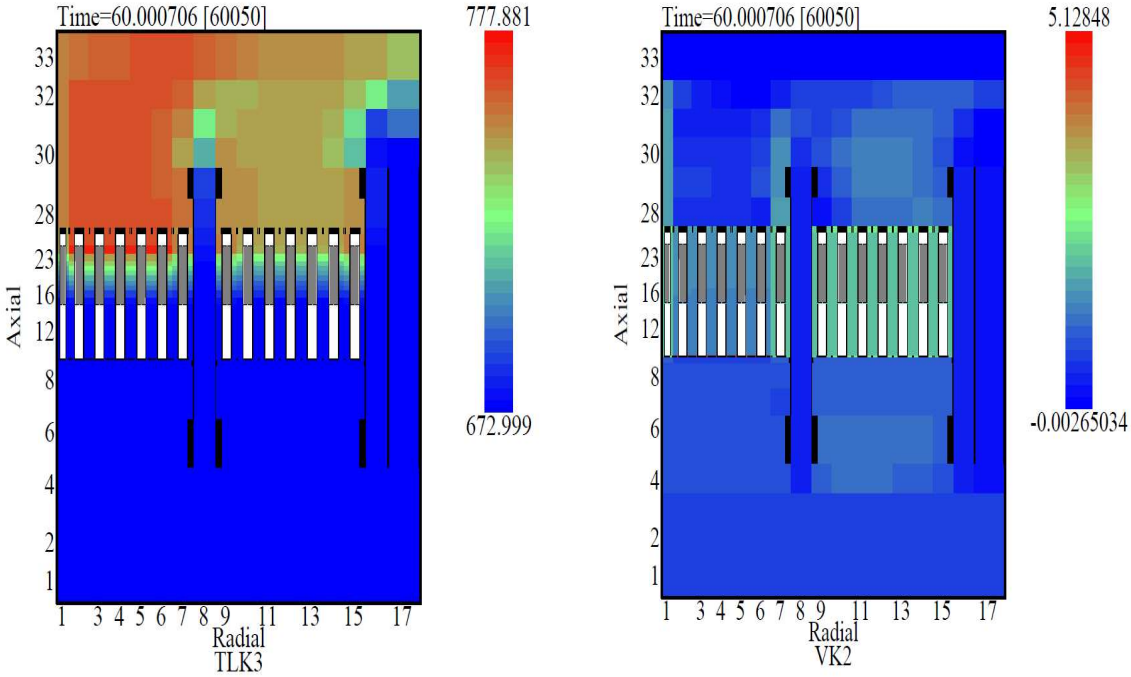


Fig. 5. Coolant temperature (left) and axial velocity distribution (right) corresponding to 65% coolant flow area blockage of all internal sub-channels.

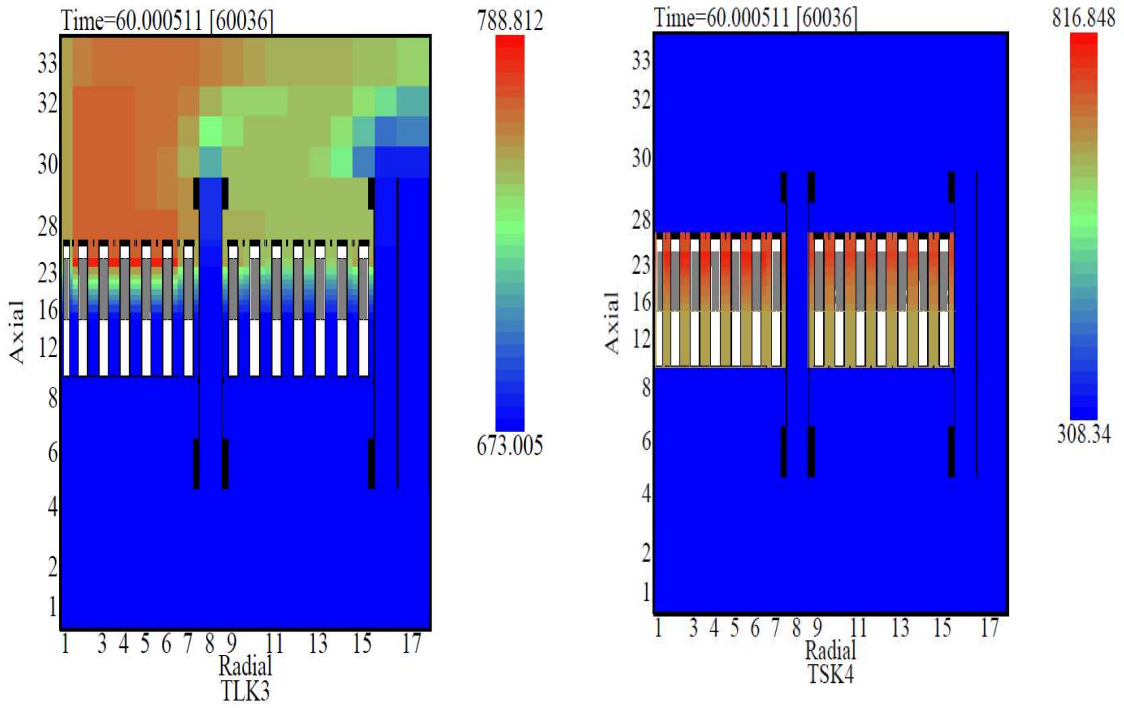


Fig. 6. Coolant temperature (left) and cladding temperature (right) distributions corresponding to 70% coolant flow area blockage of all internal sub-channels.

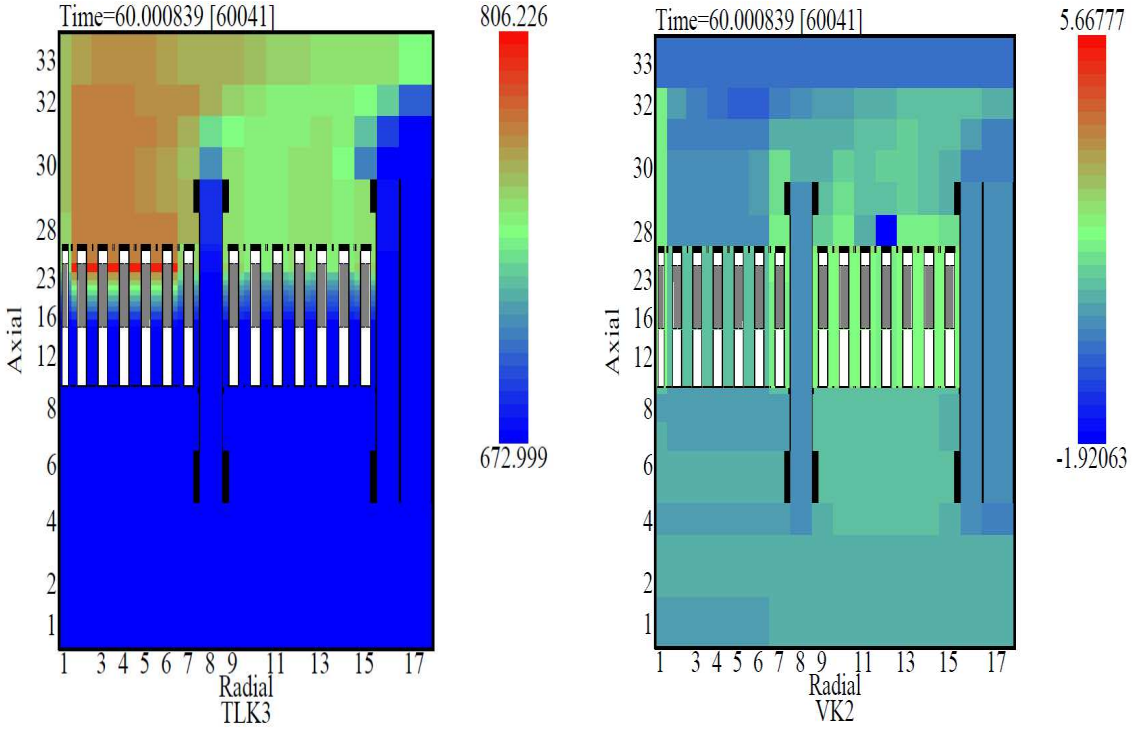


Fig. 7. Coolant temperature (left) and axial velocity distribution (right) corresponding to 75% coolant flow area blockage of all internal sub-channels.

3.2.2 Protected cases

The situation of nearly total blockages protected by the reactor scram signal was also considered in our analyses as a Design Extension Condition. The SA blockage was expected to be detected 5 seconds into the transient, well within the interval when SA coolant temperature gradient is expected to exceed 120% of its nominal value [9]. Subsequently, the delay of the reactor scram is parametrically assumed to occur 1, 2, 3, 5, and 10 seconds from the detection of the SA blockage. The corresponding reactor scrams therefore occur at 6, 7, 8, 10, and 15 seconds into the transient. Similarly to our analyses of the unprotected blockages, radial cross-flow has not been modelled in these cases. Decay heat was taken into account corresponding to the BOC conditions.

Our first results indicate that thanks to the high thermal inertia of lead, even if the shut-down is delayed by up to 5 seconds following the detection of the blockage, clad temperatures remain below the threshold for which clad ruptures initiated by fast creep would occur (~830°C [8]). On the other hand, our analyses also suggest that 10 second delay in reactor scram would likely result in systematic fuel pin clad failures possibly leading to severe core damage. In this case, preliminary indications are that residual coolant flow between 7-10% of the nominal value would be sufficient to remove the resulting decay heat such that a systematic clad damage can be effectively prevented. These qualitative conclusions are also supported by an analytical assessment of the heat balance in the modelled geometry.

It is important to note that in LFRs, in contrast to the phenomenology of SFRs, the clad ruptures and melting will occur well before a coherent coolant boiling is to be expected (T_{boil} = 1749°C at atmospheric pressure).

Conclusions

Model of seven sub-assemblies has been set-up to simulate sub-assembly blockages with the SIMMER-III code.

Our preliminary results indicate that unprotected coolant blockages of up to at least 75% of the flow cross section should be well accommodated by the ALFRED design as well as should be detectable. As for the protected transients, our results suggest that nearly total blockages could be well accommodated if the reactor is shutdown within 5 seconds from their detection (i.e., 10 seconds from the initiation of the transient). We note that for ALFRED, sudden and complete flow blockage is prevented by the SA design solution consisting of multiple inlet openings. Any other blockage caused by deposition of material will likely be gradual and can be monitored by detection of an increase of coolant outlet temperature of each SA.

However, the aforementioned qualitative conclusions would need to be confirmed by dedicated detailed analyses with the Computational Fluid Dynamics (CFD) codes. Also, the current analyses were performed in the BOC conditions and further studies are needed to investigate situations prototypical to End-of-Cycle (EOC) conditions with an adequate treatment of the generated decay heat. Moreover, in our SIMMER modelling, no radial cross flow has been assumed, for which further model improvements are necessary, including the set-up of an orifice coefficient in the cross flow direction.

Concerning the sub-assembly blockages in heavy liquid metal cooled systems in general terms, it needs to be considered that uncertainties exist in material properties at high temperatures and that knowledge of the phenomenology is still incomplete.

Specifically, in the hypothetical post-disruption phase, the question is whether fuel might

become mobilised fast enough to be effectively swept out of the core introducing a negative reactivity, which might reduce power such that the damage could be limited to the blocked SA or at least only the surrounding SAs. If not, this might be a viable precursor to severe core damage (if not protected), with possibly sizeable mechanical loads to be then adequately mitigated.

Simultaneously, conditions of the swept out fuel might need to be controlled such that any adverse impact on steam generators (or other structures) is acceptable, protecting thus the existing confinement barriers. In particular, measures might need to be implemented for the prevention & control of any possible re-criticalities and for achieving of the adequate cooling.

These aspects might require further theoretical as well as experimental investigations.

Acknowledgements

The current work was performed in the collaboration with Xue-Nong Chen and Andrei Rineiski from the Karlsruhe Institute of Technology, Institute for Nuclear and Energy Technologies (IKET).Their support with the modelling and the use of the SIMMER code is greatly acknowledged.

References

[1] Bertini, H. W., *"Descriptions of Selected Accidents that Have Occurred at Nuclear Reactor Facilities"*, Technical report ORNL/NSIC-176, Oak Ridge National Laboratory, 1980

[2] Schleisiek, K. et al., *"The Mol-7C In-Pile Local Blockage Experiments: Main Results, Conclusions, and Extrapolation to Reactor Conditions"*, Nuclear Science and Engineering, Vol. 128, No. 2, 1998

[3] Bailly, J. et al., *"The SCARABEE facility - Its main characteristics and the experimental program",* Nuclear Engineering and Design, Vol. 59, Issue 2, 1980

[4] Tuček, K. et al., "*Identification and Ranking of Safety Issues*", Deliverable D2.5, SARGEN_IV FP7 project, 2013

[5] Poplavsky, V.M. et al., *"Liquid Metal Coolants Technology for Fast Reactors",* Journal of Materials Science and Engineering B 1, pp. 913-928, 2011

[6] "*Plant Data for the Safety Analysis of the ETDR (ALFRED)"*, Technical report TEC058-2012, LEADER FP7 collaborative project, 2012

[7] Kondo, S. et al., *"SIMMER-III: An Advanced Computer Program for LMFBR Severe Accident Analysis"*, ANP'92, Tokyo, Japan, 1992

[8] Bubelis, E., *Personal communication*, 2013

[9] TD-8: *"Partial Flow Blockage in the Hottest Fuel Assembly (w/o radial Heat Transfer): SIM-LFR (KIT-G), Report on the results of analysis of DBC events for the ETDR (ALFRED)"*, DEL015-2013, LEADER FP7 collaborative project, 2013

Development of a thermal-hydraulic model for DEC transient analysis of the ALFRED design using the system code TRACE.

A. Lázaro, K. Tuček

European Commission, Joint Research Centre
Institute for Energy and Transport
Westerduinweg 3, 1755 LE, Petten, The Netherlands

1. INTRODUCTION

On the basis of technical specifications of the ALFRED design, a thermal-hydraulic model with point kinetic neutronic response model has been set up with the aim of performing preliminary assessment of the system response to selected initiating events in the Design Extension Conditions domain. As a first step, only essential parts of the design were specifically modelled. This model has been implemented in the TRACE code, upgraded with state-of-the-art thermal dynamic properties for pure lead provided by ENEA and ANSALDO experimental facilities.

The analyses form a contribution to the LEADER Deliverable DEL022.

2. CODE MODIFICATIONS

Concerning its applicability to heavy liquid metal modeling, the TRACE code is capable of performing analyses only using lead-bismuth eutectic (LBE) as a coolant in liquid state. Therefore, to perform detailed and more accurate assessments applicable to ALFRED LFR, equations of state for lead have been implemented into the TRACE source. These data are based on experiments and their evaluations carried out by ENEA-ANSALDO [1].

An exhaustive comparison of the main thermal properties was performed between the lead-bismuth correlations embedded in the TRACE source, the ones extracted from the abovementioned data, and the ones proposed in the OECD/NEA Handbook for lead and lead-bismuth eutectic [2]. Some physical quantities (as saturation temperatures and pressures) appeared to be nearly identical, so they were left unmodified. Others, for which remarkable differences had been observed, were substituted, namely: the internal energy and its derivative over temperature (Figure 1), the specific heat as a function of temperature (Figure 1), the density (Figure 2) and its derivative over temperature as a function of temperature. As there is no experimental data available for the thermal conductivity, a comparison was made between the correlations available in literature. Finally, the original correlation embedded in TRACE code was substituted by the Takamichi [1] to be consistent with other partners of the LEADER project. Figure 2 shows the comparison between the different correlations together with the relative difference between them.

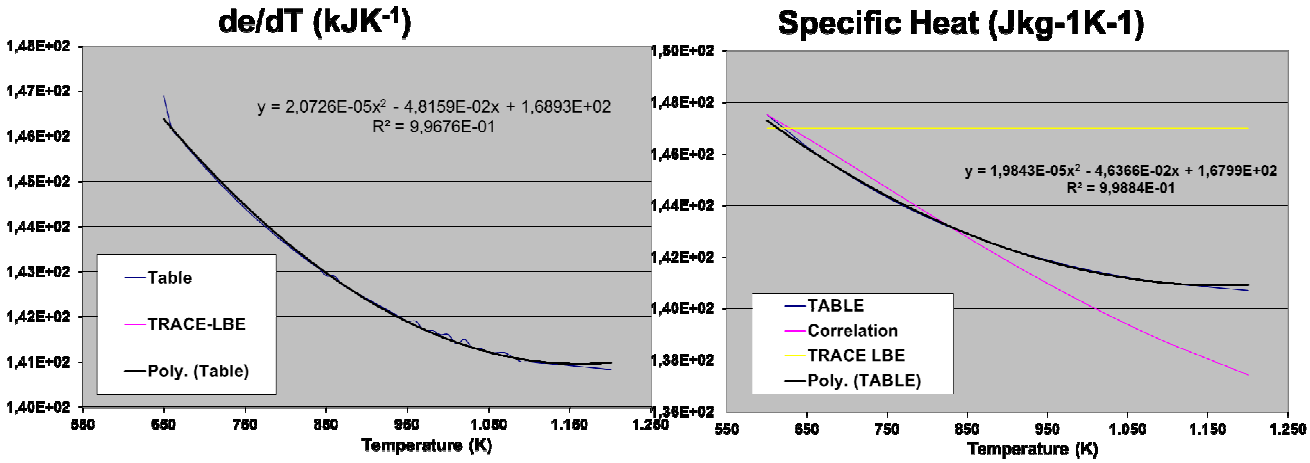


Figure 1: Left – Internal energy with displayed experimental data (blue) , the corresponding correlation (black) and in TRACE-LBE embedded correlation (magenta). Right – Specific Heat, with displayed experimental data (blue), the corresponding correlation (black), correlation given in the NEA Handbook (magenta), and in TRACE-LBE embedded correlation (yellow)

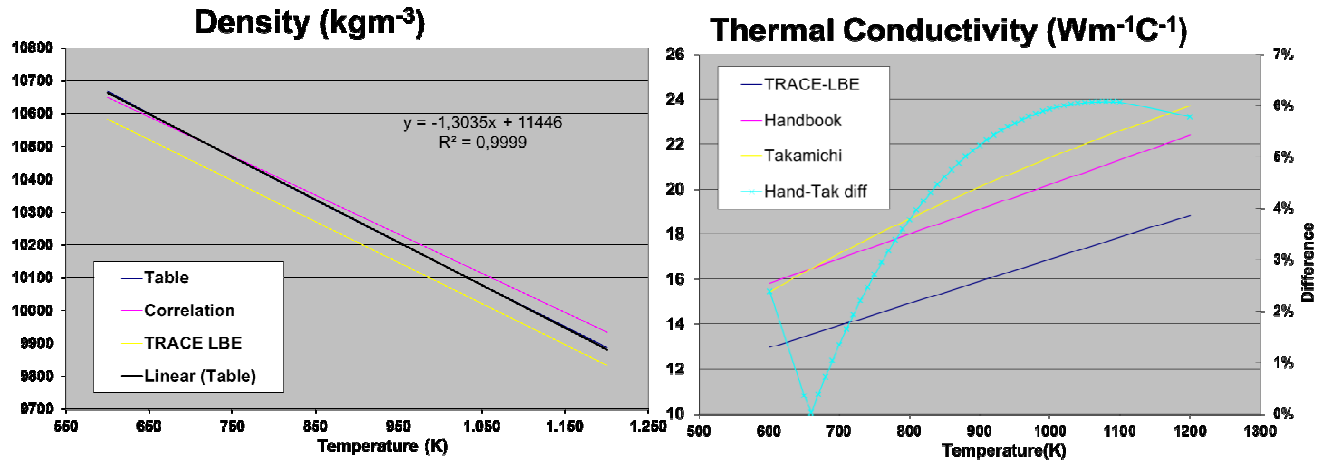


Figure 2: Left – Density - displayed are the experimental data (blue) and the corresponding correlation (black), correlation given in the NEA handbook (magenta) and in TRACE-LBE embedded correlation (yellow). Right – Thermal conductivity – displayed are in TRACE-LBE embedded correlation (blue), correlation given in the NEA handbook (magenta), the Takamichi correlation (yellow) and the relative difference between the two latter correlations.

3. MODELING

Following the technical specification of the ALFRED design [3], the main parts of the model are:

- Primary system. The primary system is composed of:

  - Three core components representing the hot fuel assembly, the average power assemblies and the core by-pass, respectively;
  - Two components representing the lower vessel parts (plena) with adjusted volumes according to the primary inventory of coolant and structures;
  - Four components representing the upper part of the vessel including the components representing the structure that carries lead flow towards the heat exchanger;
  - Heat exchangers (MHX) where heat is transferred between the primary and the secondary system.

- Secondary system. Steam generators are represented by lumped components with the design boundary conditions (i.e., water flow rate, inlet temperature, and pressure).

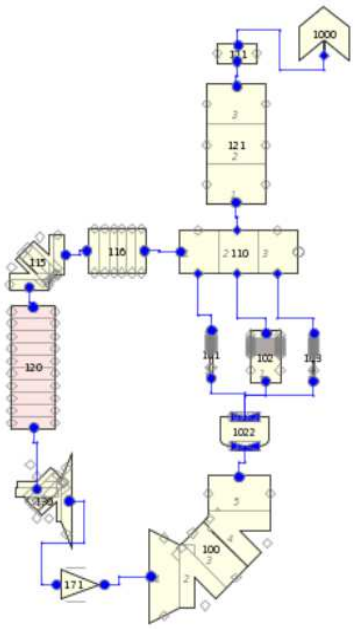


Figure 3: Nodalisation of the primary circuit of ALFRED as implemented in the TRACE code.

The point kinetics is implemented to take into account the different reactivity feedbacks relevant to the ALFRED concept. The reactivity feedbacks considered are:

- Doppler reactivity feedback;
- Coolant expansion reactivity feedback;
- Fuel expansion reactivity feedback;
- Cladding expansion reactivity feedback;
- Radial (diagrid) expansion reactivity feedback;
- Control rod insertion reactivity feedback due to their relative movement consequent to thermal expansion of control rod drivelines, primary system structures and the vessel.

4. RESULTS

4.1 Steady state analysis

Before starting with assessments of selected postulated transient initiators, a benchmarking exercise was performed among individual LEADER project partners to compare results of steady state analyses at nominal power. This was done with the objective to verify the consistency of the different codes and models used by the partners.

As the TRACE code does not contain a state-of-the-art fuel pin mechanics model, the pellet-clad gap distances and conductivities in the different axial levels of the individual modelled fuel assemblies were adopted on the basis of evaluations performed by other partners [4]. Fuel assemblies corresponding to hot fuel (peak value of power profile), inner as well as outer assemblies (with two different power values) were modelled following the core technical description.

Two core states were considered in the analysis, Beginning-of-Cycle conditions (BOC) and End-of-Cycle conditions (EOC). Table 1 shows the main plant parameters in the nominal steady state conditions for the two core configurations as predicted by the TRACE code. These values are in good agreement with results obtained by other partners.

Parameter	**BOC**	**EOC**
Reactor power (MW_{th})	300 (0.0%)	300 (0.0%)
Flow rate (kg/s)	25598 (0.0%)	25598 (0.0%)
Toutlet (°C)	491.85 (2.5%)	493.85 (2.9%)
Tmaxfuel (°C)	2139 (6.9%)	2088 (4.4%)
Tmaxclad (°C)	513 (6.7%)	513 (6.7%)
ΔPcore (bar)	0.78 (22.0%)	0.775 (22.5%)

Table 1: Plant parameters in steady state nominal conditions as predicted by the TRACE code for BOC and EOC representing the reactor power, the coolant flowrate through the core, the core outlet temperature (Toutlet), the maximum fuel (Tmaxfuel) and cladding (Tmaxclad) temperatures for the peak fuel assembly and the core pressure drop (ΔPcore). The values in brackets represent the relative differences vs. the nominal values of the design.

4.2 Transient analysis

Following the steady-state analysis, two initiating events in the Design Extension Condition domain were further analysed: the unprotected reactivity insertion transient (UTOP) and unprotected loss-of-flow (ULOF).

These transients were initiated at steady state, nominal power, and EOC conditions [5].

Consistently with the current capabilities of the TRACE code, the values of the gap distance and thermal gap conductance as defined at steady state were kept constant during the transient

calculations, which might somewhat impact our predictions of fuel temperatures during transients.

UTOP

The UTOP transient is initiated by the reactivity insertion of 250 pcm during 10 seconds. This leads to net positive reactivity in the initiation phases of the transient, resulting in an increase of the core power and correspondingly also coolant and structure temperatures. As it can be seen in Figure 4, the reactivity insertion initiates a power excursion up to a value of 730 MWth (243% Pnom). As this transient is unprotected, the system evolves to a new equilibrium state at higher power (~400 MW).

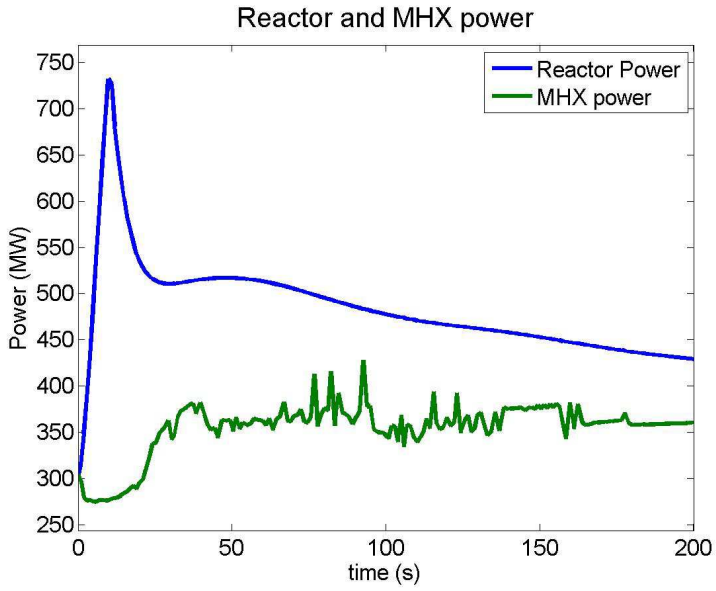


Figure 4. Core and MHX power trace - UTOP

Figure 5 shows that the increase in the temperature of the primary lead is limited as the heat transfer to the secondary side in the MHX also increases in a constant rate all along the transient.

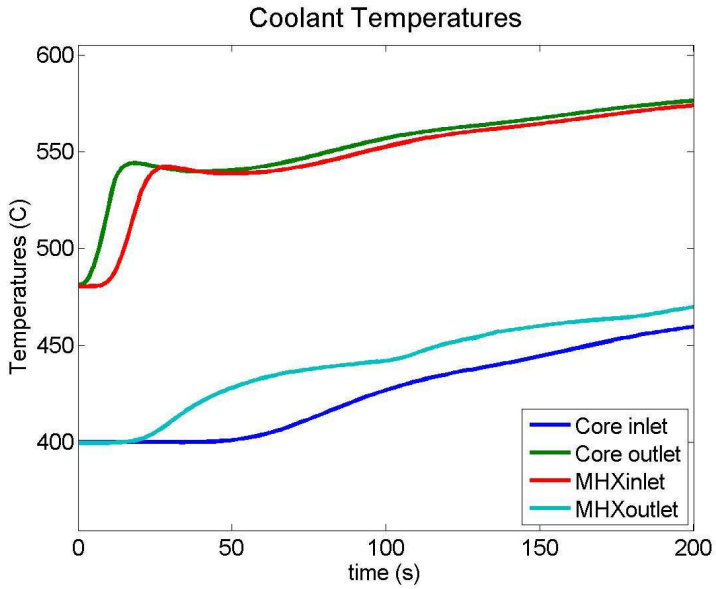


Figure 5: Coolant temperatures - UTOP

A maximum fuel temperature (Figure 6) of about 3000°C is predicted in the hot fuel assembly, which is already above the melting temperature of the mixed-oxide fuel. Consequently, fuel melting in the centre of the fuel pellet is to be expected. The maximum cladding temperature is of 625°C.

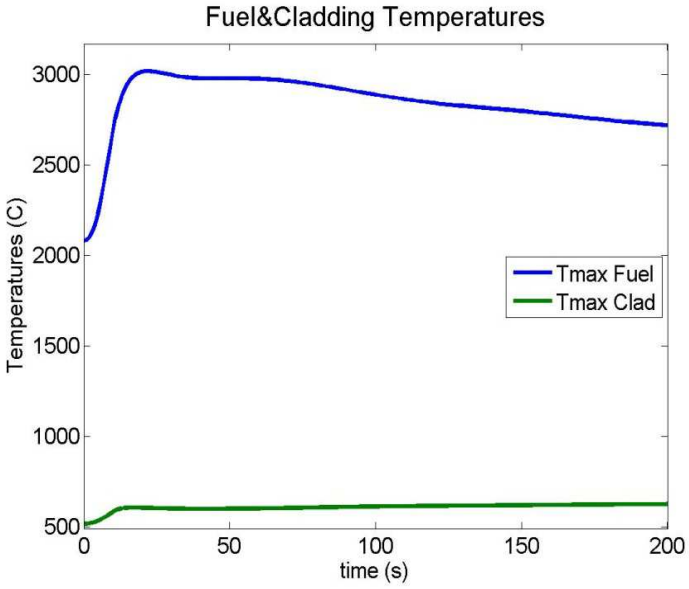


Figure 6: Fuel & Cladding temperatures - UTOP

The reactivity feedback components following the transient evolution are shown in Figure 7. The initial positive reactivity due to the reactivity insertion of 250 pcm in 10 seconds is thereafter counterbalanced mainly by negative reactivity feedbacks due to the Doppler effect and fuel expansion, together with the radial core expansion and the control rod driveline expansion, the contribution of the latter being however relatively small.

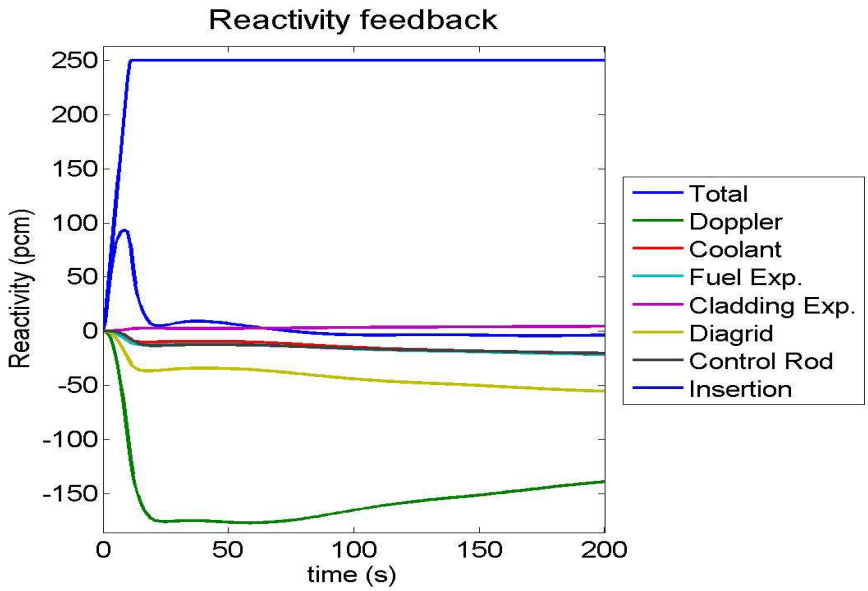


Figure 7. Reactivity feedback evolution - UTOP

ULOF

The ULOF transient is initiated by the coast-down of all primary pumps. Consequently, the system gradually evolves in a continuous decrease of primary coolant massflow until the natural convection process takes over. The natural circulation core massflow rate is of 5420 kg/s (21% of the nominal value). Figure 8 shows this core massflow evolution. The secondary circuits remain in operation in forced circulation.

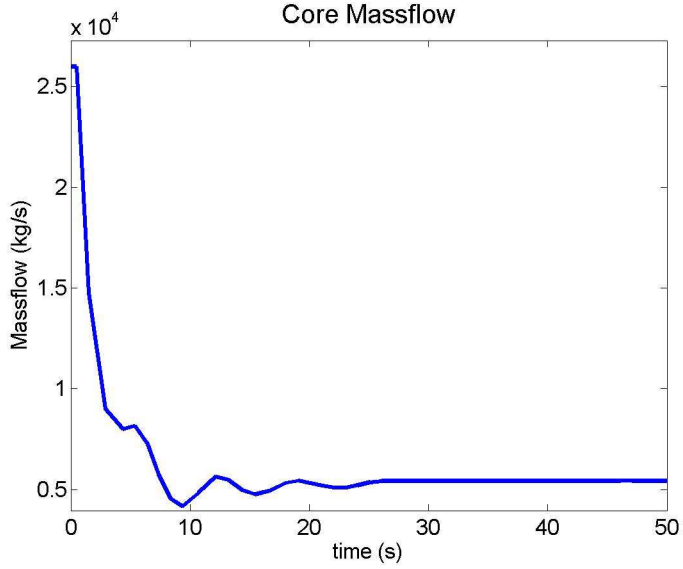


Figure 8: Core massflow - ULOF

As it can be seen in Figure 9 the transient is characterized by an abrupt increase of the primary coolant temperatures as a consequence of the reduced coolant mass flow through the core.

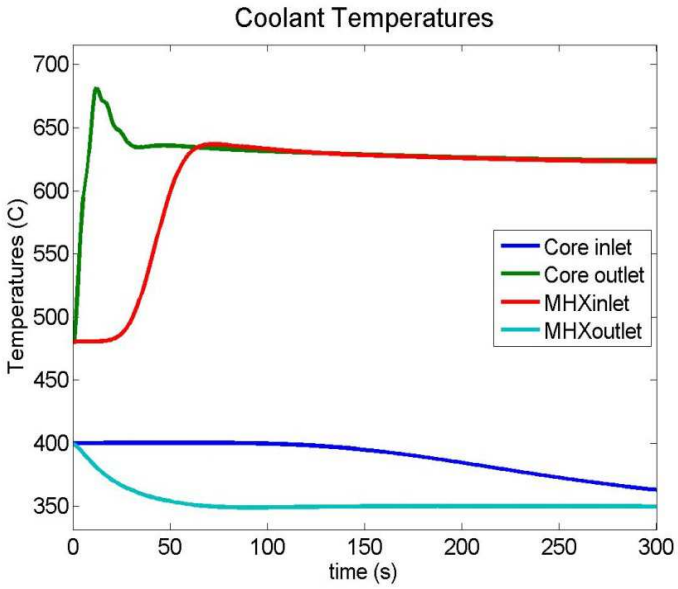


Figure 9: Coolant temperatures in the core inlet and outlet and in the MHX inlet and outlet for the hot fuel assembly.

The maximum fuel and cladding temperature is shown in Figure 10. Even though the reduced coolant mass flow results in an abrupt increase in the cladding temperature (Tmax 782°C), the safety margins can be maintained during the transient and no deterministic clad ruptures are to be expected. Equally, safety margins can be kept with respect to fuel melting or coolant boiling.

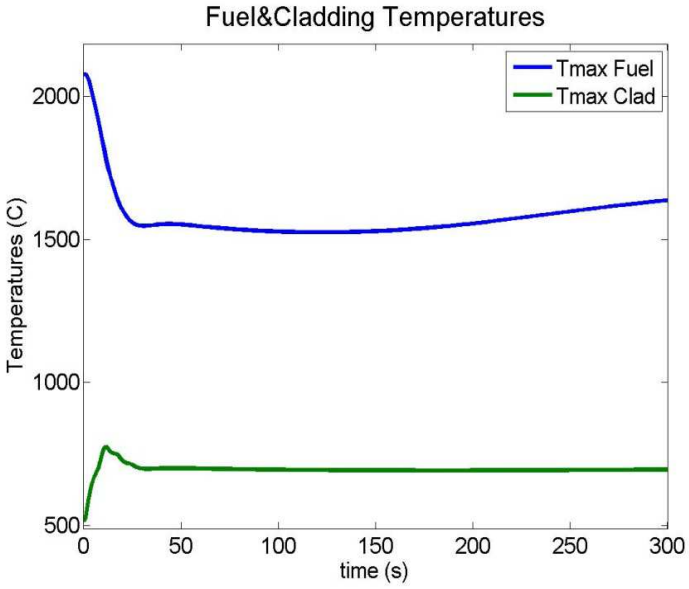


Figure 10: Fuel and cladding temperatures for the hot fuel assembly - ULOF

This increase in temperatures of coolant and structures implies the insertion of reactivity feedbacks (Figure 11), out of which dominating is the negative feedback due to the diagrid (radial) expansion. The control rod (due to the driveline expansion) and the coolant expansion effects also introduce negative reactivity, which leads to further decrease of the net reactivity.

In the longer term, however, as a consequence of decreased fuel temperatures, the positive reactivity insertion is observed due to the Doppler and fuel expansion reactivity feedbacks.

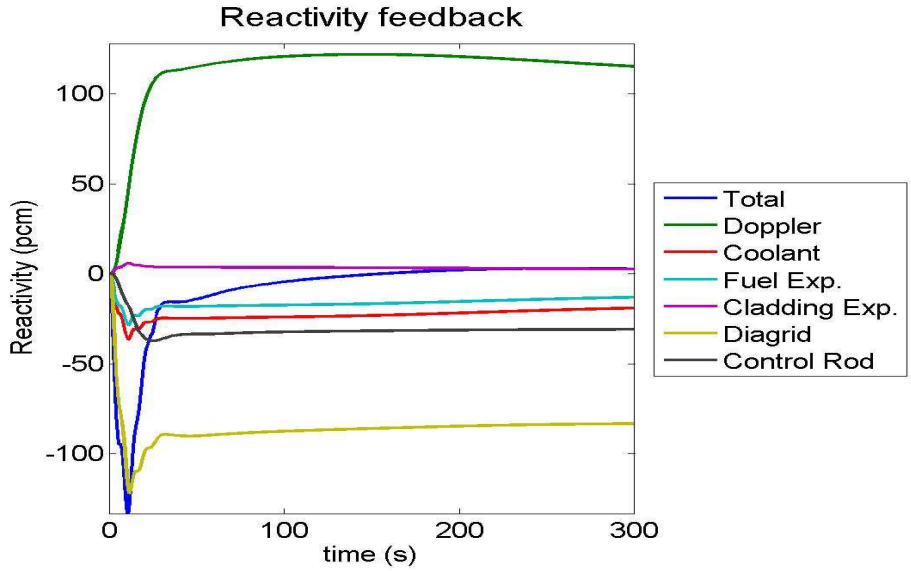


Figure 11: Reactivity feedback evolution - ULOF

Figure 12 show the core power evolution during the transient. As a consequence of the reactivity evolution, the core is subcritical during the first seconds into the transient with a remarkable decrease in power, after which the core power slowly attains a new equilibrium state at about 180 MWth (60% Pnom).

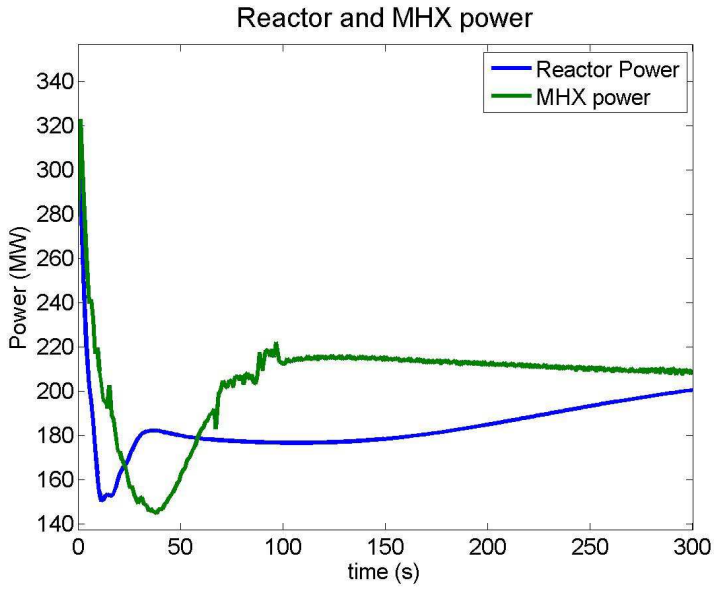


Figure 12: Core and IHX power evolution – ULOF

Thus, the analyses show that the ALFRED design is robust with respect to a ULOF transient providing sufficient grace times for corrective actions to be taken to terminate the transient.

5. CONCLUSIONS

JRC-IET developed a thermal hydraulic model of the ALFRED design and performed with it simulations of the design's behaviour during certain postulated transients in the Design Extension Conditions domain. The conclusions out of this work are following:

- The TRACE code is able to analyse the plant behaviour of Lead-cooled Fast Reactors during postulated transients, incl. design extension conditions, with minor modifications of the source code.

- The analyses indicate that the ALFRED design is, also thanks to the inherent characteristics of lead coolant, robust with respect to behaviour in postulated unprotected transients (ULOF and UTOP) providing sufficient grace times for the implementation of adequate mitigating measures.

The future work involves the development of a three-dimensional model able to analyse the particular phenomena relevant for this technology, such as effect of asymmetric control rod withdrawal or shut down of a single pump. Further developments and improvements of the fuel pin model, in particular the treatment of thermal gap conductance during the transient conditions, might also be envisaged.

6. REFERENCES

[1] Private Communication, ENEA –ANSALDO (Mr. L. Mansani) (2012)

[2] Handbook on Lead-bismuth Eutectic Alloy and Lead Properties, Materials Compatibility, Thermal-hydraulics and Technologies, Edition 2007, Chapters 2 and 3, NEA No. 6195, OECD (2007)

[3] LEADER project documentation, "Plant data for the safety analysis of the ETDR (ALFRED)", KIT-PSI (2012)

[4] Private Communication, Paul Scherrer Institute (Mr. K. Mikityuk) (2012)

[5] Bandini, G. et al., "Safety Analysis Results of Representative DEC Accidental Transients for the ALFRED Reactor", Proceedings of the International Conference on Fast Reactors and Related Fuel Cycles: Safe Technologies and Sustainable Scenarios (FR13), Paris, France (2013)

APPENDIX E

NRG Contribution to LEADER Deliverable DEL022:

a) ALFRED DEC Transient Analysis with SPECTRA Code, and b) SPECTRA Model of the ETDR ALFRED (Pag. 276)

M. M. Stempniewicz (NRG)

1 ALFRED DEC Transient Analysis with SPECTRA Code

1.1 Analyzed Transients

Eight DEC transients were analyzed. The transients are listed in Table 1. Table shows the initiating events, the reactor scram threshold and the timing of the interventions on the primary (pumps) and secondary (feedwater, MSIV and DHR) systems. The main results of the DEC transients analyzed for the EOC conditions are shown in the following sections.

Table 1 Table of main events [3]

TRANSIENT	Initiating Event	Reactor scram	Primary pump trip	MHX FW trip	MSIV closure	DHR startup
TR-4: UTOP	Insertion of 250 pcm in 10 s	No	No	No	No	No
TDEC-1: ULOF	All primary pumps coastdown	No	0 s	No	No	No
TDEC-3: ULOHS	All MHX feedwater trip	No	No	0 s	1 s	DHR-1 at 2 s (3 IC loops)
T-DEC4: ULOHS+ULOF	All primary pumps and MHXs feedwater trip	No	0 s	0 s	1 s	DHR-1 at 2 s (3 IC loops)
T-DEC5: Partial blockage in the hottest FA	10% to 87.5% blockage at the hottest FA inlet	No	No	No	No	No
TO-3: All prim. pumps stop + reduction of FW temperature	T-fw: 335→300°C in 1 s + all p. pumps stop	2 s, low pump speed	0 s	2 s	2 s	DHR-1 at 3 s (4 IC loops)
TO-6: All prim. pumps stop + increase of FW flow rate	FW-flow +20% in 25 s + all p. pumps stop	2 s, low pump speed	0 s	2 s	2 s	DHR-1 at 3 s (4 IC loops)
T-DEC6: SCS failure	Depressurization of all secondary circuits	2 s, low sec. pressure	No	2 s	No	No

1.2 Results of All Transients

1.2.1 TR-2 (UTOP) Reactivity Insertion, 250 pcm in 10 s

The Unprotected Transient Over-Power (UTOP) scenario is as follows.

- Reactivity of 250 pcm (0.7463 $) is inserted in 10 seconds.
- Reactor trip (SCRAM signal) is disabled.
- Fuel-clad linked effect - fuel expansion according to linked effect with clad temperature.

In this transients all loops are symmetrical. The model with all loops combined into one is used. The NRG SPECTRA results are shown in Figure 2 through Figure 5.

Core power is shown in Figure 2. The core power reaches 645 MW and decreases to about 460 MW.

Fuel temperatures are shown in Figure 3. The maximum fuel temperature reaches 3129 K, 2856°C at 57 s. The maximum fuel temperature exceeds for a short period the melting temperature (MOX melting point ~2940 K ~2670°C). Only local fuel melting is expected (~ 1 mm) – Figure 1.

Coolant and cladding temperatures are shown in Figure 4. The maximum cladding temperature remains below 650°C the core outlet temperature slowly increases following the temperature increase at core inlet.

The total reactivity as well as the reactivity feedbacks are shown in Figure 5. The inserted reactivity is counterbalanced mainly by negative Doppler effect induced by fuel temperature increase. Total reactivity reaches a maximum of about 80 pcm at 10 s and then reduces due to negative feedbacks.

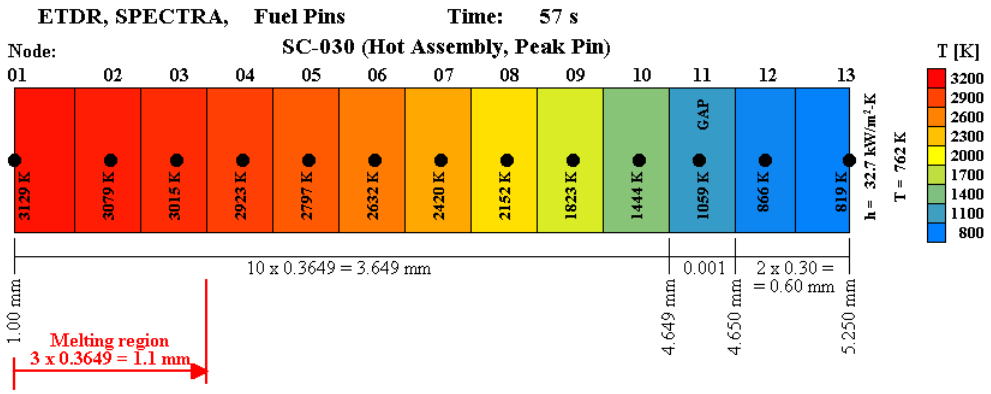


Figure 1 Maximum fuel temperatures, SPECTRA

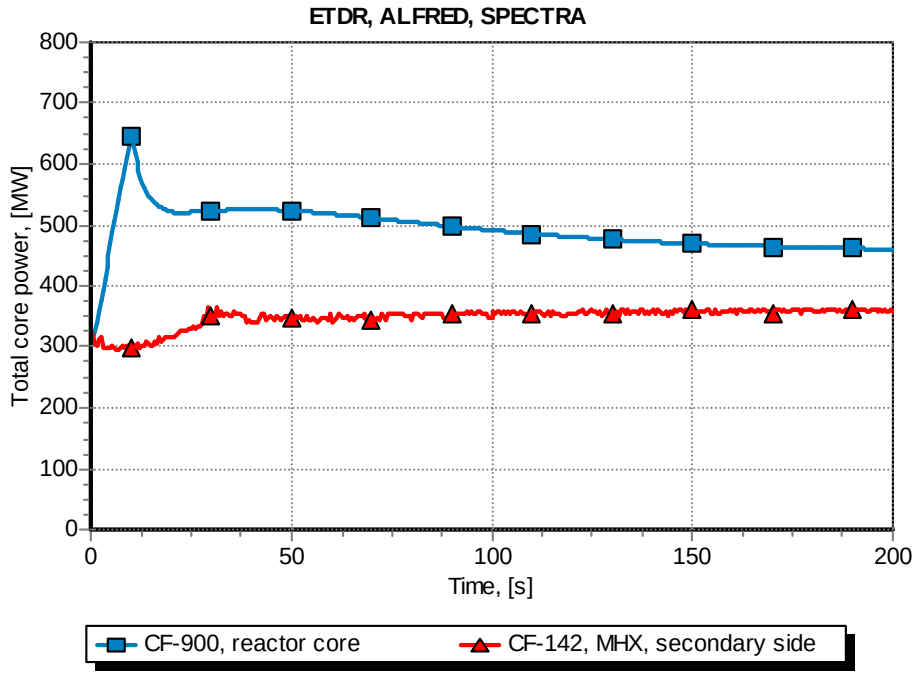


Figure 2 **Core and MHX power**

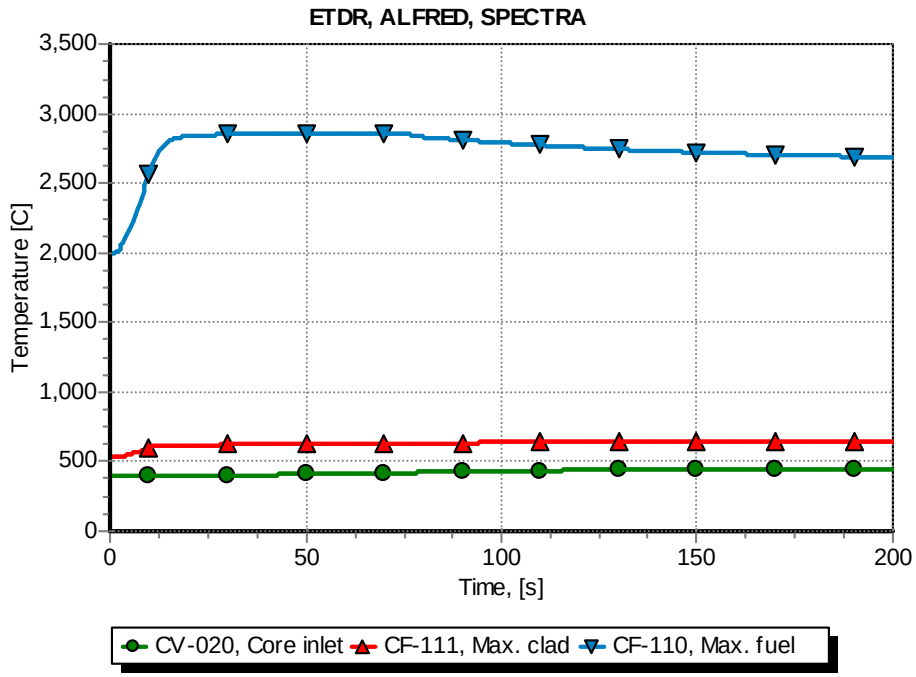


Figure 3 **Fuel temperatures**

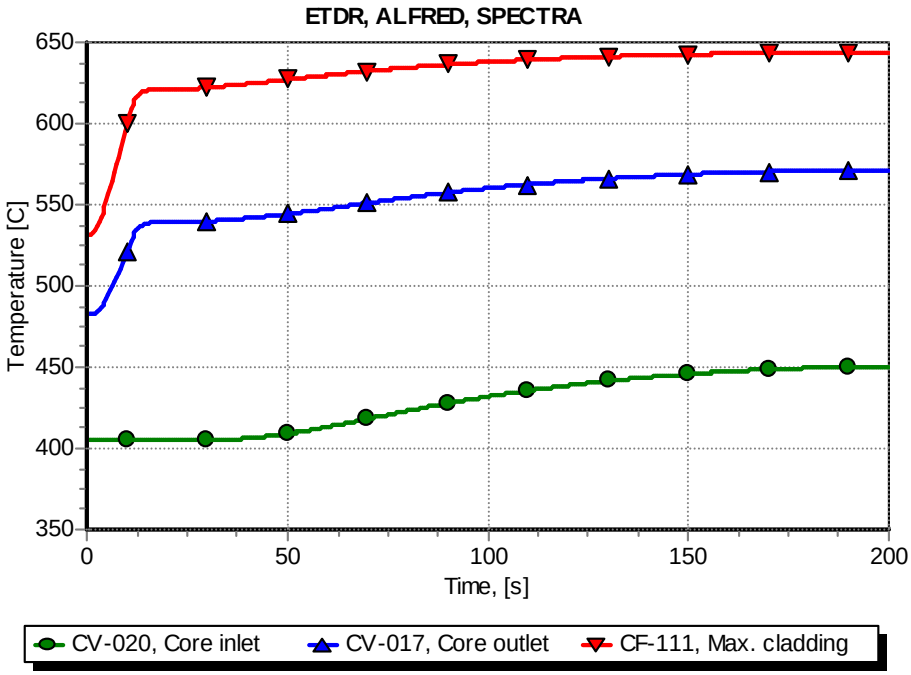


Figure 4 **Coolant temperatures**

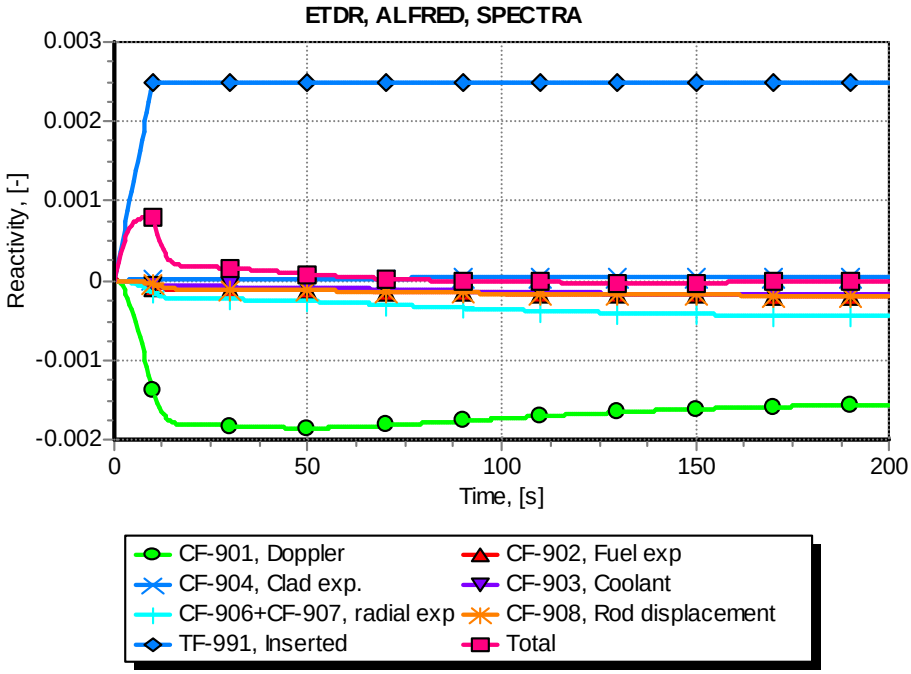


Figure 5 **Reactivities**

1.2.2 T-DEC1 (ULOF) Loss of All Primary Pumps

The Unprotected Loss of Flow (ULOF) scenario is as follows:

- Coastdown of all primary pumps. Pump speed halving time 0.56 s.
- The secondary circuits remain in operation in forced circulation
- Reactor trip (SCRAM signal) is disabled.

In this transients all loops are symmetrical. The model with all loops combined into one is used. The NRG SPECTRA results are shown in Figure 6 through Figure 10.

The core inlet flow is shown in Figure 6. After an initial small core flow rate undershot natural circulation stabilizes in the primary circuit a little above 5000 kg/s.

The core and MHX powers are shown in Figure 7. The core power initially reduces due to negative reactivity feedbacks and then stabilizes at about 210 MW, in equilibrium with the MHX power. The MHX power initially decreases due to reduced primary flow and then increases with the lead temperature increase at the MHX inlet.

The fuel, cladding, and core inlet temperatures are shown in Figure 8. The peak and average fuel temperatures reduce according to the decrease of core power level. The maximum fuel temperature stabilizes at about 1660˚C.

The coolant and cladding temperatures are shown in Figure 9.Initially the maximum core outlet temperature increases. The maximum value is 794°C. The maximum core outlet temperature stabilizes at about 600°C. The core inlet temperature slowly decreases, at 300 s it is about 360°C.

The total reactivity as well as the reactivity feedbacks are shown in Figure 10.The positive reactivity come from Doppler effect and fuel expansion and is counterbalanced by negative coolant density effect, radial expansion and control rod displacement feedbacks. Total reactivity decreases and reaches a minimum of about –92 pcm at about 10 s and then approaches zero.

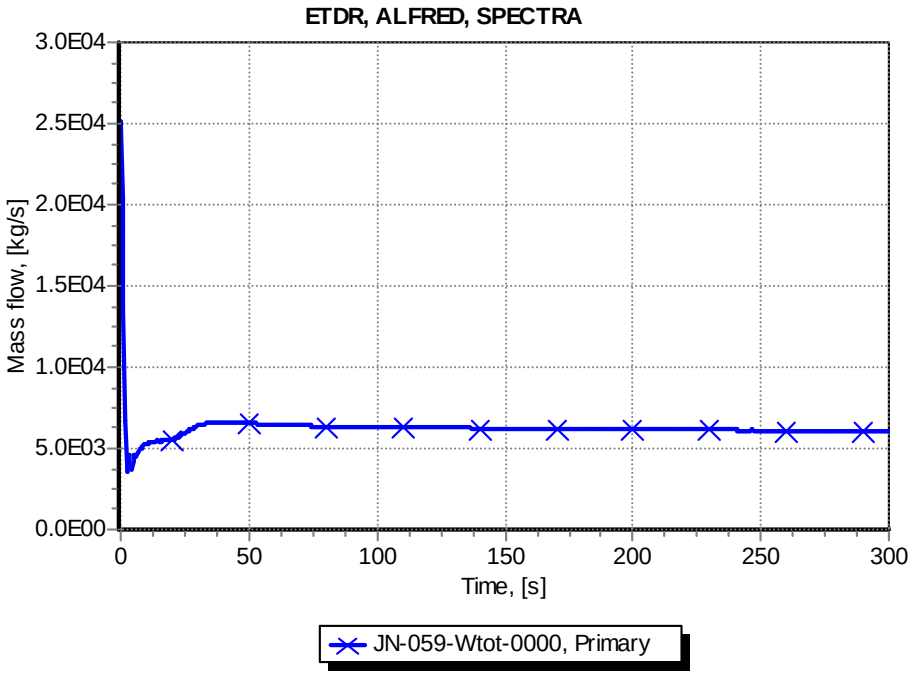


Figure 6 **Primary mass flow**

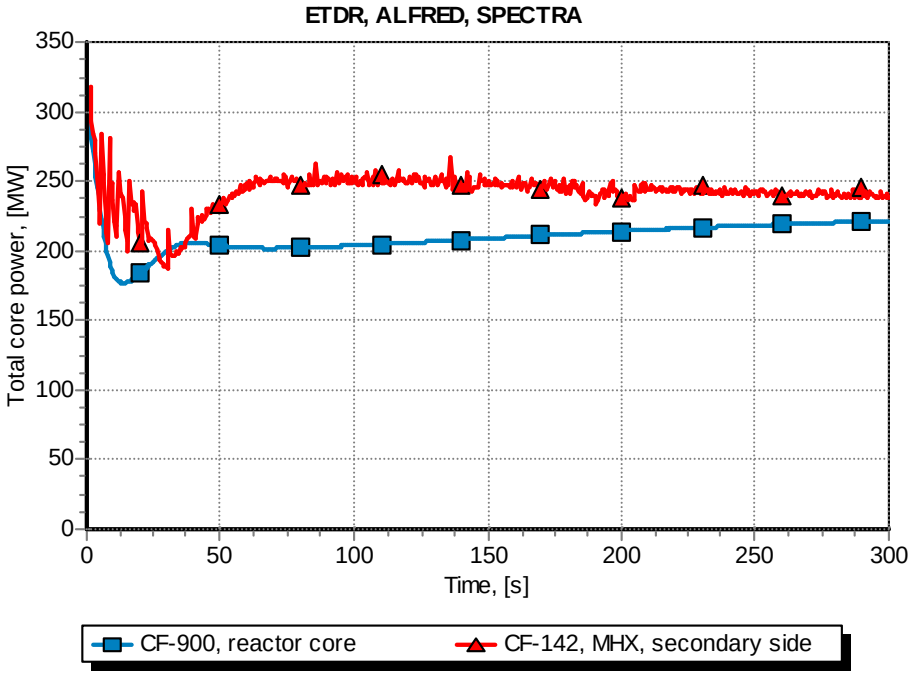


Figure7 **Core and MHX power**

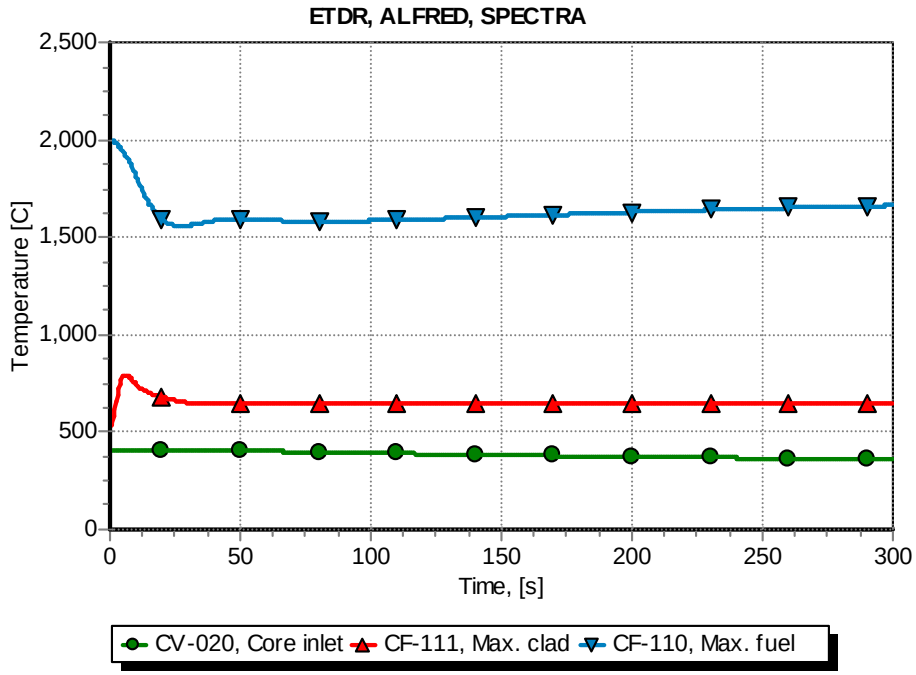


Figure 8 **Fuel, cladding, and core inlet temperatures**

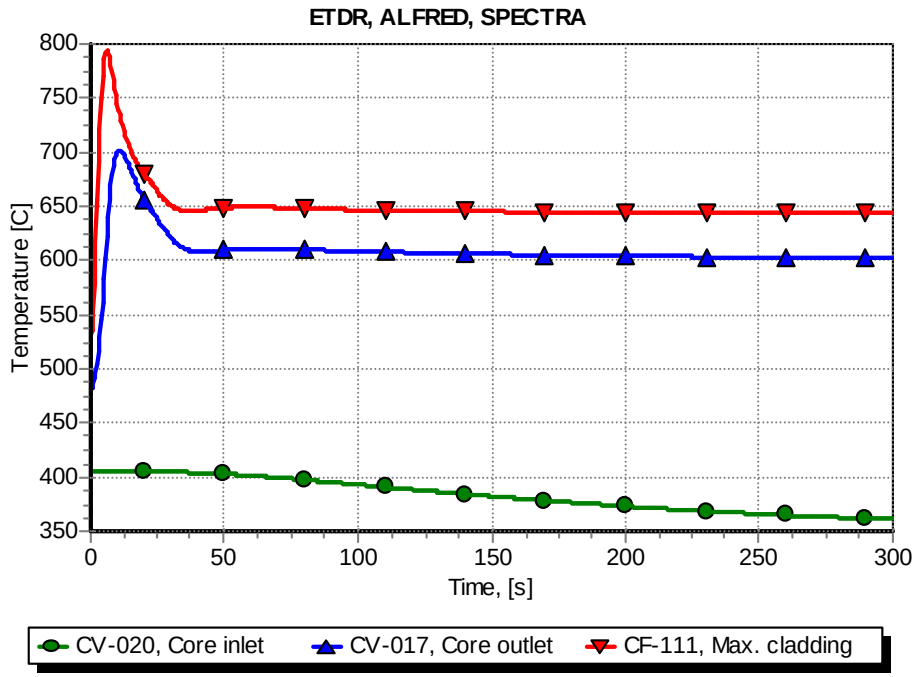


Figure 9 **Coolant and cladding temperatures**

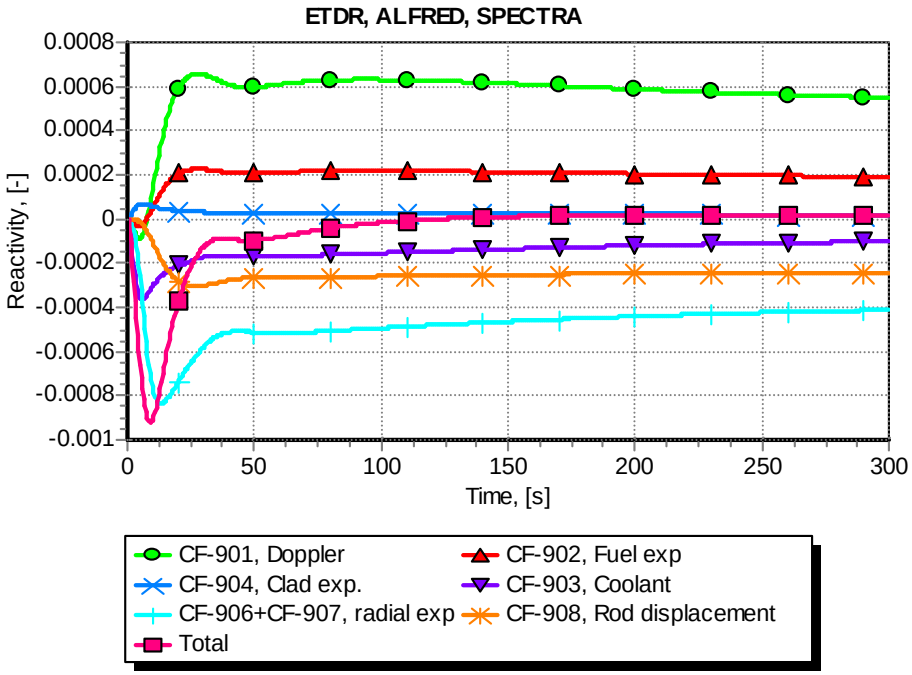


Figure 10 Total reactivity

1.2.3 T-DEC3 (ULOHS) Unprotected Loss of Heat Sink

The Unprotected Loss of Heat Sink (ULOHS) scenario is as follows.

- Loss of feedwater on all MHX-s. Mass flow halving time 1.0 s.
- MSIV closes at 0.0 s. IC valve opens at 1.0 s. Valve opening/closing time 1.0 s.
- Start up of DHR-1 (three out of four DHR-1 loops available).
- Reactor trip (SCRAM signal) is disabled.

In this transient there are three loops with IC operating and five loops with IC closed. In the model two loops are used. The first loop represents three real loops with IC-s, combined into one. The second loop represents five real loops without IC-s. The NRG SPECTRA results are shown in Figure 11 through Figure 15.

The core and MHX powers are shown in Figure 11. The core power decreases gradually. At t=3000 s the total power is 8.58 MW, consisting of 3.38 MW fission power and 5.20 MW decay power.

The coolant, cladding and vessel temperatures are shown in Figure 12. The temperatures rise to about 700˚C. No fuel rod cladding rupture nor vessel failure is expected in the medium term. Enough grace time is left to the operator to take the opportune corrective actions and bring the plant in safe conditions in the medium and long term.

The coolant, cladding and fuel temperatures are shown in Figure 13. The maximum fuel temperatures continuously decrease. At the end of calculations it is equal to 732°C. The maximum cladding temperatures slowly increases. At the end of calculations it is equal to 694°C. The core inlet temperature slowly increases. At the end of calculations it is equal to 691°C.

The total reactivity as well as the reactivity feedbacks are shown in Figure 14. The main positive feedback is from Doppler effect and fuel expansion. The main negative feedbacks are from radial expansions (diagrid, pads), coolant density, and control rod displacement. The total reactivity is constantly slightly below zero, resulting in gradual power decrease.

Figure 15 shows visualization of the IC at the start and at the end of the transient. At the end of calculations the three operating IC-s remove about 6.98 MW (3×2.33 MW) power.

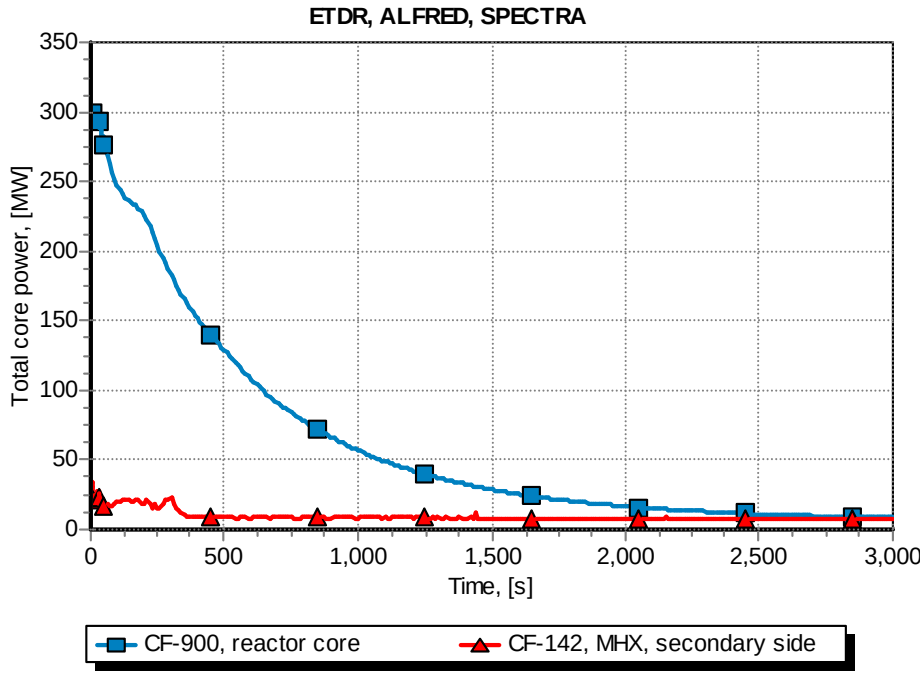


Figure 11 **Core power and MHX power**

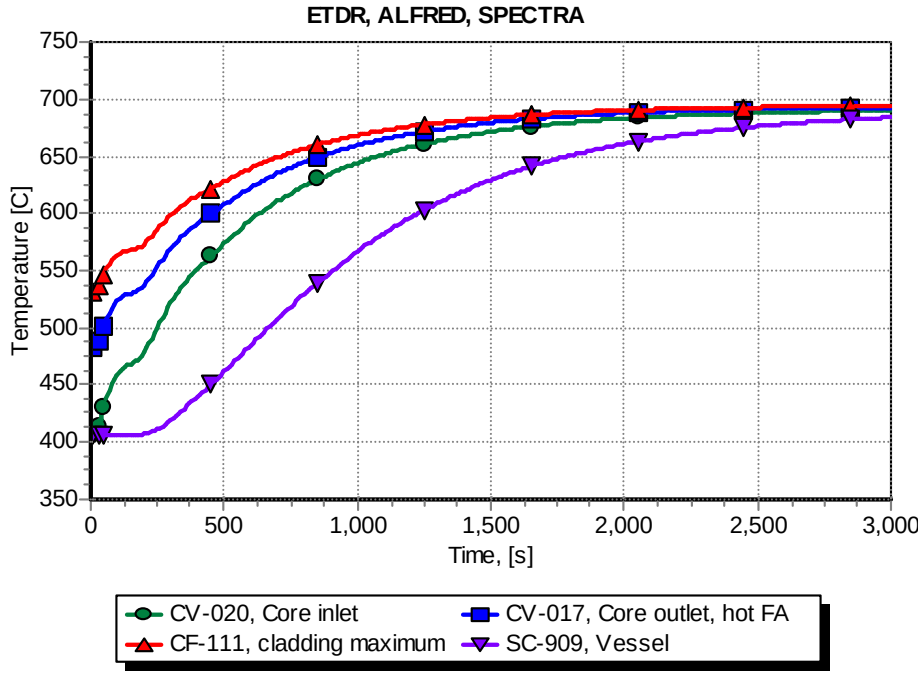


Figure 12 **Coolant, cladding, and vessel temperatures**

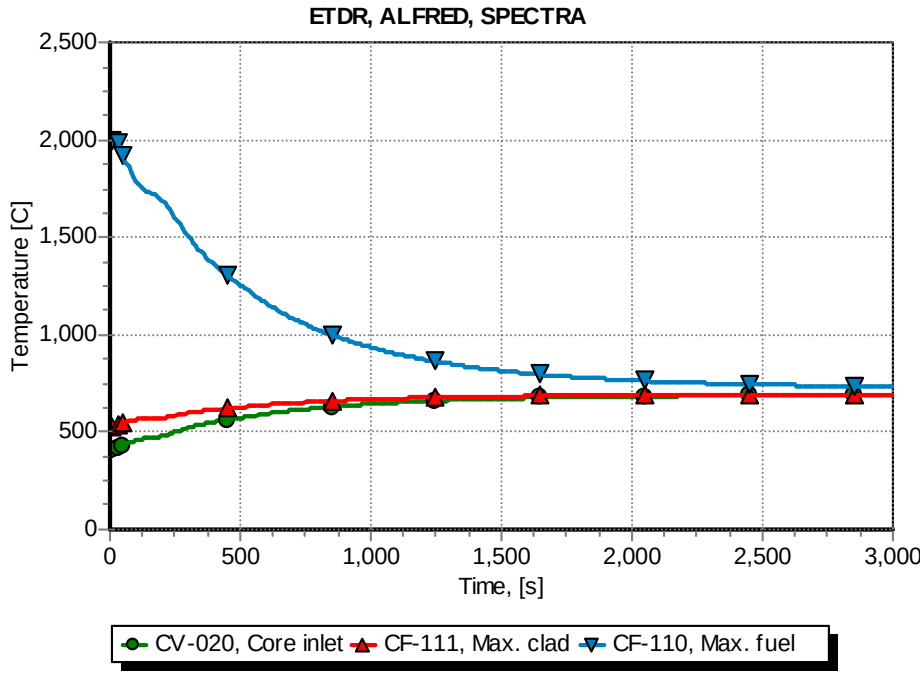


Figure 13 **Coolant, cladding, and fuel temperatures**

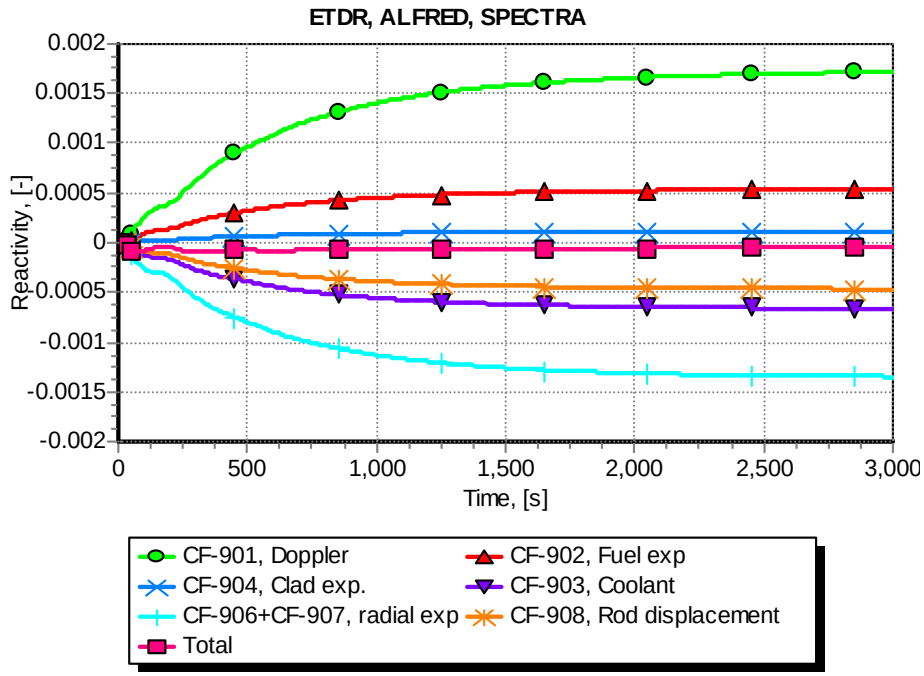


Figure 14 **Reactivities**

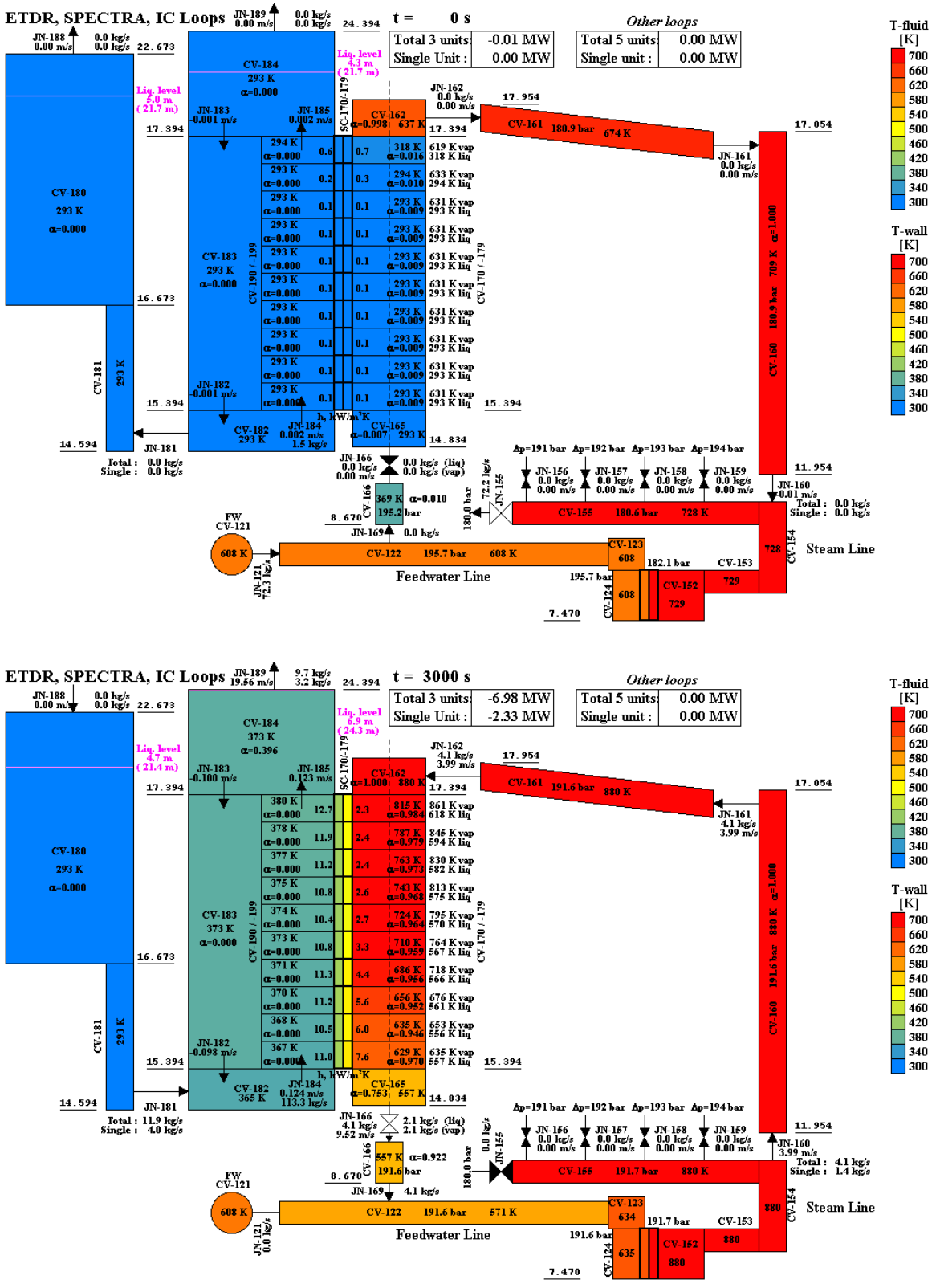


Figure 15 **Visualization of IC, SPECTRA (above) start of transient, (below) end of transient**

1.2.4 T-DEC4 (ULOHS+ULOF) Loss of Offsite Power

The Loss of offsite power (ULOHS+ULOF) scenario is as follows.

- Loss of all primary pumps. Pump speed halving time 0.56 s.
- Loss of feedwater on all MHX-s. Mass flow halving time 1.0 s.
- MSIV closes at 0.0 s. IC valve opens at 1.0 s. Valve opening/closing time 1.0 s.
- Start up of DHR-1 (three out of four DHR-1 loops available).
- Reactor trip (SCRAM signal) is disabled.

In this transient there are three loops with IC operating and five loops with IC closed. In the model two loops are used. The first loop represents three real loops with IC-s, combined into one. The second loop represents five real loops without IC-s. The NRG SPECTRA results are shown in Figure 16 through Figure 20.

The core inlet flow is shown in Figure 16. Natural circulation in primary circuit reduces down to very low value (around 1%).

Core power and MHX power are shown in Figure 17. The core power decreases gradually. At t=3600 s the total power is 10.79 MW, consisting of 5.98 MW fission power and 4.81 MW decay power. The MHX power decreases due to feedwater trip.

Coolant, cladding, and vessel temperatures are shown in Figure 18. The maximum cladding temperatures rises to about 808˚C at about 1300 s and slowly decreases to about 800˚C at the end of the run. No fuel rod cladding rupture nor vessel failure is expected in the medium term. Enough grace time is left to the operator to take the opportune corrective actions and bring the plant in safe conditions in the medium and long term.

The total reactivity as well as the reactivity feedbacks are shown in Figure 19. The main positive feedback is from Doppler effect and fuel expansion. The main negative feedbacks are from radial expansions (diagrid, pads), control rod displacement, and coolant density. The total reactivity is constantly slightly below zero, resulting in gradual power decrease.

Figure 20 shows visualization of the IC and the MHX at the end of the transient. The three operating IC-s remove about 6.24 MW (3×2.08 MW) power. The corresponding three steam generators remove similar power 6.32 MW (3×2.11 MW) from the primary system. There is practically no power removal through the remaining five steam generators. The total power is 0.08 MW (5×0.02 MW).

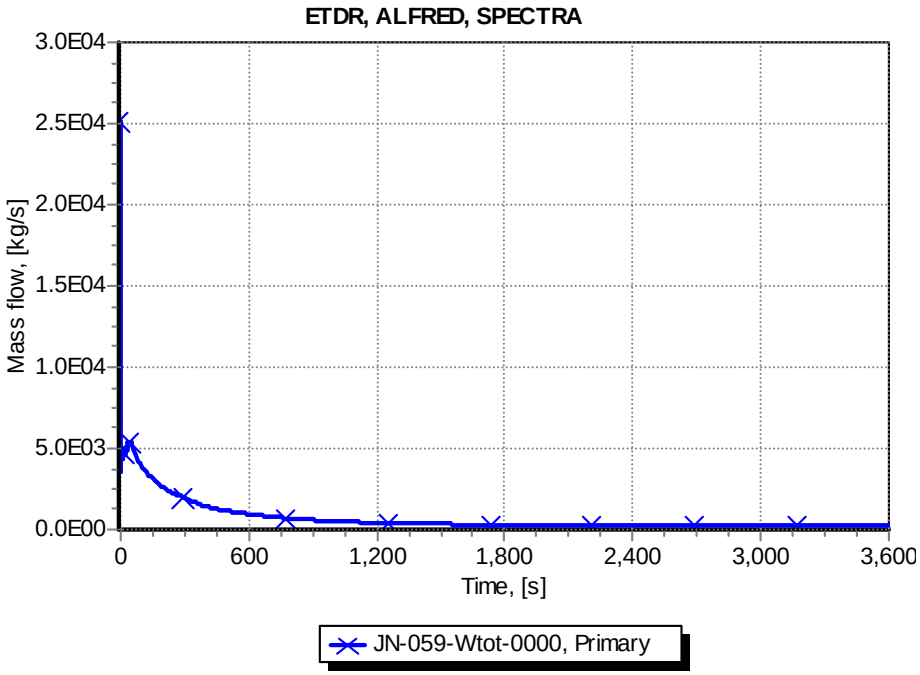


Figure 16 Core inlet flow

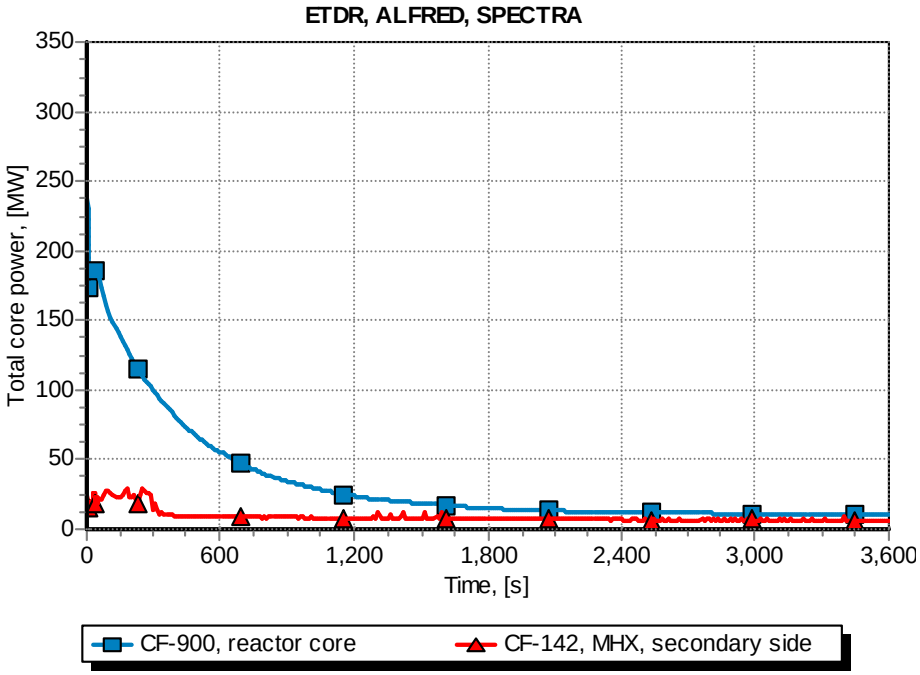


Figure 17 Core power and MHX power

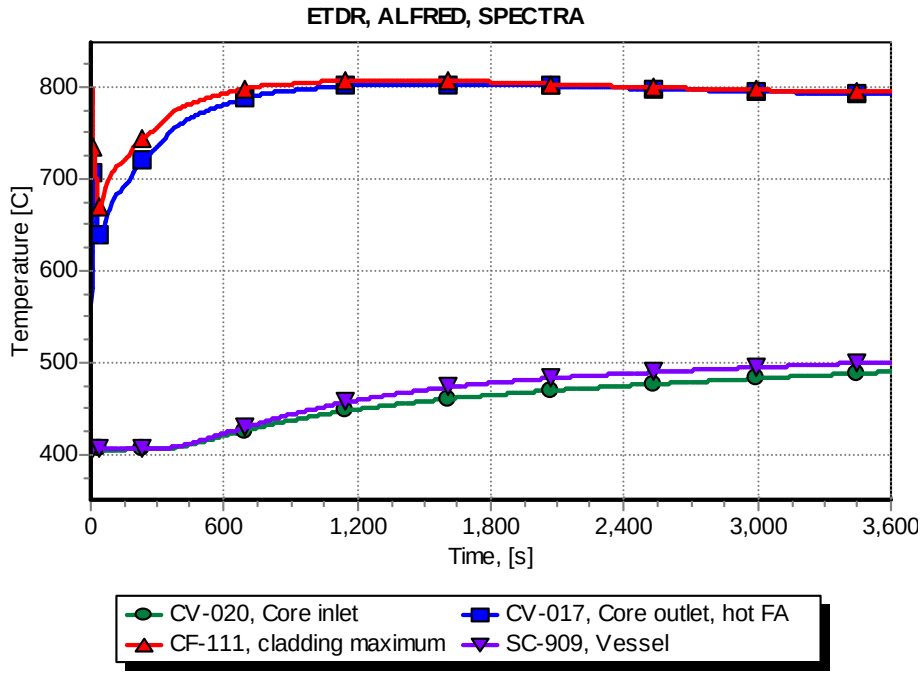


Figure 18 **Coolant, cladding, and vessel temperatures**

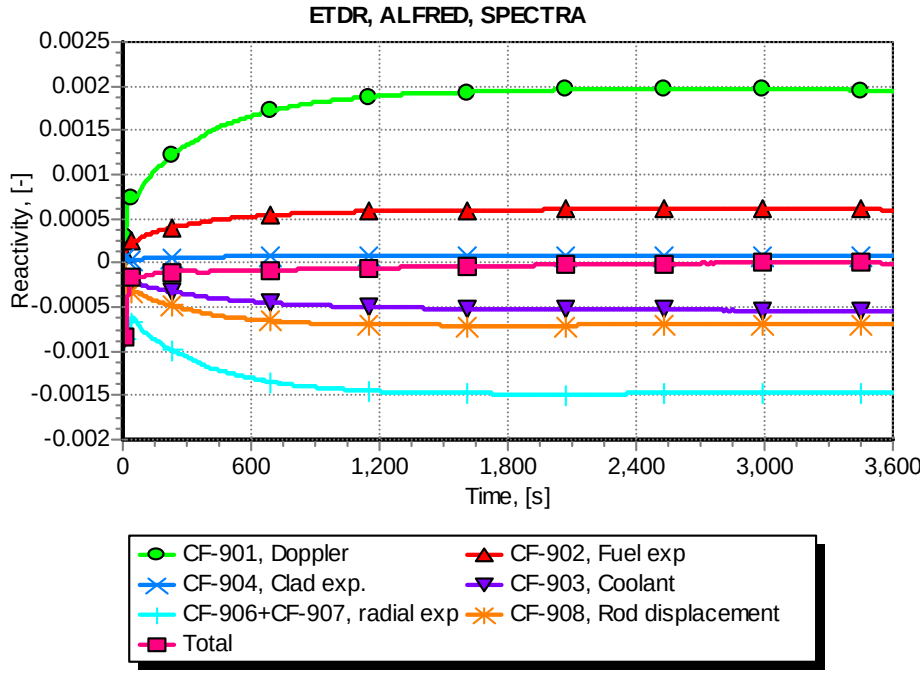
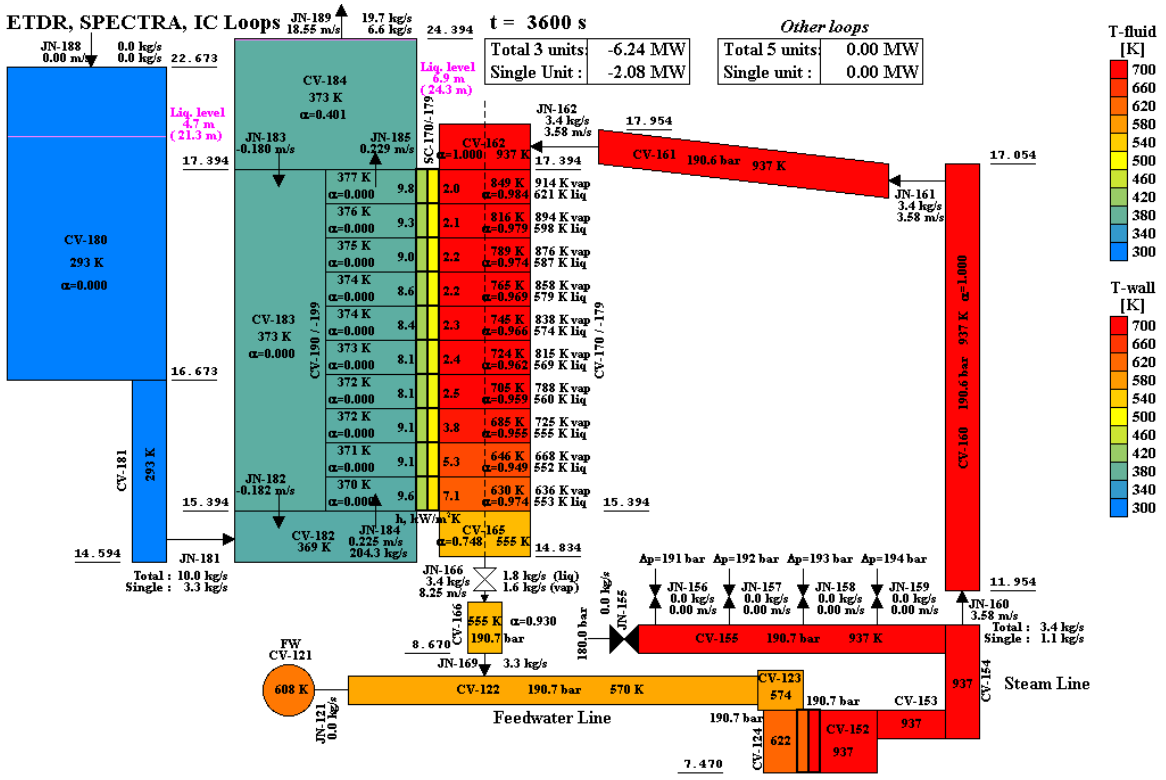


Figure 19 **Reactivities**



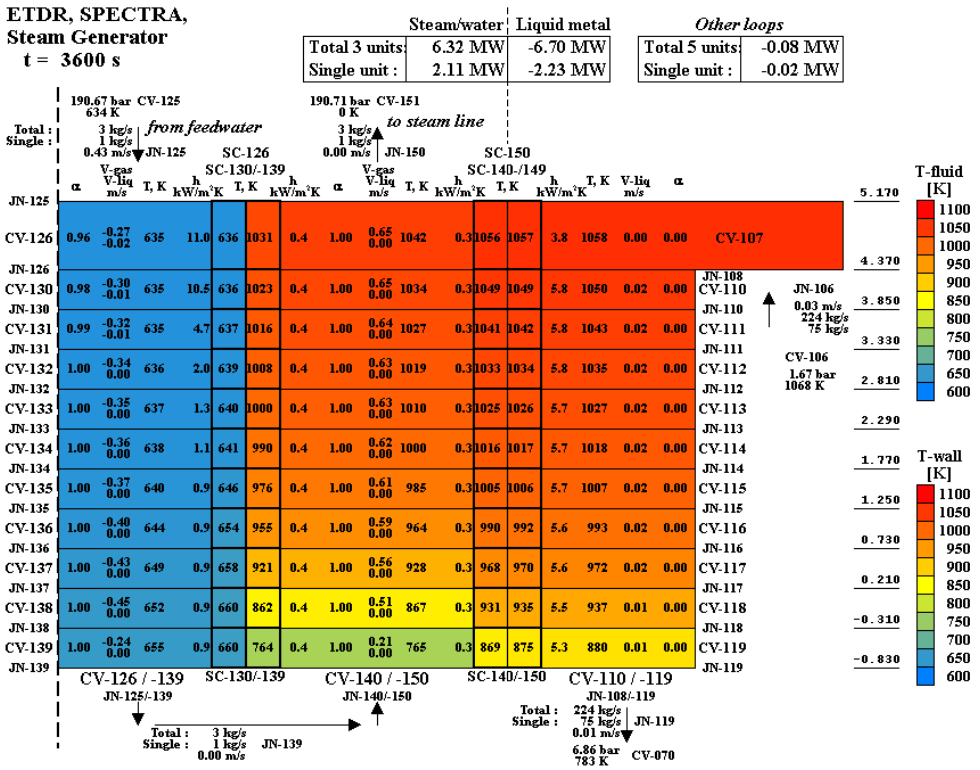


Figure 20 Visualization of IC and MHX, SPECTRA, end of transient

1.2.5 TO-3 FW Temperature Reduction

The scenario is as follows.

- Loss of one preheater, FW temperature drops from 335ºC to 300ºC in 1.0 s.
- All primary pumps coastdown at t=0.0 s, pump speed halving time 0.56 s.
- FW trip at 2.0 s. FW flow halving time 1.0 s.
- MSIV closes at 2.0 s. Closing time 1.0 s.
- Reactor trip (SCRAM signal) on low primary pump speed signal.
- Start up of HDR-1, four IC-s available.

In this transient there are three loops with IC operating and five loops with IC closed. In the model two loops are used. The first loop represents four real loops with IC-s, combined into one. The second loop represents four real loops without IC-s. The NRG SPECTRA results are shown in Figure 21 through Figure 26.

Core inlet flow is shown in Figure 21 and Figure 22. The primary mass flow decreases quickly. Natural circulation is established at about 4000 kg/s. In the long term the natural circulation flow decreases to about 800 kg/s – about 3% of the nominal flow.

Core power and MHX power are shown in Figure 23. The core power decreases to decay power after SCRAM. The MHX power is close to the IC power, about 7 MW and exceeds the decay power.

Primary coolant temperatures are shown in Figure 24. The liquid lead temperatures continuously decrease, because the power removed by the 4 IC units exceeds the decay power. The lead freezing temperature (600.6 K, 327.4˚C) is reached at MHX outlet after about 2 hours.

Coolant and cladding temperatures are shown in Figure 25. The maximum cladding temperature reaches about 650°C at about 5 s and then decreases. The core outlet temperature reaches about 580°C at about 10 s and then decreases. The core inlet temperature is stable at approximately initial values.

Figure 26 shows visualization of the IC and the MHX at the end of the transient. The four operating IC-s remove about 5.35 MW (4×1.34 MW) power. The corresponding four steam generators remove similar power 5.16 MW (4×1.29 MW) from the primary system. There is practically no power removal through the remaining four steam generators. The total power is 0.07 MW (4×0.02 MW).

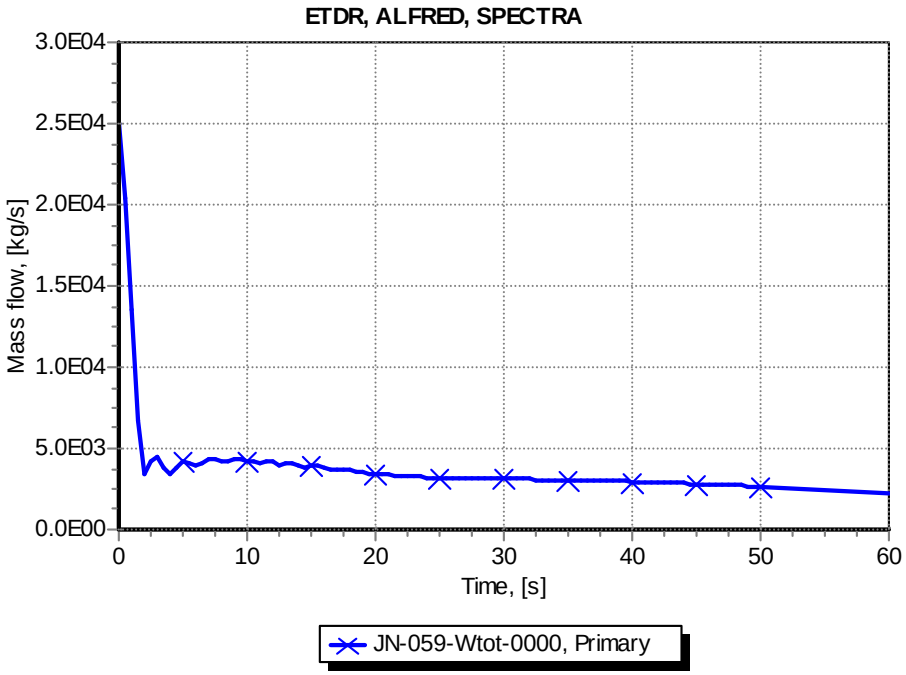


Figure 21 **Core inlet flow - short term**

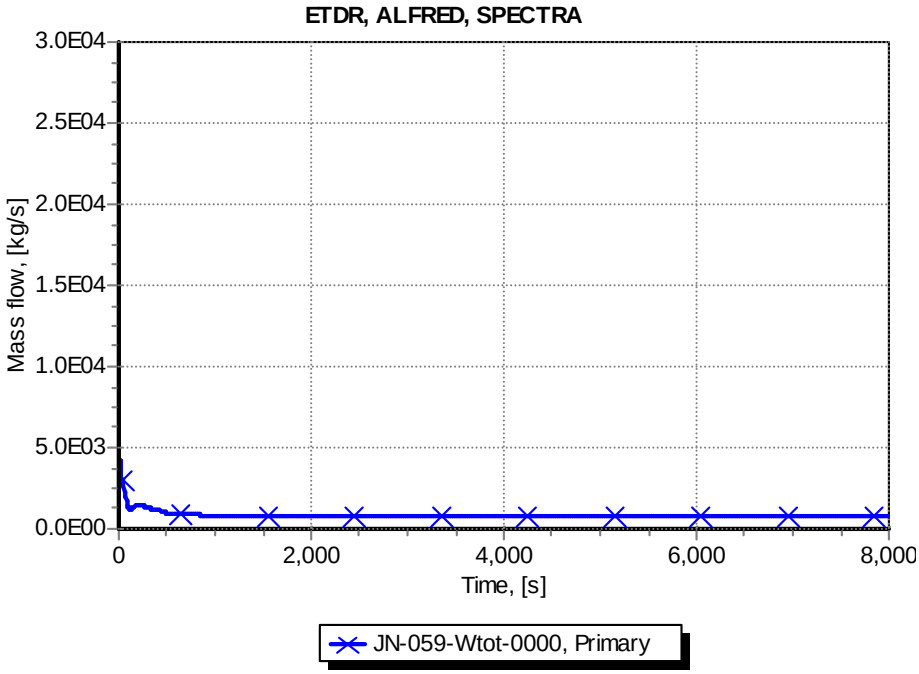


Figure 22 **Core inlet flow - long term**

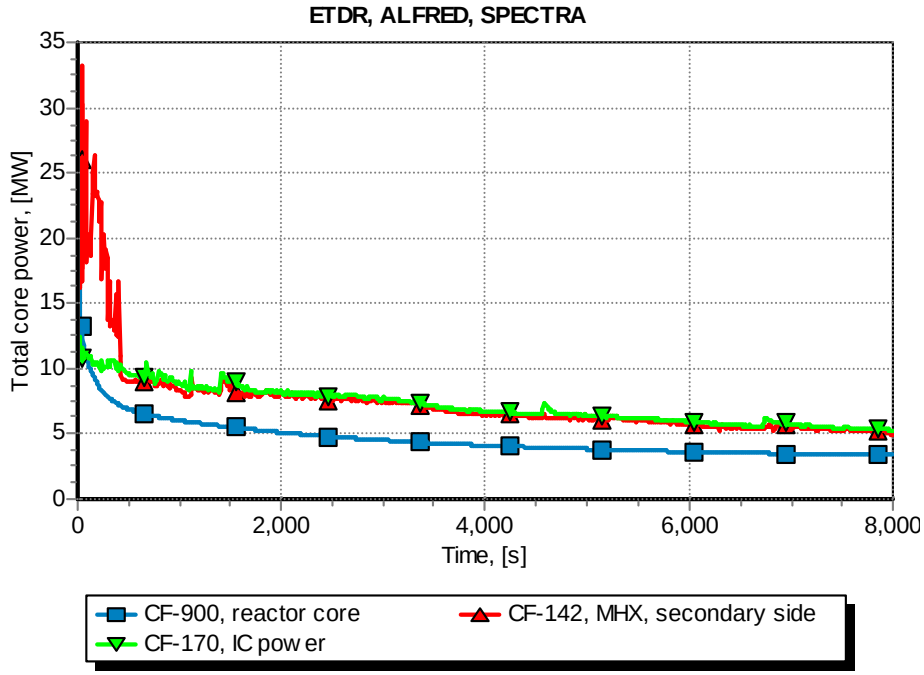


Figure 23 **Core, MHX, and IC power**

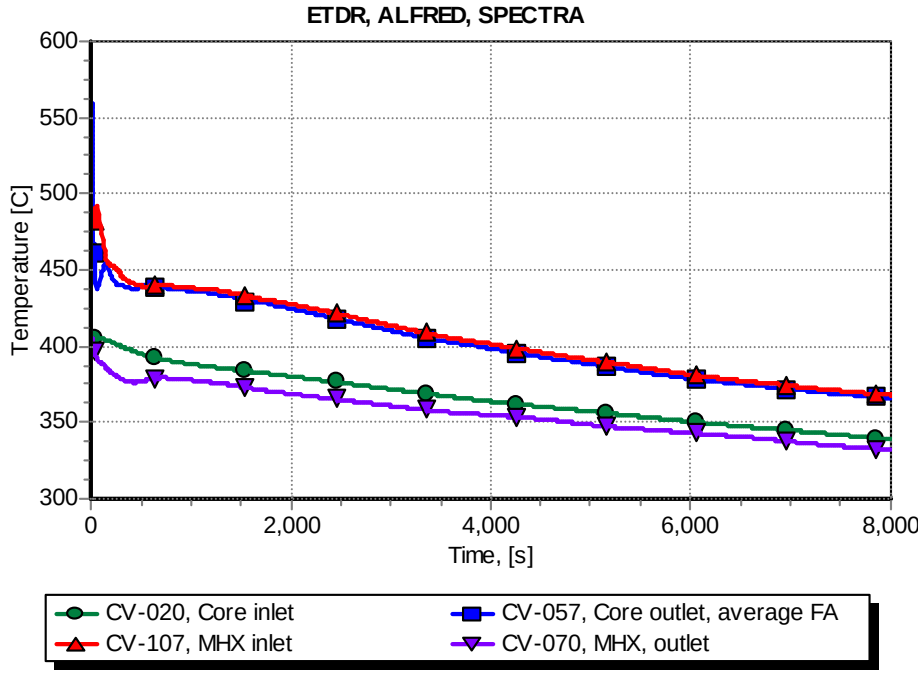


Figure 24 **Primary temperatures**

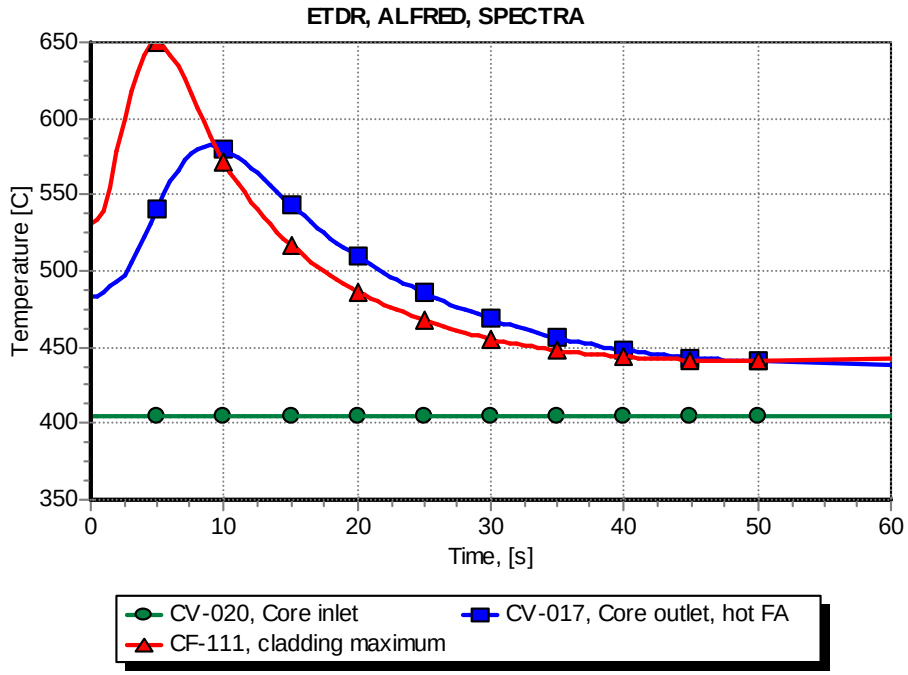


Figure 25 **Coolant and cladding temperatures**

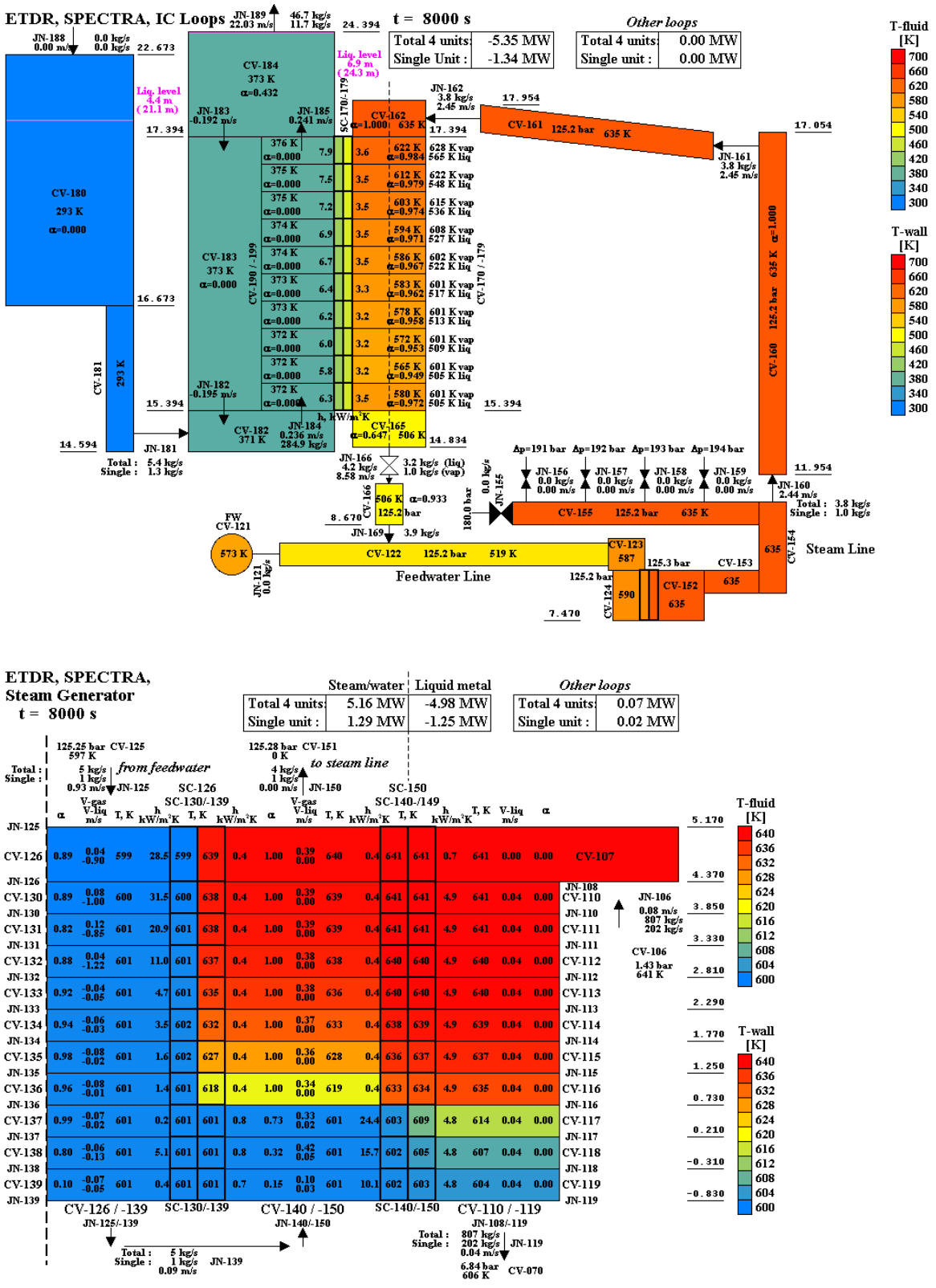


Figure 26 Visualization of IC and MHX, SPECTRA, end of transient

1.2.6 TO-6 FW Flow Increase by 20%

The scenario is as follows.

- FW flow increases by 20% in 1.0 s.
- All primary pumps coastdown at t=0.0 s, pump speed halving time 0.56 s.
- FW trip at 2.0 s. FW flow halving time 1.0 s.
- MSIV closes at 2.0 s. Closing time 1.0 s.
- Reactor trip (SCRAM signal) on low primary pump speed signal.
- Start up of HDR-1, four IC-s available.

In this transient there are three loops with IC operating and five loops with IC closed. In the model two loops are used. The first loop represents four real loops with IC-s, combined into one. The second loop represents four real loops without IC-s. The NRG SPECTRA results are shown in Figure 27 through Figure 32.

Core inlet flow is shown in Figure 27 and Figure 28. The primary mass flow decreases quickly. Natural circulation is established at about 4000 kg/s. In the long term the natural circulation flow decreases to about 800 kg/s – about 3% of the nominal flow.

Core, MHX, and IC power is shown in Figure 29. The core power decreases to decay power after SCRAM. The MHX power is close to the IC power, about 7 MW and exceeds the decay power.

Coolant temperatures are shown in Figure 30. Lead temperatures continuously decrease, because the power removed by the 4 IC units exceeds the decay power. The lead freezing temperature (600.6 K, 327.4˚C) is reached at MHX outlet after about 2 hours.

Coolant and cladding temperatures are shown in Figure 31. The maximum cladding temperature reaches about 650°C at about 5 s and then decreases. The core outlet temperature reaches about 580°C at about 10 s and then decreases. The core inlet temperature is stable at approximately initial values.

Figure 32 shows visualization of the IC and the MHX at the end of the transient. The four operating IC-s remove about 5.31 MW (4×1.33 MW) power. The corresponding four steam generators remove similar power 5.04 MW (4×1.26 MW) from the primary system. There is practically no power removal through the remaining four steam generators. The total power is 0.07 MW (4×0.02 MW).

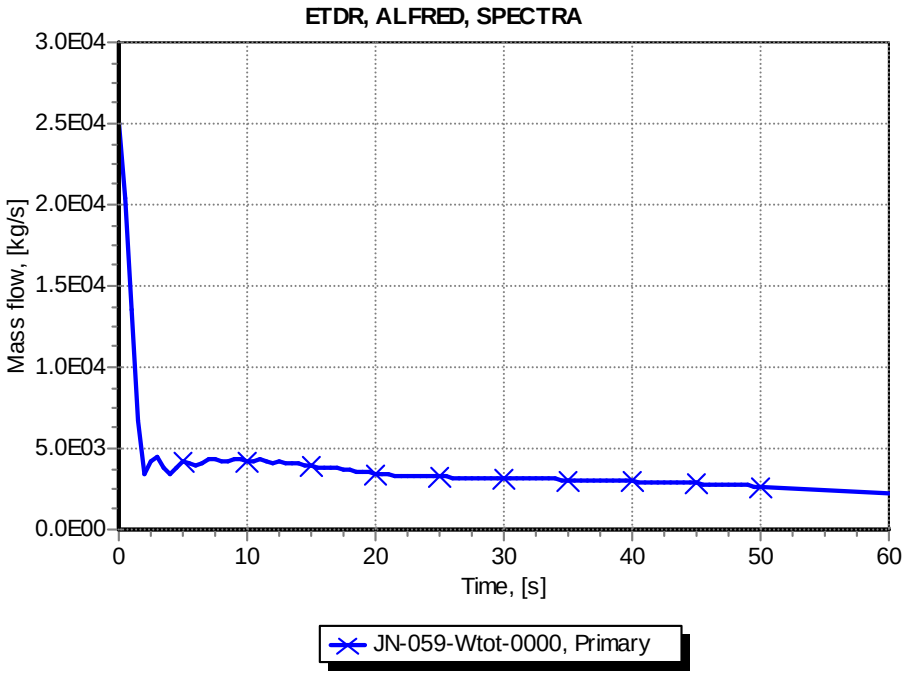


Figure 27 **Core inlet flow - short term**

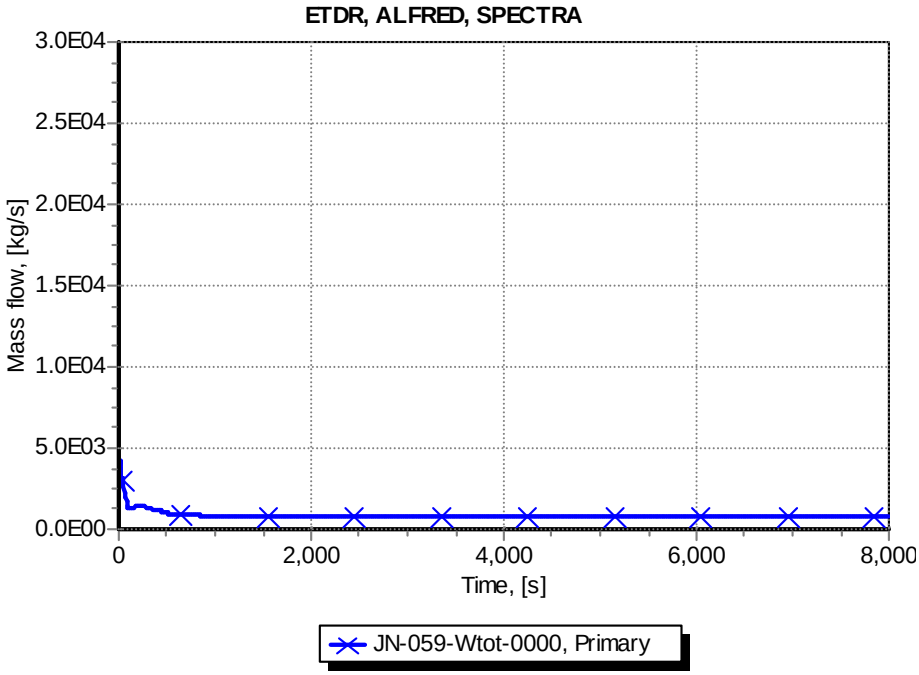


Figure 28 **Core inlet flow - long term**

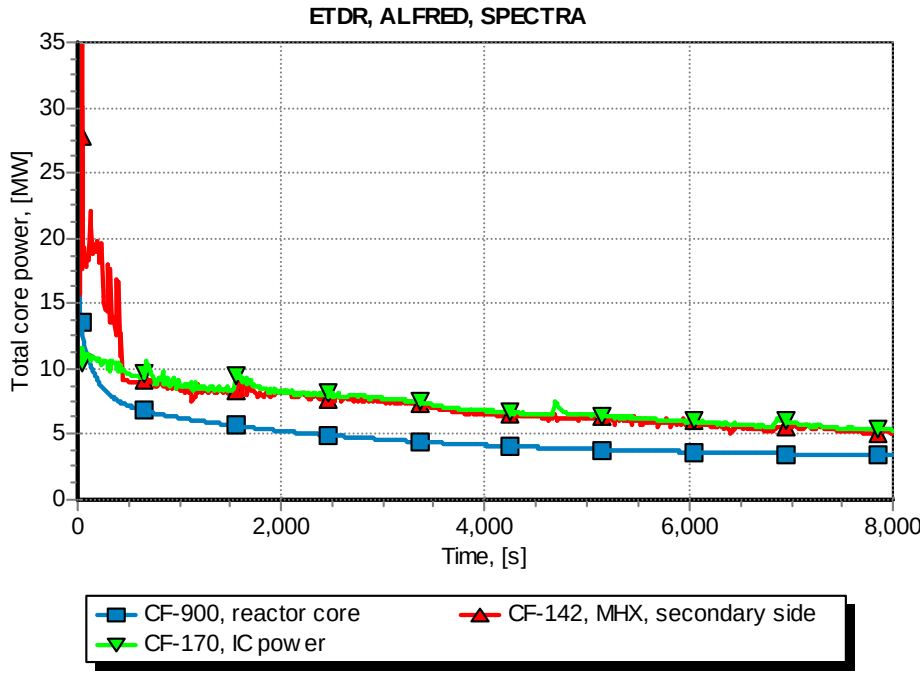


Figure 29 **Core, MHX, and IC power**

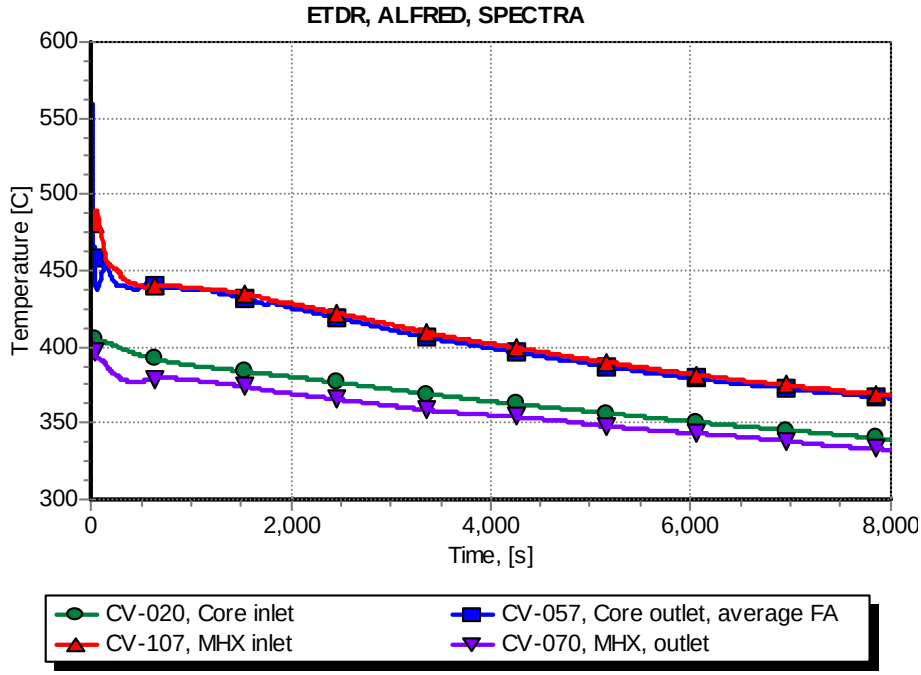


Figure 30 **Primary temperatures**

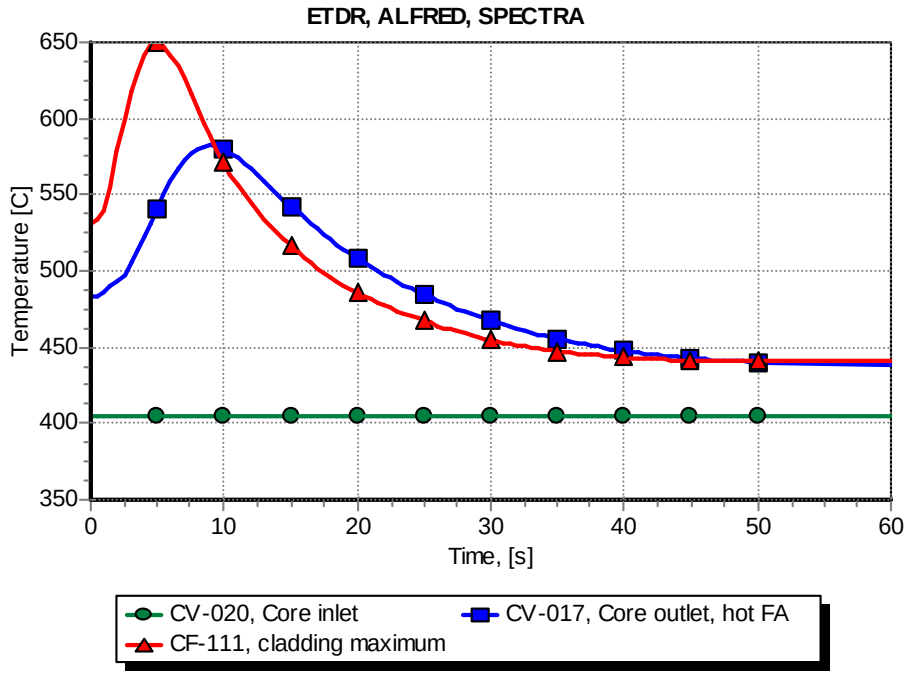
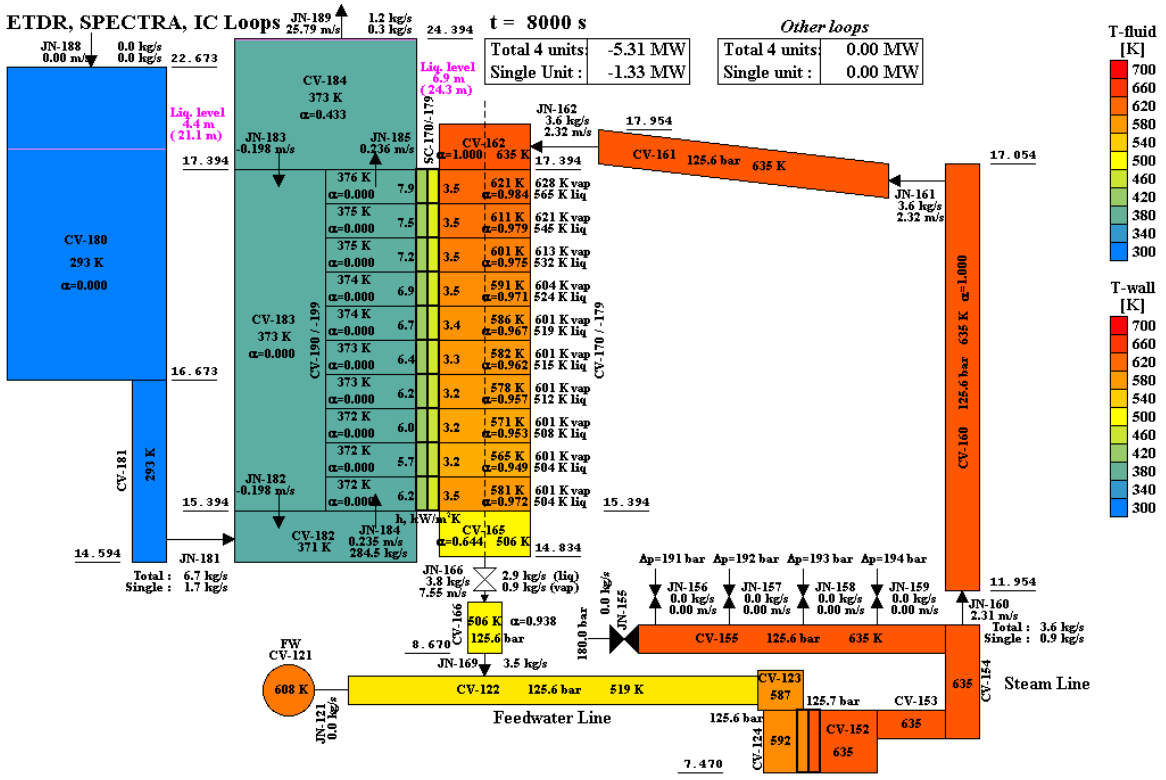


Figure 31 **Coolant and cladding temperatures**



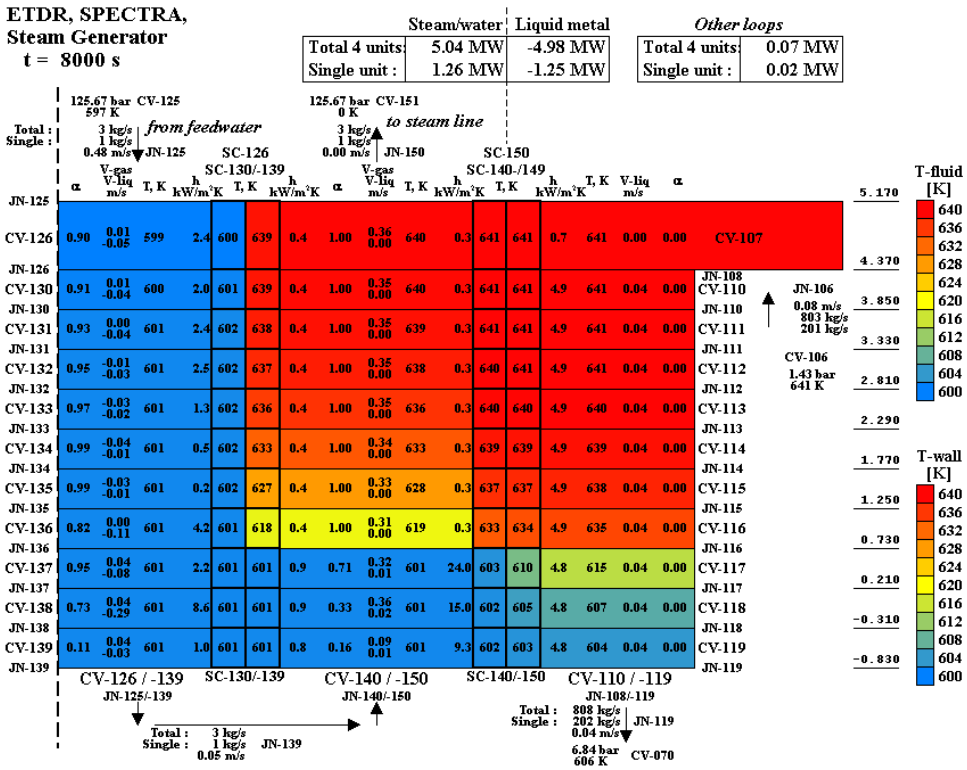


Figure 32 Visualization of IC and MHX, SPECTRA, end of transient

1.2.7 T-DEC6 SCS Failure

The T-DEC6 scenario is as follows:

- Depressurization of all secondary circuits at 0.0 s, MSDV-s open in 1.0 s, MSIV-s close in 1.0 s.
- Isolation Condensers not available.
- FW stops at t = 10.0 s. Pump speed halving time assumed 1.0 s.
- Reactor trip (SCRAM) at t = 2 s on low secondary pressure.

In this transients all loops are symmetrical. The model with all loops combined into one is used. The NRG SPECTRA results are shown in Figure 33 through Figure 39.

Secondary pressures are shown in Figure 33. The secondary pressure decreases to atmospheric in about 40 s. Core power and MHX power are shown in Figure 34. Due to reactor SCRAM at 2.0 s, the core power decreases and follows the decay power. The MHX power shortly increases to 802 MW and then decreases to about zero. Note that the height of the initial peak is very short and is strongly governed by the valve closing/opening time. In the current analyses 1.0 s was assumed for MSIV/MSDV opening/closing. If this time was 5 seconds, the peak power would be about 675 MW.

The coolant temperatures are shown in Figure 35. Lead temperatures in the core decrease to about 400°C in about 60 s. Similar lead temperatures (~400°C) are observed at the inlet and outlet of the MHX.

The fuel and cladding temperatures are shown in Figure 36 and Figure 37. The maximum fuel temperature decrease after the reactor SCRAM (at 2.0 s). The maximum cladding temperature decrease after the reactor SCRAM.

Long term power of core and MHX is shown in Figure 38. The core power follows the decay power; at 2 hours the power is 3.5 MW. The MHX power is approximately zero after about half an hour.

The long term coolant temperatures are shown in Figure 39. Because the decay heat is not removed by MHX, the temperatures rise slowly. After 2 hours the lead temperature at the core outlet is still below the initial temperature. This gives large grace time for the operator to take corrective actions (activate Isolation Condensers). The slow primary temperature increase is due to large thermal inertia of the primary system and effective mixing in the cold pool surrounding the MHX-s. In steady state (a) the pool surrounding the MHX-s is at ~670 K (400°C). Two hours into T-DEC6 (b), the pool surrounding the MHX-s is at ~730 K (450°C); similar temperature is observed in the core.

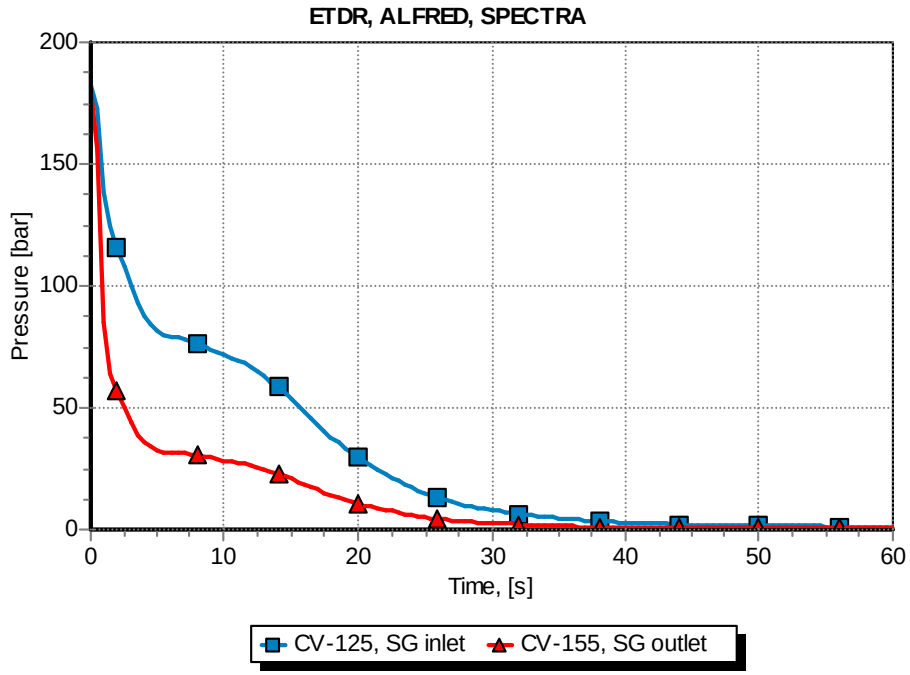


Figure 33 Secondary pressure

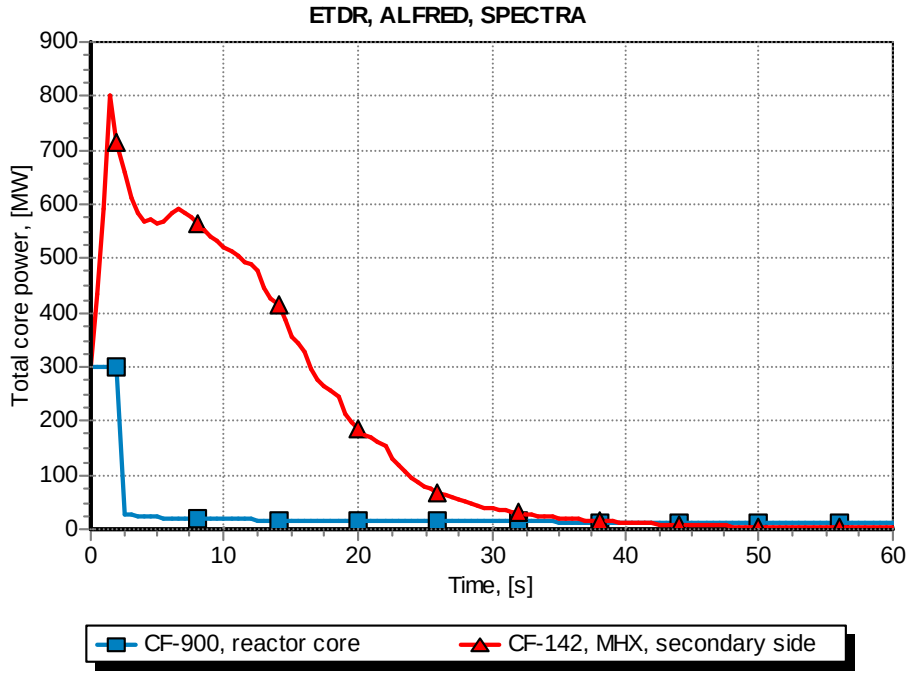


Figure 34 Core power and MHX power

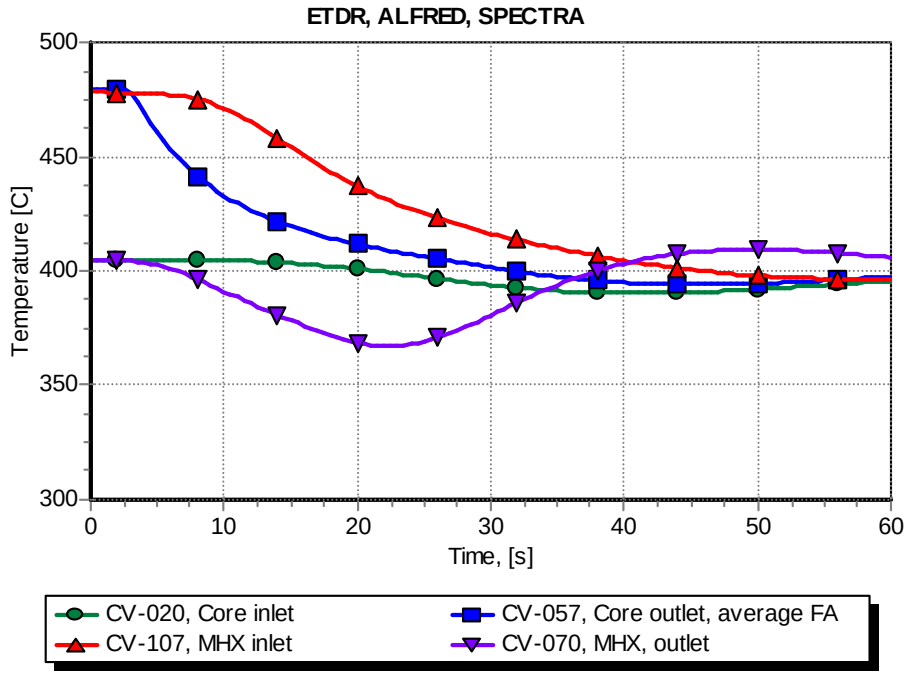


Figure 35 Coolant temperatures

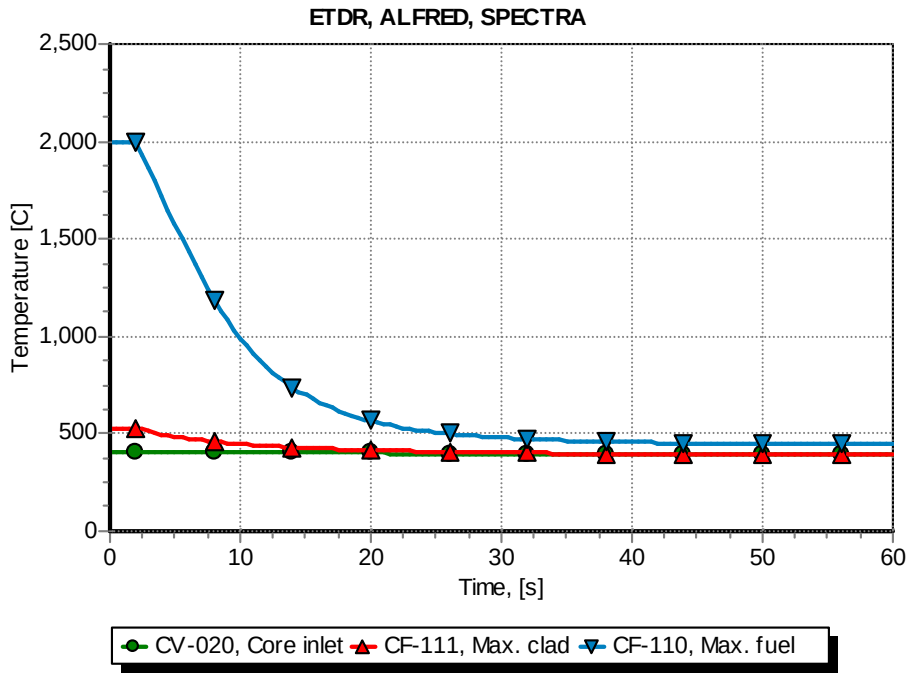


Figure 36 Fuel temperatures

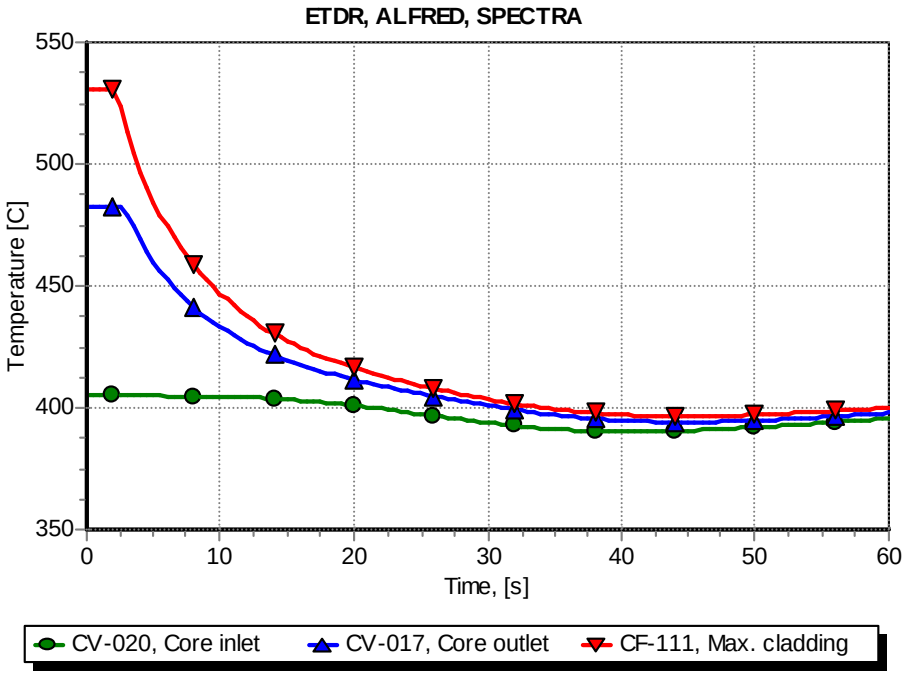


Figure 37 Cladding temperatures

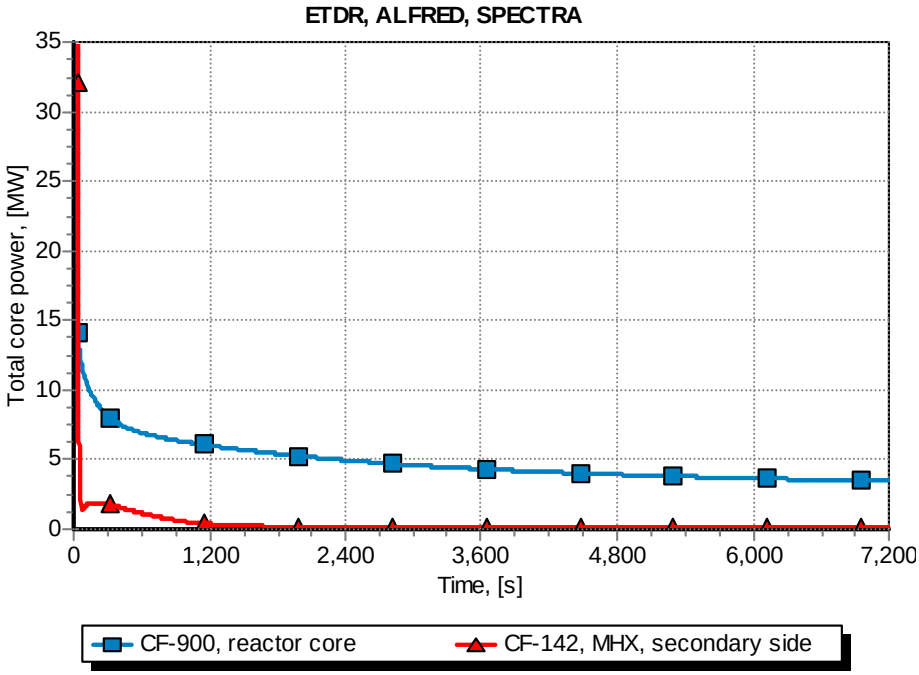


Figure 38 Core power and MHX power - long term

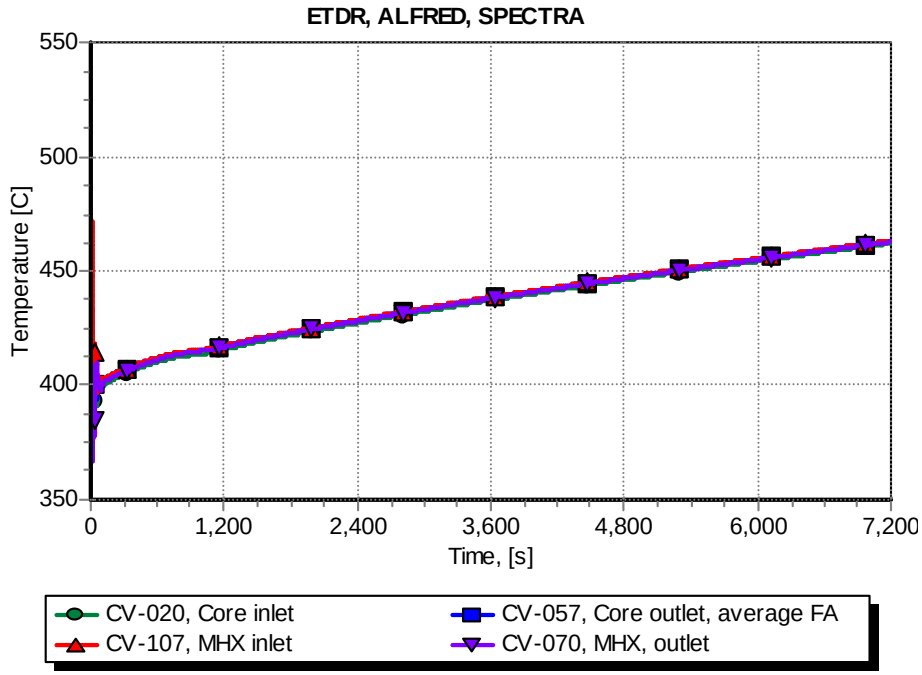


Figure 39 Coolant temperatures - long term

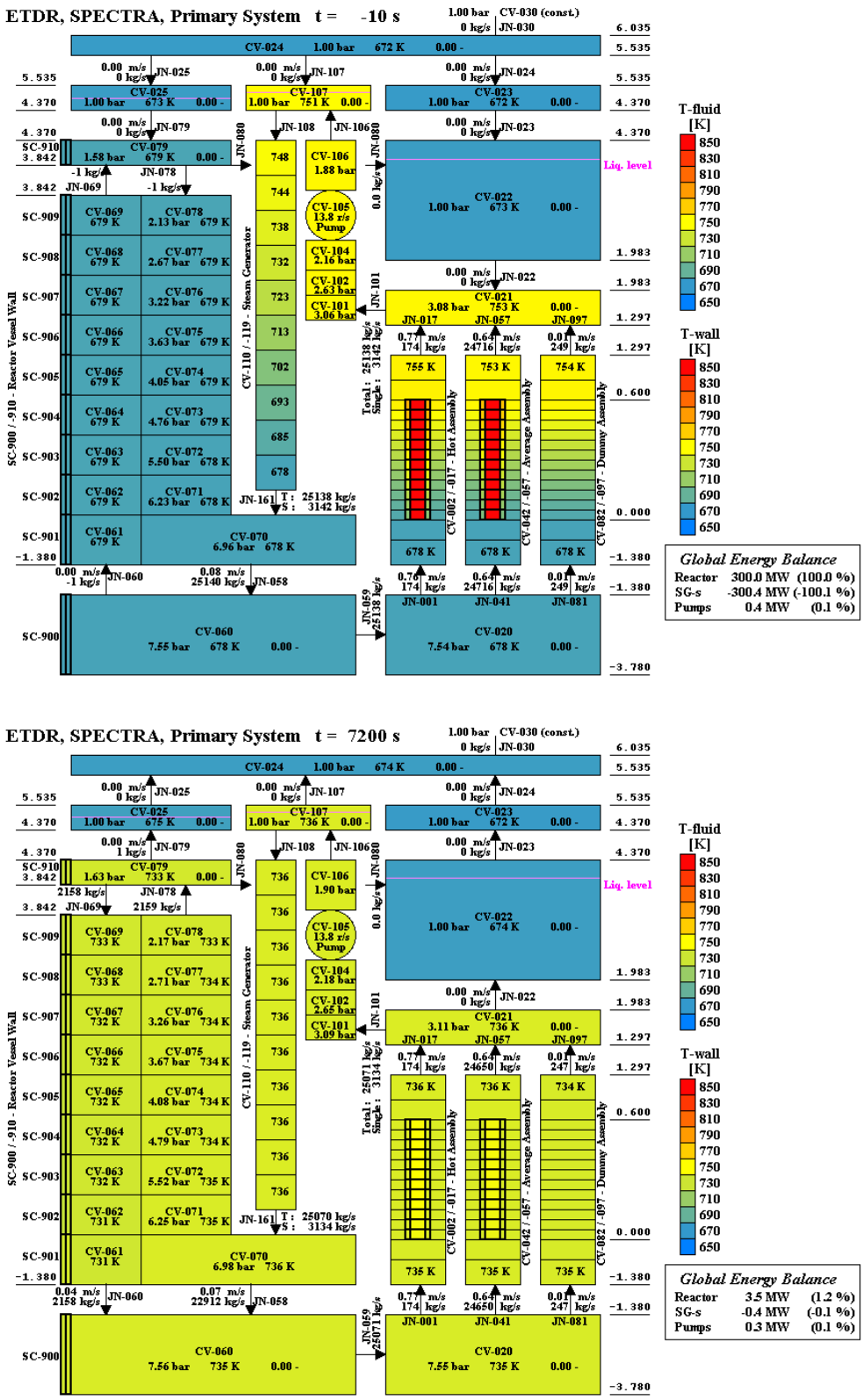


Figure 40 **Visualization of primary system at the start and end of the transient**

1.2.8 T-DEC5 Partial Blockage of Hottest Fuel Assembly

The T-DEC5 scenario is as follows

- Partial blockage of the hottest fuel assembly, inlet junction (JN-001) assumed to be blocked.
- Blockage is defined by a decrease of flow area, with constant loss factor, overall core ΔP = ~1.0 bar.
- Blockage fractions: 10, 20, 30, 40, 50, 60, 70, 80, 90, 95, 97% (subcooled boiling leading to code termination was observed for 97.5%, therefore 97% is the highest blockage reported here).
- Reactor trip (SCRAM signal) is disabled. No heat exchange with surrounding assemblies

In this transients all loops are symmetrical. The model with all loops combined into one is used. The NRG SPECTRA results are shown in Figure 41 and Figure 42. Each case is a separate run, performed for 100 s since start of blockage. During this time stable parameters are obtained.

Relative flow versus blockage fraction is shown in Figure 41. Reduction of flow rate to 50% corresponds to 75% of area reduction.

Maximum fuel, cladding, and coolant temperatures versus blockage fraction are shown in Figure 42. The maximum cladding temperature of 700˚C (973 K) is exceeded at about 85% blockage. No cladding melting is expected for blockage ≤95% (T91 clad melts at ~1720 K, ~1450˚C). No fuel melting is expected for blockage ≤90% (MOX feul melts at ~2940 K, ~2670˚C). Coolant T~580 K at 50% blockage can be detected by TC-s at assembly outlet. Note that SCRAM signal at ΔT > 1.2×nominal (=775 K, 502˚C) (blockage ≥50%) is disabled here.

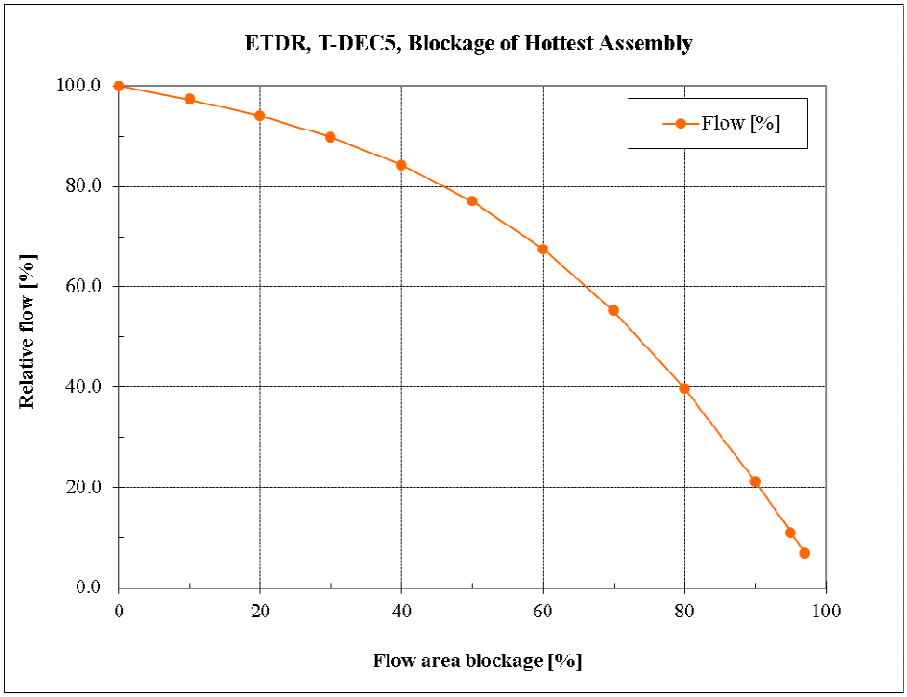


Figure 41 **Relative coolant flow**

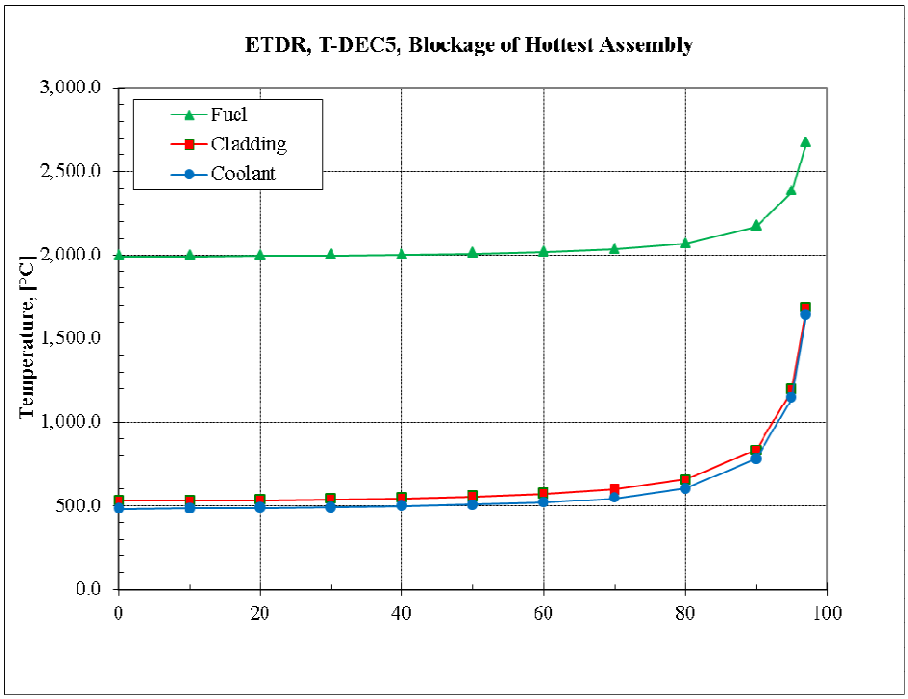


Figure 42 **Fuel, cladding, and coolant temperatures**

2 CONCLUSIONS

- Results of eight several DEC transients analyzed for the ETDR, ALFRED reactor design are shown. The results show very good intrinsic safety features of ALFRED design thanks to:
  - Good natural circulation characteristics
  - Large thermal inertia
  - Prevalent negative reactivity feedbacks

- In all analyzed transients there is no risk for significant core damage or risk for lead freezing. There is a large grace time is left to the operator to take the opportune corrective actions and bring the plant in safe conditions in the medium and long term.

Literature

[1] M.M. Stempniewicz, “SPECTRA Sophisticated Plant Evaluation Code for Thermal-Hydraulic Response Assessment, Version 3.60, August 2009, Volume 1 – Program Description, Volume 2 – User’s Guide, Volume 3 – Subroutine Description, Volume 4 - Verification and Validation”, NRG report K5024/10.101640, Arnhem, April 24, 2009.

[2] E. Bubelis, K. Mikityuk, "PLANT DATA FOR THE SAFETY ANALYSIS OF THE ETDR (ALFRED)", TEC058-2012, Revision: 0 (Draft), Issued by PSI/KIT (including contributions from ANSALDO, ENEA, EA, CEA, SRS), 30.04.2012.

[3] G. Bandini, “Analyses of Representative DEC Events of the ETDR with RELAP5”, LEADER 5th WP5 Meeting, JRC-IET, Petten, 26 february, 2013.

[4] P.A. Ushakov, A.V. Zhukov, M.M. Matyukhin, “Heat transfer to liquid metals in regular arrays of fuel elements”, High Temperature, 15, pp. 868-873, 1977.

[5] “Handbook on Lead-bismuth Eutectic Alloy and Lead Properties, Materials Compatibility, Thermal-hydraulics and Technologies”, OECD/NEA Nuclear Science Committee. ISBN 978-92-64-99002-9, 2007.

ANNEX
SPECTRA Model of ETDR ALFRED

The SPECTRA is a thermal-hydraulic system code for transient analyses in Light Water Reactors, High Temperature Reactors, and Liquid Metal Fast Reactors. The SPECTRA model of ETDR consists of the following elements:

- Primary system (liquid lead)
- Main heat exchangers (MHX), referred to also as Steam Generators (SG) and secondary system loops (8 steam/water loops)
- Decay Heat Removal (DHR) loops with Isolation Condensers (IC) heat exchangers.

Nodalization of the SPECTRA model was assumed very similar to the nodalization applied for RELAP analyses at ENEA [2]. Some simplifications in the number of nodes were made whenever possible. The EOC conditions were assumed. For modeling the gap, fuel swelling of 0.149 mm was assumed (initial gap size 0.150 mm), following RELAP model. The SPECTRA model is shortly described below.

Nodalization of the SPECTRA Model of ETDR

The nodalization of the SPECTRA model of ETDR is shown in Figure 1 through Figure 6. Figure 1 shows general overview of the reactor vessel model. Figure 2 shows the reactor core. The core consists of the following Fuel Assembles (FA):

- Hot assembly (1 FA),
  - coolant: CV-002 - CV-017 (multiplicity of 1)
  - average pin (multiplicity of 126) modeled by SC-004 through SC-015
  - peak pin (multiplicity of 1) modeled by SC-024 through SC-035
- Average assembly (170 FA),
  - coolant: CV-042 - CV-057 (multiplicity of 170)
  - average pin (multiplicity of 170×127=21590)
  - wrapper (multiplicity of 171) modeled by SC-064 - SC-075
- Dummy assembly (1 FA),
  - coolant: CV-082 - CV-097 (multiplicity of 1)
  - wrapper (multiplicity of 108) modeled by SC-084 - SC-095

Figure 3 shows the nodalization of fuel pins, including fuel, gap, and cladding. shown in Figure 4 shows nodalization of the Main Heat Exchanger (Steam Generator). Figure 5 shows nodalization of the secondary loops. Figure 6 shows the Decay Heat Removal loops with Isolation Condensers.

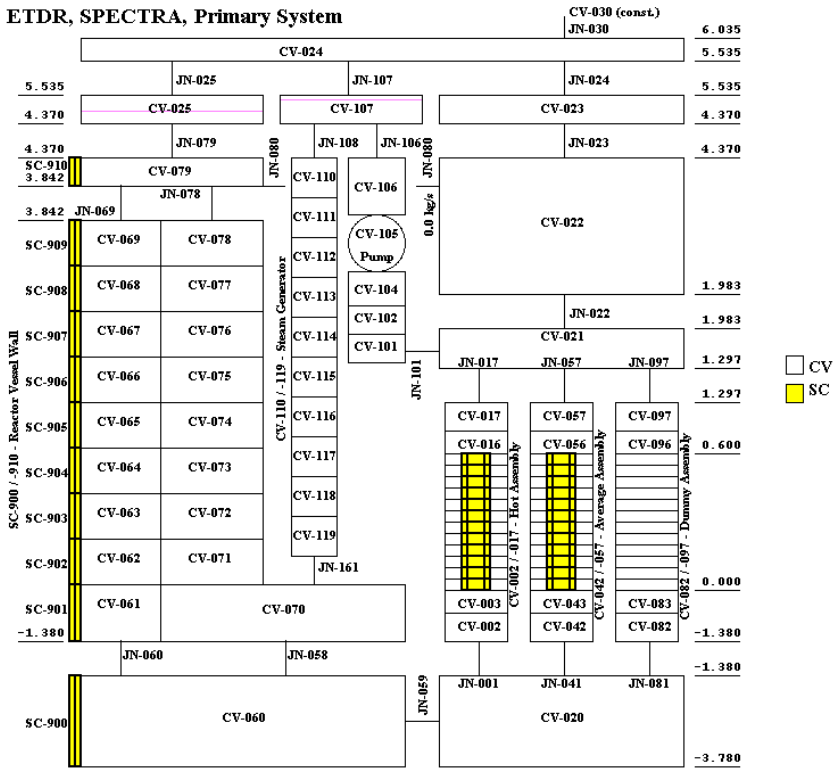


Figure 1 **Nodalization of the primary system - SPECTRA model of ETDR**

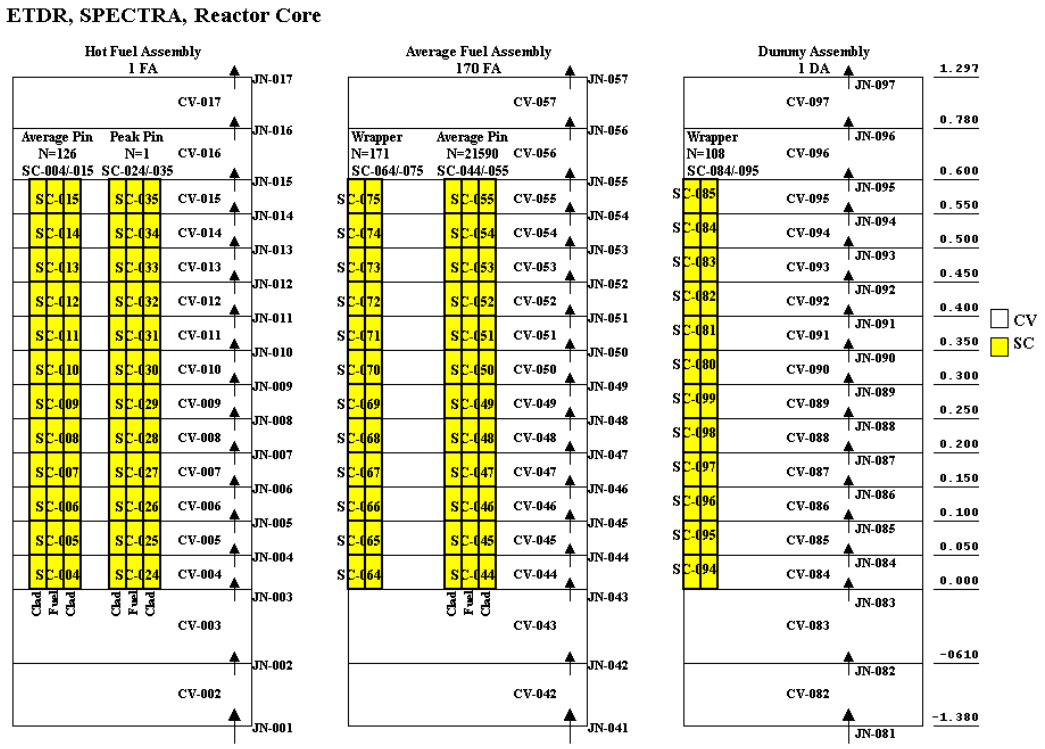


Figure 2 **Nodalization of the reactor core - SPECTRA model of ETDR**

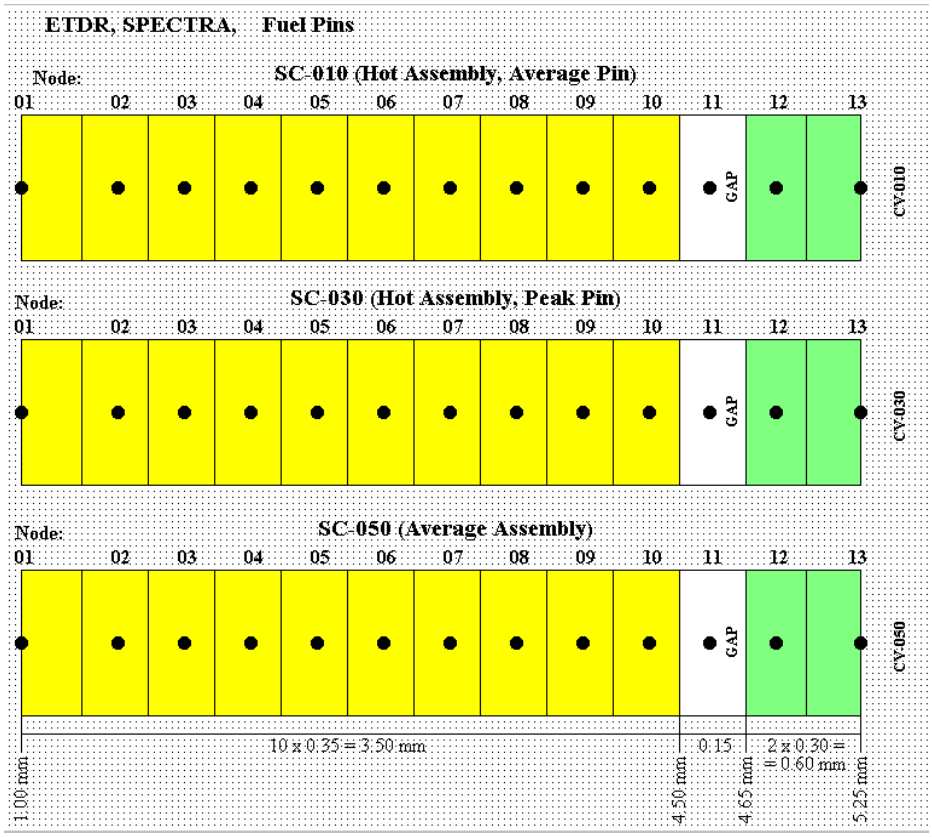


Figure 3 **Nodalization of the intermediate loops - SPECTRA model of ETDR**

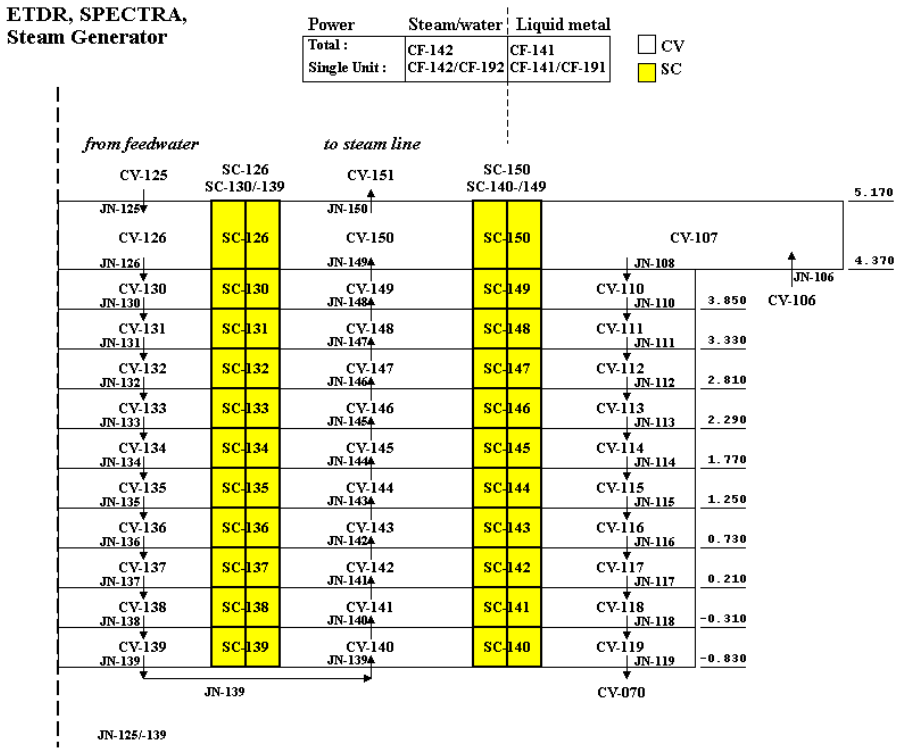


Figure 4 **Nodalization of the intermediate heat exchangers (IHX) - SPECTRA model of ETDR**

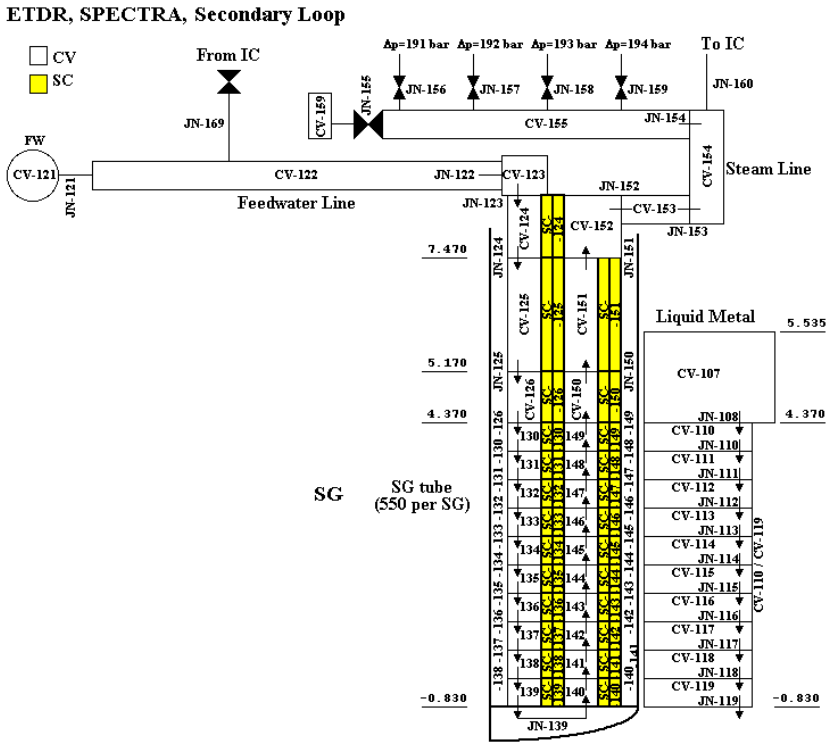


Figure 5 **Nodalization of the steam generators (SG) - SPECTRA model of ETDR**

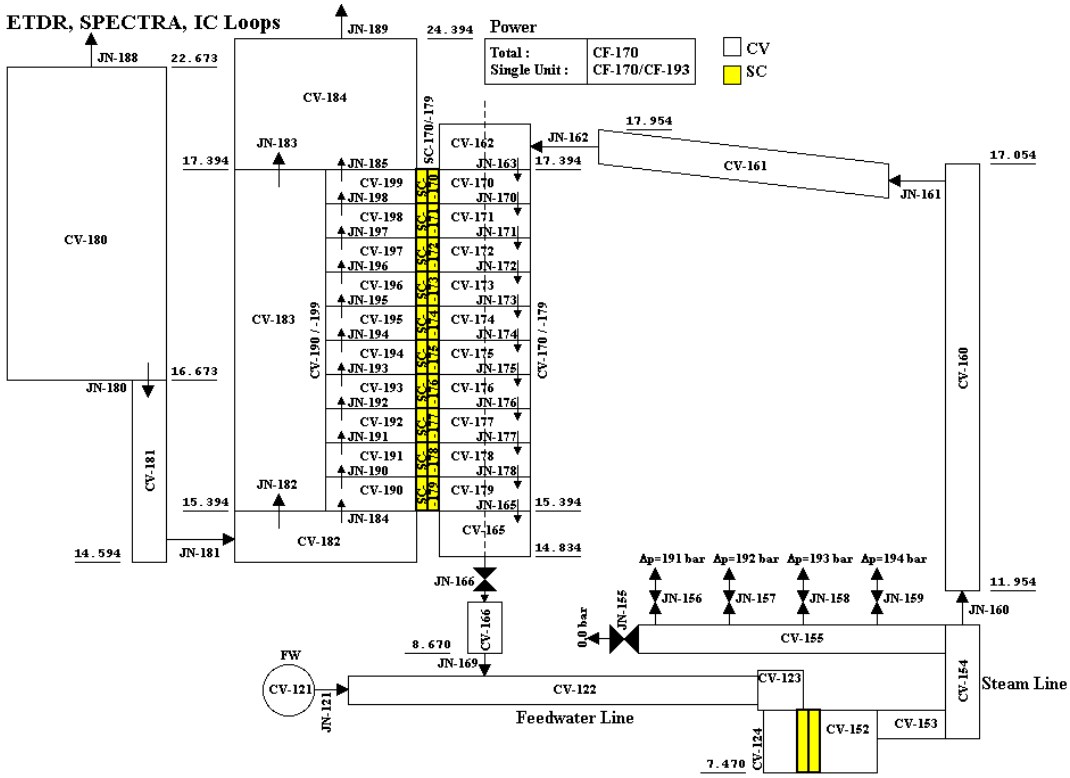


Figure 6 **Nodalization of the decay heat removal loops (DHR) - SPECTRA model of ETDR**

Heat Transfer Correlations

Whenever alternative fluids (liquid metals) are used in SPECTRA calculations, the heat transfer coefficient correlations must be defined in input. For application in the current model, the following correlation was used:

$$Nu = 7.55x - \frac{20}{x^{13}} + \frac{0.041}{x^2} \cdot Pe^{(0.56+0.19x}$$

Here $x = P/D$ (pitch to diameter ratio). The following values were used:

- Reactor Core: P/D=1.32 D = 0.00897 m hydraulic diameter (4P/A)
- MHX primary side: P/D=1.4182 D = 0.00387 m hydraulic diameter (4P/A)

For the secondary, steam/water side, the built in correlations for single phase flows, two phase flows, boiling, as well as condensation are used. The characteristic dimension are defined as follows:

- MHX secondary side: D = 0.00487 m hydraulic diameter (4P/A)
- IC condensing side: D = 2.0 m tube length (= L)
- IC boiling side: D = 0.66 m hydraulic diameter (4P/A)

Reactor Kinetics Model

The point kinetics model is used. Reactivity feedback from isotopes (Xenon, etc.) is ignored for the present calculations. The reactivity data is appropriate for the End of Life and was obtained from reference [1].

- General data
  - Prompt neutron generation time: $\Lambda = 6.296\times10^{-7}$ 1/s
  - Delayed neutron precursor data shown in Table 1.

- Average fuel temperature, T_{fuel}.
  The average fuel temperature is calculated using constant weighting factors (uniform weight - note that the values are internally normalized by the code, so the input values may be scaled by any factor):

  - Average fuel assembly (SC-044 through SC-055) W_i = 0.05

Table 1 Delayed neutron precursor data

Group number i	Yield β_i, [-]	Relative yield β_i / β	Decay constant, λ_i, [1/s]
1	5.899E-05	1.761E-02	1.250E-02
2	5.790E-04	1.728E-01	2.830E-02
3	2.180E-04	6.507E-02	4.250E-02
4	5.050E-04	1.508E-01	1.330E-01
5	1.069E-03	3.191E-01	2.925E-01
6	3.850E-04	1.149E-01	6.665E-01
7	3.740E-04	1.116E-01	1.635E+00
8	1.610E-04	4.806E-02	3.555E+00
Total, β	3.350E-3	1.0	

- The Doppler reactivity effect is calculated as follows:

$$\Delta R_D = K_D \cdot \ln(T_{fuel} / T_{fuel,0})$$

Here K_D is constant, equal to: K_D = –566 pcm/K, T_{fuel} is the average fuel temperature, and $T_{fuel,0}$ is the nominal fuel temperature (1500 K). For SPECTRA calculations the reactivity is converted to dollars and tabulated for the temperature range 400 - 3100 K. The values are shown in Table 2.

Table 2 Doppler reactivity table

T, [K]	R, [pcm]	***R*, [$]**	T, [K]	R, [pcm]	***R*, [$]**
400.0	748.11	**2.233**	1800.0	-103.19	**-0.308**
500.0	621.81	**1.856**	1900.0	-133.80	**-0.399**
600.0	518.62	**1.548**	2000.0	-162.83	**-0.486**
700.0	431.37	**1.288**	2100.0	-190.44	**-0.568**
800.0	355.79	**1.062**	2200.0	-216.77	**-0.647**
900.0	289.13	**0.863**	2300.0	-241.93	**-0.722**
1000.0	229.49	**0.685**	2400.0	-266.02	**-0.794**
1100.0	175.55	**0.524**	2500.0	-289.13	**-0.863**
1200.0	126.30	**0.377**	2600.0	-311.33	**-0.929**
1300.0	81.00	**0.242**	2700.0	-332.69	**-0.993**
1400.0	39.05	**0.117**	2800.0	-353.27	**-1.055**
1500.0	0.00	**0.000**	2900.0	-373.13	**-1.114**
1600.0	-36.53	**-0.109**	3000.0	-392.32	**-1.171**
1700.0	-70.84	**-0.211**	3100.0	-410.88	**-1.227**

The Doppler reactivity is calculated in SPECTRA as the thermal feedback, ΔR_{TF}, and may be plotted as such. For convenience, Control Function CF-901 was defined, which gives the thermal feedback shifted to give zero at nominal reactor operating condition:

$$\text{CF-901} = \Delta R_{TF} - 2.2055$$

Here R_{TF} is the reactivity from thermal feedback [$]. The additive constant, –2.2055 $ ensures that the value of CF-901 is zero at nominal reactor operating conditions.

- The axial fuel expansion effect is calculated as follows:

$$\Delta R_{axial} = c_{axial} \cdot (T_{fuel} - T_{fuel,0})$$

Here c_{axial} is the axial fuel expansion coefficient, equal to –0.155 pcm/K = -4.63×10^{-4} $/K, while T_{fuel} is the average fuel temperature, calculated as shown above.

The axial fuel expansion reactivity effect is calculated using Control Function CF-902, defined as:

$$\text{CF-902} = \Delta R_{axial} + 0.6154$$

The additive constant, +0.6154 $ ensures that the value of CF-902 is zero at nominal reactor operating conditions.

For the cases when the fuel-cladding gap is closed (transient TR-4) the “linked coefficient” is used, with cladding average temperature:

$$\Delta R_{axial} = c_{linked} \cdot (T_{clad} - T_{clad,0})$$

Here c_{linked} is the linked coefficient, equal to –0.242 pcm/K = -7.22×10^{-4} $/K, while T_{clad} is the average cladding temperature, calculated as arithmetic average of all nodes of the average fuel assembly:

$$T_{clad} = \left(\frac{1}{12}\right) \cdot \sum_{i=SC-044}^{SC-055} T_{clad,i}$$

- The coolant density feedback is calculated as follows:

$$\Delta R_{cool} = c_{cool} \cdot (T_{cool} - T_{cool,0})$$

Here c_{cool} is the coolant density coefficient, equal to –0.268 pcm/K = -8.00×10^{-4} $/K, while T_{cool} is the average coolant temperature. The average coolant temperature is calculated as arithmetic average of all nodes of the average fuel assembly:

$$T_{cool} = \left(\frac{1}{12}\right) \cdot \sum_{i=CV-044}^{CV-055} T_{cool,i}$$

The coolant density reactivity effect is calculated using Control Function CF-903, defined as:

$$CF-903 \quad = \quad -8.00\times10^{-4} \times \left(\frac{1}{12}\right) \cdot \sum_{i=CV-044}^{CV-055} T_{cool,i} \quad + \quad 0.5742$$

The additive constant, +0.5742 $ ensures that the value of CF-903 is zero at nominal reactor operating conditions.

- The axial cladding expansion effect is calculated as follows:

$$\Delta R_{clad} = c_{clad} \cdot (T_{clad} - T_{clad,0})$$

Here c_{clad} is the axial clad expansion coefficient, equal to +0.05 pcm/K = 1.49×10^{-4} $/K, while T_{clad} is the average cladding temperature. The cladding expansion reactivity effect is calculated using Control Function CF-904, defined as:

$$CF-904 \quad = \quad 1.49\times10^{-4} \times \left(\frac{1}{12}\right) \cdot \sum_{i=SC-044}^{SC-055} T_{clad,i} \quad - \quad 0.11043$$

The additive constant, –0.11043 $ ensures that the value of CF-904 is zero at nominal reactor operating conditions.

- The wrapper expansion effect is calculated as follows:

$$\Delta R_{wrap} = c_{wrap} \cdot (T_{wrap} - T_{wrap,0})$$

Here c_{wrap} is the wrapper expansion coefficient, equal to +0.026 pcm/K = $+7.76\times10^{-5}$ $/K, while T_{wrap} is the average wrapper temperature. The wrapper expansion reactivity effect is calculated using Control Function CF-905, defined as:

$$CF-905 \quad = \quad 7.76\times10^{-5} \times \left(\frac{1}{12}\right) \cdot \sum_{i=SC-064}^{SC-075} T_{clad,i} \quad - \quad 0.0557$$

The additive constant, –0.0557 $ ensures that the value of CF-905 is zero at nominal reactor operating conditions.

- The radial core expansion is caused by expansion of the diagrid, which supports the whole core. The diagrid expansion effect is calculated as follows:

$$\Delta R_{diagrid} = c_{diagrid} \cdot (T_{diagrid} - T_{diagrid,0})$$

Here $c_{diagrid}$ is the reactivity effect due to diagrid radial expansion, equal to –0.152 pcm/K = –4.54×10^{-3} \$/K, while $T_{diagrid}$ is the diagrid temperature (approximated here as the liquid temperature at the core inlet, CV-020). The diagrid expansion reactivity effect is calculated using Control Function CF-906, defined as:

$$CF-906 \quad = \quad -4.54\times10^{-4}\times T_{CV-020} \quad + \quad 0.3079$$

The additive constant, +0.3079 \$ ensures that the value of CF-906 is zero at nominal reactor operating conditions.

- The pad expansion effect is calculated as follows:

$$\Delta R_{pad} = c_{pad}\cdot(T_{pad} - T_{pad,0})$$

Here c_{pad} is the reactivity effect due to pad expansion, equal to –0.43 pcm/K = –1.28×10^{-3} \$/K, while T_{pad} is the pad temperature (approximated here as the liquid temperature at the core outlet, CV-057). The pad expansion reactivity effect is calculated using Control Function CF-907, defined as:

$$CF-907 \quad = \quad -1.28\times10^{-3}\times T_{CV-057} \quad + \quad 0.964$$

The additive constant, +0.964 \$ ensures that the value of CF-907 is zero at nominal reactor operating conditions.

- The reactivity effect caused by the change of the length of the Control Assembly (CA) in the core consists of two effects:
  - prompt effect - movement of control rod due to expansion of the CA bar mechanism when the temperature of the hot collector increases.

$$\Delta R_{CA,1} = c_{CA,1}\cdot(T_b - T_{b,0})$$

Here T_b is the temperature of the CA bar mechanism, while $c_{CA,1}$ = –0.218 pcm/K = 6.51E–4 \$/K.

  - delayed effect - vertical movement of the core due to expansion of the core support when the core support temperature changes.

$$\Delta R_{CA,2} = c_{CA,2}\cdot(T_s - T_{s,0})$$

Here T_s is the core support temperature , while $c_{CA,2}$ = –0.429 pcm/K = –1.28E–3 \$/K.

In the model only the prompt effect is taken into account; the delayed effect is neglected. The CA bar temperature is approximated as the liquid temperature above the core - CV-057.The reactivity effect is calculated using Control Function CF-908, defined as:

$$CF-908 \quad = \quad -6.52\times10^{-4}\times T_{CV-021} \quad + \quad 0.4903$$

The additive constant, +0.4901 $ ensures that the value of CF-908 is zero at nominal reactor operating conditions.

Two series of calculations were performed within the current task. The first series the reactor protection system is assumed to be unavailable (unprotected transients). For the second set of calculations, reactor protection was taken into account. The protected transients were analyzed only for those situations where unprotected transients resulted in exceeding the limit on maximum cladding temperature (700˚C). The reactor protection system (SCRAM), signals are shown in Table 3. The total reactivity worth of the SCRAM rods is 8476 pcm = 27.31 $.

Table 3 SCRAM signals

No.	Signal	Setpoint
S1	neutron flux > 120%	Q > 336 MW
S2	average assembly ΔT > 1.2×nominal	T > 772 K (499˚C)
S3	hot assembly ΔT > 1.2×nominal	T > 775 K (502˚C)
S4	low primary flow, W < 90%	W < 22230 kg/s

Steady State Results

The model was tested by running steady state calculations. The results are shown in several visualization pictures below.

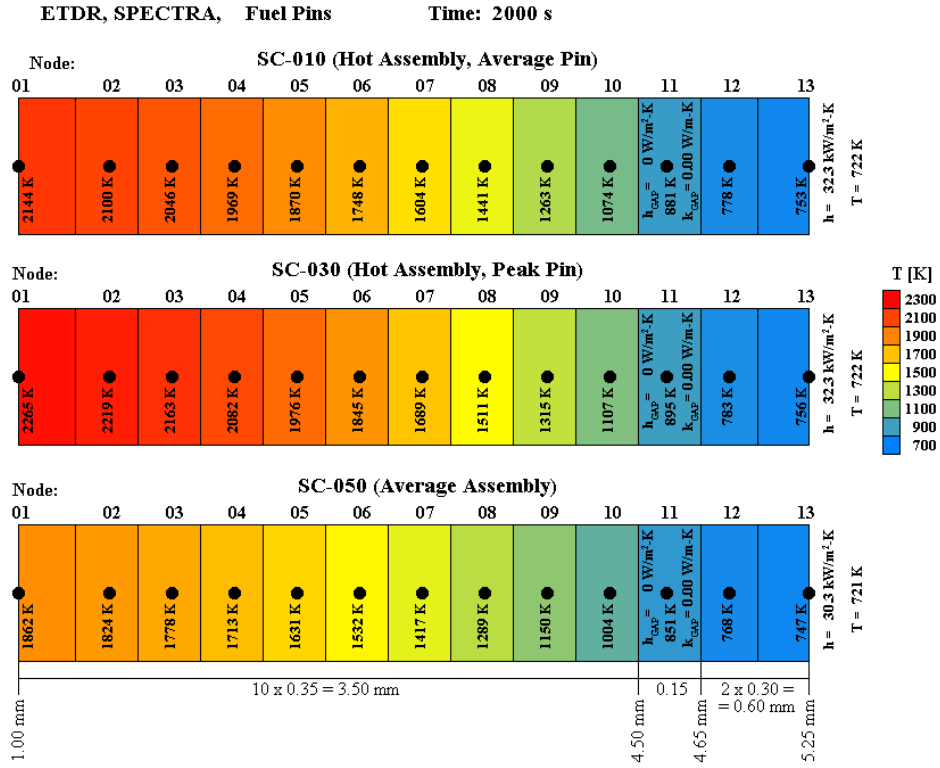


Figure 7 **Fuel pins, hot assembly and average assembly**

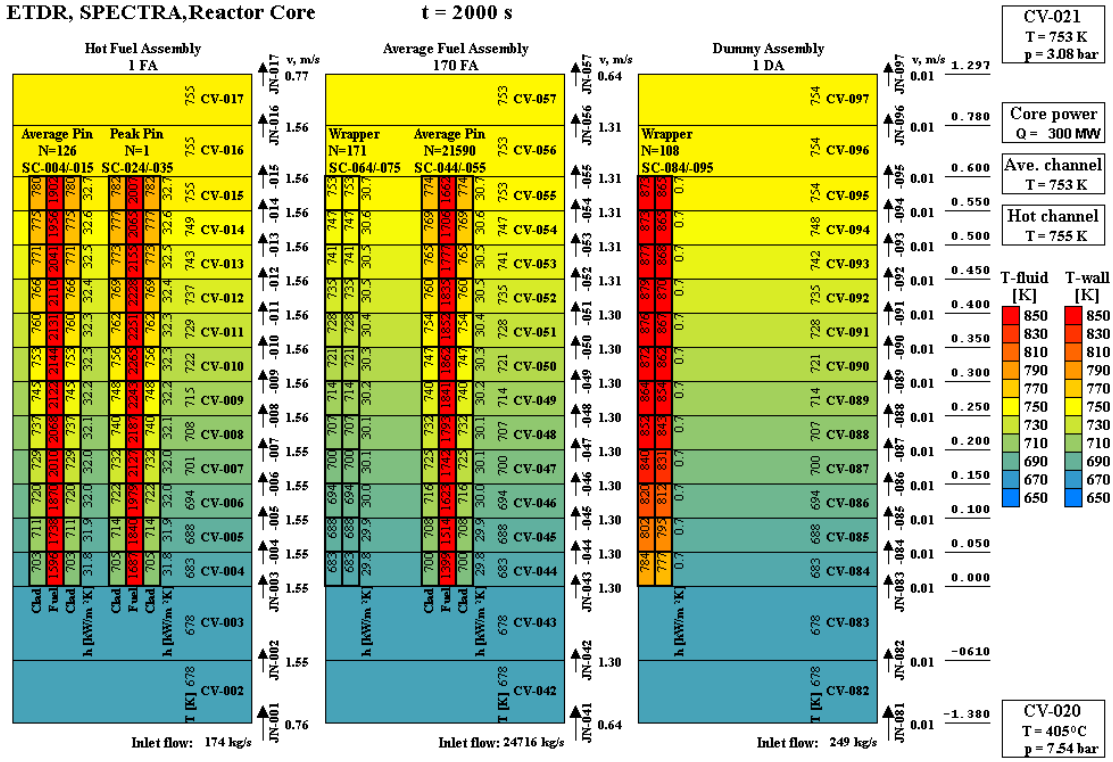


Figure 8 **Reactor core**

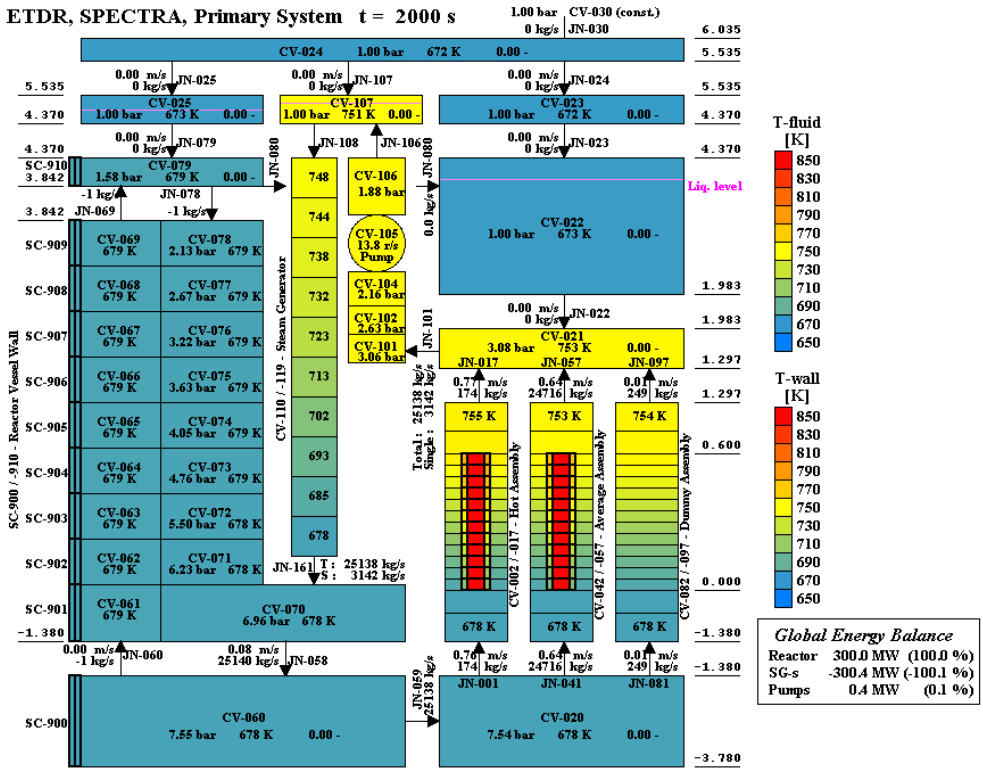


Figure 9 **Primary system**

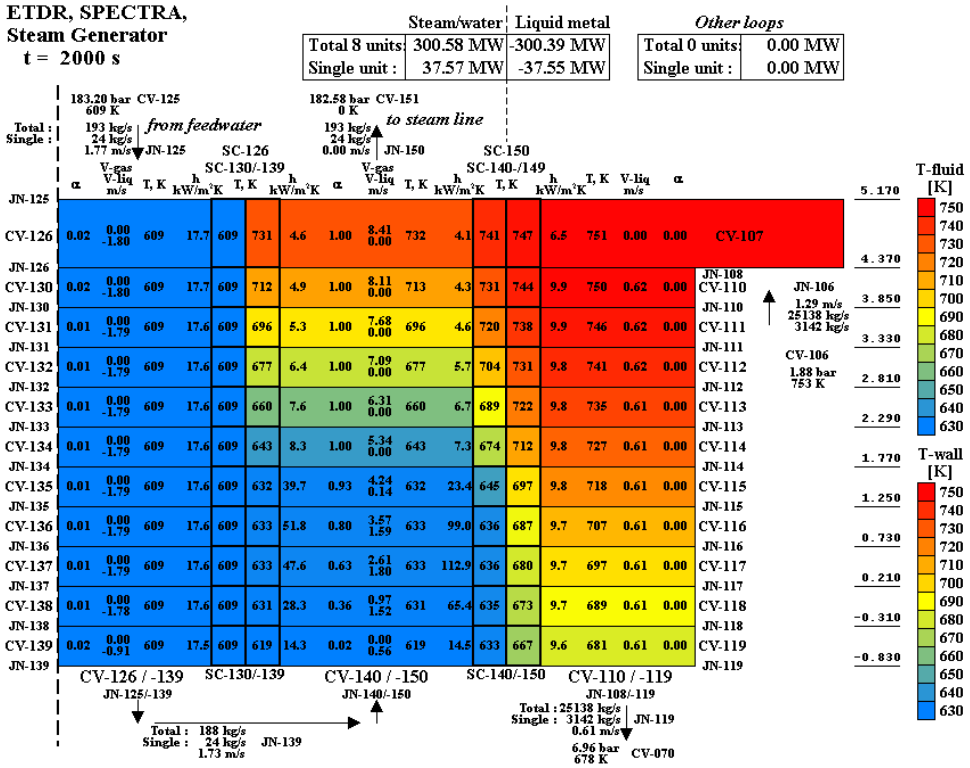


Figure 10 **MHX (Steam Generator)**

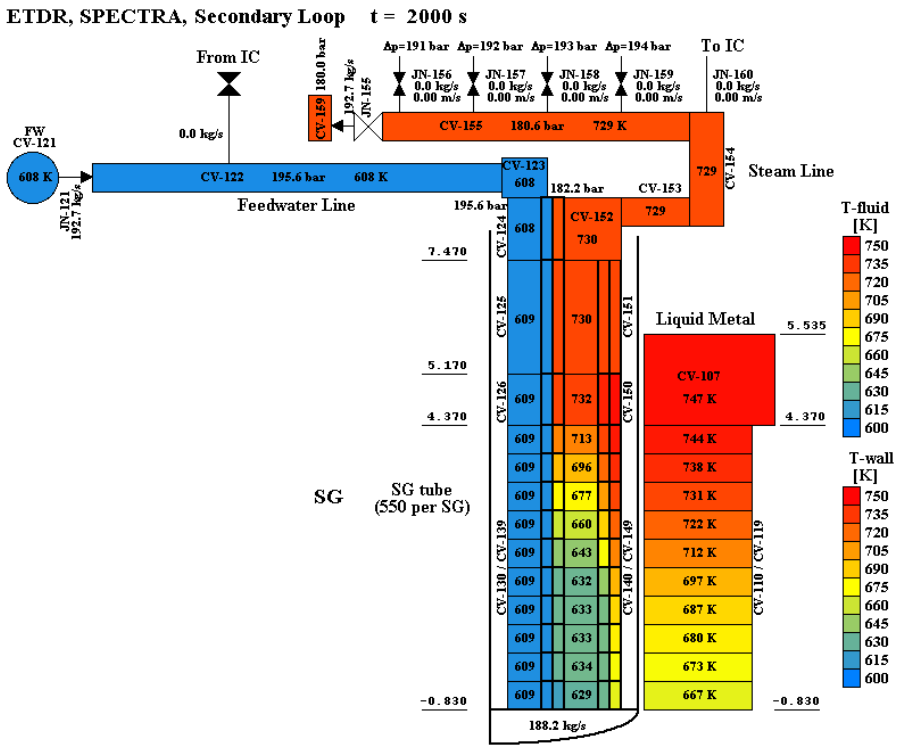


Figure 11 **Secondary loop**

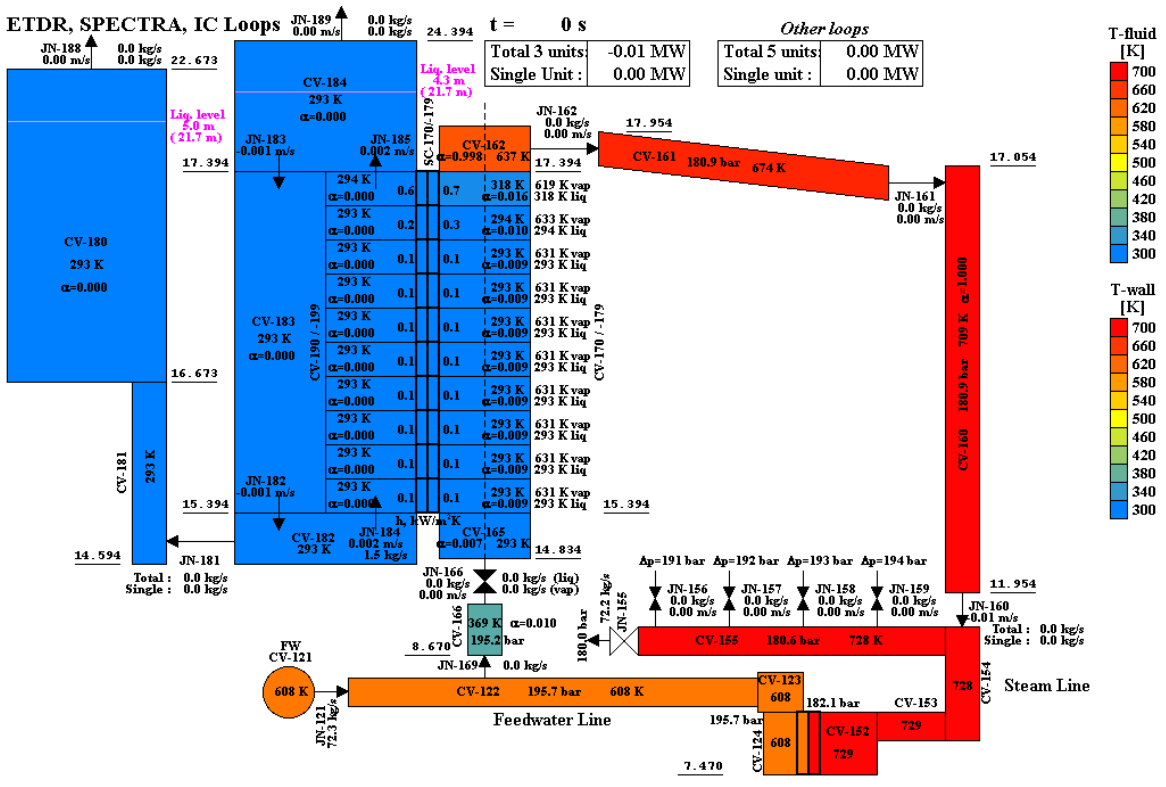


Figure 12 **Isolation Condenser loop**

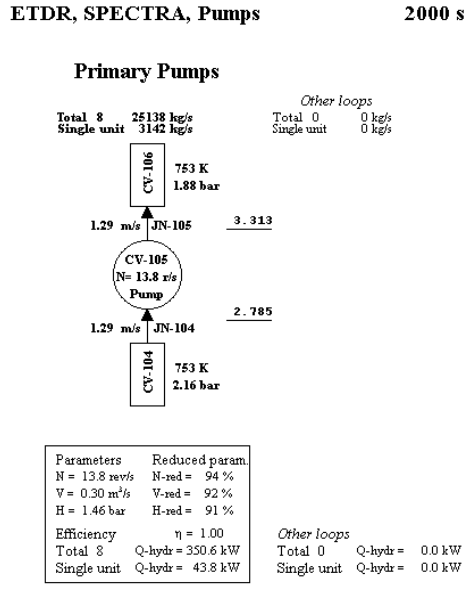


Figure 13 Pumps

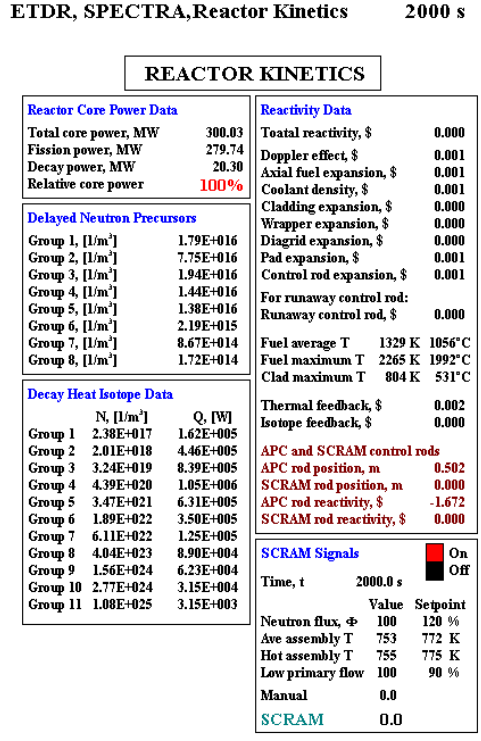


Figure 14 Reactor kinetics

Literature

[1] E. Bubelis, K. Mikityuk, "PLANT DATA FOR THE SAFETY ANALYSIS OF THE ETDR (ALFRED)", TEC058-2012, Revision: 0 (Draft), Issued by PSI/KIT (including contributions from ANSALDO, ENEA, EA, CEA, SRS), 30.04.2012.

[2] G. Bandini, “Analyses of Representative DEC Events of the ETDR with RELAP5”, LEADER 5th WP5 Meeting, JRC-IET, Petten, 26 february, 2013.

APPENDIX F

KTH Contribution to LEADER Deliverable DEL022:

a) Summary of Transient Simulation Results for ALFRED with RELAP5 Code and CFD Simulation Approach for Bubble Transport in SGTR/SGTL Event

DEC transients performed by KTH

M. Jeltsov, K. Kööp, P. Kudinov

In the framework of LEADER, under WP 5 (task 5.5), KTH has performed two transient analyses for design extended conditions.

1. **T-DEC1** – unprotected loss of forced flow
2. **T-DEC4** – unprotected loss of forced flow and loss of secondary cooling system while 3 out of 4 DHR operating.
3. **TR-4** – a transient due to reactivity insertion (enveloping SGTR, flow blockage, core compaction).

The calculations of T-DEC1 and T-DEC4 are performed using modified RELAP5 system code with Ushakov correlation. The system model is based on ENEA's RELAP5 model with slight modifications.

TR-4 analysis comprises of development of the approach to assess the risk of core voiding due to steam generator tube failure. This study focuses on small leakages in the early stage of a SG failure and aims to investigate whether a steam bubble or bubbles can be dragged from the leaking SG region to the core inlet by the flow of lead coolant. The calculation results are delayed at this moment and will be provided in the next revision of the deliverable or as a separate report to the project.

Modifications to the RELAP5 model

Obtained RELAP5 model was modified to better handle non-symmetric transients (e.g. partial pump trips). The original model was created for symmetric transients and running partial pump trip calculations resulted in RELAP5 crashes. The reason for the code crashing was identified as "*vapor phase property call error*". The location of the problem was mainly found to be in the inlet part of the steam generator (151-8), below a branch component (061-8) that connects the outlet of the pump with the steam generator and the gas plenum.

The modifications to the original model were kept to a minimum to maintain compatibility and comparability. Several combinations were explored including using pipe components, combination of pipe and branch components and changing the non-condensable gases flags in local nodes. In the end, good results were obtained by dividing the single branch component into two branches. The top branch has non-condensable gases flag activated while the lower branch has only the vapor flag. This configuration resulted in more stable calculations and allowed exploration of a larger event space.

T-DEC1

In case of unprotected loss of flow transient, all pumps are tripped at time 0 after a 1000 seconds steady state calculation. SCRAM signal is deactivated throughout the transient and secondary cooling system is kept operational.

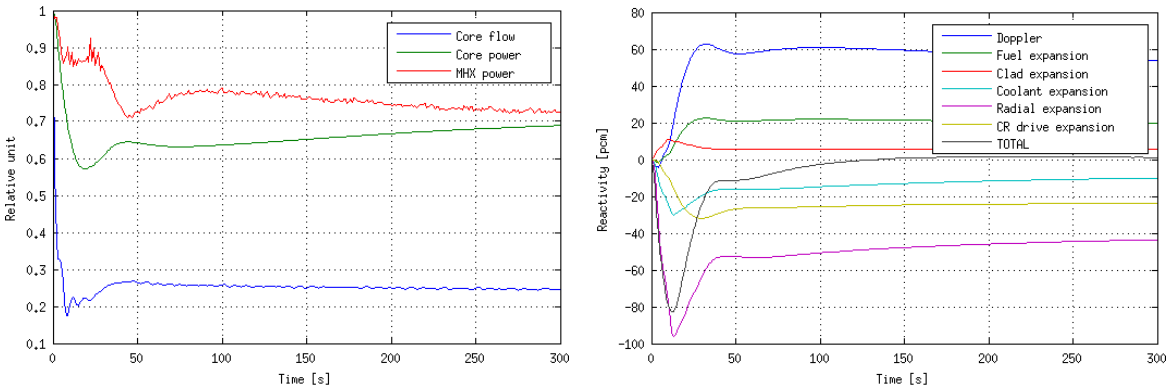


Figure 1: a) Core flow, power and MHX power in relative units
b) Reactivity components and total feedback for ULOF

The power of the reactor decreases from its initial value of 300 MW down to around 57 % in the first 20 seconds as the pumps coast down. This is largely due to the negative reactivity feedback from the radial expansion.

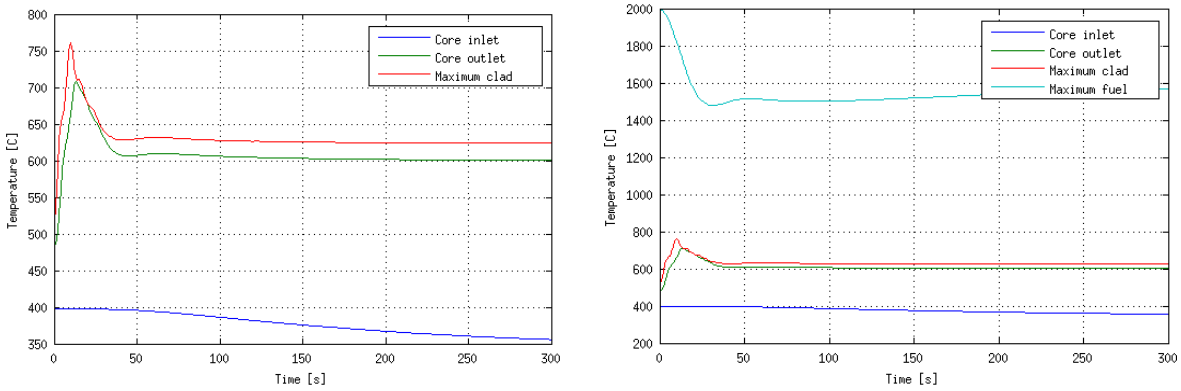


Figure 2: a) Core inlet, outlet and maximum clad temperatures
b) Same with added maximum fuel temperature for ULOF

Core outlet temperature rises steadily from its initial value of 484 degrees C to about 700 degrees C and then stabilizes around 600 degrees C as natural circulation in the system is achieved at around 24 % of the nominal mass flow. After about 50 seconds, the inlet temperature of the core starts decreasing. This is the effect of overcooling, as MHX power is still higher than that of the core. The power of the core increases because of the inlet temperature change. In the initial phase of the transient, the maximum fuel temperature decreases rapidly to about 1500 degrees C and then increases steadily with power.

Based on the simulation results, no cladding or vessel failure (see Appendix 1) is expected in case of ULOF transient.

T-DEC4

In case of unprotected loss of flow and secondary cooling system transient, all pumps are tripped at time 0 after a 1000 seconds steady state calculation, at 1 second the main steam isolation valves are closed and at 2 seconds DHR-1 (with 3 out of 4 IC loops) is initiated. SCRAM signal is deactivated throughout the transient.

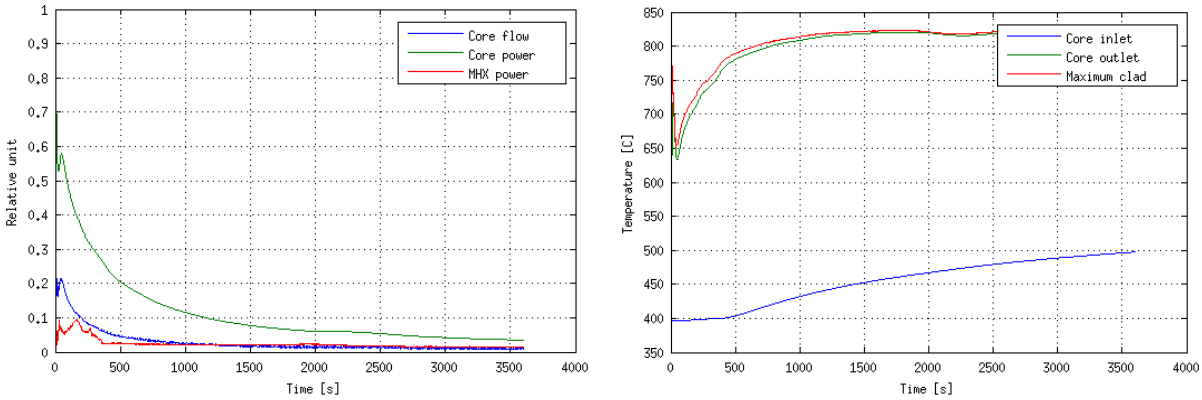


Figure 3: a) Core flow, power and MHX power in relative units
b) Reactivity components and total feedback for ULOF+ULOHS

The initial sharp decrease of the power in the first 100 seconds reduces the power from 300 MW to nearly half of that value. The power decrease continues as temperatures of the lead and cladding continue to rise. At around 20 minutes into the transient, the power of the core has decreased to 30 MW and continues to decrease due to inlet temperature rise.

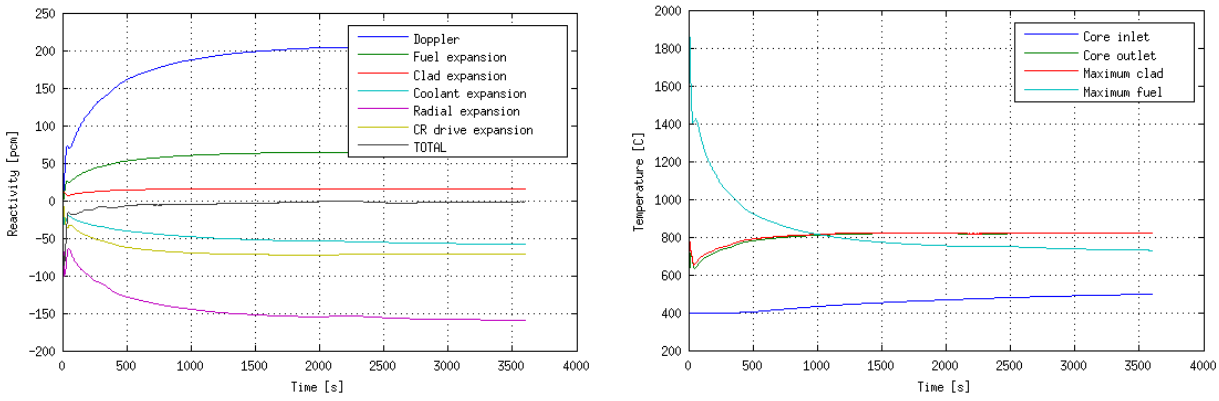


Figure 4: a) Core inlet, outlet and maximum clad temperatures
b) Same with added maximum fuel temperature for ULOF+ULOHS

The inlet temperature of the core starts steadily increasing, as the MHX is not powerful enough to remove the heat from the coolant. The inlet temperature increases 100 degrees in around 50 minutes. Dominant reactivity feedbacks are negative radial expansion and positive Doppler.

In case of ULOF+ULOHS transient, vessel temperature (see Appendix 2) continues to rise with coolant temperature and might pose an issue in the long term.

TR-4

Close proximity of steam generator to the core increases the risks associated with Steam Generator Tube Rupture/Leakage (SGTR/SGTL) such as voiding of the core and resulting reactivity insertion and/or local damage (burnout) of fuel rod cladding. Analysis of consequences of SGTL provided in present paper suggests that small bubbles of steam can be dragged by the turbulent coolant flow into the core region. Trajectories of the bubbles are determined by location of the leak, bubbles size and turbulent flow field of lead coolant. The influence of epistemic uncertainty in drag coefficient on prediction of the fraction of bubbles that can reach the core and accumulate in the primary coolant system is discussed in the paper.

Background

Discussion of different safety concerns associated with close proximity of steam generator to the core in pool type LFR design can be found in 0 and [2]. SGTR/L can become a showstopper for licensing of LFR technology, given that potential direct consequences of SGTR/L are high (core damage) and frequency is uncertain due to the lack of operational experience. To assess the risk and provide adequate defence-in-depth for SGTR/L in LFR both frequency and consequences need to be clarified. Among the safety concerns described in [2] there is a potential for core voiding that might cause reactivity insertion and local fuel damage in case of small leak from a SG tube.

Leakage of SG tube is not a new safety issue per se. Significant efforts have been undertaken to changes in the design, coolant chemistry, and adjustment of frequencies of SG inspections, to keep under control the SGTR in pressurized water reactors (PWRs). Nevertheless, analysis of available statistics [2] for PWRs shows that there were 9 cases of SG tube rupture in US during 1975-2000 and about 40 cases of SG tube leak incidents during 9 years of 1990-1998. Comparing potential for occurrence of SGTR in PWR and in LFR it is important to mention that lead, as a coolant, has higher density and is very corrosive for the structural materials. These factors generally accelerate chemical and mechanical wearing and degradation of the steam generator tubing, thus increasing frequency of SGTR occurrence.

From the PWR operational experience and from experiments performed on degraded SG tubing (e.g. [3]) it is well known that a small leak usually precede a large rupture of the tube. The leak can last for many days. In fact, EPRI guidelines [4] recommend increased monitoring if leak exceeds 20 litres per day and below that value no specific actions are recommended during normal operation of a PWR.

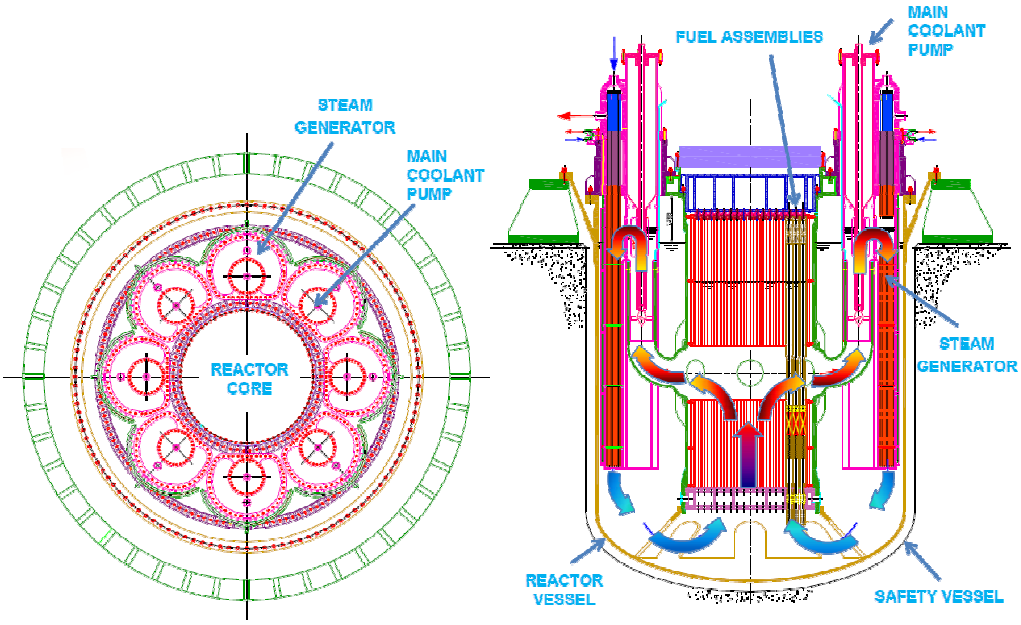


Figure 5: ALFRED reactor. View from top (left image) and vertical cross-section (right image).

The main objective of the present study is to quantify the likelihood that a steam bubble is transported in the primary coolant system to the core in case of SG tube leakage. The ALFRED (Advanced Lead cooled Fast REactor) pool-type 300MWth LFR is used as a reference design (see Figure 5) [5]. The core is submerged in the middle part of the pool and surrounded by 8 steam generators (SG), located at the top part of the pool. An axial primary pump is installed inside each SG. The SG in lead-cooled systems provides active heat removal from low-pressure heavy liquid metal on the primary side to the high-pressure water/steam on the secondary side.

General approach

A commercial CFD code Star-CCM+ version 8.02.008 [6] is used for modelling of coolant flow field and bubble transport. We are considering the steady state liquid lead flow in the primary system of the ALFRED design at nominal full power operation conditions.

The consequences of SGT leakage are studied by injecting bubbles with different diameters into the steam generator region. Bubbles are modelled as Lagrangian particles. Bubble transport to the core region is contingent upon the balance between the gravity and hydrodynamic drag forces. To account for the effects of fluctuating turbulent velocity field on the trajectories of the bubbles, a turbulent dispersion model, which employs so-called random-walk technique, is employed. A fraction of the bubbles that can reach the core region is calculated by counting the number of bubbles at the core inlet and relating this number to the total number of bubbles released. Similar approach is used to determine the fraction of bubbles that can accumulate in the primary coolant system. We vary the size of the bubbles and location of bubble injection inside the SG to identify the most dangerous bubble size and positions of the leak. The influence of epistemic uncertainty in the correlations for bubble drag in liquid lead is addressed by comparing the probabilities of bubble transport to the core obtained with different correlations.

Liquid lead thermo-physical properties were defined in Star-CCM+ as a function of temperature according to the recommended correlations in the OECD/NEA Handbook on lead/LBE technology [7].

Bubble drag coefficient

Drag force is a result of skin and form friction of a body. The most common method to mathematically model the drag force is:

$$F_D = \frac{1}{2}\rho v^2 C_D A \qquad (4)$$

The balance between drag and buoyancy forces defines the terminal rise velocity of a bubble in lead. Essentially, bubble will be dragged down by coolant flow if the terminal rise velocity of a bubble is smaller than local downward velocity of the coolant. Therefore the drag coefficient is one of the most important factors determining the bubble transport in the primary system. Verification of drag coefficient correlation for steam bubble in liquid lead is performed. For that purpose, terminal rise velocity of a steam bubble in steady liquid lead column is calculated using different drag correlations. The predicted velocity is then compared with available analytical and experimental data about the terminal rise velocity of a bubble in heavy liquid metals.

Modeling bubble motion in lead

Motion of a bubble in liquid and its terminal rise velocity have been studied extensively in the past (e.g. see reviews [8], [9]). Bubble dynamics is affected by many factors (i.e. temperature, viscosity, pressure, purity). Therefore, prediction of terminal rise velocity is not a trivial task, especially taking into account a nonlinear nature of drag coefficient versus bubble size curve (nonlinearity rises with bubble size).

In this work, Lagrangian model for bubble transport in a continuum flow field of liquid lead is used [10]. Steam inside the bubble was assumed to be incompressible and bubble size was not a function of hydrostatic pressure. Density and viscosity of the bubble gas was assumed equal to water vapour density at 100 °C under atmospheric pressure. Bubbles with diameter ranging from 0.2 mm to 10 mm are studied. This range of bubble sizes was observed in experiments performed air injection into water with different sizes and geometries of the orifice [11] and also in experiments with water injection into lead [12].

Four different drag coefficient correlations were tested:

- Schiller-Naumann – suitable for spherical, rigid particles (as it is defined in [6]).
- Modified Schiller-Naumann – Stokes law was used at low Reynolds number region.
- Rodrigue – according to author the correlation is applicable for wide range of bubble sizes and various viscous liquids [13].
- Tomiyama et al. – is reported to provide good match with the whole drag curve [8], [14].

The used correlation reads as:

$$C_D = max\left\{min\left[\frac{16}{Re_b}(1+0.15Re_b^{0.687}), \frac{48}{Re_b}\right], \frac{8}{3}\frac{Eo}{Eo+4}\right\} \quad (5)$$

Bubble terminal rise velocity was studied in a lead column of 0.5 m x 0.5 m x 5 m. The column contains 23,826 polyhedral cells with a characteristic size of about 5-7 cm. The top and the bottom surfaces of the column were defined as walls. The sidewalls of the column were defined as symmetry planes with “rebound” option for the bubbles. Lead flow field is described in Eulerian frame of reference. Steady stagnant lead at temperature of 450 °C was used in all cases. Terminal velocity of rising bubble in laminar stagnant column was determined as the bubble velocity at the column outlet.

Since there is no available experimental data on bubble terminal rise velocity in lead, the simulation results were compared to Stokes law that predicts velocity for small, spherical shape bubbles and to Mendelson’s equation that predicts velocities in surface tension- and inertia-dominated regimes [15]. Comparison of Stokes law and Mendelson equation with experimental data for bubble terminal rise velocity in mercury obtained by Mori et al. [16] is shown in Figure 6.

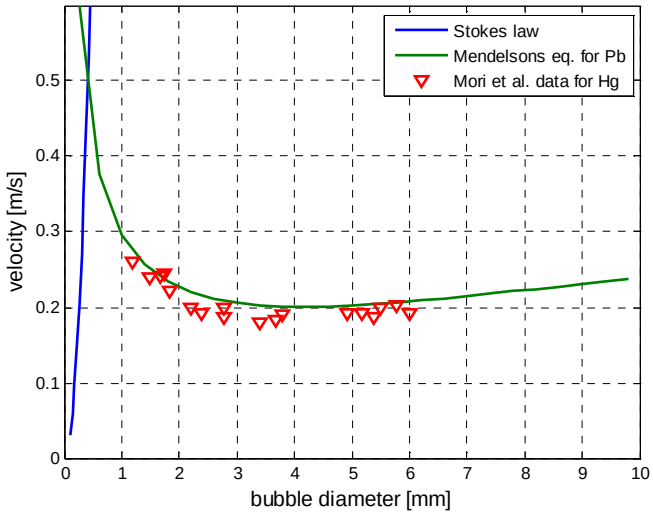


Figure 6: Bubble terminal rise velocity as a function of bubble diameter. Analytical predictions by Stokes and Mendelson laws. Experimental data for mercury.

As it can be seen, the bubble velocity is predicted reasonably well by Mendelson’s equation in the surface tension dominated regime. Small bubbles are expected to behave as solid spheres and their terminal velocity should be described by Stokes law. However, there is an uncertainty in the transition from surface tension-inertia dominated region to Stokes region.

First calculations were performed without activating turbulent dispersion model for the bubbles. Figure 7 presents the terminal rise velocities obtained using different drag correlations described in the previous section.

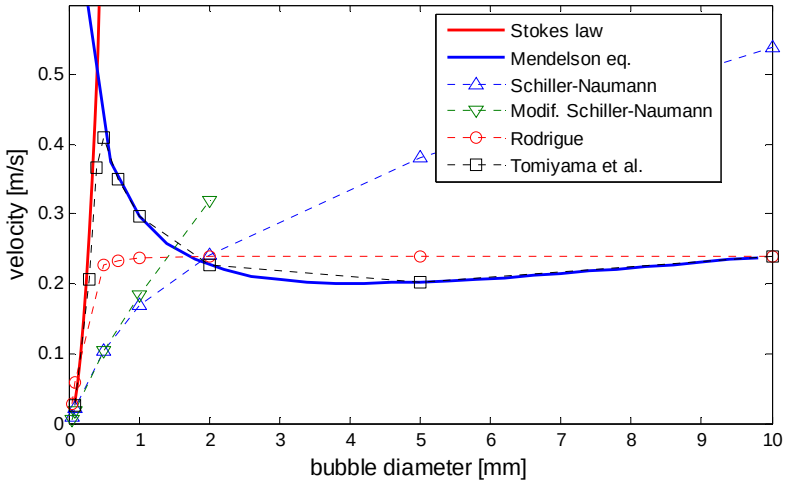


Figure 7: Bubble terminal rise velocities calculated with different drag coefficient correlations.

It can be seen that Schiller-Naumann correlation is applicable only for very small bubbles that behave as rigid spheres. The modified Schiller-Naumann correlation does not improve the results. Rodrigue's correlation shows a better agreement than Schiller-Naumann, but is still deficient in capturing the peak on the curve of terminal velocity. Tomiyama's drag correlation, which aims to match the whole drag curve, provides the best agreement with the Stokes solution and Mendelson equation for bubble rise velocities. Therefore, Tomiyama's correlation is used for the study of bubble transport in reactor conditions.

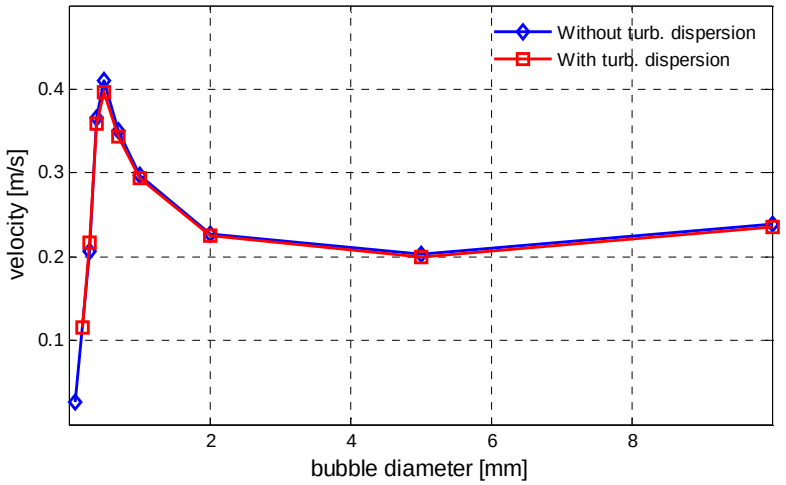


Figure 8: Bubble terminal rise velocity with and without modeling of turbulent dispersion.

A comparison between the results obtained with and without turbulent dispersion (random-walk model) was done for Tomiyama's correlation. As it appears in Figure 8, a difference between averaged terminal rise velocity of a bubble in stagnant laminar and in turbulent lead column is negligible as it is expected.

Bubble transport in the primary system

In this section we address the possibility of transport of a bubble from the steam generator to the core region in the ALFRED design at nominal operation conditions. First, we resolve the averaged steady state flow at full power operation in a realistic configuration of the primary system. Then we study behavior of individual bubbles in the flow field with Lagrangian approach, taking into account dispersion of the bubbles by turbulent vortices. The probability that a bubble of certain size can reach the core region and then stay in the primary coolant system is assessed for the bubbles released at different locations in the SG.

ALFRED nominal operational conditions

Simulation domain represents 1/8th of the whole reactor pool, comprising of an SG, a pump and a slice of the core region with corresponding sections of the hot/cold plenum and downcomer.

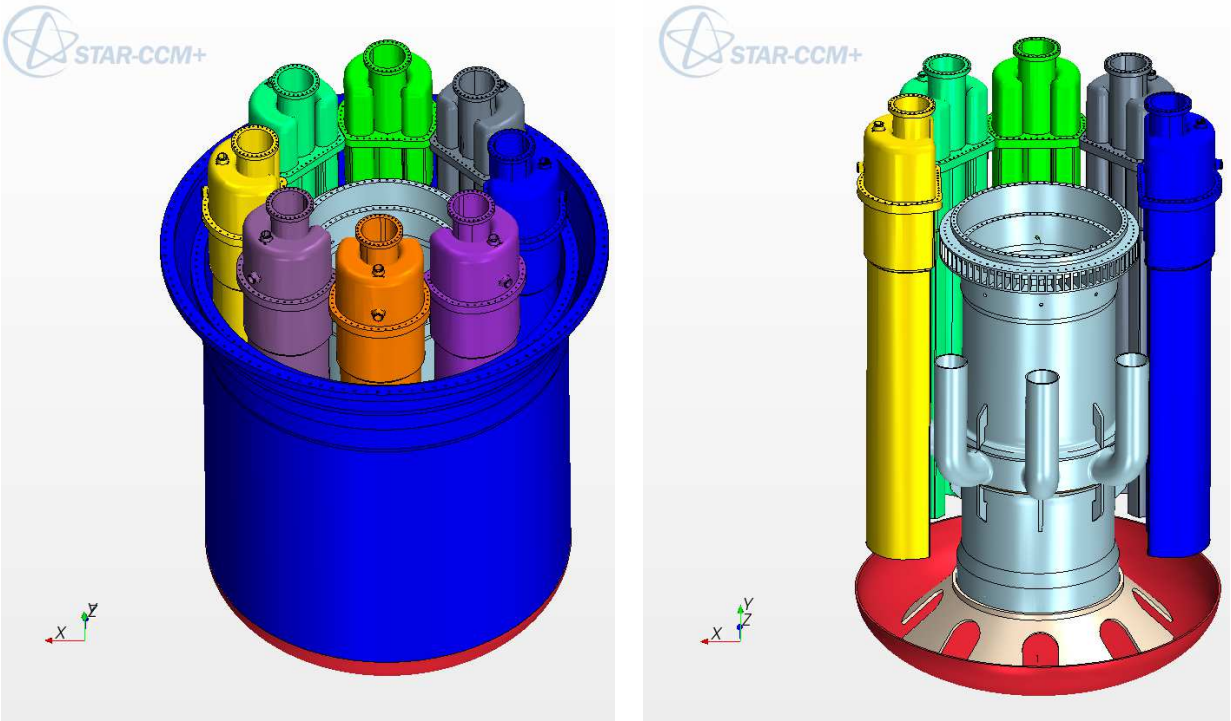


Figure 9: ALFRED 3D CAD model. Left image shows all components, right image shows internals.

CFD simulations will be set up to first achieve nominal operational conditions given by [5]. The simulations are in the phase of preparing the geometry and therefore we cannot provide any results at this moment.

Approach to estimate the fraction of bubbles reaching the core

The following three-step method is used in assessment of void accumulation rate in the core (and in the primary system). Bubbles are injected at three different height levels within the SG region simulating different leakage locations. Then the bubbles have three possibilities to

escape the system (see Figure 10) depending on their size, leak location and coolant flow characteristics:

1. Bubble escapes after injection immediately to the cold free surface above the downcomer and the SG.
2. Bubble is dragged down to the core for the first time and then escapes from the loop to the hot free surface above the core.
3. Bubble stays in the primary coolant flow, travels through the hot leg and pump and reaches the SG again. Then it emerges to the cold free surface.

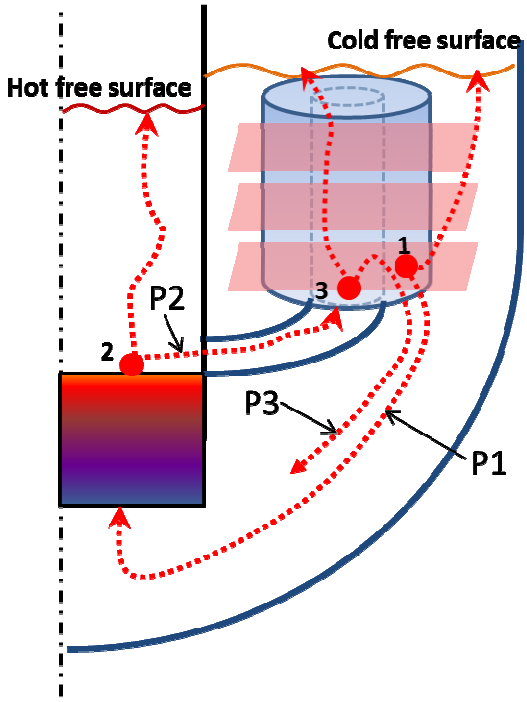


Figure 10: Illustration of different locations of bubble injection (1-3) and respective probabilities that injected bubble can stay in the loop (P1-P3).

All the bubbles which do not escape from the coolant will be carried by the coolant flow through the primary loop again to the core. In order to assess the consequences of the SGTL and different scenarios of void behaviour in the primary system we need to calculate the probabilities that a bubble will escape from the coolant given the abovementioned three possibilities.

P1 is the probability that a bubble can reach the core after entering the primary coolant flow through the SG tube leak. We calculate this probability by injecting bubbles at one of the three injection levels in the SG and counting the number of the bubbles that reach the core inlet boundary. P2 is the probability that a bubble can reach SG after passing through the core. To estimate the P2, we inject bubbles at the exit of the core and count those that escape to the hot free surface. One minus obtained fraction of the bubbles that escape from the coolant is equal to P2. Finally, P3 is the probability that a bubble stays in the primary loop after passing through the core and the pump. To calculate the P3 we inject bubbles at the exit of the pump and count those that reach the core inlet.

If leak rate and bubble size distribution in case of SGTL are known, one can estimate the total rate of void accumulation in the coolant in the form of the bubbles that are circulating in the primary system:

$$Q_{primary}(t) = Q_{leak}(t) \sum_{i=1,N} f_{d_i} P1_{d_i} P2_{d_i} P3_{d_i} \quad (6)$$

where Q_{leak} is volumetric leak rate [litres/day], $f_{d_i}, P1_{d_i}, P2_{d_i}, P3_{d_i}$ are volume fraction and respective probabilities for a bubble with size d_i, and N is the number of bubbles sizes considered in the bubble size distribution.

It is also interesting to estimate the void accumulation rate in the core (assuming that all bubbles that reach the core will stick in the core, e.g. below spacers):

$$Q_{core}(t) = Q_{leak}(t) \sum_{i=1,N} f_{d_i} P1_{d_i} \quad (7)$$

To estimate the realistic rate of void accumulation in the core one needs to consider the probability that bubble will pass or stuck in the core given detailed geometry of the core internals. This task is beyond the scope of the present work.

Future considerations

The future work foresees finishing the CAD model that is, preparing the surface for CFD meshing. Then surface and volume mesh will be created. Simulation of nominal operational flow conditions are then performed on several meshes to evaluate the mesh sensitivity and use the fastest (read: coarser) mesh.

After the solution for nominal operational conditions is resolved, Lagrangian framework is utilized to simulate bubble transport in the primary system. Then the above described methodology to estimate the void accumulation rates in the primary system and in the core are calculated.

References

[1] B.W. Spencer, “The Rush to Heavy Liquid Metal Reactor Coolants – Gimmick or Reasoned”, Proceedings of ICONE-8, 8th International Conference on Nuclear Engineering, April 2-6, 2000, Baltimore, MD USA.

[2] P. Kudinov and T.N. Dinh, “Evaluation approach and case set-up for simulation of consequences of the SGTR event”, Division of Nuclear Power Safety, Royal Institute of Technology, Stockholm, 2010.

[3] S.S. Hwang, H.P. Kim, J.S. Kim, K.E. Kasza, J. Park, and W.J. Schack, “Leak behavior of SCC degraded steam generator tubings of nuclear power plant,” *Nuclear Engineering and Design*, **235**, 2005, 2477-2484.

[4] EPRI Technical Report. “PWR Primary-To-Secondary Leak Guidelines – Revision 2,” EPRI, Palo Alto, CA: TR-104788-R2. 2000.

[5] E. Bubelis, K. Mikityuk, “Plant data for the safety analysis of the ETDR (ALFRED),” LEADER Project WP5 TEC058-2012, April, 2012.

[6] CD-adapco, *Star-CCM+ User Guide version 8.02.*

[7] “Handbook on lead-bismuth eutectic alloy and lead properties, materials compatibility, thermal-hydraulics and technologies,” OECD NEA, No. 6195, 2007.

[8] A. A. Kulkarni and J. B. Joshi, “Bubble formation and bubble rise velocity in gas-liquid systems: a review”, *Ind. Eng. Chem. Res.*, Vol. 44, 2005, 5873-5931.

[9] G. Q. Yang, Bing Du, and L. S. Fan, “Bubble formation and dynamics in gas-liquid-solid fluidization – a review”, *Chem. Eng. Sci.*, Vol. 62, 2007, 2-27.

[10] M. Jeltsov and P. Kudinov, "Simulation of steam bubble transport in primary system of pool type lead cooled fast reactors," *14th International Topical Meeting on Nuclear Reactor Thermalhydraulics (NURETH-14)*, Toronto, Ontario, Canada, September 25-29, 2011.

[11] E. Krepper, D. Lucas, and H.-M. Prasser, “On the modelling of bubbly flow in vertical pipes”, *Nucl. Eng. Des.*, Vol. 235, 2005, 597-611.

[12] A. V. Beznosov, S. S. Pinaev, D. V. Davydov, A. A. Molodtsov, T. A. Bokova, P. N. Martynov and V. I. Rachkov, “Experimental studies of the characteristics of contact heat exchange between lead coolant and the working body”, *Atomic Energy*, Vol. 98, Issue 3, 2005.

[13] D. Rodrigue, “A simple correlation for gas bubbles rising in power-law fluids”, *Can. J. Chem. Eng.*, Vol. 80, Issue 2, 2002, 289.

[14] A. Tomiyama, I. Kataoka, I. Zun, and T. Sakaguchi, “Drag coefficients of single bubbles under normal and microgravity conditions”, *JSME Int. J. Ser. D*, Vol. 41, Issue 2, 1998, 472.

[15] H. D. Mendelson, “The prediction of bubble terminal velocities from wave theory”, *A.I.Ch.E. Journal*, 13, 1967, 250.

[16] Y. Mori, K. Hijikata, and K. Kuriyama, “Experimental study of bubble motion in mercury with and without a magnetic field”, *J. Heat Transfer (Trans. ASME)*, Vol. 99, 1977, 404-410.

APPENDIX G

CIRTEN Contribution to Deliverable DEL022:

a) Analysis of the SGTR Accident for the ALFRED Reactor, and b) Summary of DBC and DEC Transient Analysis: PLOF (Loss of 1 Pump) and ULOF Transients (Pag. 349)

CIRTEN - UNIVERSITA' DI PISA
DIPARTIMENTO DI INGEGNERIA CIVILE E INDUSTRIALE

Analysis of the SGTR accident for ALFRED reactor

Authors: A. Pesetti, N. Forgione,

Reviewer: R. Lo Frano

Pisa, January 2013

Abstract

In the frame of the LEADER project (EU 7th FP), two numerical simulations, aiming to study the SGTR accident in the ALFRED reactor, have been performed at University of Pisa by the SIMMER III code. The SGTR scenario needs to be analysed, in the integrated pool type ALFRED reactor configuration, due to the serious hazard represented by the bayonet tube rupture of the SG taking place in the lead pool.

Two simulations were executed in order to evaluate the SGTR accident effects. In particular, the former was performed considering one bayonet tube rupture and the latter supposing also the rupture of the six surrounding tubes. The injected water mass flow rate, the pressure effects and the steam flow paths have been evaluated for both the tube rupture conditions analysed. The computed results provided by the SIMMER III code, show a coherent behaviour with the nature of the phenomena involved in this reference accident.

The obtained results show pressure peaks occurring in the immediate vicinity of the water injector tube exit, which disappear at short distance and do not represent a risk for the SG and core structural integrity. The code foreseen a very low quantity of steam that flows through the core for a short time interval; it does not entail a hazard of positive reactivity insertion, even if it is to be carefully taken into account for the neutronic feedback consequences.

Index

Abstract ..... **ii**

Index ..... **iii**

List of figures ..... **iv**

List of tables ..... **v**

Abbreviations ..... **v**

1 Introduction **1**

2 The ALFRED reactor **2**

2.1 Steam generator description 3

3 Steam Generator Tube Rupture accident **7**

4 Calculation domains and simulation matrix **8**

5 Obtained results **13**

5.1 Setting up of analysis conditions 13

5.2 One bayonet tube rupture 18

5.3 Seven bayonet tubes rupture 28

6 Conclusions **37**

References **39**

List of figures

Figure 2.1: Reactor configuration, vertical view (left) and top view (right) (from [1]) 2
Figure 2.2: Steam Generator arrangement (from [2]) 4
Figure 2.3: Steam Generator and Primary Pump horizontal section (from [3]) 1
Figure 2.4: SG bayonet tube detail (from [4]) 1
Figure 2.5: Main SG bayonet tube design (from [5]) 6
Figure 3.1: Steam generator, water inlet and steam outlet collectors details (from [4]) 7
Figure 3.2: Tubes pitch detail (from [3]) 8
Figure 4.1: SIMMER III geometrical model 1
Figure 4.2: Whole SIMMER III model with lead flow paths 10
Figure 4.3: Water injector tube detail for one (left)and seven (right) tubes rupture tests 12
Figure 5.1: Pressure distribution before the pumps start in the SIMMER III model 13
Figure 5.2: Lead velocity vectors after 5 s of transient 14
Figure 5.3: Lead velocity vectors after 20 s of transient 14
Figure 5.4: Lead velocity vectors after 99 s of transient 15
Figure 5.5: Total lead mass flow rate downstream the single pump, cells (22-25,49) 16
Figure 5.6: Total lead mass flow rate downstream the seven pumps, cells (64-70,49) 16
Figure 5.7: Cells to compute the SGs-core downcomer mass flow rate 17
Figure 5.8: Lead mass flow rate in the cell (35,7) 17
Figure 5.9: Total lead mass flow rate in the cells (54,5-7) 17
Figure 5.10: Detailed view of the injector tube, single SG and single pump conduct 18
Figure 5.11: Outline of the reference cells beneath the water injector pipe 18
Figure 5.12: Pressure time trends in the cells (1-6,15) 19
Figure 5.13: Zoom of the pressure peaks in the cells (1-6,15) 19
Figure 5.14: Pressure time trends in the cells (1-6,14) 20
Figure 5.15: Pressure time trends in the cells (1-6,13) 20
Figure 5.16: Pressure time trends in the cells (7,20), (13,20), and (19,20) 21
Figure 5.17: Pressure time trends in the cells (7,50), (13,50), and (19,50) 21
Figure 5.18: Pressure time trends in the cells (7,69), (13,69), and (19,69) 22
Figure 5.19: Outline of the reference cells 22
Figure 5.20: Pressure time trends in the cells (10,10), (30,10) and (45,10) 23
Figure 5.21: Pressure time trends in the cells (30,20), (45,20) and (30,69) 23
Figure 5.22: Steam distribution in the SG at different transient instants 24
Figure 5.23: Steam distribution in the SG and PP at different transient instants 25
Figure 5.24: Steam distribution in the SG and PP at different transient instants 26
Figure 5.25: Water mass flow rate time trend injected in the lead pool 27
Figure 5.26: Reference cells to analyses the vapor presence in the core 28
Figure 5.27: Pressure time trends in the cells (1-6,15) 29
Figure 5.28: Pressure time trends in the cells (1-6,14) 29
Figure 5.29: Pressure time trends in the cells (1-6,13) 30
Figure 5.30: Pressure time trends in the cells (7,20), (13,20), and (19,20) 31
Figure 5.31: Pressure time trends in the cells (7,50), (13,50), and (19,50) 31
Figure 5.32: Pressure time trends in the cells (7,69), (13,69), and (19,69) 31
Figure 5.33: Pressure time trends in the cells (10,10), (30,10) and (45,10) 32
Figure 5.34: Pressure time trends in the cells (30,20), (45,20) and (30,69) 32
Figure 5.35: Steam distribution in the SG and PP at different transient instants 33
Figure 5.36: Steam distribution in the SG, PP and 7PP at different transient instants 34
Figure 5.37: Steam distribution in ALFRED at different transient instants 34
Figure 5.38: Water mass flow rate time trends injected in the lead pool 35

Figure 5.39: Vapor flow paths 1
Figure 5.40: Void fraction time trends in the cells (37,10), (45,10) and (52,10) 36

List of tables

Table 2.1: Main parameters of the ALFRED reactor (from [1]) 3
Table 2.2: Main steam generator operation parameters (from [4]) 5
Table 4.1: Boundary conditions for the numerical simulations 12

Abbreviations

1PP	Single Primary Pump
1SG	Single Steam Generator
7PP	Seven merged Primary Pumps
7SG	Seven merged Steam Generators
ALFRED	Advanced Lead Fast Reactor European Demonstrator
DHR	Decay Heat Removal
LFR	Lead Fast Reactor
PP	Primary Pump
RV	Reactor Vessel
SG	Steam Generator
SGTR	Steam Generator Tube Rupture

1 Introduction

The present work, performed in the frame of the LEADER project (EU 7th FP), aims to analyse the effects induced by a steam generator tube rupture (SGTR) accident in the Advanced Lead Fast Reactor European Demonstrator (ALFRED). This phenomenon is considered, by the International Regulatory Bodies, as a design basis event in lead fast reactor (LFR) technology because of the safety concerns of this event due to the steam generator (SG) integrated into the main reactor vessel.

In such a reactor type, the rupture of one or more SG tubes causes the secondary coolant (water) leak into the molten lead. The vaporization of discharged water causes a propagation of the pressure waves, which determine the rapid and strong increase of pressure. The pressure could rise to values severe enough to determine structural risks for the SG itself, the core region and the vessel's integrity. It is therefore of interest to determine the loads weighing on the reactor structures. Therefore, the installation of the SG into the primary system needs to be assessed, analysing the consequences of the SGTR event. A single tube failure could induce in principle a domino effect, causing the rupture of the neighbouring tubes and an escalation of the accident. Moreover, the vapour generated in the lead-water interaction could flow through the core yielding neutronic feedback consequences.

For these reasons, the crucial issues related to the study of the SGTR in a LFR are represented by the prediction of the higher pressure values reached and the vapour flow paths in the primary system. In order to perform an evaluation of the SGTR consequences in the ALFRED reactor a numerical simulation activity has been performed with the SIMMER III code.

The SGTR phenomenon is influenced by a large number of parameters, most of which are initial conditions like the water injection pressure and temperature, the lead initial temperature and, in particular, the free volume filled with inert gas. Besides, the mixing effects of water and liquid lead constitute a key issue for studying the SGTR in a LFR.

In this work, after a brief presentation of the ALFRED reactor, the computational model developed by the SIMMER III code is described. Afterwards, the numerical results corresponding to a single and multiple steam generator bayonet tube rupture are illustrated.

2 The ALFRED reactor

ALFRED is a 300 MWth (~120 MWe) integral pool type lead cooled fast reactor. All the primary components are contained within the reactor vessel (RV), eliminating the issues related to the coolant leakage. The lead flow and cooling is performed by 8 main coolant primary pumps (PPs) and 8 steam generators (SGs), arranged as shown in fig. 2.1, where the lead flow paths are indicated by means of arrows. The lead flows upward through the core, enters in the main pumps after two elbow curves and flows downward in the SGs feeding the downcomer of the reactor vessel.

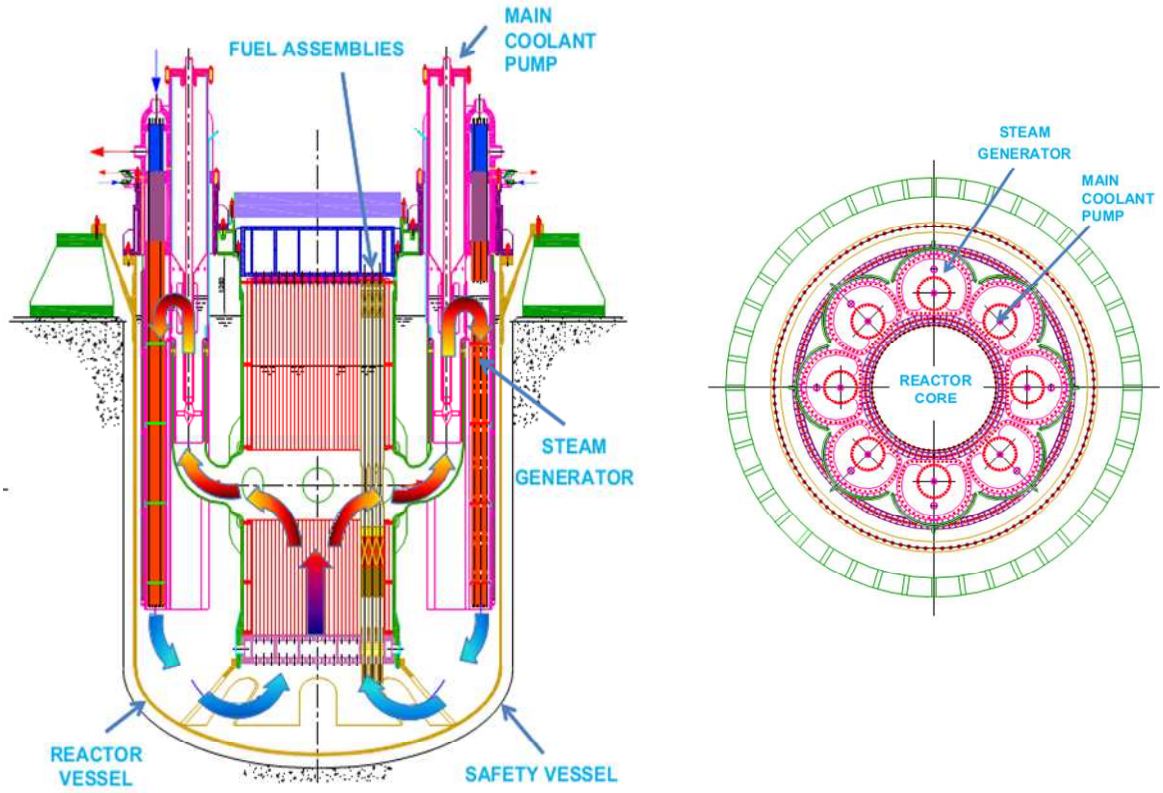


Figure 2.1: Reactor configuration, vertical view (left) and top view (right) (from [1])

The volume between the primary coolant free levels and the reactor roof is filled by the argon cover gas plenum.

ALFRED is characterized by a compact primary system arrangement, its design results in a reactor vessel, outer diameter and height of which are about 8 and 10 m, respectively.

The inlet and outlet core temperature are about 400 and 480°C respectively. With these operating temperatures, the cold collector has a sufficient margin from lead's freezing point

(327.5°C). In the future, when advanced structural-materials would be available, higher coolant temperatures could be reached, increasing the thermal efficiency significantly.
The main operating parameters of the ALFRED reactor are shown in Table 2.1.

Parameter	**Value/Type**
Electric Power	120 MW
Thermal Efficiency	~ 41 %
Primary Coolant	Pure Lead
Primary System	Pool Type, Compact
Primary Coolant Circulation	Forced by mechanical pump in normal operation, natural in emergency conditions
Primary Coolant Circulation for DHR	Natural Circulation + Pony motors
Inlet Core Temperature	400°C
Steam Generator Inlet Temperature	480°C
Fuel	MOX
Fuel Assembly	Closed hexagonal
Maximum Clad Temperature in Normal Operation	550°C
Reactor Vessel	Austenitic SS
Steam Generator	N°8, inside the reactor vessel with bayonet tubes
Primary Pumps	N°8, mechanical, in the hot collector
Internals	Removable
Inner Vessel (Core Barrel)	Cylindrical, removable

Table 2.1: Main parameters of the ALFRED reactor (from [1])

2.1 Steam generator description

The eight SGs are included in the primary cooling system according to the pool-type reactor configuration, as shown in fig. 2.1. They are distributed axi-symmetrically around the Inner Vessel, supported by the Reactor Roof and immersed in the primary coolant, as illustrated in fig. 2.2.

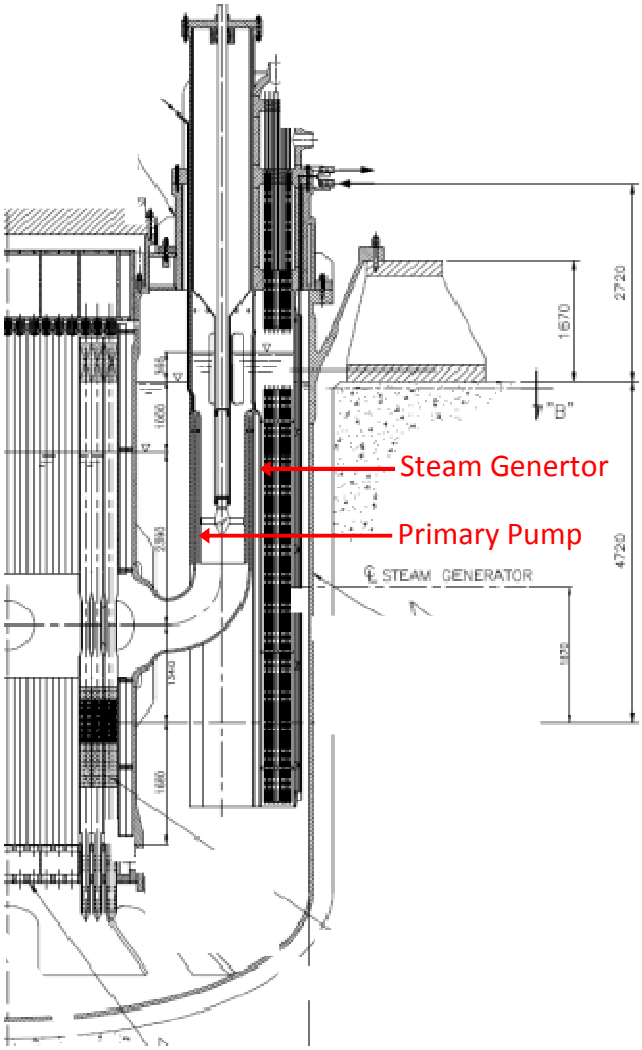


Figure 2.2: Steam Generator arrangement (from [2])

The lead flows upwards through the Primary Pump conduct and passes in the SG bayonet tubes through five vertical openings highlighted in fig. 2.3 by red arrows.

Each bayonet tube is made of four coaxial tubes with an intermediate medium between lead and water/steam, see fig. 2.4. This configuration mitigates the consequence of the SGTR accident, allowing an instantaneous identification of the broken tube.

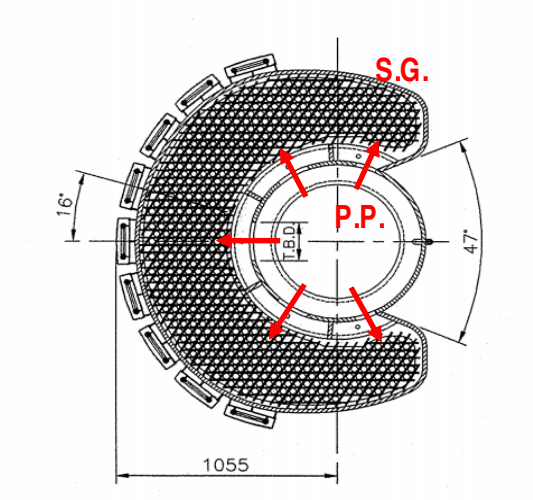


Figure 2.3: Steam Generator and Primary Pump horizontal section (from [3])

The 8 SGs are connected to two Decay Heat Removal systems (DHRs), each one consisting of four independent isolation condenser subsystems, for a total of eight isolation condensers. Three of them are sufficient to fulfill the DHR safety function.

The main SG operation parameters are reported in Table 2.2.

Parameter	**Value/Type**
Nominal reactor core power	300 MWth
Number of steam generators	8
Power removed by 1 SG	37.5 MWth
Lead (Primary System)	
SG lead inlet temperature	480°C
SG lead outlet temperature	400°C
Mass flow rate	3247.5 kg/s
Lead flow velocity	≤ 2 m/s
Water/Steam (Secondary System)	
Pressure	180 bar
Water inlet temperature	335°C
Steam Outlet temperature	450°C
Mass flow rate	24.1 kg/s
Bayonet tubes in one SG	510

Table 2.2: Main steam generator operation parameters (from [4])

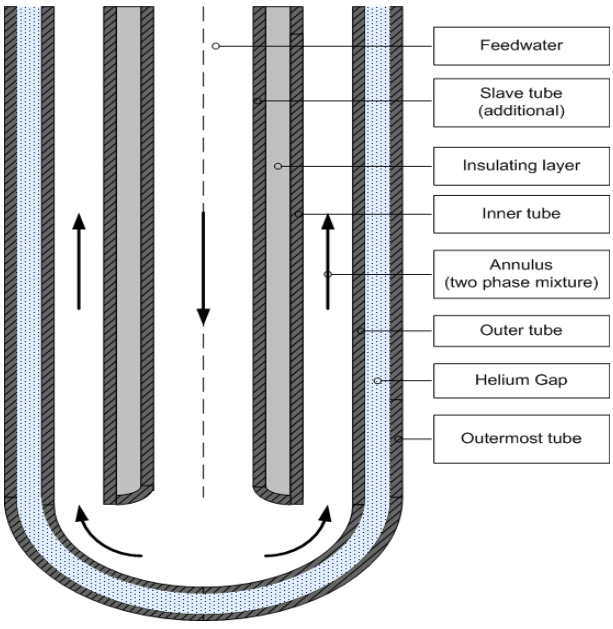


Figure 2.4: SG bayonet tube detail (from [4])

In figs. 2.4 and 2.5 are shown the layout and main characteristics of the bayonet tube inserted in the SG. The bayonet tube is composed of four tubes and is connected to three plates (figs. 2.4 and 2.5).

The water flows downward in the central tube and goes up in the outer annular conduct where evaporates receiving heat from the outer lead.

In gray, fig. 2.4, is indicated the

isolation between the inner and the slave tubes, used to avoid steam production in the water descendent path and steam condensation in the upward flow.

The region defined by outer and outermost tubes is filled by pressurized helium at intermediate pressure between inner water (180 bar) and outer lead (almost 1 bar in the higher part of the tube and 8 bar in the lower one). Hence, a variation of the helium pressure is a clear information about the damage occurred to the outer and/or outermost tube and then allows to perform a continuous water leakage monitoring. To increase the heat flux through the external safety tube, high conductivity particles (synthetic diamonds) are foreseen to be added to the helium gap.

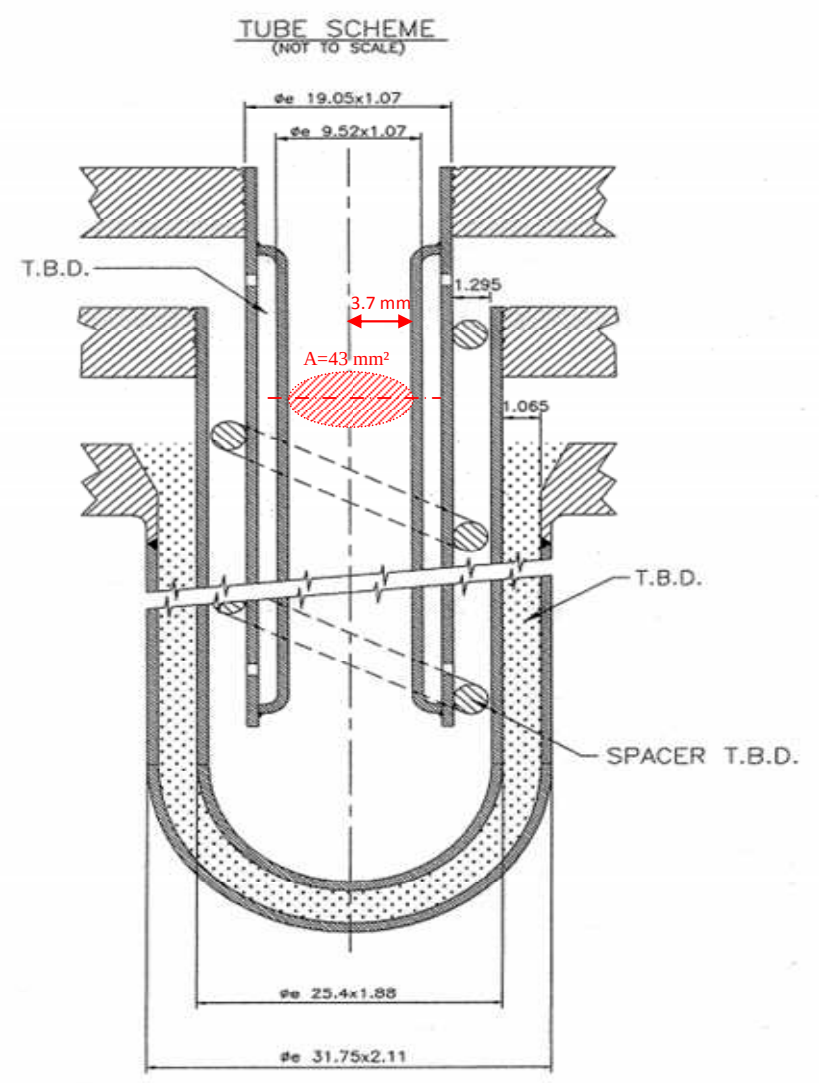


Figure 2.5: Main SG bayonet tube design (from [5])

3 Steam Generator Tube Rupture accident

The Steam Generator Tube Rupture (SGTR) accident represents a risk for the integrity of the internal structures and has great relevance for the design and safe operation of the ALFRED reactor.

The SGTR accident occurs when the structural integrity of the external safety tube (see Section 2.1) is compromised and high pressure , about 180 bar, water at a temperature about 7 K below saturation interacts with low pressure-high temperature molten lead. In these conditions a water evaporation starts and the propagation of the pressure waves could damage the neighboring tubes and can be potentially dangerous for the integrity of the steam generator.

Indeed, particular attention has been focused on the mitigation of accident consequences and reduction of the primary system pressurization. For this purpose, several solutions have been adopted in design phase. One of these consists in the installation of the water and vapor collectors outside the reactor vessel as illustrated in fig. 3.1, eliminating the collector rupture risk.

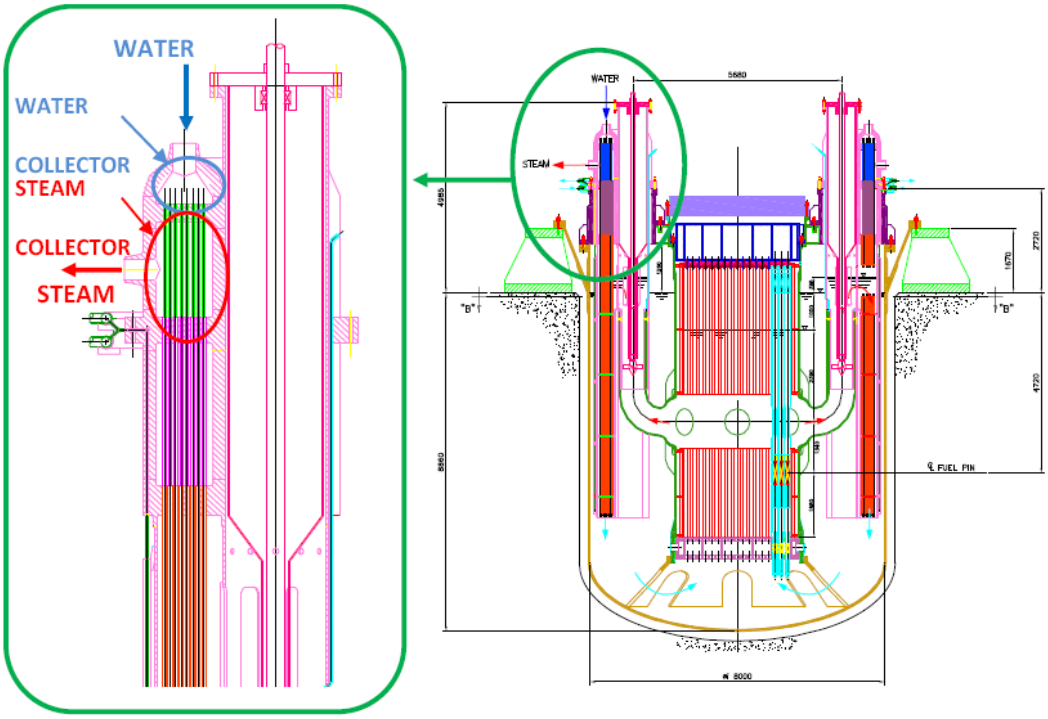


Figure 3.1: Steam generator, water inlet and steam outlet collectors details (from [4])

In the frame of safety analysis, efforts are made and addressed to understand the scenario which could develop during a steam generator tube rupture accident. In this work, two

different SGTR configurations are numerically analyzed. The former assumes the guillotine rupture of one bayonet tube and the latter considers also the 100% rupture of the six neighbor bayonet tubes (for a total of seven broken tubes), as highlighted in fig. 3.2. The accidental scenario, in which seven bayonet tubes rupture is considered to occur, constitutes an extremely rare hypothetic event that has been taken into account to perform a very conservative assessment of the SGTR consequences.

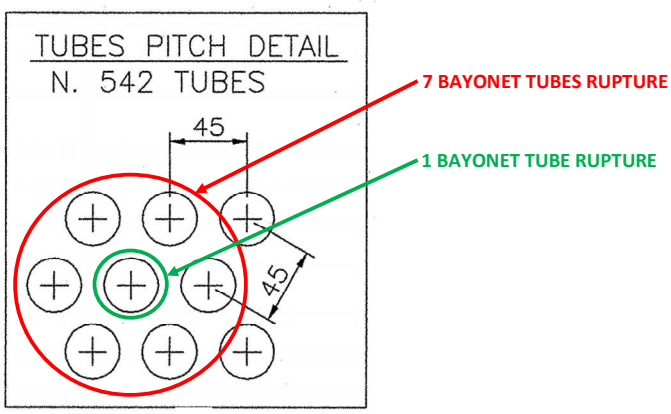


Figure 3.2: Tubes pitch detail (from [3])

The consequences of the SGTR accident are investigated by computational simulations performed by the SIMMER III code. Simmer III is a two-dimensional, three-velocity field, multi-phase, multi-component, Eulerian, fluid-dynamics code coupled with a space dependent neutron kinetics model [6-8]. It implements a two-dimensional *R*-Z cylindrical coordinate system to define the computational domain, although optionally an *X*-*Z* (one-dimensional) system could also be used. In this work, the ALFRED reactor has been modeled by an axisymmetric (*R*-*Z*) computational domain, as explained in the next section.

4 Calculation domains and simulation matrix

The analysis of the SGTR accidental transient in the ALFRED reactor has been performed modeling in a simplified and conservative way, by the SIMMER III code, the whole geometry of the ALFRED reactor. The version III of the SIMMER code, which is the two-dimensional (*R*-*Z*) axisymmetric version, compels to accept simplifications in the modeling of the non-axysimmetric ALFRED reactor.

The SIMMER III geometrical domain is shown in fig. 4.1. It is composed by 88 radial and 75 axial cells. The lead is represented in red, the water in blue, the argon (cover gas) in white, the

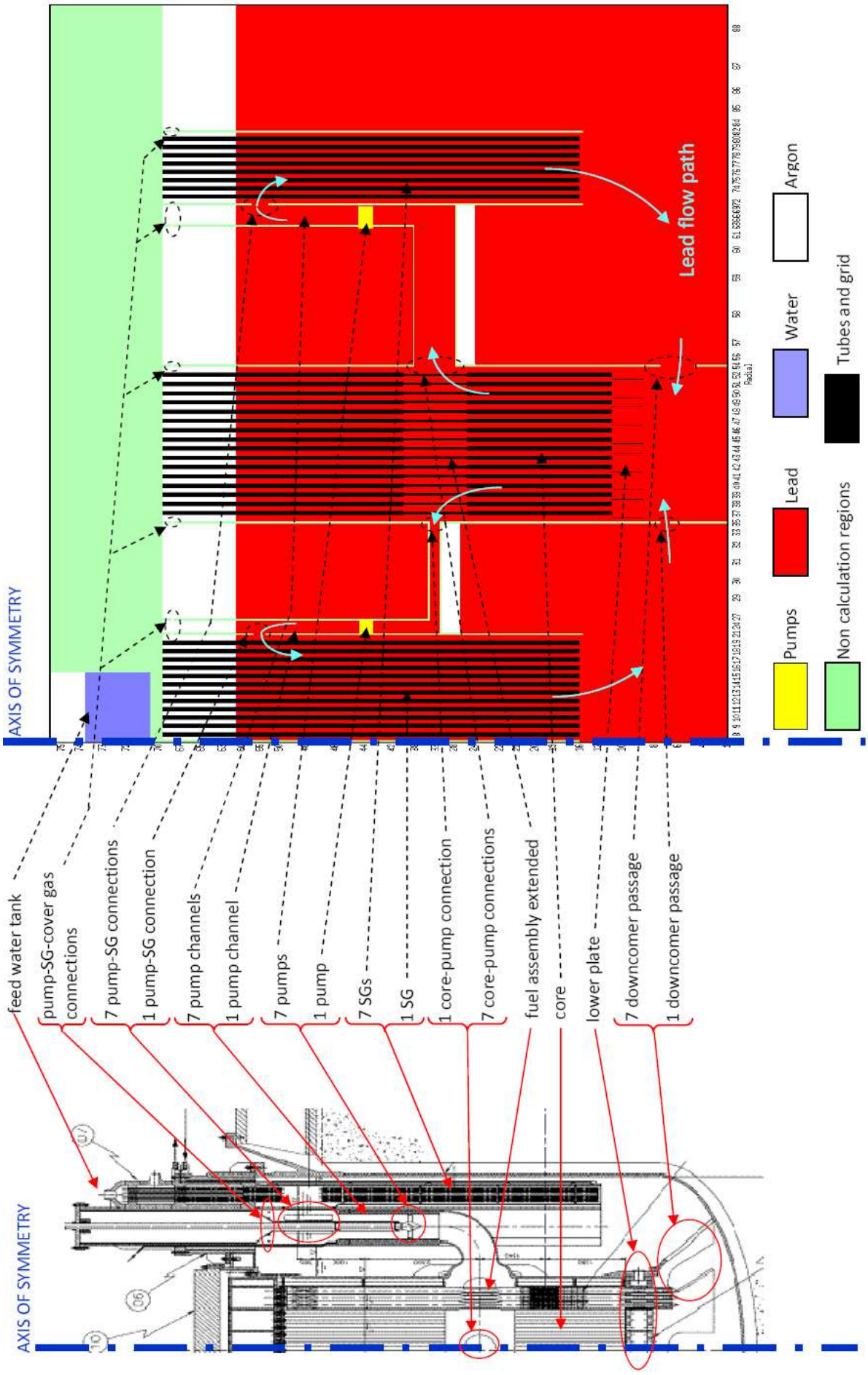


Figure 4.1: SIMMER III geometrical model

non calculation regions in light green (structural parts), pins and grids in black and pumps in yellow. The cyan arrows indicate the lead flow path. In fig. 4.1 it is possible to note as the SG, where the SGTR occurs, and its primary pump (in the following they are referred to also as 1SG and 1PP, respectively) are considered positioned near the axis of symmetry of the model. Instead, the other seven SGs (7SGs) are merged together, equally for the pumps (7PPs), and they are set in the outer region. The core is positioned between 1SG-1PP and 7PPs-7SGs.
Rotating the 2D SIMMER domain (on the right in fig. 4.1) along the axis of symmetry (blue dot-dashed line) the whole axisymmetric volumetric model is obtained, in which every cell is a toroidal volume with rectangular section. The entire diametral vertical section of the SIMMER III model, the lead flow paths (yellow arrows) and the cell grid (for figure clarity only on the left half side) are shown in fig. 4.2.

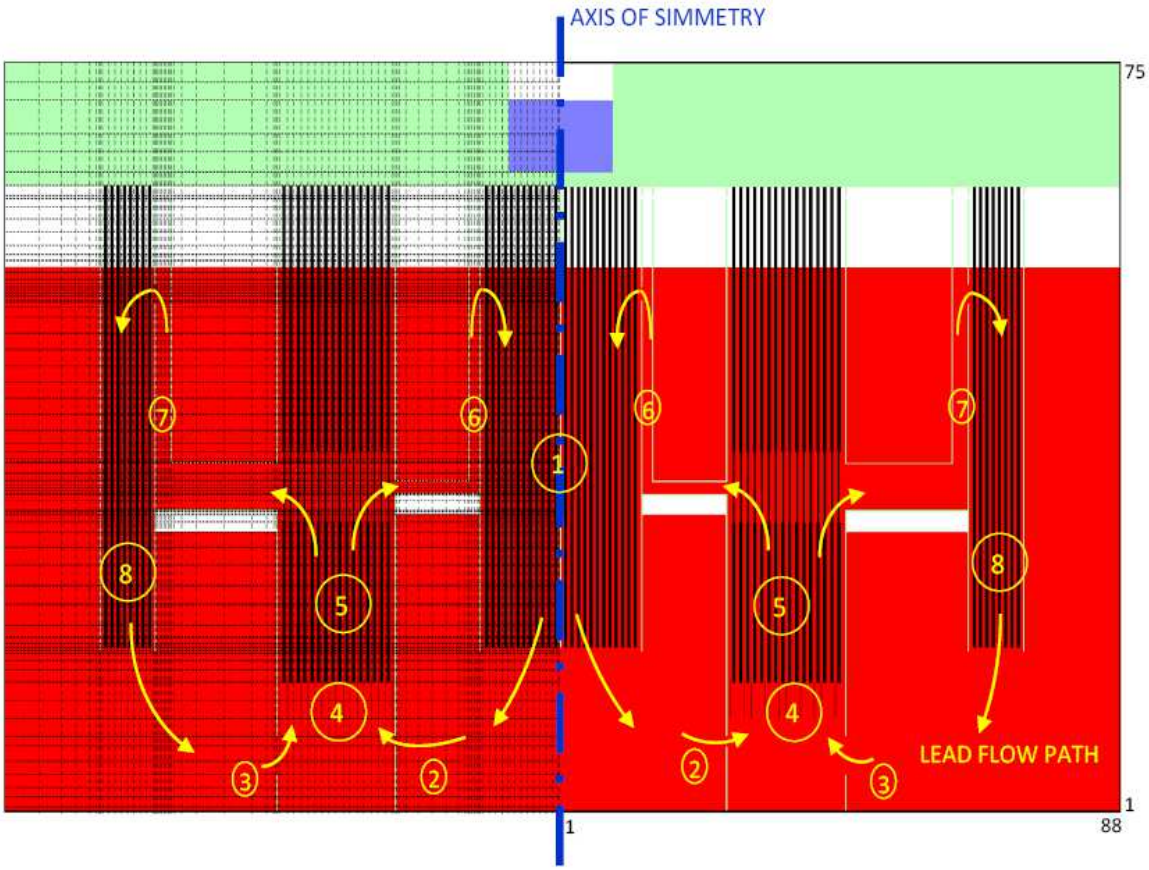


Figure 4.2: Whole SIMMER III model with lead flow paths

In the analysis of the SGTR scenario, it has been chosen to conserve the geometry of the broken bayonet tube, thus, it has been modeled by a cylindrical region of water placed in the center of the axysimmetric model. Also the water tank above the water injector has cylindrical shape; instead, all the other components and regions are annuli.

In fig. 4.2 the main reactor components are marked by numbers. Each of them was dimensioned conserving the height and the flow section area. The region (1) represents the steam generator in which the bayonet tube rupture occurs (1SG), it is an annular volume with the water tube injector positioned in the center. The black parts, inside the 1SG, are cylindrical pipes that represent the intact bayonet tubes, their number, diameter and interaxial distance are conserved. The lead flows downward in the 1SG (1) and passes through the downcomer passage, (2) in fig. 4.2, flow area of which is equal to one of eight downcomer passages, see fig. 4.1. The other seven passages are lumped in the zone (3) and are fed by seven merged steam generators (7SGs), region (8). The annular region (4) is the flow stabilizing grid, above it; the core (5) is set with the extended fuel assemblies. The lead flows upward through them and turns radially versus the axis of symmetry, passing in the single primary pump (6) and reaching the 1SG (1), and turns to the outer side versus the seven pumps (7) and the seven SGs (8). In all the regions, from (1) to (8), the flow areas have been conserved as much as the axial dimension of the components. In the region (8) have been positioned a number of pipes equal to those present in the seven steam generators (7SGs).

The pump-steam generator connections, highlighted on the left of fig. 4.1, are simulated in the SIMMER model conserving the passage area. The opening connecting 1SG (1) and 1PP (6), in fig. 4.2, is distributed on the total circumference and its flow area is equal to that of the opening called pump-steam generator connection on the left in fig. 4.1. Seven times its value is the flow area between the regions (7) and (8). It is important to note also the vents highlighted and called “pump-SG-cover gas connections” in fig. 4.1, that have been simulated in the SIMMER model as little openings in the upper part of the cover gas region, they are circled by dashed lines in fig. 4.1.

The cover gas arranged around the 1PP vertical conduct is 1/8 of the total one, the remaining 7/8 are positioned around the 7SG and the 7PP. This configuration reduces the expansion volume available around the SG where the rupture occurs and it is coherent with the objective to perform a conservative SGTR analysis.

The eight openings connecting the core to the PP, called core-pump connection in fig. 4.1, are modeled in the SIMMER code by means of both inner and outer openings above the core model. The inner opening has the same area of one real core-pump connection, instead, the outer opening has seven times that area.

The rupture disks located in the cover vessel are not simulated in the SIMMER model, also this simplification aims to perform a conservative assessment of the SGTR consequences.

In this work, the core power generation has not been simulated, because the main objectives are represented by the prediction of pressure trends and vapor flow path inside the reactor. Hence, the lead temperature was set equal to 440°C, that is the average value between the inlet and outlet core temperature.

The boundary conditions imposed in the numerical simulations, related to one and seven bayonet tubes rupture, are summarized in Table 4.1.

	One tube rupture	**Seven tubes rupture**
Lead (Primary System)		
Lead temperature	440°C	440°C
One SG mass flow rate (nominal value)	3247.5 kg/s	3247.5 kg/s
Seven SG Mass flow rate (nominal value)	22732.5 kg/s	22732.5 kg/s
Water (Secondary System)		
Injector tube diameter	7.4 mm	19.6 mm
Injector tube section area	43.01 mm²	304.80 mm²
Water injection pressure	180 bar	180 bar
Water temperature	335°C	335°C

Table 4.1: Boundary conditions for the numerical simulations

In fig. 4.3 are shown two detailed view of the water injector tube model, with the main radial dimensions, for both the analyzed SGTR scenarios. The real dimensions of a bayonet tube are reported in fig. 2.5.

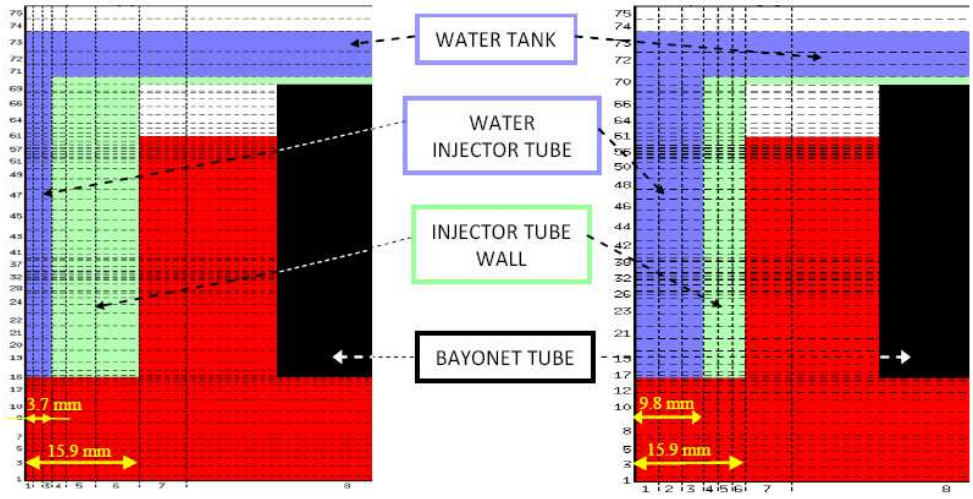


Figure 4.3: Water injector tube detail for one (left)and seven (right) tubes rupture tests

5 Obtained results

5.1 Setting up of analysis conditions

In the simulations performed by the SIMMER III code the water has been injected in the lead region after 100 s from the calculation start. This time interval constitutes the transient period to reach the ALFRED operative stationary conditions.

In the first two seconds of simulation the pumps are deactivated. This time interval is imposed to allow the right distribution of the lead pressure due to the gravity field, because initially the pressure in all the lead cells is set equal to 1 bar. In fig. 5.1 is shown the pressure distribution before the pump activation to show the gravity effect. The maximum pressure plotted is equal to 1 MPa, higher values have the same red color.

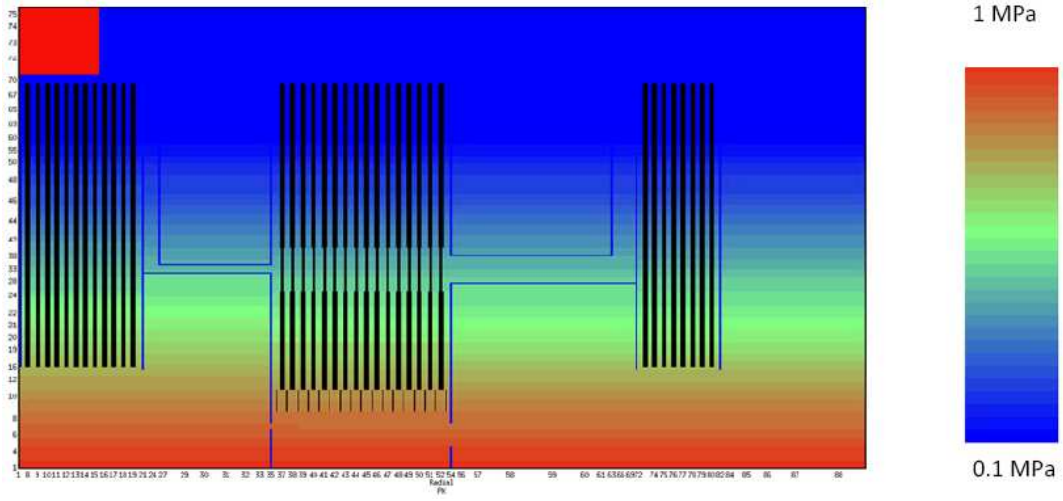


Figure 5.1: Pressure distribution before the pumps start in the SIMMER III model

After this time lapse (2 s) the pumps are activated. In the figs. 5.2, 5.3 and 5.4 are shown the lead velocity vectors after 5, 20 and 99 s of transient period, respectively. The longer velocity vectors (see figs. 5.2 and 5.3), the extremities of which are external to the plots, indicate the velocity of lead droplets dispersed in argon. Their magnitude is a common phenomenon for the SIMMER code at gas-liquid interface. They do not take place when the stationary conditions are reached, see fig. 5.4.

The conducts marked with “A” and “B” in fig. 5.2, connecting the core with the inner single pump (1PP) and the seven outer pumps (7PPs), respectively, create a roof to the below lead regions “C” and “D” (same figure). Therefore, a small volume of argon has been positioned underneath the conduct “A” and “B”, to prevent abnormal high pressure values in these regions (“C” and “D”) after the water injection activation.

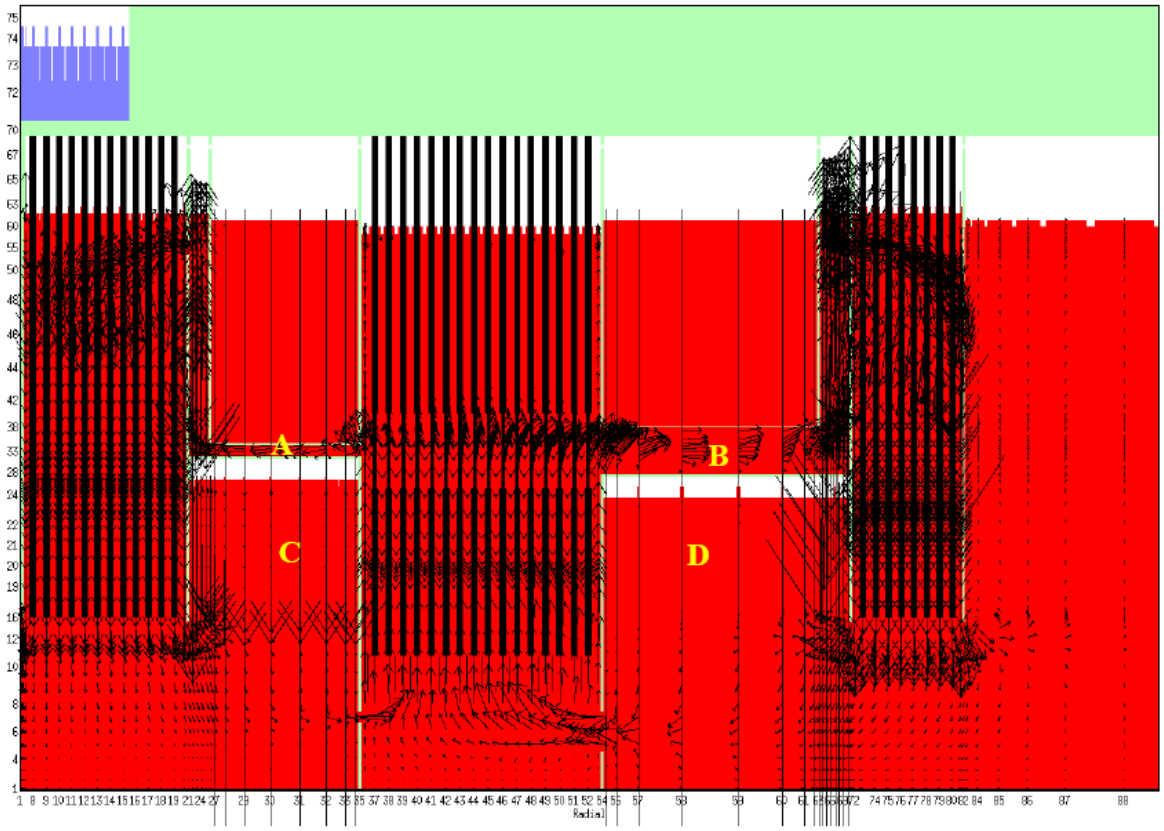


Figure 5.2: Lead velocity vectors after 5 s of transient

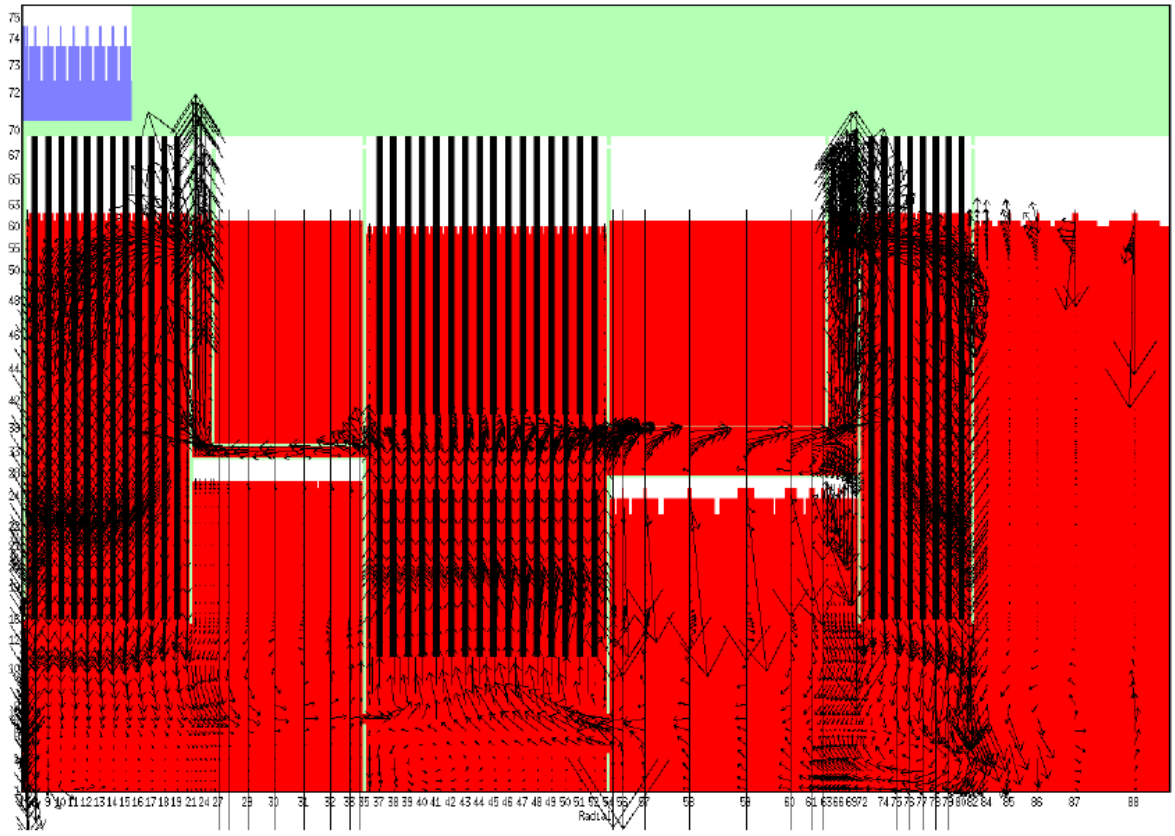


Figure 5.3: Lead velocity vectors after 20 s of transient

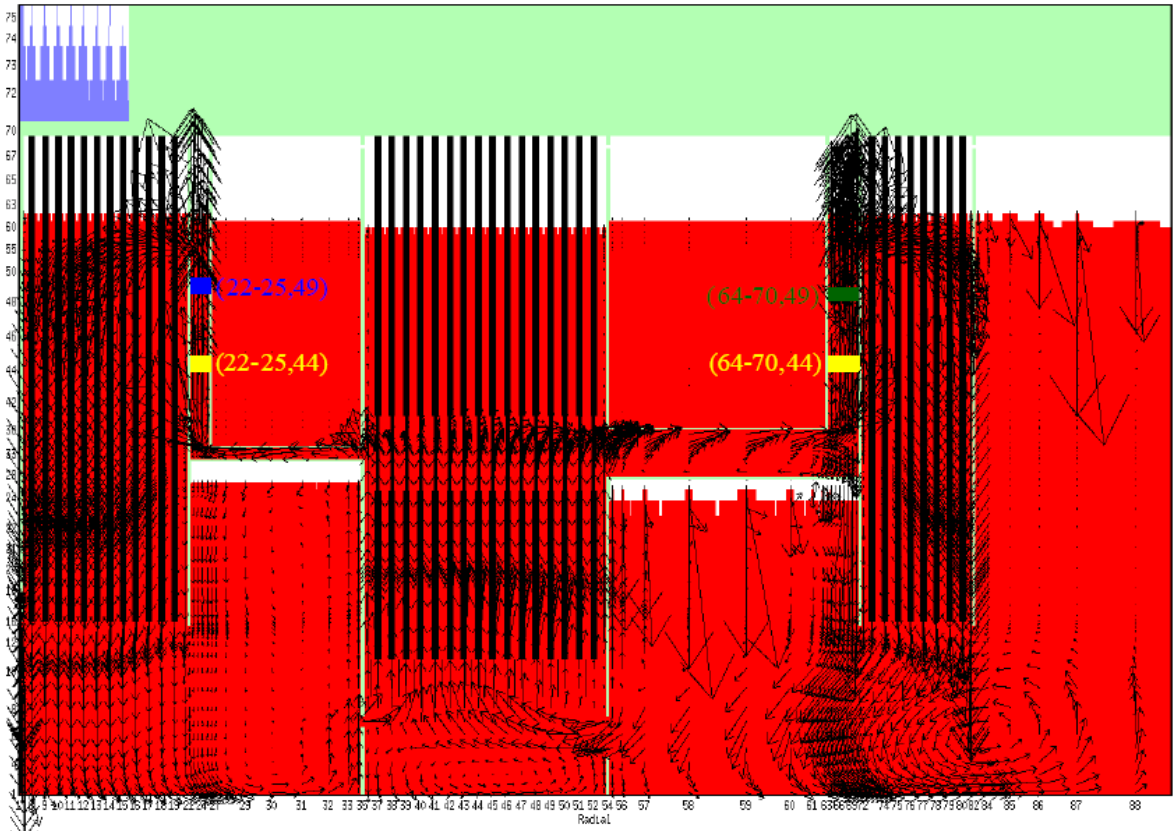


Figure 5.4: Lead velocity vectors after 99 s of transient

The document [4] reports that the lead flowing in each steam generator is equal to 3247.5 kg/s. Thus, that value corresponds to the lead mass flow rate of one single pump (1PP, cells (22-25,44) highlighted in yellow in fig. 5.4), whereas the seven merged pumps (7PPs, cells (64-70,44) in the same figure) have a lead mass flow rate equal to 7·3247.5=22732.5 kg/s. For sake of clarity, the cells (i-j,k) are located from the radial position i to j and at the axial row k. The pump heads and the pressure drops in the SIMMER model are set coherently with the main parameters of the ALFRED reactor. The suitability of the model developed is confirmed by the figs. 5.5 and 5.6, where the lead mass flow rate trends computed by the SIMMER III code are shown. In fig. 5.5 is reported the sum of the lead mass flow rate evolutions computed in the cells above 1PP: (22,49), (23,49), (24,49), (25,49) highlighted in blue in fig. 5.4, cells (22-25,49) in compact form notation. The sum of the four plotted mass flow rates, evaluated at the end of the transient period (100 s), is almost 3000 kg/s, that is in good agreement with the reference value [4].

In fig. 5.6 is shown the total lead mass flow rate trend computed by SIMMER III code in the 49th row, between the 64th and 70th radial cells (cells (64-70,49) highlighted in green in fig. 5.4). Also in this case at stationary conditions (100 s) the total lead mass flow rate (almost

23000 kg/s) downstream the seven merged pumps is in good agreement with the reference value.

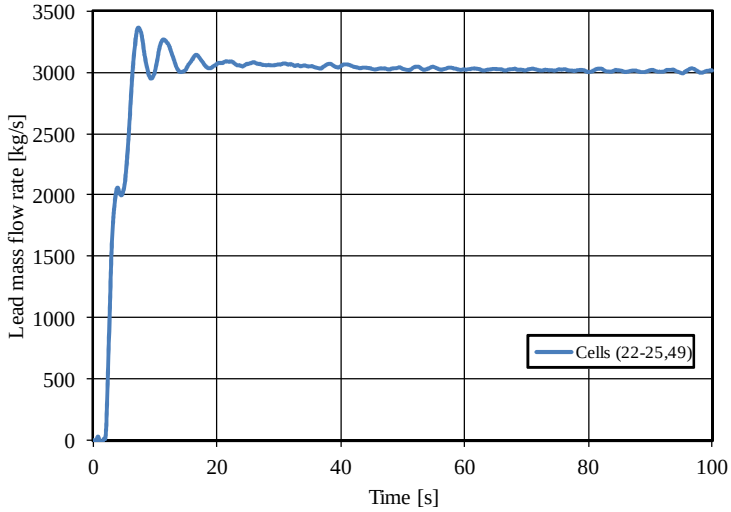


Figure 5.5: Total lead mass flow rate downstream the single pump, cells (22-25,49)

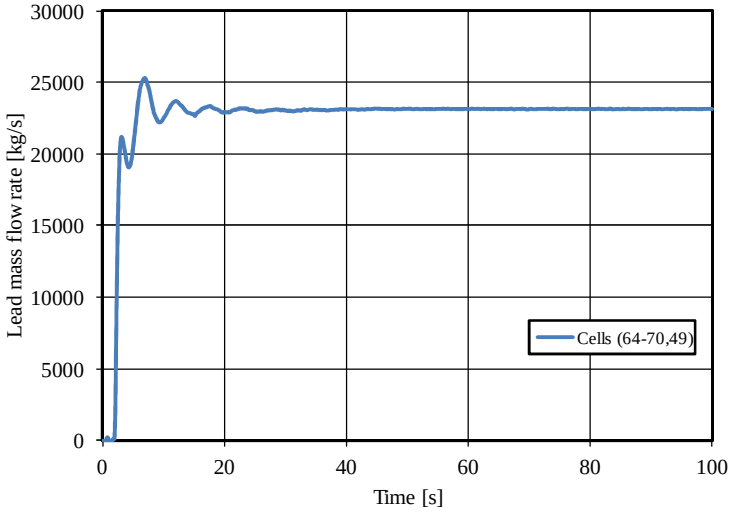


Figure 5.6: Total lead mass flow rate downstream the seven pumps, cells (64-70,49)

The lead flowing from the steam generators to the core downcomer pass through the cells (35,7) and (54,5-7), highlighted by blue circles in fig. 5.7. They are taken as reference to compute the lead mass flow rate entering the core downcomer region and their time evolutions are shown in figs. 5.8 and 5.9 during 100 s of transient.

The negative values reported in fig. 5.9 indicate that the lead flows from right to left, i.e. in the opposite direction respect to the positive radial versus (from left to right). The total mass flow rates computed at the end of the transient are in good agreement with the operational parameters presented in [4].

In the SIMMER code simulations, after the stationary flowing lead conditions have been reached (100 s), the injection of water has been activated.

In the following two sections, the analysis of the results obtained for one and seven bayonet tube rupture scenarios are described.

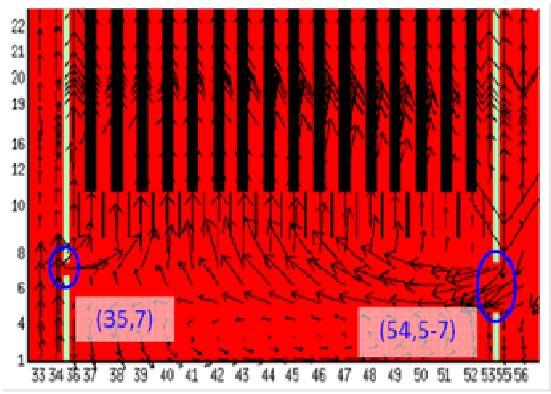


Figure 5.7: Cells to compute the SGs-core downcomer mass flow rate (35,7)(54,5-7)

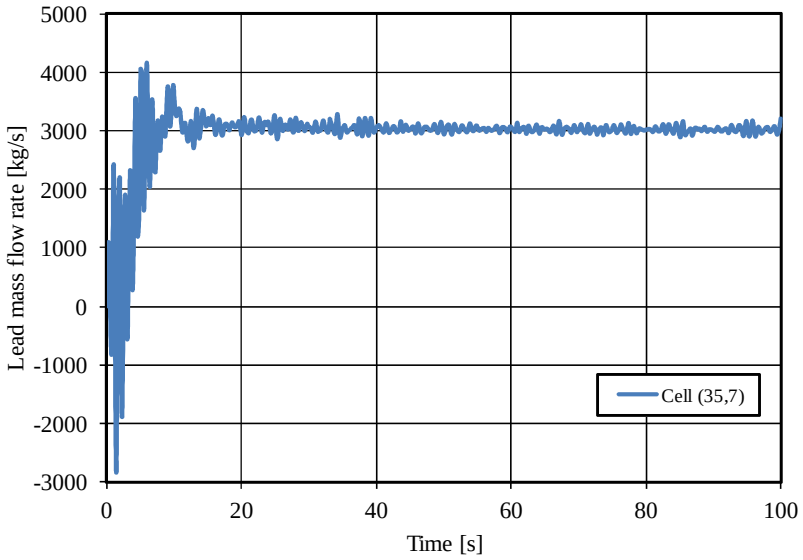


Figure 5.8: Lead mass flow rate in the cell (35,7)

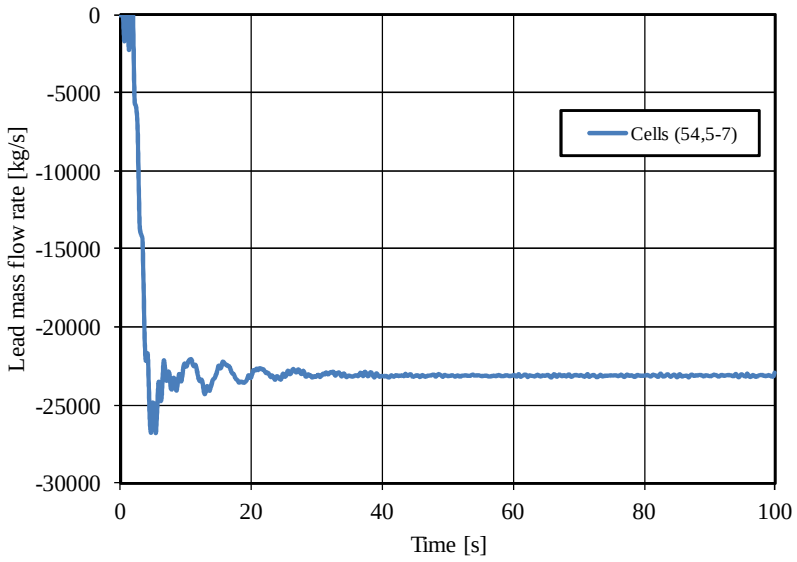


Figure 5.9: Total lead mass flow rate in the cells (54,5-7)

5.2 One bayonet tube rupture

In this section, the computational results obtained by the SIMMER III code analysing one bayonet tube rupture scenario are reported. A detailed view of the water injector tube has been previously shown by the left image in the fig. 4.3. To better understand the configuration of the injection region, in fig. 5.10 is shown a detailed view of the SIMMER model (first 26 out 88 radial cells) with the water injector and collector in blue, the wall of the water tube and other structures in light green, the single steam generator 1SG with the dummy bayonet tubes in black and, on the right, the single pump conduct delimited by light green walls. The white regions represent the cells filled by argon gas. In fig. 5.10 are also marked nine cells taken as reference to analyze the pressure behavior inside the single steam generator: cells (7,20), (13,20), (19,20), (7,50), (13,50), (19,50), (7,69), (13,69) and (19,69).

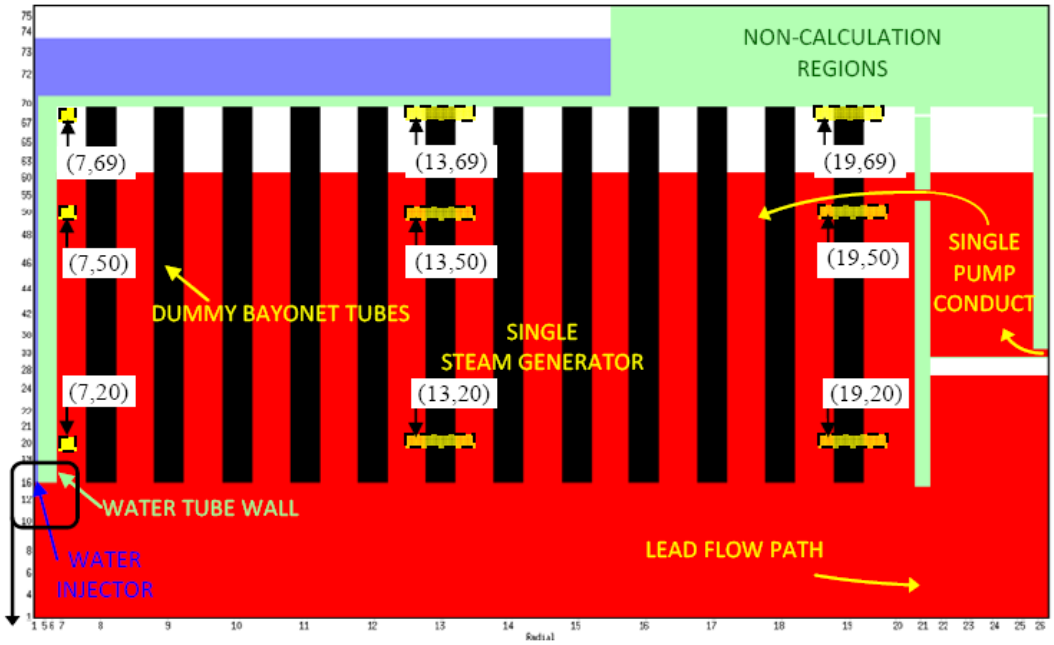
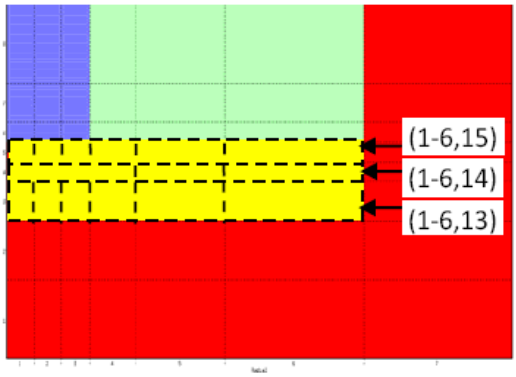


Figure 5.10: Detailed view of the injector tube, single SG and single pump conduct



The fig. 5.11 shows an enlargement of the water injection region, where the cells taken as reference to analyze the pressure behavior after the water injection activation are highlighted.

Figure 5.11: Outline of the reference cells beneath the water injector pipe

Six cells are selected in the 13th, 14th and 15th vertical rows, each group of cells is identified by compact notation in fig. 5.11. They are positioned beneath the injector tube. The pressure trends, reported in the following figures, are plotted for the time interval from the water injection instant (100 s) to almost 126 s from the simulation start.

The SIMMER calculation stopped at 126 s due to convergence problems and it has not been restarted because almost 26 s of water injection have been considered sufficient to study the consequence of the SGTR accident. In fact, the pressure increase near the rupture of the bayonet pipe take place in the first tenth of seconds after the start of water injection and the presence of rupture disks and safety valves on the vessel cover, not taken into account in the SIMMER model, limit the cover gas pressurization.

In figs. 5.12 and 5.13 are shown the pressure trends computed by the SIMMER code in the cells (1,15), (2,15), (3,15), (4,15), (5,15) and (6,15), highlighted in fig. 5.11.

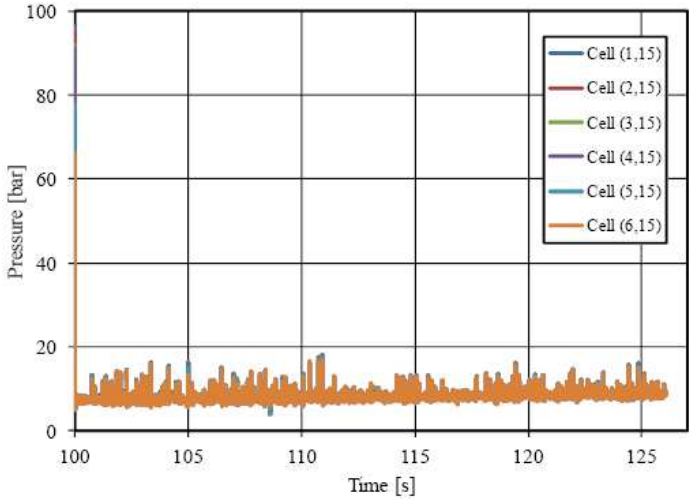


Figure 5.12: Pressure time trends in the cells (1-6,15)

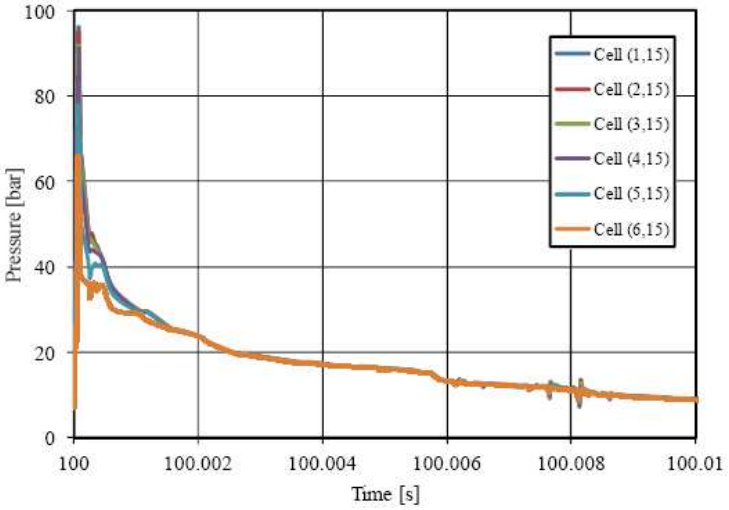


Figure 5.13: Zoom of the pressure peaks in the cells (1-6,15)

The two figures above show a pressure peak occurring in each of the considered cell. The higher pressure value is about 96 bar and has been computed in the cell (1,15), because of its nearest and central position in respect to the injector tube. In the other cells, the maximum pressure value decreases away from the cell (1,15). The peaks measured occur almost at the same instant (10^{-4} s starting from the water injection) then the pressure trends decrease rapidly to the initial value. After 2 ms and till the end of the tube rupture transient the six pressure profiles assume almost the same values. After 0.01 s starting from the water injection, the computed pressures come back to the stationary values (almost 7 bar), observed before the water injection, as shown in fig. 5.13.

The pressure vs. time trends shown in figs. 5.14 and 5.15 are computed in the first six radial cells belonging to the 14th and 13th row, respectively. Analysing these figures and fig. 5.13, it is possible to note that the cells with lower axial position have a lower and delayed pressure peak.

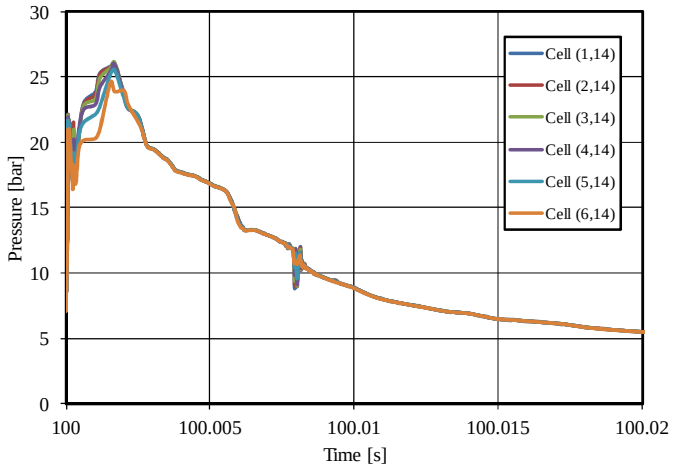


Figure 5.14: Pressure time trends in the cells (1-6,14)

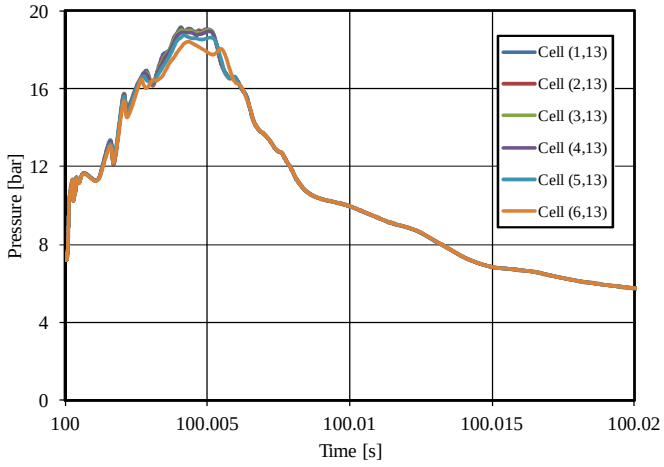


Figure 5.15: Pressure time trends in the cells (1-6,13)

In figs. 5.16, 5.17 and 5.18 are reported the pressure profiles computed by the SIMMER code in the cells indicated in fig.5.10, belonging to the 20th, 50th and 69th row, respectively. The pressure in each row is constant before the water injection and resulted equal to 6.2, 1.7 and 1 bar in the lower, middle and upper cells, respectively.

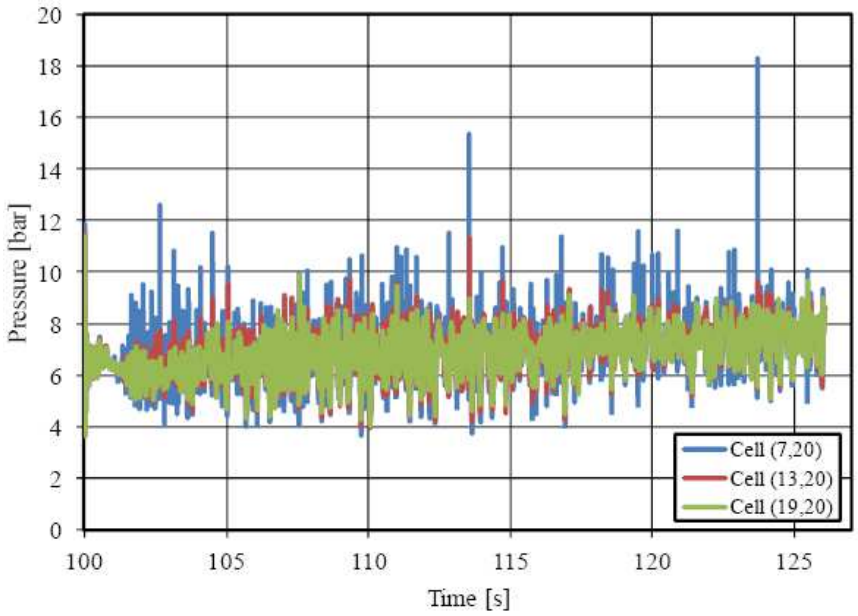


Figure 5.16: Pressure time trends in the cells (7,20), (13,20), and (19,20)

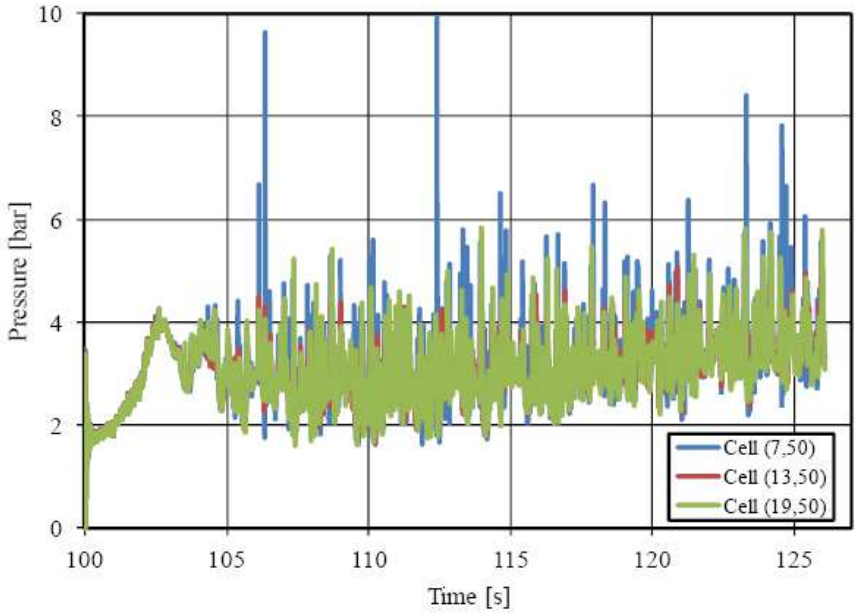


Figure 5.17: Pressure time trends in the cells (7,50), (13,50), and (19,50)

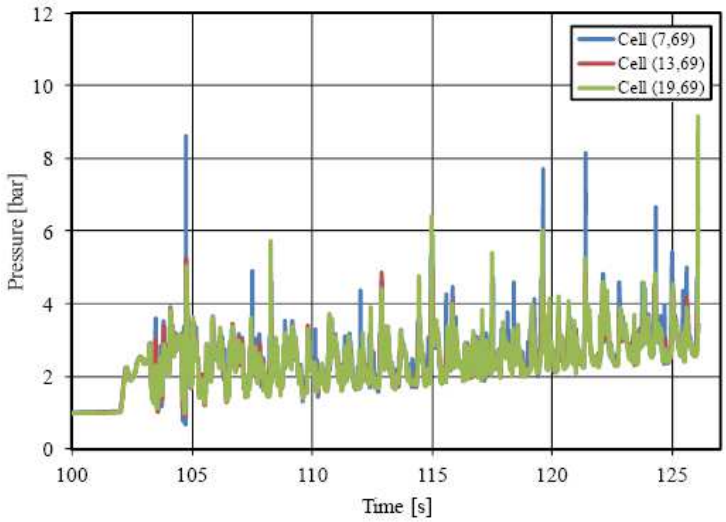


Figure 5.18: Pressure time trends in the cells (7,69), (13,69), and (19,69)

The above three figures show that the water injection modifies the pressure behavior in the single steam generator, causing a slight pressure increase in respect to the stationary conditions reached after 100 s of transient. In all these three figures it is important to note the appearance of some pressure peaks whose highest value is computed in the cell (7,20) and is almost 18 bar. It is also possible to observe that the pressure peak values decrease in the upper cells. In fig. 5.19 are marked six cells taken as reference to analyze the pressure behavior in the regions outside the single steam generator. Three cells have been selected in the lower region: (10,10), (30,10) and (45,10), their pressure time trend is shown in the fig. 5.20. The pressure profiles computed in the cells outer the SG (30,20), inside the core (45,20) and in the cover gas region (30,69) are reported in fig. 5.21.

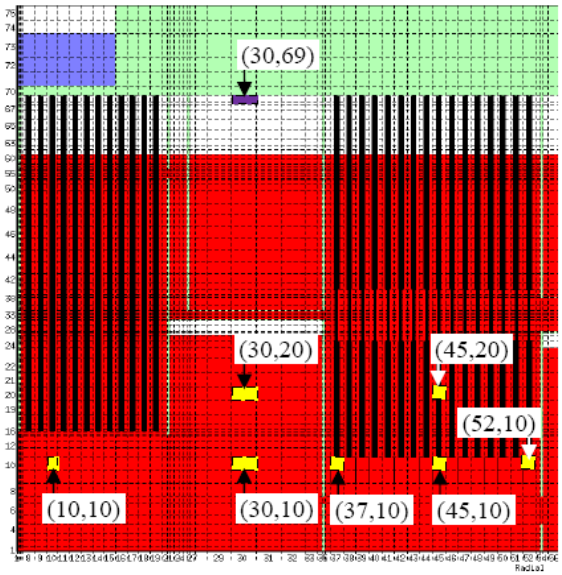


Figure 5.19: Outline of the reference cells

The figs. 5.20 and 5.21 show increasing pressure time trends with a near constant slope, their similar behavior is due to the pressurization occurred in the whole reactor model cover gas, due to the steam produced by the SGTR accident that came to the gas plenum. The calculated differences among the pressure values, at the same transient instant, for different axial positions are due to the different gravimetric load of the lead.

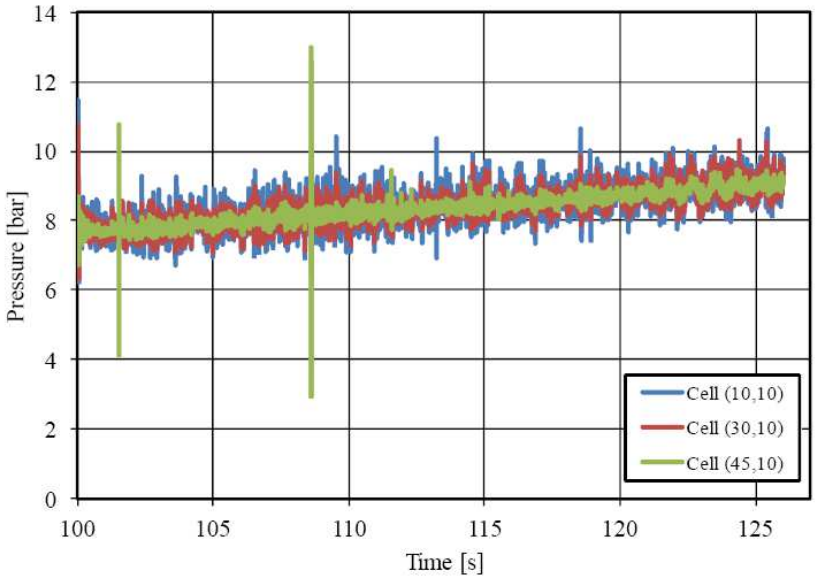


Figure 5.20: Pressure time trends in the cells (10,10), (30,10) and (45,10)

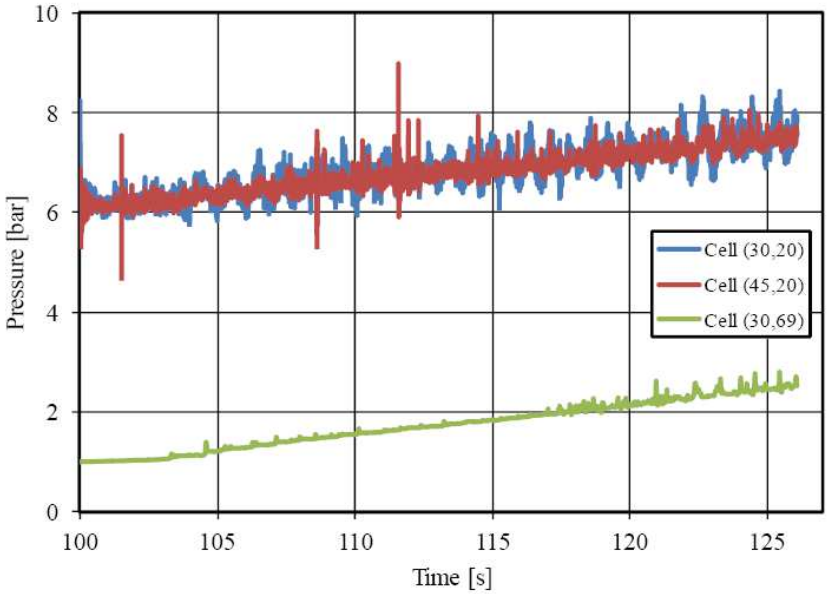


Figure 5.21: Pressure time trends in the cells (30,20), (45,20) and (30,69)

In the outer model regions, at various heights, the pressure time trends computed by the SIMMER code have a behavior similar to that shown in the above figures, in which the pressure increases of almost 1.5 bar during the 26 s of water injection transient.

In the figs. 5.22, 5.23 and 5.24 the dynamic evolution of vapor fraction into the ALFRED model, computed by the SIMMER code at different transient instants, is shown. The vapor is generated by the contact of the relatively high pressure water (180 bar and 335°C) with the hot low pressure lead (400°C and 1 bar).

The vapor distribution inside the domain, between 100 and 126 s, is summarized by nine SIMMER model images, which are included in the three figures below.

The water injected vaporizes in contact with the liquid lead at the injector tube exit region, the steam generated flows down reaching the ninth axial cell of the SIMMER model, then moves radially and goes up stratifying in the lower part of the SG (image at 100.5 s).

The vapor accumulates in this region and creates a plug of steam (101 s) that pushes up the mass of lead contained in the 1SG. When the lead reaches the SG roof (102.2 s) the cover gas has been pushed in the outer region through vents positioned in the cover gas region (see fig. 4.1), also the lead flows by these openings as shown by the image at 102.2 s. The vapor plug moves upward reaching the 1SG-1PP connection (102.8 s).

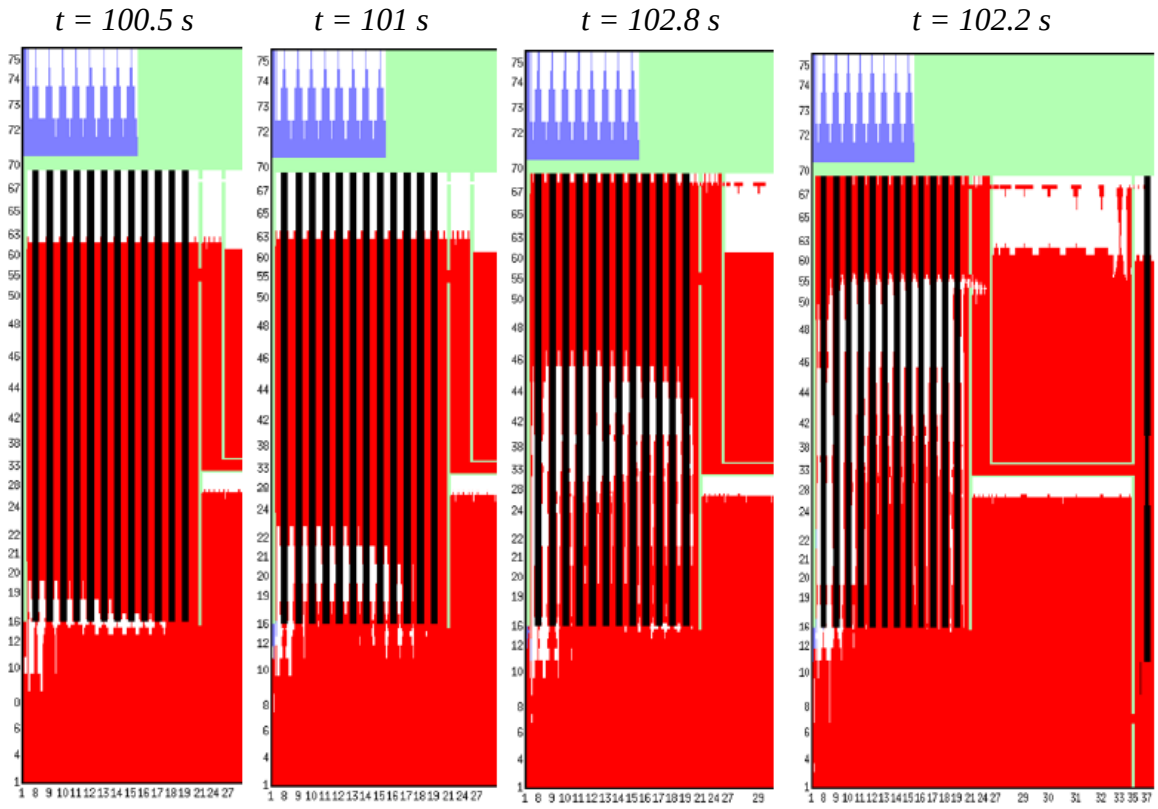


Figure 5.22: Steam distribution in the SG at different transient instants

The vapor scatters up and downward inside the vertical pump conduct, flowing through the primary pump (103.5 s in fig. 5.23). The downward movement of the vapor is arrested at

103.5 s when it reaches the upper opening that connects the PP conduct with the cover gas region. From this instant the vapor moves upward in the PP conduct and forsakes the axial cells (22-25,44) where the 1PP has been positioned. The vapor reaches the roof of the SG (104.7 s) and successively the vapor fills all the upper region of the steam generator (108 s); this configuration is maintained in the following instants (115 s, see fig. 5.24) up to the end of the computed transient (125 s).

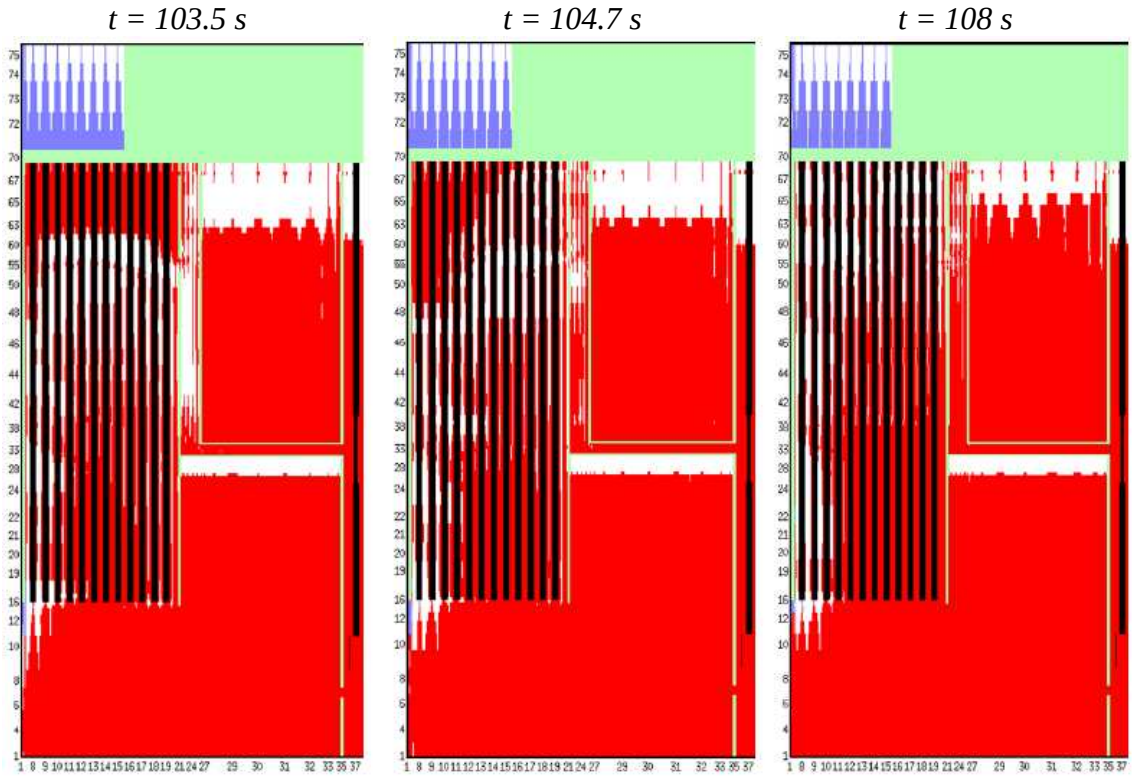


Figure 5.23: Steam distribution in the SG and PP at different transient instants

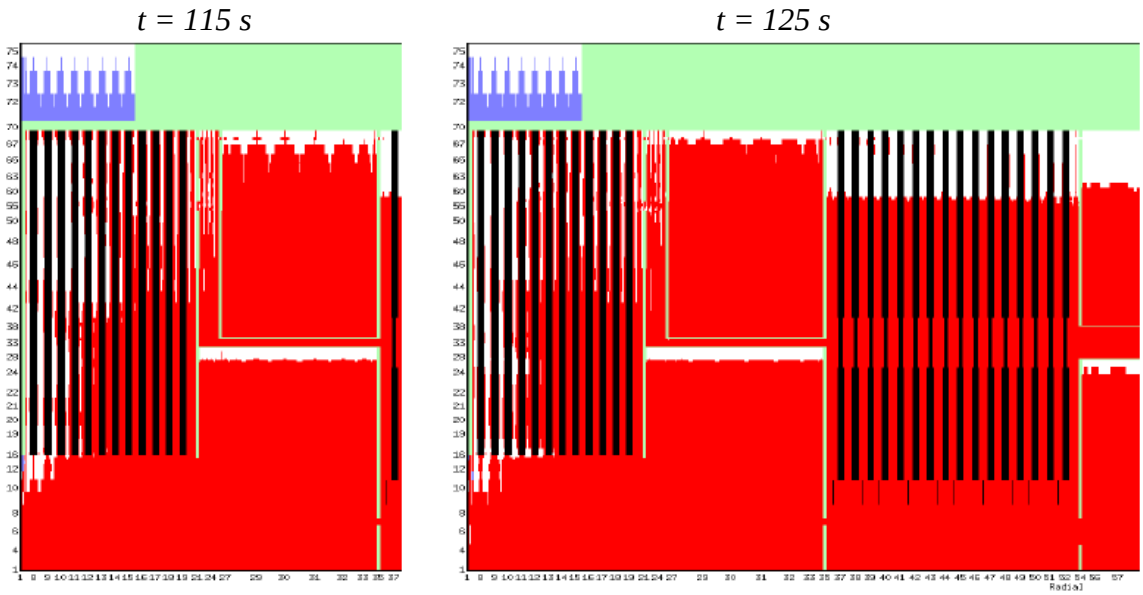


Figure 5.24: Steam distribution in the SG and PP at different transient instants

In reality, all the injected water would not vaporize instantly when contacting lead (only part of it will do so), but will be encapsulated in water vapor bubbles and transported to the cover gas region instead. This fact should be kept in mind when analyzing the simulation results.

The fig. 5.25 reports the water mass flow rate, computed by the SIMMER code, injected in the lead region through the rupture of the bayonet tube. The reported time evolution shows the water flowing through the upper surface of the cells beneath the injection orifice (1-3,15). The water mass flow rate exiting from the injector tube has been considered positive. During the 26 s of water injection the water mass flow rate value has been almost between 0.4 and 0.5 kg/s. In the modeling of the injector tube both distributed and singular pressure drops have been considered. The former represents the friction effect inside the tube and the latter (ΔP = 10 bar) is a schematization of a device (function of which is that of the Venturi nozzle implemented in the feed water of the European Lead Fast Reactor) to limit the mass flow rate exiting from the bayonet tube in case of rupture. The total mass of water injected during the entire transient (26 s) is equal to almost 11 kg.

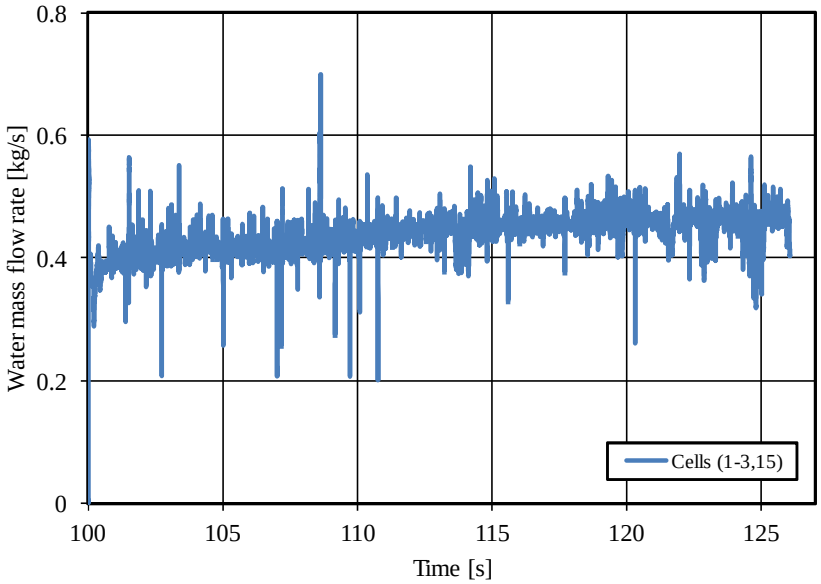


Figure 5.25: Water mass flow rate time trend injected in the lead pool

The analysis of vapor flow paths was performed on the basis of computational results obtained by the SIMMER code, to verify whether the steam do not reach the core. The steam could reach the reactor core flowing essentially through two paths, marked by “A” and “B” in fig. 5.26. The first (“A” in fig. 5.26) is constituted by the ordinary lead flow path, which could contain traces of vapor, it enters into the core by the reactor downcomer. The latter (“B” in fig. 5.26) is represented by the core-primary pump connection that could be flowed in counter-current flow by the mixture of lead-vapor. To verify whether the vapor flows into the core, the vapor void fraction has been computed by the SIMMER code in the cells (35,7) and (36-39,28), highlighted in fig. 5.26.

The results provided by the SIMMER code show that the vapor void fraction in these regions has values lower than 10^{-10}. Insignificant vapor traces (lower than 10^{-2} volume fraction) have been computed in the cells (35,31-34), see fig. 5.26, but they move upward to the cover gas and do not flow down into the core. Therefore, it is possible to conclude that in the performed numerical simulation, the steam does not enter into the reactor core.

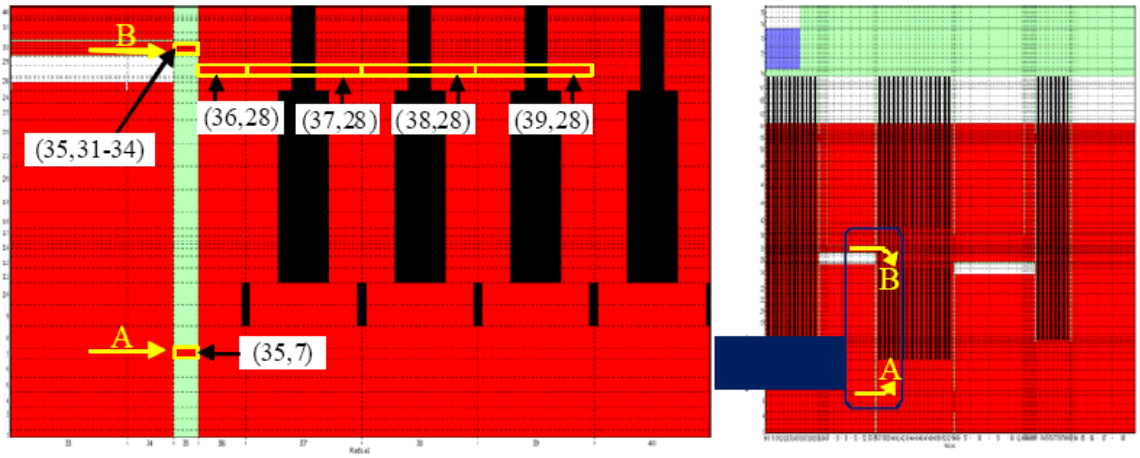


Figure 5.26: Reference cells to analyses the vapor presence in the core

5.3 Seven bayonet tubes rupture

The second SGTR accident analysed considers the rupture of one bayonet tube, as in the case studied in the section 5.2, plus the rupture of six tube positioned around it (see fig. 3.2). This configuration has been chosen to evaluate the consequence of SGTR in the very conservative case of the bayonet tube rupture propagates to the surrounding tubes, causing a so called “domino effect”.

The developed SIMMER model is almost the same as used in the single bayonet tube rupture analysis. The only difference is represented by the diameter of the water injector tube, the value of which has been set equal to 19.6 mm, in order to obtain a flow section area seven times greater than that of a single bayonet tube.

The water injector tube is coaxially positioned with the SIMMER model as previously depicted on the right image of fig. 4.3.

As in the single bayonet tube rupture accident, the water has been injected after 100 s of transient, a time interval that has been considered more than enough to reach the lead flow stationary conditions described in section 5.1.

The cells taken as reference, to evaluate by the SIMMER code the pressure time trends, are the same considered in the case of a single bayonet tube rupture accident (see sect. 5.2); this choice allows to compare the effects induced by a different water mass injected. These cells are highlighted in figs. 5.10 and 5.11.

In figs. 5.27, 5.28 and 5.29 are shown the pressure time trends computed by the SIMMER code in the first six radial cells (1-6) and three rows (13, 14 and 15) beneath the water injection orifice, in compact form the cells are specified as (1-6,15), (1-6,14) and (1-6,13).

Only the first 0.3 s of pressure time trend have been plotted to show a detailed view of the pressure peak predicted by the SIMMER code when the water injection starts.

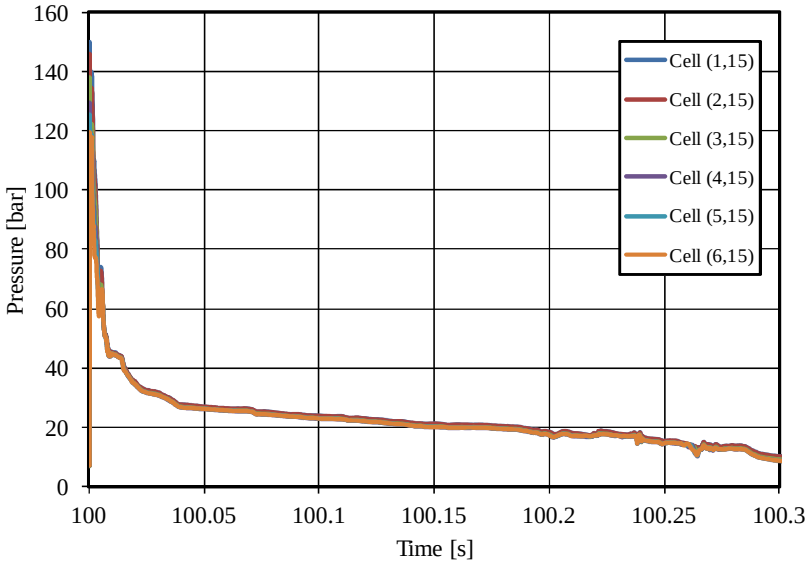


Figure 5.27: Pressure time trends in the cells (1-6,15)

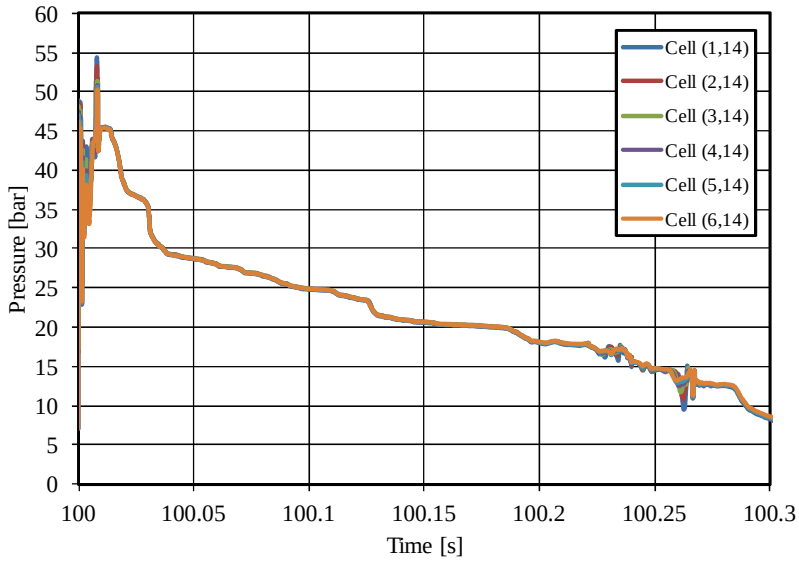


Figure 5.28: Pressure time trends in the cells (1-6,14)

The fig. 5.27 shows six pressure peaks occurred at10^{-4} s after the water injection instant (100 s), their values are much greater than those computed in case of only one bayonet tube is ruptured.

The highest pressure peak is computed in the cell (1,15), the nearest to the water injector, and its value is almost 150 bar. The figs. 5.28 and 5.29 show the pressure time trends in the cells (1-6,14) and (1-6,13), respectively. The pressure peaks computed by the SIMMER code are

lower and delayed in the further cells from the injector orifice, that is for higher radial and lower axial cell coordinates (see fig. 5.11). All the pressure trends depicted in the figs. 5.27, 5.28 and 5.29 decrease rapidly to the initial value after about 0.3 s of transient and, in each model row, are almost coincident to each other after few hundredths of a second from the peaks.

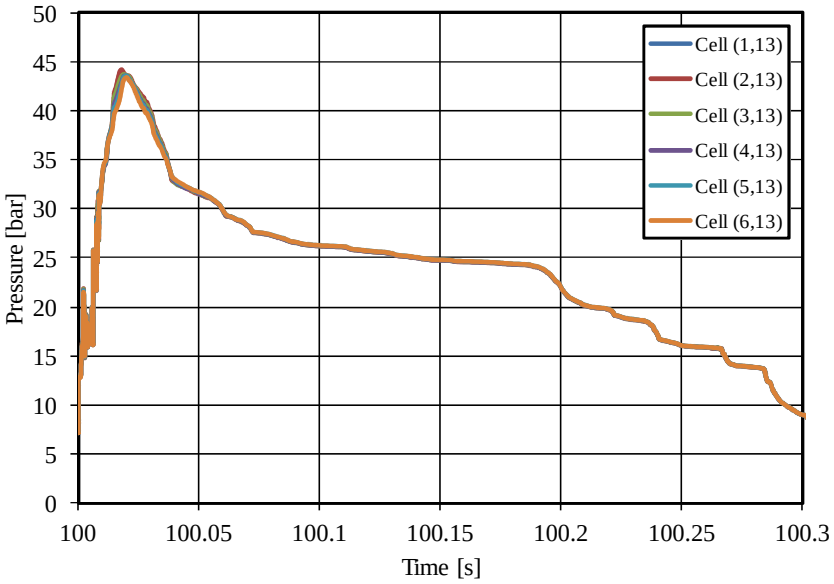


Figure 5.29: Pressure time trends in the cells (1-6,13)

The pressure behavior in the steam generator, where the bayonet tube rupture occurs, is analysed on the base of the pressure time trends computed, by the SIMMER code, in the cells marked in fig. 5.10. The pressure values calculated are shown in figs. 5.30, 5.31 and 5.32, they are referred to the cells in the 20th, 50th and 69th row, respectively. These three figures show a similar pressure increase for cells belonging to the same row and a pressure time trend slope almost constant in the entire steam generator. The slope computed is about 10 bar during 26 s of transient, that is almost five times that computed in section 5.2 (almost 2 bar during the same time interval).

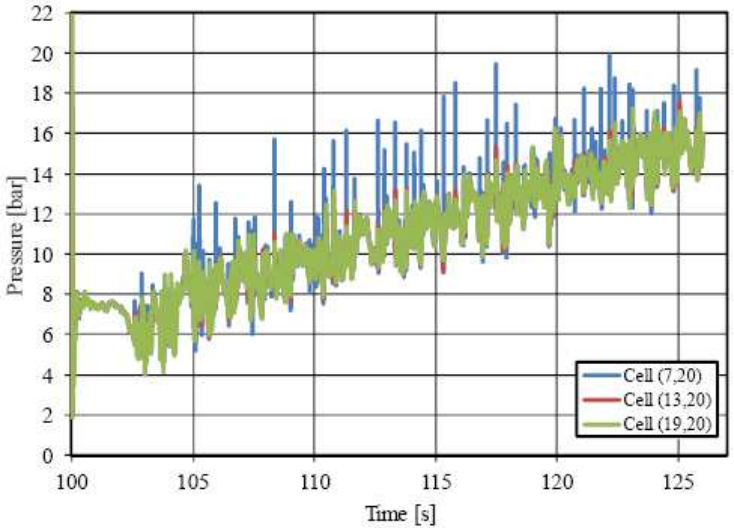


Figure 5.30: Pressure time trends in the cells (7,20), (13,20), and (19,20)

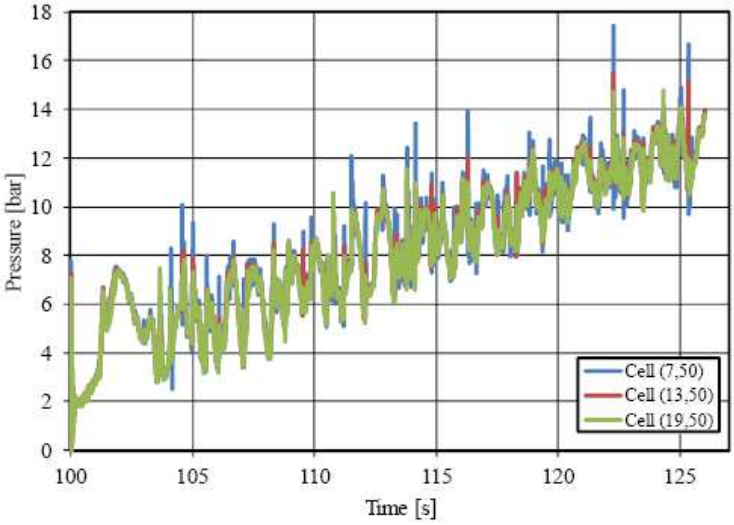


Figure 5.31: Pressure time trends in the cells (7,50), (13,50), and (19,50)

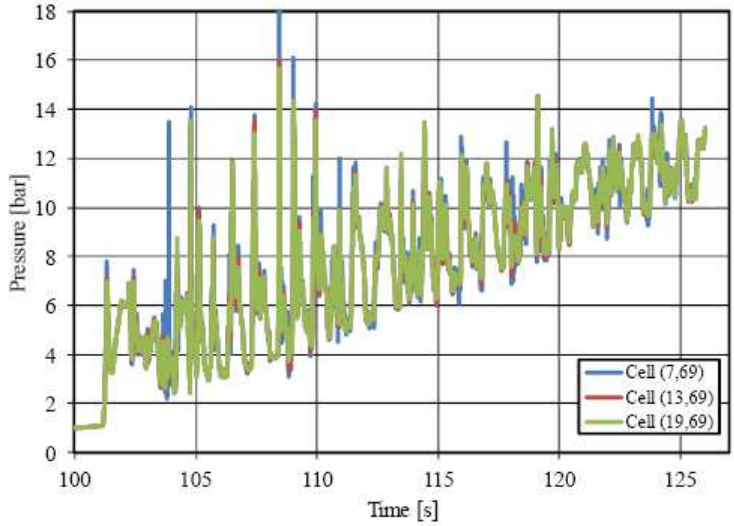


Figure 5.32: Pressure time trends in the cells (7,69), (13,69), and (19,69)

The study of the pressure behavior, in the regions surrounding the steam generator, has been performed taking as reference the six cells highlighted in fig. 5.19, that have been chosen at three different heights (row 10, 20 and 69).

The pressure time trends computed by the SIMMER code in these cells are shown in figs. 5.33 and 5.34. The higher pressure value has been computed in the cell (10,10) during the first instants of transient. The pressure profiles depicted in fig. 5.34 have the same slope, which is almost that shown in figs. 5.30, 5.31 and 5.32. Thus, the pressure increases in a similar way inside and outside the steam generator. In the outer model regions the computed pressure behaviours do not show appreciable differences in respect to the results reported in the above figures.

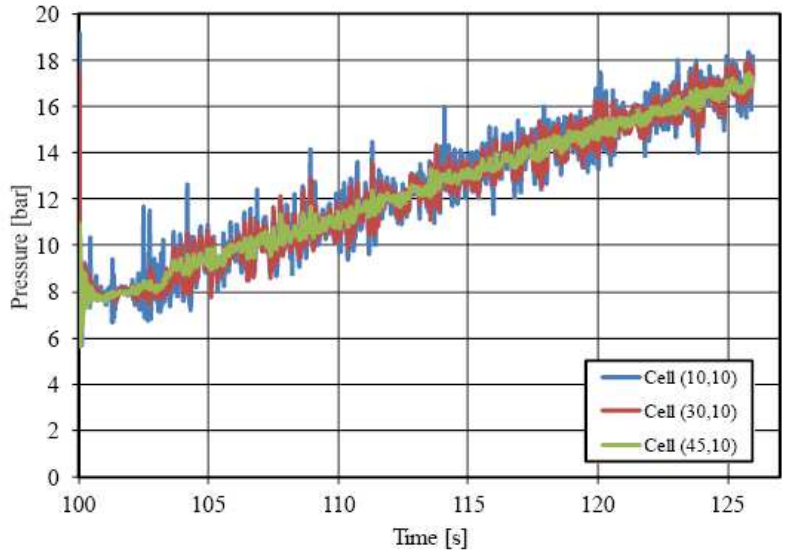


Figure 5.33: Pressure time trends in the cells (10,10), (30,10) and (45,10)

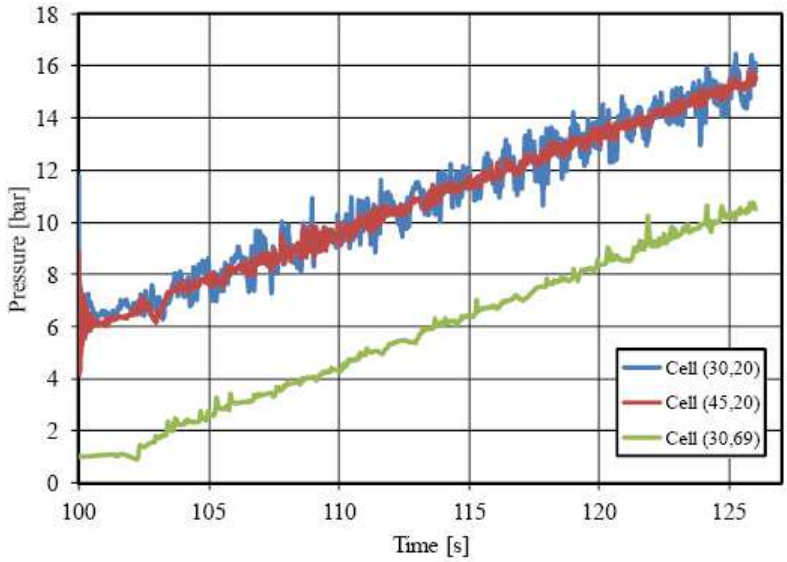


Figure 5.34: Pressure time trends in the cells (30,20), (45,20) and (30,69)

In the seven bayonet tube rupture scenario, the water injected in the lead pool is almost seven times that one injected in case of one broken tube (described in section 5.2). Thus, a greater amount of vapor is generated by the water-lead interaction in the ALFRED model. The fig. 5.35 shows the vapor behavior at three characteristic time instants during the water injection transient. The vapor generated at the water injector exit fills the lower steam generator region, creating a large plug of vapor (100.5 s, see fig. 5.35), which flows upward in the SG and lifts up the liquid lead to the SG roof (101.2 s), where the lead flows radially through the small vents that connect the SG, the PP and the outer cover gas. The vapor continues to rise and reaches the SG-PP connection (102 s) and flows upward and downward into the vertical PP conduct. In the case of one bayonet tube rupture accident the vapor exits from the PP conduct by the upper vent, but in this case the large amount of vapor generated flows away also by means of the horizontal PP-core conduct reaching the region above the core(102.3.s, see fig. 5.35).

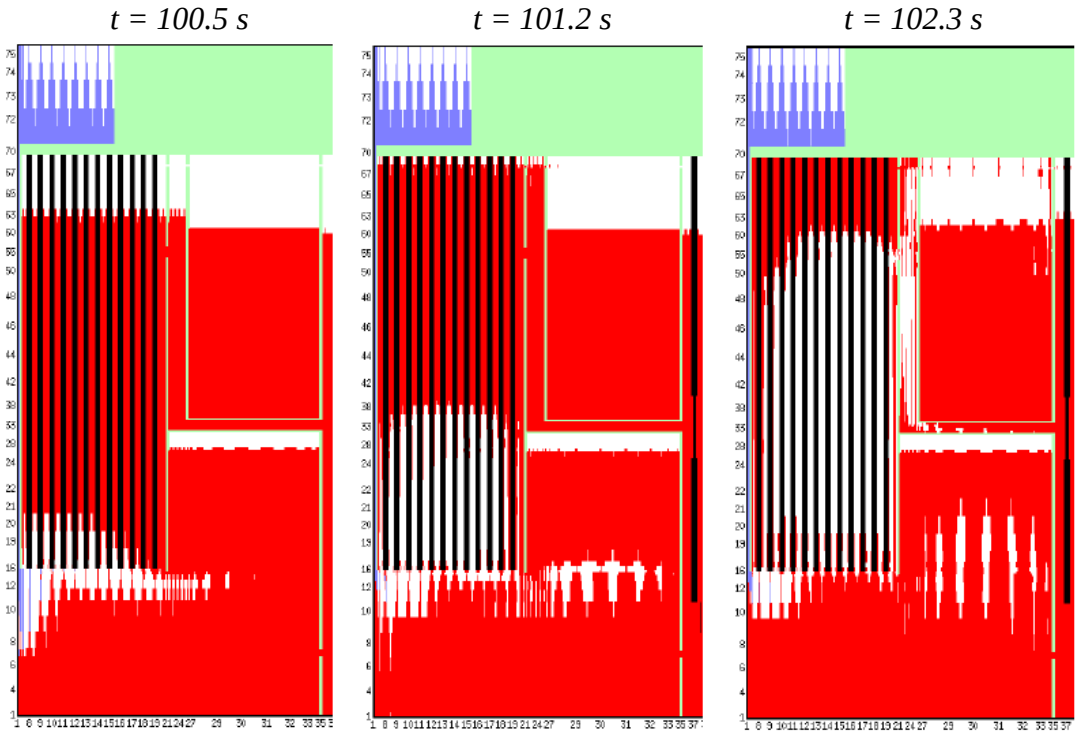


Figure 5.35: Steam distribution in the SG and PP at different transient instants

In fig. 5.36 it is shown the vapor flowing from the 1PP region to the seven merged PP region. A lot of vapor is present above the core 3 s after the water injection (left image of fig.5.36), it flows toward the upper cover gas and versus the seven SGs, thus, it does not represent an hazard for the reactivity insertion into the core. The vapor rises in the 1SG and reaches the SG upper plate, then flows out by the vents near the reactor roof (103.5 s).

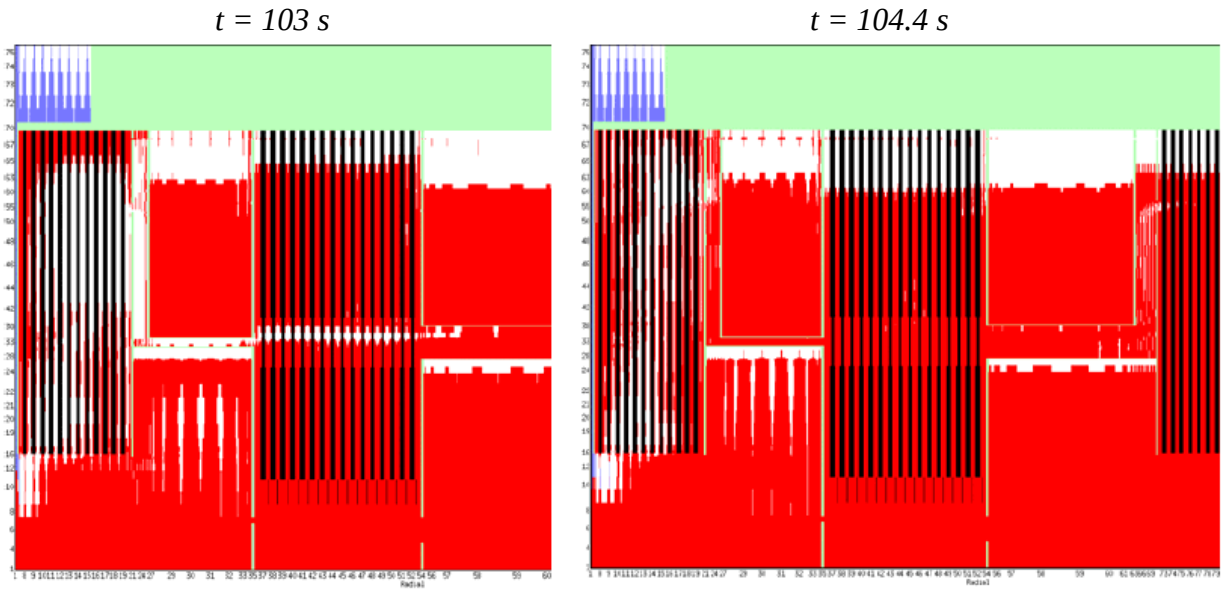


Figure 5.36: Steam distribution in the SG, PP and 7PP at different transient instants

The vapor reaches the seven merged PP (104 s) and rise in the vertical conduct entering the seven merged SGs (104.4 s, see fig. 5.36). A part of the vapor entered in the 7 SGs flows upward reaching the cover gas, the remaining vapor is dragged by the flowing lead versus the core, constituting a serious risk for the core integrity due to the reactivity feedback. After the first part of transient (almost 5 s), above analyzed, the vapor flow paths reach an almost stationary condition as shown by the fig. 5.37 at the time transient instants 115 and 125 s.

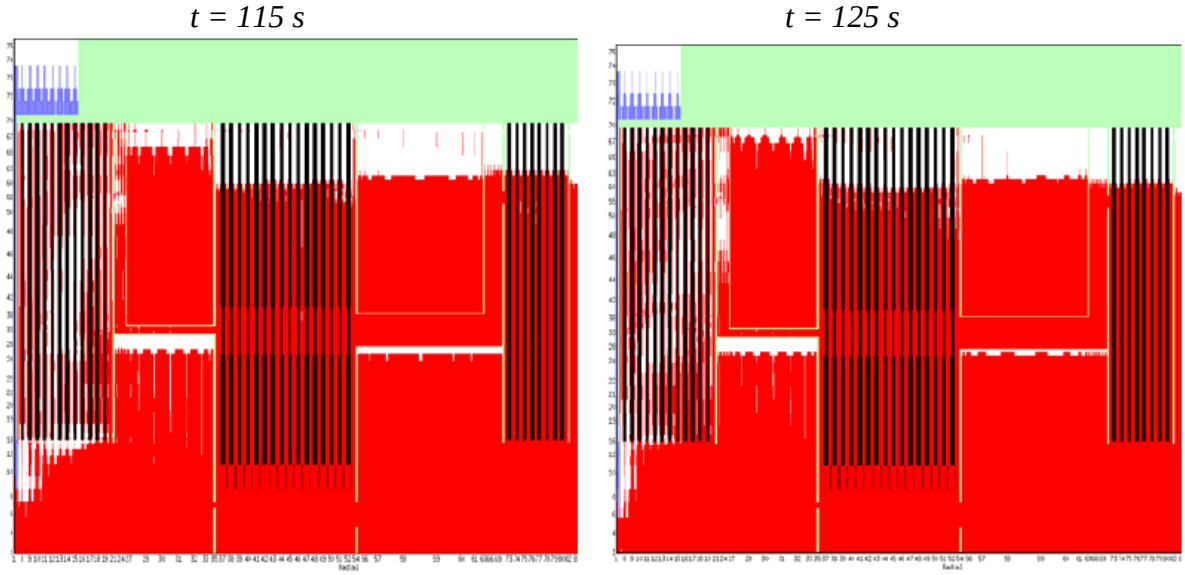


Figure 5.37: Steam distribution in ALFRED at different transient instants

The accident induced by the contemporarily rupture of seven bayonet tubes is characterized by a large amount of water injected in the lead pool. In fig. 5.38 it is reported the time trend of

the total water mass flow rate, computed by the SIMMER code, coming out from the injector tube, during 26 s of transient. It has been computed in the same way that in section 5.2. The values depicted are almost seven times higher than that reported in fig. 5.25, where one bayonet tube rupture accident has been considered.

The total water injected (during 26 s of transient) amounts at almost 80 kg.

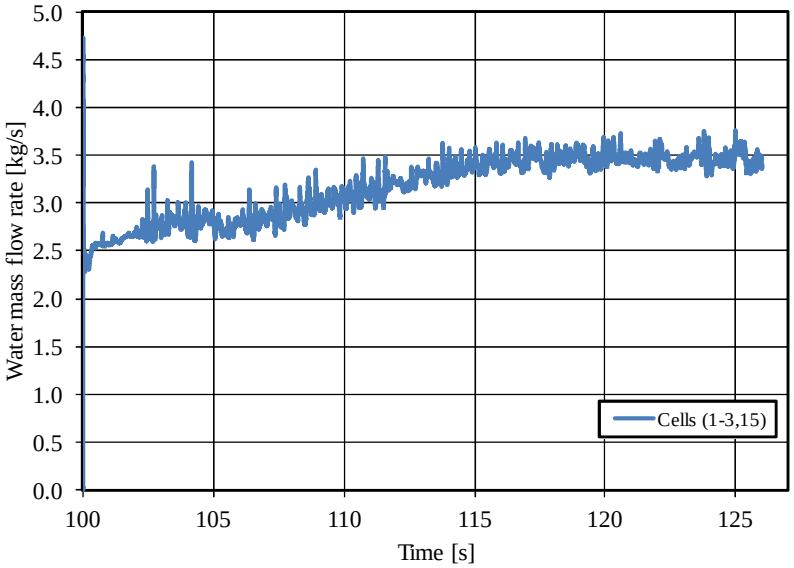


Figure 5.38: Water mass flow rate time trends injected in the lead pool

The large steam amount, generated by the water-lead interaction, flows from the lower region of the 1SG (see letter “A” in fig. 5.39) versus the upper cover gas (“C”) and the 1PP conduct (“D”), reaching the region above the core; from which it escapes upward (“E”) and toward the 7PPs-7SGs (“F”). The vapor traces, reaching the 7PPs, go up along the vertical conduct and flow partly versus the cover gas (“G”) and partly downward in the 7SGs (“H”), dragged by the lead. Few traces of vapor exit 7SGs (“I”) and flow upward, the remaining vapor reaches the core downcomer (“J”).

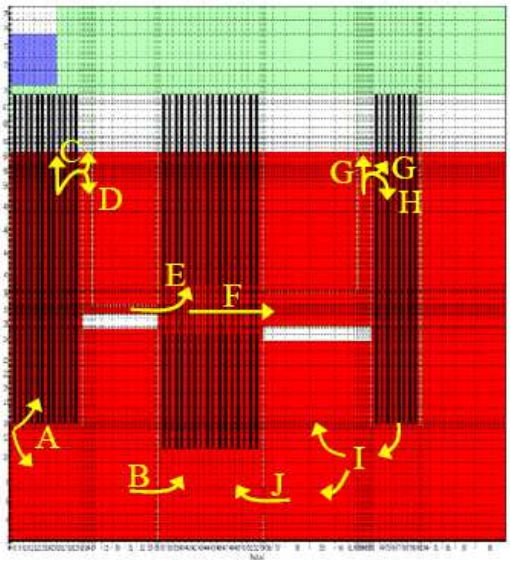


Figure 5.39: Vapor flow paths

The risk of reactivity insertion, due to the vapor flowing through the core, is represented only by the vapor flowing in the lower regions of the model (“B” and “J”), which is the only one that could enter the core, whereas the vapor above the core (“E”) moves away from the core. The vapor entering the core by “B” and “J” paths,

shown in fig. 5.39, is not visible in the figs. 5.36 and 5.37 because its concentration is relatively low.

In fig. 5.40 it is shown the void fraction computed by the SIMMER code in the cells below the core (37,10), (45,10) and (52,10), highlighted in fig. 5.19. To better analyze the steam that enters into the core by "J" path, 50 s of transient have been simulated. The SIMMER results confirm that an appreciable quantity of vapor enters only in the left part of the core (peripheral region of the core close to the SG where the accident take place), as shown by the vapor void fraction blue peak, whose maximum value is almost 0.013 (see fig. 5.40). In the center (cell (45,10)) and in the radially opposed side of the core (cell (52,10)) the void fraction computed by the SIMMER is lower than 10^{-3}. As shown in fig. 5.40 (blue trend) the vapor enters the core by "B" path only during three time interval (three blue peaks in the first 20 s of water injection), each one of almost 2 s, the first of which reaches a void fraction value almost ten times those reached in the later intervals. The vapor void fraction in the center and right cells is computed by the SIMMER code only after almost 20 s from the water injection instant; this time is in part required by the vapor to flow from the lower region of the 1SG to the core downcomer passing through the "J" path.

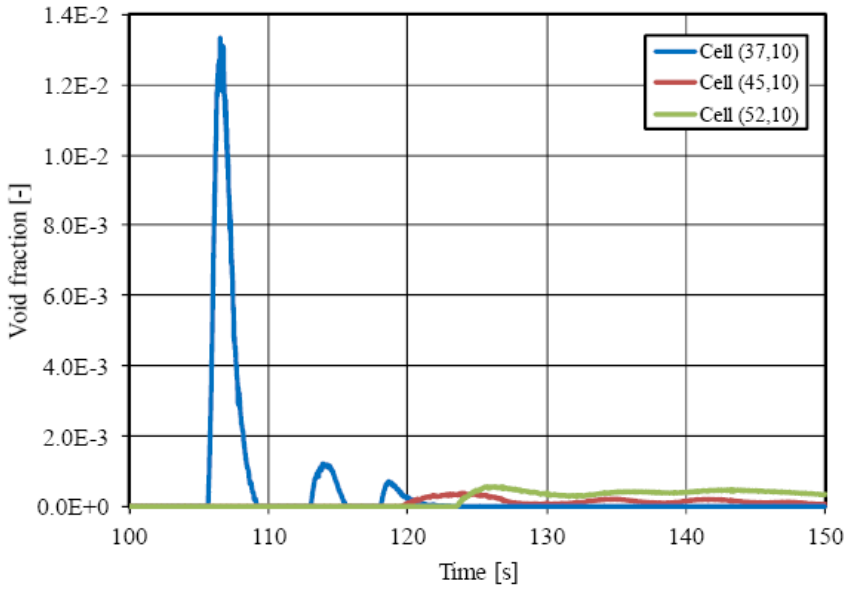


Figure 5.40: Void fraction time trends in the cells (37,10), (45,10) and (52,10)

6 Conclusions

In the frame of the LEADER project (EU 7th FP), the analysis of two SGTR accidents in the ALFRED reactor has been performed by the SIMMER III code. The SGTR scenario needs to be investigated in the ALFRED integrated pool type reactor configuration to assess the consequences of high pressure water injected in hot low pressure lead pool. In fact, the quick vapor formation represents a hazard for the internals structural integrity, exposed to the pressure waves propagation. The pressure loads induced by the bayonet tube rupture could damage the neighboring SG tubes, causing a domino effect, increasing severely the accident consequences.

The ALFRED reactor has been modelled by the axisymmetric SIMMER III code, conserving the component axial dimensions and the lead flow section areas. The broken bayonet tube is simulated by a cylindrical water injector tube, which is set coaxially to the model. All the other ALFRED components are modelled by outer annuli.

Two simulations have been performed, the former considering the rupture of only one bayonet tube and the latter assuming that also the six surrounding tubes were damaged (seven broken tubes). The two models developed by the SIMMER code differ only in the water injector tube diameter.

The first 100 s of SIMMER calculation are needed to reach the design steady state conditions; at 100 s the water injection has been activated and 26 s of water-lead interaction have been analyzed.

The highest pressure value has been computed in the cell (1,15) at the first transient instants (after some milliseconds from the water injection), beneath the water injector tube. Its value is equivalent to almost 100 and 150 bar for one and seven broken tubes, respectively.

In the SIMMER-III simulation, the water injected into the liquid metal fully vaporizes in contact with it at the injector tube exit region. In reality, all the injected water would not vaporize instantly when contacting lead (only part of it will do so), but will be encapsulated in water vapor bubbles and transported to the cover gas region instead. This fact should be kept in mind when analyzing the simulation results.

After 0.3 s starting from the water injection, the pressure peak disappears and the pressure comes back to its initial stationary value, and then increases due to the cover gas pressurization. Not so far from the injector the pressure peaks disappeared, as observed in the two simulations, and do not represent a risk for the SG and core structural integrity.

The steam generated by one bayonet tube rupture accident flows upward in the 1SG and reaches the cover gas passing through the gas vents. Instead, as consequence of the large amount of steam produced in the case of seven broken tubes, traces of steam flow from the 1SG directly and indirectly (passing through 1PP, 7PPs and 7SGs) to the core downcomer. The steam enters the core downcomer mostly by the inner path, as shown by the void fraction calculated in the cells beneath the core. The inner cell (37,10) shows a void fraction time trend, whose peak value is almost 0.013 that occurs about 6 s after the water injection instant. The outer cells, (45,10) and (52,10), have a lower void fraction peak values, which are almost equal to $5.5 \cdot 10^{-4}$ and $3.5 \cdot 10^{-4}$, respectively. They occur delayed of almost 20 s in respect to the peak measured in the inner cell, because they are caused by vapor entering in the reactor downcomer through the outer path, after having passed through the 1PP, 7PPs and 7SGs. The very low amount of vapor entering in the core, the limited vapor residence time and the negative coolant expansion reactivity effect in the optimized ALFRED reactor core do not entail a hazard of positive reactivity insertion, even if they are to be carefully taken into account for the neutronic feedback consequences.

References

1. A. Alemberti, “The ALFRED project on Lead-cooled Fast Reactor”, ESNII Conference, Advanced fission research in Horizon 2020, Brussels, 25 June 2012.
2. Ansaldo Nucleare, “ALFRED Project Reactor Block General Assembly”, CAD document no. LEADER 33 DMBX 013.
3. Ansaldo Nucleare, “ALFRED Project Steam Generator Outline”, CAD document no. LEADER 33 DMMX 020 001.
4. E. Bubelis, K. Mikityuk, “Plant Data for the Safety Analysis of the ETDR (ALFRED)”, Technical Report, PSI/KIT (including contributions from ANSALDO, ENEA, CEA, SRS, EA), April 2012.
5. Ansaldo Nucleare, “ALFRED Project Steam Generator Outline”, CAD document no. LEADER 33 DMMX 020 002.
6. AA.VV., “SIMMER III Structure model: model and method description”, Research Document, O-arai Engineering Center, Japan Nuclear Cycle Development Institute, JNC TN 9400 2004-043.
7. Morita K., et al., “SIMMER-III applications to fuel-coolant interactions”, NED. vol.189 (1999), 337-357.
8. Tobita Y., et al., “Evaluation in a CDA Energetics in the Prototype LMFBR with Latest Knowledge and Tools”, Proc.7th Int. Conf. Nuclear Engineering, (ICONE 7), Tokio, Japan, 12-23 April 1999

CIRTEN – UNIVERSITY OF PISA
DICI

Thermal-hydraulic analysis of a single primary pump trip in ALFRED reactor

G. Barone, M. Cherubini, N. Forgione

Pisa, February 2013

Abstract

The performed study deals with the thermal hydraulic investigation of the ALFRED reactor response against two selected accidents: the Unprotected Loss Of Flow (ULOF) and the Single Primary Pump (PP) trip, which concern respectively the TDEC-1 and DBC category.

In the ULOF scenario it has been assumed that all primary pumps are simultaneously stopped and neither control nor safety rods are dropped to scram the reactor. Rather the core power is driven by the reactivity feedback. In the Single PP trip, the postulated initiating event is the trip of one over eight primary pumps, also in this case the reactor power is driven by the reactivity feedbacks only.

The thermal-hydraulic evaluation of the ALFRED response has been carried out adopting the RELAP5 code and by using a suitable reactor nodalization (developed to the purpose at the UNIPI).

ULOF results to be (as foreseeable) a much challenging scenario, being the core power variation and clad temperature excursion larger than the Single PP trip. In ULOF scenario a natural circulation conditions are established with reactor mass flow rate of about 6100 kg/s, predicted peak cladding temperature is 828°C. Rather in the Single PP trip, reverse flow in the trip loop occurs and a much lower peak cladding temperature of 543°C is reached.

The obtained results may contribute (and compared) to benchmark on the treated issues.

This work was performed within the LEADER Project (Contract No. FP7-249668) under the auspices of the EU 7th Framework Program.

List of Figure

Figure 1-1: Reactor configuration– vertical view [1] 2
Figure 2-1: ALFRED reactor block configuration-vertical view (a) 6
Figure 2-2: ALFRED reactor outer vessel and cover assembly schematics [5]. 8
Figure 2-3: ALFRED inner vessel assembly schematics [5] 8
Figure 2-4: ALFRED core configuration 9
Figure 2-5: Main SG bayonet tube geometric data and design [7] 10
Figure 3-1: Sketch of ALFRED RELAP5 nodalization 13
Figure 3-2: Linear power distribution along the core active length 14
Figure 4-1: ALFRED steady state conditions, core power and total cooling power 19
Figure 4-2: ALFRED steady state conditions, reactor mass flow rate 19
Figure 4-3: ALFRED steady state conditions, lead temperature distribution along the core, average and maximum FA power 20
Figure 4-4: ALFRED steady state conditions, SG1 primary and secondary side temperature distribution along the tubes 21
Figure 4-5: ALFRED steady state conditions, SG1 quality profile along the tubes 22
Figure 4-6: ALFRED ULOF accident, reactor mass flow rate 24
Figure 4-7: ALFRED ULOF accident, Core and total cooling power 25
Figure 4-8: ALFRED ULOF accident, neutron kinetic feedbacks larger contributions to total reactivity 26
Figure 4-9: ALFRED ULOF accident, neutron kinetic feedbacks smaller contributions to total reactivity 26
Figure 4-10: ALFRED ULOF accident, lead inlet and outlet temperature in average FA and max power FA 27
Figure 4-11: ALFRED ULOF accident, clad temperature in average FA, max power FA and peak pin 28
Figure 4-12: ALFRED ULOF accident, fuel temperature in average FA, max power FA and peak pin 28
Figure 4-13: ALFRED ULOF accident, Axial temperature profile along the core active length and comparison with steady state conditions 29
Figure 4-14: ALFRED ULOF accident, SG secondary side inlet (water) and outlet (steam) temperature 30
Figure 4-15: ALFRED ULOF accident, SG primary and secondary side temperature profile along the tubes length and comparison with steady state conditions 31
Figure 4-16: ALFRED ULOF accident, SG quality profile along the tubes length and comparison with steady state conditions 31
Figure 4-17: ALFRED Single PP Trip EOC accident, primary pumps mass flow rate 34
Figure 4-18: ALFRED Single PP Trip EOC accident, reactor mass flow rate 34
Figure 4-19: ALFRED Single PP Trip EOC accident, Core and total cooling power 35
Figure 4-20: ALFRED Single PP Trip EOC accident, neutron kinetic feedbacks larger contributions to total reactivity 36
Figure 4-21: ALFRED Single PP Trip EOC accident, neutron kinetic feedbacks smaller contributions to total reactivity 36
Figure 4-22: ALFRED Single PP Trip EOC accident, lead inlet and outlet temperature in average FA and max power FA 37
Figure 4-23: ALFRED Single PP Trip EOC accident, clad temperature in average FA, max power FA and peak pin 38

Figure 4-24: ALFRED Single PP Trip EOC accident, fuel temperature in average FA, max power FA and peak pin 38
Figure 4-25: ALFRED Single PP Trip EOC accident, axial temperature profile along the core active length and comparison with steady state conditions 39
Figure 4-26: ALFRED Single PP Trip EOC accident, SG1(affected) and other SGs primary side inlet and outlet temperature 40
Figure 4-27: ALFRED Single PP Trip EOC accident, SG1(trip) and SGs secondary side inlet (water) and outlet (steam) temperature 41
Figure 4-28: ALFRED Single PP Trip EOC accident, SG1 (trip) primary and secondary side temperature profile along the tubes length and comparison with steady state conditions 42
Figure 4-29: ALFRED Single PP Trip EOC accident, SGs (not affected) primary and secondary side temperature profile along the tubes length and comparison with steady state conditions 42
Figure 4-30: ALFRED Single PP Trip EOC accident, thermodynamic quality profile of the SG1 (trip) and the 7 SGs (not affected) along the tubes length and comparison with steady state conditions 43
Figure 4-31: ALFRED Single PP Trip accident, reactor core power comparison between EOC and BOC core status 45
Figure 4-32: ALFRED Single PP Trip accident, reactor core power comparison between EOC and BOC core status – zoom 45
Figure 4-33: ALFRED Single PP Trip accident, average and hot FA core outlet temperature comparison between EOC and BOC core status 46

List of Table

Table 2-1: ALFRED reactor main parameters 7
Table 3-1: Relap5 ALFRED nodalization, adopted code resources 12
Table 3-2: Reactivity feedbacks 16
Table 4-1: ALFRED reactor, selected steady state parameters and comparison with computed values 18
Table 4-2: ALFRED ULOF accident, imposed events 23
Table 4-3: ALFRED ULOF accident, resulting sequence of events 23
Table 4-4: ALFRED Single PP Trip EOC accident, imposed events 32
Table 4-5: ALFRED Single PP Trip EOC accident, resulting sequence of events 33
Table 4-6: ALFRED Single PP Trip BOC accident, imposed events 44
Table 4-7: ALFRED Single PP Trip BOC accident, resulting sequence of events 44

Content

1 Introduction 2

2 Overview of ALFRED reactor 4

3 Computational tools 11

3.1 Adopted code description 11

3.2 Nodalization description 11

3.2.1 Hydrodynamic part 12

3.2.2 Heat structures 14

3.2.3 Neutron Kinetics 15

4 ALFRED reactor simulations 17

4.1 Steady state conditions 17

4.2 Unprotected Loss of Flow Transient 22

4.3 Single Primary Pump trip 32

4.3.1 Single Primary Pump trip simulation in EOC condition 32

4.3.2 Single Primary Pump trip simulation in BOC condition 43

5 Conclusions 47

6 References 49

1 Introduction

The ELFR option B configuration (represented in Figure 1-1) to be adopted in ALFRED differs from the LFR primary cooling system Option A mainly for the adoption of bayonet tubes type solution for the design of its SGs.

The LFR demonstrator-ALFRED is a scaled down reactor design, that may implement solutions as much as possible close to the adopted reference conceptual design but considering the essential need to proceed to construction in a short time frame.

ALFRED reactor is intended to demonstrate the feasibility of the LFR design solutions (capability of effective power production both from a safety and economic point of view) and like a "laboratory" to proof and substantiate the made technological choices .

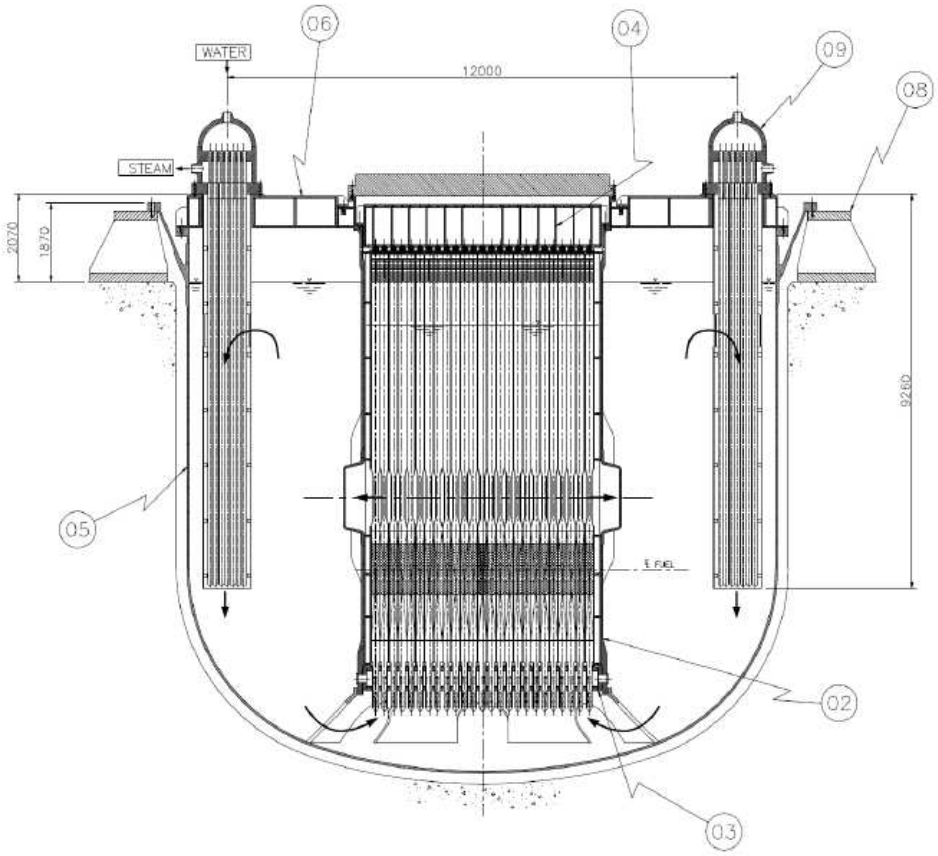


Figure 1-1: Reactor configuration– vertical view [1]

The aim of the present study, performed in the frame of the LEADER project (EU 7th FP), is to provide an evaluation of the reactor performances and the effects induced in case of Single

Pump Trip (following the simulation of steady state conditions) and Unprotected Loss Of Flow (ULOF).

Both these accident scenarios, that are the loss of one primary pump, with AC power available (TD-5) and the complete loss of forced flow plus the reactor trip fails (total ULOF considered to have low probability of occurrence, indicated as TDEC-1) have been investigated by applying an adequate computational tool (i.e. RELAP5 code) and setting up a suitable model/nodalization (implemented by CIRTEN-UNIPI), in order to analyze the safety behavior of the Pb-cooled ALFRED reactor.

In addition it is worthy to note that the protected and unprotected (these design basis and design extension conditions are indicated respectively with the acronyms DBC & DEC) transients analyzed allow to assess the safety behavior of the Pb-cooled ELFR for a range of conceivable initiators events. Moreover although the second one is characterized by a very low probability of occurrence, the intent of the transient analysis is to evaluate inherent safety characteristics and to highlight the limits of the reactor design.

The total ULOF is an unprotected accident scenario that postulates all the eight Primary Pumps fail without drop of control rods to SCRAM the reactor. As a consequence, therefore, ULOF is classified in the TDEC category according to ALFRED accident classification. The main objective of this transient is to investigate and analyze the cooling capability of the reactor systems “working” in natural circulation conditions.

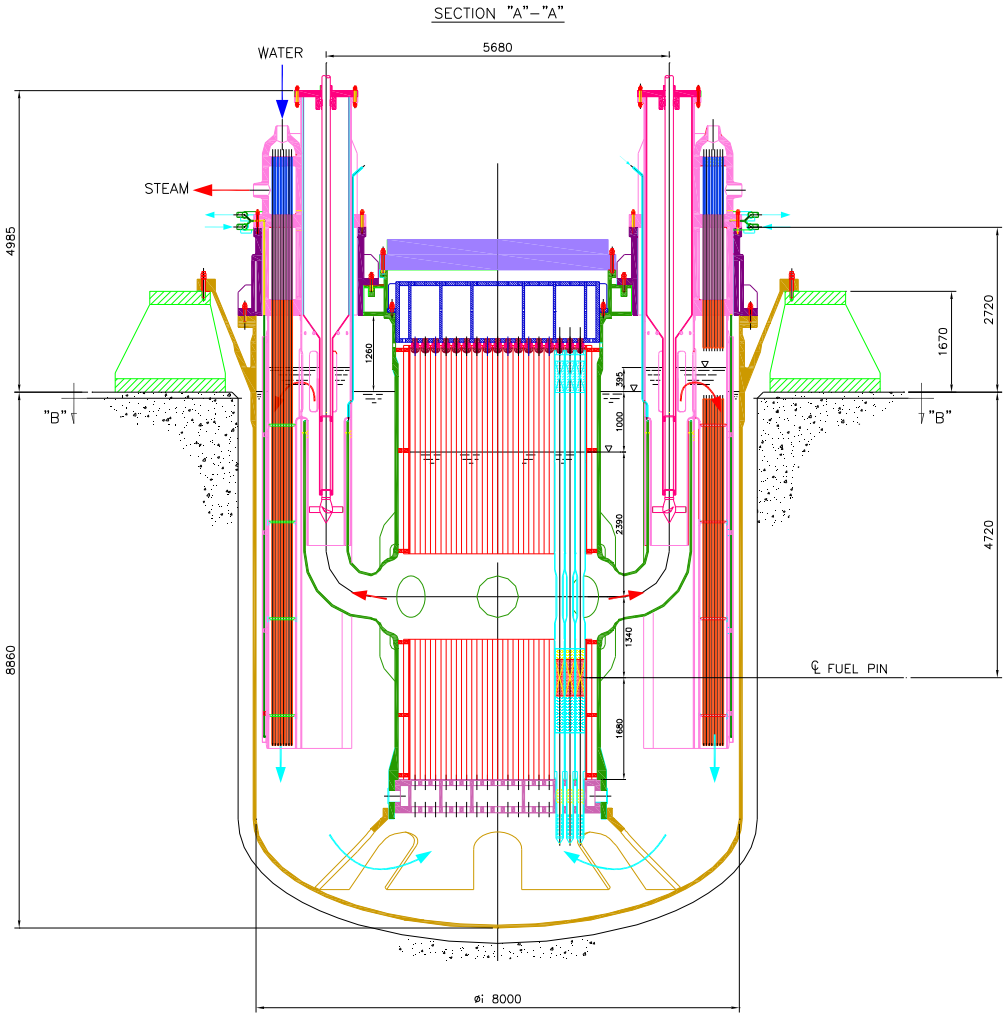
A single primary pump trip is instead postulated in the second simulated accident. This accident is surely milder than ULOF in terms of power, coolant and clad temperature variations, however much stringent limits (in compliance with Design Basis Conditions, DBC) have to be fulfilled.

Summarizing, the present study deals with thermal-hydraulic analyses of TD-5 and TDEC-1 accident scenarios. To the purpose, RELAP5 nodalization has been developed taking in consideration the main features characterizing ALFRED reactor. In what follows the considered input data related to the hydrodynamic, heat structures and neutron kinetic (including feedbacks) are also described.

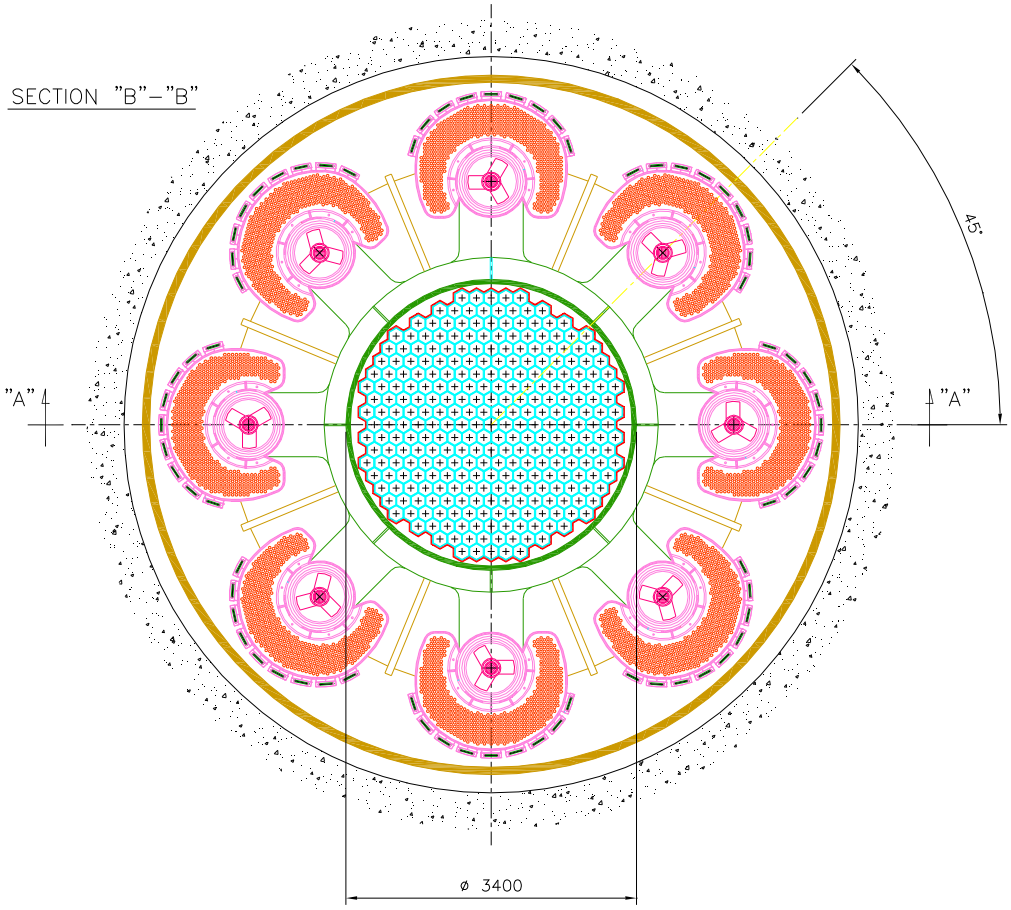
2 Overview of ALFRED reactor

Recent developments carried out in last decade (EU FWP-5, FWP-6 and FWP7) in the frame of Accelerator Driven Systems (ADS) as well as Fast Reactors, have evidenced lead as an emergent technology (due to its high boiling point, inert nature, favourable neutronics and safety characteristics) potentially complying all Gen. IV goals (with specific reference to nuclear cycle sustainability). During FP6, the conceptual viability of a large scale LFR (600 MWe) in terms of economics, safety as well as sustainability have been demonstrated by the outcome of the ELSY (European Lead System) project. Following this effort, the FP7 project named LEADER was started in April 2010 aiming mainly at providing the conceptual design of a demonstrator (ALFRED-Advanced Lead Fast Reactor European Demonstrator) based on already available industrial technology in order to shorten as much as possible the construction phase [1], [2].

The main LFR primary cooling system geometric and design parameters (briefly summarized in the following Table 1-1) are reported in [3]. The current available configuration of the primary system components (Option B as shown in Figure 1-2) consists mainly in a pool type reactor vessel, inner vessel, bayonet tubes steam generators (SGs), primary pumps, core support plate, above core structure.


SECTION "A"–"A"
WATER
5680
STEAM
4985
2720
1670
"B"
"B"
1260
395
1000
2390
4720
8860
1340
℄ FUEL PIN
1680
ø 8000

(a)



(b)

Figure 1-2: ALFRED reactor block configuration-vertical view (a) and reactor block configuration – top view, “B”-“B” cut (b) [4].

ALFRED inner vessel is constituted by the main components: the cylindrical vessel (Figure 1-4), the core lower and upper grid, having 1.5 m diameter, the main primary system components and the cover vessel (Figure 1-3).

The outer safety vessel has a torospherical bottom head. It is anchored to the reactor pit from the top, its supports allows to sustain the weight of the core and all primary components.

The main parameters of ALFRED are presented in Table 1-1 [3] below:

Parameter	Value
Thermal power	300 MWth
Thermal efficiency	45%
Primary Coolant	Pure lead
Core inlet temperature	400°C
Core outlet temperature	480°C
Fuel	MOX
Fuel cladding temperature	Maximum 550°C (nominal conditions)
Cladding material	15-15/Ti
Primary system	Pool type, compact, forced circulation (at power), natural circulation for DHR
Primary system pressure loss (in core)	0.1MPa (Unprotected Loss of Flow grace time >30 min)
Steam generators	8, integrated in the main vessel
No of SG tubes	510
SG removed power	37.5 MW (nominal conditions)
Primary pumps	8, integrated in steam generator, suction from hot collector
Secondary cycle	Water-superheated steam at 180 bar, 450°C
Reactor Vessel (inner)	Hanged, Austenitic stainless steel
Safety Vessel (outer)	Anchored to reactor pit
Reactor Internals	Removable

Table 1-1: ALFRED reactor main parameters

The reactor outer vessel (Figure 2-2) is a cylindrical vessel with a torospherical bottom head. It is anchored to the reactor pit from the top. Reactor outer vessel is closed by a roof that supports the core and all the primary components. A cone frustum welded to the bottom head has the function of bottom radial restraint of the Inner Vessel.

ALFRED Inner Vessel (see Figure 2-3) is made of 3 subassemblies [3]:

- The cylindrical vessel,
- The core lower grid,
- The core upper grid.

Cylindrical vessel is a double wall shell: the outer thick wall has a structural function, while the inner thin wall follows the core section profile. Lead flow is guided from the FAs outlet towards the PP inlet pipes by a toroidal half-ring. The Inner Vessel is fixed to the cover by bolts and is radially restrained at the bottom. ALFRED uses wrapped hexagonal Fuel Assembly (FA) weighed down (at least with primary pumps off) and supported by a lower support grid anchored to the inner vessel, as shown in Figure 1-43. FA is maintained in position laterally by the cylindrical inner vessel and from the top by springs connected to the reactor roof. No refuelling machine is foreseen inside the reactor vessel.

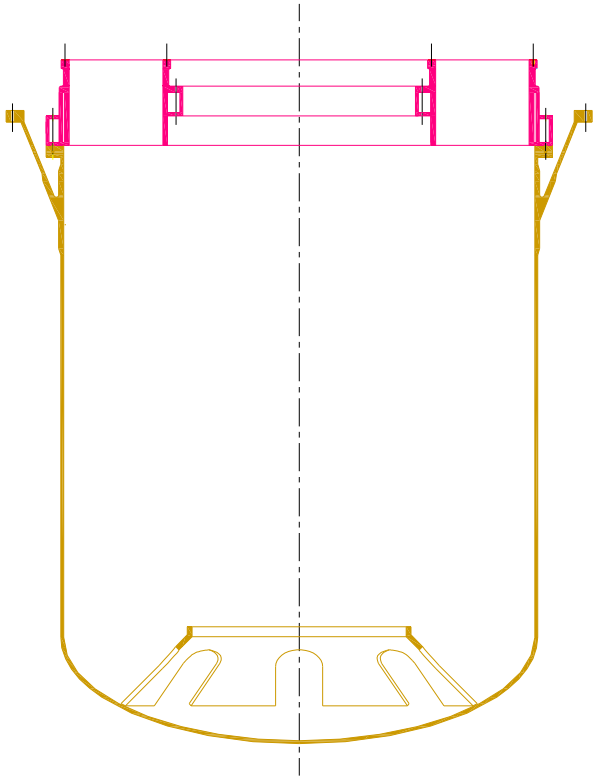


Figure 1-3: ALFRED reactor outer vessel and cover assembly schematics [5].

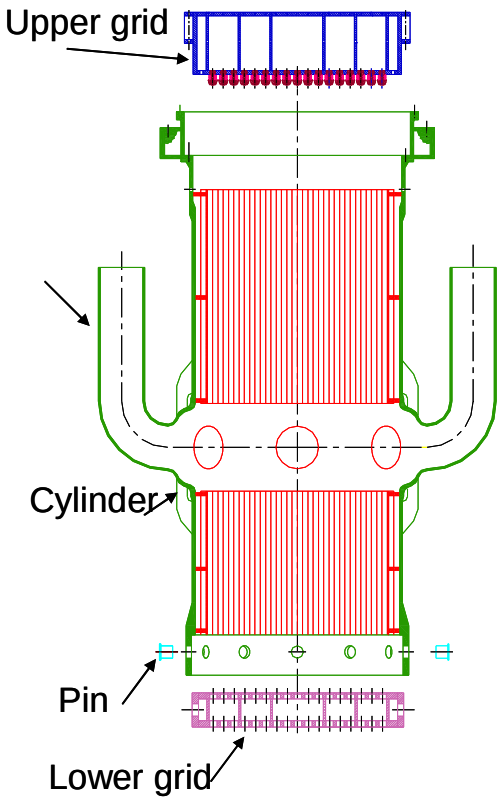


Figure 1-4: ALFRED inner vessel assembly schematics [5]

The core is constituted by 171 fuel assemblies, each of these formed by 127 fuel pins arranged in hexagonal lattice (see Figure 1-5). Active length is 0.6 m, overall rod length is 1.43 m.

The 171 FA are surrounded by 108 dummy elements which work as neutron shielding. The chain reaction is controlled by 12 control rods, shutdown of the reactor is ensured by additional 4 safety rods. B_4C enriched in ^{10}B is considered as absorber material [6].

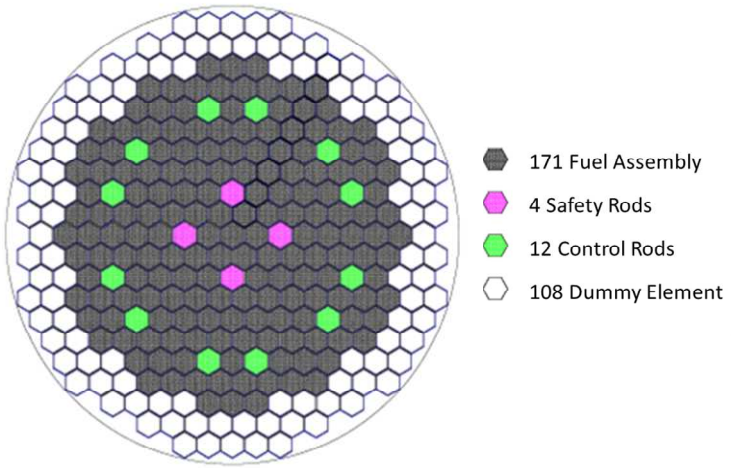


Figure 1-5: ALFRED core configuration

The lead forced circulation is maintained by eight Primary Pumps (PP), which feed eight SGs which in turn transfer the heat generated in the core to water, that represents the secondary fluid. Superheated steam is thus generated in the steam generators and directed into the turbine to be finally converted to electricity. PP suctions are in a hot header which collects lead exiting from the core. The PP are surrounded by the SG tube bundle and their housing are the SG casing and are of axial type.

ALFRED includes 8 once through double wall bayonet type steam generators. The single vertical unit (Figure 1-65) proposed consists of three concentric tubes. Starting from the inner tube, the water flows downwards and then enters the second concentric tube in up-flow where it starts to boil because of the heat exchange with the liquid lead that flows in counter-current on the tube outer surface. The tube design allows the achievement of super-heated steam. The liquid lead is not in direct contact with the second tube; the third concentric tube separates it from the steam-water tubes. This configuration allows the double physical separation between lead and water sides by means of an intermediate gap. Furthermore, by means of gap

pressurization (with Helium), a leakage check system should be introduced in order to prevent incident scenarios (SGTR detection). Two main features are requested:

- An insulating layer to avoid heat exchange (causing steam condensation) between the superheated steam that leaves the second tube and the feedwater that enters the first one.
- The achievement of superheated steam requires the selection of an appropriate high conductivity material (i.e. powders) to be placed within the gap between the second and the third tube.

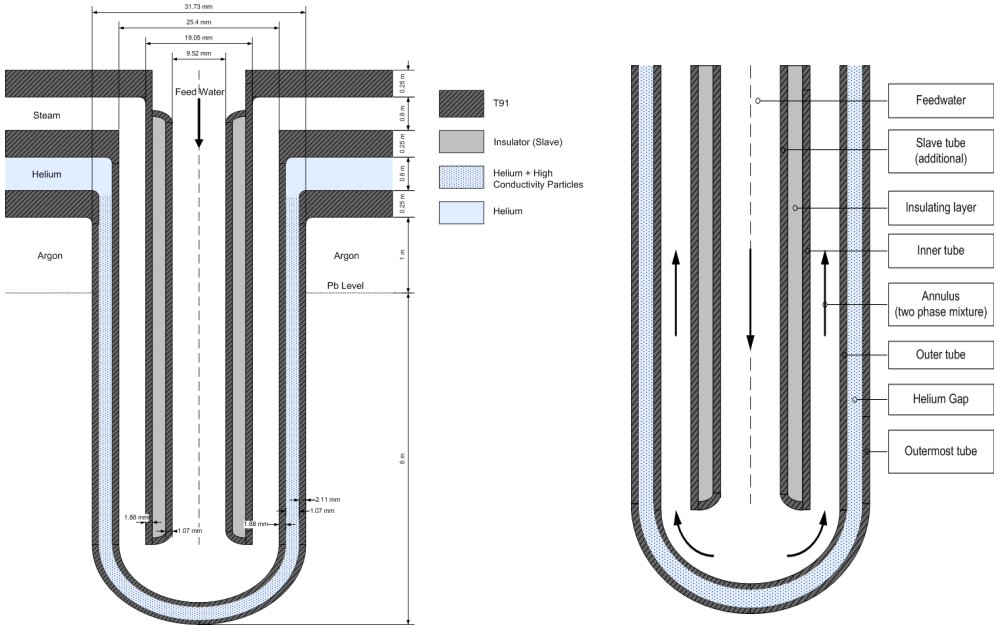


Figure 1-6: Main SG bayonet tube geometric data and design [7]

ALFRED is equipped with two redundant and diverse DHR systems operated in a passive way. Primary system features low pressure drop to enhance natural circulation which permits to have a grace time larger than 30 min in case of unprotected loss of flow.

3 Computational tools

3.1 Adopted code description

The adopted code is RELAP5/Mod3.3 in which the capability of dealing with lead has been introduced. Namely, devoted thermo-physical lead fluid properties have been constructed in a suitable form for the code use and specific convective heat transfer correlations for liquid metals have been implemented inside the code. All other capabilities, in respect to the standard RELAP5, are available in terms of hydraulic, heat conduction and 0D neutron kinetic parts [8].

3.2 Nodalization description

The nodalization developed by CIRTEN-UNIPI to simulate the behaviour of ALFRED reactor follows some general rules such as:

- slice nodalization approach;
- reference length characteristics of each sub-volume equal to about 0.1m;
- length of sub-volumes in active core region equal to 0.05 m;
- use of stacks of pipe to model specific subpart of the reactor.

The slice nodalization approach is realized cutting different parts of the reactor by common horizontal planes. In this respect the elevation of the sub-volumes is imposed equal in various reactor subparts. Such an approach is recommended when natural circulation conditions have to be simulated because it does not introduce artificial differential pressure generated by different elevation of sub-volume centre (position in which the code calculates volume thermodynamic conditions).
The characteristic length of each sub-volume, fixed at 0.1 m or 0.05 in active core region, ensures an accurate evaluation of thermophysical properties variations along the flow path. This is particularly relevant in those reactor regions where lead heat up and cool down take place and in which quite large thermal gradient is expected.
The latter rule is followed to easily check and review the input deck data.

Code resource	Value	Note
No. of volumes	2867	Primary and secondary system considered
No. of junctions	2956	Primary and secondary system considered
No. of active heat structures	48	FA and dummy elements considered
No. of heat structures	1401	Active and passive structures considered
No. of mesh points	21907	Active and passive structures considered

Table 1-2: Relap5 ALFRED nodalization, adopted code resources

3.2.1 Hydrodynamic part

The developed nodalization takes into consideration the nominal flow path recognizable in the description provided in above section. All main components are represented in the model, namely eight pumps, eight steam generators with their inlet and outlet primary side piping including also their upper free level.

Concerning the flow path in the rest of the reactor vessel, a BRANCH component collects the lead exiting the steam generators driving the primary fluid down to the lower plenum. The bottom part of the vessel is represented by a stack two PIPEs up to the core region inlet.

Lead flow path is divided into two main parts: one flowing through the FA, while the other through the PIPE stacks, which is devoted to dummies elements simulation.

The FA hydrodynamic parts are further subdivided into two parallel paths: one for the maximum sub-assembly power, one for the rest of the core. The former has the geometrical dimension of a single assembly, the latter is equivalent to all the other 170 constituting the ALFRED core. The maximum subassembly power is simulated separately with the aim of increasing the level of core simulation detail and of having a maximum value to be compared with design reactor limits (e.g. clad temperature, fuel temperature, etc.). All the other sub-assemblies are supposed to have an average power, thus they are modelled by an equivalent PIPE, in which the flow area is the equal to 170 sub-assemblies and in which proper hydraulic diameter (i.e. attaining to a single sub-assembly) is imposed.

Additional flow paths are considered to model the gap among the FA, among the dummy elements and the annular zone between the reactor and the safety vessel. The core exit is modelled again by means of two PIPEs (separated per each core zone), merged in a BRANCH which finally simulates the pump suction region (Upper Plenum).

The primary pumps are simulated by corresponding PUMP component. Being the design of ALFRED pumps not finalized [3], homologous curves adopted in the deck are taken from ELSY reactor [9]. Free level above the core exit is included too. Primary pressure is fixed by a TMDPVOL placed at the top of the Argon region.

The SG primary side shell is modelled by a single equivalent PIPE.

The SG secondary sides are modelled by a kind of “U” flow path, reproducing the bayonet configuration, in which water descending and water/steam ascending sides are considered. Feedwater is supplied by a TMDPJUN, while exiting steam pressure is fixed by a TMDPVOL. Nominal conditions are imposed in both components at steady state conditions. Neither steam lines nor isolation valves are included in the nodalization.

Figure 1-7 shows the sketch of the nodalization, only two over eight flow paths are represented. Different free levels are highlighted (blue colour is associated with the presence of lead, white colour is associated with the presence of Argon) as well as the two pipes (sub-assembly maximum power and all other sub-assemblies) forming the core (red boxes). On the secondary side the light orange identifies water flow path, rather the dark orange identifies the water/steam flow path.

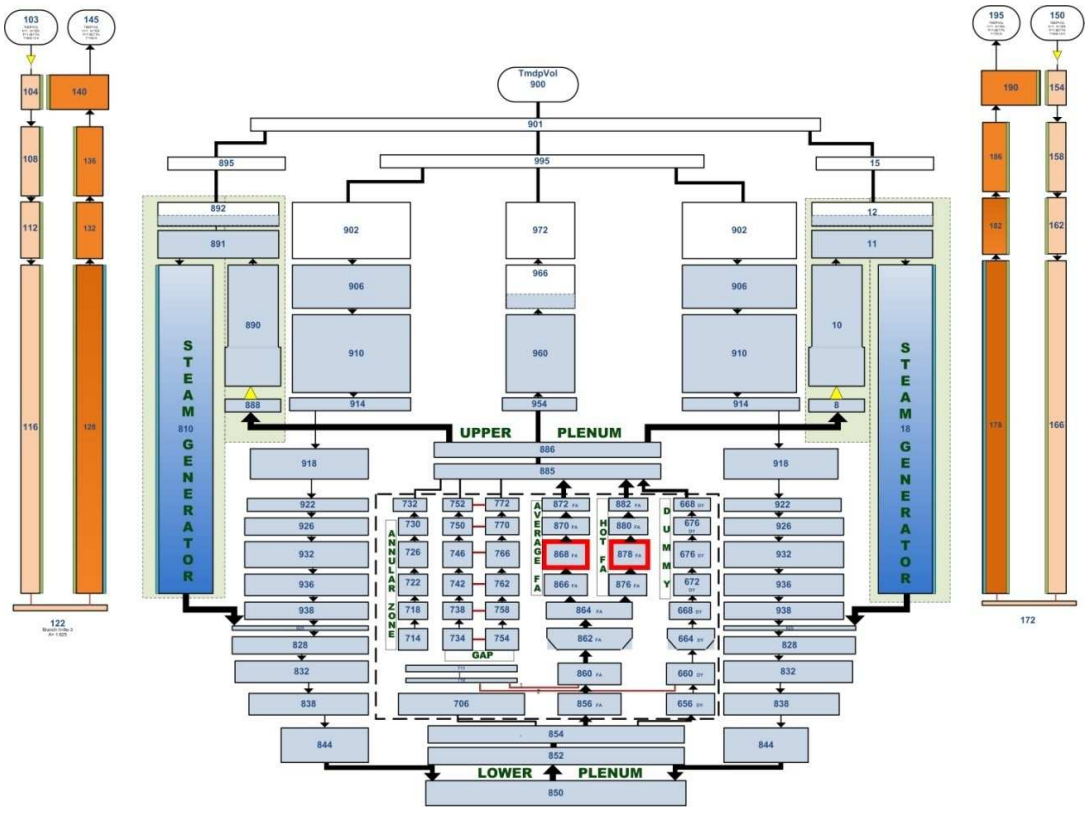


Figure 1-7: Sketch of ALFRED RELAP5 nodalization

3.2.2 Heat structures

Both active (where heat generation is simulated) and passive (where heat is not generated) heat structures are included in the input deck in order to simulate appropriate behaviour of ALFRED reactor.

Active heat structures are used to simulate the core, average FA, maximum power FA and maximum power pin (hot pin). Different power among the three core zones are accounted for by imposing corresponding power level. Peaking factors are also entered to simulate an axial power profile according to the design specification [3]. Another active heat structure is associated with the dummy elements to simulate the power generated in these elements. According to the above, the total reactor power of 300 MWth is split into two parts: 96.76 % into the core structures and 3.24 % into the dummy elements [3].

Figure 1-8 shows the linear power trend along the active length for the hot FA, the average FA and the hot pin respectively. It can be seen that the maximum linear power of 350 W/cm is reached by the hot pin slightly above the middle length; this is consistent with the maximum value foreseen in the core design [3].

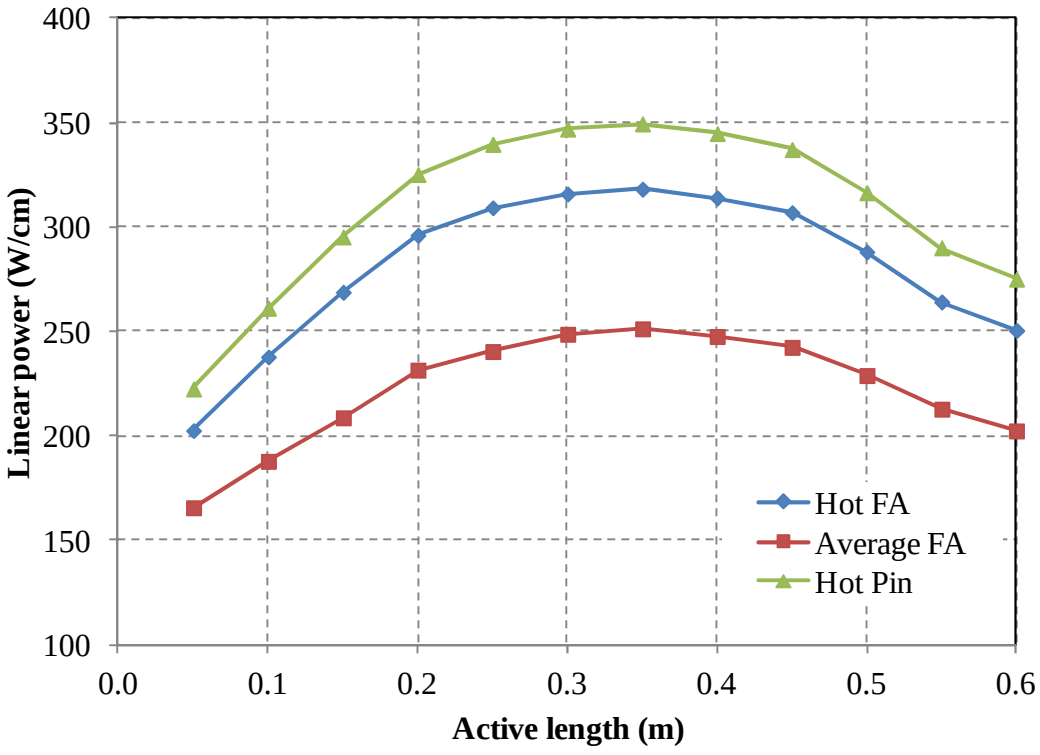


Figure 1-8: Linear power distribution along the core active length

Passive heat structures are adopted to model the heat exchanged through the SG tubes, both to the lead side and to the feedwater side.
The heat transfer between the lead flowing within the FA gap, the main lead descending flow path, and the FA boxes is taken into account by simulating the corresponding metal parts, preserving heat transfer area and total metal mass.
Concerning the SGs heat structures, a layer of insulating paint (0.05 W/(m°C)) has been introduced to reduce heat transfer between the steam generated in the outer rising annular tube and water flowing downwards in the inner descending tube (to avoid steam condensation). Exchanged power occurs between descending primary side lead and secondary water/steam, through an appropriate heat structure which includes the high conductance (corresponding to 55 times the helium thermal conductivity) powder gap foreseen in the bayonet tube design. Power is exchanged along 6 m, not considering heat transfer above SG tubes active length.
The Ushakov correlation [10] implemented in RELAP5, has been used to evaluate the lead convective heat transfer coefficient for both FAs and SGs.

3.2.3 Neutron Kinetics

The power generation is simulated by the adoption of the 0D neutron kinetic model embedded in RELAP5 code. Such a model is based on the assumption that the entire core can be "concentrated" in its centre (single point), thus inherent limitation regards the simulation of core with large diameter (in which decoupled regions can be found, e.g. in Boiling Water Reactor) or those accidents not involving the whole core (e.g. control rod ejection). In the present context the 0D approximation can be accepted (at least this is a good starting point) being the ULOF and the single PP trip affecting the whole core. In the 0D implemented model, reactivity feedbacks contributions are included too. The following reactivity feedbacks are taken into account:

- doppler;
- lead expansion;
- axial and radial clad expansion;
- axial and radial wrapper tube expansion;
- diagrid expansion;

- pad expansion;
- axial fuel expansion: free;
- control rod expansion (prompt and delayed response).

The coefficient associated to each parameter listed above is reported in Table 1-3 [3], values are provided for beginning and end of cycle (BOC and EOC respectively).

Feedback	Unit	BOC	EOC
CR and SR differential expansion – prompt response	pcm/K	-0.455	-0.218
CR and SR differential expansion – delayed response	pcm/K	-0.442	-0.211
Lead expansion coefficient*	pcm/K	-0.271	-0.268
Axial clad expansion	pcm/K	0.037	0.039
Axial wrapper tube expansion	pcm/K	0.022	0.023
Radial clad expansion	pcm/K	0.008	0.011
Radial wrapper tube expansion	pcm/K	0.002	0.003
Diagrid expansion ($T_{outlet} > T_c$) **	pcm/K	-0.147	-0.152
Diagrid expansion ($T_{outlet} < T_c$) **	pcm/K	-0.519	-0.430
Pad expansion ($T_{outlet} > T_c$) **	pcm/K	-0.415	-0.430
Pad expansion ($T_{outlet} < T_c$) **	pcm/K	0	0
Axial fuel expansion: free	pcm/K	-0.148	-0.155
Axial fuel expansion: linked	pcm/K	-0.232	-0.242
Doppler constant	pcm	-555	-566
Iron part of the Doppler constant	pcm	-74	-66
Fissile part of the Doppler constant	pcm	-481	-500

**: calculated on the whole height of the fissile sub-assemblies (the other feedbacks are calculated only in the fissile zone)*
***: the critical temperature for pads to enter in contact is* $T_c = 480 + 0.6552 * (T_{inlet} - 400)$ [°C].

Table 1-3: Reactivity feedbacks

The evaluation of the feedback is implemented in the deck by defining tables and control variables. The tables include the reactivity feedback values based on the reactivity coefficient rate, as per Table 1-3. The control variables compute the average quantities that are the table search variables. The average is (if needed) realized by weighting factors (W_i) based on the ratio P_i^2/V_i where P_i is the power produced in a cell i-th and V_i is the volume of the cell i-th. The weighting factors are normalized according to the formula:

$$W_i = P_i^2/V_i / \sum_i (P_i^2/V_i)$$

Such a normalization yields to:

$$\sum_i W_i = 1$$

4 ALFRED reactor simulations

After the description of the computational tools adopted in the present context, their application is presented hereafter.

Before starting any kind of transient simulation it should be proved that a developed reactor model is capable to correctly reproduce nominal plant conditions. The demonstration of this capability is provided in the section devoted to steady state analysis.

Two accidents are then simulated adopting RELAP5 code: ULOF and single PP trip. ULOF is simulated considering the EOC core status, rather single PP trip is simulated considering both EOC and BOC core status. The core status distinction affects the reactivity feedbacks, namely their change rate. In all the three mentioned cases Scram does not occur, hence the power change is due to the reactivity feedbacks.

4.1 Steady state conditions

The present section deals with the demonstration of the capability of the ALFRED nodalization in replicating nominal plant conditions. Three thousand seconds of a ‘null’ transient calculation is run to ensure stabilization of parameters (both of primary and secondary side) like fluid temperature, active and passive heat structures temperature distribution, mass flow rate within different reactor flow paths, etc.

A comparison between design and computed value of selected steady state quantities is provided in Table 1-4 (design data are taken from [3]). It can be seen that RELAP5 simulation results are fairly good in respect to design values; major discrepancies (around 3%) can be observed in the reactor mass flow rate. A bit less mass flow has to be set to obtain the nominal ΔT across the core. This discrepancy might be caused by the imperfection affecting the heat transfer correlation implemented in RELAP5.

Parameter	Unit	Design value	R5 result	Note
Primary side				
Nominal reactor core power	MW	300	300	Thermal power
Power removed by SG	MW	300	300	37.5 MW per each SG
Lead core inlet temperature	°C	400	400.2	
Lead core outlet temperature	°C	480	480.4	Average value
Total mass flow rate	kg/s	25980	25172	3146.5 kg/s per each pump
Secondary side				
Secondary side pressure	MPa	18	18	Steam dome
Feed water temperature	°C	335	335	
Steam outlet temperature	°C	450	451	
FW mass flow rate	kg/s	24.1	24.1	

Table 1-4: ALFRED reactor, selected steady state parameters and comparison with computed values

The following figures show the steady state simulation to demonstrate the achievement of stable nominal conditions.

Figure 1-9 shows the power balance between the core and the cooling power; apart initial oscillations, the two curves are practically overlapped demonstrating a good power balance simulated by the code. To calculate the power balance both wall to fluid (occurring in the core) and fluid to fluid (occurring in the SGs) heat transfer modalities are considered, showing the RELAP5 capabilities in dealing with both modalities fairly well also when lead is involved as primary fluid.

In Figure 1-10 the total mass flow rate is reported, as explained above, steady state value is a little bit lower than the reference one.

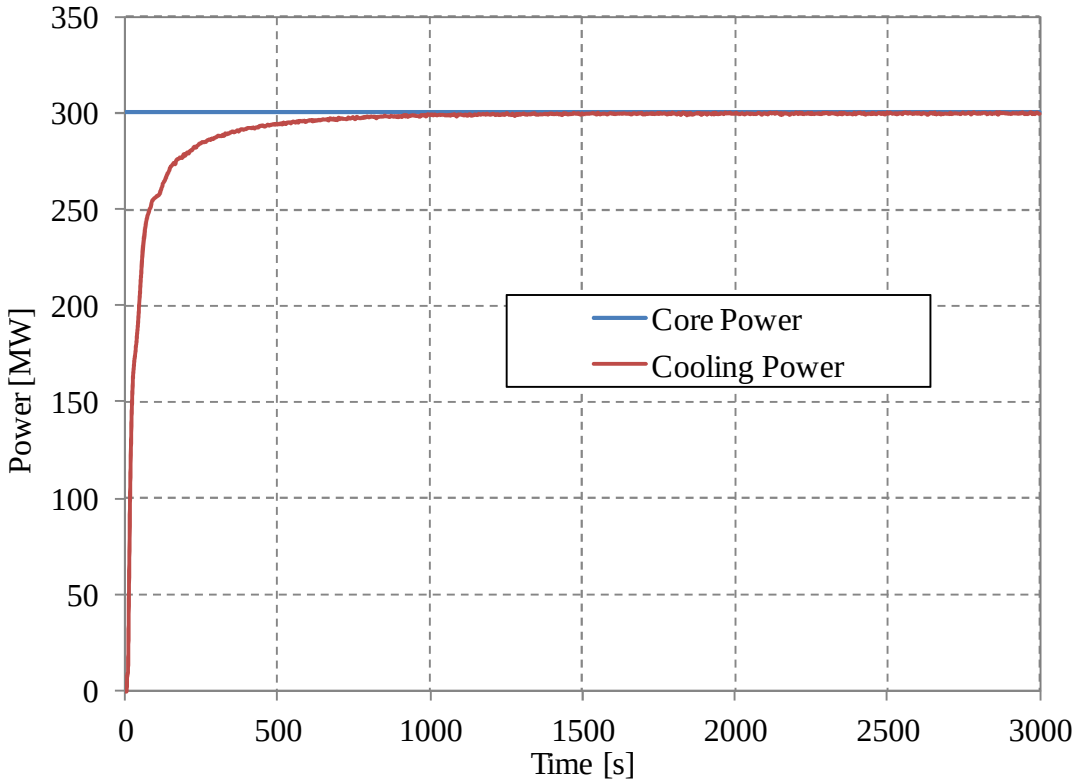


Figure 1-9: ALFRED steady state conditions, core power and total cooling power

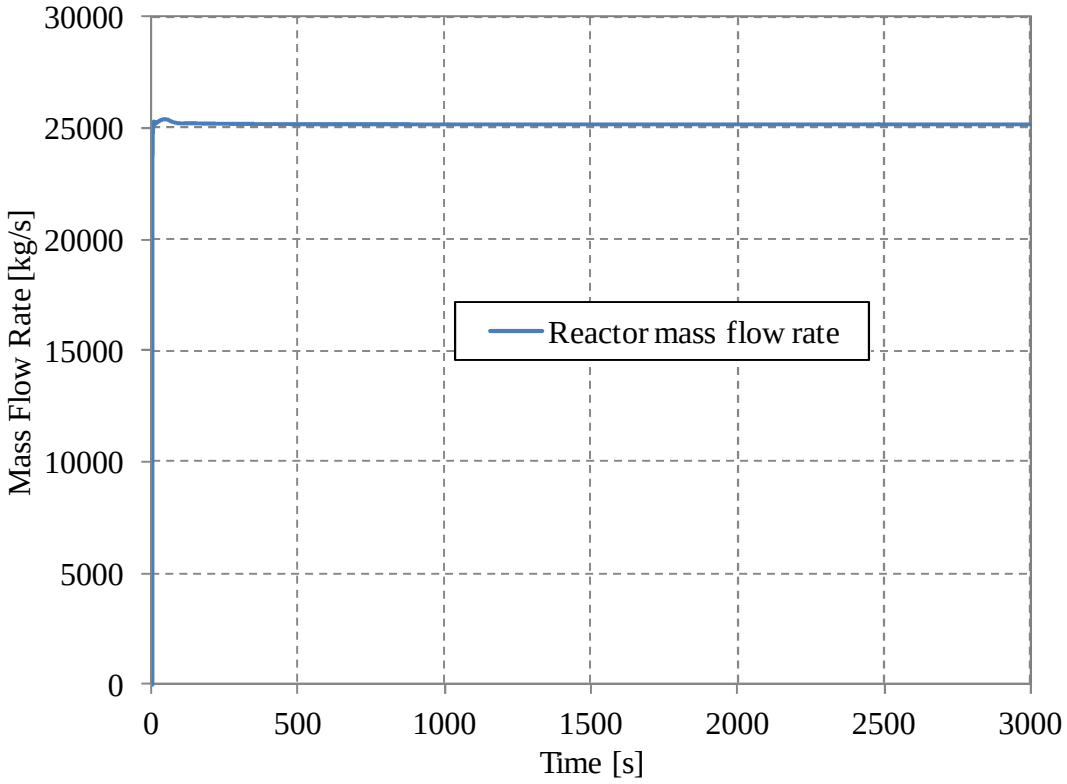


Figure 1-10: ALFRED steady state conditions, reactor mass flow rate

Figure 1-11 shows the lead temperature distribution along the active length of the core. Two curves are included reflecting data for the average and maximum FA power respectively. Inlet temperature value is equal for both curves, then due to the different peaking factors (reflecting the different axial power distribution) the one corresponding to the maximum FA power is always greater than the average FA power trend. Lead exiting temperature shows also a difference of about 20°C between the two flow paths. Such differences justify the modelling of the two parallel channels (reproducing the average and the maximum FA power respectively) as approach followed in the nodalization.

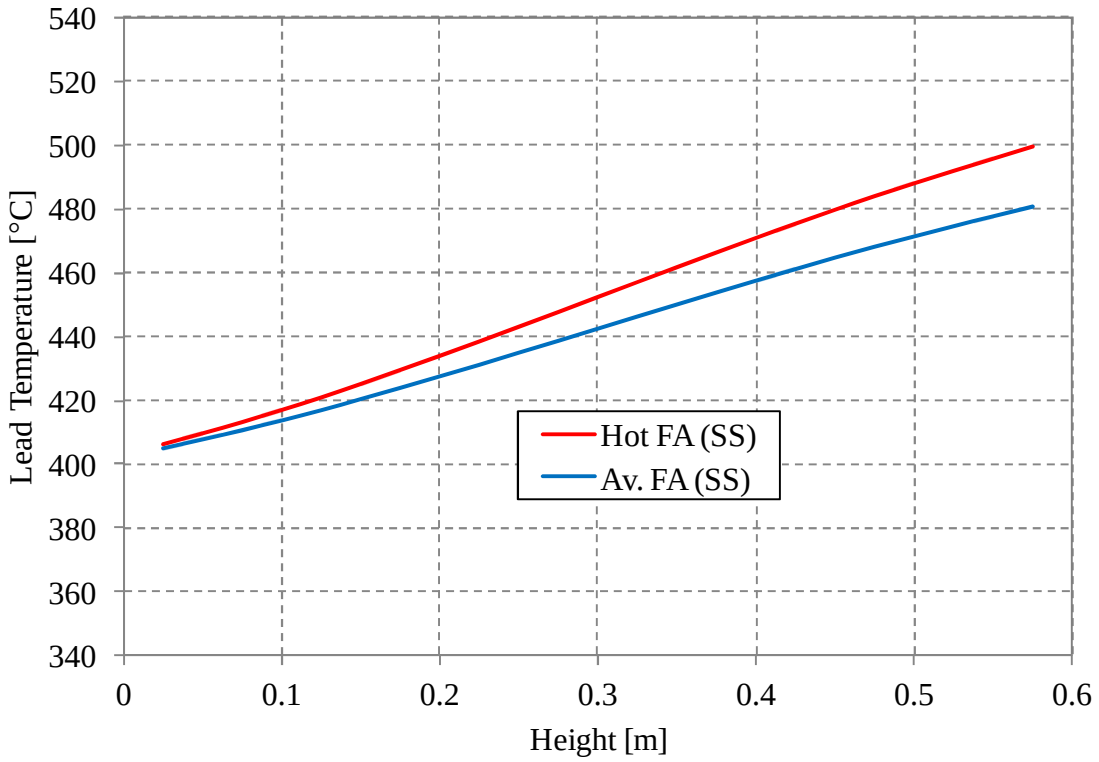


Figure 1-11: ALFRED steady state conditions, lead temperature distribution along the core, average and maximum FA power

To illustrate the thermal performance of the SG, Figure 1-12 shows SG1 primary and secondary temperature trends along the tube length. Lead enters the SGs at 480°C (inlet conditions are equal to the upper core region in which a mixing of the lead coming from all FAs occurs) and exits at 400°C. From the secondary side point of view, the water is heated up

to its saturation (saturated liquid at about 1 m), then its enthalpy increases together with the void fraction up to 3.2 m when saturated steam conditions are met. Continuing the heat exchange, the steam becomes superheated exiting at a temperature of 450°C.

In Figure 1-13 the thermodynamic equilibrium quality trend along the SG1 tube length is provided. It is clearly visible when liquid and steam saturated conditions are met (at about 0.75 and 3.0 m, from tubes inlet respectively). At the first condition the quality reaches 0, at the second it reaches 1.0.

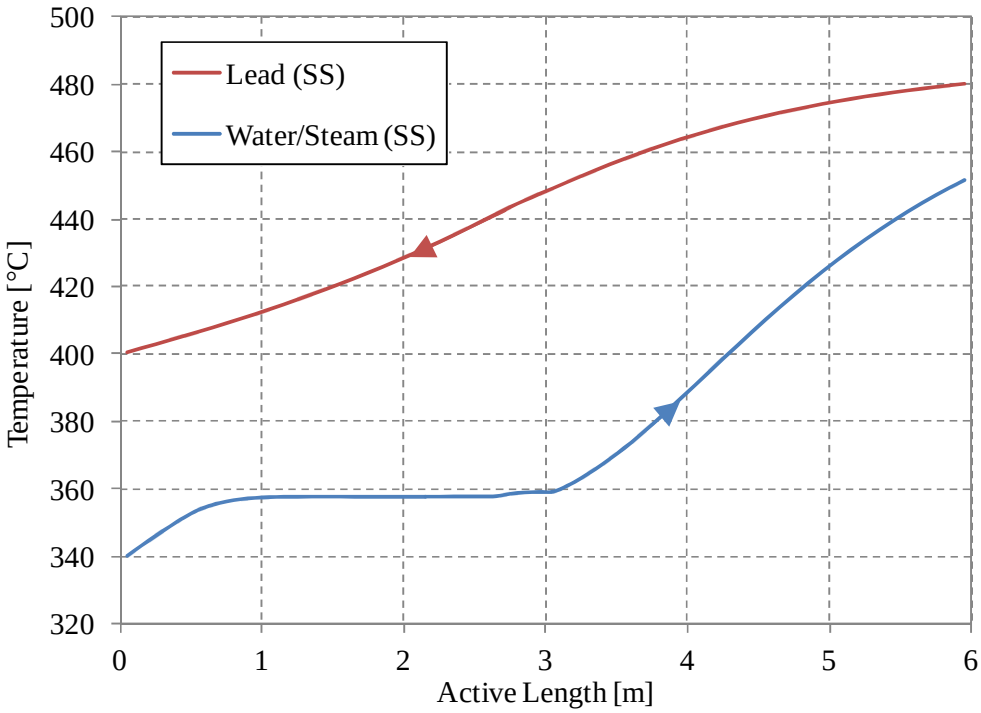


Figure 1-12: ALFRED steady state conditions, SG1 primary and secondary side temperature distribution along the tubes

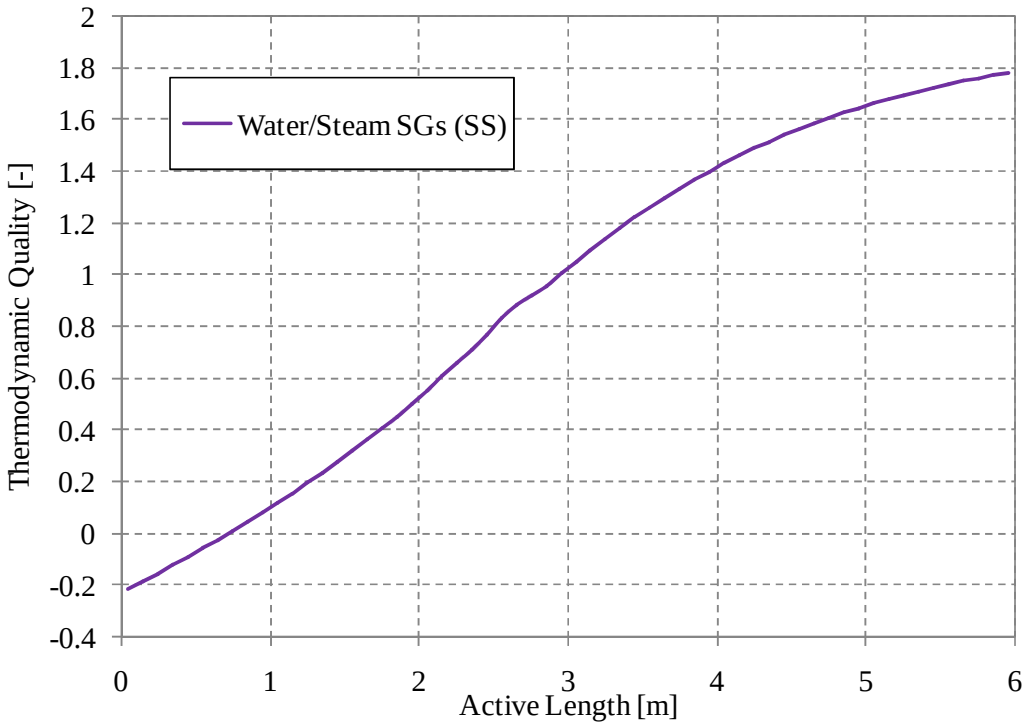


Figure 1-13: ALFRED steady state conditions, SG1 quality profile along the tubes

4.2 Unprotected Loss of Flow Transient

The present scenario aimed at testing the capability of the developed nodalization in reproducing ALFRED behaviour under natural circulation conditions. The postulated accident foresees simultaneous trip of all primary pumps, beside no scram is actuated. Core power time trend is thus driven by reactivity feedbacks only.

As mentioned in the nodalization description section, the eight PP are modelled by eight PUMP components. Hence to simulate natural circulation behaviour they are tripped simultaneously.

Regarding secondary side boundary conditions no modification in respect to nominal values is imposed (e.g. FW mass flow rate, secondary side pressure).

Core status is assumed to be at End of Cycle.

The numerical simulation ranges up to 1000 s, enough time interval to demonstrate that the reactor can withstand such a challenging transient and to obtain a new (quasi-) steady condition.

Table 1-5 and Table 1-6 provide the imposed events and the resulting sequence of events respectively. It is worth to note that the end of forced circulation occurs after 10 s from the

start of the transient, this value is consistent with other RELAP5 nodalization in which the ALFRED pumps are simulated by PUMP components, [9].

Event	Time of occurrence	Value	Note
All PP trip	0 s	-	Start of simulation of pumps coast down – initiating event
SCRAM	-	-	Unprotected accident
FW mass flow rate (per each SG)	-	24.1 kg/s	Kept as in nominal condition

Table 1-5: ALFRED ULOF accident, imposed events

Event	Time of occurrence	Value	Note
PP halved mass flow rate	>1 s	-	-
Minimum power level	20 s	170 MW	Power decrease due to neutron feedbacks
Minimum reactor mass flow rate	7 s	4025 kg/s	Approx. 1/6 of the nominal value
Maximum clad temperature	9 s	828°C	Predicted in the hot pin
Maximum fuel temperature	0 s	-	Fuel temperature decreases along the transient
Maximum core outlet lead temperature	9 s	802°C	Max power FA
Maximum difference between core and cooling power	4 s	67.7 MW	Core power > cooling power

Table 1-6: ALFRED ULOF accident, resulting sequence of events

The transient starts with the simultaneous coast down of all primary pumps. This causes a fast drop of the reactor mass flow rate (see Figure 1-14) down to about 4000 kg/s. Once the natural circulation conditions are established, the reactor mass flow rate stabilizes around a value of 6100 kg/s.

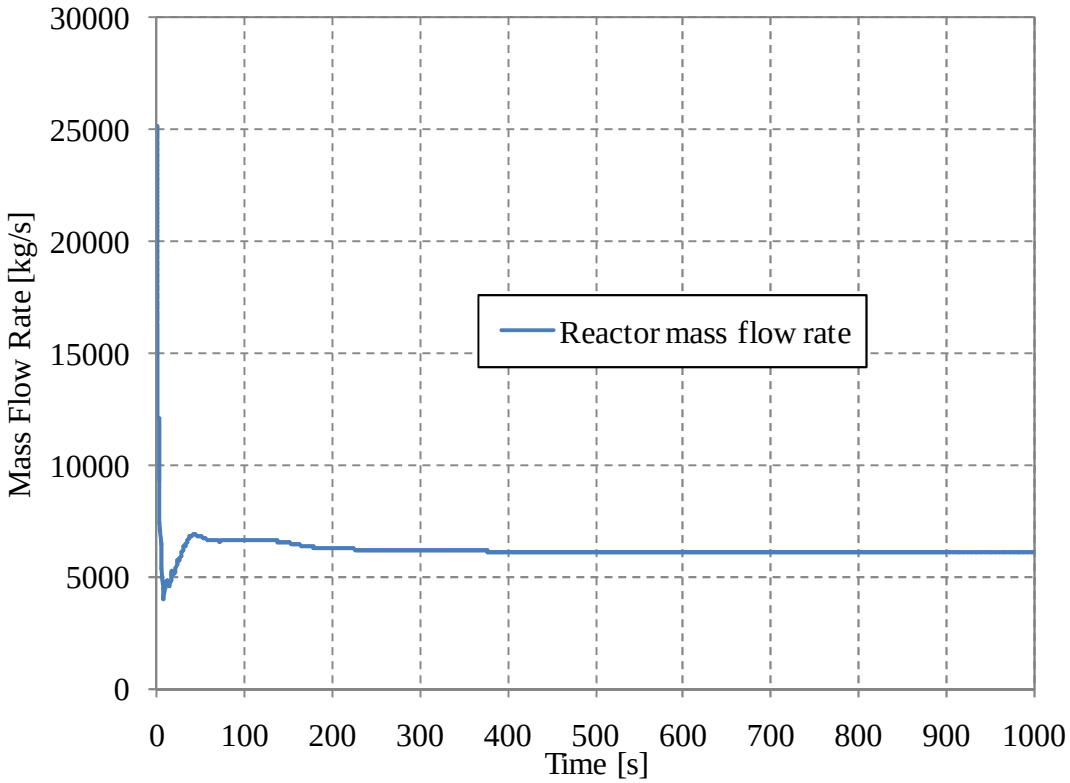


Figure 1-14: ALFRED ULOF accident, reactor mass flow rate

The core power, driven by neutron feedbacks only, experiences a drop down to about 170 MW, further it stabilizes at a level close to 225 MW, as shown in Figure 1-15. The same figure reports also the total power exchanged by all SGs (cooling power). The first drop is caused by the immediate and drastic primary mass flow rate reduction, a slow oscillatory trend of the parameter is predicted till 400 s in the transient. Oscillations are caused by the transition between forced circulation and natural circulation establishing in the reactor.

Moreover, an extra cooling is computed by the code, since that cooling power is greater than that generated in the core in the time interval 50–350 s (this is reflected in the lead temperature distribution). Further on the core power is completely transferred by the SG reaching a new steady state condition.

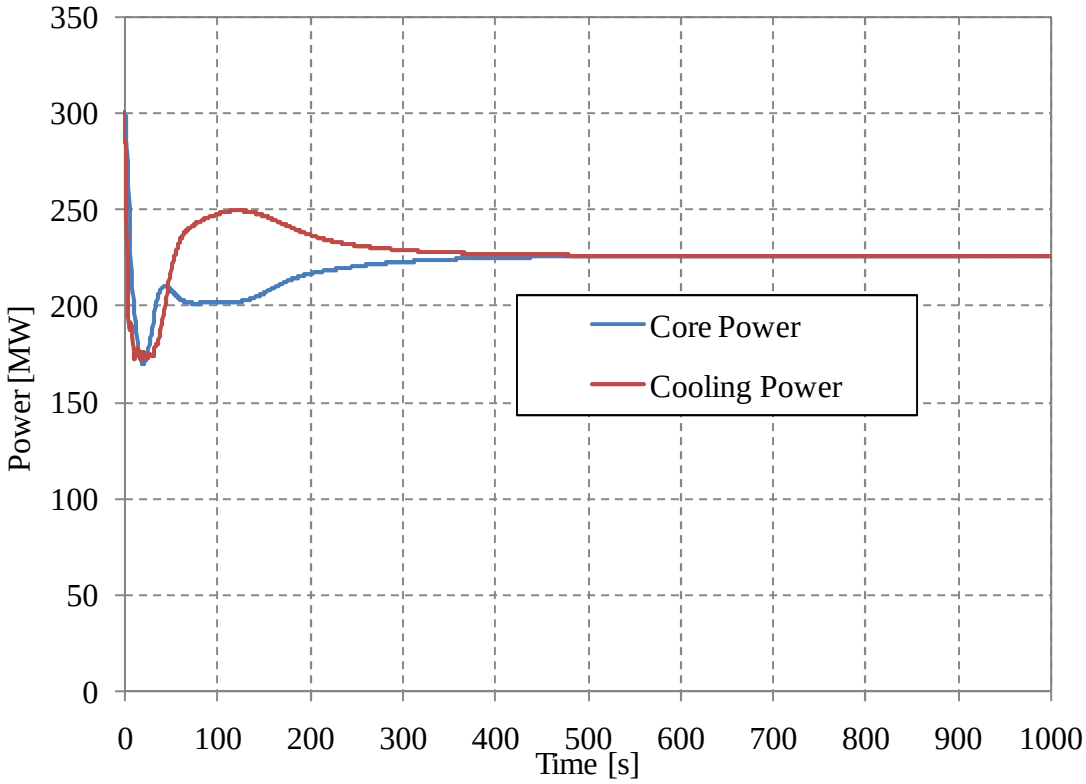


Figure 1-15: ALFRED ULOF accident, Core and total cooling power

Figure 1-16 and Figure 1-17 show all the considered contributions to the reactivity. Among the others major feedbacks can be recognized: Doppler effect which inserts a positive contribution up to about 110 pcm; pad and control rod expansion which on contrary contributes for a negative value whose minimum is about -75 pcm. The total core reactivity rapidly decreases down to -80 pcm in the first 10 s, then Doppler feedback starts to give its contribution (because of decreasing in fuel temperature due to lower power level) and the total reactivity consequently increases. At the end of the simulation (i.e. 1000 s) the total reactivity is equal to 0.0 pcm establishing new reactor conditions.

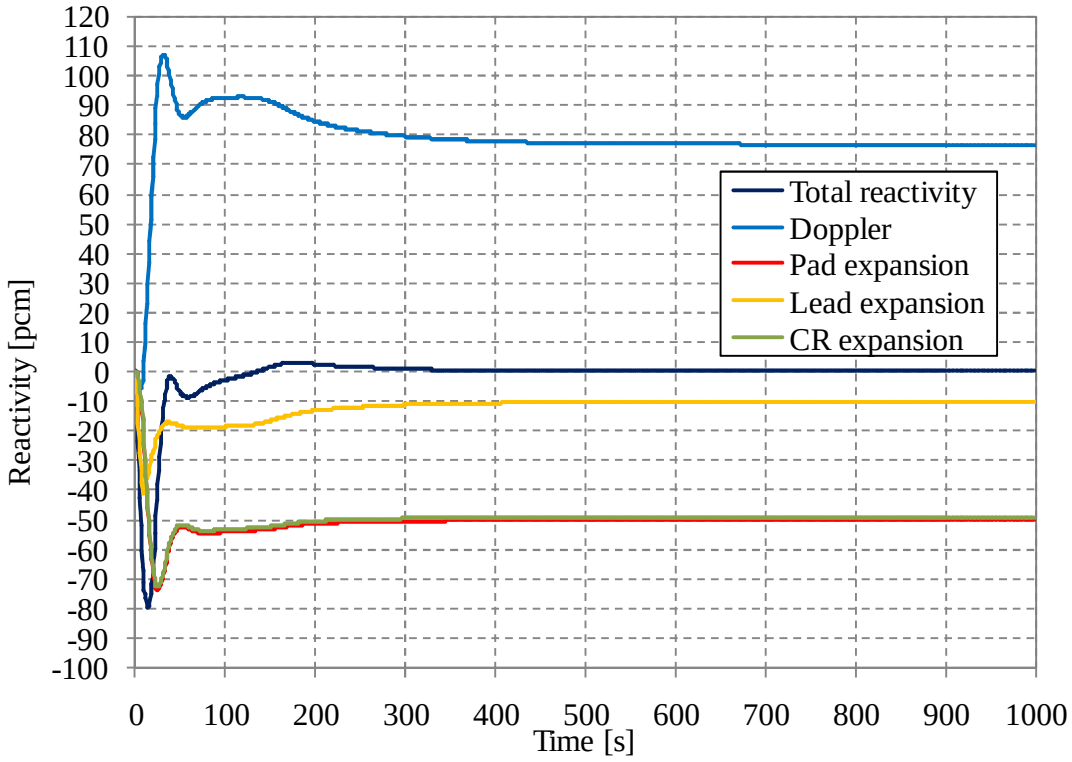


Figure 1-16: ALFRED ULOF accident, neutron kinetic feedbacks larger contributions to total reactivity

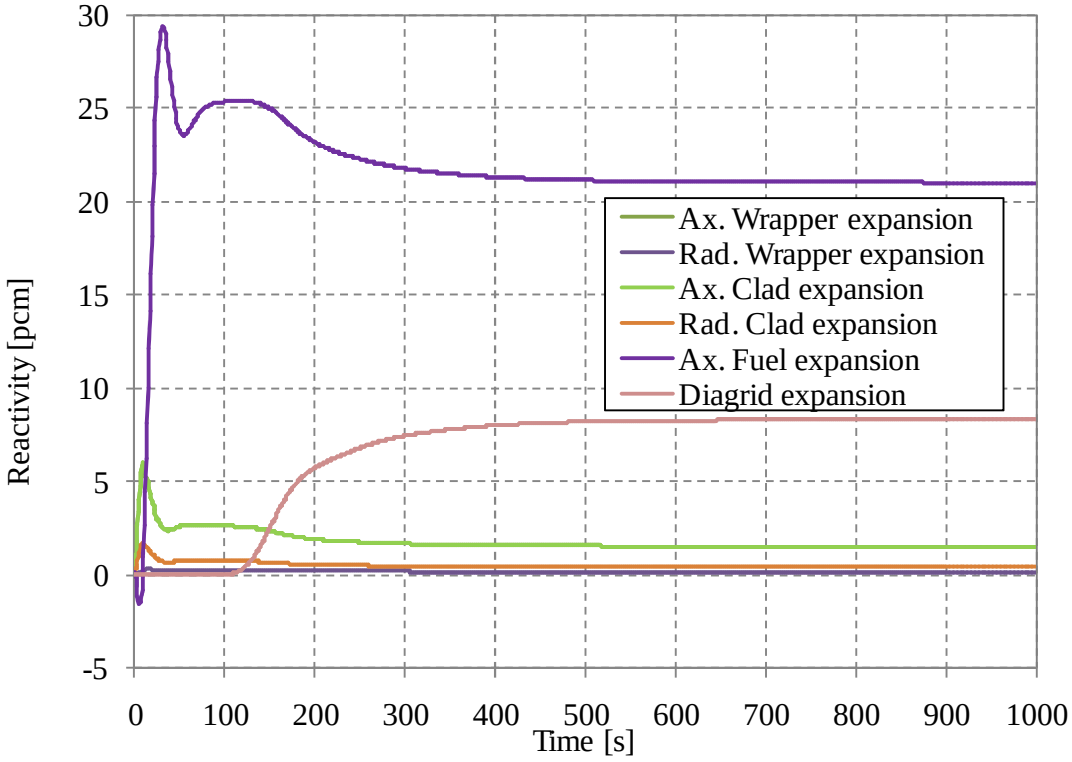


Figure 1-17: ALFRED ULOF accident, neutron kinetic feedbacks smaller contributions to total reactivity

Primary fluid temperature behaviour is shown in Figure 1-18. A steep increase of core exit temperature is due to the fast mass flow rate decrease. In the mean time core inlet temperature stays close to its nominal value (400°C), still feed by the lead nominally cooled by the SGs. Going on in the transient, inlet temperature decreases (because of extra cooling by SGs as discussed above) and a much larger (than in nominal conditions) core ΔT is established (350°C and 597°C inlet and outlet temperature respectively in the FA with average power). It should be noted that the margin from solidification threshold is sensibly reduced. Clad temperature basically follows the same trend of the lead (see Figure 1-19). A maximum value of 828°C is reached in the hot pin at 9 s.

As described above, core power decreases due to the initial negative reactivity balance. As a consequence fuel temperature decreases too, Figure 1-20. At the end of the simulation a lower (than steady state conditions) temperature is reached. A decrease of about 260°C in respect to the nominal steady state condition is computed for the FA with average power, maximum power and for the hot pin.

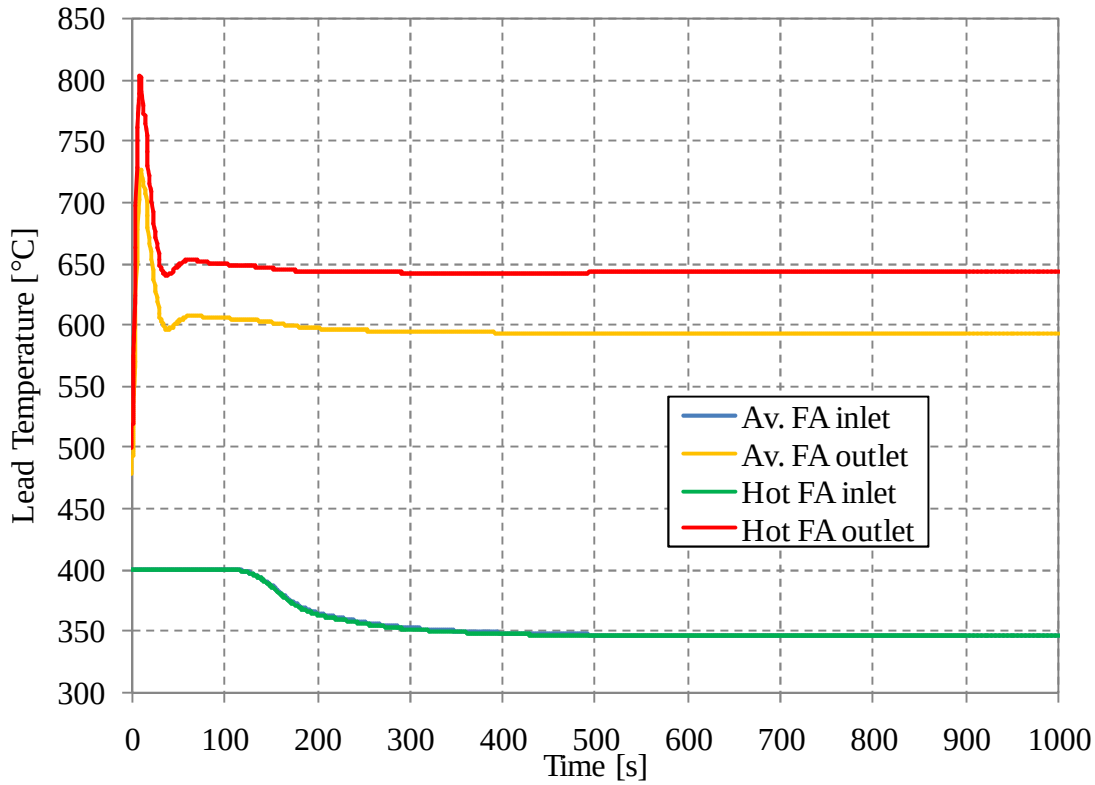


Figure 1-18: ALFRED ULOF accident, lead inlet and outlet temperature in average FA and max power FA

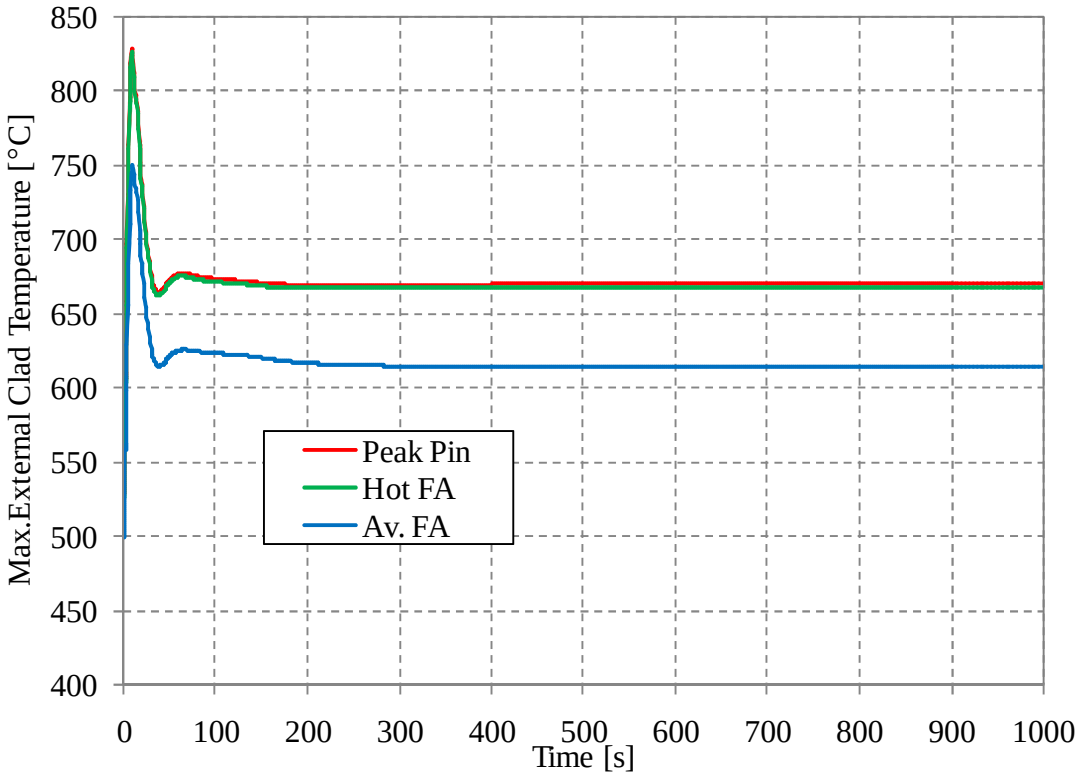


Figure 1-19: ALFRED ULOF accident, clad temperature in average FA, max power FA and peak pin

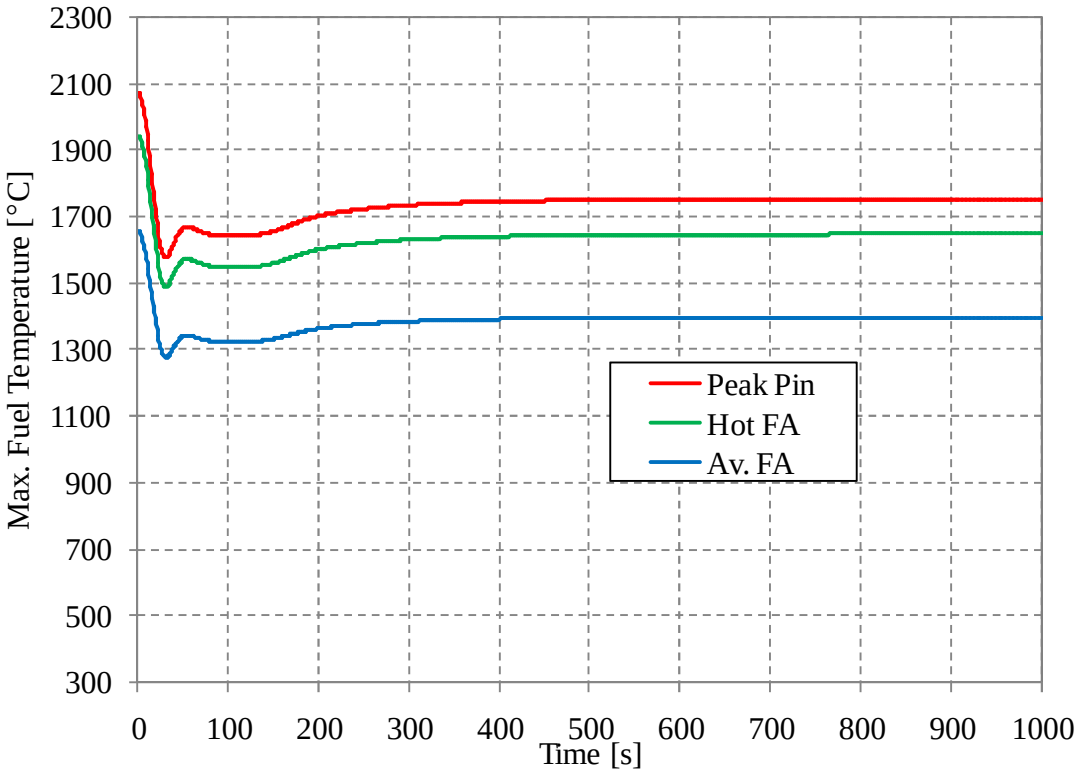


Figure 1-20: ALFRED ULOF accident, fuel temperature in average FA, max power FA and peak pin

Figure 1-21 reports the comparison between ULOF (at a time instant corresponding to the end of the simulation) and steady state conditions of the lead temperature profile along the active core length. It can be immediately noted the larger temperature jump across the core (from 80 to about 250°C) because natural circulation conditions are established at the considered time and core power is still at high value (as per hypothesis of the unprotected scenario). Beside, it increases also the difference at the core outlet between the average and maximum power FA (from about 20 to about 50°C).

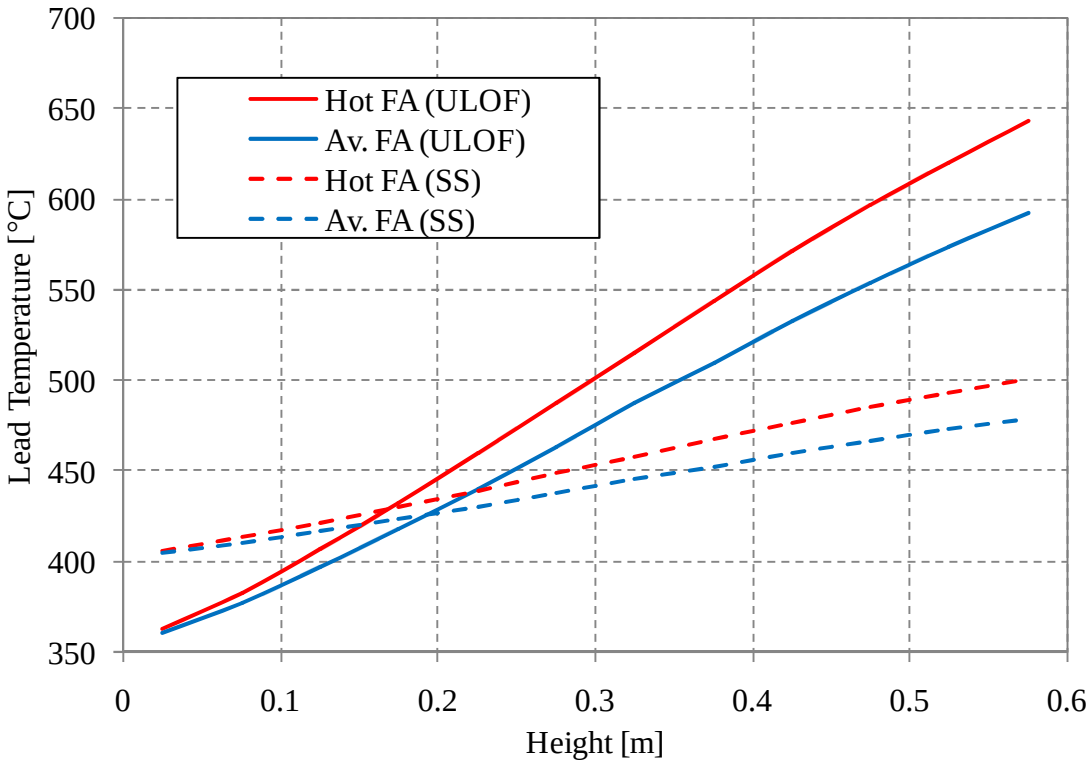


Figure 1-21: ALFRED ULOF accident, Axial temperature profile along the core active length and comparison with steady state conditions

Secondary side parameters are quite perturbed too. Due to the less power generated in the core and hence transferred by the primary side to the water flowing into the SG tubes, steam exit temperature is lower than nominal conditions, stabilizing at around 380°C. However, superheated steam (T_{sat}(180 bar) = 357°C)is still produced by the SGs (with the assumption that secondary pressure is not affected by the ULOF occurrence) as highlighted in Figure 1-22, which shows secondary side SGs inlet temperature and outlet temperature (active tube outlet and steam plenum).

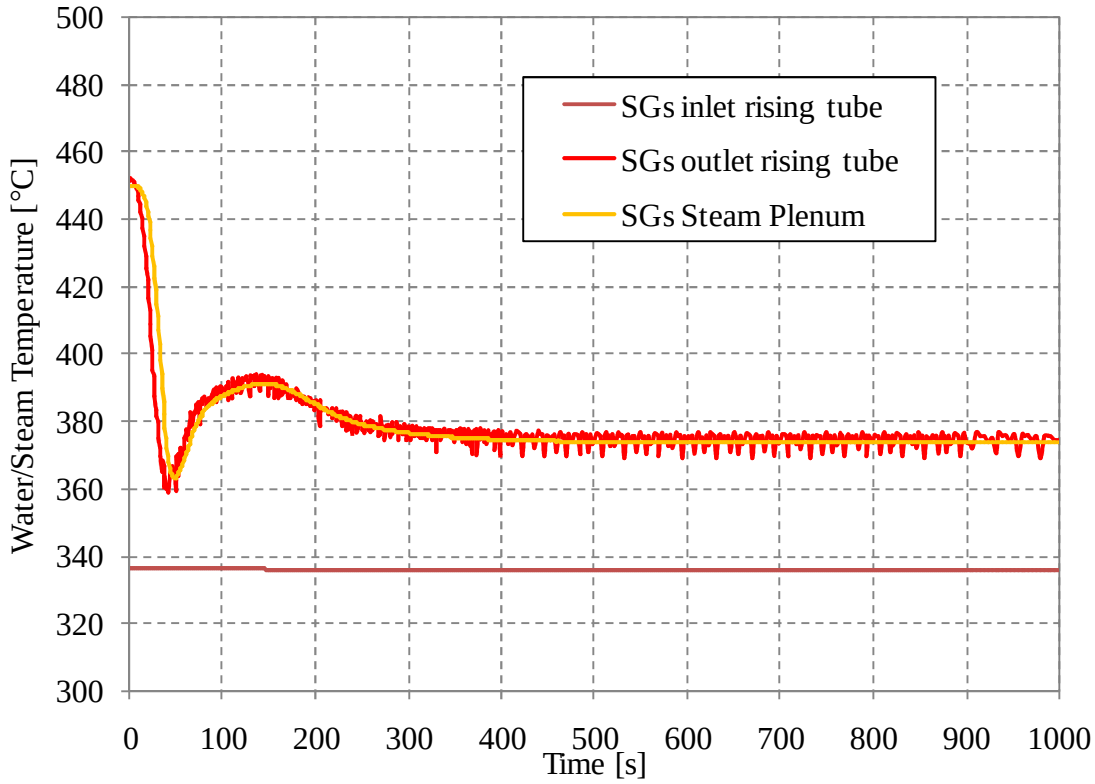


Figure 1-22: ALFRED ULOF accident, SG secondary side inlet (water) and outlet (steam) temperature

The above considerations are also confirmed observing the primary and secondary temperature profile along the SG tubes. Figure 1-23 confirms the cooling capability of the SGs in dealing with so ample lead temperature variation (continuous line) in respect to the steady state value (dashed line). Superheated steam conditions are met close to the end of the SG tubes. This last sentence is confirmed by Figure 1-24, showing the thermodynamic quality profile along the SG tubes (continuous line). Again comparison with steady state trend (dashed line) is provided. In case of ULOF, saturation conditions are reached bit ahead of the middle of the tubes, rather superheated steam conditions are reached less than 0.2 m before the tubes exit. However, it should be noted that even with a very large differential temperature at the tube inlet, saturation conditions are reached much far, from the tubes inlet, than the SG operation conditions. This because, being the reactor in natural circulation conditions, the heat transfer is lower than in normal operation (i.e. forced circulation).

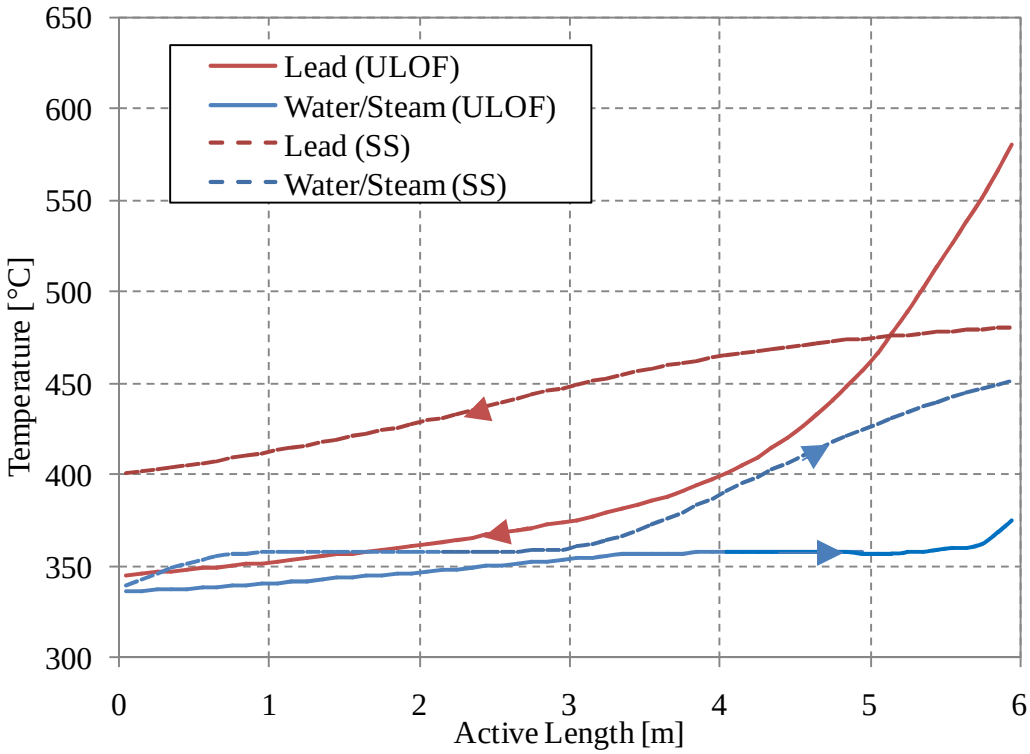


Figure 1-23: ALFRED ULOF accident, SG primary and secondary side temperature profile along the tubes length and comparison with steady state conditions

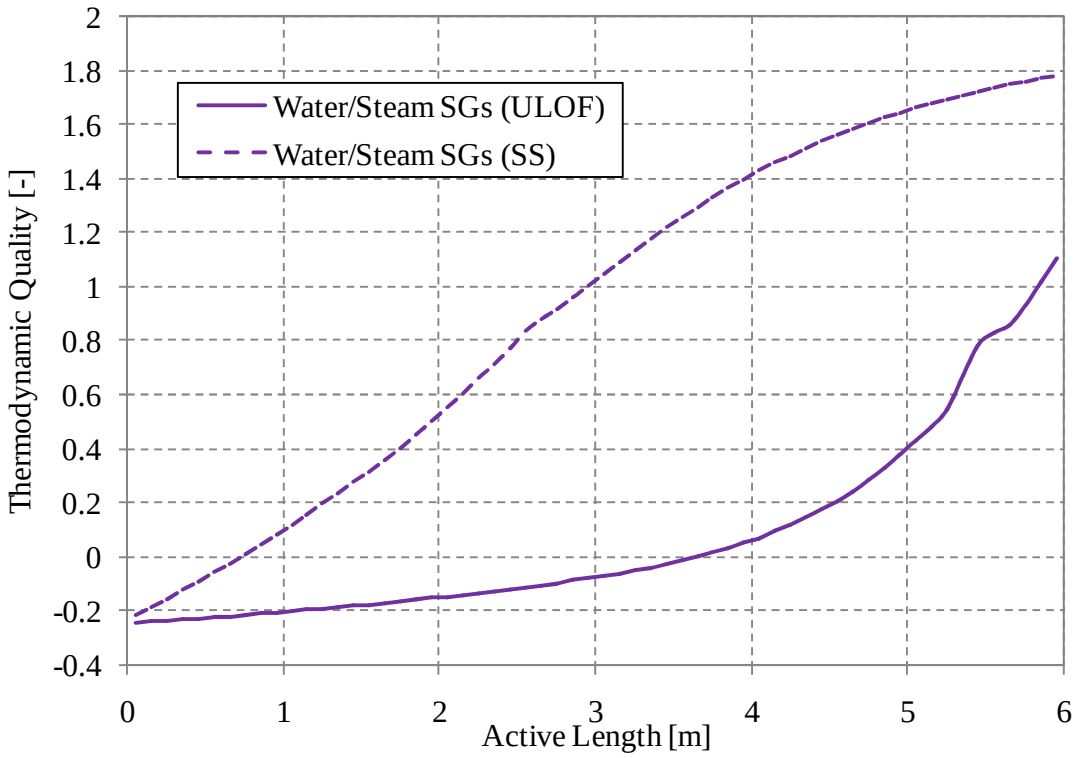


Figure 1-24: ALFRED ULOF accident, SG quality profile along the tubes length and comparison with steady state conditions

4.3 Single Primary Pump trip

As stated above, the Single Primary Pump trip has been simulated in two different core conditions, namely Beginning of Cycle (BOC) and End of Cycle (EOC). In both cases reverse flow in the affected loop is expected and no SCRAM is actuated. The two cases differentiate in the core neutronic response being the reactivity feedbacks slightly different as shown in Table 1-3.

4.3.1 Single Primary Pump trip simulation in EOC condition

The initiating event is simulated by starting the coast down of the pump in the flow path No. 1. Specific trip is set in the input deck to initiate the transient.

Core status is assumed to be at End of Cycle. The numerical simulation ranges up to 1000 s, enough time frame to demonstrate that the reactor can withstand such a transient.

Table 1-7 and Table 1-8 provide the imposed events and the resulting sequence of events respectively.

Event	Time of occurrence	Value	Note
PP1 trip	0s	-	Start of simulation of pump No. 1 coast down – initiating event
SCRAM	-	-	Not simulated
FW mass flow rate (per each SG)	-	24.1 kg/s	Kept as in nominal condition

Table 1-7: ALFRED Single PP Trip EOC accident, imposed events

As in the ULOF transient, the affected pump stops after 10 s from the accident occurrence. On the contrary the Single PP trip has a slower evolution than ULOF, as comes out from the resulting sequence of events (see Table 1-8). As an example, the maximum clad temperature is predicted at about 840 s, while the minimum core power is achieved toward the end of the transient.

Event	Time of occurrence	Value	Note
PP1 halved mass flow	>1 s	-	
Onset of flow reversal	1.2 s	-	In affected flow path
Maximum difference between core and cooling power	53 s	21 MW	Core power > cooling power
Minimum reactor mass flow rate	2 s	22580 kg/s	Approx. 93% of the nominal value
Maximum core outlet lead temperature	744 s	516°C	Max FA power
Maximum clad temperature	840 s	543°C	Predicted in the peak pin
Minimum core power	996 s	281 MW	Power decrease due to reactivity feedbacks
Maximum fuel temperature	0 s	-	Fuel temperature decreases along the transient

Table 1-8: ALFRED Single PP Trip EOC accident, resulting sequence of events

Following the postulated initiating event the mass flow rate in the affected flow path experiences a flow reversal, as high as 1000 kg/s (about 1/3 of its nominal mass flow rate), as indicated by Figure 1-25. It should be noted that such value predicted by the code is mainly affected by the adopted pump characteristics and by the pressure losses distributed along the flow paths. For the latter aspect, assumptions based on handbook, e.g. [11], shall be verified later on when the reactor will be in an advanced design stage and other (than system thermal-hydraulic code) computational tools might be involved.

The effect of a flow reversal is evident also in Figure 1-26 which shows the reactor mass flow rate. A steep decrease from nominal value down to about 23500 kg/s is predicted by the code. However, even though the reactor mass flow rate decreases down to the 93% of its nominal value, adequate cooling is ensured.

Notwithstanding the rapid variation occurring to the reactor mass flow rate, core power excursion is quite limited, although no CR or SR movement and related effect is accounted for. The overall swing in cooling power, is almost dumped in about 200 s with a minimum value of 272 MW. Indeed the core power shows a descending trend till about 850 s when the two curves are practically overlapped. From now on, a new equilibrium condition is reached because generated power is equal to the power transferred to the SGs, (see Figure 1-27) with a new power level of 281 MW.

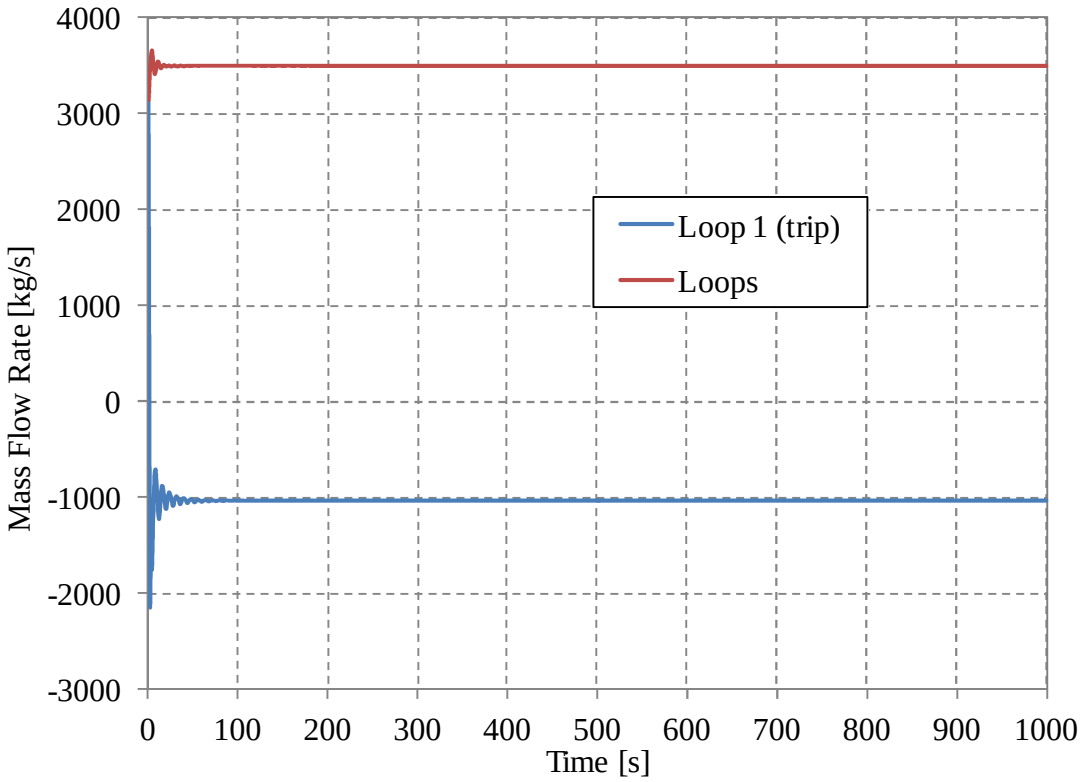


Figure 1-25: ALFRED Single PP Trip EOC accident, primary pumps mass flow rate

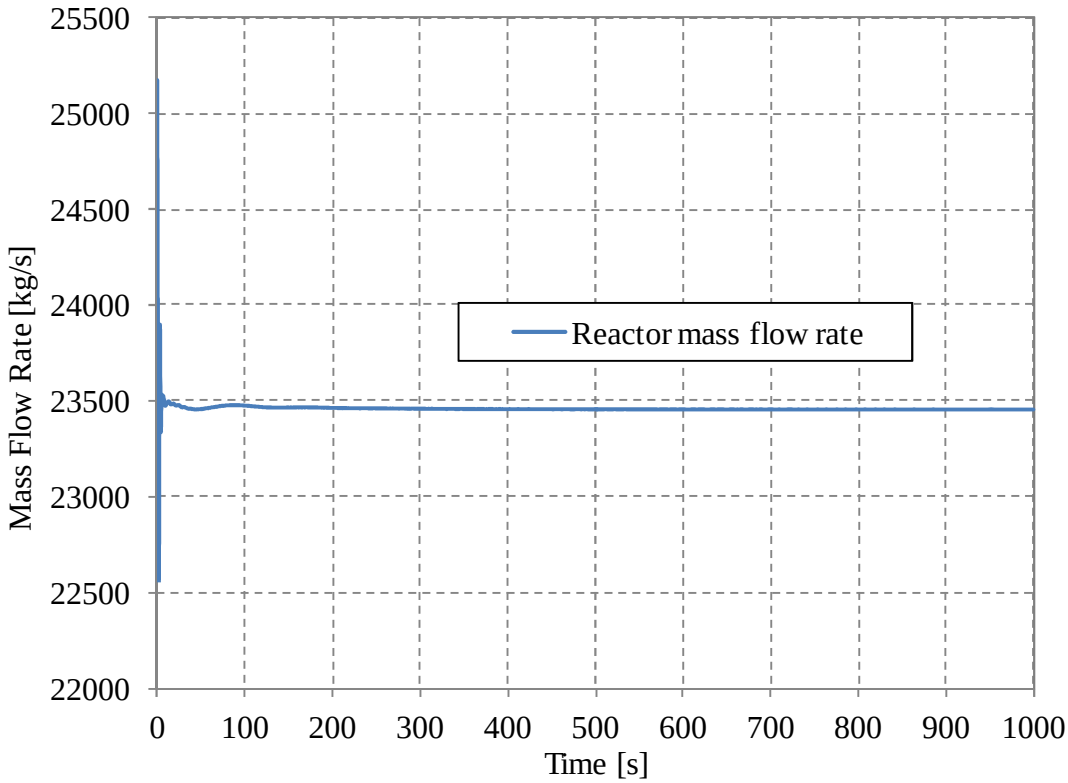


Figure 1-26: ALFRED Single PP Trip EOC accident, reactor mass flow rate

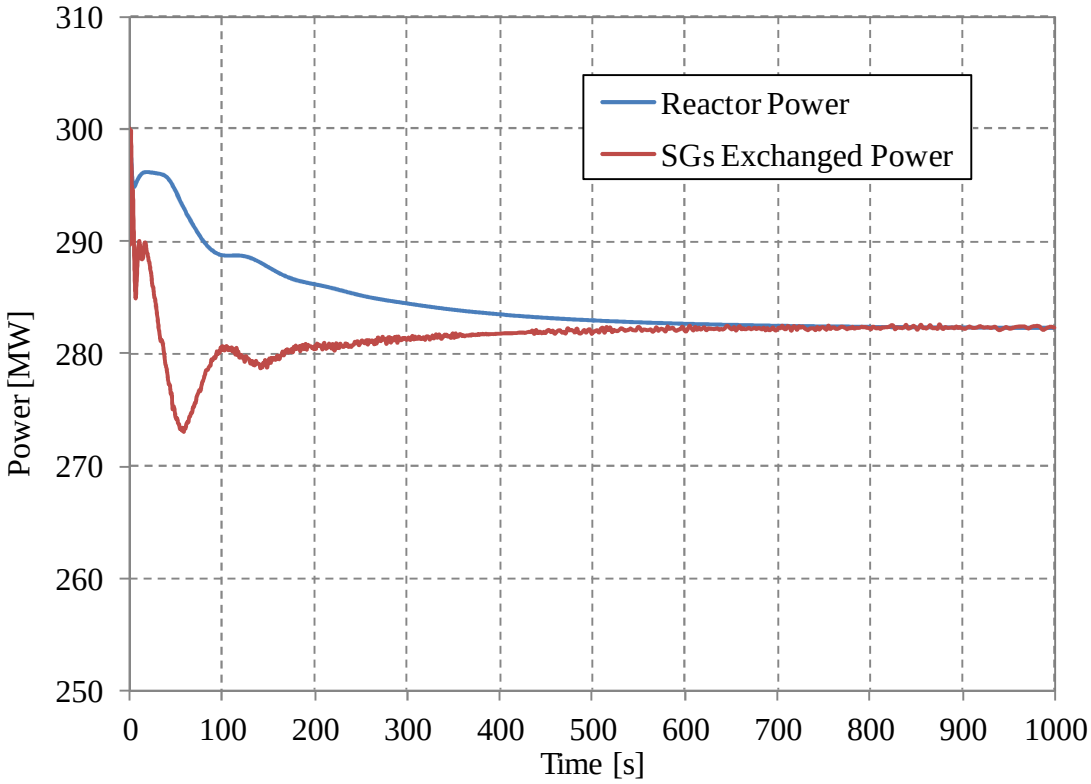


Figure 1-27: ALFRED Single PP Trip EOC accident, Core and total cooling power

The core power trend is driven by the reactivity feedbacks, whose contributions are shown in Figure 1-28 and Figure 1-29. Larger contributions come from Doppler, Pad expansion and CR/SR differential expansion (prompt and delayed response) feedbacks. Also in this concerned accident, their trend is opposite, namely positive contribution supplied by the Doppler (due to the reduction of fuel temperature caused by lower power level), negative by the Pad (due to the increase of its temperature caused by the increase of lead temperature) and CR/SRexpansion.

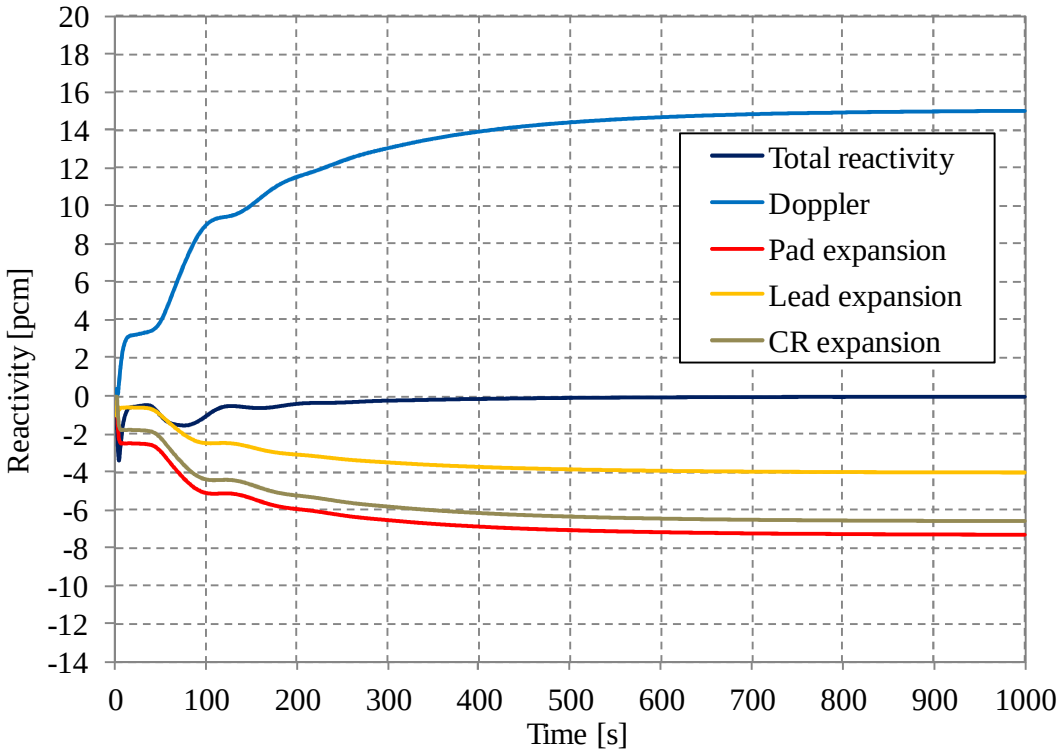


Figure 1-28: ALFRED Single PP Trip EOC accident, neutron kinetic feedbacks larger contributions to total reactivity

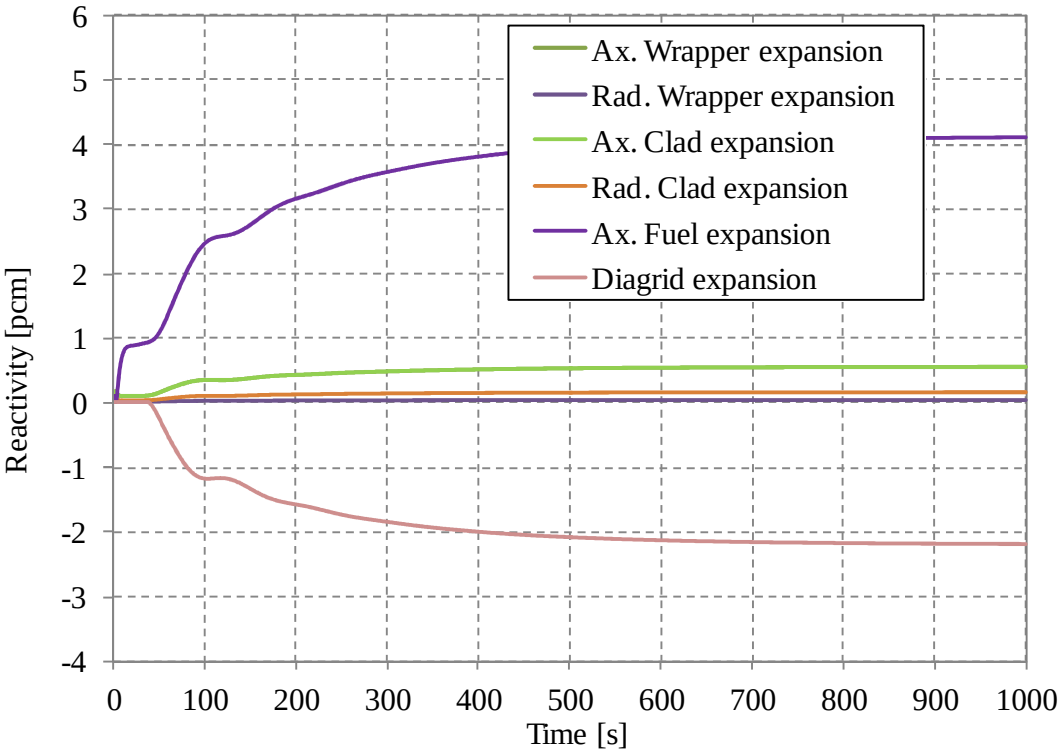


Figure 1-29: ALFRED Single PP Trip EOC accident, neutron kinetic feedbacks smaller contributions to total reactivity

Within the minor reactivity contributions again two opposite trends can be recognized attaining to axial wrapper expansion (positive) and diagrid expansion (negative). Both trends are driven by the (increased) lead temperature. Overall core reactivity laid on a value equal to zero after 600 s. Reaching such balance is mandatory for a flat trend in the core power. The lead temperature at the inlet and outlet of the FA is reported in Figure 1-30. An increase of about 15°C is computed by the code at the core outlet due to the reduction of the core mass flow rate. About 650 s are needed to achieve steady behaviour. Inlet temperature trend is similar to the outlet, both in terms of timing and variation.

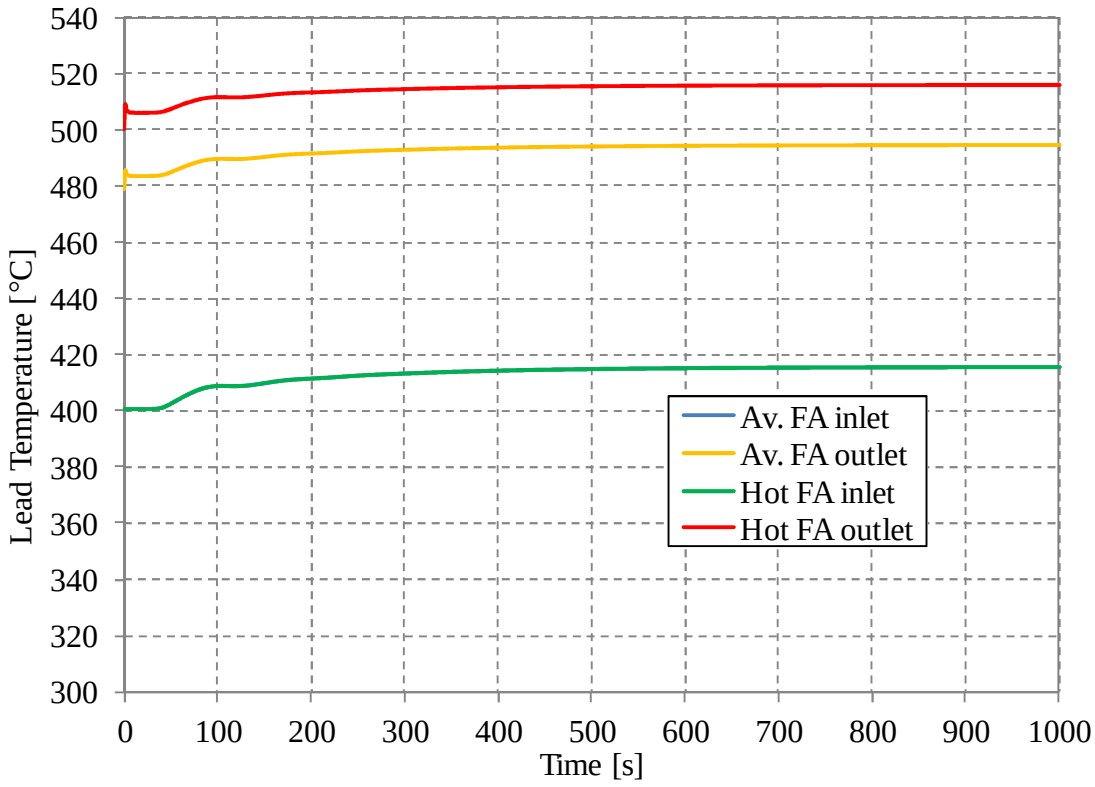


Figure 1-30: ALFRED Single PP Trip EOC accident, lead inlet and outlet temperature in average FA and max power FA

Figure 1-31 shows the maximum clad temperature which basically reflects the behaviour of the primary coolant. In this context the temperature jump is about 15°C; the new reached value does not constitute any harms for the material.

Maximum fuel temperature, shown in Figure 1-32, decreases in the first part of the transient driven by the power reduction. Further on, namely after about 650 s, the fuel temperature stabilizes at a value about 55°C (for the average FA) less than the steady state.

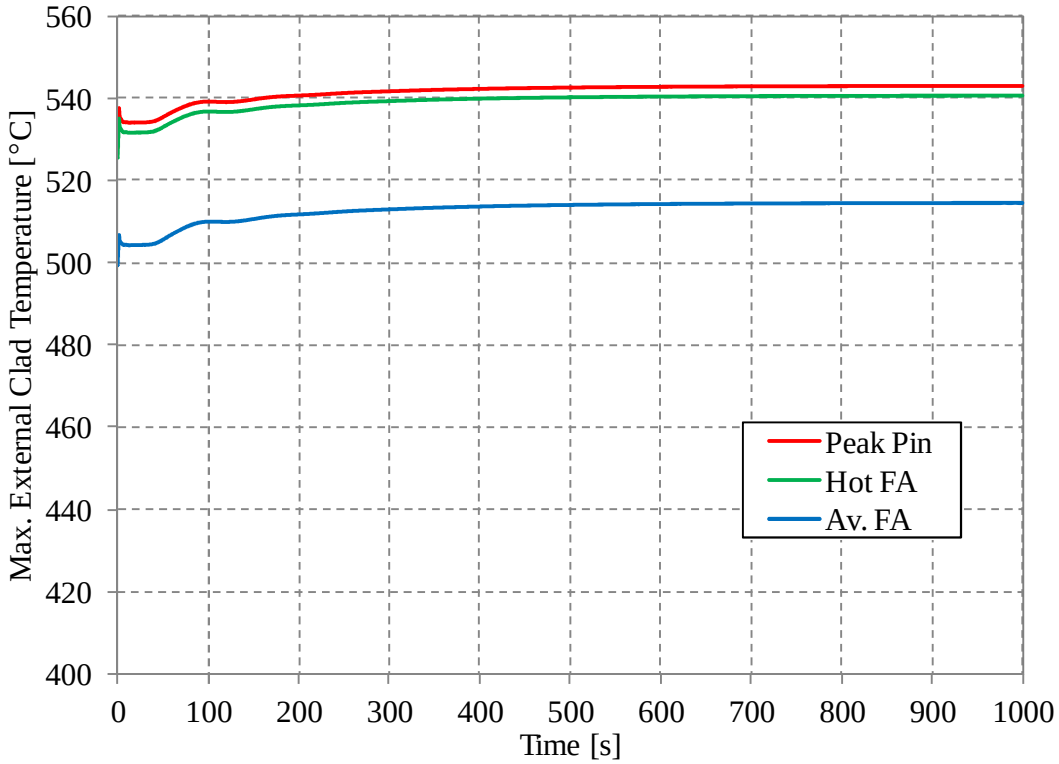


Figure 1-31: ALFRED Single PP Trip EOC accident, clad temperature in average FA, max power FA and peak pin

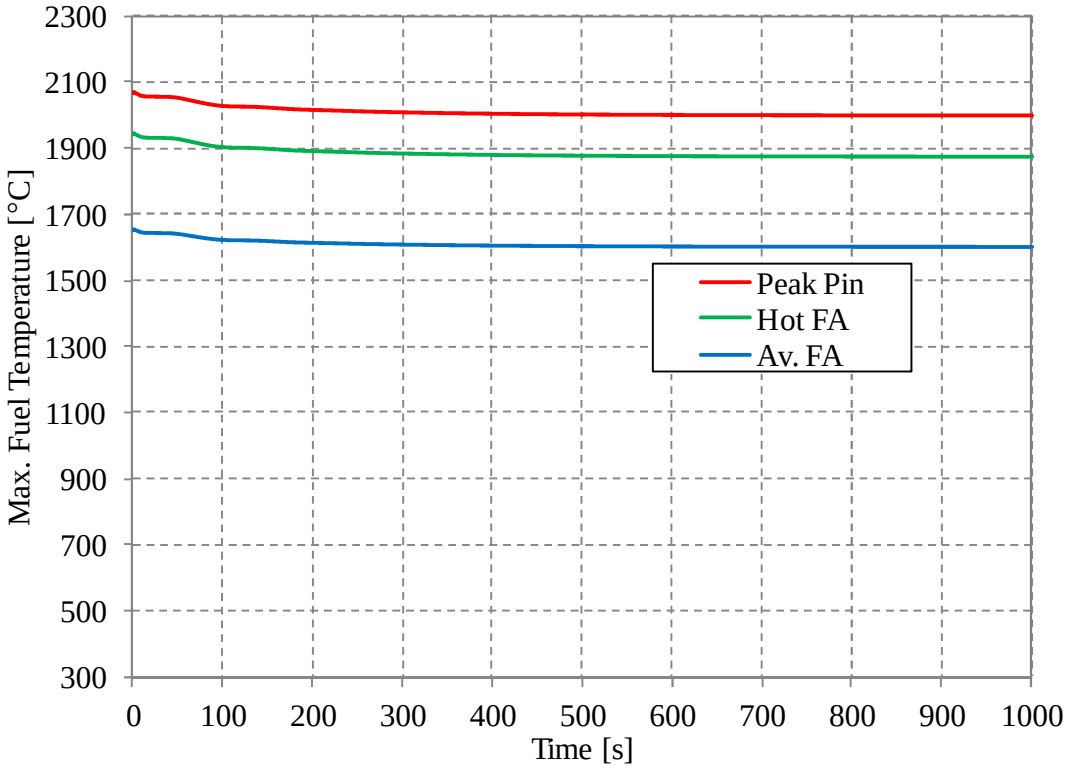


Figure 1-32: ALFRED Single PP Trip EOC accident, fuel temperature in average FA, max power FA and peak pin

Figure 1-33 compares the lead temperature distribution along the active core length between steady state conditions and Single PP trip at the end of the simulation. It can be noted that accident lead temperature profile is almost parallel to the steady state profile. The “accident” curves are shifted toward higher values of about 20°C. The increase of temperature is the results of the balance between the decrease of the reactor mass flow rate and of the core power variation.

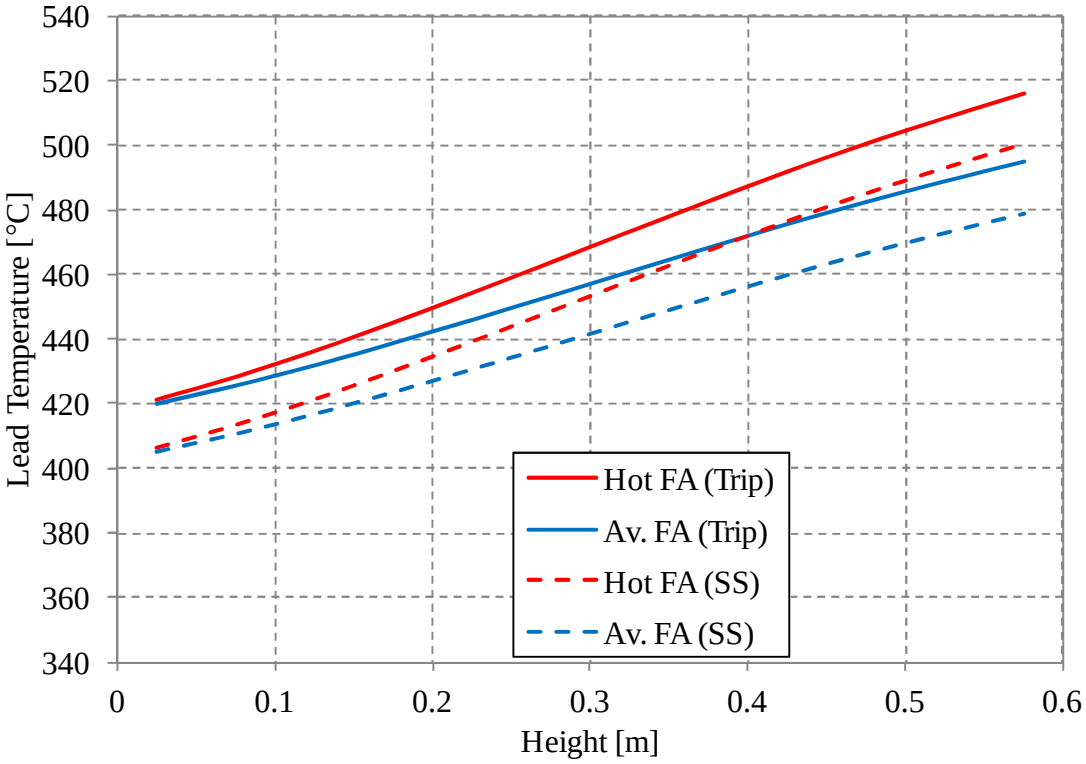


Figure 1-33: ALFRED Single PP Trip EOC accident, axial temperature profile along the core active length and comparison with steady state conditions

As previously mentioned, single PP trip results in reverse flow in the affected flow path. The effect of reverse flow is clearly visible in Figure 1-34, showing primary coolant temperature at inlet and outlet of SG1 (affected) and SGs (taken as example of unaffected flow path). Inlet temperature of SG1 drops down to about 360°C, while the outlet remains very close to the nominal value. Unaffected SGs feels the transient in the early stage during which inlet temperature increases of about 10°C, then new working conditions are established close to nominal value.

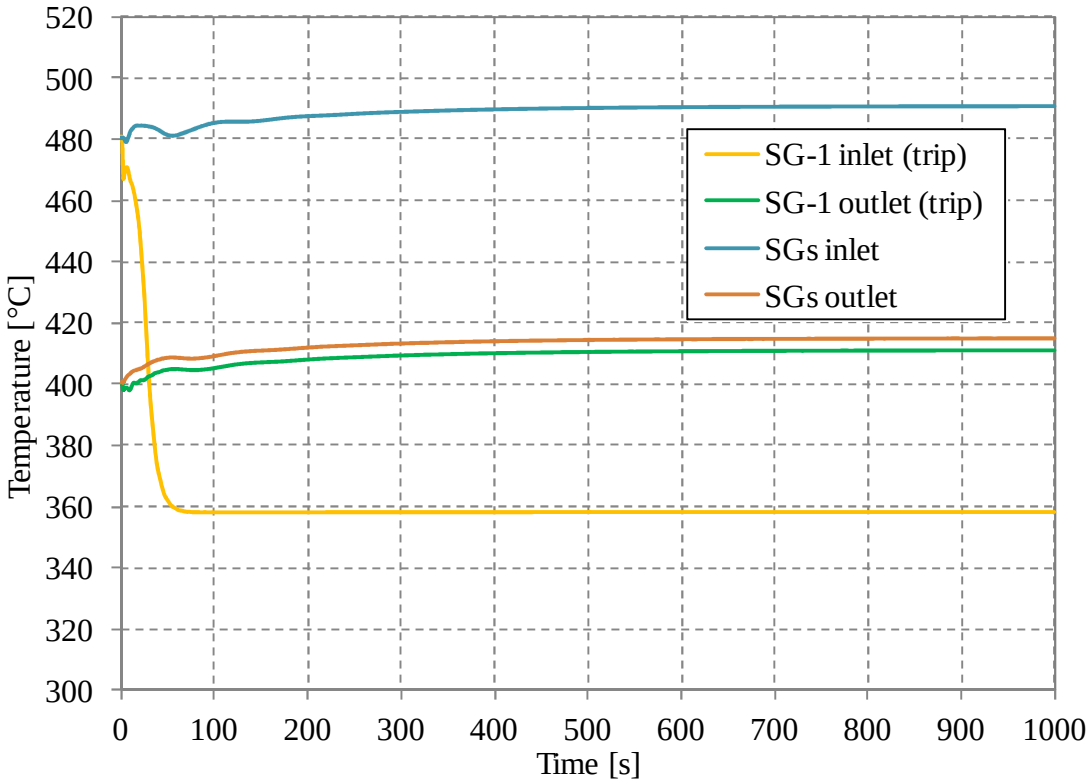


Figure 1-34: ALFRED Single PP Trip EOC accident, SG1(affected) and other SGs primary side inlet and outlet temperature

Concerning the secondary side flow characteristics, in the affected SG1, a drop of outlet temperature down to saturation value corresponding to the secondary pressure is predicted, as highlighted in Figure 1-35. Secondary side fluid enthalpy in affected loop is haltered because of the flow reversal which penalized the SG efficiency (parallel flow). Rather minimal disturbance has been evidenced in the other SGs.

The SG performance consequently to the postulated accident can be analyzed also through Figure 1-36, Figure 1-37 and Figure 1-38, showing profiles of temperature and quality at the end of the simulation. Figure 1-36 shows the primary and secondary side fluid temperature profiles along the tube length of the SG1, i.e. the trip loop SG. It can be seen the major change in the behaviour of the plotted quantities in respect to the steady state conditions, caused by the occurrence of the flow reversal. Occurrence of flow reversal can be appreciated observing that the bottom SG1 (0 m) lead temperature is higher than its value at the top (6 m). Such temperature profile induces on the secondary fluid just the achievement of saturation condition. Observing Figure 1-37, which reports the same quantities of Figure 1-36 but referred to the 7 non affected SGs, it can be seen that the profile of the plotted quantities is

similar to steady state trend. However, temperature distributions are at a higher level. This results in a larger average temperature in the lead and in an earlier achievement of superheated conditions for the steam. Finally, Figure 1-38, shows the impact of the accident on the steam thermodynamic quality of the trip loop SG1. Maximum achieved quality at the tubes outlet is bit more than 0.2 (green continuous line), far from the value obtained in steady state condition (see dashed line). On the contrary the achieved quality at other (not affected) SGs is higher than that in nominal conditions.

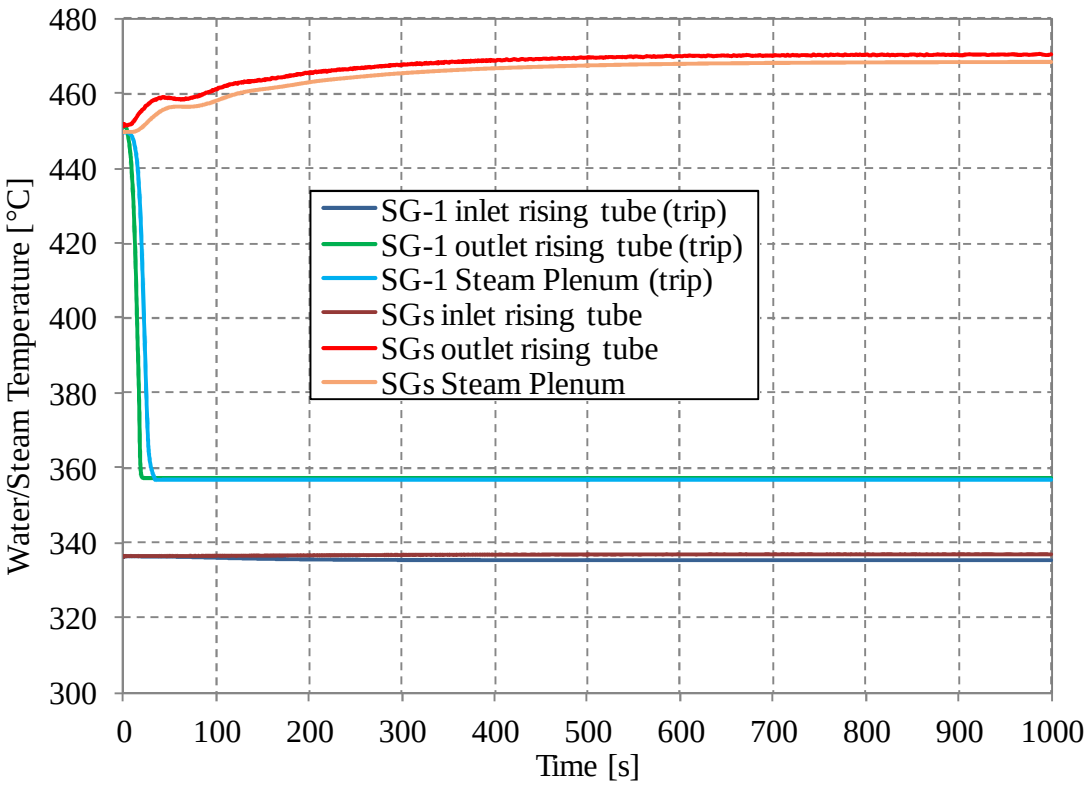


Figure 1-35: ALFRED Single PP Trip EOC accident, SG1(trip) and SGs secondary side inlet (water) and outlet (steam) temperature

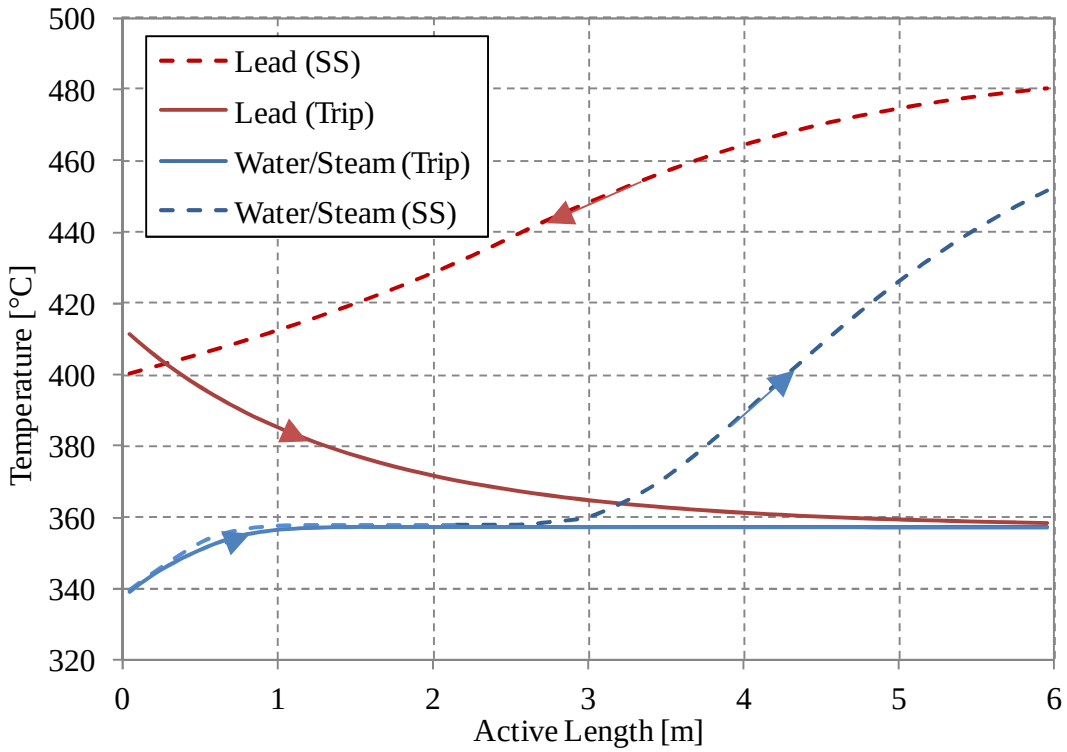


Figure 1-36: ALFRED Single PP Trip EOC accident, SG1 (trip) primary and secondary side temperature profile along the tubes length and comparison with steady state conditions

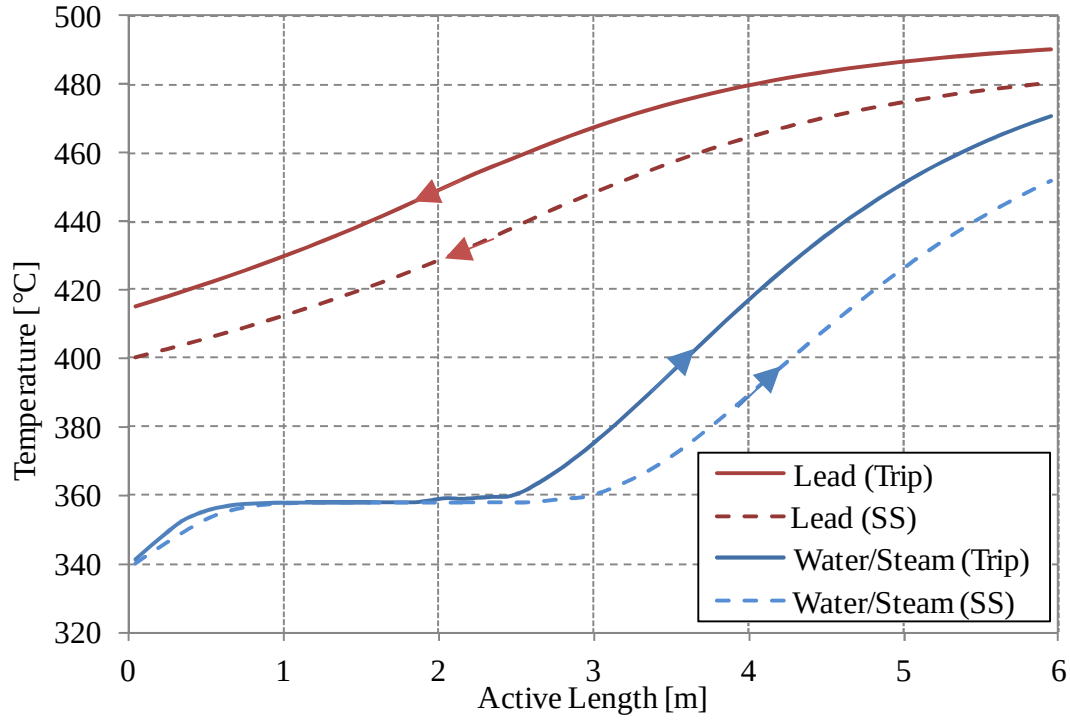


Figure 1-37: ALFRED Single PP Trip EOC accident, SGs (not affected) primary and secondary side temperature profile along the tubes length and comparison with steady state conditions

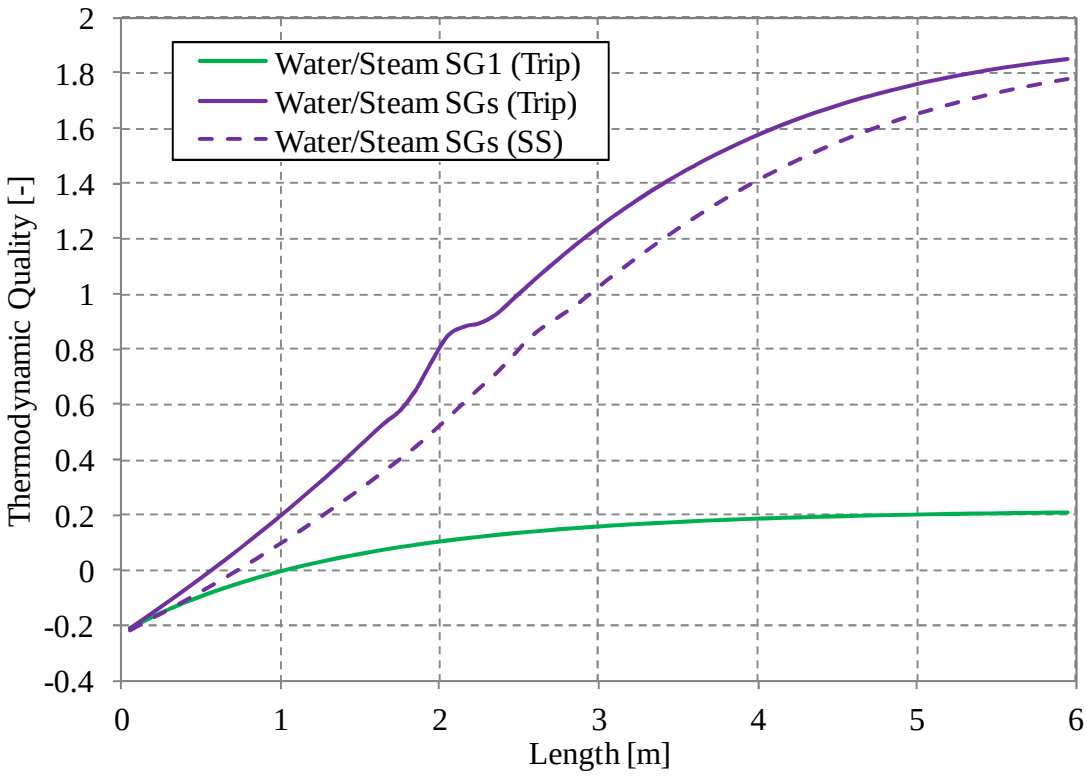


Figure 1-38: ALFRED Single PP Trip EOC accident, thermodynamic quality profile of the SG1 (trip) and the 7 SGs (not affected) along the tubes length and comparison with steady state conditions

4.3.2 Single Primary Pump trip simulation in BOC condition

The second simulation in which Beginning of Cycle core configuration is considered has been performed adopting the same nodalization, including axial peaking factor, as per the EOC case, but with different reactivity feedbacks. Namely consistent values with the selected core status are introduced in the input deck. The adoption of the same nodalization results in getting very similar response to the one illustrated for EOC core configuration.

The numerical simulation ranges up to 1000 s, enough time frame to demonstrate that the reactor can withstand such a transient. Table 1-9 and Table 1-10 provide the imposed events and the resulting sequence of events. Minor or minimal differences are visible comparing the two tables with the ones related with EOC case.

Event	Time of occurrence	Value	Note
PP1 trip	0s	-	Start of simulation of pump coast down – initiating event
SCRAM	-	-	Not simulated
FW mass flow rate (per each SG)	-	24.1 kg/s	Kept as in nominal condition

Table 1-9: ALFRED Single PP Trip BOC accident, imposed events

Event	Time of occurrence	Value	Note
PP1 halved mass flow	>1 s	-	
Onset of flow reversal	1.2 s	-	In trip loop flow path
Maximum difference between core and cooling power	54 s	21 MW	Core power > cooling power
Minimum reactor mass flow rate	2 s	22580 kg/s	Approx. 93% of the nominal value
Maximum core outlet lead temperature	716 s	512°C	Max FA power
Maximum clad temperature	764 s	542°C	Predicted in the peak pin
Minimum core power	996 s	282.5 MW	Power decrease due to neutron feedbacks
Maximum fuel temperature	0 s	-	Fuel temperature decreases along the transient

Table 1-10: ALFRED Single PP Trip BOC accident, resulting sequence of events

Rather than repeated the analysis presented for the Single PP trip EOC case, few figures comparing the achieved results assuming EOC and BOC core status are provided.

Figure 1-39 shows the comparison related with the core power between EOC (continuous line) and BOC (dashed line) case. The two curves have a very similar trend along the transient. However, BOC power level is a bit higher than EOC case due to different neutron feedbacks. The limited difference is appreciable seeing Figure 1-40 which zoom the quantities of the previous plot.

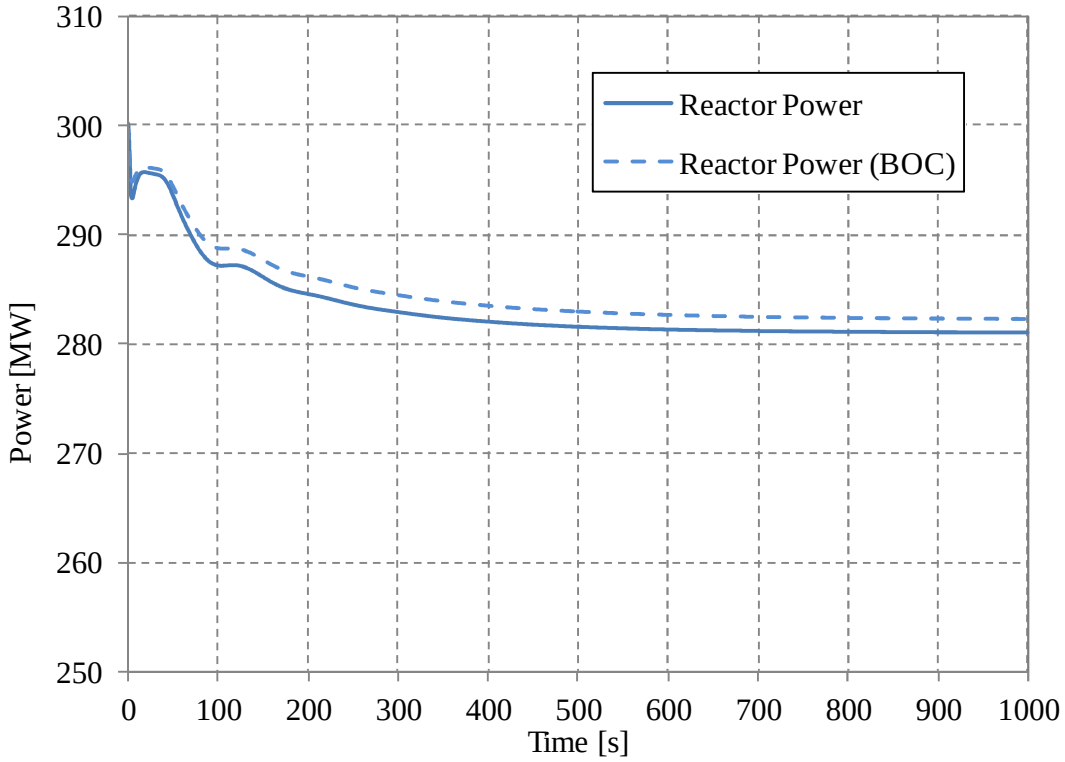


Figure 1-39: ALFRED Single PP Trip accident, reactor core power comparison between EOC and BOC core status

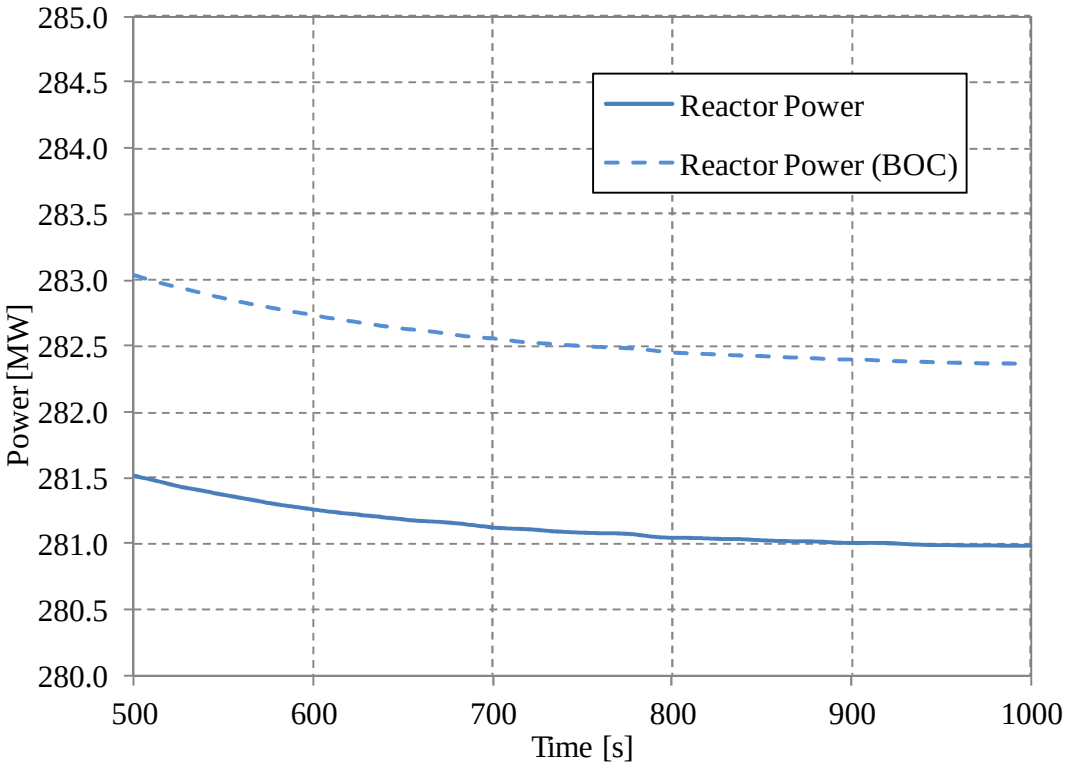


Figure 1-40: ALFRED Single PP Trip accident, reactor core power comparison between EOC and BOC core status – zoom

Regarding lead temperature trend the comparison between EOC and BOC case reflects the core power trend. In BOC case both inlet and outlet lead temperature show higher values almost along the entire simulation. Figure 1-41 compares the average and hot FA core outlet temperature for the EOC (continuous lines) and BOC (dashed lines) cases.

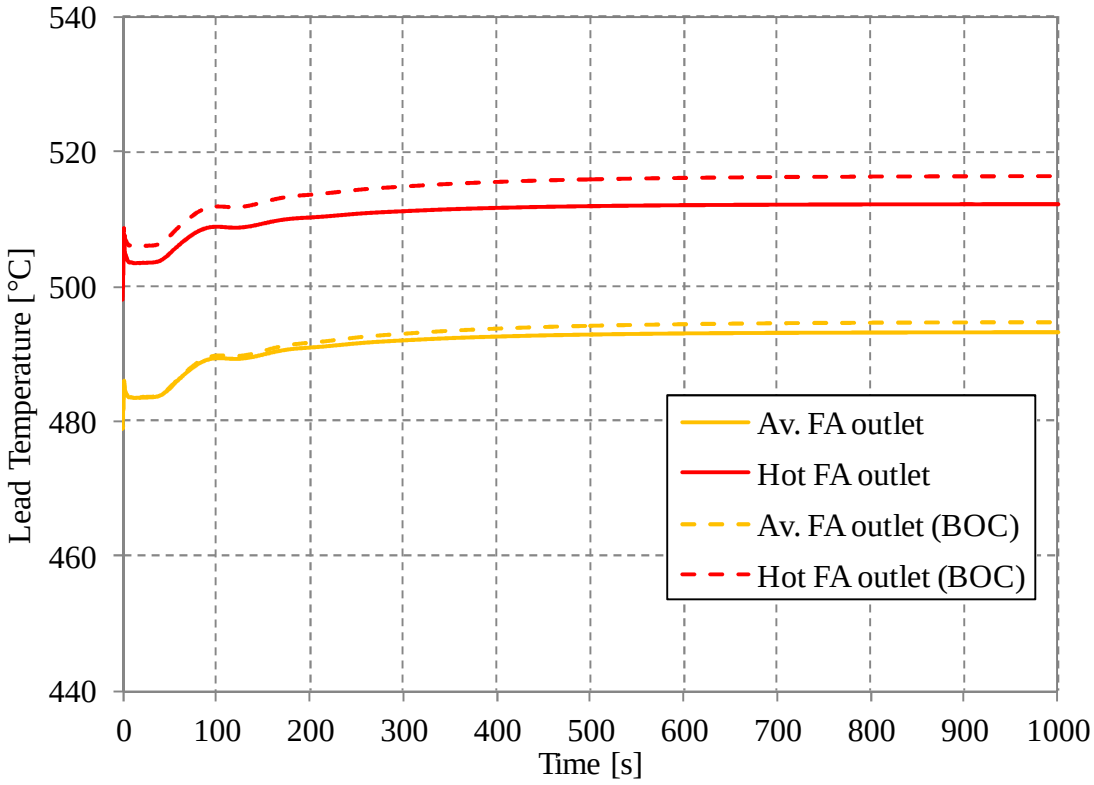


Figure 1-41: ALFRED Single PP Trip accident, average and hot FA core outlet temperature comparison between EOC and BOC core status

5 Conclusions

In the present report thermal-hydraulic simulations of ALFRED reactor has been described. Such analyses have been carried out adopting RELAP5 code and a suitable nodalization developed by CIRTEN-UNIPI.

Two accidents attaining to two classes of transients have been considered, namely Unprotected Loss of Flow for TDEC-1 category and Single Primary Pump trip for the DBC category, respectively. In addition the latter one has been analyzed at End Of Cycle and Beginning Of Cycle core conditions.

ULOF is a quite challenging scenario in which it was postulated the simultaneous coast down of all eight primary pumps without safety rods fall to scram the reactor. According to the performed simulations, natural circulation conditions are established in the ALFRED reactor, with a total mass flow rate of about 6100 kg/s. The core power is driven by reactivity feedbacks and experiences a fast drop down to 170 MW. Later during the transient, a stabilization to around 225 MW has been computed. Clad and lead core outlet temperatures show a quite rapid increase with maximum values of 828 and 802°C respectively during the first phase of the transient, after that a stabilization at about 610°C (clad) and 600°C (lead) occurs (for average FA).

Concerning the Primary Pump trip case, the PP attaining to the flow path 1 is assumed to be tripped. Soon after the end of its coast down, a reverse flow is occurring in the trip loop flow path. Consequently, overall reactor mass flow rate experience a reduction of about 7%. In this respect larger contribution to feedback effect come from the Doppler and Pad expansion. Cooling power shows a couple of oscillations during the first 200 s of the transient evolution, which are reduced soon, and finally dumped after 250 s. New steady conditions are reached at a power level of about 280 MW.

Based on the outcome of the simulation, the selected transient related to one Primary Pump trip accident does not constitute any harm concerning clad and fuel temperature, for which a slightly increase and a lower temperature is computed respectively. Stronger effects are visible in the SG attaining to the trip loop flow path in which bottom SG temperature is higher than upper temperature, because of flow reversal occurrence. In the secondary side also the outlet temperature of the same SG drops down (in respect to steady state value) to the saturation temperature.

The conclusions drawn above are applicable for both core states, namely EOC and BOC. Comparing the two transients, the general trends of the selected parameters are very similar; minor differences have been computed in terms of core power because of the differences in the reactivity feedback.

6 References

1. L. Mansani “Updated design options for the LFR reference plant”, LEADER project deliverable D01, May 2011.
2. L. Vála, C. Latgé, P. Agostini, et al. “Roadmap proposal for building knowledge and facilities needed for nuclear energy systems development” Deliverable D8.4, ADRIANA Project, 31/07/2011.
3. E. Bubelis K. Mikityuk “Plant data for the safety analysis of the ETDR (ALFRED)”, LEADER Project, TEC058-2012 rev 0, 21/05/2012.
4. Drawing LEADER33DMMX013 Rev. 0 – ALFRED Project – Reactor Block General Assembly.
5. G. Ramò and M. Reale “LEADER Task 3.3: ALFRED Reactor Block”, LEADER WP3 meeting presentation, Bologna, October 25th, 2011.
6. A. Alemberti, The ALFRED project on Lead-cooled Fast Reactor, ESNII Conference Advanced Fission Research in HORIZON 2020 European Economic And Social Committee Brussels, 25 June 2012.
7. M. Palmero and F. Fionelli “ALFRED steam generator design”, LEADER WP3 meeting presentation, Genova, May 11th, 2011.
8. RELAP5/Mod3 Code Manual, 1999 Vol. I-V, the Thermal Hydraulics Group, SCIENTECH Inc., Idaho.
9. G. Bandini, ENEA, Personal communication on ELSY pump behaviour.
10. P.A. Ushakov, A. V. Zhukov, N. M. Matyukhin, “Heat transfer to liquid metals in regular arrays of fuel elements”, High temperature, Vol.15, pp. 868-873, 1977.
11. I. E. Idelcik “Memento des pertes de charge”, ISSN 0399-4198.